Imię i nazwisko autora rozprawy: **Błażej Galiński**

Dyscyplina naukowa: **Nauki Chemiczne**

ROZPRAWA DOKTORSKA

Tytuł rozprawy w języku polskim:

Chromogeniczne pochodne azoli jako składniki warstw receptorowych czujników optycznych

Tytuł rozprawy w języku angielskim:

Chromogenic azole derivatives as components of optical sensor receptor layers

Promotor

dr hab. inż. Ewa Wagner-Wysiecka, prof. PG

Gdańsk, 2024

POLITECHNIKA GDAŃSKA

WYDZIAŁ CHEMICZNY

OŚWIADCZENIE

Autor rozprawy doktorskiej: **Błażej Galiński**

Ja, niżej podpisany, oświadczam, iż jestem świadomy, że zgodnie z przepisem art. 27 ust. 1 i 2 ustawy z dnia 4 lutego 1994 r. o prawie autorskim i prawach pokrewnych (t.j. Dz.U. z 2021 poz. 1062), uczelnia może korzystać z mojej rozprawy doktorskiej zatytułowanej:

Chromogeniczne pochodne azoli jako składniki warstw receptorowych czujników optycznych

do prowadzenia badań naukowych lub w celach dydaktycznych.[1]

Świadomy odpowiedzialności karnej z tytułu naruszenia przepisów ustawy z dnia 4 lutego 1994 r. o prawie autorskim i prawach pokrewnych i konsekwencji dyscyplinarnych określonych w ustawie Prawo o szkolnictwie wyższym i nauce (Dz.U.2021.478 t.j.), a także odpowiedzialności cywilno-prawnej oświadczam, że przedkładana rozprawa doktorska została napisana przeze mnie samodzielnie.

Oświadczam, że treść rozprawy opracowana została na podstawie wyników badań prowadzonych pod kierunkiem i w ścisłej współpracy z promotorem **dr hab. inż. Ewą Wagner-Wysiecką, prof. PG**.

Niniejsza rozprawa doktorska nie była wcześniej podstawą żadnej innej urzędowej procedury związanej z nadaniem stopnia doktora.

Wszystkie informacje umieszczone w ww. rozprawie uzyskane ze źródeł pisanych i elektronicznych, zostały udokumentowane w wykazie literatury odpowiednimi odnośnikami, zgodnie z przepisem art. 34 ustawy o prawie autorskim i prawach pokrewnych.

Potwierdzam zgodność niniejszej wersji pracy doktorskiej z załączoną wersją elektroniczną.

Gdańsk, dnia ....

podpis doktoranta

Ja, niżej podpisany, wyrażam zgodę na umieszczenie ww. rozprawy doktorskiej w wersji elektronicznej w otwartym, cyfrowym repozytorium instytucjonalnym Politechniki Gdańskiej.

Gdańsk, dnia ....

podpis doktoranta

[1] Art. 27. 1. Instytucje oświatowe oraz podmioty, o których mowa w art. 7 ust. 1 pkt 1, 2 i 4–8 ustawy z dnia 20 lipca 2018 r. – Prawo o szkolnictwie wyższym i nauce, mogą na potrzeby zilustrowania treści przekazywanych w celach dydaktycznych lub w celu prowadzenia działalności naukowej korzystać z rozpowszechnionych utworów w oryginale i w tłumaczeniu oraz zwielokrotniać w tym celu rozpowszechnione drobne utwory lub fragmenty większych utworów.
2. W przypadku publicznego udostępniania utworów w taki sposób, aby każdy mógł mieć do nich dostęp w miejscu i czasie przez siebie wybranym korzystanie, o którym mowa w ust. 1, jest dozwolone wyłącznie dla ograniczonego kręgu osób uczących się, nauczających lub prowadzących badania naukowe, zidentyfikowanych przez podmioty wymienione w ust. 1.

POLITECHNIKA GDAŃSKA

WYDZIAŁ CHEMICZNY

OPIS ROZPRAWY DOKTORSKIEJ

Autor rozprawy doktorskiej: Błażej Galiński

Tytuł rozprawy doktorskiej w języku polskim: Chromogeniczne pochodne azoli jako składniki warstw receptorowych czujników optycznych

Tytuł rozprawy w języku angielskim: Chromogenic azole derivatives as components of optical sensor receptor layers

Język rozprawy doktorskiej: polski

Promotor rozprawy doktorskiej: dr hab. inż. Ewa Wagner-Wysiecka, prof. PG

Data obrony:

Słowa kluczowe rozprawy doktorskiej w języku polskim: azol, chromojonofor, związki azowe, warstwy receptorowe, czujniki optyczne, optody

Słowa kluczowe rozprawy doktorskiej w języku angielskim: azole, chromoionophore, azo compounds, receptor layers, optical sensors, optodes

Streszczenie rozprawy w języku polskim: Głównym celem badań prowadzonych w ramach studium doktoranckiego była synteza oraz badanie właściwości chromogenicznych pochodnych azoli, makrocyklicznych i acyklicznych, jako składników warstw receptorowych czujników optycznych. Otrzymane związki zawierają w swojej strukturze resztę heterocykliczną – azol, który może uczestniczyć w tworzeniu kompleksów z jonami metali ciężkich oraz co najmniej jedno ugrupowanie azowe. Obecność grupy azowej zapewnia właściwości chromoforowe, ale także stanowi dodatkowe centrum koordynacji jonów metali poprzez jeden z dwóch atomów azotu tej grupy. Wybrane chromojonofory przetestowano pod kątem unieruchomienia ich na podłożach o różnych właściwościach hydrofobowo-lipofilowych, w celu uzyskania warstw receptorowych. Zbadana została odpowiedź spektralna i kolorymetryczna, przy zastosowaniu cyfrowej analizy obrazu, poszczególnych warstw receptorowych na obecność kationów metali ciężkich w funkcji składu warstwy receptorowej. Oczekiwanym efektem końcowym przeprowadzonych badań było określenie zależności pomiędzy właściwościami proponowanych układów gość-gospodarz w roztworze, a ich charakterystyką po unieruchomieniu na stałym podłożu. Zdefiniowanie tej zależności przyczyniło się do opracowania szybkich i niedrogich warstw receptorowych, wykorzystujących metody optyczne do oznaczania jonów metali ciężkich w próbkach wodnych.

Streszczenie rozprawy w języku angielskim: The main goal of the research conducted as part of the PhD study was the synthesis and study of the chromogenic azole derivatives, macrocyclic and acyclic, as components of optical sensor receptor layers. The obtained compounds contain a heterocyclic residue in their structure - azole, which can participate in the formation of complexes with heavy metal ions and at least one azo moiety. The presence of the azo group provides chromophoric properties, but also constitutes an additional coordination center for metal ions through one of the two nitrogen atoms of this group. Selected chromoionophores were tested for immobilization on substrates with various hydrophobic-lipophilic properties in order to obtain receptor layers. The spectral and colorimetric response of individual receptor layers to the presence of heavy metal cations was examined using digital image analysis as a function of the composition of the receptor layer. The expected end result of the conducted research was to determine the relationship between the properties of the proposed guest-host systems in solution and their characteristics after immobilization on a solid substrate. Defining this relationship contributed to the development of fast and inexpensive receptor layers using optical methods for the determination of heavy metal ions in aqueous samples.

Podstawę niniejszej dysertacji stanowią następujące publikacje:

P1 B. Galiński, E. Luboch, J. Chojnacki, E. Wagner-Wysiecka
Novel diazocrowns with pyrrole residue as lead(II) colorimetric probes, Materials **2021**, 14, 7239. https://doi.org/10.3390/ma14237239
IF_{2021} = 3,748, Q2, MNiSW 140 pkt.

P2 B. Galiński, E. Wagner-Wysiecka
Pyrrole bearing diazocrowns: Selective chromoionophores for lead(II) optical sensing, Sensors and Actuators B: Chemical **2022**, 361, 131678. https://doi.org/10.1016/j.snb.2022.131678
IF_{2022} = 8,400, Q1, MNiSW 140 pkt.

P3 B. Galiński, J. Chojnacki, E. Wagner-Wysiecka
Simple colorimetric copper(II) sensor – spectral characterization and possible applications, Spectrochimica Acta Part A: Molecular and Biomolecular Spectroscopy **2023**, 293, 122472. https://doi.org/10.1016/j.saa.2023.122472
IF_{2022} = 4,400, Q1, MNiSW 140 pkt.

P4 B. Galiński, J. Chojnacki, K. Szwarc-Karabyka, A. Małkowski, D. Sopel, A. Zwolińska, E. Wagner-Wysiecka
Chromogenic macrocycles with imidazole residue: structure vs. properties, Dyes and Pigments **2023**, 219, 111610. https://doi.org/10.1016/j.dyepig.2023.111610
IF_{2022} = 4,500, Q1, MNiSW 100 pkt.

P5 B. Galiński, E. Wagner-Wysiecka
Macrocyclic derivatives of imidazole as chromoionophores for bismuth(III)/lead(II) pair, Sensors and Actuators B: Chemical **2024**, 399, 134798. https://doi.org/10.1016/j.snb.2023.134798
IF_{2022} = 8,400, Q1, MNiSW 200 pkt.

SPIS TREŚCI

WYKAZ SKRÓTÓW 10
I. WPROWADZENIE 12
I.A. CHEMIA SUPRAMOLEKULARNA 13
I.B. CHROMOJONOFORY 22
I.C. CZUJNIKI CHEMICZNE 29
II. ZAŁOŻENIA ROZPRAWY 51
III. MATERIAŁY I METODY BADAWCZE 53
III.A. ODCZYNNIKI CHEMICZNE DO SYNTEZY 54
III.B. IDENTYFIKACJA ZWIĄZKÓW 54
III.C. BADANIE LIPOFILOWOŚCI 55
III.D. KOMPLEKSOWANIE JONÓW METALI W ROZTWORZE 55
III.E. WŁAŚCIWOŚCI KWASOWO-ZASADOWE 55
III.F. ROZTWORY SYMULOWANE 56
III.G. ROZTWORY RZECZYWISTE 56
III.H. WARSTWY RECEPTOROWE 56
III.I. ANALIZA SPEKTROFOTOMETRYCZNA W ZAKRESIE UV-VIS 57
III.J. KOLORYMETRIA OBRAZU CYFROWEGO 57
III.K. GRANICE WYKRYWALNOŚCI I OZNACZALNOŚCI 58
III.L. WPŁYW JONÓW PRZESZKADZAJĄCYCH 58
IV. KRÓTKI PRZEWODNIK PO CYKLU PUBLIKACJI 60
IV.P1 – NOWE DIAZOKORONY Z RESZTĄ PIROLU JAKO KOLORYMETRYCZNE CZUJNIKI OŁOWIU(II) (NOVEL DIAZOCROWNS WITH PYRROLE RESIDUE AS LEAD(II) COLORIMETRIC PROBES) 61
IV.P2 – DIAZOKORONY Z RESZTĄ PIROLU: SELEKTYWNE CHOMOJONOFORY DO OPTYCZNEGO WYKRYWANIA OŁOWIU(II) (PYRROLE BEARING DIAZOCROWNS: SELECTIVE CHROMOIONOPHORES FOR LEAD(II) OPTICAL SENSING) 65
IV.P3 – PROSTY KOLORYMETRYCZNY CZUJNIK MIEDZI(II): CHARAKTERYSTYKA SPEKTRALNA ORAZ MOŻLIWE ZASTOSOWANIA (SIMPLE COLORIMETRIC COPPER(II) SENSOR – SPECTRAL CHARACTERIZATION AND POSSIBLE APPLICATIONS) 68
IV.P4 – CHROMOGENICZNE MAKROCYKLICZNE AZOZWIĄZKI Z RESZTĄ IMIDAZOLU: STRUKTURA A KOLORYMETRYCZNA DETEKCJA MIEDZI(II) I OŁOWIU(II) (CHROMOGENIC AZOMACROCYCLES WITH IMIDAZOLE RESIDUE: STRUCTURE VS. PROPERTIES) 72

IV.P5 – OPTODY Z TRIOCTANU CELULOZY DO RÓWNOCZESNEGO WYKRYWANIA BIZMUTU(III) I OŁOWIU(II) (MACROCYCLIC DERIVATIVES OF IMIDAZOLE AS CHROMOIONOPHORES FOR BISMUTH(III)/LEAD(II) PAIR) 76

V. PODSUMOWANIE 79

DOKUMENTY I OŚWADCZENIA 86

PUBLIKACJE 93

P1 – NOVEL DIAZOCROWNS WITH PYRROLE RESIDUE AS LEAD(II) COLORIMETRIC PROBES 94

P1 – SUPPLEMENTARY MATERIALS 112

P2 – PYRROLE BEARING DIAZOCROWNS: SELECTIVE CHROMOIONOPHORES FOR LEAD(II) OPTICAL SENSING 149

P2 – SUPPLEMENTARY MATERIALS 161

P3 – SIMPLE COLORIMETRIC COPPER(II) SENSOR – SPECTRAL CHARACTERIZATION AND POSSIBLE APPLICATIONS 173

P3 – SUPPLEMENTARY MATERIALS 194

P4 – CHROMOGENIC AZOMACROCYCLES WITH IMIDAZOLE RESIDUE: STRUCTURE VS. PROPERTIES 217

P4 – SUPPLEMENTARY MATERIALS 232

P5 – MACROCYCLIC DERIVATIVES OF IMIDAZOLE AS CHROMOIONOPHORES FOR BISMUTH(III)/LEAD(II) PAIR 260

P5 – SUPPLEMENTARY MATERIALS 273

WYKAZ SKRÓTÓW

ACN	acetonitryl (ang. **ac**eto**n**itrile)
AU	sztuczny mocz (ang. **a**rtificial **u**rine)
BBPA	adypinian bis(1-butylopentylu) (ang. **b**is(1-**b**utyl**p**entyl)**a**dipate)
CC	chusteczki do prania **C**olour **C**atcher
CD	cyklodekstryna (ang. **c**yclo**d**extrin)
CTA	trioctan celulozy (ang. **c**ellulose **t**ri**a**cetate)
DCM	dichlorometan (ang. **di**chloro**m**ethane)
DMF	N,N'-dimetyloformamid (ang. **di**methyl**f**ormamide)
DMSO	dimetylosulfotlenek (ang. **di**methyl **s**ulf**o**xide)
DMSO-d_6	deuterowany dimetylosulfotlenek
DBP	ftalan dibutylu (ang. **di**b**u**tyl **p**hthalate)
DOP	ftalan bis(2-etyloheksylu) (ang. **di**o**c**tyl **p**hthalate)
DOS	sebacynian bis(2-etyloheksylu) (ang. **di**o**c**tyl **s**ebacate)
EDTA	kwas etylenodiaminotetraoctowy (ang. **e**thylene**d**iamine**t**etraacetic **a**cid)
ISE	elektrody jonoselektywne (ang. **i**on **s**elective **e**lectrode)
ISO	optody jonoselektywne (ang. **i**on **s**elective **o**ptodes)
KTClPB	tetrakis(*p*-chlorofenylo)boran potasu (ang. potassium tetrakis(4-chlorophenyl)borate)
LOD	granica wykrywalności (ang. **l**imit **o**f **d**etection)
LOQ	granica oznaczalności (ang. **l**imit **o**f **q**uantity)
MeOH	metanol (ang. methanol)
NMR	magnetyczny rezonans jądrowy (ang. **n**uclear **m**agnetic **r**esonance)
NPOE	eter 2-nitrofenylowo-oktylowy (ang. 2-**n**itro**p**henyl **o**ctyl **e**ther)
PBS	buforowana fosforanem sól fizjologiczna (ang. **p**hosphate **b**uffered **s**aline)
PE	polietylen (ang. **p**oly**e**thylene)
PTFE	poli(tetrafluoroetylen) (ang. **p**oly(**t**etra**f**loro**e**thylene)
PET	poli(tereftalan etylenu) (ang. **p**oly(**e**thylene **t**erephthalate))
PG-PS	szkło porowate modyfikowane polistyrenem (ang. **p**orous **g**lass modified with **p**oly**s**tyrene**)**
PMMA	poli(metakrylan metylu) (ang. **p**oly(**m**ethyl **m**eth**a**crylate))

PP	polipropylen (ang. **p**oly**p**ropylene)
PVC	poli(chlorek winylu) (ang. **p**oly(**v**inyl **c**hloride))
SBF	symulowany płyn ustrojowy (ang. **s**imulated **b**ody **f**luid)
TCM	chloroform (ang. **t**ri**c**hloro**m**ethane)
TEG	glikol trietylenowy (ang. **t**ri**e**thylene **g**lycol)
THF	tetrahydrofuran (ang. **t**etra**h**ydro**f**uran)
W%	wydajność reakcji makrocyklizacji

I. WPROWADZENIE

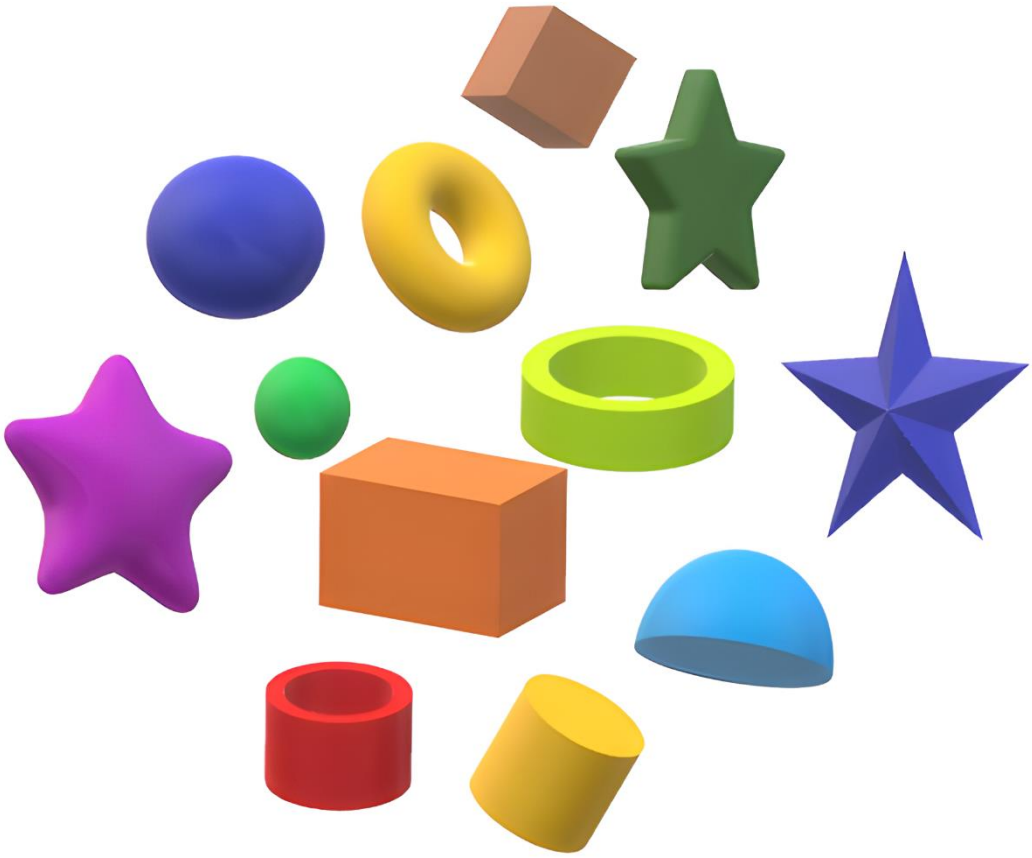

I.A. CHEMIA SUPRAMOLEKULARNA

Termin „chemia supramolekularna" został po raz pierwszy przedstawiony w 1978 roku przez Jean-Marie Lehna, który zdefiniował „supercząsteczkę" jako zorganizowaną złożoną całość utworzoną z połączenia dwóch lub więcej związków chemicznych utrzymywanych razem przez siły międzycząsteczkowe [1]. Chemia supramolekularna miała obejmować badanie tych złożonych jednostek i ich oddziaływań międzycząsteczkowych. Badania i wkład J. M. Lehna oraz Charlesa Pedersena i Donalda Crama w tę nową dziedzinę zostały uhonorowane Nagrodą Nobla w 1987 roku [2-4].

Jednak względnie późne zdefiniowanie tego terminu nie oznacza, że chemia supramolekularna nie istniała wcześniej. Właściwie chemię supramolekularną można odnaleźć już w pierwszych stadiach istnienia Ziemi: od wiązań wodorowych w cząsteczkach wody, po złożone układy enzym-substrat w organizmach żywych. Oddziaływania międzycząsteczkowe obejmują między innymi oddziaływania: jon-jon, dipol-jon, pary jonowe, wiązania wodorowe, koordynację metali, oddziaływania hydrofobowe, siły van der Waalsa, oddziaływania π-π , CH-π, kation-π, anion-π i efekty elektrostatyczne [5]. Te różne typy oddziaływań umożliwiają cząsteczkom łączenie się i organizowanie w złożone struktury, przyczyniając się do tworzenia makroskopowego świata.

Podstawy chemii supramolekularnej sięgają końca XIX wieku, kiedy to opracowano niektóre z najbardziej podstawowych koncepcji dla tego obszaru badań. I tak w 1893 roku Alfred Werner sformułował ideę chemii koordynacyjnej [6], rok później Emil Fischer przedstawił koncepcję „zamka i klucza" (ang. lock-and-key) [7], czyli teorię według której cząsteczka substratu pasuje przestrzennie do centrum aktywnego enzymu, tak jak klucz do zamka, a Villiers odkrył pierwsze cząsteczki gospodarzy – cyklodekstryny (CD) [8-10]. Natomiast kilka lat później Paul Ehrlich opracował koncepcję receptorów i stwierdził, że każda cząsteczka może oddziaływać na organizm ludzki tylko wtedy, gdy występuje w formie związanej („Corpora non agunt nisi fixata") [11-15]. Z czasem kilka z tych koncepcji zostało udoskonalonych i zmodyfikowanych np. w 1903 roku Schardinger scharakteryzował trzy naturalnie występujące CD (α, β i γ) jako cykliczne oligosacharydy, które różnią się między sobą liczbą jednostek glukozowych (rys. I.1) [16-18], a w 1958 roku Daniel Koshland sformułował teorię dopasowania indukowanego, czyli mechanizmu opierającego się na dopasowaniu kształtu enzymu do substratów i przekształceniu ich w produkty [19]. Model indukowanego dopasowania zapewnia bardziej dynamiczny opis tworzenia wiązań, w porównaniu z raczej statyczną zasadą „zamka i klucza", a zatem jest w stanie lepiej wyjaśnić różne zjawiska, w tym np. kooperatywność enzymów. Ponadto niemieckie słowo oznaczające

„supramolekułę" pojawiło się w literaturze już w 1937 roku, kiedy Wolf i jego współpracownicy wprowadzili termin „Übermolekül" do opisania niektórych oddziaływań międzycząsteczkowych w układach takich jak np. dimery kwasów karboksylowych [20-23]. Jednakże dopiero definicja chemii supramolekularnej podana przez Lehna, jako „chemia poza cząsteczką" sprawiła, że dziedzina ta wyłoniła się jako nowa dyscyplina i zaczęto definiować podstawy chemii supramolekularnej jaką znamy dzisiaj [24].

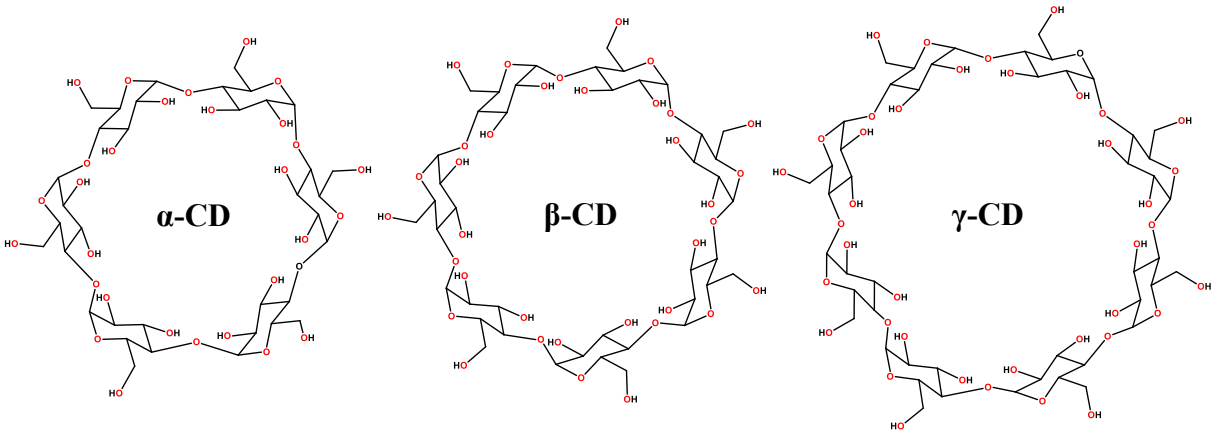

Rys. I.1. Struktury chemiczne naturalnie występujących CD [16-18].

Obecnie chemia supramolekularna obejmuje szeroki obszar badań, który jest powiązany także z innymi dyscyplinami takimi jak fizyka, inżynieria materiałowa czy biologia. Każda z tych dziedzin przyczyniła się do poszerzenia obszaru badań chemii supramolekularnej, co również przełożyło się na chemię molekularną i doprowadziło do pojawienia się chemii adaptacyjnej, która wykorzystuje różnorodność układów chemicznych zarówno na poziomie molekularnym, jak i supramolekularnym, w celu osiągnięcia adaptacji, na drodze procesu samoorganizacji [25-27].

Chemia supramolekularna zajmuje się trzema głównymi obszarami, z których pierwszy dotyczy rozpoznania molekularnego. Rozpoznawanie molekularne można zdefiniować jako wiązanie pomiędzy cząsteczką substratu i cząsteczką receptora. Zatem dana cząsteczka rozpoznaje swoją cząsteczkę partnerską w sposób selektywny i wiąże się z nią, tworząc kompleks gość-gospodarz [28, 29]. Przykład rozpoznania molekularnego w przyrodzie można znaleźć we wspomnianym wcześniej modelu zamka i klucza Fischera.

Według Fischera zamek lub inaczej gospodarz byłby enzymem z określoną dziurką od klucza lub miejscem aktywnym, podczas gdy klucz lub gość byłby specyficznym substratem. Tylko klucz o odpowiedniej wielkości zmieściłby się w dziurce od klucza, co oznacza, że tylko określony substrat, a nie inny, będzie wiązał się z enzymem, zgodnie z zasadą rozpoznawania

molekularnego (rys. I.2). Mechanizm ten jest podstawą wielu reakcji biochemicznych zachodzących w organizmach żywych [30-33].

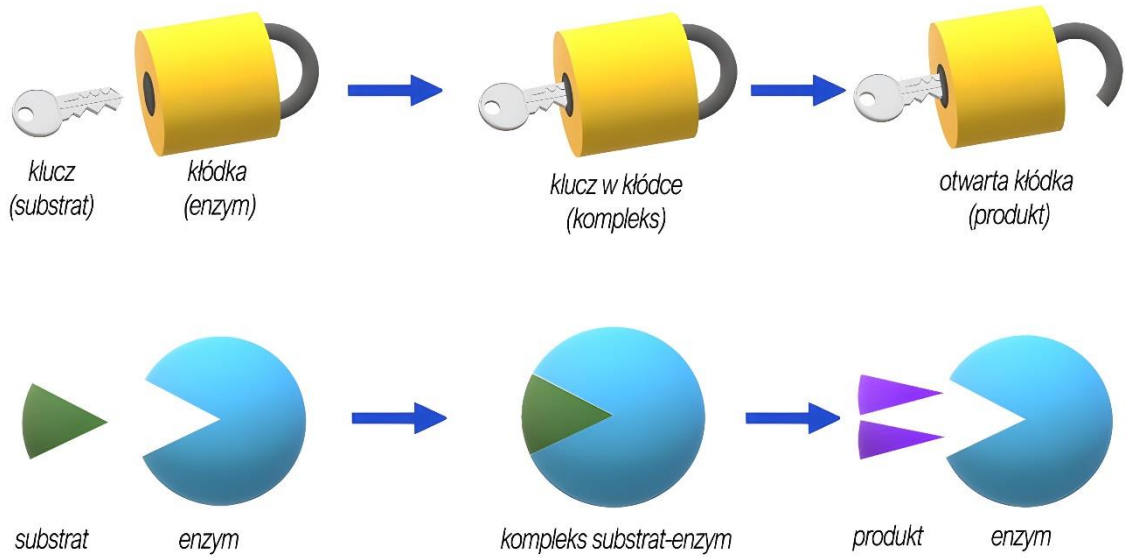

Rys. I.2. Model „zamka i klucza" oraz schemat działania enzymu.

Drugi kierunek badań koncentruje się na projektowaniu oraz syntezie cząsteczek o konkretnej strukturze przestrzennej takich jak np. etery koronowe [34-41], katapinandy [42-45], kryptandy [46-48], podandy [49-51], etery lariatowe [52-55], sferandy [56-62], kawitandy [63-65], karcerandy [66-68], cyklodekstryny [69-73]; cyklofany [74-77], superfany [78-80], kryptofany [81-83], kaliksareny [84-91], pillarareny [92-94], kukurbiturile [95-99], torandy [100, 101], rotaksany [102-106], katenany [107-111], węzły molekularne [112-116], klatki molekularne [117, 118] czy też wirniki molekularne [119-123]. Przykłady wyżej wymienionych związków zostały przedstawione na rysunku I.3.

W 2016 roku przyznano Nagrodę Nobla w dziedzinie chemii trzem naukowcom: Jean-Pierrowi Sauvage, Sir J. Fraserowi Stoddart oraz Bernardowi R. Ferindze, jako drugiej generacji chemików supramolekularnych, którzy zajmują się projektowaniem oraz otrzymywaniem maszyn molekularnych [124-126].

Trzecim obszarem chemii supramolekularnej jest badanie samoorganizacji cząsteczek. Samoorganizacja molekularna to spontaniczne tworzenie supracząsteczek o określonych kształtach i właściwościach, złożonych z cząsteczek połączonych w wyniku oddziaływań niekowalencyjnych [127-130]. Micele, folie, żele, membrany, a także nanostruktury są przykładami systemów samoorganizujących się.

I

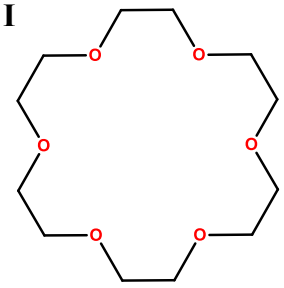

II

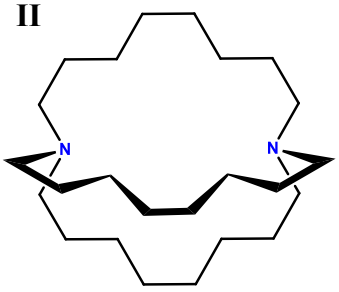

III

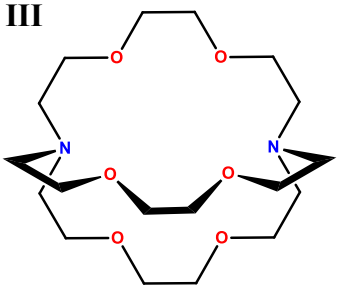

IV

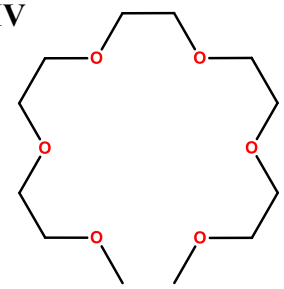

V

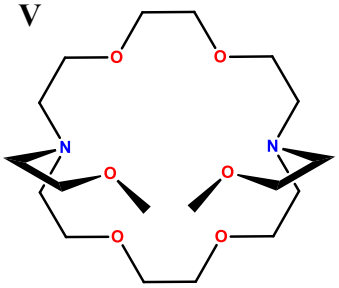

VI

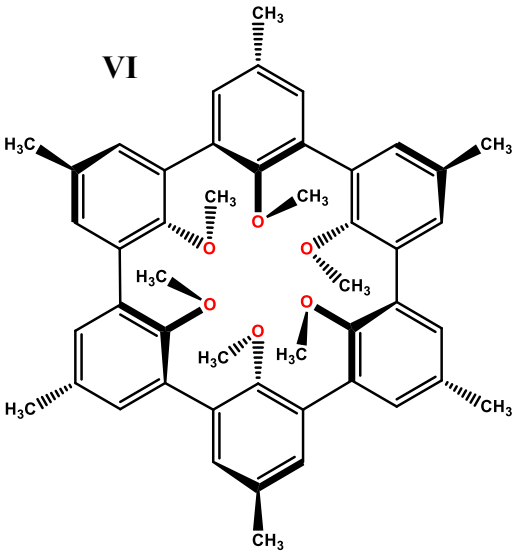

VII

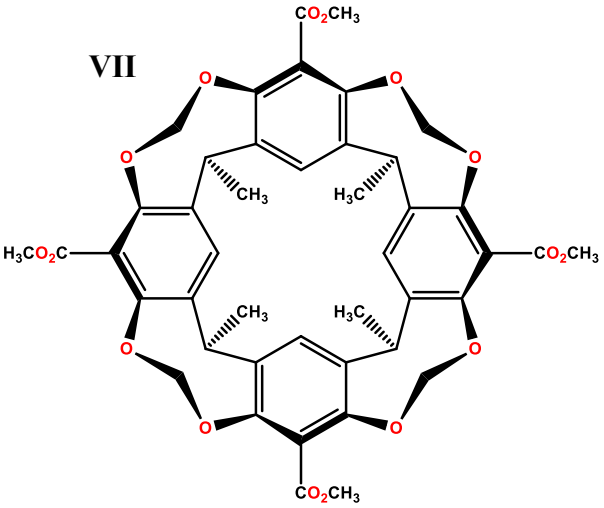

VIII

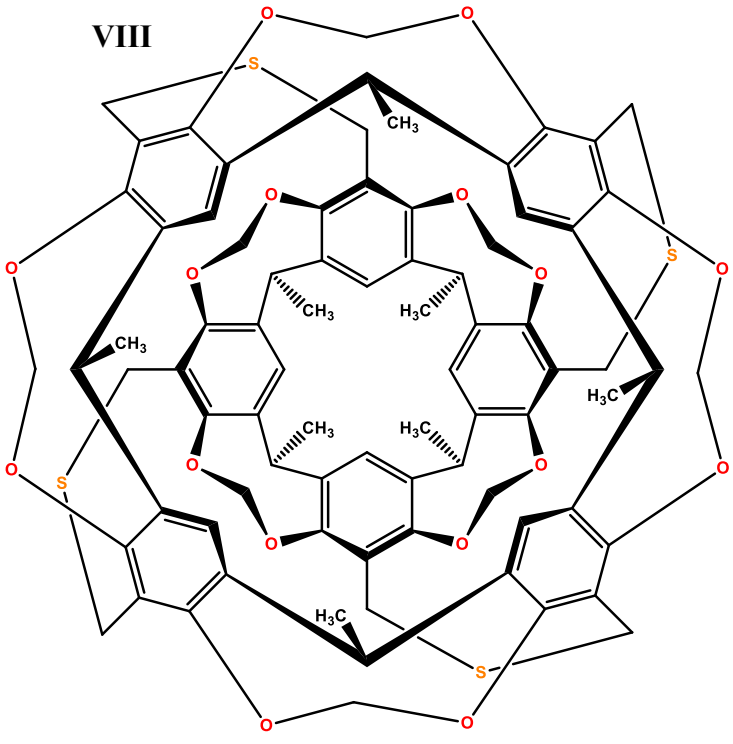

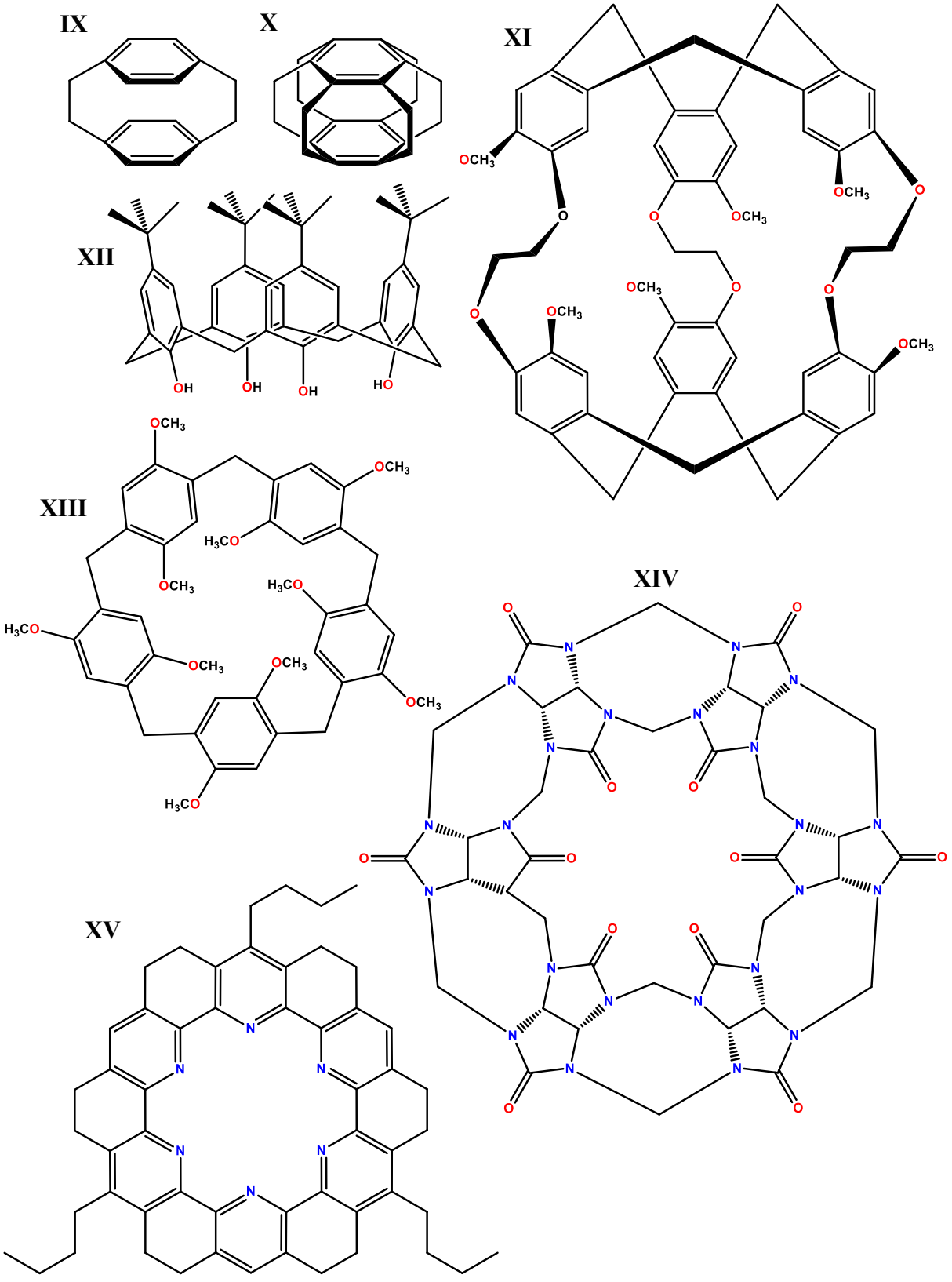

Rys. I.3. Przykłady receptorów molekularnych: **I** – 18-korona-6 [37]; **II** – 1,10-diazabicyklo[8.8.8]heksakozan [42-44]; **III** – [2.2.2]kryptand [46, 47]; **IV** – dimetoksypentaetylenoglikol [49]; **V** – *N,N'*-di-2-metoksyetyl-4,13-diaza-18-korona-6 [55]; **VI** – sferand [56-58]; **VII** – kawitand [63]; **VIII** – karcerand [66]; **IX** – [2.2]paracyklofan [75]; **X** – [2_6]superfan [78]; **XI** – kryptofan [81]; **XII** –*p-tert*-butylokaliks[4]aren [84].**XIII** – pillar[5]aren [92]; **XIV** – kukurbit[6]uril [96]; **XV** – torand [100].

LITERATURA

1. J.–M. Lehn, *Cryptates: inclusion complexes of macropolycyclic receptor molecules*, Pure Appl. Chem. **1978**, 50, 871–892;
2. J.–M. Lehn, *Supramolecular chemistry–scope and perspectives molecules, supermolecules, and molecular devices (Nobel lecture)*, Angew. Chem. Int. Ed. Engl. **1988**, 27, 89–112;
3. D.J. Cram, *The design of molecular hosts, guests, and their complexes (Nobel lecture)*, Angew. Chem. Int. Ed. Engl. **1988**, 27, 1009–1020;
4. C.J. Pedersen, *The discovery of crown ethers (Nobel lecture)*, Angew. Chem. Int. Ed. Engl. **1988**, 27. 1021–1027;
5. F. Huang, E.V. Anslyn, *Introduction: supramolecular chemistry*, Chem. Rev. **2015**, 115, 6999–7000;
6. A. Werner, *Beitrag zur Konstitution anorganischer Verbindungen*, Zeitschrift für anorganische Chemie **1893**, 3, 267–330;
7. E. Fischer, *Einfluss der Configuration auf die Wirkung der Enzyme*, Ber. Dtsch. Chem. Ges. **1894**, 27, 2985–2993;
8. A. Villiers, *Sur la transformation de la fécule en dextrine par le ferment butyrique*, C. R. Acad. Sci. **1891**, 112, 435–437;
9. A. Villiers, *Sur la fermentation de la fécule par l'action du fermentbutyrique*, C. R. Acad. Sci. **1891**, 112, 536–538;
10. A. Villiers, *Sur le monde d'action du ferment butyrique dans la transformation de le fecule en dextrine*, C. R. Acad. Sci. **1891**, 113, 144–147;
11. E.J. Ariens, A.M. Simonis, *A molecular basis for drug action*, J. Pharm. Pharmacol. **1964**, 16, 137–157;
12. L. Pelner, *Corpora non agunt nisi fixata. Maxim behind all of Ehrlich's great discoveries*, N. Y. State J. Med. **1972**, 72, 620–624;
13. A.M. Silverstein, *Paul Ehrlich's Passion: The Origins of His Receptor Immunology*, Cell. Immunol. **1999**, 194, 213–221;
14. C.–R. Prull, *Part of a scientific master plan? Paul Ehrlich and the origins of his receptor concept*, Med. Hist. **2003**, 47, 332–356;
15. A.H. Maehle, *A binding question: the evolution of the receptor concept*, Endeavour **2009**, 33, 135–140;
16. F. Schardinger, *Uber die Zulässigkeit des Warmhaltens von zum Gebuß bestimmten Nahrungsmittel mittelst Wärme speichernder Apparate, sog. Thermophore*, Wien. Klin. Wochenschr. **1903**, 16, 468–479;
17. F. Schardinger, *Über Thermophile Bakterien aus verschiedenen Speisen und Milch, sowie über einige Umsetzungsprodukte derselben in kohlenhydrathaltigen Nährlösungen, darunter krystallisierte Polysaccharide (Dextrine) aus Stärke*, Z. Lebensm. Unters. Forsch. **1903**, 6, 865–880;
18. F. Schardinger, *Bildung kristallisierter polysaccharide (dextrine) aus stärkekleister durch microben*, Zentralbl. Bakteriol. Parasitenk. Abt. II. **1911**, 29, 188–197;
19. D. Koshland, *Application of a Theory of Enzyme Specificity to Protein Synthesis*, Proc. Natl. Acad. Sci. U.S.A. **1958**, 44, 98–104
20. K.L. Wolf , H. Prahm, H. Harms, *Über den Ordnungszustand der Moleküle in Flüssigkeiten*, Z. Phys. Chem. Abt. B **1937**, 36B, 237–287;
21. H. Danken, K.L. Wolf, *Über Verbrennungswärmen und innermolekulare Ordnungszustände*, Z. Phys. Chem. Abt. B **1938**, 38B, 441–450;
22. K.L. Wolf , H. Danken, K. Merkel, *Über Übermolekülbildung*, Z. Phys. Chem. Abt. B **1940**, 46, 287–312;
23. K.L. Wolf, G. Metzger, *Übermolekül–Bildung und Übermolekül–Gleichgewichte*, Justus Liebigs Ann. Chem. **1949**, 563, 157–176;
24. J.–M. Lehn, *Supramolecular Chemistry: Receptors, Catalysts, and Carriers*. Science **1985**, 227, 849−856;
25. J.–M. Lehn, *Perspectives in Chemistry—Steps towards Complex Matter*, Angew. Chem. Int. Ed. **2013**, 52, 2836–2850;
26. J.–M. Lehn, *Perspectives in Chemistry—Aspects of Adaptive Chemistry and Materials*, Angew. Chem. Int. Ed. **2015**, 54, 3276–3289;
27. J.–M. Lehn, *Supramolecular chemistry: Where from? Where to?*, Chem. Soc. Rev. **2017**,46, 2378–2379;
28. D.J. Cram, J.M. Cram, *Host–Guest Chemistry: Complexes between organic compounds simulate the substrate selectivity of enzymes*, Science **1974**, 183, 803–809;
29. E.P. Kyba, R.C. Helgeson, K. Madan, G.W. Gokel, T.L. Tarnowski, S.S. Moore, D.J. Cram, *Host–guest complexation. 1. Concept and illustration*, J. Am. Chem. Soc. **1977**, 99, 8, 2564–2571;
30. H.–J. Schneider, A.K. Yatsimirsky, *Selectivity in supramolecular host–guest complexes*, Chem. Soc. Rev. **2008**, 37, 263–277;
31. H.–J. Schneider, *Binding Mechanisms in Supramolecular Complexes*, Angew. Chem. Int. Ed. **2009**, 48, 3924–3977;
32. J.C. Mejuto, J. Simal–Gandara, *Host–Guest Complexe*, Int. J. Mol. Sci. **2022**, 23, 15730;
33. P.B. Crowley, *OriginsoftheHost−GuestTerminology*, Cryst. Growth Des. **2023**, 23, 8469−8473;
34. C.J. Pedersen, *Cyclic polyethers and their complexes with metal salts*, J. Am. Chem. Soc. **1967**, 89, 2495–2496;
35. C.J. Pedersen, *Cyclic polyethers and their complexes with metal salts*, J. Am. Chem. Soc. **1967**, 89, 7017–7036;
36. C.J. Pedersen, *Macrocyclic Polyethers: Dibenzo–18–crown–6 Polyether and Dicyclohexyl–18–crown–6 Polyether*, Org. Synth. **1972**, 52, 66–69;
37. J.L. Atwood, S.G. Bott, A.W. Coleman, K.D. Robinson, S.B. Whetstone, C.M. Means *The oxonium cation in aromatic solvents. Synthesis, structure, and solution behavior of [$H3O^+$·18-crown-6][Cl-H-Cl]*, J. Am. Chem. Soc. **1987**, 109, 8100–8101;
38. G.W. Gokel, W.M. Leevy, M.E. Weber, *Crown Ethers: Sensors for Ions and Molecular Scaffolds for Materials and Biological Models*, Chem. Rev. **2004**, 104, 2723–2750;
39. F. Nicoli, M. Baroncini, S. Silvi, J. Groppi, A. Credi, *Direct synthetic routes to functionalised crown ethers*, Org. Chem. Front., **2021**, 8, 5531–5549;

40. F. Ullah, T.A. Khan, J. Iltaf, S. Anwar, M.F.A. Khan, M.R. Khan, S. Ullah, M. Fayyaz ur Rehman, M. Mustaqeem, K. Kotwica–Mojzych, , M. Mojzych, *Heterocyclic Crown Ethers with Potential Biological and Pharmacological Properties: From Synthesis to Applications*, Appl. Sci. **2022**, 12, 1102;
41. Z. Qi, Y. Qin, J. Wang, M. Zhao, Z. Yu, Q. Xu, H. Nie, Q. Yan, Y. Ge, *The aqueous supramolecular chemistry of crown ethers*, Front. Chem. **2023**, 11, 1119240;
42. H.E. Simmons, C.H. Park, *Macrobicyclic amines. I. Out–in isomerism of 1,(k + 2)–diazabicyclo[k.l.m]alkanes*, J. Am. Chem, Soc. **1968**, 90, 2428–2429;
43. H.E. Simmons, C.H. Park, *Macrobicyclic amines. II. Out–out in–in prototropy in 1, (k + 2)–diazabicyclo [k.l.m] alkaneammonium ions*. J. Am. Chem, Soc. **1968**, 90, 2429–2431;
44. H.E. Simmons, C.H. Park, *Macrobicyclic amines. III. Encapsulation of halide ions by in, in–1,(k + 2)–diazabicyclo[k.l.m.]alkane ammonium ions*, J. Am. Chem, Soc. **1968**, 90, 2431–2432;
45. B. Dietrich, *Design of anion receptors: Applications*, Pure Appl. Chem. **1993**, 65, 1457–1464;
46. B. Dietrich, J.M. Lehn, J.P. Sauvage, *Diaza–polyoxa–macrocycles et macrobicycles*, Tetrahedron Lett. **1969**, 10, 2885–2888;
47. B. Dietrich, J.M. Lehn, J.P. Sauvage, *Les Cryptates*, Tetrahedron Lett. **1969**, 10, 2889–2892;
48. J.–M. Lehn, *Cryptates: macropolycyclic inclusion complexes*, Pure Appl. Chem. **1977**, 49, 857–870;
49. F. Vögtle, E. Weber, *Multidentate acyclic neutral ligands and their complexation*, Angew. Chem. Int. Ed. Engl. **1979**, 18, 753–776;
50. T. Iimori, W.C. Still, A.L. Rheingold, D.L. Staley, *Podand ionophores. A new class of nonmacrocyclic yet preorganized hosts for cations*, J. Am. Chem. Soc. **1989**, 111, 3439–3440;
51. E.S. Filatova, O.V. Fedorova, G.L. Rusinov, V.N. Charushin, *Synthesis and properties of heterocycle–containing podands*, Chem. Heterocycl. Comp. **2021**, 57, 971–983;
52. G.W. Gokel, D.M. Dishong, C.J. Diamond, *Lariat ethers. Synthesis and cation binding of macrocyclic polyethers possessing axially disposed secondary donor groups*, J. Chem. Soc., Chem. Commun. **1980**, 1053–1054;
53. G.W. Gokel, K.A. Arnold, M. Delgado, L. Echeverria, V.J. Gatto, D.A. Gustowski, J. Hernandez, A. Kaifer, S.R. Miller, L. Echegoyen, *Lariat ethers: from cation complexation to supramolecular assemblies*, Pure App. Chem. **1988**, 60, 461–465;
54. G.W. Gokel, *Lariat ethers: from simple sidearms to supramolecular systems*, Chem. Soc. Rev. **1992**, 21, 39–47;
55. M.R. Gokela, M. McKeevera, J,W. Meisela, S. Negina, M.B. Patela, S. Yina, G.W. Gokel, *Crown ethers having side arms: a diverse and versatile supramolecular chemistry*, J. Coord. Chem. **2021**, 74, 14–39;
56. D.J. Cram, T. Kaneda, R.C. Helgeson, G.M. Lein, *Spherands – ligands whose binding of cations relieves enforced electron–electron repulsions*, J. Am. Chem. Soc. **1979**, 101, 6752–6754
57. K.N. Trueblood, C.B. Knobler, E. Maverick, R.C. Helgeson, S.B. Brown, D.J. Cram, *Spherands, the first ligand systems fully organized during synthesis rather than during complexation*, J. Am. Chem. Soc. **1981**, 103, 5594–5596;
58. G.M. Lein, D.J. Cram, *Spherand complexation and decomplexation rates with sodium and lithium picrates, and activation parameters for decomplexation*, J. Chem. Soc. Chem. Commun. **1982**, 301–304;
59. D.J. Cram, I.B. Dicker, C.B. Knobler, K.N. Trueblood, *Spherand hosts containing cyclic urea units*, J. Am. Chem. Soc. **1982**, 104, 6828–6830;
60. D.J. Cram, I.B. Dicker, M. Lauer, C.B. Knobler, K.N. Trueblood, *Host–guest complexation. 32. Spherands composed of cyclic urea and anisyl units*, J. Am. Chem. Soc. **1984**, 106, 7150–7167;
61. D.J. Cram, T. Kaneda, R.C. Helgeson, B.S. Brown, C.B. Knobler, E. Maverick, K.N. Trueblood, *Host–guest complexation. 35. Spherands, the first completely preorganized ligand systems*, J. Am. Chem. Soc. **1985**, 107, 3645–3657;
62. D.J. Cram, G.M. Lein, *Host guest complexation. 36. Spherand and lithium and sodium–ion complexation rates and equilibria*, J. Am. Chem. Soc. **1985**, 107, 3657–3668;
63. J.R. Moran, S. Karbach, D.J. Cram, *Cavitands: synthetic molecular vessel*, J. Am. Chem. Soc. **1982**, 104, 21, 5826–5828;
64. D.J. Cram, *Cavitands: organic hosts with enforced cavities*, Science **1983**, 219, 1177–1183;
65. Y.–J. Zhu, M.–K. Zhao, J. Rebek, Y. Yu, *Recent Advances in the Applications of Water–soluble Resorcinarene–based Deep Cavitands*, ChemistryOpen **2022**, 11, e202200026;
66. D.J. Cram, S. Karbach, Y.H. Kim, L. Baczynskyj, G.W. Kallemeyn, *Shell closure of two cavitands forms carcerand complexes with components of the medium as permanent guests*, J. Am. Chem. Soc. **1985**, 107, 2576–2576;
67. H.–I. Choi, D.J.,] Cram, C.B. Knobler, E.F. Maverick, *Characterization of cavities in carcerands*, Pure Appl. Chem. **1993**, 65, 539–543;
68. F. Liu, R.C. Helgeson, K.N. Houk, *Building on Cram's Legacy: Stimulated Gating in Hemicarcerands*, Acc. Chem. Res. **2014**, 47, 2168–2176;
69. J. Szejtli, *Introduction and General Overview of Cyclodextrin Chemistry*, Chem. Rev. **1998**, 98, 5, 1743–1754;
70. E.M.M. Del Valle, *Cyclodextrins and their uses: a review*, Process Biochem. **2004**, 39, 1033–1046;
71. G. Crini, *Review: A History of Cyclodextrins*, Chem. Rev. **2014**, 114, 21, 10940–10975;
72. G. Crini, *Twenty years of dextrin research: a tribute to Professor Hans Pringsheim (1876–1940)*, J. Incl. Phenom. Macrocycl. Chem. **2020**, 98, 11–27;
73. N. Morin–Crini, S. Fourmentin, E. Fenyvesi, E. Lichtfouse, G. Torri, M. Fourmentin, G. Crini, 130 years of cyclodextrin discovery for health, food, agriculture, and the industry: a review, Environ. Chem. Lett. **2021**, 19, 2581–2617;
74. C. Brown, A. Farthing, *Preparation and Structure of Di–p–Xylylene*, Nature **1949**, 164, 915–916;
75. D.J. Cram, H. Steinberg, *Macro Rings. I. Preparation and Spectra of the Paracyclophanes*, J. Am. Chem. Soc. **1951**, 73, 5691–5704;

76. D.J. Cram, J.M. Cram, *Cyclophane chemistry: bent and battered benzene rings*, Acc. Chem. Res. **1971**, 4, 204–21;
77. I. Roy, A.H.G. David, P.J. Das, D.J. Pe, J.F. Stoddart, *Fluorescent cyclophanes and their applications*, Chem. Soc. Rev., **2022**, 51, 5557–5605;
78. Y. Sekine, M. Brown, V. Boekelheide *[2.2.2.2.2.2]*(1,2,3,4,5,6)*Cyclophane: superphane*, J. Am. Chem. Soc. **1979**, 101, 3126–3127;
79. R. Gleiter, D. Kratz, *"Super" phanes*, Acc. Chem. Res. **1993**, 26, 311–318;
80. A. Li, Y. Liu, W. Zhou, Y. Jiang, Q. He, *Superphanes: Facile and efficient preparation, functionalization and unique properties*, Tetracherdon Chem **2022**, 1, 100006;
81. J. Gabard, A. Collet, *Synthesis of a (D3)–bis(cyclotriveratrylenyl) macrocage by stereospecific replication of a (C3)–subunit*, J. Chem. Soc., Chem. Commun. **1981**, 1137–1139;
82. T. Briotion, J.P. Dutasta, *Cryptophanes and Their Complexes—Present and Future*, Chem. Rev. **2009**, 109, 1, 88–130;
83. S. Kancherla, J.H. Hansen, *Synthesis of cryptophanes: recent advances*, Eur. J. Org. Chem. **2024**, e202301050;
84. C.D. Gutsche, R. Muthukrishnan, Calixarenes. 1. Analysis of the product mixtures produced by the base–catalyzed condensation of formaldehyde with para–substituted phenols, J. Org. Chem. **1978**, 43, 25, 4905–4906;
85. C.D. Gutsche, *Calixarenes*, Acc. Chem. Res. **1983**, 16, 161–170;
86. E. van Dienst, W.I.I. Bakker , J.F.J. Engbersen, W. Verboom, D.N. Reinhoudt *Calixarenes, chemical chameleon*, Pure Appl. Chem. **1993**, 65, 387–392;
87. P. Timmerman, W. Verboom, D.N. Reinhoudt, *Resorcinarenes*, Tetrahedron **1996**, 52, 2663–2704;
88. D. Diamond, A.M. McKervey, *Calixarene–based sensing agents*, Chem. Soc. Rev. **1996**, 25,15–24;
89. E.S. Espanol, M.M. Villamil, *Calixarenes: Generalities and Their Role in Improving the Solubility, Biocompatibility, Stability, Bioavailability, Detection, and Transport of Biomolecules*, Biomolecules **2019**, 9, 90;
90. R. Kumar, A. Sharma, H. Singh, P. Suating, H.S. Kim, K. Sunwoo, I. Shim, B.C. Gibb, J.S. Kim, *Revisiting Fluorescent Calixarenes: From Molecular Sensors to Smart Materials*, Chem. Rev. **2019**, 119, 9657–9721;
91. C.H.W. Haase, *Path to Industrial Production of Calix[8 and 4]arenes*, J. Org. Chem. **2020**, 85, 603–611;
92. T. Ogoshi, S. Kanai, S. Fujinami, T. Yamagishi, Y. Nakamoto, *para–Bridged Symmetrical Pillar[5]arenes: Their Lewis Acid Catalyzed Synthesis and Host–Guest Property*, J. Am. Chem. Soc. **2008**, 130, 5022–5023;
93. J.–F. Chen, J.–D. Ding, T,–B, Wei, K. Wada, T. Ogoshi, *Pillararenes: fascinating planar chiral macrocyclic arenes*, Chem. Commun. **2021**, 57, 9029–9039;
94. K. Wada, T. Ogoshi, *Functionalization of pillar[n]arenes towards optically responsive systems via host–guest interactions*, Mater. Chem. Front. **2024**;
95. R. Behrend, E. Meyer, F. Rusche, I. Ueber Condensationsproducte aus Glycoluril und Formaldehyd, Justus Liebigs Ann. Chem. **1905**, 339, 1–37;
96. W.A. Freeman, W.L. Mock, N.Y. Shih, *Cucurbituril*, J. Am. Chem. Soc. **1981**, 103, 24, 7367–7368;
97. J. Lagona, P. Mukhopadhyay, S. Chakrabarti., L. Isaacs, Dr.*The Cucurbit[n]uril Family*, Angew. Chem. Int. Ed. **2005**, 44, 4844–4870;
98. E. Masson, X. Ling, R. Joseph, L. Kyeremeh–Mensaha, X. Lu, *Cucurbituril chemistry: a tale of supramolecular success*, RSC Adv. **2012**, 2, 1213–1247;
99. S.J. Barrow, S. Kasera, M.J. Rowland, J. del Barrio, O.A. Scherman, *Cucurbituril–Based Molecular Recognition*, Chem. Rev. **2015**, 115, 12320–12406;
100. T.W. Bell, A. Firestone, *Torands: rigid toroidal macrocycles. Calcium sequestration by a member of this new ligand class*, J. Am. Chem. Soc. **1986**, 108, 8109–8111;
101. T.W. Bell, P.J. Cragg, M.G.B. Drew, A. Firestone, A.D.–I. Kwok, J. Liu, R.T. Ludwig, A.T. Papoulis, *Synthesis of new torands and new uses for old torands*, Pure Appl. Chem. **1993**, 65, 361–366;
102. I.T. Harrison, S. Harrison, *Synthesis of a stable complex of a macrocycle and a threaded chain*, J. Am. Chem. Soc. **1967**, 89, 22, 5723–5724;
103. J.A. Bravo, F.M. Raymo, J.F. Stoddart, A.J.P. White, D.J. Williams, *High Yielding Template–Directed Syntheses of [2]Rotaxanes*, Eur. J. Org. Chem. **1998**, 1998, 2565–2571;
104. M. Xue, Y. Yang, X. Chi, X. Yan, F. Huang, *Development of Pseudorotaxanes and Rotaxanes: From Synthesis to Stimuli–Responsive Motions to Applications*, Chem. Rev. **2015**, 115, 15, 7398–7501;
105. K. Yang, S. Chao, F. Zhang, Y. Pei, Z. Pei, *Recent advances in the development of rotaxanes and pseudorotaxanes based on pillar[n]arenes: from construction to application*, Chem. Commun. **2019**, 55, 13198–13210;
106. J.S.W. Seale, Y. Feng, L. Feng, R.D. Astumian, J.F. Stoddart, *Polyrotaxanes and the pump paradigm*, Chem. Soc. Rev. **2022**, 51, 8450–8475;
107. M. Cesario, C.O. Dietrich–Buchecker, J. Guilhem, C. Pascard, J.P. Sauvage, *Molecular structure of a catenand and its copper(I) catenate: complete rearrangement of the interlocked macrocyclic ligands by complexation*, J. Chem. Soc. Chem. Commun. **1985**, 244–247;
108. P.R. Ashton, C.L. Brown, E.J.T. Chrystal, T.T. Goodnow, A.E. Kaifer, K.P. Parry, D. Philp, A.M.Z. Slawin, N. Spencer, J.F. Stoddart, D.J. Williams, *The self–assembly of a highly ordered [2]catenane*, J. Chem. Soc. Chem. Commun. **1991**, 634–639;
109. G. Guz–Ramirez, D.A. Leigh, A.J. Stephens, *Catenanes: Fifty Years of Molecular Links*, Angew. Chem. Int. Ed. **2015**, 54, 6110–6150;
110. H.Y. Au–Yeung, Y. Deng, *Distinctive features and challenges in catenane chemistry*, Chem. Sci. **2022**, 13, 3315–3334;
111. L. Zhang, Y. Qiu, W.–G. Liu, H. Chen, D. Shen, B. Song, Ka. Cai, H. Wu, Y. Jiao, Y. Feng, J.S.W. Seale, C. Pezzato, J. Tian, Y. Tan, X.–Y. Chen, Q.–H. Guo, C.L. Stern, D. Philp, R.D. Astumian, W.A. Goddard III, J.F. Stoddart *An electric molecular motor*, Nature **2023**, 613, 280–286;
112. C.O. Dietrich–Buchecker, J.–P. Sauvage, *A Synthetic Molecular Trefoil Knot*, Angew. Chem. Int. Ed. Engl. **1989**, 28, 189–192;

113. R.F. Carina, C. Dietrich–Buchecker, J.–P. Sauvage, *Molecular Composite Knots*, J. Am. Chem. Soc. **1996**, 118, 38, 9110–9116;
114. R.S. Forgan, J.–P. Sauvage, J.F. Stoddart, *Chemical Topology: Complex Molecular Knots, Links, and Entanglements*, Chem. Rev. **2011**, 111, 9, 5434–5464;
115. K.E. Horner, M.A. Miller, J.W. Steed, P.M. Sutcliffe, *Knot theory in modern chemistry*, Chem. Soc. Rev. **2016**, 45, 6432–6448;
116. L. Wu, M. Tang, L. Jiang, Y. Chen, L. Bian, J. Liu, S. Wang, Y. Liang, Z. Liu, *Synthesis of contra–helical trefoil knots with mechanically tuneable spin–crossover properties*, Nature Synthesis **2023**, 2, 17–25;
117. L. Tapia, I. Alfonso, J. Sola, *Molecular cages for biological applications*, Org. Biomol. Chem. **2021**, 19, 9527–9540;
118. G. Monta–Gonzalez, F. Sancenon, R. Martinez–Manez, V. Marti–Centelles, *Purely Covalent Molecular Cages and Containers for Guest Encapsulation*, Chem. Rev. **2022**, 122, 16, 13636–13708;
119. T.R. Kelly, H. De Silva, R.A. Silva, *Unidirectional rotary motion in a molecular system*, Nature **1999**, 401, 150–152;
120. N. Koumura, R.W.J. Zijlstra, R.A. van Delden, N. Harada, B.L. Feringa, *Light–driven monodirectional molecular rotor*, Nature **1999**, 401, 152–155;
121. G.S. Kottas, L.I. Clarke, D. Horinek, J. Michl, *Artificial Molecular Rotors*, Chem. Rev. **2005**, 105, 4, 1281–1376;
122. J. Michl, E.C.H. Sykes, *Molecular Rotors and Motors: Recent Advances and Future Challenges*, ACS Nano **2009**, 3, 5, 1042–1048;
123. A. Mondal, R. Toyoda, R. Costil, B.L. Feringa, *Chemically Driven Rotatory Molecular Machines*, Angew. Chem. Int. Ed. **2022**, 61, e202206631;
124. B.L. Feringa, *The art of building small: from molecular switches to motors (Nobel lecture)*, Angew. Chem. Int. Ed. **2017**, 56, 11060–11078;
125. J.–P. Sauvage, *From chemical topology to molecular machines (Nobel lecture)*, Angew. Chem. Int. Ed. **2017**, 56, 11080–11093;
126. J.F. Stoddart, *Mechanically interlocked molecules (mims)–molecularshuttles, switches, and machines (Nobel lecture)*, Angew. Chem. Int. Ed. **2017**, 56, 11094–11125;
127. K. Ariga, J.P. Hill, M.V. Lee, A. Vinu, R. Chavret, S. Acharya, *Challenges and breakthroughs in recent research on self–assembly*, Sci. Tech. Adv. Mat. **2008**, 9, 014109;
128. A. Wang, J. Huang, Y. Yan, *Hierarchical molecular self–assemblies: construction and advantages*, Soft Matter, **2014**, 10, 3362–3373;
129. K. Ariga, M. Nishikawa, T. Mori, J. Takeya, L.K. Shrestha, J.P. Hill, *Self–assembly as a key player for materials nanoarchitectonics*, Sci. Tech. Adv. Mat. **2019**, 20, 51–95;
130. S. Yadav, A.K. Sharma, P. Kumar, *Nanoscale Self–Assembly for Therapeutic Delivery,* Front. Bioeng. Biotechnol. **2020**, 8, 127;

I.B. CHROMOJONOFORY

Znaczny obszar chemii supramolekularnej koncentruje się na otrzymywaniu i badaniu właściwości syntetycznych receptorów [131-140]. I tak na przykład receptory jonów mogą być projektowane jako układy zawierające w swoje strukturze ugrupowania zdolne do tworzenia kompleksów z jonami metali oraz mogą zawierać grupy chromo-/fluoroforowe, co przekłada się na otrzymywanie jonoforów i chromo-/fluorojonoforów [141-172]. Chromojonofory zdefiniowane przez J.P. Dixa i F. Vögtle'a [173] są jednocześnie pierwszymi związkami, które zawierały w swojej strukturze etery koronowe i umożliwiały fotometryczne oznaczanie jonów metali alkalicznych [174]. Chromogeniczne i fluorogeniczne receptory znajdują zastosowanie m.in. w szeroko pojętej analityce np. jako wskaźniki analityczne, odczynniki wykorzystywane w obrazowaniu komórkowym, w analizie enancjomerów, a także jako komponenty szybkich testów do badania próbek wodnych o znaczeniu biologicznym oraz środowiskowym [175-194]. Na rysunku I.4 został przedstawiony schemat idei chromogenicznych receptorów molekularnych.

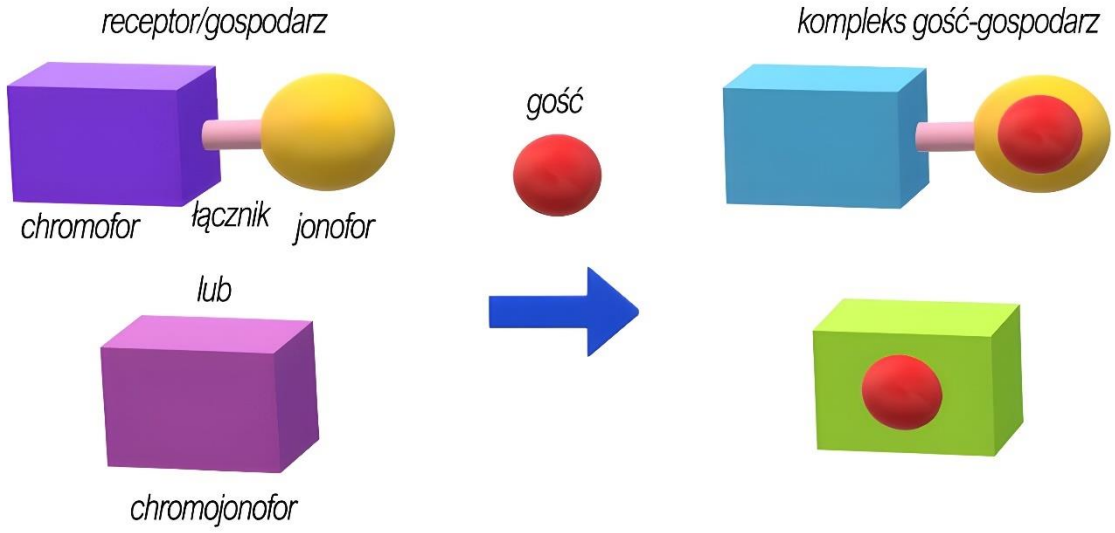

Rys. I.4. Schemat idei chromogenicznych receptorów molekularnych.

Wśród często wykorzystywanych struktur o właściwościach fluoro-/chromoforowych lub fluoro-/chromojonforowych można wymienić m.in. porfiryny, rodaminę, kumarynę, chinolinę, benzotiazol, indol, 1,8-naftalimid, piren, antracen, tetrafenyloeten, iminy – w tym diimid perylenu, tiomocznik, zasady Shiffa oraz BODIPY (ang. **bo**ron-**dipy**rromethene) (rys. I.5) [141-172, 175-194].

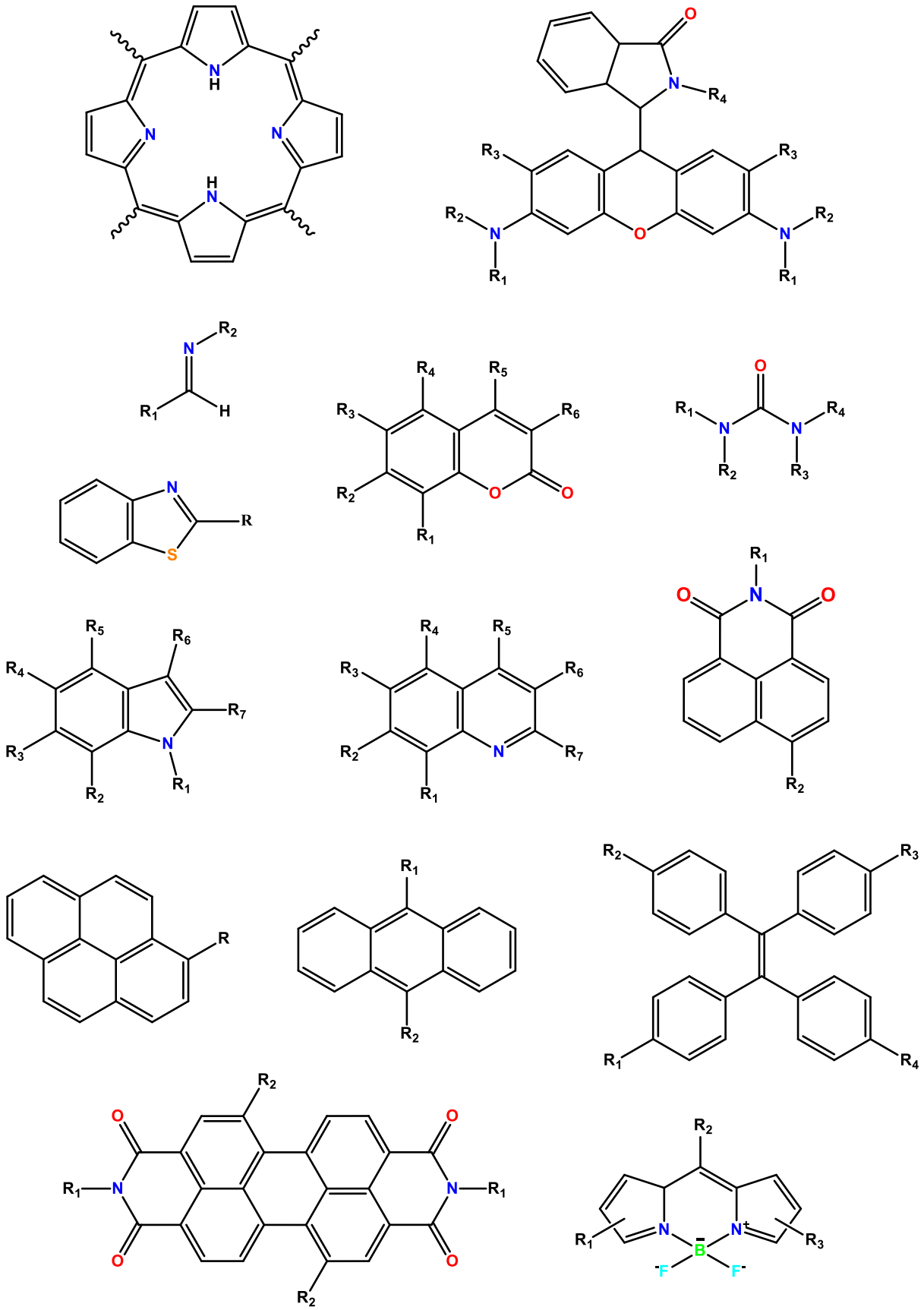

Rys. I.5. Przykłady jednostek o właściwościach fluoro-/chromoforowych lub fluoro-/chromojonforowych [141-172, 175-194].

Jako związki receptorowe wykorzystywane są również chromo-/fluorojonofory zawierające w swojej strukturze reszty heterocykliczne [195-199], w szczególności azole. Opisywane są one jako jedne z najlepszych układów do wykrywania i oznaczania jonów metali ciężkich [200, 201], a także anionów [202]. Chromogeniczny charakter receptorów można osiągnąć poprzez wprowadzenie odpowiedniej grupy funkcyjnej - chromoforu. Jedną z najpowszechniejszych, najwygodniejszych i najbardziej użytecznych funkcjonalizacji związków, które mają pełnić rolę chromogenicznych receptorów, jest wprowadzenie jako grupy chromoforowej grupy azowej. Związki azowe mogą występować w postaci dwóch izomerów geometrycznych: *cis* (Z) i *trans* (E), które mogą przekształcać się zarówno fotochemicznie jak i termicznie [203, 204]. Izomery charakteryzują się dobrze rozdzielonymi pasmami absorpcji w obszarze promieniowania UV-Vis i posiadają różne właściwości fizyczne, takie jak stała dielektryczna oraz współczynnik załamania światła [205]. Związki te są również aktywne elektrochemicznie i mogą działać jako jednostki funkcjonalne, jeśli zostaną wprowadzone do materiałów elektrochromowych, których właściwości mogą być stymulowane zmianą potencjału. Ponadto szczególne właściwości spektralne związków azowych tj. obecność donorowego atomu azotu oraz, co ważne, stosunkowo nieskomplikowana synteza pochodnych azowych, sprzyja ich zastosowaniu w warstwach receptorowych wielu układów czujnikowych [206-212].

W literaturze można znaleźć wiele przykładów chromojonoforów, także makrocyklicznych zawierających ugrupowania azowe (rys. I.6) [213]. Wykazano, że makrocykliczne pochodne bisazowe zawierające reszty pirolu lub imidazolu w obrębie makropierścienia wykazują czułość na jony ołowiu(II) zarówno w roztworze (acetonitryl i jego mieszaniny z wodą) [214-216], jak i jako nośniki jonów ołowiu(II) w polimerowych membranach inkluzyjnych [217, 218], a także w membranowych elektrodach jonoselektywnych czułych na jony ołowiu(II), w których zastosowano je jako jonofory [219, 220]. Natomiast makrocykliczne pochodne imidazolu unieruchomione na podłożu krzemionkowym otrzymywanym metodą zol-żel, traktowane jako elementy czujników optycznych, selektywnie rozpoznają jony miedzi(II) w roztworach wodnych [221, 222].

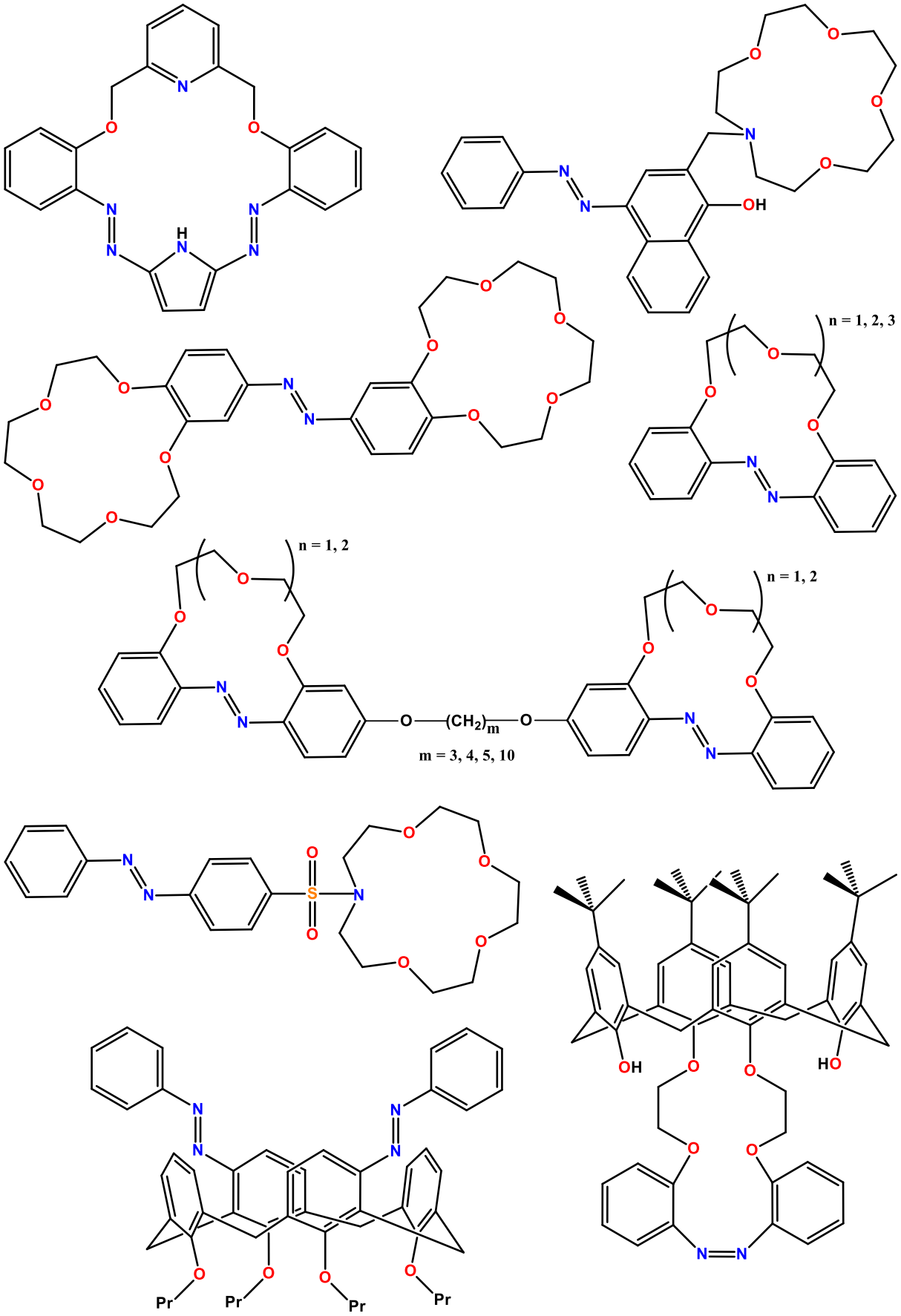

Rys. I.6. Przykłady związków makrocyklicznych zawierających w swojej strukturze wiązanie azowe [213].

LITERATURA

131. A.K. Yundi, *Macrocycles: lessons from the distant past, recent developments, and future directions*, Chem. Sci., **2015**, 6, 30–49;
132. N. Busschaert, C. Caltagirone, W.V. Rossom, P.A. Gale, *Applications of Supramolecular Anion Recognition*, Chem. Rev. **2015**, 115, 8038–8155;
133. P.A. Gale, E.N.W. Howe, X. Wu, *Anion Receptor Chemistry*, Chem **2016**, 1, 351–422;
134. P.A. Gale, E.N.W. Howe, X. Wu, M.J. Spooner, *Anion receptor chemistry: Highlights from 2016*, Coord. Chem. Rev. **2018**, 375, 333–372;
135. C. Jiang, Z. Song, L. Yu, S. Ye, H. He, *Fluorescent probes based on macrocyclic hosts: Construction, mechanism and analytical applications*, Trends Anal. Chem. **2020**, 133, 116086;
136. C., Lijun, S.N. Berry, X. Wu, E.N.W. Howe, P.A. Gale, *Advances in Anion Receptor Chemistry*, Chem **2020**, 6, 61–141;
137. G.T. Williams, C.J.E. Haynes, M. Fares, C. Caltagirone, J.R. Hiscock, P.A. Gale, *Advances in applied supramolecular technologies*, Chem. Soc. Rev. **2021**,50, 2737–2763;
138. L.K. Macreadie, A.M. Gilchrist, D.A. McNaughton, W.G. Ryder, M. Fares, P.A. Gale, *Progress in anion receptor chemistry*, Chem **2022**, 8, 46–118;
139. D.A. McNaughton, W.G. Ryder, A.M. Gilchrist, P. Wang, M. Fares, X. Wu, P.A. Gale, *New insights and discoveries in anion receptor chemistry*, Chem **2023**, 9, 3045–3112;
140. Y. Sasaki, T. Minami, *Methodologies for Spontaneous Preparation of Chemosensors and Their Arrays Using Off–the–Shelf Reagents*, ChemNanoMat **2024**, 10, e202300492;
141. H.N. Kim, W.X. Ren, J.S. Kim, J. Yoon, *Fluorescent and colorimetric sensors for detection of lead, cadmium, and mercury ions*, Chem. Soc. Rev. **2012**, 41, 3210–3244;
142. N. Kumar, I. Leray, A. Depauw, *Chemically derived optical sensors for the detection of cesium ions*, Coord. Chem. Rev. **2016**, 310, 1–15;
143. A.V.S. Piriya, P. Joseph, K.S.C.G. Daniel, S. Lakshmanan, T. Kinoshita, S. Muthusamy, *Colorimetric sensors for rapid detection of various analytes*, Mater. Sci. Eng. C **2017**, 78, 1231–1245;
144. D. Wu, A.C. Sedgwick, T. Gunnlaugsson, E.U. Akkaya, J. Yoon, T.D. James, *Fluorescent chemosensors: the past, present and future*, Chem. Soc. Rev., **2017**, 46, 7105–7123 ;
145. B. Kaur, N. Kaur, S. Kumar, *Colorimetric metal ion sensors – A comprehensive review of the years 2011–2016*, Coord. Chem. Rev. **2018**, 358, 13–69;
146. S. Suganya, S. Naha, S. Velmathi, *A Critical Review on Colorimetric and Fluorescent Probes for the Sensing of Analytes via Relay Recognition from the year 2012–17*, ChemistrySelect **2018**, 3, 7231–7268;
147. M. Taghizadeh–Behbahani, B. Hemmateenejad, M. Shamsipur, *A Mini Review on Organic Chemosensors for Cation Recognition (2013–19)*, Chem. Pap. **2018**, 72, 1239–1247;
148. P.A. Gale, C. Caltagirone, *Fluorescent and colorimetric sensors for anionic species*, Coord. Chem. Rev. **2018**, 354, 2–27;
149. S. Upadhyay, A. Singh, R. Sinha, S. Omer, K. Negi, *Colorimetric chemosensors for d–metal ions: A review in the past, present and future prospect*, J. Mol. Struct. **2019**, 1193, 89–102;
150. S. Chakraborty, M. Mandal, S. Rayalu, *Detection of iron (III) by chemo and fluoro–sensing technology*, Inorg. Chem. Commun. **2020**, 121, 108189;
151. S. Chakraborty, S. Rayalu, *Detection of nickel by chemo and fluoro sensing technologies*, Spectrochim. Acta A Mol. Biomol. Spectrosc. **2021**, 245, 118915;
152. S. Chakraborty, S. Paul, P. Roy, S. Rayalu, *Detection of cyanide ion by chemosensing and fluorosensing technology*, Inorg. Chem. Commun. **2021**, 128, 108562;
153. P.R. Dongare, A.H. Gore, *Recent Advances in Colorimetric and Fluorescent Chemosensors for Ionic Species: Design, Principle and Optical Signalling Mechanism*, ChemistrySelect **2021**, 6, 5657–5669;
154. D.A. McNaughton, M. Fares, G. Picci, P.A. Gale, C. Caltagirone, *Advances in fluorescent and colorimetric sensors for anionic species*, Coord. Chem. Rev. **2021**, 427, 213573;
155. S. Xiong, M.V.N. Kishore, W. Zhou, Q. He, *Recent advances in selective recognition of fluoride with macrocyclic receptors*, Coord. Chem. Rev. **2022**, 461, 214480;
156. U. Manna, G. Das, A. Hossain, *Insights into the binding aspects of fluoride with neutral synthetic receptors*, Coord. Chem. Rev. **2022**, 455, 214357;
157. P. Kaur, K. Singh, *Analyte Detection: A Decade of Progress in the Development of Optical/Fluorescent Sensing Probes*, Chem. Rec. **2022**, 23, e202200184;
158. T. Chopra, S. Sasan, L. Devi, R. Parkesh, K.K. Kapoor, *A comprehensive review on recent advances in copper sensors*, Coord. Chem. Rev. **2022**, 470, 214704;
159. S.K. Manna, S. Mondal, B. Janaa, K. Samanta, *Recent advances in tin ion detection using fluorometric and colorimetric chemosensors*, New J. Chem. **2022**, 16, 7309–7328;
160. J.S Algethami, *A Review on Recent Progress in Organic Fluorimetric and Colorimetric Chemosensors for the Detection of Cr^{3+}/$^{6+}$Ions*, Crit. Rev. Anal. Chem. **2022**, 26, 1–21;
161. H.M. Al–Saidi, S. Khan, *A Review on Organic Fluorimetric and Colorimetric Chemosensors for the Detection of Ag(I) Ions*, Crit. Rev. Anal. Chem. **2022**, 17, 1–27;
162. D. Sadananda, A.M.M. Mallikarjunaswamy, C.N. Prashantha, R. Mala, K. Gouthami, L. Lakshminarayana, L.F.R. Ferreira, M. Bilal, A. Rahdar, S.I. Mulla, *Recent development in chemosensor probes for the detection and imaging of zinc ions: a systematic review*, Chem. Pap. **2022**, 76, 5997–6015;

163. S. Krishnamoorthy, P. Ganasan, *Spectrophotometric, Spectrofluorometric and Colorimetric Sensing of Ce^{4+} Ions Using Organic Molecules – A Review*, Crit. Rev. Anal. Chem. **2022**, 26, 1–12;
164. M. Mansha, S.A. Khan, A. Aziz, A.Z. Khan, S. Ali, M. Khan, *Optical Chemical Sensing of Iodide Ions: A Comprehensive Review for the Synthetic Strategies of Iodide Sensing Probes, Challenges, and Future Aspects*, Chem. Record **2023**, 22, e202200059;
165. S. Chakraborty, *Detection of fluoride ion by chemosensing and fluorosensing technology*, Results Chem. **2023**, 6, 100994;
166. K.H. Alharbi, *A Review on Organic Colorimetric and Fluorescent Chemosensors for the Detection of Zn(II) Ions*, Crit. Rev. Anal. Chem. **2023**, 53, 1472–1488;
167. H.M. Al–Saidi, *Recent advancements in organic chemosensors for the detection of Pb^{2+}: a review*, Chem. Pap. **2023**, 77, 4807–4822;
168. K.M. Trevino, C.R. Wagner, E.K. Tamura, J. Garci, A.Y. Louie, *Small molecule sensors for the colorimetric detection of Copper(II): A review of the literature from 2010 to 2022*, Dyes Pigm. **2023**, 214, 110881;
169. M.M. Alhamami, J.S. Algethami, S. Khan, *A Review on Thiazole Based Colorimetric and Fluorimetric Chemosensors for the Detection of Heavy Metal Ions*, Crit. Rev. Anal. Chem. **2023**, 8, 1–15;
170. N. Goswami, S. Naithani, J. Mangalam, T. Goswami, R. Dubey, P. Kumar, P. Kumar, S. Kumar, *Fluorescent and chromogenic organic probes to detect group 10 metal ions: design strategies and sensing applications*, Dalton Trans. **2023**, 52, 14704–14732;
171. G. Kaur, I. Singh, R. Tandon, N. Tandon, *Recent advancements in coumarin based colorimetric and fluorescent chemosensors*, Inorg. Chem. Commun. **2023**, 158, 111480;
172. G. Picci, R. Montis, A.M. Gilchrist, P.A. Gale, C. Caltagirone, *Fluorescent and colorimetric sensors for anions: Highlights from 2020 to 2022*, Coord. Chem. Rev. **2024**, 501, 215561;
173. . J.P. Dix, F. Vögtle, *Neue Chromoionophore*, Chem. Ber. **1981**, 114, 638–651;
174. . H.G. Loehr, F. Vögtle, *Chromo– and fluoroionophores. A new class of dye reagents,* Acc. Chem. Res. **1985**, 18, 65–72;
175. E.V. Anslyn, *Supramolecular Analytical Chemistry*, J. Org. Chem. **2007**, 72, 3, 687–699;
176. L. You, D. Zha, E.V. Anslyn, *Recent Advances in Supramolecular Analytical Chemistry Using Optical Sensing*, Chem. Rev. **2015**, 115, 15, 7840–7892;
177. H. Sharma, N. Kaur, A. Singh, A. Kuwar, N. Singh, *Optical chemosensors for water sample analysis*, J. Mater. Chem. C **2016**, 4, 5154–5194;
178. I.V. Kolesnichenko, E.V. Anslyn, *Practical applications of supramolecular chemistry*, Chem. Soc. Rev., **2017**, 46, 2385–2390;
179. G. Fukuhara, *Analytical supramolecular chemistry: Colorimetric and fluorimetric chemosensors*, J. Photochem. Photobiol. C Photochem. Rev. **2020**, 42, 100340;
180. X. Zheng, W. Cheng, C. Ji, J. Zhang, M. Yin, *Detection of metal ions in biological systems: A review*, Rev. Anal. Chem. **2020**, 39, 231–246;
181. S. Chakraborty, V. Ravindran, P.V. Nidheesh, S. Rayalu, *Optical Sensing of Copper and Its Removal by Different Environmental Technologies*, ChemistrySelect **2020**, 5, 10432–10474;
182. J.P. Vareda, A.J.M. Valente, L. Duraes, *Ligands as copper and nickel ionophores: Applications and implications on wastewater treatment*, Adv. Colloid Interface Sci. **2021**, 289, 102364;
183. Z. Li, H. Lin, L. Wang, L. Cao, J. Sui, K. Wang, *Optical sensing techniques for rapid detection of agrochemicals: Strategies, challenges, and perspectives*, Sci. Total Environ. **2022**, 838, 156515;
184. I.M. El–Sewify, A. Radwan, N.H. Elghazawy, W. Fritzschec, H.M.E. Azzazy, *Optical chemosensors for environmental monitoring of toxic metals related to Alzheimer's disease*, RSC Adv. **2022**,12, 32744–32755;
185. G.M. Abu–Taweel, M.M. Ibrahim, S. Khan, H.M. Al–Saidi, M. Alshamrani, F.A. Alhumaydhi, S.S. Alharthi, *Medicinal Importance and Chemosensing Applications of Pyridine Derivatives: A Review*, Crit. Rev. Anal. Chem. **2022**, 20, 1–18;
186. A. Kumar , Virender, M. Saini, B. Mohan, Shayoraj, M. Kamboj, *Colorimetric and fluorescent Schiff base sensors for trace detection of pollutants and biologically significant cations: A review (2010–2021)*, Microchem. J. **2022**, 181, 107798;
187. S, Saha, R, Alam, *Recent developments in the creation of a single molecular sensing tool for ternary iron (III), chromium (III), aluminium (III) ionic species: A review*, Luminescence **2022**, 38, 1026–1046;
188. H.N.N. Kumar, D.H. Nagaraju, Z. Yhobu, P. Shivakumar, K.S.M. Kumara, S. Budagumpi, B.M. Praveen, *Recent advances in on–site monitoring of heavy metal ions in the environment*, Microchem. J. **2022**, 182, 107894;
189. S. Paul, R. Das, P. Banerjee, *Recent endeavours in the development of organo chromo–fluorogenic probes towards the targeted detection of the toxic industrial pollutants Cu^{2+} and CN^{-}: recognition to implementation in sensory device*, Mater. Chem. Front. **2022**, 6, 2561–2595;
190. R. Iftikhar, I. Parveen, A. Khalid ,A. Mazhar, M.S. Iqbal, G.M. Kamal, F. Hafeez, A.L. Pang, M. Ahmadipour, *Small organic molecules as fluorescent sensors for the detection of highly toxic heavy metal cations in portable water*, J. Environ. Chem. Eng. **2023**, 11, 109030;
191. L. Motiei, D. Margulies, *Molecules that Generate Fingerprints: A New Class of Fluorescent Sensors for Chemical Biology, Medical Diagnosis, and Cryptography*, Acc. Chem. Res. **2023**, 56, 1803–1814;
192. R. Lalitha, S. Velmathi, *A Study of Small Molecule–Based Rhodamine–Derived Chemosensors and their Implications in Environmental and Biological Systems from 2012 to 2021: Latest Advancement and Future Prospects*, J. Fluoresc. **2024**, 34, 15–118;
193. M. Rajasekar, P. Baskaran, J. Mary, S. Meenambigai, M. Selvam, *Review of current developments in rhodamine derivatives–based photoresponsive chemosensors for ion detection*, Inorg. Chem. Commun. **2024**, 162, 112143;

194. P.C. Wanniarachchi, K.G.U. Kumarasinghe, C. Jayathilake, *Recent advancements in chemosensors for the detection of food spoilage*, Food Chem. **2024**, 436, 137733;
195. S. Kashyap, R. Singh, U.P. Singh, *Inorganic and organic anion sensing by azole family members*, Coord. Chem. Rev. **2020**, 417, 21369;
196. M.–C. Ríos, N.–F. Bravo, C.–C. Sancheza, J. Portilla, *Chemosensors based on N–heterocyclic dyes: advances in sensing highly toxic ions such as CN^- and Hg^{2+}*, RSC Adv. **2021**, 11, 34206–34234;
197. R.S. Fernandes, N.S. Shetty, P. Mahesha, S.L. Gaonkar, *A Comprehensive Review on Thiophene Based Chemosensors*, J. Fluoresc. **2021**, 32, 19–56;
198. N. Bin Darwish, A. Kurdi, S. Alshihri, T. Tabbakh, *Organic heterocyclic–based colorimetric and fluorimetric chemosensors for the detection of different analytes: a review (from 2015 to 2022)*, Mater. Today Chem. **2023**, 27, 101347;
199. O.F. Al Sharif, L.M. Nhari, R.M. El–Shishtawy, A.M. Asiri, *Imidazole–based fluorophores: Synthesis and applications*, Mater. Today Chem. **2023**, 29, 101453;
200. F. Ahmed, H. Xiong, *Recent developments in 1,2,3–triazole–based chemosensors*, Dyes Pigm. **2021**, 185, 108905;
201. R. Nagarajan, C. Varadaraju, K. Hwan Lee, *Recent advancements in the role of N–Heterocyclic receptors on heavy metal ion sensing*, Dyes Pigm. **2021**, 191, 109331;
202. S. Kashyap, R. Singh, U.P. Singh, *Inorganic and organic anion sensing by azole family members*, Coord. Chem. Rev. **2020**, 417, 213369;
203. H.M.D. Bandarab, S.C. Burdette, *Photoisomerization in different classes of azobenzene*, Chem. Soc. Rev. **2012**, 41, 1809–1825;
204. M. Younis, S. Ahmad, A. Atiq, M.A. Farooq, M.–H. Huang, M. Abbas, Recent *Progress in Azobenzene–Based Supramolecular Materials and Applications*, Chem. Rec. **2023**, 23, e202300126;
205. H. Chen, W. Chen, Y. Lin, Y. Xie, S.H. Liu, J. Yin, *Visible and near–infrared light activated azo dyes*, Chin. Chem. Lett. **2021**, 32, 2359–2368;
206. W.–C. Geng, H. Sun, D.–S. Guo, *Macrocycles containing azo groups: recognition, assembly and application*, J. Incl. Phenom. Macrocycl. Chem. **2018**, 92, 1–79;
207. S. Benkhaya, S. Mrabet, A. El Harfi, *Classifications, properties, recent synthesis and applications of azo dyes*, Heliyon **2020**, 6, e03271;
208. R.I. Alsantali, Q. Alam Raja, A.Y.A. Alzahrani, A. Sadiq, N. Naeem, E. Ullah Mughal, M.M. Al–Rooqi, N. El Guesmi, Z. Moussa, S.A. Ahmed, *Miscellaneous azo dyes: a comprehensive review on recent advancements in biological and industrial applications*, Dyes Pigm. **2022**, 199, 110050;
209. P. Mishra, P. Sethi, N. Sharma, J. Sharma, *Macrocyclic scaffold: A boon in advancement of sensor technology – review*, Mater. Today Chem. **2022**, 71, 370–376;
210. F. Eltaboni, N. Bader, R. El–Kailany, N. Elsharif, A. Ahmida, *Chemistry and Applications of Azo Dyes: A Comprehensive Review*, J. Chem. Rev. **2022**, 4, 313–330;
211. R. Khanum, R.A. Shoukat Ali, H.R. Rangaswamy, S.R. Santhosh Kumar, A.G. Prashantha, A.S. Jagadisha, *Recent review on Synthesis, spectral Studies, versatile applications of azo dyes and its metal complexes*, Results Chem. **2023**, 5, 100890;
212. K.R. Damade, D.H. More, *Azo Based Chromogenic Sensor: An Approach for Naked Eye Detection of Biologically Relevant Anions and Metal Cations*, Mini–Rev. Org. Chem. **2024**, 21, 514–526;
213. E. Wagner–Wysiecka, N. Łukasik, J.F. Biernat, E. Luboch, *Azo group(s) in selected macrocyclic compounds*, J. Incl. Phenom. Macrocycl. Chem. **2018**, 91, 189–257;
214. E. Wagner–Wysiecka, E. Luboch, M. Jamrógiewicz, J.F. Biernat, *Chromogenic macrocyclic derivatives of azoles—synthesis and properties*, Tetrahedron **2003**, 59, 4415–4420;
215. E. Wagner–Wysiecka, E. Luboch, M.S. Fonari, *The Synthesis, X–ray Structure and Metal Cation Complexation Properties of Colored Crown with Two Heterocyclic Residues as a Part of Macrocycle*, Pol. J. Chem. **2008**, 82, 1319–1330;
216. E. Luboch, E. Wagner–Wysiecka, T. Rzymowski, M.S. Fonari, R. Kulmaczewski, *Pyrrole azocrown ethers – synthesis, crystal structures, and fluorescence properties*, Tetrahedron **2011**, 67, 1862–1872;
217. M. Ulewicz, K. Sadowska, J.F. Biernat, *Facilitated transport of Zn (II), Cd (II) and Pb (II) across polymer inclusion membranes doped with imidazole azocrown ethers*, Physicochem. Probl. Miner. Process. **2007**, 41, 133–143;
218. M. Ulewicz, J. Szczygielska–Tao, J.F. Biernat, *Selectivity of Pb(II) transport across polymer inclusion membranes doped with imidazole azothiacrown ethers*, J. Membr. Sci. **2009**, 344, 32–38;
219. E. Luboch, E. Wagner–Wysiecka, M. Fainerman–Melnikova, L.F. Lindoy, J.F. Biernat, *Pyrrole Azocrown Ethers. Synthesis, Complexation, Selective Lead Transport and Ion–Selective Membrane Electrode Studies*, Supramol. Chem. **2006**, 18, 593–601;
220. E. Wagner–Wysiecka, M. Jamrógiewicz, M.S. Fonari, J.F. Biernat, *Azomacrocyclic Derivatives of Imidazole: Synthesis, Structure, and Metal Ion Complexation Properties*, Tetrahedron **2007**, 63, 4414–4421;
221. E. Wagner–Wysiecka, E. Luboch, M. Jamrógiewicz, J. Szczygelska–Tao, J.F. Biernat, *Metallochromic Azole Macrocyclic Reagents*, Ann. Pol. Chem. Soc. **2005**, 4, 11–14;
222. K. Kledzik, M. Jamrógiewicz, M. Gwiazda, E. Wagner–Wysiecka, J. Jezierska, J. Biernat, A.M. Kłonkowski, *Optical recognition elements. Macrocyclic imidazole chromoionophores entrapped in silica xerogel*, Mat. Sci. Pol. **2007**, 25, 1041–1051;

I.C. CZUJNIKI CHEMICZNE

Według IUPAC czujnik chemiczny to urządzenie, które przekształca informacje chemiczne, począwszy od stężenia określonego składnika próbki, po ogólny skład matrycy, w sygnał użyteczny analitycznie [223]. Wymienione powyżej informacje chemiczne mogą być uzyskiwane jako wynik odpowiedniej reakcji chemicznej analitu lub wynikać ze zmiany właściwości fizycznych badanego systemu będących skutkiem utworzenia kompleksu. Czujniki chemiczne zawierają dwie podstawowe jednostki funkcjonalne: chemicznie selektywną warstwę receptorową oraz element przetwornikowy. W warstwie receptorowej informacja chemiczna jest przekształcana w formę energii, która może być mierzona przez element przetwornikowy. Natomiast przetwornik konwertuje energię przenoszącą informacje chemiczne o próbce, w użyteczny analitycznie sygnał. Przetwornik jako taki nie wykazuje selektywności chemicznej. W zależności od generowanego sygnału można je podzielić [224, 225] na różne grupy m.in. optyczne - wykorzystujące zjawiska takie jak absorbcja, fluorescencja, luminescencja czy refrakcja, które są wynikiem interakcji analitu z warstwą receptorową; elektrochemiczne – wykorzystują zjawiska zachodzące na granicy analit-elektroda, w sygnał użyteczny analitycznie. Takie efekty mogą być stymulowane przepływem prądu elektrycznego lub mogą powodować spontaniczne oddziaływanie w warunkach prądu zerowego; elektryczne – oparte na pomiarach, w których nie zachodzą procesy elektrochemiczne, a sygnał wynika ze zmiany właściwości elektrycznych spowodowanych oddziaływaniem z analitem; grawimetryczne - przekształcają zmianę masy na odpowiednio zmodyfikowanej powierzchni w zmianę właściwości materiału nośnego (zmiana masy jest spowodowana akumulacją analitu); magnetyczne – oparte są na zmianie magnetycznych właściwości analizowanego układu; termiczne – oparte są na pomiarze efektu cieplnego określonej reakcji chemicznej lub zjawiska fizycznego np. adsorpcji. Czujniki chemiczne stanowią grupę najszerzej przebadanych nowoczesnych narzędzi analitycznych, które mogą służyć do wykrywania oraz oznaczania jonów, a także przy zastosowaniu odpowiednio selektywnego receptora cząsteczek obojętnych [226-240].

Czujniki optyczne stanowią grupę czujników chemicznych, w których sygnał analityczny jest generowany w wyniku oddziaływania promieniowania elektromagnetycznego z materią. Do tej grupy należą m.in. optody [241-245]. Zasada działania optody może opierać się na kilku zjawiskach optycznych obejmując różne regiony promieniowania elektromagnetycznego – od promieniowania UV poprzez zakres widzialny, aż do podczerwieni. Czujniki optyczne oparte na (chromo)- lub (fluoro)jonoforach, do których zaliczane są

jonoselektywne optody (ISO) [246-252], są szczególnie ważne ze względu na możliwość wykrywania analitów w zakresie promieniowania UV-Vis, mniejszą podatność na zakłócenia elektromagnetyczne, a także mogą osiągać niższe wartości granicy wykrywalności (LOD) niż ich analogi – jonoselektywne elektrody (ISE) [253]. Na rysunku I.7 zostały przedstawione przykłady mechanizmów wykrywania jonów w ISO.

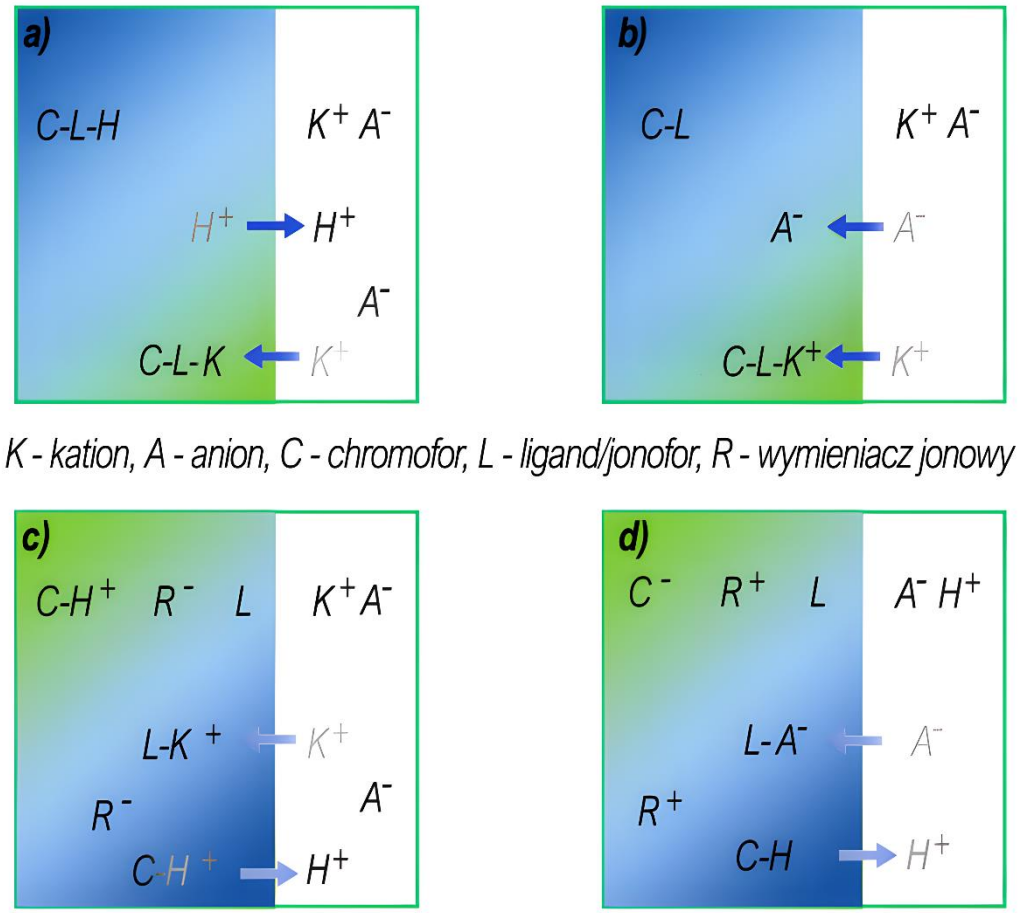

Rys. I.7. Przykładowe mechanizmy wykrywania jonów w ISO poprzez: a) i b) – generowanie sygnału optycznego oparte na wymianie jonowej za pomocą chromojonoforu, unieruchomionego w warstwie receptorowej, selektywnego na dany jon lub w wyniku współekstrakcji anionu/chromojonoforu, który ulega deprotonowaniu; c) i d) – zastosowanie chromoforu selektywnego względem jonów wodorowych w układzie z selektywnym jonoforem, co umożliwia selektywną ekstrakcję jonu docelowego do organicznej fazy czujnikowej poprzez wymianę lub współekstrakcję z jonem wodorowym związanym z chromojonoforem [238].

Polimery syntetyczne są zwykle tanie i otrzymywane na masową skalę. Ze względu na szeroki asortyment polimerów o różnych właściwościach, takich jak elastyczność, przezroczystość, rozciągliwość itp. mogą być odpowiednimi nośnikami dla receptorów. Klasyczne optody zawierające fluoro- lub chromojonofory (lub jonofor i wskaźnik) są bardzo często otrzymywane przy użyciu poli(chlorku winylu) jako matrycy polimerowej i badane poprzez pomiar zmiany absorbancji i/lub fluorescencji spowodowanej obecnością analitu.

Pierwsze doniesienia o optodach na bazie PVC wykorzystujących układ jonofor-wskaźnik, pochodzą z początku lat 90 XX wieku i zostały opracowane przez zespół Wilhelma Simona [254-260]. Zaproponowane optody stosowano do analizy próbek wodnych w celu wykrywania: kationów wapnia, ołowiu(II), cynku(II), srebra(I), rtęci(II), uranylu [261-266], anionów wodorosiarczanowych [267], ale również jako optyczne czujniki gazowe amoniaku [268, 269]. Ponadto stwierdzono możliwość zastosowania optod bazujących na PVC do wykrywania oraz oznaczania jonów sodu czy potasu, w bardziej złożonych układach takich jak ludzkie osocze [270, 271]. Wraz z czasem optody zyskały na popularności na całym świecie, co potwierdza wzrost liczby publikowanych prac o tej tematyce (Tabela I.1A i I.1B) [272-344]. Ze względu na to, że optody bazujące na PVC wymagają dodatkowego podłoża w postaci szklanych płytek, na które są nanoszone, wraz z postępem techniki oraz możliwości analizy kolorymetrycznej zaproponowano optody PVC, w których szklane podłoże zastąpiono papierem [345-353], poli(tereftalanem etylenu) (PET) [354, 355] a także bazując na najnowszych doniesieniach, możliwe jest otrzymanie optod PCV bez dodatkowego podłoża [356].

Wśród najpopularniejszych polimerów stosowanych w czujnikach optycznych szeroko stosowana, poza poli(chlorkiem winylu), jest acetylowana celuloza. Trioctan celulozy (CTA) może być stosowany jako surowiec do wytwarzania tworzyw sztucznych, włókien i folii, takich jak klisze fotograficzne. Ponadto folia CTA może być stosowana jako porowate podłoże dla czujników optycznych i nie wymaga zastosowania dodatkowego podłoża, tak jak ma to miejsce przy optodach PVC. W pierwszych doniesieniach o tego typu czujnikach optycznych na bazie triacetylocelulozy, używano jako materiału wyjściowego odpadowych taśm fotograficznych, na powierzchni których chromojonofor unieruchamiano fizycznie lub poprzez kowalencyjne związanie z podłożem (Tabela I.2) [357-397]. Tego typu rozwiązania wykorzystują materiał odpadowy o doskonałych właściwościach optycznych i mechanicznych, jako nośnik barwnych receptorów. Membrany te reagują na obecność analitu zmieniając barwę, a to można wykryć „gołym okiem” lub zmierzyć spektrofotometrycznie. Jednak wraz ze zmniejszającym się obrotem taśm fotograficznych zaczęto stosować do otrzymywania optod trioctan celulozy w postaci granulatu [398-408].

Tabela I.1A. Przykłady optod na bazie PCV do wykrywania i oznaczania jonów metali.

Chromofor / jonofor / chromojonofor	Kation	Zakres liniowej odpowiedzi [mol/dm^3]	Granica wykrywalności [mol/dm^3]	Lit.
5,10,15,20-tetrafenyloporfiryna	Hg(II)	$2{,}3\times10^{-7}$ – $4{,}5\times10^{-5}$	$4{,}0\times10^{-8}$	[278]
pirydyno-2-tiol + chromojonofor I (ETH 5294)	Hg(II)	$2{,}0\times10^{-9}$ – $2{,}0\times10^{-5}$	$4{,}0\times10^{-10}$	[293]
tiazolo-2-tiol + chromojonofor I (ETH 5294)	Hg(II)	$2{,}0\times10^{-10}$ – $1{,}5\times10^{-5}$	$5{,}0\times10^{-11}$	[294]
heksatiacyklooktadekan + chromojonofor V	Hg(II)	$2{,}1\times10^{-7}$ – $1{,}2\times10^{-4}$	$2{,}0\times10^{-7}$	[297]
1,15-diaza-3,4,12,13-dibenzo-8-oksa-16,18-pirydyno-5,1-ditiacyklooktadekano-2,14-dion + chromojonofor V	Hg(II)	$1{,}0\times10^{-12}$ – $8{,}6\times10^{-4}$	$5{,}3\times10^{-13}$	[310]
7-[(2-metylo-1H-indol-3-yl)metylo]-5,6,7,8,9,10-heksahydro-2H-1,13,4,7,10-benzodioksatriazacyklopentadekano-3,11-(4H,12H)-dion + chromojonofor I (ETH5294)	Hg(II)	$4{,}5\times10^{-13}$ – $4{,}7\times10^{-4}$	$3{,}5\times10^{-13}$	[311]
7-(1H-imidazol-1-ylmetylo)-5,6,7,8,9,10-heksahydro-2H-1,13,4,7,10-benzodioksatriaza cyklopentadekano-3,11-(4H,12H)-dion + chromojonofor I (ETH5294)	Hg(II)	$7{,}2\times10^{-13}$ – $4{,}7\times10^{-4}$	$1{,}8\times10^{-13}$	[312]
di(tiofenylo)-4,4′-metylenodianilina + chromojonofor I (ETH 5294)	Hg(II)	$2{,}5\times10^{-13}$ – $1{,}0\times10^{-5}$	$3{,}4\times10^{-14}$	[318]
jonofor III (ETH 5435) + chromojonofor VII (ETH 5418)	Pb(II)	$5{,}0\times10^{-9}$ – $5{,}0\times10^{-5}$	$3{,}2\times10^{-12}$	[263]
dibenzodiaza-18-korona-6 + 1-(2-pirydylazo)-2-naftol	Pb(II)	$1{,}0\times10^{-8}$ – $5{,}0\times10^{-5}$	$1{,}0\times10^{-8}$	[279]
difenylokarbazon	Pb(II)	$6{,}9\times10^{-6}$ – $1{,}1\times10^{-2}$	$6{,}5\times10^{-6}$	[295]
jonofor IV selektywny na ołów(II) + chromojofor ETH 5294	Pb(II)	$6{,}2\times10^{-8}$ – $5{,}0\times10^{-5}$	$2{,}5\times10^{-8}$	[299]
2-[6-(3-metylo-3-fenylocyklobutylo)-7H-[1,2,4]triazolo[3,4-b]tiadiazin-3-yl]-fenol	Pb(II)	$5{,}0\times10^{-8}$ – $3{,}8\times10^{-4}$	$2{,}2\times10^{-8}$	[301]
BODIPY	Pb(II)	$1{,}0\times10^{-5}$ –$1{,}0\times10^{-1}$	$1{,}0\times10^{-6}$	[324]
4-(tiazol-2-yldiazenylo)benzeno-1,3-diol	Pb(II)	$6{,}0\times10^{-9}$ – $8{,}0\times10^{-5}$	$1{,}8\times10^{-9}$	[344]
heksatia-18-korona-6 + 1,2-benzo-3-octadekanoylimino-7-dietyloaminofenyloksazyna	Ag(I)	$5{,}0\times10^{-9}$ – $5{,}0\times10^{-5}$	$1{,}0\times10^{-9}$	[282]
7-(1H-benzimidazol-1-ylmetylo)-5,6,7,8,9,10-heksahydro-2H-1,13,4,7,10-benzodioksatriaza cyklopentadekano-3,11-(4H,12H)-dion + chromojonofor I (ETH 5294)	Ag(I)	$1{,}0\times10^{-11}$ – $8{,}9\times10^{-5}$	$2{,}8\times10^{-12}$	[307]
7-(1H-benzimidazol-1-ylmetylo)-5,6,7,8,9,10-heksahydro-2H-1,13,4,7,10-benzodioksatriaza cyklopentadekano-3,11-(4H,12H)-dion + chromojonofor I (ETH 5294)	Ag(I)	$2{,}3\times10^{-11}$ – $1{,}1\times10^{-3}$	$9{,}5\times10^{-12}$	[309]
2-[(benzo[*d*]tiazol-2-ylimino)metylo]fenol	Ag(I)	$4{,}8\times10^{-9}$ – $1{,}0\times10^{-5}$	$1{,}5\times10^{-9}$	[333]

Tabela I.1B. Przykłady optod na bazie PCV do wykrywania i oznaczania jonów metali cd.

Chromofor / jonofor / chromojonofor	Kation	Zakres liniowej odpowiedzi [mol/dm^3]	Granica wykrywalności [mol/dm^3]	Lit.
(N′1E,N′2E)–N′1,N′2–di(pirydyn–2–ylmetyleno)oksalohydrazyd	Cu(II)	$1{,}6\times10^{-6}$ – $3{,}2\times10^{-5}$	$8{,}1\times10^{-7}$	[322]
N,N′-di(2-hydroksynaftenoaldehyd)-1,3-fenylenodiimina	Cu(II)	$2{,}3\times10^{-8}$ – $8{,}2\times10^{-6}$	$5{,}0\times10^{-9}$	[323]
1,1′-2,2′-(1,2-fenyleno)bis(eten-2,1-diyl)dinanaftalen-2-ol	Cu(II)	$8{,}0\times10^{-6}$ – $1{,}3\times10^{-4}$	$4{,}0\times10^{-7}$	[326]
1,2-di(*o*-salicylidodiminofenylotio)eten	Ni(II)	$1{,}0\times10^{-5}$ – $5{,}0\times10^{-3}$	$8{,}5\times10^{-6}$	[303]
5-(2′,4′-dimetylofenyloazo)-6-hydroksypyrimidyn-2,4-dion	Ni(II)	$2{,}0\times10^{-8}$ – $5{,}1\times10^{-5}$	$6{,}1\times10^{-9}$	[341]
4-(p-nitrofenyloazo)pirokatechina	Th(IV)	$8{,}7\times10^{-6}$ – $2{,}0\times10^{-4}$	$6{,}0\times10^{-6}$	[288]
chlorowodorek midodryny	Th(IV)	$1{,}0\times10^{-6}$ – $1{,}2\times10^{-5}$	$9{,}9\times10^{-7}$	[327]
4-(5-bromo-2-pyridylazo)-5-(dietyloamino)fenol	Tl(III)	$2{,}6\times10^{-6}$ – $4{,}5\times10^{-4}$	$1{,}1\times10^{-6}$	[298]
4-(2-pyridylazo)rezorcynol	Tl(III)	$3{,}1\times10^{-6}$ – $4{,}7\times10^{-4}$	$1{,}8\times10^{-6}$	[319]
4-(5-bromo-2-pyridylazo)-N,N-dietylo-3-hydroksyanilina	Sm(III)	$2{,}6\times10^{-6}$ – $2{,}6\times10^{-4}$	$1{,}9\times10^{-6}$	[296]
1,1′-(iminodi(metan-1-yl-1-ylidien))-dinaften-2-ol	Fe(III)	$1{,}0\times10^{-9}$ – $1{,}0\times10^{-3}$	$6{,}2\times10^{-10}$	[313]
chlorowodorek midodryny	U(VI)	$5{,}0\times10^{-7}$ – $1{,}0\times10^{-5}$	$1{,}9\times10^{-7}$	[327]
amino-4-(3-nitrofenyloazo)pyridyn-3-ol	Sn(IV)	$3{,}0\times10^{-8}$ – $6{,}4\times10^{-6}$	$8{,}0\times10^{-9}$	[331]
kwas 5-[*o*-karboksyfenyloazo]-2,4-dihydroksybenzoesowy	Co(II)	$5{,}0\times10^{-8}$ – $4{,}5\times10^{-5}$	$1{,}5\times10^{-8}$	[335]
5-(2′,4′-dimetylofenyloazo)-6-hydroksy-pyrimidyn-2,4-dion + chromojonofor I (ETH 5294)	Zn(II)	$5{,}0\times10^{-9}$ – $2{,}5\times10^{-5}$	$1{,}6\times10^{-9}$	[336]
6-[4-(2,4-dihydroksyfenylodiazenylo)fenylo]-2-okso-4-fenylo-1,2-dihydropirydyno-3-cyjan + chromojonofor V	Cd(II)	$5{,}0\times10^{-12}$ – $2{,}5\times10^{-5}$	$1{,}6\times10^{-12}$	[337]
6-[4-(2,4-dihydroksyfenylodiazenylo)fenylo]-2-okso-4-fenylo-1,2-dihydropirydyno-3-cyjan + chromojonofor I (ETH 5294)	Sb(III)	$2{,}5\times10^{-8}$ – $4{,}0\times10^{-5}$	$7{,}0\times10^{-9}$	[338]
kwas 1-(2-benzotiazolylazo)-2-hydroksy-3-naftalenowy	Mo(VI)	$8{,}5\times10^{-8}$ – $4{,}4\times10^{-5}$	$2{,}5\times10^{-8}$	[339]
4-(4′-chlorobenzylidenoimino)-3-mehyl-5-tio-1,2,4-triazol	Te(IV)	$4{,}7\times10^{-5}$ – $1{,}2\times10^{-3}$	$1{,}4\times10^{-5}$	[356]

Tabela I.2. Zestawianie optod na bazie CTA do wykrywania i oznaczania jonów metali.

Chromofor / jonofor / chromojonofor	Kation	Zakres liniowej odpowiedzi [mol/dm^3]	Granica wykrywalności [mol/dm^3]	Lit.
4-(2-pyridylazo)-rezorcynol	Hg(II)	$5{,}0\times10^{-6}$ – $3{,}4\times10^{-3}$	$1{,}5\times10^{-6}$	[367]
4-hydroksysalofen	Hg(II)	$1{,}0\times10^{-6}$ – $1{,}0\times10^{-2}$	$1{,}3\times10^{-7}$	[370]
l-(2-pirydylazo)-2-naftol	Hg(II)	$1{,}0\times10^{-6}$ – $1{,}0\times10^{-3}$	$8{,}0\times10^{-7}$	[371]
tetratia–12–korona–4 + chromojonofor I	Hg(II)	$1{,}0\times10^{-9}$ – $9{,}5\times10^{-5}$	$8{,}1\times10^{-10}$	[380]
difenylotiokarbazon	Hg(II)	$7{,}5\times10^{-7}$ – $9{,}7\times10^{-6}$	$1{,}0\times10^{-7}$	[363]
indygokarmin	Hg(II)	$2{,}4\times10^{-5}$ – $4{,}7\times10^{-4}$	$7{,}2\times10^{-6}$	[381]
5-(2',4'-dimetylofenyloazo)-6-hydroksypyrimidyno-2,4-dion	Hg(II)	$5{,}0\times10^{-9}$ – $4{,}0\times10^{-7}$	$1{,}5\times10^{-9}$	[387]
5,6-dimetylo-1-(4 metylobenzylo)-2-*p*-tolylo-1H-benzimidazol	Hg(II)	$5{,}0\times10^{-7}$ – $5{,}0\times10^{-5}$	$1{,}0\times10^{-7}$	[391]
żółcień tiazolowa G	Hg(II)	$1{,}0\times10^{-7}$ – $3{,}2\times10^{-5}$	$1{,}0\times10^{-8}$	[393]
kwas 2-amino-cyklopentano-1-ditiokarboksylowy	Pb(II)	$1{,}0\times10^{-6}$ – $5{,}0\times10^{-1}$	$6{,}9\times10^{-7}$	[369]
4-hydroksysalofen	Pb(II)	$1{,}0\times10^{-7}$ – $1{,}0\times10^{-3}$	$8{,}6\times10^{-8}$	[373]
difenylotiokarbazon	Pb(II)	$2{,}4\times10^{-6}$ – $2{,}7\times10^{-5}$	$7{,}2\times10^{-7}$	[384]
difenylotiokarbazon	Cu(II)	$8{,}3\times10^{-7}$ – $1{,}6\times10^{-5}$	$2{,}0\times10^{-7}$	[365]
1-fenylo-1,2-propanodiono-2-oksym tiosemikarbazydu	Cu(II)	$7{,}5\times10^{-6}$ – $2{,}0\times10^{-4}$	$8{,}0\times10^{-7}$	[374]
6-bromo-3-(2-metylo-2,3-dihydrobenzo[d]tiazol-2-yl)-2H-chroman-2 on	Cu(II)	$7{,}0\times10^{-7}$ – $1{,}0\times10^{-4}$	$2{,}5\times10^{-7}$	[386]
kwas 2-amino-cyklopentano-1-ditiokarboksylowy	Ni(II)	$5{,}0\times10^{-6}$ – $1{,}0\times10^{-3}$	$5{,}2\times10^{-7}$	[361]
1-tlenek-1-*p*-tolylo-3-(3-(trifluorometylo)fenylo)triazyna	Ni(II)	$1{,}2\times10^{-9}$ – $7{,}3\times10^{-5}$	$1{,}0\times10^{-9}$	[385]
1-acenaftochinono-1-tiosemikarbazyd	Ni(II)	$5{,}0\times10^{-10}$ – $2{,}0\times10^{-5}$	$1{,}0\times10^{-10}$	[390]
4-hydroksysalofen	Cd(II)	$1{,}0\times10^{-6}$ – $5{,}0\times10^{-2}$	$5{,}3\times10^{-7}$	[372]
kwas 2-amino-cyklopentano-1-ditiokarboksylowy	Cd(II)	$3{,}0\times10^{-6}$ – $3{,}4\times10^{-4}$	$1{,}0\times10^{-6}$	[379]
czerwień pirogalolu	Co(II)	$1{,}7\times10^{-6}$ – $1{,}5\times10^{-4}$	$3{,}6\times10^{-7}$	[364]
3,4-dihydroksyantrachinon-2-sulfonian sodu	Zr(IV)	$2{,}1\times10^{-6}$ –$4{,}6\times10^{-5}$	$8{,}8\times10^{-7}$	[368]
thorin	Th(IV)	$6{,}5\times10^{-6}$ – $9{,}9\times10^{-5}$	$1{,}9\times10^{-6}$	[375]
4-hydroksysalofen	La(III)	$1{,}0\times10^{-6}$ – $1{,}0\times10^{-2}$	$1{,}0\times10^{-7}$	[378]
cyjanina eriochromowa R	V(IV)	$9{,}9\times10^{-7}$ – $8{,}3\times10^{-5}$	$1{,}0\times10^{-7}$	[388]
moryna	Fe(III)	$1{,}1\times10^{-9}$ – $4{,}7\times10^{-5}$	$4{,}2\times10^{-11}$	[394]
2-(2'-hydroksynaftyloazo)benzotiazol	Cr(III)	$3{,}0\times10^{-9}$ – $5{,}0\times10^{-5}$	$8{,}5\times10^{-10}$	[396]

Wśród innych polimerów można rozważyć również polimery termoplastyczne, które ulegają zmiękczeniu pod wpływem temperatury, dzięki czemu można je formować i kształtować. Klasyczne polimery termoplastyczne stosowane do konstrukcji warstw czujnikowych to: polietylen (PE) [409], polipropylen (PP) [410], polistyren (PS) [411], poli(metakrylan metylu) (PMMA) i politereftalan etylenu (PET). W przeciwieństwie do innych polimerów zapewniają one odporność chemiczną na rozpuszczalniki organiczne, mniejszą przepuszczalność gazów oraz szeroki zakres sztywności. Dzięki tym właściwościom tworzywa termoplastyczne są chętnie wybierane jako matryce polimerowe optod [412]. Największa liczba doniesień naukowych, z użyciem poli(metakrylanu metylu) jako matrycy, wskazuje je jako kolorymetryczne czujniki pH [413, 414], a także do wykrywania innych jonów [415-425] oraz związków takich jak np. kwas askorbinowy [426], heparyna [427], rodamina [428], barwniki do żywności [429], antyoksydanty [430] czy glukoza [431].

W ostatnim czasie oprócz wspomnianego wyżej papieru [432-444], wykorzystuje się inne równie proste podejścia do otrzymywania materiałów czujnikowych takie jak np. zastosowanie tekstyliów [445-452], również w postaci pojedynczych nici [453-467] oraz różnego rodzaju matryc polimerowych np. nylon [468, 469]. Optody oparte na niedrogich materiałach mają duże znaczenie ekonomiczne. Takie podejście sprawdza się dobrze także w przypadku badania mętnych próbek czy próbek biologicznych, zawierających jako składniki matrycy wielkocząsteczkowe substancje takie jak białka (ale również krwinki w przypadku analizy krwi pełnej), gdzie zastosowany materiał optody zapewnia oddzielenie innych składników próbki od analitu [470].

W literaturze proponowane są również rozwiązania bazujące na otrzymywaniu warstw receptorowych przy zastosowaniu biodegradowalnych polimerów takich jak np. skrobia [471-475], chitozan [476, 477], żelatyna [478-480], czy poli(alkohol winylowy) [481-489], które znajdują zastosowanie głównie w czujnikach pH-metrycznych, co również można wykorzystać jako inteligentne materiały do monitorowania świeżości żywności. Natomiast optody na bazie agarozy [490-494] poza powyższym zastosowaniem, mogą również pełnić rolę matryc polimerowych do wykrywania oraz oznaczania jonów metali [495-503].

Z komercyjnie dostępnych materiałów, które mogą pełnić rolę podłoży dla receptorów, warto również wspomnieć o chusteczkach do prania typu Colour Catcher (CC), które mają za zadanie wyłapywać cząsteczki związków barwnych w czasie prania, aby nie doszło do zafarbowania tkanin. Materiał ten jest tani oraz łatwo dostępny w sprzedaży, a ze względu na właściwości absorbujące stanowi również interesujące rozwiązanie dla optod, gdyż w prosty sposób można osadzić na jego powierzchni chromojnofory [504]. Do tej pory CC zastosowano

między innymi jako warstwy receptorowe do wykrywania: siarczków oraz tioli [505], jonów metali [506-508], fluorków [509], monitorowania świeżości mięs [510-512], a także oznaczania zawartości etanolu w napojach [513]. Również popularne są bawełniane płatki [514] oraz patyczki kosmetyczne, które mogą być wykorzystywane do szybkiego wykrywania oraz ilościowego oznaczana analitów np. siarczków [515], cyjanków [516-518], siarczanów(IV) [519], azotanów(III) [520], jonów metali [521-525], cysteiny [526, 527] oraz enzymów [528, 529].

Podstawowym elementem warstwy receptorowej jest jonofor/chromojonofor, ale istotną rolę, oprócz materiału który stanowi matrycę dla receptorów, odgrywają pozostałe jej składniki wśród których można wymienić plastyfikator oraz sól lipofilową. Na wielkość generowanego sygnału ma wpływ rodzaj oraz ilość poszczególnych składników użytych do otrzymania optod, które między innymi mogą wpływać na takie parametry jak: czas odpowiedzi, selektywność, czułość czy zakres liniowej odpowiedzi [530-536].

Optody można miniaturyzować do mikro- i nanoskali [537-544], co pozwala na wykorzystanie ich do pomiarów bezpośrednio w komórkach i tkankach. Poza klasycznymi optodami proponowane są również inne rozwiązania wytwarzania czujników optycznych np. z wykorzystaniem hydrożeli [545-554], nanoemulsji [555-557], nanosfer [558-566], nanokapsuł [567], nanogąbek [568] czy nanokostek [569].

Oddziaływanie analitu z receptorem generuje sygnał optyczny [570], który jest mierzalny metodami spektrofotometrycznymi, ale także za pomocą aplikacji mobilnych [571-574] wykorzystujących cyfrową analizę barwną obrazów [575-581]. Obserwowalna „gołym okiem” zmiana koloru materiału czujnika czyni z nich przyjazne, wygodne i przenośne urządzenia analityczne [582-588].

Ze względu na zmianę barwy optod widoczną „gołym okiem”, detekcję można przeprowadzić poprzez analizę barwy i zastosowanie jej zmiany w procedurach analitycznych. Jak wykazano, nowoczesne algorytmy analizy obrazu pozwalają obecnie na badanie poziomów wybranych jonów na podstawie zmiany barwy materiału czujnika, co skutkuje prostą metodą ich wykrywania i wyznaczania [589, 590]. Większość obrazów optod jest rejestrowana lub przetwarzana na skalę barwną, najczęściej RGB lub HSV, gdzie można określić wartości poszczególnych kanałów barwnych RGB lub bezpośrednio wartości odcieni [591-594]. Natomiast zastosowanie odpowiedniego modelu matematycznego umożliwia zastosowanie cyfrowej analizy obrazu nawet w przypadku niespełniania przez układ prawa Lamberta-Beera [595].

Obserwowany w literaturze trend wzrastającego zainteresowania względnie prostymi, ekonomicznie korzystnymi, a co więcej skutecznie konkurującymi na przykład pod względem czułości, granic oznaczalności z metodami instrumentalnymi takimi jak atomowa spektroskopia absorpcyjna/emisyjna (AAS/AES) czy spektrometria mas z plazmą indukcyjnie sprzężoną (ICP-MS), czujnikami optycznymi był jedną z przyczyn wyboru tematyki badawczej. Wśród opisanych w literaturze rozwiązań stosunkowo niewielka ich liczba dotyczy zastosowania chromojonoforów o makrocyklicznej budowie jako jonoselektywnych składników warstw receptorowych. Można oczekiwać, że wprowadzenie makrocyklicznego chromojonoforu do jonoselektywnej membrany wpłynie istotnie na właściwości materiałów czujnikowych, w tym na przykład na ich selektywność. Była to kolejna przesłanka by podjąć badania nad możliwościami zastosowania chromogenicznych związków makrocyklicznych w warstwach receptorowych czujników optycznych.

LITERATURA

223. A. Hulanicki, S. Glab, F. Ingman, *Chemical sensors definitions and classification*, Pure Appl. Chem. **1991**, 63, 1247–1250;
224. B.F. Myasoedov, *Chemical sensors (review)*, Russ. Chem. Bull. **1992**, 41, 383–387;
225. S.C. Kishore, K. Samikannu, R. Atchudan, S. Perumal, T.N.J.I. Edison, M. Alagan, A.K. Sundramoorthy, Y.R. Lee, *Smartphone–Operated Wireless Chemical Sensors: A Review*, Chemosensors **2022**, 10, 55;
226. E. Bakker, P. Buhlmann, E. Pretsch, *Carrier–Based Ion–Selective Electrodes and Bulk Optodes. 1. General Characteristics*, Chem. Rev. **1997**, 97, 3083–3132;
227. P. Buhlmann, E. Pretsch, E. Bakker, *Carrier–Based Ion–Selective Electrodes and Bulk Optodes. 2. Ionophores for Potentiometric and Optical Sensors*, Chem. Rev. **1998**, 98, 1593–1688;
228. E. Bakker, Y. Qin, *Electrochemical Sensors*, Anal. Chem. **2006**, 78, 3965–3984;
229. A.E. Stashkova, M.A. Peshkova, K.N. Mikhelson, *Single–ion activity: Optical sensing vs. electrochemical sensing*, Sens. Actuators B Chem. **2015**, 207, 346–350;
230. S.A. Ferguson, M.E. Meyerhoff, *Advances in electrochemical and optical polyion sensing: A review*, Sens. Actuators B Chem. **2018**, 272, 643–654;
231. P. Devi, A. Thakur, R.Y. Lai, S. Saini, R. Jain, P. Kumar, *Progress in the materials for optical detection of arsenic in water*, Trends Anal. Chem. **2019**, 110, 97–115;
232. E. Zdrachek, E. Bakker, *From Molecular and Emulsified Ion Sensors to Membrane Electrodes: Molecular and Mechanistic Sensor Design*, Acc. Chem. Res. **2019**, 52, 1400–1408;
233. X.–D. Wang, O.S. Wolfbeis, *Fiber–Optic Chemical Sensors and Biosensors (2015–2019)*, Anal. Chem. **2020**, 92, 1, 397–430;
234. A. Steinegger, O.S. Wolfbeis, S.M. Borisov, *Optical Sensing and Imaging of pH Values: Spectroscopies, Materials, and Applications*, Chem. Rev. **2020**, 120, 22, 12357–12489;
235. V. Mani, T. Beduk, W. Khushaim, A.E. Ceylan, S. Timur, O.S. Wolfbei, K.N. Salama, *Electrochemical sensors targeting salivary biomarkers: A comprehensive review*, TrAC Trends Anal. Chem. **2021**, 135, 116164;
236. J. Baranwal, B. Barse, G. Gatto, G. Broncova, A. Kumar, *Electrochemical Sensors and Their Applications: A Review*, Chemosensors **2022**, 10, 363;
237. P. Panda, S. Chakroborty, *Optical sensor technology and its application in detecting environmental effluents: a review*, Int. J. Environ. Anal. Chem. **2022**;
238. K.J. Robinson, Y. Soda, E. Bakker, *Recent improvements to the selectivity of extraction–based optical ion sensors*, Chem. Commun. **2022**, 58, 4279–4287;
239. A. Barhoum, S. Hamimed, H. Slimi, A. Othmani, F.M. Abdel–Haleem, M. Bechelany, *Modern designs of electrochemical sensor platforms for environmental analyses: Principles, nanofabrication opportunities, and challenges*, Trends Environ. Anal. Chem. **2023**, 38, e00199;
240. R. Sun, Y. Li, T. Du, Y. Qi, *Recent advances in integrated dual–mode optical sensors for food safety detection*, Trends Food Sci. Tech. **2023**, 135, 14–31;
241. C. McDonagh, C.S. Burke, B.D. MacCraith, *Optical Chemical Sensors*, Chem. Rev. **2008**, 108, 400–422;
242. H.H. Qazi, A. Bakar bin Mohammad, M. Akram, *Recent Progress in Optical Chemical Sensors*, Sensors **2012**, 12, 16522–16556;
243. R. Pizzoferrato, *Optical Chemical Sensors: Design and Applications*, Sensors **2023**, 23, 5284;
244. A.V. Kalinichev, S.E. Ziegera, K. Koren, *Optical sensors (optodes) for multiparameter chemical imaging: classification, challenges, and prospects*, Analyst **2024**, 149, 29–45;
245. S.F.F.S. Yaacob, A. Olasupo, F. B.M. Suah, *Polymer inclusion membranes based Optode: Recent advances and perspectives*, Trends Anal. Chem. **2024**, 171, 117498;
246. E. Bakker, M. Lerchi, T. Rosatzin, B. Rusterholz, W. Simon, *Synthesis and characterization of neutral hydrogen ion–selective chromoionophores for use in bulk optodes*, Anal. Chem. Acta **1993**, 278, 211–225;
247. U.E. Spichiger–Keller, *Ion– and substrate–selective optode membranes and optical detection modes*, Sens. Actuators B Chem. **1997**, 38, 68–77;
248. H. Hisamoto, K. Suzuki, *Ion–selective optodes: current developments and future prospects*, TrAC Trends Anal. Chem. **1999**, 18, 513–524;
249. G. Mistlberger, G.A. Crespo, E. Bakker, *Ionophore–Based Optical Sensors*, Annu. Rev. Anal. Chem. **2014**, 7, 483–512;
250. K.N. Mikhelson, M.A. Peshkova, *Advances and trends in ionophore–based chemical sensors*, Russ. Chem. Rev. **2015**, 84, 555–578;
251. X. Du, X. Xie, *Ion–Selective optodes: Alternative approaches for simplified fabrication and signaling*, Sens. Actuators B Chem. **2021**, 335, 129368;
252. Z. Chen, Z. Zhang, J. Qi, J. You, J. Ma, L. Chen, *Colorimetric detection of heavy metal ions with various chromogenic materials: Strategies and applications*, J. Hazard. Mater. **2023**, 441, 129889;
253. E. Bakker, M. Willer, E. Pretsch, *Detection limit of ion–selective bulk optodes and corresponding electrodes*, Anal. Chim. Acta **1993**, 282, 265–271;
254. W.E. Morf, K. Seiler, B. Lehmann, C. Behringer, K. Hartman, W. Simon, *Carriers for chemical sensors: Design features of optical sensors (optodes) based on selective chromoionophores*, Pure Appl. Chem. **1989**, 61, 1613–1618;
255. P.C. Hauser, P.M. J. Perisset, S.S.S. Tan, W. Simon, *Optode for bulk–response membranes*, Anal. Chem. **1990**, 62, 1919–1923;
256. K. Seiler, W. Simon, *Theoretical aspects of bulk optode membranes*, Anal. Chim. Acta **1992**, 266, 73–87;
257. K. Seiler, W. Simon, *Principles and mechanisms of ion–selective optodes*, Sens. Actuators B Chem. **1992**, 6, 295–298;

258. E. Bakker, W. Simon, *Selectivity of ion–sensitive bulk optodes*, Anal. Chem. **1992**, 64, 1805–1812;
259. U. Spichiger, W. Simon, E. Bakker, M. Lerchi, P. Buhlmann, J.–P. Haug, M. Kuratli, S. Ozawa, S. West, *Optical sensors based on neutral carriers*, Sens. Actuators B Chem. **1993**, 11, 1–8;
260. U.E. Spichiger, D. Freiner, E. Bakker, T. Rosatzin, W. Simon, *Optodes in clinical chemistry: potential and limitations*, Sens. Actuators B Chem. **1993**, 11, 263–271;
261. W.E. Morf, K. Seiler, B. Rusterholz, W. Simon, *Design of a novel calcium–selective optode membrane based on neutral ionophores*, Anal. Chem. **1990**, 62, 738–742;
262. T. Rosatzin, P. Holy, K. Seiler, B. Rusterholz, W. Simon, *Immobilization of components in polymer membrane–based calcium–selective bulk optodes*, Anal. Chem. **1992**, 64, 2029–2035;
263. M. Lerchi, E. Bakker, B. Rusterholz, W. Simon, *Lead–selective bulk optodes based on neutral ionophores with subnanomolar detection limits*, Anal. Chem. **1992**, 64, 1534–1540;
264. K. Wang, K. Seiler, B. Rusterholz, W. Simon, *Characterization of an optode membrane for zinc(II) incorporating a lipophilized analogue of the dye 4–(2–pyridylazo)resorcinol*, Analyst, **1992**, 117, 57–60;
265. M. Lerchi, E. Reitter, W. Simon, E. P, D.A. Chowdhury, S. Kamata, *Bulk Optodes Based on Neutral Dithiocarbamate Ionophores with High Selectivity and Sensitivity for Silver and Mercury Cations*, Anal. Chem. **1994**, 66, 1713–1717;
266. M. Lerchi, E. Reitter, W. Simon, Uranyl ion–selective optode based on neutral ionophores, Fresenius J. Anal. Chem. **1994**, 348, 272–276;
267. M. Kuratli, M. Badertscher, B. Rusterholz, W. Simon, *Bisulfite addition reaction as the basis for a hydrogensulfite bulk optode*, Anal. Chem. **1993**, 65, 3473–3479;
268. S. Ozawa, P.C. Hauser, K. Seiler, S.S.S. Tan, W.E. Morf, W. Simon, *Ammonia–gas–selective optical sensors based on neutral ionophores*, Anal. Chem. **1991**, 63, 640–644;
269. S.J. West, S. Ozawa, K. Seiler, S.S.S. Tan, W. Simon, *Selective ionophore–based optical sensors for ammonia measurement in air*, Anal. Chem. **1992**, 64, 533–540;
270. K. Wang, K. Seiler, W.E. Morf, U.E. Spichiger, W. Simon, E. Lindner, E. Pungor, *Characterization of Potassium–Selective Optode Membranes Based on Neutral Ionophores and Application in Human Blood Plasma*, Anal. Sci. **1990**, 6, 715–720;
271. K. Seiler, K. Wang, E. Bakker, W.E. Morf, B. Rusterholz, U.E. Spichiger, W. Simon, *Characterization of sodium–selective optode membranes based on neutral ionophores and assay of sodium in plasma*, Clin. Chem. **1991**, 37, 1350–1355;
272. I. Murkovic, I. Oehme, G.J. Mohr, T. Ferber, O.S. Wolfbeis, *Optode membrane for continuous measurement of silver ions*, Microchim. Acta **1995**, 121, 249–258;
273. E. Wang, M.E. Meyerhoff, V.C. Yang, *Optical Detection of Macromolecular Heparin via Selective Coextraction into Thin Polymeric Films*, Anal. Chem. **1995**, 67, 3, 522–527;
274. G.J. Mohr, I. Murkovic, F. Lehmann, C. Haider, O.S. Wolfbeis, *Application of potential–sensitive fluorescent dyes in anion and cation–sensitive polymer membranes*, Sens. Actuators B Chem. **1997**, 39, 239–245;
275. I. Murkovic, O.S. Wolfbeis, *Fluorescence–based sensor membrane for mercury (II) detection*, Sens. Actuators B Chem. **1997**, 39, 246–251;
276. G.J. Mohr, F. Lehmann, R. Ostereich, I. Murkovic, O.S. Wolfbeis, *Investigation of potential–sensitive fluorescent dyes for application in nitrate sensitive polymer membranes*, Fresenius J. Anal. Chem. **1997**, 357, 284–291;
277. S. O'Neill, S. Conway, J. Twellmeyer, O. Egan, K. Nolan, D. Diamond, *Ion–selective optode membranes using 9–(4–diethylamino–2–octadecanoatestyryl)–acridine acidochromic dye*, Anal. Chim. Acta **1999**, 398, 1–11;
278. W.H. Chan, R.H. Yang, K.M. Wang, *Development of a mercury ion–selective optical sensor based on fluorescence quenching of 5,10,15,20–tetraphenylporphyrin*, Anal. Chim. Acta **2001**, 444, 261–269;
279. N. Alizadeh, A. Moemeni, M. Shamsipur, *Poly(vinyl chloride)–membrane ion–selective bulk optode based on 1,10–dibenzyl–1,10–diaza–18–crown–6 and 1–(2–pyridylazo)–2–naphthol for Cu^{2+} and Pb^{2+} ions*, Anal. Chim. Acta **2002**, 464, 187–196;
280. W. Zhang, E. Rozniecka, E. Malinowska, P. Parzuchowski, M.E. Meyerhoff, *Optical Chloride Sensor Based on Dimer−Monomer Equilibrium of Indium(III) Octaethylporphyrin in Polymeric Film*, Anal. Chem. **2002**, 74, 17, 4548–4557;
281. W. Qin, P. Parzuchowski, W. Zhang, M.E. Meyerhoff, *Optical Sensor for Amine Vapors Based on Dimer−Monomer Equilibrium of Indium(III) Octaethylporphyrin in a Polymeric Film*, Anal. Chem. **2003**, 75, 2, 332–340;
282. M. Shamsipur, S. Rouhani, A. Mohajeri, M.R. Ganjali, *PVC–membrane ion–selective bulk optode for Ag+ ion based on hexathia–18–crown–6 and 1,2–benzo–3–octadecanoylimino–7–diethylaminophenoxazine*, Anal. Bioanal. Chem. **2003**, 375, 692–697;
283. I. Murkovic Steinberg, A. Lobnik, O.S. Wolfbeis, *Characterisation of an optical sensor membrane based on the metal ion indicator Pyrocatechol Violet*, Sens. Actuators B Chem. **2003**, 90, 230–235;
284. M. Shamsipur, J. Tashkhourian, H. Sharghi, *Development of a PVC–membrane ion–selective bulk optode, for UO_2^{2+} ion, based on tri–n–octylphosphine oxide and dibenzoylmethane*, Anal. Bioanal. Chem. **2005**, 382, 1159–1162;
285. I.H.A. Badr, M.E. Meyerhoff, *Highly selective single–use fluoride ion optical sensor based on aluminum(III)–salen complex in thin polymeric film*, Anal. Chim. Acta. **2005**, 553, 169–176;
286. I.H.A. Badr, M.E. Meyerhoff, *Fluoride–Selective Optical Sensor Based on Aluminum(III)−Octaethylporphyrin in Thin Polymeric Film: Further Characterization and Practical Application*, Anal. Chem. **2005**, 77, 6719–6728;
287. I.H.A. Badr, M.E. Meyerhoff, *Highly Selective Optical Fluoride Ion Sensor with Submicromolar Detection Limit Based on Aluminum(III) Octaethylporphyrin in Thin Polymeric Film*, J. Am. Chem. Soc. **2005**, 127, 5318–5319;
288. A. Safavi, M. Sadeghi, *Design and evaluation of a thorium (IV) selective optode*, Anal. Chim. Acta **2006**, 567, 184–188;

289. Y. Takahashi, T. Hayashita, T.M. Suzuki, *Test Strips for Lead(II) Based on a Unique Color Change of PVC-film Containing O-Donor Macrocycles and an Anionic Dye*, Anal. Sci. **2007**, 23, 147–150;
290. Y. Kang, J.W. Kampf, M.E. Meyerhoff, *Optical fluoride sensor based on monomer–dimer equilibrium of scandium(III)–octaethylporphyrin in a plasticized polymeric film*, Anal. Chim. Acta **2007**, 598, 295–303;
291. A. Safavi, M. Sadeghi, *A PVC–membrane bulk optode for gallium(III) ion determination*, Talanta **2007**, 71, 339–343;
292. I. Murkovic Steinberg, S. Milardovic, *Chromogenic radical based optical sensor membrane for screening of antioxidant activity*, Talanta **2007**, 71, 1782–1787;
293. B. Khezri, M.K. Amini, A.R. Firooz, *An optical chemical sensor for mercury ion based on 2–mercaptopyrimidine in PVC membrane*, Anal. Bioanal. Chem. **2008**, 390, 1943–1950;
294. M.K. Amini, B. Khezri, A.R. Firooz, *Development of a highly sensitive and selective optical chemical sensor for batch and flow–through determination of mercury ion*, Sens. Actuators B Chem. **2008**, 131, 470–478;
295. A.A. Ensafi, M. Fouladgar, *Development a Simple PVC Membrane Bulk Optode for Determination of Lead Ions in Water Samples*, Sens. Lett. **2009**, 7, 177–184;
296. M. Fouladgar, A.A. Ensafi, *A Novel Optical Chemical Sensor to Determine Samarium Ions in Aqueous Solutions*, Sens. Lett. **2009**, 7, 1135–1140;
297. A.A. Ensafi, M. Fouladgar, *A sensitive and selective bulk optode for determination of Hg(II) based on hexathiacyclooctadecane and chromoionophore*, Sens. Actuators B Chem. **2009**, 136, 326–331;
298. M. Fouladgar, A.A. Ensafi, *A novel optical chemical sensor for thallium(III) determination using 4–(5–bromo–2–pyridylazo)–5–(diethylamino)–phenol*, Sens. Actuators B Chem. **2010**, 143, 590–594;
299. C. Bualom, W. Ngeontae, S. Nitiyanontakit, P. Ngamukot, A. Imyim, T. Tuntulani, W. Aeungmaitrepirom, *Bulk optode sensors for batch and flow–through determinations of lead ion in water samples*, Talanta **2010**, 82, 660–667;
300. A. Kavanagh, R. Byrne, D. Diamond, A. Radu, *A two–component polymeric optode membrane based on a multifunctional ionic liquid*, Analyst, **2011**, 136, 348–353;
301. N. Aksuner, *Development of a new fluorescent sensor based on a triazolo–thiadiazin derivative immobilized in polyvinyl chloride membrane for sensitive detection of lead(II) ions*, Sens. Actuators B Chem. **2011**, 157, 162–168;
302. J. Zhu, J. Zhai, X. Li, Y. Qin, *Applications of hydrophobic room temperature ionic liquids in ion–selective optodes*, Sens. Actuators B Chem. **2011**, 159, 256–260;
303. B. Rezaei, H. Hadadzadeh, A. Azimi, *Nickel(II) Selective PVC–Based Membrane Sensor Using a Schiff Base*, Int. J. Spectrosc. **2011**, 746372;
304. L. Xie, Y. Qin, H.–Y. Chen, *Polymeric Optodes Based on Upconverting Nanorods for Fluorescent Measurements of pH and Metal Ions in Blood Samples*, Anal. Chem. **2012**, 84, 1969–1974;
305. M. Bamsey, A. Berinstain, M. Dixon, *Development of a potassium–selective optode for hydroponic nutrient solution monitoring*, Anal. Chim. Acta **2012**, 737, 72–82;
306. M. Ghaedi, J. Tashkhourian, M. Montazerozohori, A.A. Pebdani, S. Khodadoust, *Design of an efficient uranyl ion optical sensor based on 1'–2,2'–(1,2–phenylene)bis(ethene–2,1–diyl)dinaphthalen–2–ol*, Mater. Sci. Eng. C **2012**, 32, 1888–1892;
307. A.R. Firooz, A.A. Ensafi, N. Kazemifard, H. Sharghim, *A highly sensitive and selective bulk optode based on benzimidazol derivative as an ionophore and ETH5294 for the determination of ultra trace amount of silver ions*, Talanta **2012**, 101, 171–176;
308. Y. Ge, J. Zhu, W. Zhao, Y. Qin, *Ion–selective optodes based on near infrared fluorescent chromoionophores for pH and metal ion measurements*, Sens. Actuators B Chem. **2012**, 166–167, 480–484;
309. A.R. Firooz, A.A. Ensafi, N. Kazemifard, R. Khalifeh, *Development of a highly sensitive and selective optical sensor for determination of ultra–trace amount of silver ions*, Sens. Actuators B Chem. **2013**, 176, 598–604;
310. A.R. Firooz, A.A. Ensafi, Z. Hajyani, *A highly sensitive and selective bulk optode based on dithiacyclooctadecane derivative incorporating chromoionophore V for determination of ultra trace amount of Hg(II)*, Sens. Actuators B Chem. **2013**, 177, 710–716;
311. A.R. Firooz, A.A. Ensafi, K. Karimi, R. Khalifeh, *Specific sensing of mercury(II) ions by an optical sensor based on a recently synthesized ionophore*, Sens. Actuators B Chem. **2013**, 185, 84–90;
312. A.R. Firooz, A.A. Ensafi, K. Karimi, H. Sharghi, *Development of a specific and highly sensitive optical chemical sensor for determination of Hg(II) based on a new synthesized ionophore*, Mater. Sci. Eng. C **2013**, 33, 4167–7172;
313. M. Bagher–Gholivand, A. Babakhanian, M. Mohammadi, P. Moradi, S.H. Kiaie, *Novel optical bulk membrane sensor and its application for determination of iron in plant and cereal samples*, J. Food Compos. Anal. **2013**, 29, 144–150;
314. M.T. Bamsey, A. Berinstain, M.A. Dixon, *Calcium–selective optodes for the management of plant nutrient solutions*, Sens. Actuators B Chem. **2014**, 190, 61–91;
315. J. Wu, Y. Qin, *Polymeric optodes based on upconverting nanorods for fluorescence measurements of Pb^{2+} in complex samples*, Sens. Actuators B Chem. **2014**, 192, 51–55;
316. C. Yang, T. Liu, Y. Xu, Y. Qin, *Fluorescent ion optodes based on calixarene functionized boron dipyrromethene chromoionophore for simultaneous measurement of multi–electrolytes in biological samples*, Sens. Actuators B Chem. **2014**, 192, 423–428;
317. S. Yang, Y. Wo, M.E. Meyerhoff, *Polymeric optical sensors for selective and sensitive nitrite detection using cobalt(III) corrole and rhodium(III) porphyrin as ionophores*, Anal. Chim. Acta **2014**, 843, 89–96;
318. A.R. Firooz, A.A. Ensafi, K.S. Hoseini, N. Kazemifard, *Development of a highly sensitive and selective mercury optical sensor based on immobilization of bis(thiophenal)–4,4'–methylenedianiline on a PVC membrane*, Mater. Sci. Eng. C **2014**, 38, 73–78;
319. A.A. Ensafi, M. Fouladgar, *A new sensitive optical bulk test–system for thallium based on pyridylazo resorcinol*, J. Anal. Chem. **2014**, 69, 143–148;

320. M. Ghaedi, A. Shahamiri, S. Hajati, B. Mirtamizdoust, *A novel PVC–membrane optical sensor for high sensitive and selective determination of Cu^{2+} ion based on synthesized (E)–N'–(pyridin–2–ylmethylene)isonicotin–ohydrazide*, J. Mol. Liq. **2014**, 199, 483–488;
321. Y. Liu, J. Zhu, Y. Xu, Y. Qin, D. Jiang, *Boronic Acid Functionalized Aza–Bodipy (azaBDPBA) based Fluorescence Optodes for the Analysis of Glucose in Whole Blood*, ACS Appl. Mater. Interfaces **2015**, 7, 11141–11145;
322. M. Ghaedi, A. Shahamiri, B. Mirtamizdoust, S. Hajati, F. Taghizadeh, *A novel polyvinyl chloride–membrane optical sensor for the determination of Cu^{2+} ion based on synthesized (N'1E,N'2E)–N'1,N'2–bis(pyridine–2–ylmethylene)oxalohydrazide: Experimental design and optimization*, Spectrochim. Acta A Mol. Biomol. Spectrosc. **2015**, 138, 878–884;
323. M. Jamshidi, M. Ghaedi, K. Dashtian, M. Montazerozohori, S. Hajati, *Schiff Base Impregnated Plasticized Polyvinyl Chloride Optical Sensor for Selective and Efficient Detection of Copper (II) Ion: Central Composite Design*, IEEE Sens. J. **2015**, 15, 6604–6610;
324. Y. Li, Y. Xu, J. Wu, Y. Qin, D. Jiang, *Rational design of piperidine functionalized boron–dipyrromethene as fluorescent chromoionophore for ion–selective optodes*, Sens. Actuators B Chem. **2016**, 232, 37–42;
325. F.M. Abdel–Haleem, *Highly selective thiourea–based bulk optode for determination of salicylate in spiked urine samples, Aspirin® and Aspocid®*, Sens. Actuators B Chem. **2016**, 233, 257–262;
326. M. Ghaedi, J. Tashkhourian, M. Montazerozohori, M.N. Biyareh, B. Sadeghian, *Highly selective and sensitive determination of copper ion by two novel optical sensors*, Arab. J. Chem. **2017**, 10, 2319–2326;
327. O.A. Elhefnawy, *A new optical sensor for spectrophotometric determination of uranium (VI) and thorium (IV) in acidic medium*, Radiochim. Acta **2017**;
328. F.M. Abdel–Haleem, M.S. Rizk, *Highly selective thiocyanate optochemical sensor based on manganese(III)–salophen ionophore*, Mater. Sci. Eng. C **2017**, 75, 682–687;
329. E. Horak, P. Kassal, M. Hranjec, I. Murković Steinberg, *Benzimidazole functionalised Schiff bases: Novel pH sensitive fluorescence turn–on chromoionophores for ion–selective optodes*, Sens. Actuators B Chem. **2018**, 258, 415–423;
330. F.M. Abdel–Haleem, R.M. El Nashar, *Calixarene–doped PVC polymeric films as size–selective optical sensors: Monitoring of salicylate in real samples*, Spectrochim. Acta A Mol. Biomol. Spectrosc. **2018**, 201, 98–104;
331. A.A. Gouda, A.S. Amin, *Design of a novel optical sensor for determination of trace amounts of tin in food and in environmental samples*, Int. J. Environ. Anal. Chem. **2020**, 102, 7313–7328;
332. N.V.Pokhvishcheva, M.A. Peshkova, *Ionic Liquids as Plasticizers for Optodes*, Moscow Univ. Chem. Bull. **2020**, 75, 115–120;
333. H.H. El–Feky, A.M. Askar, A.S. Amin, *Quantification of silver in several samples using a new ionophore polymer membrane as an optical sensor*, RSC Adv. **2021**, 11, 35300–35310;
334. M.M. Taha, M.S. Rizk, M.A. Zayed, F.M. Abdel–Haleem, A. Barhoum, *Non–Enzymatic Phenylboronic Acid–Based Optode Membrane for Glucose Monitoring in Serums of Diabetic Patients and in the Culture Medium of Human Embryos*, Sens. **2022**, 22, 7135;
335. H. H. El–Feky, A.S. Amin, E.M.I. Moustafa, *Utilization of a plasticized PVC optical sensor for the selective and efficient detection of cobalt(ii) in environmental samples*, RSC Adv. **2022**, 12, 18431–18440;
336. A.S. Amin, S. El–Bahy, H.H. El–Feky, *Utility of 5–(2',4'–dimethylphenylazo)–6–hydroxy–pyrimidine–2,4–dione in PVC membrane for a novel green optical chemical sensor to detect zinc ion in environmental samples*, Anal. Biochem. **2022**, 643, 114579;
337. E.M.I. Moustafa, A.S. Amin, M.A. El–Attar, *A highly selective bulk optode based on 6–{4–(2,4–dihydroxy–phenyl)diazenyl)phenyl}–2–oxo–4–phenyl–1,2–dihydro–pyridine–3–carbonitrile incorporating chromoionophore V for determination of nano levels of cadmium*, Anal. Biochem. **2022**, 654, 114835;
338. I.M.I. Moustafa, A.S. Amin, E. Darwish, *A novel bulk optode for ultra–trace detection of antimony coupled with spectrophotometry in food and environmental samples*, Talanta Open **2023**, 7, 100197;
339. A.S. Amin, S.M. El–Bahy, A.M.E. Hassan, *Construction of an optical sensor for molybdenum determination based on a new ionophore immobilized on a polymer membrane*, J. King Saud Univ. Sci. **2023**, 35, 102592;
340. A.M.E. Hassan,R.F. Alshehri, S.M. El–Bahy, A.S. Amin, M. Aish, *A modified selective optical sensor for selenium determination based on incorporating xylenol orange in a poly(vinyl chloride) membrane*, RSC Adv. **2023**,13, 34618–34629;
341. R.F. Alshehri, A.S. Amin, E.R. Darwish, *Ultrasensitive and highly selective detection of nickel ion by two novel optical sensors*, Anal Bioanal Chem **2023**, 415, 5695–5707;
342. R.F. Alshehri, A.S. Amin, M. Aish, *PVC–DOS membrane immobilized with 2–amino–4–(3–chloro–phenylazo) pyridine–3–ol for environmentally friendly detection of Cd(II) ions*, Chem. Data Coll. **2023**, 48, 101098;
343. R.F. Alshehri, H.H. El–Feky, A.M. Askar, A.S. Amin, M. Aish, *Utilization of a novel PVC– optical sensor for high sensitive and selective determination of zinc ion in real samples*, Spectrochim. Acta A Mol. Biomol. **2024**, 305, 123424,
344. R.F. Alshehri, A.S. Amin, E.R. Darwish, *Introducing an innovative immobilized optode based on PVC–ETH–5294 matrix for environmentally friendly sensing of lead ions*, Talanta Open **2024**, 9, 100285;
345. L. Lvova, C. Di Natale, R. Paolesse, L. Giorgi, V. Fusi, A. Garau, V. Lippolis, *Photographic Detection of Cadmium(II) and Zinc(II) Ions*, Procedia Eng. **2016**, 168, 346–350;
346. L. Lvova, C. Guanais Gonçalves, L. Prodi, M. Sgarzi, N. Zaccheroni, M. Lombardo, A. Legin, C. Di Natale, R. Paolesse, *Systematic approach in Mg^{2+} ions analysis with a combination of tailored fluorophore design*, Anal. Chim. Acta **2017**, 988, 96–103;
347. H. Shibata, T.G. Henares, K. Yamada, K. Suzukia, D. Citterio, *Implementation of a plasticized PVC–based cation–selective optode system into a paper–based analytical device for colorimetric sodium detection*, Analyst, **2018**, 143, 678–686;

348. L. Lvova, E. Acciari, F. Mandoj, G. Pomarico, C. Di Natale, R. Paolesse, *Crown–Porphyrin Ligand for Optical Sensors Development*, Proc. **2018**, 2, 922;
349. L. Lvova, E. Acciari, F. Mandoj, G. Pomarico, R. Paolesse, *Fast Optical Sensing of Metals: A Case Study of Cu^{2+} Assessment in Soils*, ECS J. Solid State Sci. Technol. **2020**, 9, 061004;
350. A. Garau, L. Lvova, E. Macedi, G. Ambrosi, M.C. Aragoni, M. Arca, C. Caltagirone, S. J. Coles, M. Formica, V. Fusi, L. Giorgi, F.Isaia, V. Lippolis, J.B. Ortond, R. Paolesse, *N_2S_2 pyridinophane–based fluorescent chemosensors for selective optical detection of Cd^{2+} in soils*, New J. Chem., **2020**, 44, 20834–20852;
351. M. Phichi, A. Imyim, T. Tuntulani, W. Aeungmaitrepirom, *Paper–based cation–selective optode sensor containing benzothiazole calix[4]arene for dual colorimetric Ag^{+} and Hg^{2+} detection*, Anal. Chim. Acta **2020**, 1104, 147–155;
352. S. Wirojsaengthong, D. Aryuwananon, W. Aeungmaitrepirom, B. Pulpoka, T. Tuntulani, *A colorimetric paper–based optode sensor for highly sensitive and selective determination of thiocyanate in urine sample using cobalt porphyrin derivative*, Talanta **2021**, 231, 122371;
353. D. Paderni, E. Macedi, L. Lvova, G. Ambrosi, M. Formica, L. Giorgi, R. Paolesse, V. Fusi, *Selective Detection of Mg^{2+} for Sensing Applications in Drinking Water*, Chem. Eur. J. **2022**, 28, e202201062;
354. T. Mizuta, K. Sueyoshi, T. Endo, H. Hisamoto, *Ionic liquid–based dye: A "Dyed plasticizer" for rapid and highly sensitive anion optodes based on a plasticized PVC membrane*, Sens. Actuators B Chem. **2018**, 258, 1125–1130;
355. T. Mizuta, S. Takai, T. Nishihata, Kenji Sueyoshi, T. Endoa, H. Hisamoto, *A lipophilic ionic liquid–based dye for anion optodes: importance of dye lipophilicity and application to heparin measurement*, Analyst, **2020**,145, 5430–5437;
356. M. Aish, R.F. Alshehr, A.S. Amin, E.R. Darwish, *Exploring the design and performance of a tellurium optical sensor utilizing a plasticizer–free polymer inclusion membrane*, Food Chem. **2024**, 439, 138112;
357. Y. Kostov, S. Tzonkov, *Membranes for optical pH sensors*, Anal. Chim. Acta **1993**, 280, 15–19;
358. A. Safavi, M. Pakniatn, *Dipicrylamine–modified triacetylcellulose membrane for optical pH and potassium ion measurement*, Anal. Chim. Acta **1996**, 335, 227–233;
359. A. Safavi, H. Abdollahi, *Optical sensor for high pH values*, Anal. Chim. Acta **1998**, 367, 167–173;
360. A.A. Ensafi, A. Kazemzadeh, *Monitoring nitrite with optical sensing films*, Microchem. J. **2002**, 72, 193–199;
361. A.A Ensafi, M Bakhshi, *New stable optical film sensor based on immobilization of 2–amino–1–cyclopentene–1–dithiocarboxylic acid on acetyl cellulose membrane for Ni(II) determination*, Sens. Actuators B Chem. **2003**, 96, 435–440;
362. A. Safavi, M. Bagheri, *Novel optical pH sensor for high and low pH values*, Sens. Actuators B Chem. **2003**, 90, 143–150;
363. A. Safavi, M. Bagheri, *Design and characteristics of a mercury (II) optode based on immobilization of dithizone on a triacetylcellulose membrane*, **2004**, 99, 608–612;
364. A.A. Ensafi, A. Aboutalebi, *A versatile stable cobalt optical sensor based on pyrogallol red immobilization on cellulose acetate film*, Sens. Actuators B Chem. **2005**, 105, 479–483;
365. A. Safavi, M. Bagheri, *Design of a copper (II) optode based on immobilization of dithizone on a triacetylcellulose membrane*, Sens. Actuators B Chem. **2005**, 107, 53–58;
366. M. Shamsipur, J. Tashkhourian, H. Sharghi, *Development of Sulfide-Selective Optode Membranes Based on Immobilization of Methylene Blue on Optically Transparent Triacetylcellulose Film*, Instrum. Sci. Technol. **2005**, 33, 703–714;
367. A.A. Ensafi, M. *Fouladgar, Development of a mercury optical sensor based on immobilization of 4–(2–pyridylazo)–resorcinol on a triacetylcellulose membrane*, Sens. Actuators B Chem. **2006**, 113, 88–93;
368. A. Abbaspour, L. Baramakeh, *Novel zirconium optical sensor based on immobilization of Alizarin Red S on a triacetylcellulose membrane by using principle component analysis artificial neural network*, Sens. Actuators B Chem. **2006**, 114, 950–956;
369. A.A. Ensafi, Z.N. Isfahani, *Determination of Lead Ions by an Optical Sensor Based on 2–Amino–Cyclopentene–1–Dithiocarboxylic Acid*, IEEE Sens. J. **2007**, 7, 1112–1117;
370. A.A. Ensafi, F.A. Katiraei, S. Meghdadi, *Highly selective optical sensor for mercury assay based on covalent immobilization of 4–hydroxy salophen on a triacetylcellulose membrane*, Sens. Actuators B Chem. **2008**, 133, 84–90;
371. A.A. Ensafi, M. Fouladgar, *Development of a Spectrophotometric Optode for the Determination of Hg(II)*, IEEE Sens. J. **2008**, 8, 347–353;
372. A.A. Ensafi, S. Meghdadi, E. Fooladgar, *Development of a New Selective Optical Sensor for Cd(II) Ions Based on 4–Hydroxy Salophen*, IEEE Sens. J. **2008**, 8, 1794–1800;
373. A.A. Ensafi, A.K. Far, S. Meghdadi, *Highly selective optical–sensing film for lead(II) determination in water samples*, J. Hazard. Mater. **2009**, 172, 1069–1075;
374. M.A. Chamjangali, S. Soltanpanah, N. Goudarzi, *Development and characterization of a copper optical sensor based on immobilization of synthesized 1–phenyl–1,2–propanedione–2–oxime thiosemicarbazone on a triacetylcellulose membrane*, Sens. Actuators B Chem. **2009**, 138, 251–256;
375. S. Rastegarzadeh, N. Pourreza, I. Saeedi, *An optical chemical sensor for thorium (IV) determination based on thorin*, J. Hazard. Mater. **2010**, 173, 110–114;
376. G. Absalan, M. Asadi, S. Kamran, S. Torabi, L. Sheikhian, *Design of a cyanide ion optode based on immobilization of a new Co(III) Schiff base complex on triacetylcellulose membrane using room temperature ionic liquids as modifiers*, Sens. Actuators B Chem. **2010**, 147, 31–36;
377. A.A. Ensafi, M. Amini, *A highly selective optical sensor for catalytic determination of ultra–trace amounts of nitrite in water and foods based on brilliant cresyl blue as a sensing reagent*, Sens. Actuators B Chem. **2010**, 147, 61–66;
378. A.A. Ensafi, E. Fooladgar, *Selective lanthanum ions optical sensor based on covalent immobilization of 4–hydroxysalophen on a hydrolyzed triacetylcellulose membrane*, J. Anal. Chem. **2011**, 66, 865–870;

379. A.A. Ensafi, Z.N. Isfahani, *A simple optical sensor for cadmium ions assay in water samples using spectrophotometry*, J. Anal. Chem. **2011**, 66, 151–157;
380. A.R. Firooz, M. Movahedi, A.A. Ensafi, *Selective and sensitive optical chemical sensor for the determination of Hg(II) ions based on tetrathia–12–crown–4 and chromoionophore I*, Sens. Actuators B Chem. **2012**, 171–172, 492–498;
381. H. Tavallali, E. Shaabanpur, P. Vahdati, *A highly selective optode for determination of Hg (II) by a modified immobilization of indigo carmine on a triacetylcellulose membrane*, Spectrochim. Acta A Mol. Biomol. Spectrosc. **2012**, 89, 216–221;
382. A.A. Ensafi, M. Amini, *Highly selective optical nitrite sensor for food analysis based on Lauth's violet–triacetyl cellulose membrane film*, Food Chem. **2012**, 132, 1600–1606;
383. H. Montaseri, S. Yousefinejad, *Design of an optical sensor for the determination of cysteine based on the spectrophotometric method in a triacetylcellulose film: PC–ANN application*, Anal. Methods **2014**, 6, 8482–8487;
384. H. Tavallali, L. Dorostghoal, *Design and evaluation of a lead (II) optical sensor based on immobilization of dithizone on triacetylcellulose membrane*, Int. J. Chemtech Res. **2014**, 6, 3179–3186;
385. K. Alizadeh, B. Rezaei, E. Khazaeli, *A new triazene–1–oxide derivative, immobilized on the triacetylcellulose membrane as an optical Ni^{2+} sensor*, Sens. Actuators B Chem. **2014**, 193, 267–272;
386. E. Pourbasheer, S. Morsali, A. Banaei, S. Aghabalazadeh, M.R. Ganjali, P. Norouzi, *Design of a novel optical sensor for determination of trace amounts of copper by UV/vis spectrophotometry in the real samples*, J. Ind. Eng. Chem. **2015**, 26, 370–374;
387. A.S. Amin, *Application of a triacetylcellulose membrane with immobilizated of 5–(2',4'–dimethylphenylazo)–6–hydroxypyrimidine–2,4–dione for mercury determination in real samples*, Sens. Actuators B Chem. **2015**, 221, 1342–1347;
388. M.M. Bordbar, H. Khajehsharifi, A. Solhjoo, *PC–ANN assisted to the determination of Vanadium (IV) ion using an optical sensor based on immobilization of Eriochorome Cyanine R on a triacetylcellulose film*, Spectrochim. Acta A Mol. Biomol. Spectrosc. **2015**, 151, 225–231;
389. G. Alberti, S. Re, A.M.C. Tivellia, R. Biesuz, *Smart sensory materials for divalent cations: a dithizone immobilized membrane for optical analysis*, Analyst **2016**, 141, 6140–6148;
390. K. Alizadeh, N.A. Rad, *A New Optical Sensor for Selective Monitoring of Nickel Ion Based on A Hydrazone Derivative Immobilized on the Triacetyl Cellulose Membrane*, J. Anal. Bioanal. Tech. **2016**, 7, 322;
391. A. Mosadeghei Fard, G.H. Vatankhah, *Design and Evaluation of a Mercury (II) Optode Based on Immobilization of 5, 6 Dimethyl–1–(4 methyl benzyl)–2–paratolyl–1H–benzimidazole (DMBPTBI) on a Triacetylcellulose Membrane and Determination in Various Samples*, J. Phys. Theor. Chem. **2017**, 14, 133–142;
392. M.G.K. Salmani, G.H. Rounaghi, M. Chamsaz, *An optical sensor for determination of low pH values based on covalent immobilization of Congo red on triacetyl cellulose films via epichlorohydrin*, Sens. Actuators B Chem. **2018**, 254, 177–181;
393. M.G.K. Salmani, G.H. Rounaghi, M. Chamsaz, *A selective and sensitive optode for determination of Hg^{2+} ion based on covalent immobilization of thiazole yellow on triacetyl cellulose films*, Sens. Actuators B Chem. **2018**, 256, 968–975;
394. A.R. Firooz, M. Movahedi, H. Sabzyan, *A new selective optode for the determination of iron(III) based on the immobilization of morin on triacetylcellulose: A combined experimental and computational study*, Mater. Sci. Eng. C **2019**, 94, 410–416;
395. M. Shafiee, A. Larki, A.Y. Faal, *Fabrication of an Optochemical Sensor Based on Triacetylcellulose Polymer for Colorimetric Determination of Trinitrotoluene*, Propellants Explos. Pyrotech. **2019**, 44, 1–8;
396. H.H. El–Fekya, S.M. El–Bahy, A.M.E. Hassan, A.S. Amin, *Utility of a novel optical sensor design for ultra–trace detection of chromium colorimetrically in real environmental samples*, Int. J. Environ. Anal. Chem. **2023**, 103, 4031–4048;
397. M. Saadati, *A simple method for colourimetric determination of silver using a home–made double beam photometer*, S. Afr. J. Chem. **2023**, 77, 19–23;
398. Y. Tharakeswar, Y. Kalyan, B. Gangadhar, K.S. Kumar, G.R. Naidu, *Optical Chemical Sensor for Screening Cadmium(II) in Natural Waters*, J. Sens. Tech. **2012**, 2, 68–74;
399. M.Y. Abdelaal, T.R. Sobahi, R.M. El–Shishtawy, *Chromophoric thin film based on cellulose triacetate blends for sensing metal ions*, C. R. Chim. **2014**, 17, 557–562;
400. N. Thakur, S.A. Kumar, K.S.A. Kumar, A.K. Pandey, S.D. Kumar , A.V.R. Reddy, *Development of a visual optode sensor for onsite determination of Hg(II)*, Sens. Actuators B Chem. **2015**, 211, 346–353;
401. N. Hassana, A.S. Amin, *Membrane optode for uranium(VI) preconcentration and colorimetric determination in real samples*, RSC Adv. **2017**, 7, 46566–46574;
402. N. Łukasik, E. Wagner–Wysiecka, *Salicylaldimine–based receptor as a material for iron(III) selective optical sensing*, J. Photochem. Photobiol. A Chem **2017**, 346, 318–326;
403. Z. Al–Mallah, A.S. Amin, *Utilization of a triacetylcellulose membrane to immobilize 5–(2',4'–dimethylphenylazo)–6–hydroxypyrimidine–2,4–dione for erbium determination in real samples*, J. Ind. Eng. Chem. **2018**, 63, 281–287;
404. P.S. Kulkarni, P.V. Ramekar, S.D. Kulkarni, *An optical sensor for selenite determination in aqueous samples*, J. Anal. Sci. Tech. **2018**, 9, 2;
405. N. Łukasik, E. Wagner–Wysiecka, A. Małachowska, *Iron(III)–selective materials based on a catecholbearing amide for optical sensing*, Analyst, **2019**,144, 3119–3127;
406. Z. Arif, R. Munandar, E. Rohaeti, M. Rafi, *Detection of Hexavalent Chromium Ion in Waterby Optode Membrane*, Indones. J. Chem. Stud. **2023**, 2, 76–82;
407. E.R. Darwish, R.F. Alshehri, A.S. Amin, M. Aish, *Development of an innovative optical sensor to detect extremely low levels of chromium in real samples using colorimetric methods*, Environ. Sci. Adv. **2024**, 3, 274–289;

408. Z. Arif, S. Sugiarti, E. Rohaeti, I. Batubara, *A Sensor (Optode) Based on Cellulose Triacetate Membrane for Fe(III) Detection in Water Samples*, Chemistry **2024**, 6, 81–94;
409. Q. Zhang, X. Wang, V. Decker, M.E. Meyerhoff, *Plasticizer–Free Thin–Film Sodium–Selective Optodes Inkjet–Printed on Transparent Plastic for Sweat Analysis*, ACS Appl. Mater. Interfaces **2020**, 12, 25616–25624;
410. E.K. Wujcika, S.E. Duirk, G.G. Chasec, C.N. Monty, *A visible colorimetric sensor based on nanoporous polypropylene fiber membranes for the determination of trihalomethanes in treated drinking water*, Sens. Actuators B Chem. **2016**, 223, 1–8;
411. A.R.M. Salcedo, F.B. Sevilla III, *Colorimetric determination of mercury vapor using smartphone camera–based imaging*, Instrum. Sci. Technol. **2018**, 46, 450–462;
412. C. Dincer, R. Bruch, E. Costa–Rama, M.T.F. Abedul, A. Merkoçi, A. Manz, G.A. Urban, F. Guder, *Disposable Sensors in Diagnostics, Food, and Environmental Monitoring*, Adv. Mater. **2019**, 31, e1806739;
413. N.A. Gavrilenko, N.V. Saranchina, A.V. Sukhanov, D.A. Fedan, *Reversible pH–sensitive element based on bromocresol Purple immobilized into the polymethacrylate matrix*, Mendeleev Commun. **2018**, 28, 450–452;
414. O. Voskoboynikova, A. Sukhanov, A. Duerkop, *Optical pH Sensing in Milk: A Small Puzzle of Indicator Concentrations and the Best Detection Method*, Chemosensors **2021**, 9, 177;
415. N.A. Gavrilenko, N.V. Saranchina, *Analytical Properties of 1–(2–Pyridylazo)–2–Naphthol Immobilized on a Polymethacrylate Matrix*, J. Anal. Chem. **2009**, 64, 226–230;
416. S.V. Muravyov, N.A. Gavrilenko, A.S. Spiridonova, S.V. Silushkin, P.G. Ovchinnikov, *Colorimetric scales for chemical analysis on the basis of transparent polymeric sensors*, J. Phys. Conf. Ser. **2010**, 238, 012051;
417. N.A. Gavrilenko, N.V. Saranchina, A.V. Sukhanov, M.A. Gavrilenko, E.V. Zenkova, *Colorimetric Polymethacrylate Sensor*, Adv. Mat. Res. **2014**, 880, 19–24;
418. N.A. Gavrilenko, N.V. Saranchina, M.A. Gavrilenko, *A Colorimetric Sensor Based on a Polymethacrylate Matrix with Immobilized 1–(2–Pyridylazo)–2–Naphthol for the Determination of Cobalt*, J. Anal. Chem. **2015**, 70, 1475–1479;
419. N.A. Gavrilenko, N.V. Saranchina, D.A. Fedan, M.A. Gavrilenko, *Solid–Phase Spectrophotometric Iodometric Determination of Nitrite and Selenium(IV) Using a Polymethacrylate Matrix*, J. Anal. Chem. **2017**, 72, 546–550;
420. N.A. Gavrilenko, N.V. Saranchina, A.V. Sukhanov, D.A. Fedan, M.A. Gavrilenko, *Kinetic Determination of Thiocyanate by the Reaction of Bromate with Crystal Violet Immobilized in a Polymethacrylate Matrix*, J. Anal. Chem. **2018**, 73, 849–899;
421. E.V. Urazov, M.A. Gavrilenko, M.K. Belikov, *Colorimetric Determination of Metal Ions Using Smartphone*, Key Eng. Mater. **2018**, 769, 235–241;
422. N.V. Saranchina, A.A. Dudkina, MM. Gavrilenko, N.A. Gavrilenko, *A Simple Method for Colorimetric and Naked–Eye Detection of Mercury in Fish Products*, Mater. Sci. Forum **2019**, 970, 219–226;
423. N.V. Saranchina, E.V. Urazov, M.M. Gavrilenko, N.A. Gavrilenko, *Automation of Optical Control of Metal Ions in Liquid Using a Smartphone*, Mater. Sci. Forum **2019**, 970, 290–296;
424. N.V. Saranchina, Y.G. Slizhov, Y.M. Vodova, N.S. Murzakasymova, A.M. Ilyina, N.A. Gavrilenko M.A. Gavrilenko, *Smartphone–based colorimetric determination of fluoride anions using polymethacrylate optode*, Talanta **2021**, 226, 122103;
425. E.M.I. Moustafa, A.S. Amin, E.R. Darwis, *Optical chemical sensor of Gd(iii) based on 5–(2'–bromophenyl– azo)–6–hydroxypyrimidine–2,4–dione immobilized on poly(methyl methacrylate) and 2–nitrophenyloctylether matrix*, RSC Adv. **2022**, 12, 26090–26098;
426. N.A. Gavrilenko, A.V. Sukhanov, O.V. Mokhova, *Redox and Acid–Base Properties of 2,6–Dichlorophenolindophenol Immobilized on a Polymethacrylate Matrix*, J. Anal. Chem. **2010**, 65, 17–20;
427. M.A. Gavrilenko, N.A. Gavrilenko, *Colorimetric sensor for the determination of low–molecular–weight heparyn*, Mendeleev Commun. **2017**, 27, 419–420;
428. N.A. Gavrilenko, N.V. Saranchina, E.A. Kambarova, E.V. Urazov, M.A. Gavrilenko, *Colorimetric and fluorescent sensing of rhodamine using polymethacrylate matrix*, Spectrochim. Acta A Mol. Biomol. Spectrosc. **2019**, 220, 117106;
429. A.A. Dudkina, T.N. Volgina, N.V. Saranchina, N.A. Gavrilenko, M.A. Gavrilenko, *Colorimetric determination of food colourants using solid phase extraction into polymethacrylate matrix*, Talanta **2019**, 202, 186–189;
430. N.V. Saranchina, A.A. Damzina, Y.E. Ermolaev, E.V. Urazov, N.A. Gavrilenko, M.A. Gavrilenko, *Determination of antioxidant capacity of medicinal tinctures using cuprac method involving Cu(II) neocuproine immobilized into polymethacrylate matrix*, Spectrochim. Acta A Mol. Biomol. Spectrosc. **2020**, 240, 118581;
431. S.K. Bragina, O.A. Bazhenova, M.M. Gavrilenko, M.V. Chubik, N.V. Saranchina, T.N. Volgina, N.A. Gavrilenko, *Digital image colorimetry method for determination of glucose using silver nanoparticles immobilized into polymethacrylate matrix*, Mendeleev Commun. **2023**, 33, 261–263;
432. X. Wang, Y. Qina, M.E. Meyerhoff, *Paper–based plasticizer–free sodium ion–selective sensor with camera phone as a detector*, Chem. Commun. **2015**, 51, 15176–15179;
433. X. Wang, Q. Zhang, C. Nam, M. Hickner, M. Mahoney, M.E. Meyerhoff, *An Ionophore–Based Anion–Selective Optode Printed on Cellulose Paper*, Angew. Chem. Int. Ed. **2017**, 56, 11826–11830;
434. P. Kassal, M.D. Steinberg, E. Horak, I. Murković Steinberg, *Wireless fluorimeter for mobile and low cost chemical sensing: A paper based chloride assay*, Sens. Actuators B Chem. **2018**, 275, 230–236;
435. S.A. Ferguson, X. Wang, M. Mahoney, M.E. Meyerhoff, *Detection and Quantification of Polyquaterniums via Polyion–Sensitive Ion–Selective Optodes Inkjet Printed on Cellulose Paper*, Anal. Sci. **2018**, 34, 45–50;
436. Y. Soda, H. Shibata, K. Yamada, K. Suzuki, D. Citterio, *Selective Detection of K^+ by Ion–Selective Optode Nanoparticles on Cellulosic Filter Paper Substrates*, ACS Appl. Nano Mater. **2018**, 1, 1792–1800;
437. Y. Soda, D. Citterio, E. Bakker, *Equipment–Free Detection of K^+ on Microfluidic Paper–Based Analytical Devices Based on Exhaustive Replacement with Ionic Dye in Ion–selective Capillary Sensors*, ACS Sens. **2019**, 4, 670–677;

438. A. D'Andreaa, G. Pomaricoa, S. Nardisa, R. Paolessea, C. Di Nataleb, L. Lvova, *Chemical traffic light: A self–calibrating naked–eye sensor for fluoride*, J. Porphyrins Phthalocyanines **2019**, 23, 117–124;
439. P. Kassal, M. Sigurnjak, I. Murković Steinberg, *Paper–based ion–selective optodes for continuous sensing: Reversible potassium ion monitoring*, Talanta **2019**, 193, 51–55;
440. H. Shibata, Y. Hiruta, D. Citterio, *Fully inkjet–printed distance–based paper microfluidic devices for colorimetric calcium determination using ion–selective optodes*, Analyst **2019**, 144, 1178–1186;
441. L. Lvova, G. Pomarico, F. Mandoj, F. Caroleo, C. Di Natale, K.M. Kadish, S. Nardis, *Smartphone coupled with a paper–based optode: Towards a selective cyanide detection*, J. Porphyrins Phthalocyanines **2020**, 24, 964–972;
442. P. Kamnoet, W. Aeungmaitrepirom, R.F. Menger, C.S. Henry, *Highly selective simultaneous determination of Cu(II), Co(II), Ni(II), Hg(II), and Mn(II) in water samples using microfluidic paper–based analytical devices*, Analyst **2021**, 146, 2229;
443. Y. Cui, R. Wang, B. Brady, X. Wang, *Fully inkjet–printed paper–based Pb^{2+} optodes for water analysis without interference from the chloramine disinfectant*, Anal. Bioanal. Chem. **2022**, 414, 7585–7595;
444. W. Tan, L. Zhang, P. Jarujamrus, J.C.G. Doery, W. Shen, *Improvement strategies on colorimetric performance and practical applications of Paper–based analytical devices*, Microchem. J. **2023**, 180, 107562;
445. J. Lin, Z. Tan, J. Zhang, L. Wang, *Preparation and properties of Fe(II)–ion–sensitive colour–changing fabric*, Color. Tech. **2015**, 131, 131–135;
446. G. Baysal, S. Onder, I. Gocek, L. Trabzon, H. Kızıl, F.N. Kök, B.K. Kayaoglu, *Design and fabrication of a new nonwoven–textile based platform for biosensor construction*, Sens. Actuators B Chem. **2015**, 208, 475–484;
447. F. Fattahia, M. Shariati–Rad, *A cotton pad–based sensor for the detection and determination of trihalomethanes in water by the colorimetric method*, Anal. Methods **2020**,12, 1779–1785;
448. B. Brady, R. Wang, R. Cheong, X. Wang, *Digital printing of selective and reversible ion optodes on fabrics: toward smart clothes for epidermal chemical sensing*, Analyst **2021**, 146, 6119;
449. H. Ramlow, K.L. Andrade, A.P.S. Immich, *Smart textiles: an overview of recent progress on chromic textiles*, J. Textile Inst. **2021**, 112, 152–471;
450. Y.K. Park, H.J. Oh, H.D. Lee, J.J. Lee, J.H. Kim, W. Lee, *Facile and eco–friendly fabrication of a colorimetric textile sensor by UV–induced photografting for acidic gas detection*, J. Environ. Chem. Eng. **2022**, 10, 108508;
451. X. Jiang, Z. Zhao, Y.X. Liao, C. Tang, P.–L. Tremblay, T. Zhang, *A recyclable colorimetric sensor made of waste cotton fabric for the detection of copper ions*, Cellulose **2022**, 29, 5103–515;
452. X. Jiang, C. Tang, Z. Zhao, Y.X. Liao, J. Zhao, J. Hu, H. Zhang, Q. Yu, P.–L. Tremblay, T. Zhang, *Cationic Waste Cotton Fabric for the Adsorptive Colorimetric Detection of Chromium Ion Traces*, ACS Sustainable Chem. Eng. **2023**, 11, 6610–6618;
453. R. Konwarh, P. Gupta, B.B. Mandal, *Silk–microfluidics for advanced biotechnological applications: A progressive review*, Botech. Adv. **2016**, 34, 845–858;
454. P. Jarujamrus, N. Malahom, S. Puchum, R. Meelapsom, M. Amatatongchai, A. Siripinyanond, S. Chairam, C. Kulsing, *Complexometric and argentometric titrations using thread–based analytical devices*, Talanta **2018**, 183, 228–236;
455. A. Gonzalez, M. Gaines, L.Y. Gallegos, R. Guevara, F.A. Gomez, *Thread–paper, and fabric enzyme–linked immunosorbent assays (ELISA)*, Methods **2018**, 146, 58–65;
456. Y.D. Li, H.H. Chai, S.J. Zhang, Z.S. Lu, C.M. Li, L. Yu, *Sensitive and portable colorimetric detection of copper in water by cotton thread based pre–concentration*, Mircochem. J. **2019**, 148, 735–742;
457. R.E. Owyeung, M.J. Panzer, S.R. Sonkusale, *Colorimetric Gas Sensing Washable Threads for Smart Textiles*, Sci. Rep. **2019**, 9, 5607;
458. X. Weng, Y. Kang, Q. Guo, B. Peng, H. Jiang, *Recent advances in thread–based microfluidics for diagnostic applications*, Biosens. Bioelectro. **2019**, 132, 171–185;
459. M.M. Erenas, B. Carrillo–Aguilera, K. Cantrell, S. Gonzalez–Chocano, I.M.P. de Vargas–Sansalvador, I. de Orbe–Paya, L.F. Capitan–Vallvey, *Real time monitoring of glucose in whole blood by smartphone*, Biosens. Bioelectro. **2019**, 136, 47–52;
460. M.J. Arroyo, M.M. Erenas, I. de Orbe–Paya, K. Cantrell, J.A. Dobado, P. Ballester, P. Blondeau, A. Salinas–Castillo, L.F. Capitán–Vallvey, *Thread based microfluidic platform for urinary creatinine analysis*, Sens. Actuators B Chem. **2020**, 305, 127407;
461. N. Promphet, J.P. Hinestroza, P. Rattanawaleedirojn, N. Soatthiyanon, K. Siralertmukul, P. Potiyaraj, N. Rodthongkum, *Cotton thread–based wearable sensor for non–invasive simultaneous diagnosis of diabetes and kidney failure*, Sens. Actuators B Chem. **2020**, 321, 128549;
462. W.T. Suarez, M.O.K. Franco, L.F. Capitán–Vallvey, M.M. Erenas, *Chitosan–modified cotton thread for the preconcentration and colorimetric trace determination of Co(II)*, Microchem. J. **2020**, 158, 105137;
463. P. Singhaphan, F. Unob, *Thread–based platform for nitrite detection based on a modified Griess assay*, Sens. Actuators B Chem. **2021**, 327, 128938;
464. P. Punnoy, P. Preechakasedkit, C. Aumnate, N. Rodthongkum, P. Potiyaraj, N. Ruecha, *Polyvinyl alcohol/starch modified cotton thread surface as a novel colorimetric glucose sensor*, Mater. Lett. **2021**, 299, 130076;
465. S. Damodara, Y. Zhu, P.R. Selvaganapathy, *Patterned threads as solid–state reagent storage and delivery medium for automated periodic colorimetric monitoring of the environment*, Microfluid Nanofluid. **2021**, 25, 93;
466. D. Agustini, F.R. Caetano, R.F. Quero, J.A.F. da Silva, M.F. Bergamini, L.H. Marcolino–Junior, D.P. de Jesus, *Microfluidic devices based on textile threads for analytical applications: state of the art and prospects*, Anal. Methods **2021**,13, 4830–4857;
467. T. Saiboh, N. Malahom, A. Prakobkij, K. Seebunrueng, M. Amatatongchai, S. Chairam, Y. Sameenoi, P. Jarujamrus, *Visual detection of formalin in food samples by using a microfluidic thread–based analytical device*, Microchem. J. **2023**, 190, 108685;

468. L. Wang, X. Xie, J. Zhaia, E. Bakker, *Reversible pH–independent optical potassium sensor with lipophilic solvatochromic dye transducer on surface modified microporous nylon*, Chem. Commun. **2016**, 52, 14254–14257;
469. X. Wang, Y. Zhou, V. Decker, M. Meyerhoff, M. Sund, Y. Cui, *Plasticizer–free and pH–independent ion–selective optode films based on a solvatochromic dye*, Anal. Methods, **2020**,12, 2547–2550;
470. J. Kramer, R. Kang, L.M. Grimm, L.D. Cola, P. Picchetti, F. Biedermann, Molecular Probes, *Chemosensors, and Nanosensors for Optical Detection of Biorelevant Molecules and Ions in Aqueous Media and Biofluids*, Chem. Rev. **2022**, 122, 3459–3636;
471. R.A. Talja, H. Helen, Y.H. Roos, K Jouppila, *Effect of type and content of binary polyol mixtures on physical and mechanical properties of starch–based edible films*, Carbohydr. Polym. **2008**, 71, 269–276;
472. C.L. Luchese, N. Sperotto, J.C. Spada, I.C. Tessaro, *Effect of blueberry agro–industrial waste addition to corn starch–based films for the production of a pH–indicator film*, Int. J. Biol. Macromol. **2017**, 104, 11–18;
473. C.L. Luchese, V.F. Abdalla, J.C. Spada, I.C. Tessaro, *Evaluation of blueberry residue incorporated cassava starch film as pH indicator in different simulants and foodstuffs*, Food Hydrocoll. **2018**, 82, 209–218;
474. C.L. Luchese, J.M.F. Pavoni, J.C. Spada, I.C. Tessaro, *Influence of Blueberry and Jaboticaba Agroindustrial Residue Particle Size on Color Change of Corn Starch Based Films Submitted to Different pH Values Solution*, J. Renew. Mater. **2019**, 7, 235–243;
475. R. Andretta, C.L. Luchese, I.C. Tessaro, J.C. Spada, *Development and characterization of pH–indicator films based on cassava starch and blueberry residue by thermocompression*, Food Hydrocoll. **2019**, 93, 317–324;
476. M. Alizadeh–Sani, E. Mohammadian, J.–W. Rhim, S. Mahdi Jafari, *pH–sensitive (halochromic) smart packaging films based on natural food colorants for the monitoring of food quality and safety*, Trends Food Sci. Technol. **2020**, 105, 93–144;
477. M. Chen, T. Yan, J. Huang, Y. Zhou, Y. Hu, *Fabrication of halochromic smart films by immobilizing red cabbage anthocyanins into chitosan/oxidized–chitin nanocrystals composites for real–time hairtail and shrimp freshness monitoring*, Int. J. Biol. Macromol. **2021**, 179, 90–100;
478. M.I. Shaik, M.F. Azhari, N.M. Sarbon, *Gelatin–Based Film as a Color Indicator in Food–Spoilage Observation: A Review*, Foods **2022**, 11, 3797;
479. P. Ezati, A. Khan, J.–W. Rhim, *Resazurin–impregnated gelatin–based indicator for intelligent packaging applications*, Colloids Surf. A Physicochem. Eng. Asp. **2023**, 675, 131950;
480. S. Tavakoli, E. Mubango, L. Tian, Y. Bohoussou ŃDri, Y. Tan, H. Hong, Y. Luo, *Novel intelligent films containing anthocyanin and phycocyanin for nondestructively tracing fish spoilage*, Food Chem. **2023**, 402, 134203;
481. Z. Liu, F. Lou, T. Chen, *Polymeric pH indicators immobilized PVA membranes for optical sensors of high basicity based on a kinetic proces*, Anal. Chim. Acta **2004**, 519, 147–153;
482. Z. Liu, J. Liu, T. Chen, *Phenol red immobilized PVA membrane for an optical pH sensor with two determination ranges and long–term stability*, Sens. Acctuactor B Chem. **2005**, 107, 311–316;
483. L.R. Magnaghi, G. Alberti, C. Milanese, P. Quadrelli, R. Biesuz, *Naked–Eye Food Freshness Detection: Innovative Polymeric Optode for High–Protein Food Spoilage Monitoring*, ACS Food Sci. Technol. **2021**, 1, 165–175;
484. L.R. Magnaghi, F. Capone, G. Alberti, C. Zanoni, B. Mannucci, P. Quadrelli, R. Biesuz, *EVOH–Based pH–Sensitive Optode Array and Chemometrics: From Naked–Eye Analysis to Predictive Modeling to Detect Milk Freshness*, ACS Food Sci. Technol. **2021**, 1, 819–828;
485. L.R. Magnaghi, C. Zanoni, G. Alberti, P. Quadrelli, R. Biesuz, *Towards intelligent packaging: BCP–EVOH@ optode for milk freshness measurement*, Talanta **2022**, 241, 123230;
486. L.R. Magnaghi, C. Zanoni, G. Alberti, P. Quadrelli, R. Biesuz, *Freshness Traffic Light for Fish Products: Dual–Optode Label to Monitor Fish Spoilage in Sales Packages*, ACS Food Sci. Technol. **2022**, 2, 1030–1038;
487. L.R. Magnaghi, C. Zanoni, E. Bancalari, J.H. Saadoun, G. Alberti, P. Quadrelli, Raffaela Biesuz, *pH–Sensitive Sensors at Work on Poultry Meat Degradation Detection: From the Laboratory to the Supermarket Shelf*, AppliedChem **2022**, 2, 128–141;
488. H. Wu, C. Jiao, S. Li, Q. Li, Z. Zhang, M. Zhou, X. Yuan, *A Facile Strategy for Development of pH–Sensing Indicator Films Based on Red Cabbage Puree and Polyvinyl Alcohol for Monitoring Fish Freshness*, Foods **2022**, 11, 3371;
489. L.R. Magnaghi, G. Alberti, C. Zanoni, M. Guembe–Garcia, P. Quadrelli, R. Biesuz, *Chemometric–Assisted Litmus Test: One Single Sensing Platform Adapted from 1–13 to Narrow pH Ranges*, Sensors **2023**, 23, 1696;
490. P. Hashemi, M.M. Abolghasemi, *Preparation of a novel optical sensor for low pH values using agarose membranes as suport*, Sens. Actuators B Chem. **2006**, 115, 49–53;
491. P. Hashemi, R.A. Zarjani, M.M. Abolghasemi, A. Olin, *Agarose film coated glass slides for preparation of pH optical sensors*, Sens.Actuators B Chem. **2007**, 121, 396–400;
492. P. Hashemi, R.A. Zarjani, *A wide range pH optical sensor with mixture of Neutral Red and Thionin immobilized on an agarose film coated glass slide*, Sens. Actuators B Chem. **2008**, 135, 112–115;
493. R. Heydari, M. Hosseini, A. Amraei, A. Mohammadzadeh, *Preparation of a novel pH optical sensor using orange (II) based on agarose membrane as suport*, Mat. Sci. Eng. C **2016**, 61, 333–337;
494. K. Alizadeh, B. Rezaei, H. Nemati, *A new optical pH sensor based on a mixture of Alizarin and Orange dyes immobilized on an agarose membrane*, MethodX **2023**, 11, 102462;
495. P. Hashemi, M.M. Abolghasemi, K. Alizadeh, R.A. Zarjani, *A calmagite immobilized agarose membrane optical sensor for selective monitoring of* Cu^{2+}, Sens. Actuators B Chem. **2008**, 129, 332–338;
496. K. Alizadeh, R. Parooi, P. Hashemi, B. Rezaei, M.R. Ganjali, *A new Schiff's base ligand immobilized agarose membrane optical sensor for selective monitoring of mercury ion*, J. Hazard. Mat. **2011**, 1794–1800;
497. P. Hashemi, M. Hosseini, K. Zargoosh, K. Alizadeh, *High sensitive optode for selective determination of* Ni^{2+} *based on the covalently immobilized thionine in agarose membrane*, Sens. Actuators B Chem. **2011**, 153, 24–28;

498. K. Zargoosh, F.F. Babadi, *Highly selective and sensitive optical sensor for determination of Pb^{2+} and Hg^{2+} ions based on the covalent immobilization of dithizone on agarose membrane*, Spectrochim. Acta A Mol. Biomol. Spectrosc. **2015**, 137, 105–110;
499. F.N. Serenjeh, P. Hashemi, A.R. Ghiasvand, F. Rasolzadeh, *A new optical sensor for selective quantitation of uranium by the immobilization of arsenazo III on an agarose membrane*, Anal. Methods **2016**, 8, 4181–4187;
500. F. Rasolzadeh, P. Hashemi, B. Rezaei, *Aryl triazene derivative immobilized on agarose membrane for selective optical sensing and quantitation of Ni^{2+} in water*, J. Iran Chem. Soc. **2019**, 16, 1283–1289;
501. K. Alizadeh, B. Rezaei, E. Khazaeli, *An agarose based optical membrane sensor for selective monitoring of trace nickel ions*, J. Photochem. Photobiol. A Chem. **2021**, 417, 113371;
502. A.S. Amin, H.H. El–Feky, N. Hassan, *A novel sensor for the selective monitoring of trace ytterbium ions using an agarose–based optical membrane*, RSC Adv. **2022**, 12, 26620–26629;
503. M. Aish, R.F. Alshehrib, A.S. Amin, *Construction of an optical sensor for copper determination in environmental, food, and biological samples based on the covalently immobilized 2–(2–benzothiazolylazo)–3–hydroxyphenol in agarose*, RSC Adv. **2023**, 13, 24777–24788;
504. G. Alberti, C. Zanoni, L.R. Magnaghi, R. Biesuz, *Disposable and Low–Cost Colorimetric Sensors for Environmental Analysis*, Int. J. Environ. Res. Public Health **2020**, 17, 8331;
505. G. Alberti, V.M. Nurchi, L.R. Magnaghi, R. Biesuz, *A portable, disposable, and low–cost optode for sulphide and thiol detection*, Anal. Methods **2019**,11, 4464–4470;
506. R. Biesuz, V.M. Nurchi, L.R. Magnaghi, G. Alberti, *Inexpensive Alizarin Red S–based optical device for the simultaneous detection of Fe(III) and Al(III)*, Microchem. J. **2019**, 149, 104036;
507. G. Alberti, C. Zanoni, L.R. Magnaghi, R. Biesuz, *Low–cost, disposable colourimetric sensors for metal ions detection*, J. Anal. Sci. Technol. **2020**, 11, 30;
508. F. Caroleo, G. Magna, C. Damiano, M. Cavalleri, E. Gallo, C. Di Natale, R. Paolesse, *Colour Catcher® sheet beyond the laundry: A low–cost support for realizing porphyrin–based mercury ion sensors*, Sens. Actuators B Chem. **2022**, 364, 131900;
509. F. Caroleo, G. Magna, S. Nardis, A. Catini, V. Allegra, C. Di Natale, R. Paolesse, *Silicon corrole functionalized color catcher strips for fluoride ion detection*, Chem. Eng. J. Adv. **2023**, 14, 100478;
510. L.R. Magnaghi, F. Capone, C. Zanoni, G. Alberti, P. Quadrelli, R. Biesuz, *Colorimetric Sensor Array for Monitoring, Modelling and Comparing Spoilage Processes of Different Meat and Fish Foods*, Foods **2020**, 9, 684;
511. L.R. Magnaghi, G. Alberti, P. Quadrelli, R. Biesuz, *Development of a Dye–Based Device to Assess Poultry Meat Spoilage. Part I: Building and Testing the Sensitive Array*, J. Agric. Food Chem. **2020**, 68, 12702−12709;
512. L.R. Magnaghi, G. Alberti, F. Capone, C. Zanoni, B. Mannucci, P. Quadrelli, R. Biesuz, *Development of a dye–based device to assess the poultry meat spoilage. Part II: Array on act*, J. Agric. Food Chem. **2020**, 68, 12710–12718;
513. I. Safarik, J. Prochazkova, *Semiquantitative color catcher and smartphone–based analysis of synthetic food dyes in alcohol containing beverages*, Talanta **2023**, 262, 124686;
514. N.A. Bumagina, A.A. Ksenofontov, E.V. Antina, M.B. Berezin, *The new role of dipyrromethene chemosensor for absorbance–ratiometic and fluorescence "turn–on" sensing Zn^{2+} ions in water–organic solutions and real water samples*, Spectrochim. Acta A Mol. Biomol. Spectrosc. **2024**, 307, 123663;
515. K.B.A. Ahmed, M. Mariappan, A. Veerappan, *Nanosilver cotton swabs for highly sensitive and selective colorimetric detection of sulfide ions at nanomolar level*, Sens. Actuators B Chem. **2017**, 244, 831–836;
516. Rajamanikandan, M. Ilanchelian, *β–Cyclodextrin protected gold nanoparticle based cotton swabs as an effective candidate for specific sensing of trace levels of cyanide*, Anal. Methods **2019**, 11, 97–104;
517. C. Nandhini, P.S. Kumar, K. Poongodi, R. Shanmugapriya, K.P. Elango, *Development of simple imine based probe for selective fluorescent cyanide sensing with red–emission in solid and solution phases*, J. Mol. Liq. **2021**, 327, 114833;
518. V. Hemalatha, V. Vijayakumar, *A highly selective colorimetric sensing of CN^- ion by a hydrazine appended Schiff base and its application in detection of CN^- ion present in tobacco and food samples*, Inorg. Chem. Commun. **2022**, 144, 109894;
519. C. Khamkhajorn, S. Pencharee, J. Jakmunee, N. Youngvises, *Smartphone–based colorimetric method for determining sulfites in wine using a universal clamp sample holder and microfluidic cotton swab–based analytical device*, Microchem. J. **2022**, 174, 107055;
520. T. Anton–Canovas, F. Alonso, *The Eschenmoser's Salt as a Formylation Agent for the Synthesis of Indolizinecarbaldehydes and Their Use for Colorimetric Nitrite Detection*, Angew Chem Int Ed Engl. **2023**, 62, e202215916;
521. S. Erdemir, O. Kocyigit, S. Malkondu, *Optical and quantitative detection of Ca^{2+} ion by an calix[4]arene–isophorone incorporated fluorometric and colorimetric probe*, J. Photochem. Photobiol. A Chem. **2022**, 425, 113713;
522. G. Prabakaran, G. Narmatha, A. Thangamani, P.B. Raja, R. Karthick, G. Velraj, R.S. Kumar, A.I. Almansour, K. Perumal, R. Nandhakumar, *A thiophene built chalcone as fluorescent chemosensor for silver ions and their applications in strip–paper, ointments, and bio–imaging*, J. Photochem. Photobiol. A Chem. **2023**, 444, 114984;
523. S. Erdemir, D.Aydin, O. Kocyigit, *Nanomolar "Turn–On" Hg^{2+} detection by a fluorescein based fluorescent probe: DFT calculations, bioimaging and on–site assay kit studies* **2023**, 310, 128376;
524. H.N. Genc, O.G. Yasar, S.N.K. Elma, F.N. Arslan, I Yilmaz, A. Sirit, *Naked–eye colorimetric and switch–on fluorescence chemosensor based on a rhodamine derivative for Hg^{2+}: Smartphone device, test–kit and food sample applications*, J. Photochem. Photobiol. A Chem. **2023**, 438, 114558;
525. M. Nelson, F. Predih, A.M. Kubendran, G. Santhalingam, B. Ashokkumar, S. Ayyanar, *Design, synthesis, experimental investigations, theoretical corroborations, and distinct applications of a futuristic fluorescence chemosensor for the unveiling of Zn^{2+} ions*, J. Mol. Struct. **2023**, 1281, 134991;

526. Z.–F. Hu, L. Dou, J. Zhang, Y. Zhang, Y.–X. Sun, W.–K. Dong, *A novel "on–off–on" halogen–substituted bis(salamo)–like fluorogenic chemosensor for sequentially identifying Cu^{2+} ions and cysteine*, Inorg. Chem. Acta **2022**, 541, 121090;
527. V. Kavitha, P. Viswanathamurthi, J. Haribabu, C. Echeverria, *An aqueous mediated ultrasensitive facile probe incorporated with acrylate moiety to monitor cysteine in food samples and live cells*, Spectrochim. Acta A Mol. Biomol. Spectrosc. **2023**, 293, 122447;
528. R. Dutta, S. Makhaik, P. Zhao, K.G. Cruz, K.–W. Park, H. Liu, T.L. Andrew, J.A. Hardy, S. Thayumanavan, *Colorimetric Cotton Swab for Viral Protease Detection*, Anal. Chem. **2022**, 94, 12699–12705;
529. G.–Q. Zhang, H. Chang, Z. Gao, Y.–P. Deng, S. Zeng, L. Shang, D. Ding, Q. Liu, *Neuraminidase–Activatable NIR Fluorescent Probe for Influenza Virus Ratiometric Imaging in Living Cells and Colorimetric Detection on Cotton Swabs*, ACS Materials Lett. **2023**, 5, 722–729;
530. X. Xie, *Renovating the chromoionophores and detection modes in carrier–based ion–selective optical sensors*, Anal. Bioanal. Chem. **2016**, 408, 2717–2725;
531. A.V. Kalinichev, A. Frosinyuk, M.A. Peshkova, K.N. Mikhelson, *The impact of ion association in the optode phase to the dynamic range and the sensitivity of the response of ion–selective bulk optodes*, Sens. Actuators B Chem. **2017**, 249, 123–130;
532. D.I. Dekina, A.V. Kalinichev, N.V. Pokhvishcheva, M.A. Peshkova, K.N. Mikhelson, *Effects of quantitative composition of the sensing phase in the response of ionophore–based optical sensors*, Sens. Actuators B Chem. **2018**, 277, 535–543;
533. A. Kalinichev, M. Peshkova, N. Pokhvishcheva, K. Mikhelson, *Ion–Selective Optical Sensors: A New Look at Well–Established Techniques of Signal Acquisition*, Proc. **2018**, 2, 825;
534. A.V. Kalinichev, N.V. Pokhvishcheva, M.A. Peshkova, *Influence of Electrolyte Coextraction on the Response of Indicator–Based Cation–Selective Optodes*, ACS Sens. **2020**, 5, 3558–3567;
535. A.V. Siamionau, V.V. Egorov, *Determination of Single–Ion Partition Coefficients between Water and Plasticized PVC Membrane Using Equilibrium–Based Techniques*, Membranes **2022**, 12, 1019;
536. N.V. Pokhvishcheva, I.S. Prozherin, A.V. Kalinichev, M.A. Peshkova, *Response Patterns of Chromoionophore–Based Bulk Optodes Containing Lipophilic Electrolytes: Toward Background–Independent pH–Sensing*, ACS Sens. **2023**, 8, 3086–3094;
537. X. Xie, J. Zhai, G.A. Crespo, E. Bakker, *Ionophore–Based Ion–Selective Optical NanoSensors Operating in Exhaustive Sensing Mode*, Anal. Chem. **2014**, 86, 8770–8775;
538. X. Xie, E. Bakker, *Ion selective optodes: from the bulk to the nanoscale*, Anal. Bioanal. Chem. **2015**, 407, 3899–3910;
539. C. Zhu, M. Huang, J. Lan, L.W. Chung, X. Li, X. Xie, *Colorimetric Calcium Probe with Comparison to an Ion–Selective Optode*, ACS Omega **2018**, 3, 12476–12481;
540. E. Stelmach, K. Kłucińska, K. Maksymiuk, A. Michalska, *Rational design of nanoptodes architecture – Towards multifunctional sensors*, Talanta **2019**, 196, 226–230;
541. Y. Cui, J. Zhai, Y. Wanga, X. Xie, *Polymersome–based ion–selective nano–optodes containing ionophores*, Sens. Diagn. **2023**, 2, 1286–1291;
542. A. Konefał, P. Piątek, K. Maksymiuk, A. Michalska, *Looking into the ion–selective nanoptode bulk – Alternative mechanism of optical signal transduction for ratiometric ion–selective probes applicable in broad pH range*, Sens. Actuators B Chem. **2023**, 391, 134022;
543. F. Ghasemi, N. Fahimi–Kashani, A. Bigdeli, A.H. Alshatteri, S. Abbasi–Moayed, S.H. Al–Jaf, M.Y. Merry, K.M. Omer, M.R. Hormozi–Nezhad, *Paper–based optical nanosensors – A review*, Anal. Chim. Acta **2023**, 1238, 340640;
544. Y. Cui, J. Zhai, Y. Wanga, X. Xie, *Polymersome–based ion–selective nano–optodes containing ionophores*, Sens. Diagn. **2023**, 2, 1286–1291;
545. X. Du, J. Zhou, J. Shi, B. Xu, *Supramolecular Hydrogelators and Hydrogels: From Soft Matter to Molecular Biomaterials*, Chem. Rev. **2015**, 115, 13165–13307;
546. R. Dong, Y. Pang, Y. Su, X. Zhu, *Supramolecular hydrogels: synthesis, properties and their biomedical applications*, Biomater. Sci., 3, **2015**, 937–954;
547. X. Du, J. Zhai, X. Li, Y. Zhang, N. Li, X. Xie, *Hydrogel–Based Optical Ion Sensors: Principles and Challenges for Point–of–Care Testing and Environmental Monitoring*, ACS Sens. **2021**, 6, 1990–2001;
548. X. Sun, S. Agate, K.S. Salem, L. Lucia, L. Pal, *Hydrogel–Based Sensor Networks: Compositions, Properties, and Applications—A Review*, ACS Appl. Bio Mater. **2021**, 4, 1, 140–162;
549. L. Li, R. Sun, R. Zheng, Y. Huang, *Anions–responsive supramolecular gels: A review*, Mater. Des. 205, **2021**, 109759;
550. S. Panja, A. Panja, K. Ghosh, *Supramolecular gels in cyanide sensing: a review*, Mater. Chem. Front. **2021**, 5, 584–602;
551. S. Bernhard, M.W. Tibbitt, *Supramolecular engineering of hydrogels for drug delivery*, Adv. Drug Deliv. Rev. **2021**, 171, 240–256;
552. K. Vollmecke, R. Afroz, S. Bierbach, L.J. Brenker, S. Frucht, A. Glass, R, Giebelhaus, A. Hoppe, K. Kanemaru, M, Lazarek, L. Rabbe, L. Song, A.V. Suarez, S. Wu, M. Serpe, D. Kuckling, *Hydrogel–Based Biosensors*, Gels **2022**, 8, 768;
553. J.A. Sanchez–Fernandez, *Structural Strategies for Supramolecular Hydrogels and Their Applications*, Polym. **2023**, 15, 1365;
554. D. Tripathy, A.S. Gadtya, S. Moharana, *Supramolecular Gel, Its classification, preparation, properties, and applications: A review*, Polym.–Plast. Technol. Mater. **2023**, 62, 306–326;
555. L. Wang, E. Bakker, *A tunable detection range of ion–selective nano–optodes by controlling solvatochromic dye transducer lipophilicity*, Chem. Commun. **2019**, 55, 12539–12542;

556. K. Maki, R. Oishi, T. Mizuta, K. Sueyoshi, T. Endoa, H. Hisamoto, *Chloride ion–selective dye liquid nanoemulsion: improved sensor performance due to intermolecular interactions between dye and ionophore*, Analyst, **2022**, 147, 1529–1533;
557. S. Oka, K. Sueyoshi, T. Endo, H. Hisamoto, *Nanoemulsion–based silver ion–selective optode based on colorimetrically silver ion–responsive ionic liquid–based dye*, Anal. Sci. **2023**, 39, 1249–1256;
558. X. Xie, J. Zhai, E. Bakker, *pH Independent Nano–Optode Sensors Based on Exhaustive Ion–Selective Nanospheres*, Anal. Chem. **2014**, 86, 2853–2856;
559. J. Zhai, X. Xie, E. Bakker, *Ion–Selective Optode Nanospheres as Heterogeneous Indicator Reagents in Complexometric Titrations*, Anal. Chem. **2015**, 87, 2827–2831;
560. X. Xie, E. Bakker, *Determination of Effective Stability Constants of Ion–Carrier Complexes in Ion Selective Nanospheres with Charged Solvatochromic Dyes*, Anal. Chem. **2015**, 87, 11587–11591;
561. K. Kłucińska, E. Stelmach, P. Bartosińska, A. Kisiel, K. Maksymiuk, A. Michalska, *Critical assessment of polymeric nanostructures used as colorimetric ions probes*, Mater. Sci. Eng. C **2018**, 92, 69–76;
562. E. Stelmach, B. Kaczmarczyk, K. Maksymiuk, A. Michalska *Tailoring polythiophene cation–selective optodes for wide pH range sensing*, Talanta **2020**, 211, 120663;
563. R. Wang, X. Du, X. Ma, J. Zhaic, X. Xie, *Ionophore–based pH independent detection of ions utilizing aggregation–induced effects*, Analyst, **2020**,145, 3846–3850;
564. L. Deng, J. Zhai, X. Du,, X. Xie, *Ionophore–Based Ion–Selective Nanospheres Based on Monomer–Dimer Conversion in the Near–Infrared Region*, ACS Sens. **2021**, 6, 3, 1279–1285;
565. A. Konefał, P. Piątek, B. Paterczyk, K.Maksymiuk, A. Michalska, *Ionophore based optical sensors using hydrophilic polymer matrix – Ratiometric, pH independent ion–selective optodes*, Talanta **2023**, 253, 124038;
566. A. Konefał, P. Piątek, K. Maksymiuk, A. Michalska, *Looking into the ion–selective nanoptode bulk – Alternative mechanism of optical signal transduction for ratiometric ion–selective probes applicable in broad pH range*, Sens. Actuators B Chem. **2023**, 391, 134002;
567. A. Kisiel, K. Maksymiuk, A. Michalska, *Capsules as ion–selective optodes – Maximizing sensitivity of ion–selective optodes*, Sens. Actuators B Chem. **2018**, 273, 1730–1734;
568. A. Kisiel, D. Kałuża, B. Paterczyk, K. Maksymiuk, A. Michalska, Quantifying plasticizer leakage from ion–selective membranes – a nanosponge approach, Analyst, **2020**, 145, 2966–2974;
569. E. Stelmach, E. Nazaruk, K. Maksymiuk, A. Michalska, *Cubosome Based Ion–Selective Optodes–Toward Tunable Biocompatible Sensors*, Anal. Chem. **2021**, 93, 13106–13111;
570. X. Wang, C. Shen, C. Zhou, Y. Bu, X. Yan, *Methods, principles and applications of optical detection of metal ions*, Chem. Eng. J. **2021**, 417, 129125;
571. K.E. McCrackena, J.–Y. Yoon, *Recent approaches for optical smartphone sensing in resource–limited settings: a brief review*, Anal. Methods **2016**, 8, 6591–6601;
572. S. Di Nonno, R. Ulber, *Smartphone–based optical analysis systems*, Analyst **2021**, 146, 2749–2768;
573. R. Sivakumar, N.Y. Lee, *Recent progress in smartphone–based techniques for food safety and the detection of heavy metal ions in environmental water*, Chemosphere **2021**, 275, 130096;
574. L. Ciaccheri, B. Adinolfi, A.A. Mencaglia, A.G. Mignani, *Smartphone–Enabled Colorimetry*, Sensros **2023**, 23, 5559;
575. L.F. Capitán–Vallvey, N. López–Ruiz, A. Martínez–Olmos, M.M. Erenas, A.J. Palma, *Recent developments in computer vision–based analytical chemistry: A tutorial review*, Anal. Chim Acta **2015**, 899, 23–56;
576. D. Yusufu, A. Mills, *Spectrophotometric and Digital Colour Colourimetric (DCC) analysis of colour–based indicators*, Sens. Actuators B Chem. **2018**, 273, 1187–1194;
577. A.V. Kalinichev, N.V. Pokhvishcheva, M.A. Peshkova, *Novel color standards for digital color analysis of optochemical sensor arrays*, Talanta **2019**, 197, 638–644;
578. G.M. Fernandes, W.R. Silva, D.N. Barreto, R.S. Lamarca, P.C.F.L. Gomes, J.F. Petruci, A.D. Batista, *Novel approaches for colorimetric measurements in analytical chemistry – A review*, Anal. Chim. Acta **2020**, 1135, 187–203;
579. N.Y. Tiuftiakov, A.V. Kalinichev, N.V. Pokhvishcheva, M.A. Peshkova, *Digital color analysis for colorimetric signal processing: Towards an analytically justified choice of acquisition technique and color space*, Sens. Actuators B Chem. **2021**, 344, 130274;
580. Y. Fan, J. Li, Y. Guo, L. Xie, G. Zhang, *Digital image colorimetry on smartphone for chemical analysis: A review*, Measurement **2021**, 171, 108829;
581. G. Carvalho Oliveira, C.C.S. Machado, D.K. Inacio, J.F.D.S. Petruci, S.G. Silva, *RGB color sensor for colorimetric determinations: Evaluation and quantitative analysis of colored liquid samples*, Talanta 241, **2022**, 123244;
582. H. Xiao–Wei, Z. Xiao–Bo, S. Ji–Yong, L. Zhi–Hua, Z. Jie–Wen, *Colorimetric sensor arrays based on chemo–responsive dyes for food odor visualization*, Trends Food Sci. Technol. **2018**, 81, 90–107;
583. M. Rezazadeh, S. Seidi, M. Lid, S. Pedersen–Bjergaard, Y. Yamini, *The modern role of smartphones in analytical chemistry*, Trends Analyt. Chem. **2019**, 118, 548–555;
584. T. Alawsi, G. Proietti Mattia, Z. Al–Bawi, R. Beraldi, *Smartphone–based colorimetric sensor application for measuring biochemical material concentration*, Sens. Bio–Sens. Res. **2021**, 32, 100404;
585. O. Kap, V. Kılıç, J.G. Hardy, N. Horzum, *Smartphone–based colorimetric detection systems for glucose monitoring in the diagnosis and management of diabetes*, Analyst **2021**, 146, 2784–2806;
586. S. Krishnan, Z.Q. Syed, *Colorimetric Visual Sensors for Point–of–needs Testing*, Sens. Actuators Rep. **2022**, 4, 100078;
587. P. Yadav, L. Yadav, H. Laddha, M. Agarwal, R. Gupta, *Upsurgence of smartphone as an economical, portable, and consumer–friendly analytical device/interface platform for digital sensing of hazardous environmental ions*, Trends Enviro. Anal. Chem. **2022**, 36, e00177;
588. S. Soares, G.M. Fernandes, F.R.P. Rocha, *Smartphone–based digital images in analytical chemistry: Why, when, and how to use*, Trends Analyt. Chem. **2023**, 168, 117284;

589. K. Koren, S.E. Zieger, *Optode Based Chemical Imaging—Possibilities, Challenges, and New Avenues in Multidimensional Optical Sensing*, ACS Sens. **2021**, 6, 1671–1680;
590. S.E. Zieger, P.D. Jones, K. Koren, *Noise versus Resolution in Optical Chemical Imaging—How Reliable Are Our Measurements?*, ACS Omega **2022**, 7, 11829−11838;
591. J. Zhai, X. Xie, T. Cherubini, E. Bakker, *Ionophore–Based Titrimetric Detection of Alkali Metal Ions in Serum*, ACS Sens. **2017**, 2, 606–612;
592. A.V. Kalinichev, N.V. Pokhvishcheva, M.A. Peshkova, *Novel color standards for digital color analysis of optochemical sensor arrays*, Talanta **2019**, 197, 638–644;
593. Y. Soda, E. Bakker, *Colorimetric ratiometry with ion optodes for spatially resolved concentration analysis*, Anal. Chim. Acta **2021**, 1154, 338225;
594. N.G. Ghalehjoughi, R. Wang, S. Kelley, X. Wang, *Ultrasensitive Ionophore–Based Liquid Sensors for Colorimetric Ion Measurements in Blood*, Anal. Chem. **2023**, 95, 12557–12564;
595. Y. Soda, K.J. Robinson, T.J. Cherubini, E. Bakker, *Colorimetric absorbance mapping and quantitation on paper–based analytical devices*, Lab Chip **2020**, 20, 1441–1448;

II. ZAŁOŻENIA ROZPRAWY

Tytuł przedstawionej rozprawy doktorskiej: „Chromogeniczne pochodne azoli jako składniki warstw receptorowych czujników optycznych" opisuje najbardziej namacalny efekt badań zrealizowanych w ramach pracy doktorskiej, a przedstawionych szczegółowo w załączonych publikacjach **P1** – **P5** oraz kolejnych rozdziałach dysertacji – krótkich przewodnikach po odpowiednich publikacjach.

Celem prac prowadzonych w ramach realizacji pracy doktorskiej było:

1. otrzymanie z możliwie dużą wydajnością nowych związków, stanowiących potencjalne chromogeniczne receptory jonów o znaczeniu biologicznym/środowiskowym;
2. zbadanie natury oddziaływań receptor-jon metodami spektroskopowymi;
3. porównanie właściwości nowootrzymanych związków z właściwościami otrzymanych wcześniej w zespole makrocyklicznymi związkami bisazowymi zawierającymi w swojej strukturze resztę azolu;
4. analizę wpływu rodzaju azolu w strukturze związku na jego właściwości kompleksujące;
5. badanie wpływu otoczenia chemicznego na powinowactwo do jonów;
6. przygotowanie warstw receptorowych i określenie ich podstawowych parametrów, a także zaproponowanie ich potencjalnego zastosowania oraz porównanie z udokumentowanymi w literaturze rozwiązaniami.

III. MATERIAŁY I METODY BADAWCZE

III.A. ODCZYNNIKI CHEMICZNE DO SYNTEZY

Użytymi do syntezy substratami były: 1,4-dibromobutan (Sigma Aldrich), 1,5-dibromopentan (Sigma Aldrich), 1,10-dibromodekan (Sigma Aldrich), 2-nitrofenol (Sigma Aldrich), 2-amino-4-nitrofenol (Sigma Aldrich), pirol (Sigma Aldrich), imidazol (Sigma Aldrich), 4-metyloimidazol (Sigma Aldrich) oraz azotan(III) sodu (POCH). Innymi odczynnikami wykorzystanymi do przeprowadzenia syntez były: bezwodny węglan potasu (POCH), wodorotlenek potasu (POCH), wodzian hydrazyny roztwór 80% (Sigma Aldrich), kwas solny 35-38% (POCH). Przeprowadzając syntezę korzystałem z rozpuszczalników zakupionych w firmie POCH tj. dimetyloformamidu, metanolu oraz propan-2-olu.

Postęp reakcji śledziłem przy pomocy chromatografii cienkowarstwowej (TLC) stosując płytki aluminiowe pokryte żelem krzemionkowym 60 F_{254} (Merck). Natomiast produkty z mieszaniny reakcyjnej izolowałem stosując chromatografię kolumnową, gdzie fazą stacjonarną był żel krzemionkowy 60 (0,063-0,200 mm) (Merck), a fazą ruchomą rozpuszczalniki: dichlorometan (POCH), aceton (POCH) oraz ich mieszaniny.

III.B. IDENTYFIKACJA ZWIĄZKÓW

Identyfikację otrzymanych związków przeprowadziłem na podstawie analizy widm ^{1}H oraz ^{13}C NMR (deuterowane rozpuszczalniki: DMSO, chloroform, aceton) zarejestrowanych na spektrometrze Varian INOVA 500 (częstotliwość 500 MHz), znajdującym się w Laboratorium Magnetycznego Rezonansu Jądrowego, mieszczącym się na Wydziale Chemicznym Politechniki Gdańskiej. Widma w podczerwieni (film) zarejestrowałem przy użyciu spektrometru IS10 Thermo Spectronic, znajdującego się w Katedrze Chemii i Technologii Materiałów Funkcjonalnych Wydziału Chemicznego Politechniki Gdańskiej. Widma mas zarejestrowano na aparacie AutoSpec Premier Waters (EI) w Instytucie Chemii Organicznej PAN w Warszawie. Widma absorpcyjne w zakresie UV-Vis rejestrowałem wykorzystując spektrofotometr Unicam UV-300. Pomiary prowadzone były w kuwetach kwarcowych o dł. drogi optycznej 1 cm. Widma emisyjne zarejestrowałem przy użyciu spektrofluorymetru AMINCO-Bowman Series 2 (kuwety kwarcowe 1 cm, szerokość szczeliny wzbudzenia i emisji 16 nm).

III.C. BADANIE LIPOFILOWOŚCI

Lipofilowość związków określiłem wykorzystując metodę chromatograficzną [596, 597], stosując płytki szklane pokryte żelem krzemionkowym 60 RP-18 F_{254} (Merck) oraz układ metanol:woda 9:1 (v/v) jako fazę ruchomą. Natomiast jako wzorce użyłem plastyfikatory o znanej lipofilowości: adypinian bis(butylopentylu) (BBPA, ≥98,0%, Sigma Aldrich), ftalan dibutylu (DBP, ≥99.0% Sigma Aldrich), ftalan bis(2-etyloheksylu) (DOP, ≥99.5%, Sigma Aldrich), sebacynian bis(2-etyloheksylu) (DOS, ≥97.0%, Sigma Aldrich), eter 2-nitrofenylowo-oktylowy (NPOE, ≥99.0%, Sigma Aldric).

III.D. KOMPLEKSOWANIE JONÓW METALI W ROZTWORZE

W badaniach równowagi kompleksowania wykorzystywałem acetonitryl (LiChrosolv MERCK), DMSO (POCH), metanol (POCH), oraz ich mieszaniny z wodą, a także dichlorometan (POCH). We wszystkich eksperymentach w środowisku wodnym wykorzystywałem wodę dejonizowaną (o przewodności < 1 μS·cm-1, HydroLab Polska). Kompleksowanie kationów metali badałem wykorzystując odpowiednie sole: chlorany(VII) (Sigma Aldrich), azotany(V) (POCH) i chlorki (POCH); metali 1 i 2 grupy układu okresowego oraz metali ciężkich. Wartości stałych komlpeksowania (logK) wyznaczyłem za pomocą programu OPIUM [598] na podstawie danych z miareczkowań spektrofotometrycznych badanych roztworów. Natomiast stechiometrię kompleksów potwierdzałem wykorzystując metodę stosunku molowego oraz metodę Joba [599-601].

III.E. WŁAŚCIWOŚCI KWASOWO-ZASADOWE

Właściwości kwasowo-zasadowe badałem stosując kwas *p*-toluenosulfonowy (POCH) oraz wodorotlenek tetra-n-butyloamoniowy (Fluka), w przypadku rozpuszczalników organicznych, a także kwas solny (POCH) i wodorotlenek sodu (POCH), w roztworach wodnych. Również w tym wypadku, w celu wyznaczenia stałych równowagi korzystałem z programu OPIUM.

III.F. ROZTWORY SYMULOWANE

Składniki wykorzystane do otrzymania buforowanej fosforanem soli fizjologicznej (PBS) [602], symulowanego płynu ustrojowego (SBF) [603] oraz sztucznego moczu (AU) [604]: chlorek sodu (POCH), wodorowęglan sodu (POCH), węglan sodu (POCH), wodorofosforan sodu (POCH), diwodorofosforan sodu (POCH), siarczan sodu (POCH), chlorek potasu (POCH), wodorofosforan potasu (POCH), diwodorofosforan potasu (POCH), chlorek magnezu (POCH), siarczan magnezu (POCH), chlorek wapnia (POCH), chlorek amonu (POCH), tris(hydroksymetylo)aminometan (Fluka), cytrynian sodu (POCH), szczawian potasu (POCH), mocznik (POCH), kreatynina (Sigma Aldrich) oraz kwas moczowy (Sigma Aldrich).

III.G. ROZTWORY RZECZYWISTE

Próbki rzeczywiste stanowiły: wody technologiczne z sektora ciepłowniczego, wody pitne oraz wody wodociągowe z województwa pomorskiego i warmińsko-mazurskiego.

Roztwory wzorcowe wykorzystane w celu określenia możliwości zastosowania otrzymanych układów do oznaczania jonów w próbkach rzeczywistych: roztwór wzorcowy azotanu(V) ołowiu(II) w HNO_3 (1000 mg/L Pb, Merck), roztwór wzorcowy azotanu(V) miedzi(II) w HNO_3 (1000 mg/L Cu, Merck), roztwór wzorcowy azotanu(V) bizmutu(III) w HNO_3 (1000 mg/L Bi, Merck), certyfikowany roztwór kalibracyjny iCAP Q/Qnova (Analytika).

III.H. WARSTWY RECEPTOROWE

Warstwy receptorowe otrzymywałem poprzez fizyczne unieruchomienie chromojonoforów na powierzchni odpowiedniego podłoża, które stanowiły: pytki aluminiowe pokryte żelem krzemionkowy 60 (0,063-0,200 mm) (Merck), pytki aluminiowe pokryte tlenkiem glinu 60 (Merck), pytki aluminiowe pokryte celulozą (Merck), włókno szklane (Whatman GF/C, Schleicher & Schuell), poliamid-6 (adsorbent TLC, Macherey-Nagel), szkło porowate modyfikowane polistyrenem (M_w ~ 120000, 0,075-0,125 mm, Corning) (PG-PS), filtr celulozowy (nr 5, Whatman) oraz bawełniane patyczki kosmetyczne. Natomiast optody polimerowe otrzymałem wykorzystując: trioctan celulozy (Acros Organics/Sigma Aldrich), poli(chlorek winylu) (PVC, wysokocząsteczkowy, Sigma Aldrich), glikol trietylenowy (TEG, ≥99,0%, Merck), BBPA (≥98,0%, Sigma Aldrich), DBP (≥99.0%, Sigma Aldrich), DOP (≥99.5%, Sigma Aldrich), DOS (≥97.0%, Sigma Aldrich), NPOE (≥99.0%, Sigma Aldrich), tetrakis(p-chlorofenylo)boran potasu (KTClPB, ≥98.0%, Fluka), chloroform (POCH), dichlorometan (POCH) i tetrahydrofuran (THF, ≥99.5%, Sigma Aldrich).

III.I. ANALIZA SPEKTROFOTOMETRYCZNA W ZAKRESIE UV-VIS

W celu określenia zależności zmian sygnału analitycznego - absorbancji - od stężenia badanego analitu wykorzystywałem zależność, że różnica w wartości absorbancji ΔA odnosi się do wartości absorbancji tworzącego się kompleksu z badanym związkiem (A) oraz wartości absorbancji odpowiadającej ligandowi (A_0), przy długości fali odpowiadającej maksimum absorpcji tworzonego kompleksu.

Natomiast w przypadku badania warstw receptorowych o różnym składzie, wartości generowanego sygnału (ΔA) przez optody, obliczyłem stosując wzór:

$$\Delta A = \left(\frac{A_{\lambda_{\max X}}}{A_{\lambda_{max}}}\right) - \left(\frac{A_{\lambda_{\max X}}}{A_{\lambda_{max}}}\right)_0$$

gdzie $A_{\lambda max}$ to wartość absorbancji przy długości fali odpowiadającej maksimum absorpcji chromojonoforu w membranie, $A_{\lambda max\ X}$ to wartość absorbancji przy długości fali odpowiadającej maksimum absorpcji kompleksu chromojonoforu z badanym analitem w membranie, a indeks dolny *0* przypisany jest do wartości membrany przed kontaktem z roztworem analitu.

III.J. KOLORYMETRIA OBRAZU CYFROWEGO

Badanie kolorymetryczne roztworów związków/optod polegało na wykonaniu zdjęć roztworów/membran (przy użyciu smartfona) przed i po kontakcie z badanym analitem. Na początku zdjęcia wykonywałem w przygotowanym przeze mnie przenośnym „studiu fotograficznym", a następnie w zakupionym namiocie bezcieniowym 23 x 23 x 23 cm (PULUZ, Photography Light Box, Shenzhen Puluz Technology Limited), w celu zapewnienia powtarzalności zdjęć przy tych samych warunkach oświetlenia. Następnie zdjęcia kadrowałem do wielkości odpowiadającej objętości zajętej przez roztwór w kuwecie kwarcowej lub membrany zanurzonej w badanym roztworze. W kolejnym kroku zdjęcia poddawałem obróbce przy użyciu komercyjnie dostępnej aplikacji na urządzenia mobilne analizującej barwę Color Analysis lub bezpłatnego oprogramowania ImageJ [605-608].

W obu przypadkach generowana była wartość barwy w skali RGB (czerwona (R), zielona (G) oraz niebieska (B)), dla całego zdjęcia z uwzględnieniem ich procentowego udziału. Na podstawie otrzymanych wartości RGB wyliczyłem zależności barwne dla roztworów/optod przed (R_0, G_0, B_0) i po kontakcie z badanym analitem (R, G, B) w postaci:

- różnicy w barwie [609]:

$$\Delta R = |R_0 - R| \qquad \Delta G = |G_0 - G| \qquad \Delta B = |B_0 - B|$$

- stosunku barwy [610]:

R/G R/B G/R G/B B/R B/G

- zmiany barwy [611-614]:

$$\Delta E_{RGB} = \sqrt{(R_0 - R)^2 + (G_0 - G)^2 + (B_0 - B)^2}$$

- intensywności barwy [615]:

$$I_R = -log\left(\frac{R_0}{R}\right) \qquad I_G = -log\left(\frac{G_0}{G}\right) \qquad I_B = -log\left(\frac{B_0}{B}\right)$$

III.K. GRANICE WYKRYWALNOŚCI I OZNACZALNOŚCI

Granice wykrywalności (LOD) [616-619] obliczałem wykorzystując wyrażenie:

$$LOD = \frac{3\sigma}{k}$$

gdzie σ jest odchyleniem standardowym ślepej próby, a k jest nachyleniem funkcji liniowej A = f(c), lub w przypadku kiedy A = log(f(c)) równanie miało postać:

$$LOD = 10^{\frac{3\sigma - b}{k}}$$

gdzie b jest wartością odpowiadającą punktowi przecięcia równania linii prostej z osią y.

Natomiast granica oznaczalności (LOQ) [616-619] wyrażona była jako 3,3-krotność LOD.

III.L. WPŁYW JONÓW PRZESZKADZAJĄCYCH

Wpływ jonów przeszkadzających na odpowiedź spektrofotometryczną oraz kolorymetryczną wobec badanego analitu wyrażałem jako wartość bezwzględną odpowiedzi:

$$RR\% = \left|\frac{X - X_0}{X_0}\right| \times 100\%$$

gdzie X_0 to wartość absorbancji lub zależności barwy w obecności badanego analitu, a X to wartość absorbancji lub zależności barwy w obecności badanego analitu oraz jonu/ów przeszkadzającego/ych.

LITERATURA

596. O. Dinten, U.E. Spichiger, N. Chaniotakis, P. Gehrig, B. Rusterholz, W.E. Morf, W. Simon, *Lifetime of neutral–carrier–based liquid membranes in aqueous samples and blood and the lipophilicity of membrane components*, Anal. Chem. **1991**, 63, 596–603;
597. E. Luboch, M. Jeszke, M. Szarmach, N. Łukasik, *New bis(azobenzocrown)s with dodecylmethylmalonyl linkers as ionophores for sodium selective potentiometric sensors*, J. Incl. Phenom. Macrocycl. Chem. **2016**, 86, 323–335;
598. M. Kyvala, I. Lukes, *Program Package "OPIUM"*. Online: https://web.natur.cuni.cz/~kyvala/opium.html (dostęp na 22 Luty 2024);
599. P. Job, *Formation and Stability of Inorganic Complexes in Solution*, Ann. Chim. **1928**, 10. 113–203;
600. Z.D. Hill, P. MacCarthy, *Novel approach to Job's method: An undergraduate experiment*, J. Chem. Educ. **1986**, 63, 162–167;
601. J.S. Renny, L.L. Tomasevich, E.H. Tallmadge, D.B. Collum, *Method of Continuous Variations: Applications of Job Plots to the Study of Molecular Associations in Organometallic Chemistry*, Angew. Chem. Int. Ed. **2013**, 52, 11998–12013;
602. Cold Spring Harbor Laboratory Press, *Phosphate–buffered saline (PBS)*. Online: http://cshprotocols.cshlp.org/content/2006/1/pdb.rec8247 (dostęp na 22 Luty 2024);
603. T. Kokubo, H. Kushitani, S. Sakka, T. Kitsugi, T. Yamamuro, *Solutions able to reproduce in vivo surface–structure changes in bioactive glass–ceramic A–W*, J. Biomed. Mater. Res. **1990**, 24 721–734;
604. N. Sarigul, F. Korkmaz, I. Kurultak, *A New Artificial Urine Protocol to Better Imitate Human Urine*, Sci. Rep. **2019**, 9, 20159;
605. W.S. Rasband, ImageJ, U.S. National Institutes of Health, Bethesda, Maryland, USA, https://imagej.net/ij/, 1997–2024;
606. M.D. Abramoff, P.J. Magalhaes, S.J. Ram, *Image Processing with ImageJ*, Biophotonics Int. **2004**, 11, 36–42;
607. C.A.Schneider, W.S. Rasband, K.W. Eliceiri, *NIH Image to ImageJ: 25 years of image analysis*, Nat. Methods **2012**, 9, 671–675;
608. A.B. Schroeder, E.T.A. Dobson, C.T. Rueden, P. Tomancak, F. Jug, K.W. Eliceiri, *The ImageJ ecosystem: Open–source software for image visualization, processing, and analysis*, Protein Sci. **2021**, 30, 234–249;
609. M. Hong, B. Zeng, M. Li, X. Xu, G. Chen, *An ultrasensitive conformation–dependent colorimetric probe for the detection of mercury(II) using exonuclease III–assisted target recycling and gold nanoparticles*, Microchim. Acta **2018**, 185, 72;
610. G. Prabakaran, R. Vickram, K. Velmurugan, C.I.David, S.P.M. Paul, R.S. Kumar, A.I. Almansour, K. Perumal, A. Abiram, J. Prabhu, R. Nandhakumar, *A lead selective dimeric quinoline based fluorescent chemosensor and its applications in milk and honey samples, smartphone and bio–imaging*, Food Chem. **2022**, 395, 133617;
611. N.A. Gavrilenko, S.V. Muravyov, S.V. Silushkin, A,S. Spiridonova, *Polymethacrylate optodes: A potential for chemical digital color analysis*, Measurement **2014**, 51, 464–469;
612. S.V. Muravyov, A.S. Spiridonova, N.A. Gavrilenko, P.F. Baranov, L.I. Khudonogova, *A Digital Colorimetric Analyzer for Chemical Measurements on the Basis of Polymeric Optodes*, Instrum. Exp. Tech. **2016**, 59, 592–600;
613. S.V. Muravyov, N.A. Gavrilenko, N.V. Saranchina, P.F. Baranov, *Polymethacrylate Sensors for Rapid Digital Colorimetric Analysis of Toxicants in Natural and Anthropogenic Objects*, IEEE Sens. J. **2019**, 19, 4765–4772;
614. D. Kim, S.J. Kim, H.–T. Ha, S. Kim, *Smartphone–based image analysis coupled to paper–based colorimetric devices*, Curr. Appl. Phys. **2020**, 20, 1013–1018;
615. H. James, K.C. Honeychurch, *Digital Image Colorimetry Smartphone Determination of Acetaminophen*, J. Chem. Educ. **2024**, 101, 187–196;
616. L.A. Currie, *Nomenclature in evaluation of analytical methods including detection and quantification capabilities1: (IUPAC Recommendations 1995)*, Anal. Chim. Acta **1999**, 391, 105–126;
617. L.A. Currie, Detection and quantification limits: origins and historical overview, Anal. Chim. Acta **1999**, 391, 127–134;
618. A. Shrivastava, *Methods for the determination of limit of detection and limit of quantitation of the analytical methods*, Chron. Young Sci. **2011**, 2, 21–25;
619. T. Little, *Method Validation Essentials, Limit of Blank, Limit of Detection, and Limit of Quantitation*, BioPharm Int. **2015**, 28, 48–51;

IV. KRÓTKI PRZEWODNIK PO CYKLU PUBLIKACJI

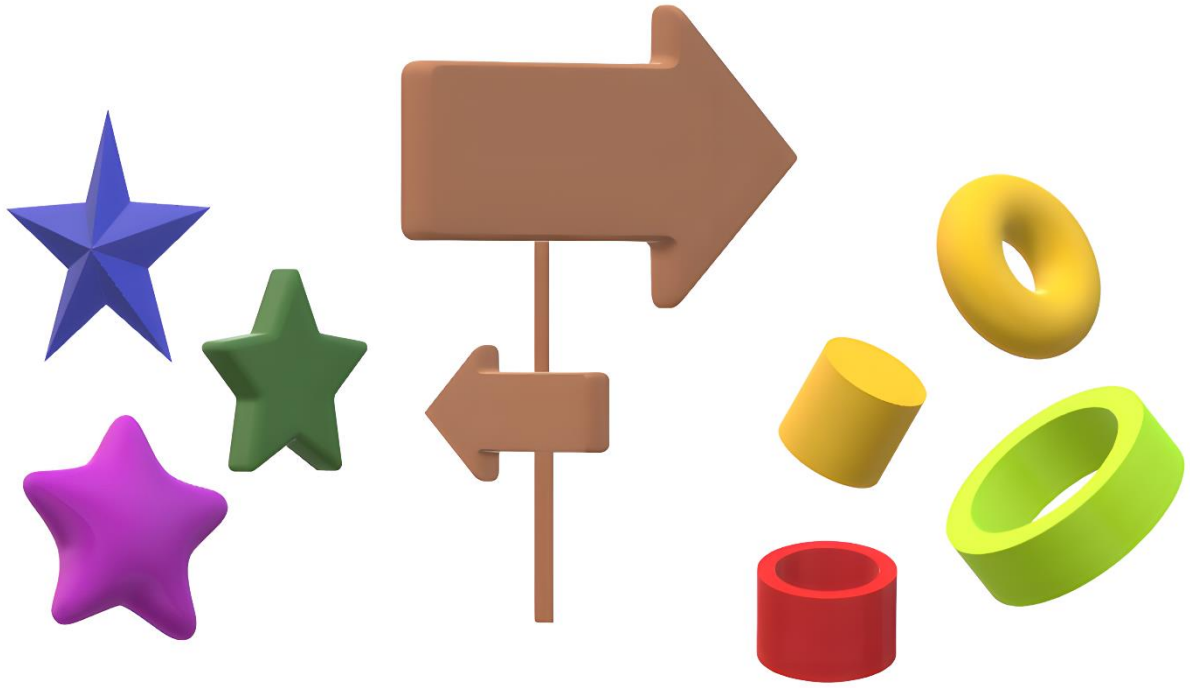

IV.P1 – NOWE DIAZOKORONY Z RESZTĄ PIROLU JAKO KOLORYMETRYCZNE CZUJNIKI OŁOWIU(II) (NOVEL DIAZOCROWNS WITH PYRROLE RESIDUE AS LEAD(II) COLORIMETRIC PROBES)

W pracy przedstawiono syntezę nowych makrocyklicznych związków bisazowych (**1** i **2**) z resztą pirolu, które stanowią analogi tlenowych związków **3** i **4** otrzymanych wcześniej w zespole (rys. IV.1) [214, 219].

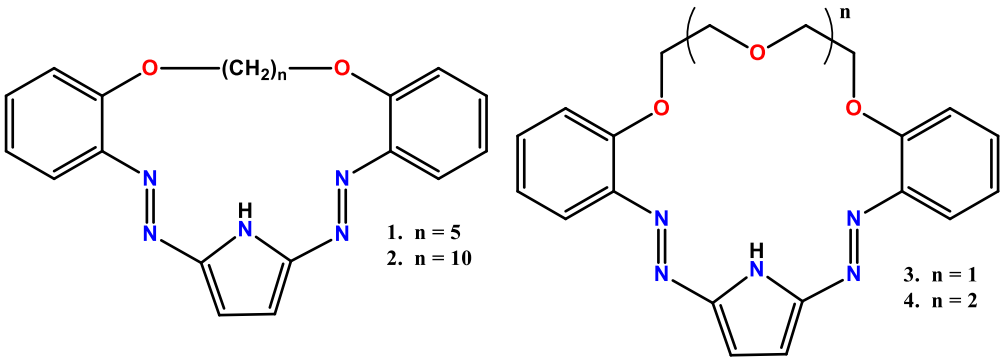

Rys. IV.1. Makrocykliczne pochodne pirolu: **1**, **2** – nowootrzymane związki z łańcuchem węglowodorowym; **3**, **4** – związki z łańcuchem oligoeterowym, otrzymane wcześniej w zespole [214, 219].

Nowe 18- oraz 23-członowe makrocykliczne związki **1** i **2** otrzymałem z zadowalającą wydajnością na poziomie 25 – 30%, w reakcji sprzęgania soli bisdiazoniowych z pirolem bazując na wcześniej opracowanych procedurach syntetycznych [214, 219, 220, 620, 621]. Reakcję przeprowadziłem przy zastosowaniu techniki wysokich rozcieńczeń (ang. high dilution) [622-624], która pozwoliła na otrzymanie związków makrocyklicznych, których wydajności mieszczą się w granicach typowych wydajności dla tej grupy związków (19 – 42%).

Pochodne **1** oraz **2** zostały otrzymane w celu zbadania wpływu zmiany struktury chromojonoforu, polegającej na zastąpieniu atomów tlenu w łańcuchu polieterowym grupami metylenowymi, na ich właściwości kompleksujące.

W celu charakteryzacji chromojonoforów dodatkowo wyznaczyłem wartości lipofilowości ($\log P_{TLC}$) dla badanych makrocykli **1** – **4**, wykorzystując metodę chromatografii cienkowarstwowej w układzie odwróconych faz, aby określić wpływ tego parametru na oddziaływanie z podłożem (matrycą polimerową), na którym chromojonofory będą unieruchamiane w warstwach receptorowych czujników optycznych. Zgodnie z postawioną hipotezą badawczą otrzymałem wyższe wartości $\log P_{TLC}$ (rys. IV.2) dla związków makrocyklicznych **1** i **2** zawierających łańcuch węglowodorowy niż dla ich oligoeterowych analogów **3** i **4**.

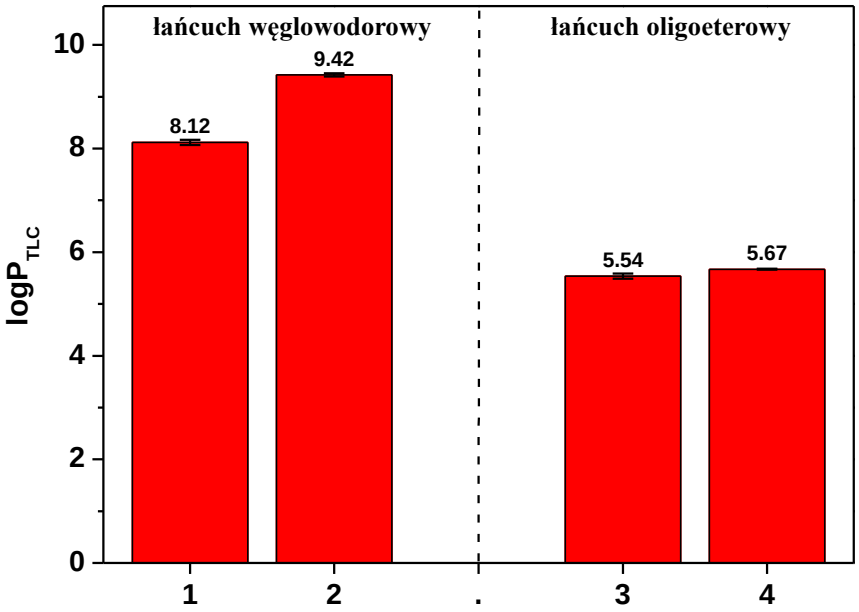

Rys. IV.2. Zestawienie wartości lipofilowości $logP_{TLC}$ związków **1** – **4**.

W celu określenia natury oddziaływania związków **1** – **4** z jonami w roztworze przeprowadziłem badania spektroskopowe (NMR, MS). Wykazałem, że nowootrzymane związki **1** i **2** tworzą kompleksy z jonami metali ciężkich i wykazują się większą selektywnością w stosunku do jonów ołowiu(II) w porównaniu do związków **3** i **4**. Można to wytłumaczyć mniejszą liczbą twardych centrów koordynacji, atomów tlenu, co wpływa na preferencyjne kompleksowanie miękkich jonów metali ciężkich. Wykazałem selektywność odpowiedzi barwnej i spektrofotometrycznej badanych związków na obecność jonów ołowiu(II) w roztworze rozpuszczalnika organicznego (acetonitryl) oraz mieszaninie tego rozpuszczalnika z wodą.

Wykorzystując spektrofotometrię UV-Vis określiłem stechiometrię kompleksów badanych związków z jonami ołowiu(II), wykazując tworzenie się w warunkach pomiaru kompleksu typu podwójnej kanapki (ang. triple-decker sandwich) [625-628] dla tej grupy związków (ligand:kation, 3:2). Tworzenie tego typu kompleksów potwierdziły także eksperymenty przeprowadzone z wykorzystaniem spektrometrii mas oraz spektroskopii protonowego rezonansu jądrowego. Na rysunku IV.3 przedstawiłem strukturę kompleksu typu podwójnej kanapki związku **3** z jonami ołowiu(II).

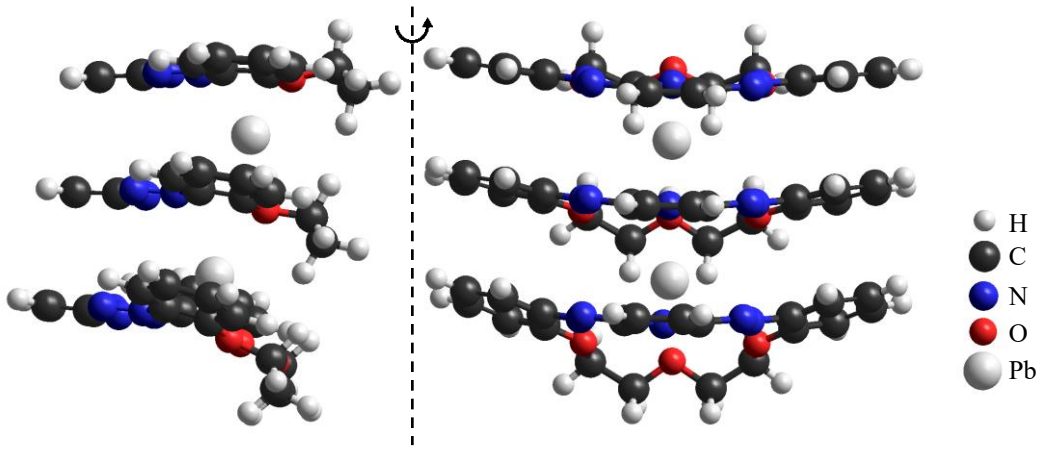

Rys. IV.3. Proponowana struktura kompleksu triple-decker sandwich związku **3** z jonami ołowiu(II) wygenerowana w programie HyperChem [629].

Wyznaczyłem wartości stałych trwałości kompleksów (logK) nowootrzymanych związków makrocyklicznych **1** oraz **2** z jonami ołowiu(II) i porównałem te wartości z wartościami oligoeterowych analogów **3** oraz **4** (rys. IV.4). Porównując wartości logK dla 18-członowych związków makrocyklicznych **1** i **3** można zauważyć, że jony ołowiu(II) są silniej wiązane przez makrocykl **1** (logK 19.22±0.05) z łańcuchem węglowodorowym niż przez oligoeterową pochodną **3** (logK 18.10±0.01). Natomiast 21-członowy związek **4** wiąże ołów(II) silniej (logK 21,0±0,09) niż związek **2** o 23-członowym pierścieniu (logK 18,37±0,01). Wynika to prawdopodobnie z faktu, że wbudowanie długiego, elastycznego łańcucha węglowodorowego może wpływać na wielkość wnęki makrocyklu **2** i czynić ją bardziej porównywalną do wnęki 18-członowych koron **1** i **3**.

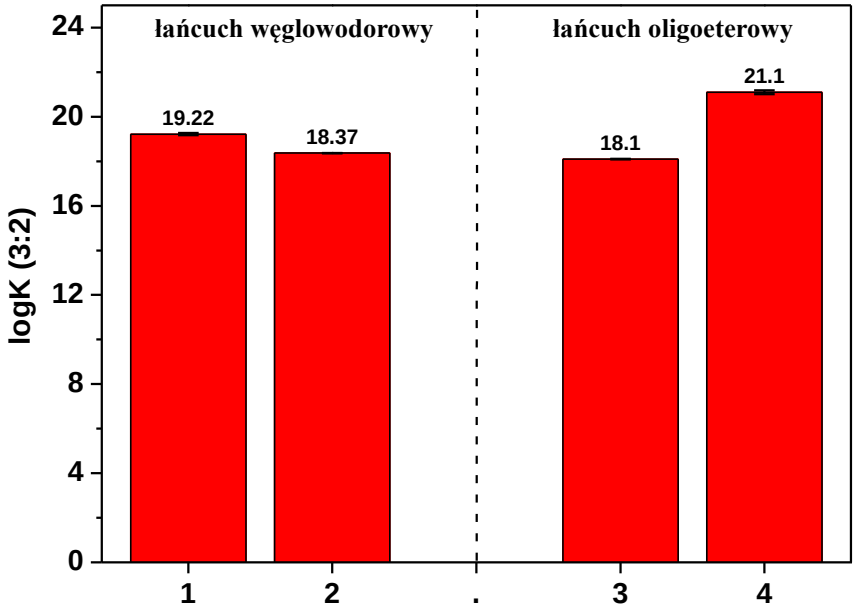

Rys. IV.4. Porównanie wartości stałych trwałości kompleksów typu triple-decker sandwich tworzonych przez makrocykliczne pochodne **1** – **4** z jonami ołowiu(II) [219].

Makrocykliczne pochodne **1** oraz **2** przetestowałem jako chromojonofory w warstwach receptorowych czujników optycznych unieruchamiając je na powierzchni włókna szklanego, w celu zastosowania jako wskaźników w szybkich testach jakościowych na jony metali ciężkich. Otrzymałem także warstwy receptorowe na bazie PCV do wykrywania jonów ołowiu(II). Uzyskane, w ramach tych rozpoznawczych prac, wyniki były na tyle obiecujące, że skierowały moje badania na wykorzystanie diazokoron **1** – **4** jako potencjalnych chromojonoforów w optodach czułych na jony ołowiu(II), czego efektem jest następna publikacja (**P2**).

IV.P2 – DIAZOKORONY Z RESZTĄ PIROLU: SELEKTYWNE CHOMOJONOFORY DO OPTYCZNEGO WYKRYWANIA OŁOWIU(II) (PYRROLE BEARING DIAZOCROWNS: SELECTIVE CHROMOIONOPHORES FOR LEAD(II) OPTICAL SENSING)

Rezultatem kontynuowanych badań nad makrocyklicznymi związkami bisazowymi jest publikacja **P2** „Diazokorony z resztą pirolu: selektywne chromojonofory do optycznego wykrywania ołowiu(II)". Celem dalszych, bardziej szczegółowych, badań nad tą grupą związków było: określenie możliwości ich zastosowania w warstwach receptorowych czujników optycznych; zaproponowanie najbardziej obiecującego składu warstwy receptorowej; określenie możliwości wykrywania oraz oznaczania analitów przy użyciu otrzymanych optod, w próbkach modelowych i rzeczywistych; a także zaproponowanie zależności właściwości kompleksujących od struktury związków oraz otoczenia chemicznego (roztwór/unieruchomienie w matrycy polimerowej).

Warstwy receptorowe czujników optycznych z wykorzystaniem chromojonoforów **1** – **4** (rys. IV.1) oraz CTA (wybrany także ze względu na właściwości mechaniczne membran), jako matrycy polimerowej, zostały zaproponowane na podstawie szeregu szczegółowych badań, które miały na celu dobranie najkorzystniejszego składu membrany pod względem generowanego sygnału, czasu odpowiedzi oraz zakresu liniowej odpowiedzi. W tym celu sprawdziłem wpływ: rodzaju plastyfikatora jak i jego ilość; rodzaju rozpuszczalnika, w którym rozpuszczane były składniki warstwy receptorowej; ilości oraz rodzaju chromojonoforów; a także dodatku soli lipofilowej. Na tej podstawie dobrałem skład membrany, dla której wyznaczyłem parametry tj. czas odpowiedzi, możliwość regeneracji, wpływ jonów przeszkadzających, sposób oraz czas przechowywania, zakres liniowej odpowiedzi.

W tabeli IV.1 zestawiłem: wartości stałych trwałości (log K) kompleksów (triple-decker) makrocyklicznych pochodnych **1** – **4** z jonami ołowiu (II), wartości logarytmów ze współczynników podziału ($\log P_{TLC}$) oraz zakresy liniowej odpowiedzi spektrofotometrycznej oraz kolorymetrycznej na obecność jonów ołowiu(II) optod (zależność od logarytmu ze stężenia jonów ołowiu(II)). Wartości logK dla związków **3** oraz **4** oraz zakres liniowej odpowiedzi EJS zawierającej związek **4** jako jonofor zostały zaczerpnięte z literatury [219].

Tabela. IV.1. Zestawienie wartości logK, $logP_{TLC}$ oraz zakresów liniowej odpowiedzi [219].

	logK	$logP_{TLC}$	Zakres liniowej odpowiedzi EJS	Zakres liniowej odpowiedzi optody	Zakres liniowej odpowiedzi optody (ΔE_{RGB})
1	19,22±0,05	8,12±0,05	-	-	-
2	18,37±0,01	9,42±0,03	-	$7{,}69\times10^{-5} – 1{,}83\times10^{-3}$	$7{,}69\times10^{-5} – 1{,}83\times10^{-3}$
3	18,10±0,01*	5,54±0,05	-	$8{,}05\times10^{-8} – 2{,}24\times10^{-5}$ c $7{,}86\times10^{-6} – 3{,}83\times10^{-4}$	$7{,}79\times10^{-7} – 2{,}07\times10^{-4}$
4	21,10±0,09*	5,67±0,01	$1{,}00\times10^{-6} – 1{,}58\times10^{-2}$ a * $1{,}00\times10^{-5} – 2{,}51\times10^{-3}$ b *	$2{,}02\times10^{-6} – 2{,}02\times10^{-4}$	$5{,}05\times10^{-5} – 5{,}05\times10^{-3}$

a – plastyfikator NPOE; b – plastyfikator BBPA; c – zależność ΔA od stężenia jonów ołowiu(II); * - dane literaturowe [219]

Jak można zauważyć wartość logK dla 21-członowego związku **4** jest największa, co sugeruje, że dla tego związku tworzy się najbardziej trwały kompleks z jonami ołowiu(II), w porównaniu z pozostałymi badanymi chromojonoforami. Związek ten został także wcześniej przetestowany w zespole jako jonofor w membranowych elektrodach jonoselektywnych [219]. Zakres prostoliniowej odpowiedzi EJS zawierającej w membranie (PCV) związek **4** jest większy niż dla optody, której membrana (CTA) zawierała **4**, co sugeruje lepsze zastosowanie związku **4** w EJS niż optodzie. Natomiast porównując zakres liniowej odpowiedzi optody **3** z innymi zbadanymi optodami oraz EJS **4**, można stwierdzić, że pomimo węższego zakresu liniowej odpowiedzi możliwe jest oznaczanie niższych stężeń jonów ołowiu(II). Ponadto zakres liniowej odpowiedzi spektrofotometrycznej dla optod pokrywa się z liniowym zakresem odpowiedzi uzyskanym dla analizy kolorymetrycznej obrazu cyfrowego (ΔE_{RGB} jako sygnał analityczny).

Badając azowe związki makrocykliczne **1** – **4** o różnej wielkości pierścienia, różniące się rodzajem łącznika (łańcuch węglowodorowy lub oligoeterowy) wykazałem, że najlepsze właściwości, biorąc pod uwagę liniowy zakres odpowiedzi i granicę wykrywalności, wykazuje materiał czujnika, w którym w matrycy na bazie CTA zastosowano 18-członową pochodną zawierającą ugrupowanie oligoeterowe – związek **3**. Jak wykazano we wcześniejszych badaniach związek ten był nieefektywnym jonoforem w membranowych elektrodach jonoselektywnych opartych na membranie z PCV, w której krystalizował [219]. Bardziej hydrofilowa matryca, jaką stanowi trioctan celulozy okazała się być korzystnym rozwiązaniem, aby wykorzystać potencjał selektywności w stosunku do jonów ołowiu(II) dla omawianego chromojonoforu. Jak wykazałem, pochodne **1** oraz **2** o większej lipofilowości w tej matrycy sprawdzają się znacznie gorzej lub nie sprawdzają się w ogóle (związek **1** o tej samej wielkości makropierścienia co pochodna **3** krystalizuje w membranie z trioctanu celulozy – rys. IV.5).

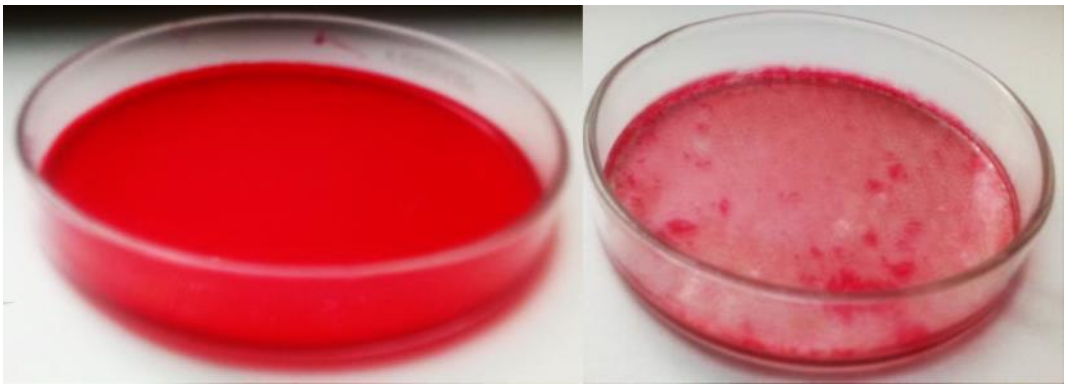

Rys. IV.5. Po lewej zdjęcie optody na bazie CTA ze związkiem **3**, a po prawej zdjęcie optody z wykrystalizowanym w membranie związkiem **1**

Otrzymana optoda może być potencjalnie zastosowana do wykrywania i oznaczania ołowiu(II) w wodnych próbkach środowiskowych na poziomie ppb, jako szybki test jakościowy dzięki wyraźnej zmianie barwy materiału z czerwonego na niebieski w obecności jonów ołowiu(II) (rys. IV.6). Może być także zastosowana do ilościowego oznaczania ołowiu(II) z zastosowaniem detekcji spektrofotometrycznej jak i z wykorzystaniem cyfrowej analizy barwy za pomocą urządzeń mobilnych.

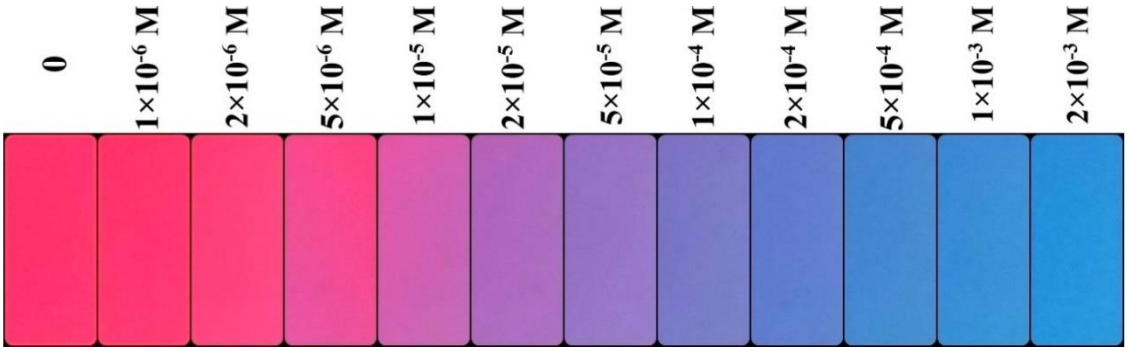

Rys. IV.6. Zmiana barwy optody ze związkiem **3** w obecności jonów ołowiu(II).

Badania, które przeprowadziłem stosując makrocykliczne pochodne bisazowe z resztą pirolu, jako składniki warstw receptorowych czujników optycznych, do tej pory nie były prowadzone i stanowią istotny element nowości zaprezentowany w niniejszej pracy doktorskiej.

IV.P3 – PROSTY KOLORYMETRYCZNY CZUJNIK MIEDZI(II): CHARAKTERYSTYKA SPEKTRALNA ORAZ MOŻLIWE ZASTOSOWANIA (SIMPLE COLORIMETRIC COPPER(II) SENSOR – SPECTRAL CHARACTERIZATION AND POSSIBLE APPLICATIONS)

Następna publikacja powstała w wyniku prac nad otrzymaniem nowych makrocyklicznych związków z resztą pirolu, zawierających dodatkowo grupy nitrowe w pierścieniach benzenowych – co miało stanowić istotny element nowości w tej grupie związków. Jednakże w wyniku wielokrotnie przeprowadzonych reakcji sprzęgania soli diazoniowej 2-amino-4-nitrofenolu z pirolem, nie udało mi się rozdzielić z mieszaniny reakcyjnej dipodstawionego pirolu [630], który w następnym etapie mógłby stanowić substrat w reakcji makrocyklizacji na drodze syntezy Williamsona. Otrzymałem jednak z zadowalającą wydajnością (~73 %) związek acykliczny **5** (rys. IV.7).

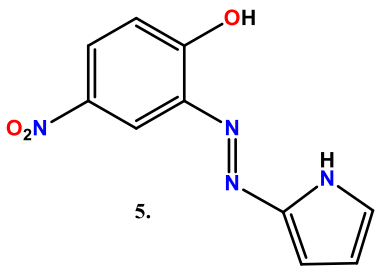

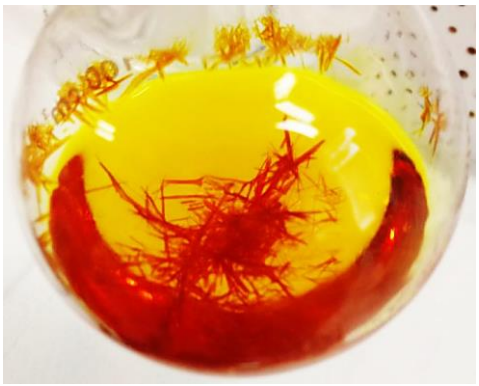

Rys. IV.7. Wzór strukturalny związku **5** (2-[(2-hydroksy-5-nitrofenylo)diazenylo]pirolu) oraz zdjęcie w trakcie jego krystalizacji z dichlorometanu.

W literaturze można znaleźć prace na temat zastosowania heteroaromatycznych acyklicznych związków hydroksyazowych jako chromojonoforów (rys. IV.8) [631-639].

Otrzymana pochodna strukturalnie wydała się na tyle interesująca, że postanowiłem zbadać jej właściwości kompleksujące i określić możliwości zastosowania tego związku w warstwach receptorowych czujników optycznych. Do tej pory w zespole acykliczne chromogeniczne związki azowe nie były badane pod tym kątem.

Pierwsze prace skupiały się na zbadaniu natury oddziaływań receptor-jon metodami spektroskopowymi (UV-Vis, NMR) w rozpuszczalnikach organicznych oraz ich mieszaninach z wodą, w celu wyznaczenia stechiometrii tworzących się kompleksów oraz wartości stałych trwałości ich kompleksów w zależności od otoczenia chemicznego.

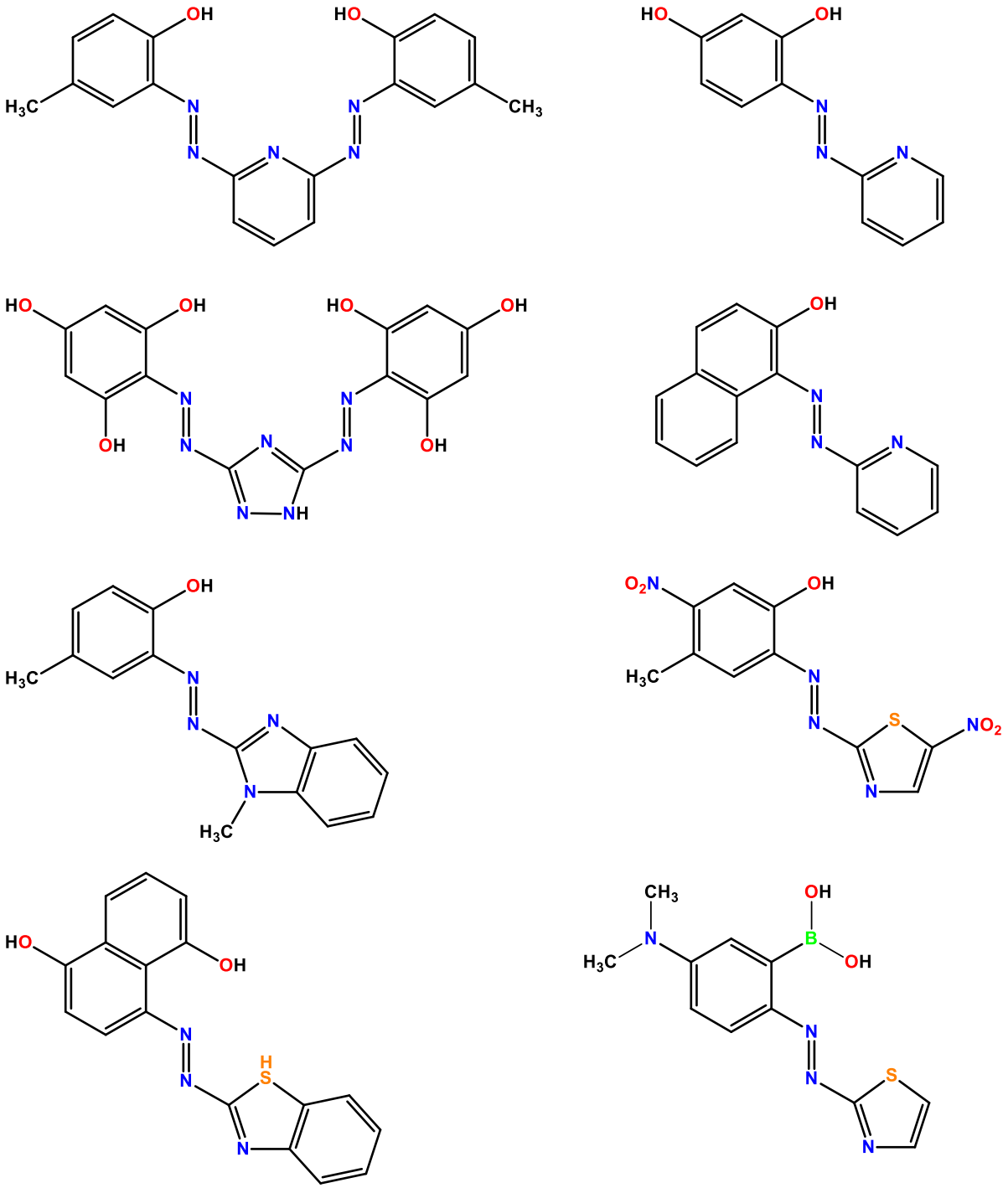

Rys. IV.8. Przykłady heteroaromatycznych acyklicznych związków hydroksyazowych [631-639].

Wstępne badania procesu kompleksowania jonów wykazały, że związek **5**, o względnie prostej budowie, selektywnie tworzy kompleksy z jonami miedzi(II), czemu towarzyszy niezwykle charakterystyczna zamiana barwy jego roztworów także w zawierających nawet 90% wody jako rozpuszczalnik z żółtej na purpurową (rys. IV.9).

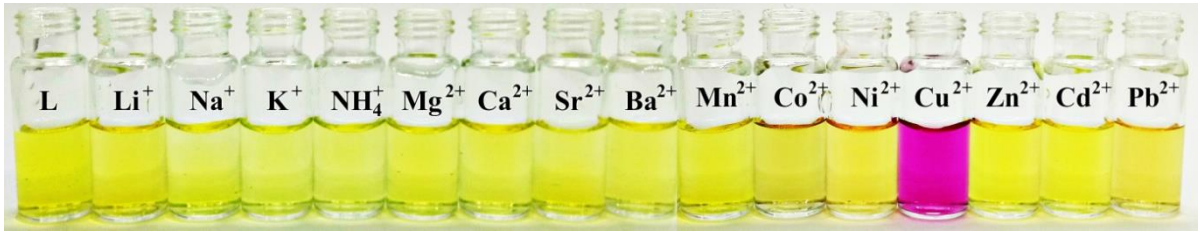

Rys. IV.9. Zmiana barwy roztworu związku **5** w mieszaninie woda:DMSO (9:1, v/v) w obecności chlorków metali.

Wykazałem, że w warunkach miareczkowania spektrofotometrycznego prowadzonego w metanolu oraz dimetylosulfotlenku związek **5** tworzy kompleksy z jonami miedzi(II) o stechiometrii 1:1 o wartościach stałych trwałości (logK) odpowiednio 5,21±0,02 oraz 5,42±0,06. Zbadałem także wpływ obecności wody w mieszaninie rozpuszczalników na siłę wiązania jonów miedzi(II), a także efekt przeciwjonu na tworzenie kompleksów wykazując, że kompleksy z chlorkiem miedzi(II) mają wyższe wartości stałych trwałości niż w przypadku gdy stosowany jest chloran(VII) miedzi(II). Jest to korzystne jeśli weźmie się pod uwagę rozpowszechnienie chlorków w przyrodzie, a rozważa się zastosowanie danego układu do celów analitycznych. Wykazałem także selektywność chromojonoforu **5** na jony miedzi(II), w stosunku do innych jonów metali, również w złożonych matrycach modelowych takich jak symulowany płyn ustrojowy (SBF) czy sztuczny mocz (AU).

Poza badaniami w roztworze przeprowadziłem szereg prób unieruchomienia acyklicznej chromogenicznej pochodnej **5** na różnych podłożach, w celu określenia zastosowania tego związku jako składnika kolorymetrycznych warstw jonoselektywnych. Były to m.in. eksperymenty, w których unieruchomiłem chromojonofor poprzez adsorpcję na włóknie szklanym, podłożu papierowym oraz bawełnianych patyczkach kosmetycznych (rys. IV.10). Również w takich warunkach obserwowałem selektywną charakterystyczną zmianę barwy z żółtej na purpurową. Wykazałem, że tak otrzymane narzędzia analityczne mogą potencjalnie służyć do oznaczania półilościowego miedzi(II) w roztworach wodnych.

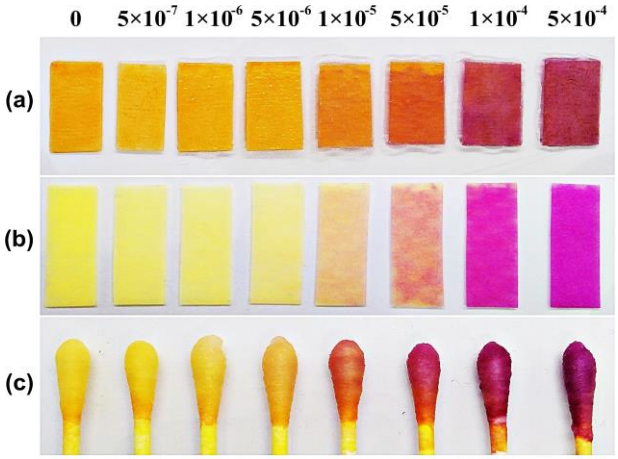

Rys. IV.10. Zmiana barwy w obecności roztworów zawierających jony miedzi(II): (a) filtru celulozowego; (b) włókna szklanego; (c) bawełnianych patyczków kosmetycznych; na których został fizycznie unieruchomiony związek **5**.

Ponadto otrzymałem warstwy receptorowe ze związkiem **5** na bazie CTA, jednak ze względu na bardziej hydrofilowy charakter niż związki makrocykliczne **1** – **4**, ulega on stopniowemu wymyciu z membrany. Jednak poprzez zmniejszenie ilości plastyfikatora oraz zwiększenie ilości soli lipofilowej, procent wymycia związku z warstwy receptorowej zmalał na tyle, że możliwe było 10-krotne przetestowanie zastosowania jednej optody do wykrywania oraz oznaczania miedzi(II) w próbkach wodnych na poziomie stężeń 10^{-8} mol/dm^3.

IV.P4 – CHROMOGENICZNE MAKROCYKLICZNE AZOZWIĄZKI Z RESZTĄ IMIDAZOLU: STRUKTURA A KOLORYMETRYCZNA DETEKCJA MIEDZI(II) I OŁOWIU(II) (CHROMOGENIC AZOMACROCYCLES WITH IMIDAZOLE RESIDUE: STRUCTURE VS. PROPERTIES)

Czwarta publikacja miała na celu zbadanie wpływu rodzaju reszty heterocyklicznej w makropierścieniu na właściwości kompleksujące pochodnych makrocyklicznych będących przedmiotem rozprawy. W tym celu otrzymałem związki **6** – **9** (rys IV.11) zawierające w swojej strukturze imidazol lub 4-metyloimidazol (analogi otrzymanych wcześniej pochodnych zawierających resztę pirolu) oraz łańcuchy węglowodorowe, różniące się między sobą jedną grupą metylenową. Zastosowałem technikę wysokiego rozcieńczenia otrzymując związki makrocykliczne z wydajnościami 24 – 40%, co jest wydajnością niższą niż opisano dla oligoeterowych analogów zawierających w swojej strukturze imidazol i porównywalną dla makrocykli z 4-metyloimidazolem [214, 220].

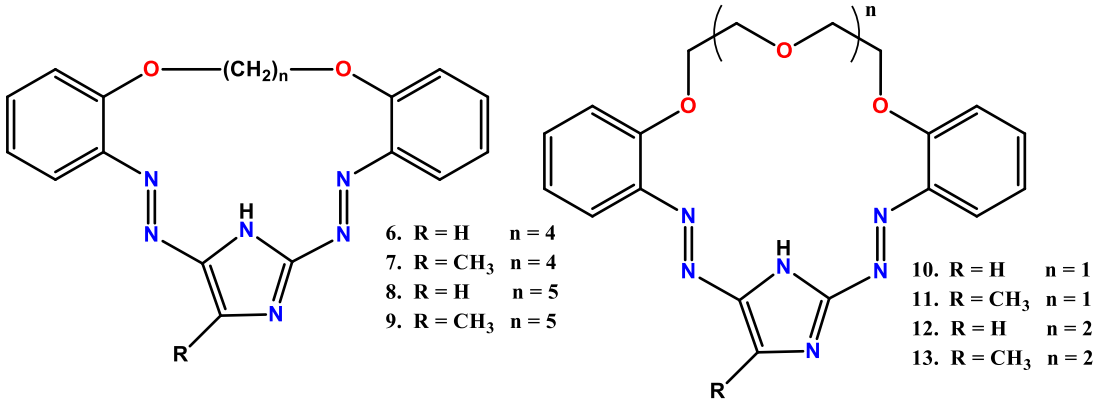

Rys. IV.11. Wzory nowych związków makrocyklicznych **6** – **9** zawierających węglowodorowy łańcuch oraz makrocykli **10** – **13** z oligoetoerowym łańcuch w strukturze [214, 220].

Związki **6 - 9** z resztą imidazolu/4-metyloimidazolu są analogami badanych wcześniej makrocyklicznych pochodnych **1** i **2** (rys. IV.1) zawierających resztę pirolu. Wykazują także podobieństwo strukturalne do makrocyklicznych pochodnych **10** – **13** zawierających łańcuch oligoeterowy (rys. IV.11) [214, 220]. Dla kilku z tych pochodnych przeprowadzono badania dotyczące kompleksowania jonów w roztworze oraz przetestowano je jako jonofory w membranowych (PVC) elektrodach jonoselektywnych czułych na jony ołowiu(II). Czujniki te charakteryzowały się jednak bardzo krótkimi czasami życia oraz wąskim zakresem liniowej odpowiedzi, a także niektóre z jonoforów wymywały się z membrany. Było to m.in. jednym z powodów otrzymania bardziej lipofilowych pochodnych w trakcie realizacji niniejszej pracy doktorskiej.

Mając na celu ogólną charakterystykę makrocyklicznych pochodnych bisazowych zawierających resztę azolu, dla nowootrzymanych związków **6** – **9** oraz ich oligoeterowych analogów przeprowadziłem eksperymenty, w których wyznaczyłem wartości współczynnika podziału $logP_{TLC}$ (analogicznie jak dla pirolowych pochodnych, opisanych wcześniej). Wykazałem, że pochodne zawierające łańcuch węglowodorowy są bardziej lipofilowe niż ich tlenowe analogi – rys. IV.12; co potwierdza początkowe założenia.

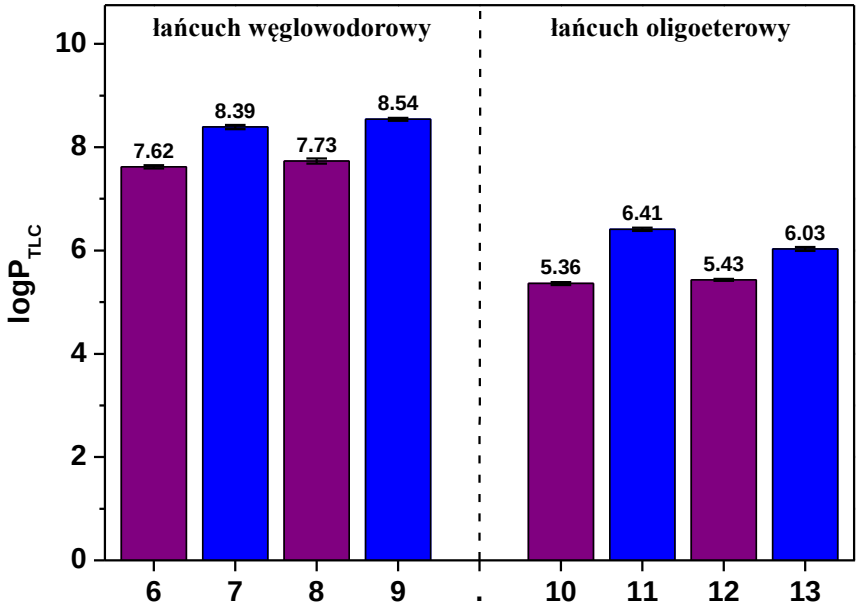

Rys. IV.12. Zestawienie wartości lipofilowości $logP_{TLC}$ makrocykli **6** – **9** i **10** – **13** (fioletowy – pochodne z resztą imidazolu; niebieski – pochodne z resztą 4-metyloimidazolu).

Badałem zdolność otrzymanych pochodnych do kompleksowania jonów metali w roztworze stwierdzając, że pochodne te cechują się większą selektywnością w stosunku do jonów metali ciężkich niż ich oligoeterowe analogi **10** – **13**. W warunkach miareczkowania spektrofotometrycznego w acetonitrylu tworzą kompleksy jedynie z jonami miedzi(II) i ołowiu(II). Co również jest zgodne z założeniami, czyli zmniejszeniem liczby atomów tlenu stanowiących twarde centra koordynacji. Przeprowadzone badania wykazały, że makrocykliczne związki bisazowe z resztą imidazolu oraz 4-metyloimidazolu analogicznie jak ich pirolowe analogi tworzą w acetonitrylu kompleksy z jonami ołowiu(II) o stechiometrii 3:2. Tworzenie kompleksów typu triple-decker wykazałem także w mieszaninie acetonitryl: woda (9:1). Przy czym 10% procentowy dodatek wody wpłynął na obniżenie wartości trwałości kompleksów logK z jonami ołowiu(II) (rys. IV.13), co również potwierdza istotny wpływ otoczenia na właściwości kompleksujące związków koronowych [640].

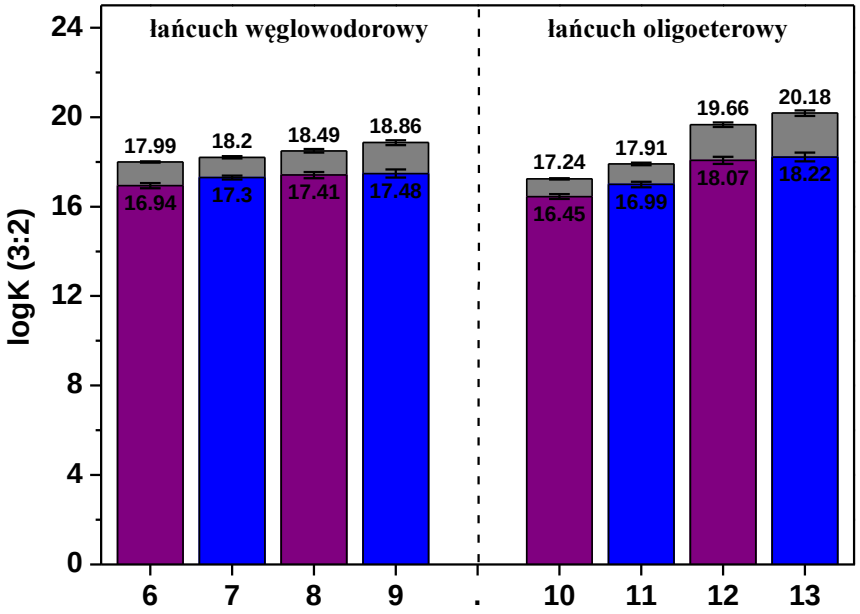

Rys. IV.13. Porównanie wartości stałych trwałości kompleksów typu triple-decker sandwich tworzonych przez makrocykliczne pochodne **6** – **9** i **10** – **13** z jonami ołowiu(II), w roztworze ACN oraz mieszaninie ACN:woda (9:1, v/v) (fioletowy – pochodne z resztą imidazolu; niebieski – pochodne z resztą 4-metyloimidazolu).

Poszukując możliwości zastosowania powyższych związków w warstwach receptorowych innych niż matryce polimerowe, otrzymałem warstwy czujnikowe wykorzystując komercyjnie dostępne szkło porowate modyfikowane polistyrenem (PG-PS). Dla tak otrzymanych warstw jonoselektywnych obserwowałem selektywną zmianę barwy w obecności kationów metali ciężkich, a mianowicie ołowiu(II) i miedzi(II). Bardziej obiecujące właściwości miały jednak te układy, w których wykorzystałem oligoeterowe pochodne. 18-członowy związek zawierający resztę 4-metyloimidazolu (**11**) unieruchomiony na porowatym szkle wydaje się być obiecującym chromojonoforem czułym na jony ołowiu(II) (rys. IV.14) zaś 21-członowa korona (**12**) z resztą imidazolową wykazuje czułość na jony miedzi(II).

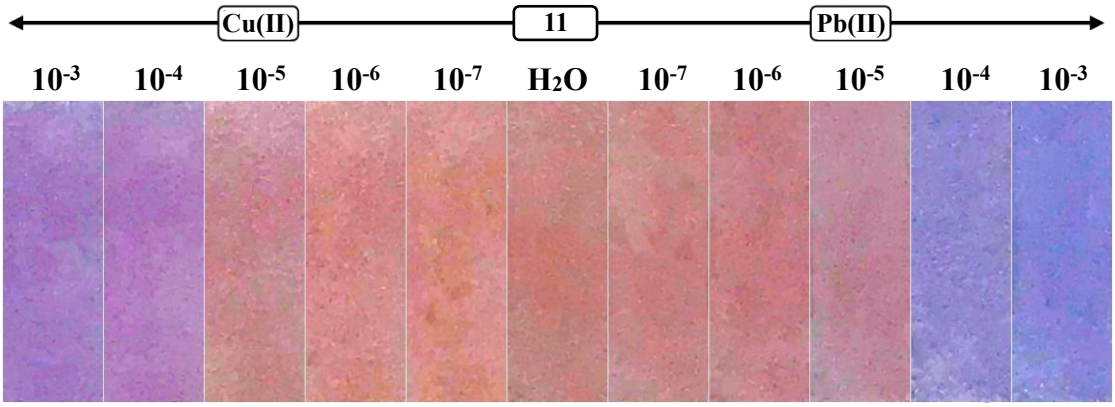

Rys. IV.14. Zmiana barwy warstwy receptorowej ze związkiem **11** w obecności jonów miedzi(II) oraz ołowiu(II), stężenia podane w mol/dm^3.

Makrocykliczne pochodne z resztą imidazolu lub 4-metyloimidazolu zostały zastosowane po raz pierwszy jako składniki warstw receptorowych czujników optycznych. Natomiast lipofilowe pochodne są aktualnie badane w zespole jako składniki membran elektrod jonoselektywnych.

IV.P5 – OPTODY Z TRIOCTANU CELULOZY DO RÓWNOCZESNEGO WYKRYWANIA BIZMUTU(III) I OŁOWIU(II) (MACROCYCLIC DERIVATIVES OF IMIDAZOLE AS CHROMOIONOPHORES FOR BISMUTH(III)/LEAD(II) PAIR)

Ostatnią publikacją składającą się na cykl publikacji jest praca pt. „Optody z trioctanu celulozy do równoczesnego wykrywania bizmutu(III) i ołowiu(II)". Badania zawarte w tej publikacji prowadzone były równolegle z badaniami opisanymi w publikacji **P4**.

Postanowiłem zbadać właściwości makrocyklicznych pochodnych 18-członowych pochodnych zawierających łańcuch oligoeterowy zawierających imidazol lub 4-metyloimidazol (związek **10** oraz **11** – rys. IV.11) jako chromojonofory w optodach na bazie CTA. W celu porównania z właściwościami materiałów czujnikowych, w których zastosowałem makrocykliczne pochodne pirolu badałem odpowiedź na obecność jonów ołowiu(II). Rozszerzyłem jednak badania o inne jony metali.

Analogicznie jak w przypadku opisanych wcześniej badań w pierwszej kolejności zbadałem właściwości kompleksujące w roztworze. Jako rozpuszczalnik organiczny doskonale mieszający się z wodą, a jednocześnie zapewniający wystarczającą rozpuszczalność związków makrocyklicznych **10** oraz **11** wybrałem DMSO [641, 642]. Wykazałem, że roztwory związków **10** oraz **11** selektywnie zmieniają barwę nie tylko w obecności soli ołowiu(II) (co było oczekiwane), ale także w obecności soli bizmutu(III). Obserwowana zmiana barwy jest związana z tworzeniem kompleksów typu triple-decker, co wykazałem stosując spektroskopię absorpcyjną w zakresie UV-Vis oraz spektroskopię protonowego rezonansu jądrowego.

Wykazałem, że związki **10** oraz **11** w warunkach miareczkowania spektrofotometrycznego w mieszaninie DMSO:woda tworzą kompleksy z jonami ołowiu(II) oraz bizmutu(III) o porównywalnych, wysokich ($\log K > 17$) wartościach stałych trwałości. Zgodnie z doniesieniami literaturowymi jest to bardzo pożądana cecha dla układów stosowanych jako radioterapeutyki, do których należy bizmut-212 i bizmut-213. Izotopy te charakteryzują się jednak stosunkowo krótkimi okresami półtrwania (odpowiednio 61 i 46 min.). Dlatego jako generator *in situ* ^{212}Bi proponuje się zastosowanie radionuklidów o dłuższym okresie półrozpadu, takich jak ^{212}Pb (okres półtrwania 10,6 h) [643, 644]. Dzięki temu okres półtrwania radioaktywnego bizmutu-212 może zostać wydłużony do kilkunastu godzin.

W celu określenia potencjalnego zastosowania związków **10** oraz **11** do badania próbek wodnych (czyli hipotetycznie również płynów ustrojowych) unieruchomiłem je w warstwie receptorowej na bazie CTA. Otrzymane membrany, podobnie jak w mieszaninie DMSO:woda cechowały się czułością na jony ołowiu(II) oraz bizmutu(III). Korzystnym efektem zmiany

otoczenia chemicznego z rozpuszczalnika na matrycę polimerową jest większe przesunięcie pasm absorpcyjnych dla tworzących się kompleksów. Oznacza to bardzie widoczne, łatwiej dostrzegalne – także gołym okiem zmiany barwy w obecności badanych jonów (rys. IV.15).

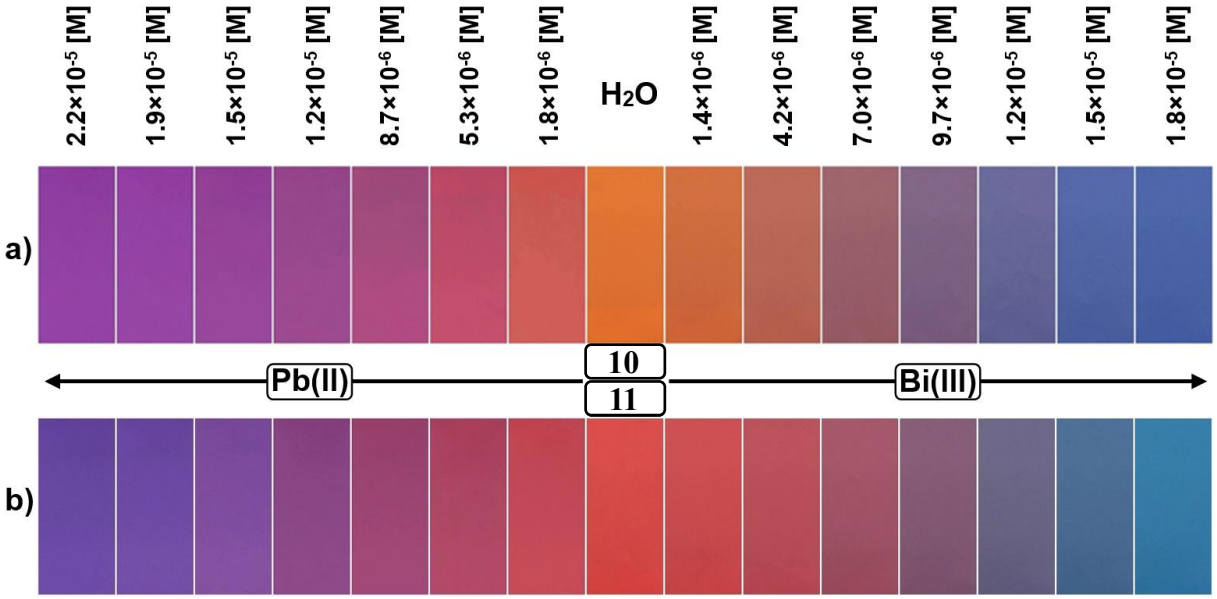

Rys. IV.15. Zmiana barwy optod ze związkiem: a) **10** i b) **11**; w obecności azotanu(V) ołowiu(II) i bizmut(III).

Skład membran (ilość chromojonoforu, plastyfikatora, soli lipofilowej) optymalizowałem uwzględniając m.in. generowaną wartość zmiany sygnału analitycznego, zakres liniowej odpowiedzi, czas życia optod. Wykazałem, że otrzymane materiały czujnikowe optod są czułe na jony bizmutu(III) oraz ołowiu(II) umożliwiając potencjalne oznaczanie tych jonów z detekcją spektrofotometryczną oraz kolorymetryczną na poziomie stężeń 10^{-7} mol/dm^3. Wykazałem także, że możliwe jest wykorzystanie zaproponowanych optod do oznaczania bizmutu(III) oraz ołowiu(II) obok siebie z zastosowaniem detekcji spektrofotometrycznej. Jest to szczególnie interesujące ze względu na potencjalne zastosowania w analityce medycznej– co jednak wykraczało poza ramy zrealizowanej pracy doktorskiej.

LITERATURA

214. E. Wagner–Wysiecka, E. Luboch, M. Jamrógiewicz, J.F. Biernat, *Chromogenic macrocyclic derivatives of azoles—synthesis and properties*, Tetrahedron **2003**, 59, 4415–4420;
219. E. Luboch, E. Wagner–Wysiecka, M. Fainerman–Melnikova, L.F. Lindoy, J.F. Biernat, *Pyrrole Azocrown Ethers. Synthesis, Complexation, Selective Lead Transport and Ion–Selective Membrane Electrode Studies*, Supramol. Chem. **2006**, 18, 593–601;
220. E. Wagner–Wysiecka, M. Jamrógiewicz, M.S. Fonari, J.F. Biernat, *Azomacrocyclic Derivatives of Imidazole: Synthesis, Structure, and Metal Ion Complexation Properties*, Tetrahedron **2007**, 63, 4414–4421;
620. J.F. Biernat, M. Bocheńska, *Proton–ionizable crown compounds. 10. Preparation and structural studies of macrocyclic ligands containing two sulfonamide units and with seventeen to twenty–six ring members*, J. Heterocycl. Chem. **1987**, 24, 1077–1083;
621. E. Luboch, V.C. Kravtsov, A. Konitz, *Reductive cyclization products of 1,2–bis(2–nitrophenoxy)ethanes. X–ray structures of 10–membered azoxycrown ether stereoisomers and the sodium iodide complex of a 20–membered azoazoxycrown*, J. Supramol. Chem. **2001**, 1, 101–110;
622. B. Dietrich, J.M. Lehn, J.P. Sauvage, J. Blanzat, *Cryptates—X: Syntheses et proprietes physiques de systemes diaza–polyoxa–macrobicycliques*, Tetrahedron, **1973**, 29, 1629–1645;
623. V. Marti–Centelles, M.D. Pandey, M.I. Burguete, S.V. Luis, *Macrocyclization Reactions: The Importance of Conformational, Configurational, and Template–Induced Preorganization*, Chem. Rev. **2015**, 115, 8736–8834;
624. F. Esteve, B. Altava, S.V. Luis, E. Garcia–Verdugo, *Tools and new metric (Macrocyclization Environmental Impact – MEI) to tackle the sustainability of macrocyclization reactions*, Catal. Today **2024**, 426, 114407;
625. H. Sitzmann, M.D. Walter, G. Wolmershäuser, *A triple–decker sandwich complex of barium*, Angew. Chem. Int. Ed. **2002**, 41, 2315–2316;
626. Q.F. Liu. *Preparation and Characterization of a Novel Gadolinium Triple–Decker Sandwich–Type Complex with Tetrabenzoporphyrin Ligand*, Adv. Mat. Res. **2013**, 690–693, 573–576;
627. M. Piesch, F. Dielmann, S. Reichl, M. Scheer, *A general pathway to heterobimetallic triple–decker complexes*, Chem. Eur. J. **2020**, 26, 1518–1524;
628. S.P. Babailov, M.A. Polovkova, G.A. Kirakosyan, A.G. Martynov, E.N. Zapolotsky, Y.G. Gorbunova, *NMR thermosensing properties on binuclear triple–decker complexes of terbium(III) and dysprosium(III) with 15–crown–5–phthalocyanine*, Sens. Actuators A Phys. **2021**, 331, 112933;
629. M. Froimowitz, *HyperChem: a software package for computational chemistry and molecular modeling*, BioTechniques **1993**, 14, 1010–1013;
630. Y. Li, B.O. Patrick, D. Dolphin, *Near-Infrared Absorbing Azo Dyes: Synthesis and X-ray Crystallographic and Spectral Characterization of Monoazopyrroles, Bisazopyrroles, and a Boron−Azopyrrole Complex*, J. Org. Chem. **2009**, 74, 5237–5243;
631. V.K. Gupta, S.K. Shoora, L.K. Kumawat, A.K. Jain, *A highly selective colorimetric and turn–on fluorescent chemosensor based on 1–(2–pyridylazo)–2–naphthol for the detection of Aluminium (III) Ions*, Sens. Actuators B Chem. **2015**, 209, 15–24;
632. D. Sarkar, A.K. Pramanik, T.K. Mondal, *Benzimidazole based ratiometric and colourimetric chemosensor for Ni(II)*, Spectrochim. Acta Part A: Mol. Biomol. Spectrosc. **2016**, 153, 397;
633. S. Biswas, S. Acharyya, D. Sarkar, S. Gharami, T.K. Mondal, *Novel pyridyl based azo–derivative for the selective and colorimetric detection of nickel(II)*. Spectrochim. Acta Part A: Mol. Biomol. Spectrosc. **2016**, 159, 157–162;
634. Q. Zhao, H. Yuan, X. Xu, L. Hu, P. Gong, Z. Yan, *A D–π–A–π–D organic conjugated molecule with multiple chelating points: Spectral property and its reversible visual sensing Cu^{2+}*, Dyes Pigm. **2019**, 165, 217–222;
635. H. Tavallali, G. Deilamy-Rad, M.A. Karimi, E. Rahimy, *A novel dye-based colorimetric chemosensors for sequential detection of Cu^{2+} and cysteine in aqueous solution*, Anal. Biochem. **2019**, 583, 113376;
636. Z.T. Al-Khateeb, F.F. Karam, K. Al-Adilee, *Synthesis and characterization of some metals complexes with new heterocyclic azo dye ligand 2-[2-(5-nitrothiazolyl)azo]-4- methyl-5-nitrophenol and their biological activities*, J. Phys.: Conf. Ser. **2019**, 1294, 052043;
637. Y. Suzuki, A. Ikeda, K. Ohno, T. Fujihara, T. Sugaya, K. Ishihara, *o-Azophenylboronic Acid-Based Colorimetric Sensors for d-Fructose: o-Azophenylboronic Acids with Inserted Protic Solvent Are the Key Species for a Large Color Change*, J. Org. Chem. **2020**, 85, 9680–9693;
638. M. Ghorbanian, S. Asghari, M. Tajbakhsh, *A new benzothiazole azo dye colorimetric chemosensor for detecting Pb^{2+} ion*, Spectrochim. Acta Part A: Mol. Biomol. Spectrosc. **2023**, 296, 122652;
639. Z. Wang, J. Liu, L. Zhang, W. Nie, J. Liu, J. Yang, Y. Li, *Copper (II)–azo complex modified hydrogel: A sensitive colorimetric sensor for visual detection of H_2S gas*, Sens. Actuators B Chem. **2023**, 376, 132968;
640. M. Hercigonja, B. Milovanović, M. Etinski, M. *Petković, ecorated crown ethers as selective ion traps: Solvent's role in crown's preference towards a specific ion*, J. Mol. Liq. **2023**, 381, 121791;
641. J. Catalan, C. Diaz, F. Garcia–Blanco, *Characterization of Binary Solvent Mixtures of DMSO with Water and Other Cosolvents*, J. Org. Chem. **2001**, 66, 5846–5852;
642. B. Yang, X. Cao, C.Wang, S. Wang, C. Sun, *Investigation of hydrogen bonding in Water/DMSO binary mixtures by Raman spectroscopy*, Spectrochim. Acta A Mol. Biomol. Spectrosc. **2020**, 228, 117704;
643. K. Yong, M.W. Brechbiel, *Towards Translation of 212Pb as a Clinical Therapeutic; Getting the Lead In!*, Dalton Trans. **2011**, 40, 6068−6076;
644. G. Montavon, A. Le Du, J. Champion, T. Rabungb, A. Morgenstern, *DTPA complexation of bismuth in human blood serum*, Dalton Trans. **2012**, 41, 8615−8623.

V. PODSUMOWANIE

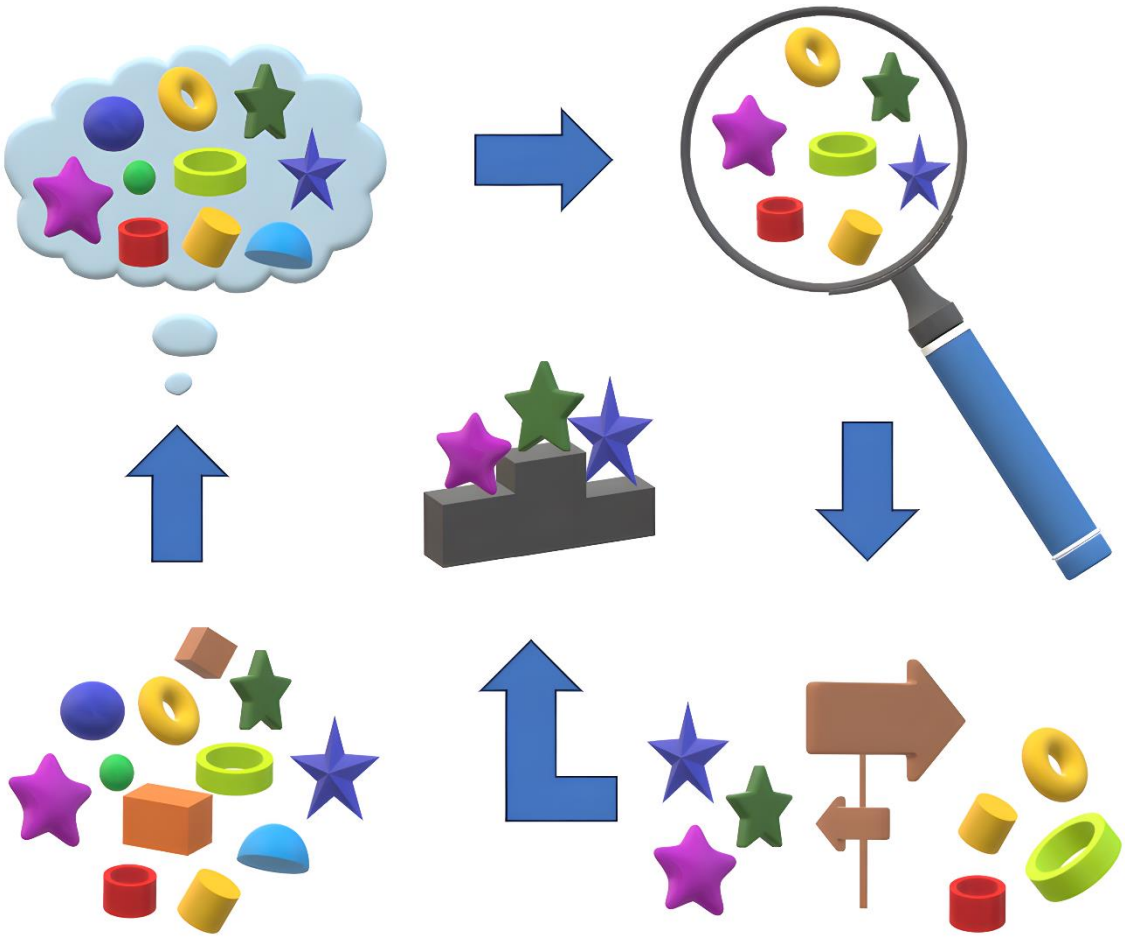

Podczas realizacji pracy doktorskiej zbadałem właściwości 13 chromogenicznych związków (rys. V.1.) zawierających w swojej strukturze ugrupowania azowe oraz reszty heterocykliczne w postaci pirolu lub imidazolu, jako potencjalnych chromojonoforów w warstwach receptorowych. Nowootrzymane związki jak (**1**, **2**, **5** – **9**) i wcześniej otrzymane w zespole (**3**, **4**, **10** – **13**), ale nie zbadane do tej pory jako receptory w warstwach receptorowych czujników optycznych do wykrywania oraz oznaczania jonów metali ciężkich, zostały przetestowane na różnych podłożach takich jak sączki papierowe, włókno szklane, bawełniane patyczki, PVC, CTA czy PG-PS. Przeprowadzone badania oraz ich wyniki, zostały przedstawione w publikacjach **P1** – **P5** i zebrane we wcześniejszych rozdziałach, wraz z materiałami pomocniczymi stanowiącymi podstawę niniejszej dysertacji.

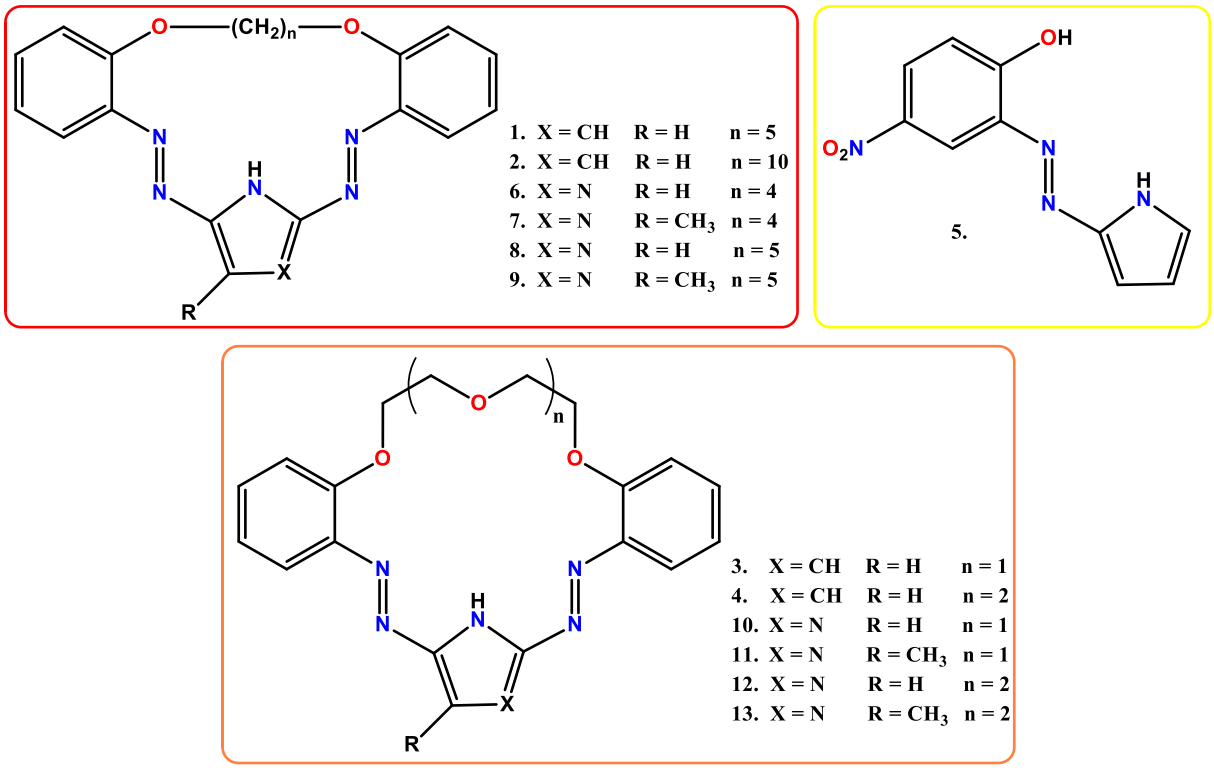

Rys. V.1. Wzory nowootrzymanych związków oraz wcześniej otrzymanych w zespole.

W ramach realizacji pracy doktorskiej otrzymałem 6 nowych związków makrocyklicznych (**1**, **2**, **6** – **9**) zawierających w swojej strukturze węglowodorowe łańcuchy oraz jeden acykliczny hydroksyazozwiązek (**5**), z grupą nitrową zlokalizowaną w pierścieniu benzenowym. Przedstawiłem syntezę nowych diazokoron z wykorzystaniem techniki wysokiego rozcieńczenia, a także związku acyklicznego **5**. Wydajności reakcji makrocyklizacji (W%) nowootrzymanych związków oraz otrzymanych wcześniej w zespole zestawiłem na rysunku V.2.

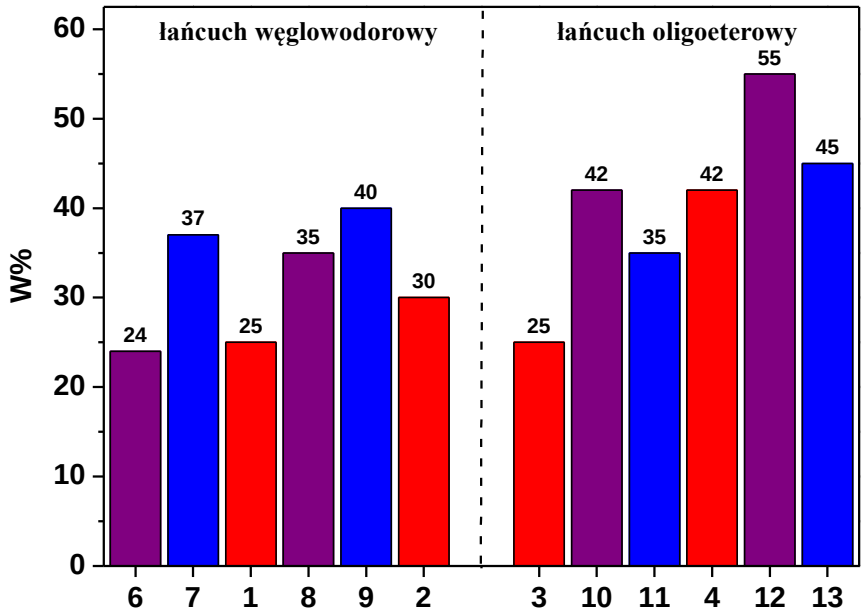

Rys. V.2. Wydajność reakcji makrocyklizacji nowootrzymanych związków oraz wcześniej otrzymanych w zespole (czerwony – pochodne zawierające resztę pirolu; fioletowy - pochodne zawierające resztę imidazolu; niebieski – pochodne zawierające resztę 4-metyloimidazolu).

Z porównania wydajności reakcji makrocyklizacji można wnioskować, że pochodne zawierające łańcuch oligoeterowy otrzymywane są w ogólności z większymi, niż ich analogi z łącznikiem węglowodorowym, wydajnościami.

Wyznaczyłem wartości lipofilowości ($logP_{TLC}$) dla nowootrzymanych związków oraz zestawiłem je z tlenowymi analogami (**3**, **4**, **10** – **13**), w celu określenia możliwości zastosowania tych makrocyklicznych chromojonoforów w warstwach receptorowych czujników optycznych oraz określenia ich powinowactwa do podłoża. Związki zawierające w swojej strukturze węglowodorowy łańcuch charakteryzują się – zgodnie z oczekiwaniami – wyższymi wartościami lipofilowości niż ich tlenowe analogi (rys. V.3). Wraz ze zwiększeniem liczby grup CH_2 w łańcuchu wzrasta wartość $logP_{TLC}$, co przekłada się na większe powinowactwo związków do podłoży o charakterze hydrofobowym. Ponadto wartości $logP_{TLC}$ można uszeregować pod względem występującego w strukturze azolu, gdyż związki zawierające imidazol charakteryzują się niższymi wartości lipofilowści niż makrocykle z resztą pirolu, które to natomiast mają niższe wartości $logP_{TLC}$ od chrmojonoforów z 4-metyloimidazolem. Warto jednak wspomnieć, że w przypadku związków z oligoeterowym łańcuchem również potwierdza się powyższa reguła z jednym wyjątkiem, gdyż 18-członowy makrocykl z 4-metyloimidazolem (**11**) posiada najwyższą wartość lipofilowości wśród tej grupy związków.

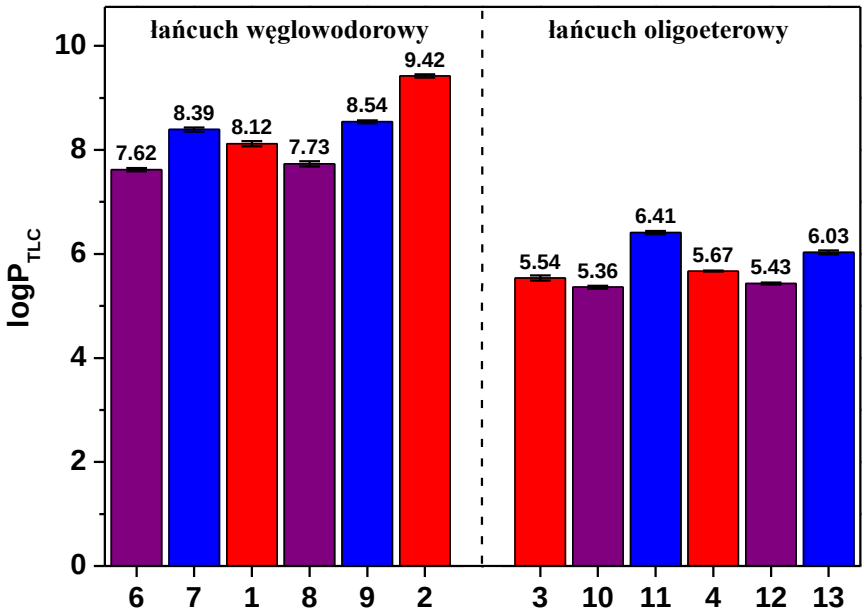

Rys. V.3. Zestawienie wartości $logP_{TLC}$ związków **1** – **4** i **6** – **13** (czerwony – pochodne zawierające resztę pirolu; fioletowy - pochodne zawierające resztę imidazolu; niebieski – pochodne zawierające resztę 4-metyloimidazolu).

Wyznaczyłem wartości stałych trwałości (logK) kompleksów z jonami metali ciężkich, na które badane związki wykazywały selektywność. W przypadku związków makrocyklicznych, potwierdzono przy wykorzystaniu technik spektroskopowych, że wszystkie tworzą z jonami ołowiu(II) kompleksy o stechiometrii 3:2 ligand:ołów(II), co odpowiada kompleksowi tak zwanej „podwójnej kanapki" (ang. triple decker sandwich complex). W przypadku wartości logK kompleksów związków makrocyclicznych można zauważyć, że dla 18-członowych makrocykli z węglowodorowym łańcuchem wyznaczono wyższe wartości stałych trwałości niż dla ich tlenowych analogów (rys. V.4). Ponadto tak jak w przypadku $logP_{TLC}$ widać zależność wartości logK od rodzaju azolu występującego w strukturze związku, jednak w tym wypadku wartości stałej trwałości z jonami ołowiu(II) rosną od imidazolu przez 4-metyloimidazol po pirol. Najwyższe wartości logK posiadają 21-członowe związki (**4**, **12**, **13**) w powyższym szeregu.

Makrocykle zawierające w swojej strukturze imidazol oraz 4-metyloimidazol, tworzą kompleksy z jonami miedzi(II), jednak w przypadku 17-, 18- i 21 członowych związków nie było możliwe wyznaczenie wiarygodnych wartości stałych trwałości kompleksów z jonami miedzi(II) na podstawie miareczkowania spektrofotometrycznego w acetonitrylu.

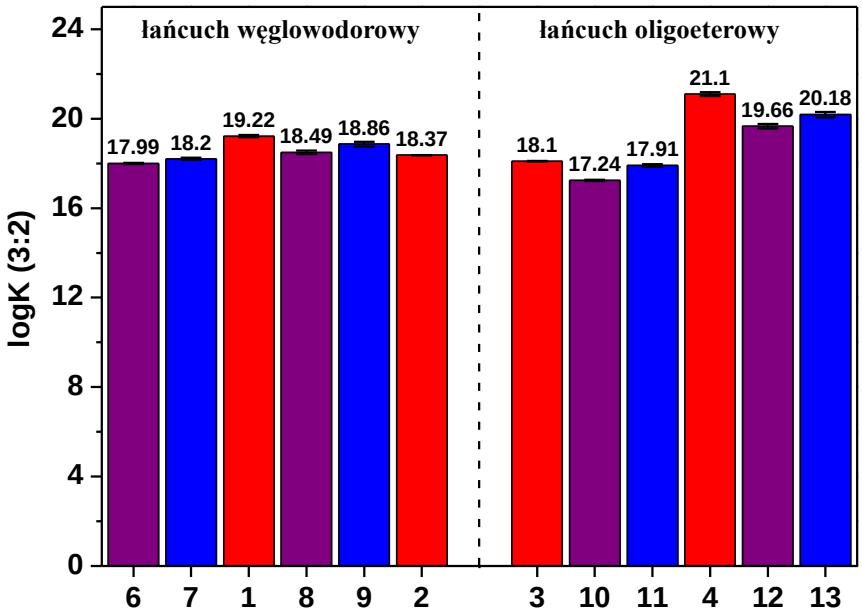

Rys. V.4. Zestawienie wartości stałych trwałości kompleksów logK związków **1** – **4** i **6** – **13** z jonami ołowiu(II) (czerwony – pochodne zawierające resztę pirolu; fioletowy - pochodne zawierające resztę imidazolu; niebieski – pochodne zawierające resztę 4-metyloimidazolu).

W publikacji **P1** oraz **P4** przedstawiłem potencjalne zastosowania badanych związków jako receptorów unieruchomionych na różnego rodzaju podłożach do szybkiego wykrywania oraz ilościowego oznaczania jonów metali ciężkich. Badanymi podłożami jak już wyżej wspomniałem były sączki papierowe, włókno szklane, bawełniane patyczki czy PG-PS. W przypadku makrocykli zawierających w swojej strukturze pirol (związek **1** i **2**) unieruchomionymi na włóknie szklanym, poza ilościowym oznaczaniem jonów ołowiu(II), było możliwe również wykrywanie jonów miedzi(II), niklu(II) oraz cynku(II). Co przekłada się na mniejszą selektywności w stosunku do jonów ołowiu(II) na tym podłożu. Natomiast na podłożu PG-PS unieruchomiłem makrocykliczne związki z resztą imidazolu oraz 4-metyloimidazolu, jednak warstwy receptorowe z 17-członowym makrocyklami (**6** i **7**) nie wykazywały zmiany barwy w obecności badanych jonów metali ciężkich. Pozostałe związki mogą znaleźć zastosowanie do wykrywania oraz ilościowego oznaczania jonów miedzi(II) oraz ołowiu(II), gdyż unieruchomione na PG-PS zmieniają barwę z pomarańczowej/czerwonej na fioletową w obecności jonów miedzi(II) oraz niebieską w obecności jonów ołowiu(II). Jednakże nie jest możliwe równoczesne wykrywanie obu tych jonów obok siebie.

W **P2** zbadałem wpływ poszczególnych składników warstwy receptorowej, której matrycę stanowił CTA, na wartość generowanego sygnału optycznego w postaci zmiany absorbancji (ΔA) oraz zmiany barwy (ΔE_{RGB}). Sprawdziłem wpływ stosowanego rozpuszczalnika używanego do rozpuszczenia składników membrany, rodzaj oraz ilość

plastyfikatora, ilość chromojonoforu, a także wpływ dodatku soli lipofilowej. Wszystkie wymienione składniki w mniejszym lub większym stopniu wpływały na wartość generowanego sygnału. Po skomponowaniu składu optod badałem parametry tj. wpływ pH, możliwość regeneracji, czas odpowiedzi, odtwarzalność, możliwość przechowywania, wpływ jonów przeszkadzających, zakres liniowej odpowiedzi czy detekcja kolorymetryczna, aby określić możliwość zastosowania otrzymanych membran. Niestety nie było możliwości otrzymania optody ze związkiem **1** ze względu na to, że krystalizował w matrycy polimerowej z CTA. Taką samą tendencję do krystalizacji wykazywały związki **8** i **9**, ze względu na co w późniejszym czasie poszukiwałem innego podłoża do unieruchomienia tych makrocykli (**P4**). CTA ze względu na hydrofilowo-hydrofobowy charakter stanowił odpowiednią matrycę dla badanych związków z resztą pirolu. Jednakże w przypadku 23-członowego makrocyklu z węglowodorowym łańcuchem o wysokiej wartość $\log P_{TLC}$ związek ten lepiej oddziaływał w matrycy PVC (**P1**) niż CTA, co objawiło się większą zmianą absorbancji oraz bardziej wyraźną zmianą barwy, w obecności jonów ołowiu(II) przy tym samym stężeniu. Natomiast najlepsze wyniki otrzymałem dla optody z 18-członowym makrocyklem **3**, który unieruchomiony w matrycy CTA pozwala na wykrywanie oraz oznaczanie jonów ołowiu(II) na poziomie ppb. Ponadto możliwe jest zastosowanie analizy kolorymetrycznej z wykorzystaniem aplikacji mobilnej na telefon, gdyż wraz ze wzrostem stężenia zauważalna „gołym okiem" jest zmiana barwy z czerwonej przez fioletową do niebieskiej.

W **P5** przeanalizowałem możliwości wykrywania jonów bizmutu(III) przez związek **10** oraz **11**, także w podejściu jednoczesnego oznaczania tego jonu wraz z jonami ołowiu(II). Poprzedzające unieruchomienie w membranie badania wykazały, że w roztworze DMSO:woda 1:1, makrocykle **10** oraz **11** tworzą kompleksy z jonami bizmutu(III), co jest związane ze znacznymi zmianami w widmach absorpcyjnych przekładającymi się na dobrze widoczną „gołym okiem" zmianę barwy. Badane związki zostały unieruchomione w matrycy polimerowej CTA, jednak skład membrany został w pewnym stopniu zmieniony pod względem ilości użytej soli lipofilowej, w porównaniu do wyżej opisanych rozwiązań. Większa ilość KTClPB wpłynęła na ograniczenie wymywania chromojonoforów z membrany, jednak przełożyło się to na czas odpowiedzi optody, a także na zakres liniowej odpowiedzi i wartość generowanego sygnału. W obecności jonów bizmutu(III) następowała zmiana barwy z pomarańczowej/czerwonej na niebieską, a w obecności jonów ołowiu(II) na fioletową. Wykazałem, że ze względu na położenie maksimów absorbcji tych kompleksów przy innych długościach fali oraz większe batochromowe przesunięcie pasma kompleksów z jonami

bizmutu(III), możliwe jest oznaczanie ilościowe jonów bizmutu(III) i ołowiu(II) z zastosowaniem detekcji spektrofotometrycznej.

Natomiast w **P3** zostały przedstawione badania nad właściwościami hydroksyazozwiązku **5**, który jak wykazałem, selektywnie tworzy kompleks o stechiometrii 1:1 z jonami miedzi(II) w DMSO oraz jego mieszaninach z wodą. Dla związku **5** ze względu na niewielki rozmiar cząsteczki oraz brak węglowodorowego łańcucha, została otrzymana najniższa wartość lipofilowości ($logP_{TLC}$ = 3,41±0,05) wśród badanych związków, co miało wpływ na późniejsze badania mające na celu unieruchomienie związku na różnego rodzaju podłożach. Związek **5** unieruchomiony zarówno na sączku papierowym, włóknie szklanym jak i na bawełnianych patyczkach, cechuje się selektywnością w stosunku do jonów miedzi(II) oraz pozwala na ilościowe oznaczanie tego jonu, dzięki bardzo dobrze widocznej zmianie barwy z żółtej na purpurową. W celu oznaczania ilościowego jonów miedzi(II) otrzymałem optody z wykorzystaniem CTA jako matrycy. W tym wypadku acykliczny związek **5** ze względu na wspomnianą wcześniej niską wartość lipofilowości wymywał się z membrany, jednak dodatek soli lipofilowej w postaci KTClPB oraz zmniejszenie ilości plastyfikatora, pozwoliły na 10-krotne użycie membrany po regeneracji w EDTA, ze zmniejszonym wymyciem chromojonoforu z optody. Hydroksyazozwiązek unieruchomiony w matrycy CTA tak jak wcześniej wykazałem dla mieszanin DMSO z wodą, cechują się selektywnością w stosunku do jonów miedzi(II) i w ich obecności zmienia barwę z żółtej na purpurową.

Przeprowadzone przeze mnie badania potwierdzają potencjalne zastosowanie badanych związków jako chromojonoforów w warstwach receptorowych czujników optycznych do wykrywania oraz oznaczania jonów metali ciężkich, przy zastosowaniu technik spektroskopowych oraz cyfrowej analizy kolorymetrycznej obrazu. W zależności od zastosowanego otoczenia chemicznego w postaci podłoża na którym zostanie unieruchomiony receptor można sterować selektywnością nowootrzymanych układów. Ponadto zaproponowane warstwy receptorowe są: względnie proste do otrzymania, pod względem syntezy związku oraz samych optod; tanie ze względu na niewielką ilość niedrogich składników; w większości można je regenerować, co przekłada się na możliwość wielokrotnego użytku; trwałe w czasie (z zastrzeżeniem przechowywania w roztworze membran CTA po pierwszym użyciu); umożliwiają detekcję półilościową „gołym okiem” oraz ilościową przy zastosowaniu aplikacji mobilnej na telefon do analizy barwy; a także posiadają niskie granice wykrywalności zarówno spektrofotometryczne jak i kolorymetryczne.

PUBLIKACJE O ZASIĘGU MIĘDZYNARODOWYM

Lp.	Rok	Autorzy	Tytuł	Czasopismo	IF / MNiSW
1	2020	E. Wagner-Wysiecka N. Łukasik A. Okuniewski B. Galiński	Ion recognition properties of new pyridine-2,6-dicarboxamide bearing propeller-like pendant residues: multi-spectroscopic approach	Monatshefte für Chemie – Chemical Monthly	1,451 / 40
2	2021	B. Galiński E. Luboch J. Chojnacki E. Wagner-Wysiecka	Novel diazocrowns with pyrrole residue as lead(II) colorimetric probes	Materials	3,748 / 140
3	2022	B. Galiński E. Wagner-Wysiecka	Pyrrole bearing diazocrowns: Selective chromoionophores for lead(II) optical sensing	Sensors and Actuators B: Chemical	8,400 / 140
4	2023	B. Galiński, J. Chojnacki, E. Wagner-Wysiecka	Simple colorimetric copper(II) sensor – spectral characterization and possible applications	Spectrochimica Acta Part A: Molecular and Biomolecular Spectroscopy	4,400 / 140
5	2023	B. Galiński J. Chojnacki K. Szwarc-Karabyka A. Małkowski D. Sopel A. Zwolińska E. Wagner-Wysiecka	Chromogenic macrocycles with imidazole residue: structure vs. properties	Dyes and Pigments	5,122 / 100
6	2024	B. Galiński E. Wagner-Wysiecka	Macrocyclic derivatives of imidazole as chromoionophores for bismuth(III)/lead(II) pair	Sensors and Actuators B: Chemical	8,400 / 200

KONFERENCJE KRAJOWE

Lp.	Rok	Autorzy	Tytuł	Konferencja	Typ
1	2017	E. Luboch E. Wagner-Wysiecka N. Łukasik B. Galiński	Chromofluorojonoforowe hydroxyazobenzokorony: izomeria i zdolność kompleksowania jonów	60. Zjazd Naukowy Polskiego Towarzystwa Chemicznego	Współautor posteru
2	2018	N. Łukasik E. Wagner-Wysiecka A. Okuniewski B. Galiński	Synteza i badanie właściwości kompleksujących nowej pochodnej kwasu pirydyno-2,6-dikarboksylowego	61. Zjazd Naukowy Polskiego Towarzystwa Chemicznego	Współautor posteru
3	2019	B. Galiński E. Wagner-Wysiecka	Makrocykliczne związki bisazowe z resztą pirolu jako chromogeniczne materiały czujnikowe do wykrywania i oznaczania jonów ołowiu(II)	62. Zjazd Naukowy Polskiego Towarzystwa Chemicznego	Poster
4	2019	E. Wagner-Wysiecka N. Łukasik B. Galiński E. Luboch J.F. Biernat	Makrocykliczne pochodne bisazowe z resztą pirolu jako uniwersalne kompleksony	62. Zjazd Naukowy Polskiego Towarzystwa Chemicznego	Współautor komunikatu
5	2021	B. Galiński M. Szwed E. Wagner-Wysiecka	Hydroksyazowe pochodne azoli: chromogeniczne receptory jonów metali ciężkich w warstwach receptorowych czujników optycznych	63. Zjazd Naukowy Polskiego Towarzystwa Chemicznego	Komunikat
6	2023	B. Galiński M. Aszyk A. Harasim E. Wagner-Wysiecka	Kompleksy miedzi(II) z chromogenicznymi pochodnymi pirolu jako układy IDA do wykrywania i oznaczania cysteiny	65. Zjazd Naukowy Polskiego Towarzystwa Chemicznego	Poster
7	2023	E. Wagner-Wysiecka B. Galiński E. Luboch J. Chojnacki	Związki azowe z resztą heterocykliczną - synteza, właściwości i zastosowania	65. Zjazd Naukowy Polskiego Towarzystwa Chemicznego	Współautor komunikatu

DZIAŁALNOŚĆ NA RZECZ POPULARYZOWANIA NAUKI

- Bałtycki Festiwal Nauki 2019 r. – przygotowanie i uczestnictwo w imprezach „Magiczny świat barw i luminescencji" oraz „Nie taka chemia straszna jak ją malują – warsztaty dla młodych chemików";
- Udział w Dniach Otwartych PG w 2021 r. oraz 2022 r. – przygotowanie materiałów i prezentacji pt. "Od związków chemicznych do materiałów optycznych i ich zastosowań" – współautor P. Szulc;
- Opracowanie materiałów dydaktycznych oraz prowadzenie zajęć laboratoryjnych z uczniami szkoły średniej w ramach grantu pt. „Chemia bez granic – warsztaty fizyko-chemiczne dla uczniów szkół średnich";
- Opracowanie instrukcji do ćwiczeń laboratoryjnych pt. „Analityczna chemia supramolekularna" – współautorzy: dr inż. Radosław Pomećko, dr hab. inż. Ewa Wagner-Wysiecka prof. PG;
- Opracowanie instrukcji do ćwiczeń laboratoryjnych pt. „Chemia, właściwości i zastosowania wybranych materiałów: materiały czujnikowe, materiały do wytwarzania, magazynowania i konwersji energii" – współautorzy: D. Roda, P. Szulc, M. Wtulich, Z. Zarach, dr hab. inż. Ewa Wagner-Wysiecka prof. PG.

OŚWIADCZENIA WSPÓŁAUTORÓW

Gdańsk, 28.02.2024

Mgr inż. Błażej Galiński
Katedra Chemii i Technologii Materiałów Funkcjonalnych
Wydział Chemiczny Politechniki Gdańskiej
ul. Narutowicza 11/12, 80-233 Gdańsk

OŚWIADCZENIE

Niniejszym oświadczam, że w pracach:

P1) Błażej Galiński, Elżbieta Luboch, Jarosław Chojnacki, Ewa Wagner-Wysiecka, *Novel diazocrowns with pyrrole residue as lead(II) colorimetric probes*, Materials **2021**, 14, 7239;

P2) Błażej Galiński, Ewa Wagner-Wysiecka, *Pyrrole bearing diazocrowns: Selective chromoionophores for lead(II) optical sensing*, Sensors and Actuators B: Chemical **2022**, 361, 131678;

P3) Błażej Galiński, Jarosław Chojnacki, Ewa Wagner-Wysiecka, *Simple colorimetric copper(II) sensor – spectral characterization and possible applications*, Spectrochimica Acta Part A: Molecular and Biomolecular Spectroscopy **2023**, 293, 122472;

P4) Błażej Galiński, Jarosław Chojnacki, Katarzyna Szwarc-Karabyka, Aadrian Małkowski, Diana Sopel, Aagniesza Zwolińska, Ewa Wagner-Wysiecka, *Chromogenic macrocycles with imidazole residue: structure vs. properties*, Dyes and Pigments **2023**, 219, 111610;

P5) Błażej Galiński, Ewa Wagner-Wysiecka, *Macrocyclic derivatives of imidazole as chromoionophores for bismuth(III)/lead(II) pair*, Sensors and Actuators B: Chemical **2024**, 399, 134798;

Mój wkład był zgodny z deklaracją w części „Author Contributions”/”CRediT authorship contribution statement” zamieszczoną na końcu treści odpowiednich publikacji i obejmował:

- udział przy zaplanowaniu eksperymentów;
- zaplanowanie oraz przeprowadzenie syntez;
- zbadanie natury oddziaływań metodami spektroskopowymi UV-Vis;
- przygotowanie, optymalizację oraz zbadanie warstw receptorowych;
- stworzenie przenośnego „studia fotograficznego”;
- wyznaczenie zależności generowanego sygnału umożliwiającej porównywanie optod o różnym składzie;
- udział przy zaprojektowaniu eksperymentów z wykorzystaniem technik NMR i MS, oraz analizie odpowiednich widm;
- udział przy interpretowaniu wyników i tworzeniu manuskryptu, a także jego korekt.

Błażej Galiński

Gdańsk, 28.02.2024

Dr hab. inż. Ewa Wagner-Wysiecka, prof. PG
Katedra Chemii i Technologii Materiałów Funkcjonalnych
Wydział Chemiczny Politechniki Gdańskiej
ul. Narutowicza 11/12, 80-233 Gdańsk

OŚWIADCZENIE

Niniejszym oświadczam, że w pracach:

P1) Błażej Galiński, Elżbieta Luboch, Jarosław Chojnacki, Ewa Wagner-Wysiecka, *Novel diazocrowns with pyrrole residue as lead(II) colorimetric probes*, Materials **2021**, 14, 7239;

P2) Błażej Galiński, Ewa Wagner-Wysiecka, *Pyrrole bearing diazocrowns: Selective chromoionophores for lead(II) optical sensing*, Sensors and Actuators B: Chemical **2022**, 361, 131678;

P3) Błażej Galiński, Jarosław Chojnacki, Ewa Wagner-Wysiecka, *Simple colorimetric copper(II) sensor – spectral characterization and possible applications*, Spectrochimica Acta Part A: Molecular and Biomolecular Spectroscopy **2023**, 293, 122472;

P4) Błażej Galiński, Jarosław Chojnacki, Katarzyna Szwarc-Karabyka, Adrian Małkowski, Diana Sopel, Agnieszka Zwolińska, Ewa Wagner-Wysiecka, *Chromogenic macrocycles with imidazole residue: structure vs. properties*, Dyes and Pigments **2023**, 219, 111610;

P5) Błażej Galiński, Ewa Wagner-Wysiecka, *Macrocyclic derivatives of imidazole as chromoionophores for bismuth(III)/lead(II) pair*, Sensors and Actuators B: Chemical **2024**, 399, 134798;

Mój wkład w powstanie powyższych publikacji był zgodny z deklaracją w części „Author Contributions”/”CRediT authorship contribution statement” zamieszczoną na końcu treści powyższych publikacji, a związany był z pełnieniem funkcji kierownika zespołu badawczego – polegał na koordynacji planowania badań, wsparciu merytorycznym doktoranta, korekcie manuskryptów wraz z materiałami uzupełniającymi oraz odpowiedziami na recenzje.

Jednocześnie jako autor korespondencyjny oświadczam, że:

- udział studentów realizujących pod moją opieką prace magisterskie: Diany Sopel, Agnieszki Zwolińskiej oraz Adriana Małkowskiego w publikacji **P4** polegał na przeprowadzeniu rozpoznawczych badań, które pozwoliły na wyselekcjonowanie odpowiednich podłoży oraz wstępną charakterystykę otrzymanych warstw receptorowych;
- udział Katarzyny Szwarc-Karabyki w publikacji **P4** polegał na rejestracji widm NMR oraz wsparciu autorów w ich interpretacji.

Udział doktoranta w powstanie powyższych publikacji jest wiodący.

Ewa Wagner-Wysiecka

Gdańsk, 26.02.2024

Prof. dr hab. inż. Elżbieta Luboch
Katedra Chemii i Technologii Materiałów Funkcjonalnych
Wydział Chemiczny Politechniki Gdańskiej
ul. Narutowicza 11/12, 80-233 Gdańsk

OŚWIADCZENIE

Niniejszym oświadczam, że w pracy:

P1) Błażej Galiński, Elżbieta Luboch, Jarosław Chojnacki, Ewa Wagner-Wysiecka, *Novel diazocrowns with pyrrole residue as lead(II) colorimetric probes*, Materials **2021**, 14, 7239

mój udział polegał na konsultowaniu metod i warunków prowadzenia syntezy badanych pochodnych pirolu i współudziale w pisaniu ostatecznej wersji publikacji.

Elżbieta Luboch

Prof. dr hab. inż. Elżbieta Luboch

Gdańsk, 22.02.2024

Prof. dr hab. inż. Jarosław Chojnacki
Katedra Chemii Nieorganicznej
Politechnika Gdańska
Ul. G.Narutowicza 11/12, 80-233 Gdańsk

Oświadczenie

Oświadczam, że w pracach:

Błażej Galiński, Elżbieta Luboch, Jarosław Chojnacki, Ewa Wagner-Wysiecka, *Novel diazocrowns with pyrrole residue as lead(II) colorimetric probes*, Materials **2021**, 14, 7239;

Błażej Galiński, Jarosław Chojnacki, Ewa Wagner-Wysiecka, *Simple colorimetric copper(II) sensor – spectral characterization and possible applications*, Spectrochimica Acta Part A: Molecular and Biomolecular Spectroscopy **2023**, 293, 122472;

Błażej Galiński, Jarosław Chojnacki, Katarzyna Szwarc-Karabyka, Adrian Małkowski, Diana Sopel, Agniesza Zwolińska, Ewa Wagner-Wysiecka, *Chromogenic macrocycles with imidazole residue: structure vs. properties*, Dyes and Pigments **2023**, 219, 111610.

wchodzących w skład cyklu publikacji, stanowiącego podstawę rozprawy doktorskiej Pana mgra Błażeja Galińskiego, mój udział polegał na wykonaniu rentgenowskiej analizy strukturalnej dostarczonych monokryształów oraz przygotowaniu krystalograficznego opisu metody badawczej oraz opisu wyznaczonych struktur, będących składnikami akapitów„Experimental" oraz „Results and Discussion".

Prof. dr hab. inż. Jarosław Chojnacki

PODPIS ZAUFANY
JAROSŁAW
CHOJNACKI
22.02.2024 11:25:14 [GMT+1]
Dokument podpisany elektronicznie
podpisem zaufanym

PUBLIKACJE

P1 – NOVEL DIAZOCROWNS WITH PYRROLE RESIDUE AS LEAD(II) COLORIMETRIC PROBES

materials

MDPI

Article

Novel Diazocrowns with Pyrrole Residue as Lead(II)Colorimetric Probes

Błażej Galiński [1], Elżbieta Luboch [1], Jarosław Chojnacki [2] and Ewa Wagner-Wysiecka [1,*]

[1] Department of Chemistry and Technology of Functional Materials, Faculty of Chemistry, Gdańsk University of Technology, Narutowicza Street 11/12, 80-233 Gdańsk, Poland; blazej.galinski@pg.edu.pl (B.G.); elzluboc@pg.edu.pl (E.L.)
[2] Department of Inorganic Chemistry, Faculty of Chemistry, Gdańsk University of Technology, Narutowicza Street 11/12, 80-233 Gdańsk, Poland; jaroslaw.chojnacki@pg.edu.pl
* Correspondence: ewa.wagner-wysiecka@pg.edu.pl

Abstract: Novel 18- and 23-membered diazomacrocycles were obtained with satisfactory yields by diazocoupling of aromatic diamines with pyrrole in reactions carried under high dilution conditions. X-ray structure of macrocycle bearing five carbon atoms linkage was determined and described. Compounds were characterized as chromogenic heavy metal ions receptors. Selective color and spectral response for lead(II) was found in acetonitrile and its mixture with water. Complexation properties of newly obtained macrocycles with a hydrocarbon chain were compared with the properties of their oligoether analogs. The influence of the introduction of hydrocarbon residue as a part of macrocycle on the lead(II) binding was discussed. Selective and sensitive colorimetric probe for lead(II) in aqueous acetonitrile with detection limit 56.1 μg/L was proposed.

Keywords: azomacrocycle; pyrrole; synthesis; ion recognition; lead(II) complexation; chromoionophore

Citation: Galiński, B.; Luboch, E.; Chojnacki, J.; Wagner-Wysiecka, E. Novel Diazocrowns with Pyrrole Residue as Lead(II)Colorimetric Probes. *Materials* **2021**, *14*, 7239. https://doi.org/10.3390/ma14237239

Academic Editor: Anastasios J. Tasiopoulos

Received: 19 October 2021
Accepted: 22 November 2021
Published: 26 November 2021

Publisher's Note: MDPI stays neutral with regard to jurisdictional claims in published maps and institutional affiliations.

1. Introduction

Heavy metals—like lead(II)—are highly toxic to humans and bioaccumulate in aquatic systems having harmful effects on the environment [1–3]. Lead poisoning (saturnism) has been present throughout the history of mankind. Lead was one of the first metals widely used (e.g., fishing nets, domestic utensils, etc.) due to its ease of extraction and its ductility. Exposure to lead is often claimed to contribute to the fall of the Roman Empire. Mental disorders called "painter's colic" or "painter's madness" displayed by some of the great masters, including Michelangelo and Caravaggio, are also attributed to lead poisoning. The possibility of lead poisoning is also mentioned in the case of famous composers Beethoven and Händel [4,5]. Lead exposure causes dysfunction of blood and nervous systems. Lead is also easily precipitating in the brain, kidneys and reproductive system. Poisoning with lead can also cause anemia and brain damage and finally death [6–8]. Nowadays, lead poisoning is rarely seen in developed countries, but it still represents a major environmental problem in certain areas, also in tap water in communities with older service lines and older household plumbing containing lead. The regulatory guidelines' value given for drinking water by the WHO is 0.01 mg/L [9].

As the most common methods of determination of lead(II) at trace levels, atomic absorption spectrometry (AAS) or inductively coupled plasma optical emission spectrometry (ICP-OES) can be mentioned. These and other analytical methods [10–13] enable accurate and precise detection and determination of lead(II) in various types of samples at different concentration levels, but there is still essential need for competitive, easy to use, low cost, fast and reliable methods which can be applied also in on site tests. These requirements are, in many cases, met by optical sensors [14–16] in which a selective ion receptor is incorporated in the sensing layer or acts as selective complexing reagent in a solution.

Lead(II) is a borderline acid in HSAB theory, forming complexes in various coordination modes with many ligands [17], also mixed with N,O macrocyclic ones [18]. Spectrophotometric and naked-eye detection and determination of lead(II) are often based on selective complex formation between a metal ion and a chromogenic sensing molecule with defined donor atom number and arrangement. For example, acyclic azo compound 1,5-dimethyl-2-phenyl-4-((2,3,4-trihydroxyphenyl)diazenyl)-1H-pyrazol-3(2H)-one was proposed for the spectrophotometric determination of lead(II) by a surfactant-sensitized method based on the ternary complexes formation with a detection limit of 0.3 μg/mL (1.45×10^{-6} M) [19]. Another example was described by Wang and Chen [20]. Azo dye was found to form a magenta colored complex with lead(II) in acetonitrile-water (1:1) mixture of stability constant value log*K* 4.66. Azoderivative was used in test strips for determination of lead(II) in untreated wastewaters and freshwaters at ppm level. In this respect, macrocyclic azo compounds, discriminating ions according to their size, serve as a group of molecules of interesting sensing properties and applications [21,22]. Due to presence of an azo moiety, macrocycle-metal cation interaction can be followed by the change of absorption spectra in the visible range of electromagnetic radiation [23–28]. Until now, a series of chromogenic crown ethers with two azo groups and phenol [23], pyrrole [24–27] or imidazole [28] residue as a part of macrocycle were synthesized and studied in our group as metal cation complexation agents in solution and as ionophores in membrane ion selective electrodes. Diazocrowns with pyrrole residue, bearing three nitrogen donor atoms (one of each azo group and nitrogen of pyrrole moiety), were described for the first time in 2003 [24]. Their functionalized derivatives were found to have high lead(II) affinity in solution and in membrane systems [24–27].

A property of these compounds, i.e., showing an easy to measure color change upon lead(II) complexation, prompted us to synthesize new macrocyclic derivatives of expected affinity towards heavy metal cations to obtain selective and sensitive probes for lead(II) detection and determination. Macrocyclic receptors with mixed N,O donor atoms bridged with oligoether or hydrocarbon linkage were investigated also to find out more about the possible nature of lead(II) binding by this class of compounds.

2. Materials and Methods

2.1. General

All chemicals of the highest available purity were purchased from commercial sources and used without further purification. TLC aluminum sheets covered with silica gel 60 F254 and glass plates 60 RP-18 F_{254} were purchased from Merck (Germany). For column chromatography, silica gel 60 (0.063–0.200 mm) from Merck (Germany) was used. ^{1}H and ^{13}C spectra were recorded on a Varian INOVA 500 spectrometer (Palo Alto, CA, USA) at 500 MHz and 125 MHz, respectively. Chemical shifts are reported as δ (ppm) values in relation to TMS. EILR and EIHR mass spectra of crowns were recorded on an AutoSpec Premier (Waters) instrument (Milford, MA, USA). For registration of ESI-LR spectra of lead(II) complexes and MS/MS experiments, API 3000 (Applied Biosystems, Warrington, Cheshire, UK) (equipped with ESI ion source), a triple-quadrupole mass spectrometer was used. FTIR spectra (film) were taken on a Nicolet iS10 apparatus (Thermo Fisher Scientific, Waltham, MA, USA). For UV–VIS measurements, an UNICAM UV 300 series apparatus (Spectronic Unicam, Leeds, UK) was used. Spectroscopic measurements were carried out in 1 cm quartz cuvettes in acetonitrile (LiChrosolv®, Merck, Germany). For recovery studies, Standard Reference Solution of lead(II) 1000 ppm (Merck, Germany) was used. Lead(II) concentration for comparative studies was determined using the ICP-OES method with iCAP 7400 Analyzer (Thermo Fisher Scientific, Waltham, MA, USA).

Glass microfiber filter (Whatman GF/C) (Schleicher & Schuell, Dassel, Germany) was used for test strips preparation. For optodes preparation PVC (Fluka, Switzerland), potassium tetrakis(4-chlorophenyl)borate (≥98%, Fluka, Switzerland), 2-nitrophenyl octyl ether (NPOE) (≥99%, Sigma-Aldrich, Switzerland), THF (≥99.5%, Sigma-Aldrich, St. Louis MO, USA) were used.

2.2. *Synthesis of Crowns* **3** *and* **4**

2.2.1. 1,5-bis(2-nitrophenoxy)pentane (**7**) and 1,10-bis(2-nitrophenoxy)decane (**8**)

Compounds **7** and **8** were prepared analogously as described in the literature [29,30]. A mixture of 2-nitrophenol (2.24 g, 16 mmol), 1,5-dibromopentane (2.07 g, 9 mmol) or 1,10-dibromodecane (2.70 g, 9 mmol) and anhydrous potassium carbonate (2.22 g, 16 mmol) in dry dimethylformamide (6 mL) were stirred and heated at 140 °C for 2 h. The mixture was diluted with cooled water (120 mL) to precipitate crude dinitro derivatives 7 or 8. Pure compounds **7** and **8** were obtained after crystallization from propan-2-ol (20 mL). **7**: yield 2.23 g (80%), light beige solid, mp 82–83 °C (lit. mp 83 °C) [30], **8**: yield 2.78 g (83%), light beige solid, mp 75–77 °C. (lit. mp 76 °C) [30].

2.2.2. 1,5-bis(2-aminophenoxy)pentane (**5**) and 1,10-bis(2-aminophenoxy)decane (**6**)

Compounds **5** and **6** were obtained using protocols described in the literature [24–27]. The reaction mixture containing compound **7** (2.80 g, 8 mmol) or **8** (3.33 g, 8 mmol) and propan-2-ol (50 mL) together with a Pd/C catalyst was magnetically stirred and heated in an oil bath at 58 °C. Aqueous hydrazine solution (80%) was added to the reaction mixture in 4 portions (0.5 mL each). Five hours after the last portion of hydrazine was added, the solution was filtered off to separate the catalyst. The solvent was evaporated under the reduced pressure. Amines were crystallized from propan-2-ol. **5**: yield 2.00 g (87%), white flakes, mp 60–61 °C (lit. mp 61 °C) [30]. **6**: yield 2.70 g (95%), white flakes, mp 66–67 °C. (lit. mp 67 °C) [30].

Compounds **1** and **2** were synthesized analogously to previous protocol [24], and the identity of material was confirmed by comparison of TLC and spectral properties with original samples of crowns deposited in our lab.

2.2.3. Preparation of New Diazocrown **3** and **4**

The synthesis of diazocrown **3** and **4** was based on a high dilution approach [24–27]. Three solutions were prepared:

- A: Diaminopodand **5** or **6** (1 mmol) and concentrated hydrochloric acid (0.5 mL) in water (20 mL) (DMF or THF in needed amount can be added to increase solubility of amines);
- B: Sodium nitrite (2 mmol) in water (30 mL);
- C: Pyrrole (1 mmol, 0.07 mL) and sodium hydroxide (0.20 g, 5 mmol) in water (30 mL).

All solutions were cooled in an ice bath to 0–5 °C. Solution B was added portionwise to solution A to obtain the bisdiazonium salt. The combined solutions A-B were left for 30 min in an ice bath. After this time, solutions A-B and C were added dropwise to deionized water (300 mL) at pH ~10 (NaOH), within 30 min, ensuring intensive stirring of the reaction system. The pH was controlled during the addition of solutions to the reaction container. After 2 h, the ice bath was removed, and the mixture was left for 24 h at room temperature. The precipitate was filtered off under reduced pressure. Products were isolated by column chromatography using initially dichloromethane and finally dichloromethane:acetone (10:1, *v/v*) as eluent. Compound **3** crystallizes from petroleum ether, **4** crystallizes from n-hexane.

Compound **3**: Yield 0.092 g (25%), red solid. mp 254–257 °C (with decomposition). TLC: Rf = 0.91 (chloroform), 0.47 (dichloromethane:n-hexane, 100:1). ^{1}H NMR (d-chloroform, 500 MHz), δ (ppm): 1.96–1.99 (4H, m), 2.09–2.14 (2H, m), 4.24 (4H, t, J = 5.5 Hz), 7.01 (2H, t, J = 7.5 Hz), 7.07 (2H, d, J = 8.8 Hz), 7.07 (2H, s), 7.40 (2H, dt, J1 = 8 Hz, J2 = 1.5 Hz), 7.79 (2H, dd, J1 = 8.5 Hz, J2 = 1.5 Hz), 10.17 (1H, s, NH). ^{13}C NMR (d6-DMSO, 125 MHz) δ (ppm): 23.9, 30.8, 40.4, 40.6, 40.8, 68.5, 114.8, 115.4, 116.5, 121.1, 133.8, 141.2, 146.7, 157.3. FTIR (crystalline film, cm^{-1}): 3450, 2940, 2871, 1585, 1488, 1456, 1371, 1275, 1232, 1150, 756. UV–VIS (acetonitrile): λ_{max} = 508 nm, $\varepsilon_{max} = 2.22 \times 10^4$. HRMS [EI]: found 375.1702 calculated for: $C_{21}H_{21}N_5O_2$ 375.1695.

Compound **4**: Yield 0.131 g (30%), red solid, mp 223–225 °C (with decomposition). TLC: Rf = 0.74 (chloroform), 0.51 (dichloromethane:n-hexane, 100:1). ^{1}H NMR (d6-DMSO, 500 MHz) δ (ppm): 1.27–1.42 (12H, m), 1.76 (4H, t, J = 6.6 Hz), 4.17 (4H, t, J = 6.1 Hz), 7.05

(2H, t, J = 7.6 Hz), 7.18 (2H, s), 7.24 (2H, d, J = 8.2 Hz), 7.41–7.44 (4H, m), 11.40 (1H, s, NH). ^{13}C NMR (d6-DMSO, 125 MHz) δ (ppm): 25.3, 28.0, 28.4, 28.8, 40.2, 69.5, 115.1, 116.7, 117.9, 121.2, 132.4, 143.8, 147.2, 155.6. IR (film, cm^{-1}): 3418, 2920, 2851, 1588, 1489, 1455, 1389, 1277, 1241, 1158, 749. UV–VIS (acetonitrile): λ_{max} = 495 nm, $\varepsilon_{max} = 2.15 \times 10^4$. HRMS [EI]: 445.2481 calculated for: $C_{26}H_{31}N_5O_2$ 445.2478.

NMR and mass spectra of **3** and **4** are shown in Supplementary Materials (Figures S1 and S2).

2.2.4. Preparation of Solid Complexes of Crowns **1–4** with Lead(II) Perchlorate

Samples for MS and FTIR analyses were prepared by dissolving of the crowns and lead(II) perchlorates in a molar ratio 3:2 in acetonitrile and left for solvent evaporation. ^{1}H NMR and MS spectra are included in Supplementary Materials (Figures S1, S2 and S11–S14).

2.3. Lipophilicity Determination

The lipophilicity values (log P_{TLC}) of chromoionophores **1–4** were estimated by TLC method [31,32] using reverse phase chromatography (RP18) with a mixture of methanol: water (9:1, *v/v*) as the mobile phase. As standards bis(1-butylpentyl)adipate (BBPA) (≥98.0%, Sigma Aldrich, Switzerland), 2-nitrophenyl octyl ether (NPOE) (≥99.0%, Sigma Aldrich, Switzerland), bis(2-ethylhexyl)sebacate (DOS) (≥97.0%, Sigma Aldrich, Germany), bis(2-ethylhexyl)phthalate (DOP) (≥97.0%, Fluka, Switzerland) and di-n-butylphthalate (DBP) (≥97.0%, Fluka, Switzerland) were used.

2.4. X-ray Structure Determination

Diffraction intensity data for **3** were collected on an IPDS 2T dual beam diffractometer (STOE & Cie GmbH, Darmstadt, Germany) at 120.0(2) K with MoKα radiation of a micro-focus X-ray source (GeniX 3D Mo High Flux, Xenocs, Sassenage, France, 50 kV, 1.0 mA, and λ = 0.71069 Å). Investigated crystals were thermostated under a nitrogen stream at 120 K using the CryoStream-800 device (Oxford CryoSystem, Oxford, UK) during the entire experiment. Data collection and data reduction were controlled by using the X-Area 1.75 program (STOE, 2015). Due to low absorption coefficient no absorption correction was performed. The structure was solved using intrinsic phasing implemented in SHELXT and refined anisotropically using the program packages Olex2 [33] and SHELX-2015 [34]. Positions of the C–H hydrogen atoms were calculated geometrically taking into account isotropic temperature factors. All H-atoms were refined as riding on their parent atoms with the usual restraints, including N-H atom (with AFIX 43) which does not take part in hydrogen bonding. Structure of **3** was refined with no special treatment. Crystallographic data reported in this paper have been deposited with the Cambridge Crystallographic Data Centre as supplementary publication No. CCDC 2081633 (Appendix A). The data can be obtained free of charge from The Cambridge Crystallographic Data Centre via www.ccdc.cam.ac.uk/structures (accessed on 12 October 2021). Details are included in Supplementary Materials including Figures S15 and S16 and Table S2).

2.5. Cation Binding Studies

Cation binding for crowns **1–4** was studied by UV–VIS titration in acetonitrile. The stock solutions of crowns (~10^{-4} M) and metal perchlorates (~10^{-2} M) were prepared by weighting the respective quantities of them and dissolving in acetonitrile in volumetric flasks. The cation binding constant values (log*K*) were calculated with the use of OPIUM [35] program on the basis of titration experiment data. The influence of interfering ions on spectrophotometric response towards lead(II) was expressed as the absolute value of relative response $RR\% = |[(A - A_0) / A_0]| \times 100\%$, where A_0 stands for absorbance of solution of crowns **1–4** in the presence of lead(II) perchlorate (equimolar to crown amount) and A absorbance value measures just after addition of interfering metal perchlorate in 10-fold excess to lead(II) perchlorate.

Limits of detection (LOD) for lead(II) were calculated using equation: LOD = 3σ/k, where σ is the standard deviation of the blank and k is the slope of the linear function A = f([Pb(II)]).

2.6. Preparation of Sensing Layers

2.6.1. Test Strips

Solutions of newly obtained crowns **3** (2.9×10^{-4} M) and **4** (3.1×10^{-4} M) in acetonitrile were poured into a chromatographic chamber, into which a strip of glass microfiber filter was placed, similar to the procedure used with the TLC plates. After 5 min, strips were taken out, and solvent was evaporated in a stream of hot air.

2.6.2. Optodes

The membrane cocktail was prepared by weighing out potassium tetrakis(4-chlorophenyl)borate (0.5 mg, 0.3% *w*/*w*), crown ether **3** or **4** (1.0 mg, 0.6% *w*/*w*), polyvinyl chloride (50 mg, 32.2% *w*/*w*) and NPOE (104 mg, 66.9% *w*/*w*). The components were dissolved in 1 mL of THF, and aliquots (90 µL) were deposited onto glass plates (9 × 45 mm) which were washed before use with nitric acid (10^{-1} M), acetone and propan-2-ol. After solvent evaporation (24 h), the resulting sensing membranes were used for naked-eye detection of lead(II).

3. Results and Discussion

3.1. Synthesis

New 18- and 23-membered macrocycles (compounds **3** and **4**) were synthesized by azocoupling of bisdiazonium salts with pyrrole analogously to previously described protocols (Scheme 1) [24–27]. Reaction carried out under high dilution conditions gave desired compounds with macrocyclization yield 25 and 30% for **3** and **4**, respectively, which seems to be within typical yields (19–42%) for this group of compounds [24–27].

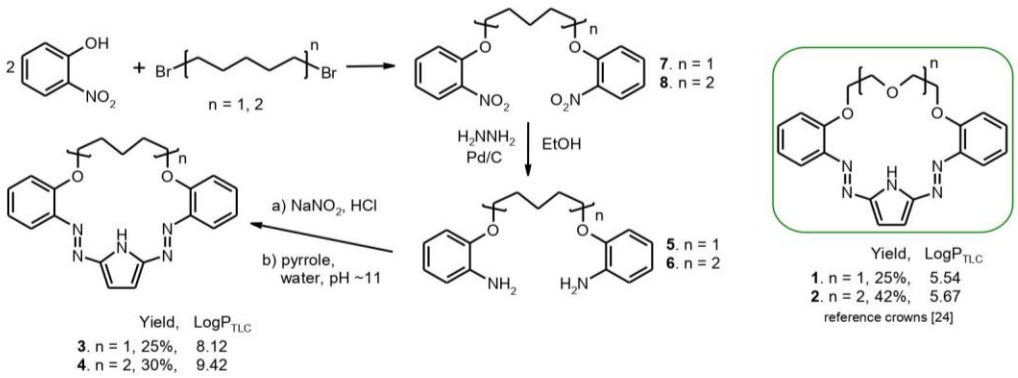

Scheme 1. Synthetic route of new macrocycles **3** and **4** and formulas of reference crowns **1** and **2** (right) [24]. Yields of macrocyclization and determined values of $logP_{TLC}$ are given.

For the first time for this class of compounds, lipophilicity values (log P_{TLC}) are reported here. The values of log P_{TLC} obtained by the RP-TLC method [30,31] (Scheme 1, Figure S10) as could be expected are higher for hydrocarbon chain bearing macrocycles **3** and **4** than for their oligoether analogs **1** and **2**.

Described earlier [24–27] pyrrole derivatives bearing oligoether chain as a part of macrocycle were found to form complexes with metal cations in acetonitrile and acetonitrile-water mixtures with preferential lead(II) cations affinity among all investigated metal cations (alkali, alkaline earth and heavy metal ions). Compounds **1** and **2** in acetonitrile (Scheme 1), treated here as reference compounds, form with lead(II) perchlorate double-sandwich type complexes of 3:2 stoichiometry (crown:Pb) of relatively high stability constants values (log K) 18.10 ± 0.01 and 21.10 ± 0.09 [25], respectively. The previous studies [24–27] showed that lead(II) complex formation, including spectral and color changes,

is dependent among others on the macrocycle size and the type of substituents both in benzene rings and the modification of the oligoether moiety. Here we tested other than the previously described modification of the skeleton of the pyrrole bearing chromogenic crown ethers, namely, introducing a hydrocarbon chain instead of oligoether linkage.

3.2. X-ray Structure of **3**

Suitable for X-ray analysis, crystals of macrocycle **3** were obtained by crystallization from petroleum ether solution and studied by single crystal X-ray diffraction (for details see Supplementary Materials).

Compound **3** forms thin plate, red crystals, with symmetry of the orthorhombic system, the space group *Pbca* (no. 61). The asymmetric unit contains one molecule, and the whole unit cell is built from eight molecules, Z = 8. Most of the bond lengths and angles are in the expected ranges (Figure 1, details in Supplementary Materials), including the hydrocarbon chain C11–C15.

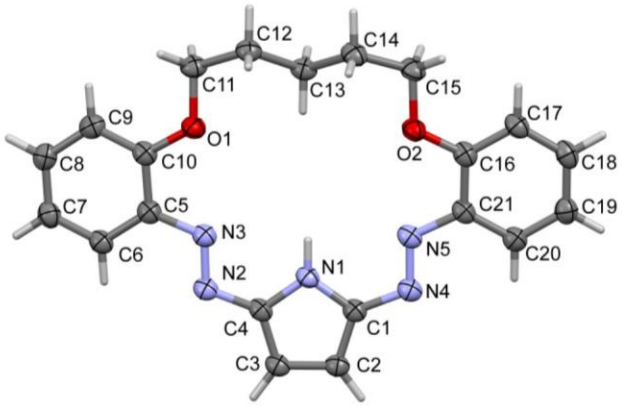

Figure 1. Molecular view of **3** showing atom labelling scheme.

Based on short interatomic distances, one may assume the mostly double character of N2-N3, N4-N5 bonds and the aromatic character of the pyrrolic ring. The molecule is essentially flat with an expected folding of the -C_5H_{10}- linker (ap, sc, -ap, ap, -sc, -ap), (Figure 2), (ap—antiperiplanar, sc—synclinal). The dihedral angle between the phenyl rings C5-C10 and C16-C21 is equal to 17.56 (9)°, which shows some deviation from planarity. The internal cavity offers Lewis base donor electron pairs on O1, O2, N3 and N5 atoms (hydrogen bond acceptors) as well as N-H group which is a potential hydrogen bonding donor. The size of the crown interior may be estimated by diagonal O . . . N atom distances which are equal to O1 . . . N5 5.720 Å and O2 . . . N3 5.602 Å. It is noteworthy that the bond C13-H13A is directed to the center of the hole, similarly to the N-H bond.

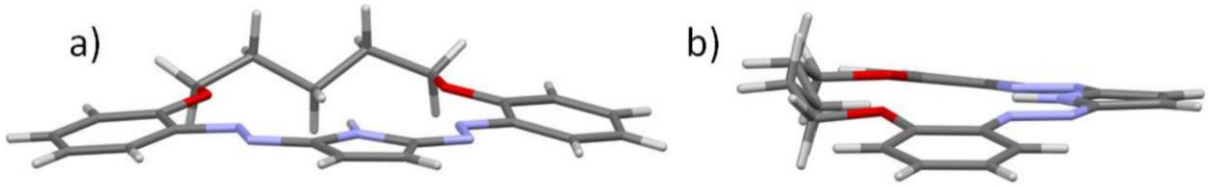

Figure 2. Projections of compound **3**, showing kinked conformation of the molecule: (**a**) front view, (**b**) side view. Subsequent torsions in the linker chain are (ap, sc, -ap, ap, -sc, -ap). More precisely: C10-O1-C11-C12 170.67 (15), O1-C11-C12-C13 57.5 (2), C11-C12-C13-C14 -174.57 (16), C12-C13-C14-C15 179.94 (16), C13-C14-C15-O2 -57.9 (2), C14-C15-O2-C16 -170.87 (16).

Crystal packing is dependent mainly on weak non-covalent interactions since no hydrogen bonding is available for the molecules. Shortest inter-ring (i.e., ring centroids) distances as short as 3.3603(8) are reported by PLATON, but this is observed for centers of 18- or 22-membered macrocyclic rings and should be disregarded. Nevertheless, some

true stackings of pyrrole N1-C1-C4 and benzene C16-C21 rings are also found, (Centroid distance 3.7913(11) Å, dihedral angle between the planes $\alpha = 7.92(10)^\circ$, slippage 2.093 Å). Other interactions are mainly of the van der Waals type. Crystal packing in 3 is shown in Figure S16. For details see Supplementary Data.

3.3. Heavy Metal Cation Complexation Studies

On the basis of qualitative tests carried out in acetonitrile, it was found that compounds **3** and **4** show a color change in the presence of: *p*-toluenesulfonic acid (TsOH), tetra-n-butylammonium hydroxide (TBAOH), nickel(II), copper(II), zinc(II) and lead(II) perchlorates (Figure 3). No changes were observed in the presence of alkali and alkaline earth metal perchlorates.

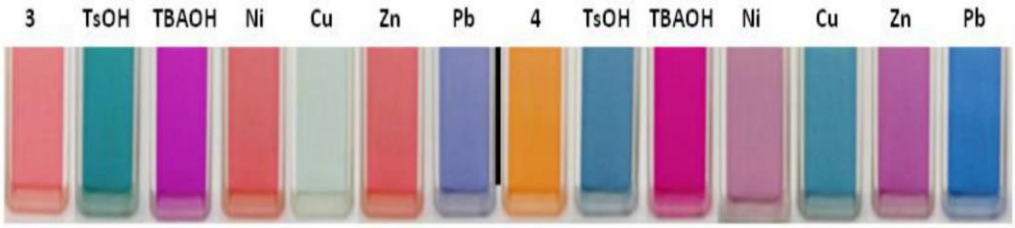

Figure 3. Qualitative probes showing color change of crowns **3** (2.01×10^{-5} M) and **4** (3.75×10^{-5} M) solutions (acetonitrile) in the presence of excess (added as solid substances, saturated solution) of *p*-toluenesulfonic acid (TsOH), tetra-n-butylammonium hydroxide (TBAOH) and nickel(II), copper(II), zinc(II) and lead(II) perchlorates in acetonitrile (photo was taken just after addition of the excess of acid, base and perchlorates).

As it is shown in Figure 3, the color of solutions of macrocycles **3** and **4** changes in the presence of heavy metal perchlorates. For both compounds, the presence of zinc(II) and nickel(II) perchlorates causes comparable color changes, just after their addition, to red for **3** and to purple for **4**. The presence of copper(II) turns the color of solutions to blue. Besides copper(II), significant color change is observed in the presence of lead(II) perchlorate: from red to deep blue for **3** and from orange to blue for **4**. Color changes are the result of the change of UV–VIS spectra, namely, formation of absorption band (Figure 4) at 610 and 605 nm, (spectral shift 102 and 110 nm), for **3** and **4,** respectively. Clear isosbestic points can indicate one complex under equilibrium.

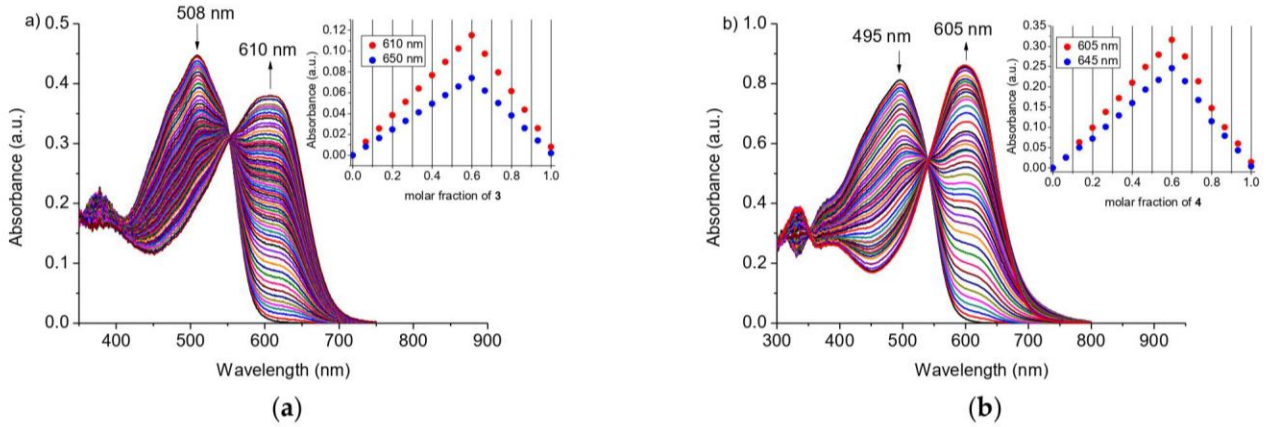

Figure 4. Changes in absorption spectra of crowns **3** and **4** upon titration with lead(II) perchlorate: (**a**) **3** ($c_3 = 2.01 \times 10^{-5}$ M; $c_{Pb} = 0$–2.61×10^{-5} M); (**b**) **4** ($c_4 = 3.75 \times 10^{-5}$ M; $c_{Pb} = 0$–5.75×10^{-5} M) in acetonitrile. Insets: Job's plots for lead(II) perchlorate and crowns **3** and **4** in acetonitrile.

Job's plots for lead(II) systems with **3** and **4** (Figure 4, insets) show apparent x_{max} value at 0.6 corresponding to the formation of 3:2 (crown:Pb) complex in acetonitrile.

Analysis of UV–VIS titration data with OPIUM [35] software also gives the best fit for 3:2 (crown:Pb) system with stability constant (log*K*) values 19.22 ± 0.05 and 18.37 ± 0.01 for **3** and **4,** respectively. The same model of lead(II) binding was proposed for previously studied macrocycles **1** and **2** [25] (Table S1). When comparing log*K* values (Table S1) for 18-membered crowns **1** and **3,** it is worth noting that lead(II) is bound stronger by macrocycle **3** (log*K* 19.22 ± 0.05) with hydrocarbon chain than by oligoether bearing derivative **1** (log*K* 18.10 ± 0.01). Contrary to this, 21-membered crown **2** binds lead(II) stronger (log*K* 21.0 ± 0.09) than compound **4** of 23-membered ring (log*K* 18.37 ± 0.01).

Thus, it can be assumed that incorporation of a long, flexible hydrocarbon chain can affect the size of the macrocycle cavity of **4** and makes it more comparable to cavity of 18-membered crowns **1** and **3**.

Complexes of 3:2 stoichiometry—triple-decker sandwich type—were reported for a significant number of systems including various types of ligands and metal centers. This type of complexes are common in transition metal chemistry [36] and lanthanides [37]. Moreover, for barium, such sandwich complex was reported [38]. An analogous model of lead(II) binding can be assumed for investigated here diazocrowns bearing pyrrole moiety. It can be confirmed by X-ray measurements, but unfortunately so far, suitable monocrystals of lead(II) complexes have not been obtained yet. ^{1}H NMR spectra of crown **2** and **4** in the presence of lead(II) perchlorate were registered in DMSO-d_6 due to low solubility of crowns in acetonitrile in required for experiment concentrations (Figure 5, Figures S3a,b and S4a,b). As solvent type can strongly influence the complexation equilibrium, spectra registered in DMSO do not bring the clear evidence for 3:2 complex formation in DMSO. However, two sets of signals in ^{1}H NMR spectra of compounds **2** and **4** registered in the presence of lead(II) perchlorate are observed. It means that in solution, ligands are not equivalent, at least on the NMR timescale. The resonances of "free" crowns **2** and **4** and their lead(II) complexes are shown in spectra of expanded range in Figures S5, S3b and S4b. The downfield shift of the signal of proton (marked as D in Figures S3b and S4b) of aromatic ring in *ortho* position to azo group can be a result of the engagement of one nitrogen of azo group in complex formation. Oxygen atoms of oligoether residue or linking hydrocarbon moiety seem also to participate in lead(II) binding as signals of these protons being also shifted and not equivalent. Interestingly, in the spectrum registered for compound **2,** significant change for signal of pyrrole CH protons (Figure 5) is observed. In the presence of lead(II) perchlorate, two signals are observed. One of them is slightly (0.05 ppm) upfielded—which could point to deprotonation of the pyrrole moiety upon lead(II) complexation. The second signal of pyrrole residue, observed at 7.36 ppm, is shifted towards the higher ppm values of 0.14 comparing the signal in spectrum of the "free" crown. This, coming along with deshielded N-H proton signal (+1.48 ppm), can point to the formation of a stronger hydrogen bonding system in complex than that in "free" crown. The shift of signal of N-H proton in hydrocarbon linked derivative **4** upon lead(II) complexation is lower (+0.26 ppm).

The investigation of nature of metal complexes and organometallic compounds with MS spectrometry is often challenging [39]. MS spectra of complexes of crowns **1**–**4** with lead(II) were registered using ESI ionization method in positive ions mode (acetonitrile as a solvent). Observed under measurement conditions peaks of m/z 1636 for compound **3** (Figure S1e) and m/z 1847 for compound **4** (Figure S2e) can correspond to complexes of 3:2 stoichiometry of composition corresponding to two ionized crowns, one non-ionized macrocycle, two lead(II) cations and one perchlorate anion (Table 1). Analogous peaks were observed in spectra of complexes of crown **1** (m/z 1644) and crown **2** (m/z 1776). Peak m/z 1948 in spectrum of **4** corresponds to three macrocyles with one being ionized, two lead cations and two perchlorate anions. Analogous peaks were also detected in ESI spectra of crowns **1** and **2**: m/z 1745 and 1876, respectively. This confirms the possibility of formation of complexes of proposed stoichiometry in acetonitrile solution, which was proposed on the basis of Job's plots obtained from UV–VIS measurements. However, besides mentioned above ions, under mass spectra measurement conditions, a number of other ionic species

were detected (Table 1) that may be the result yet another ionization of complexes under MS measurements (e.g., peaks corresponding to 3:3 stoichiometry) and the fragmentation of the above. Theoretically calculated and experimental isotope patterns of assigned peaks are shown in Supplementary Data (Figure S11–S14).

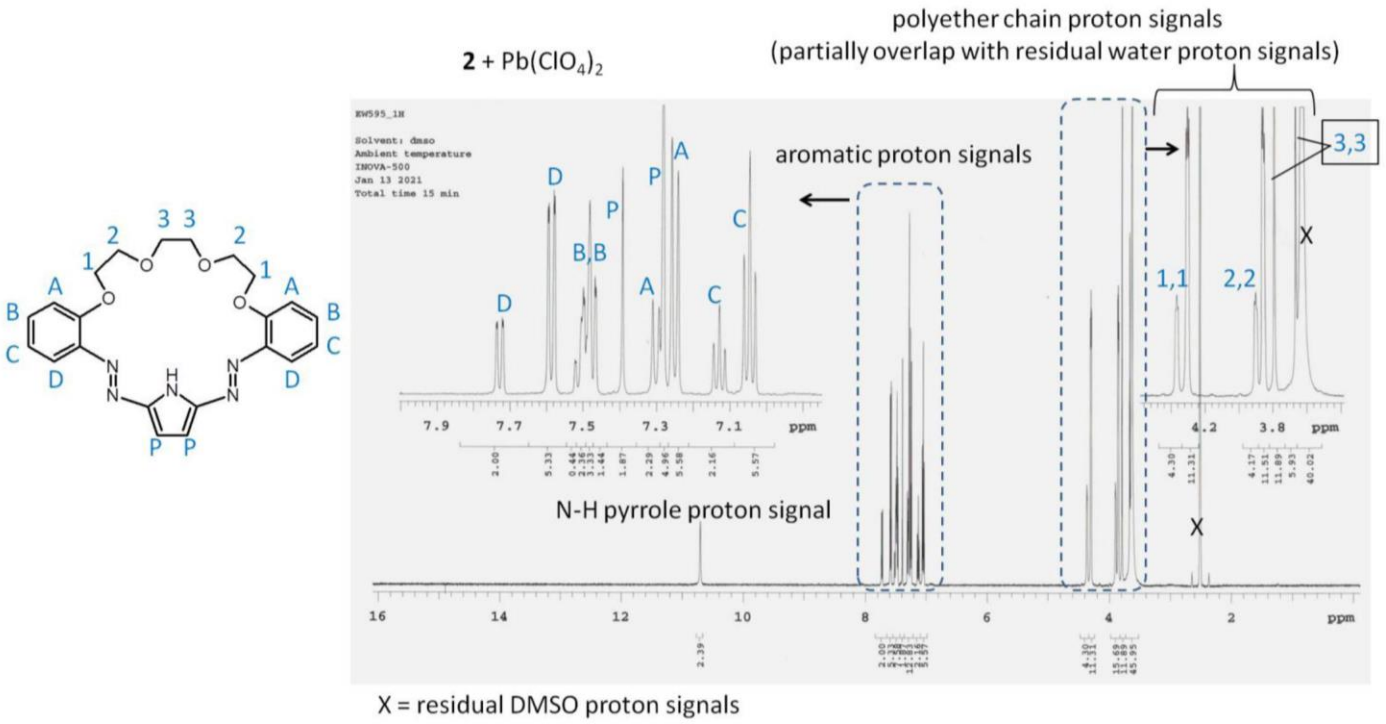

Figure 5. ^{1}H NMR spectrum of **2** (1.1×10^{-2} M) in the presence of lead(II) perchlorate, molar ratio of components—crown:lead(II) perchlorate 3:2 (DMSO-d_6).

Table 1. Ionic species in ESI MS (positive mode) spectra of complexes of crowns **1–4** with lead(II).

Crown	Model	m/z *	Figure
1	$[3(C_{20}H_{18}N_5O_3)^-][3Pb^{2+}][2ClO_4^-]$	1950	S11a
	$[2C_{20}H_{19}N_5O_3][(C_{20}H_{18}N_5O_3)^-][2Pb^{2+}][2ClO_4^-]$	1745	S11b
	$[2(C_{20}H_{18}N_5O_3)^-][C_{20}H_{19}N_5O_3][2Pb^{2+}][ClO_4^-]$	1644	S11c
	$[2(C_{20}H_{18}N_5O_3)^-][2Pb^{2+}][ClO_4^-]$	1267	S11d
	$[(C_{20}H_{18}N_5O_3)^-][Pb^{2+}]$	584	S11e
2	$[3(C_{22}H_{22}N_5O_4)^-][3Pb^{2+}][2ClO_4^-]$	2082	S12a
	$[2C_{22}H_{23}N_5O_4][(C_{22}H_{22}N_5O_4)^-][2Pb^{2+}][2ClO_4^-]$	1876	S12b
	$[2(C_{22}H_{22}N_5O_4)^-][C_{22}H_{23}N_5O_4][2Pb^{2+}][ClO_4^-]$	1776	S12c
	$[2(C_{22}H_{22}N_5O_4)^-][2Pb^{2+}][ClO_4^-]$	1355	S12d
	$[(C_{22}H_{22}N_5O_4)^-][Pb^{2+}]$	628	S12e
3	$[3(C_{21}H_{20}N_5O_2)^-][3Pb^{2+}][2ClO_4^-]$	1944	S13a
	$[2(C_{21}H_{20}N_5O_2)^-][C_{21}H_{21}N_5O_2][2Pb^{2+}][ClO_4^-]$	1638	S13b
	$[2(C_{21}H_{20}N_5O_2)^-][2Pb^{2+}][ClO_4^-]$	1263	S13c
	$[(C_{21}H_{20}N_5O_2)^-][C_{21}H_{21}N_5O_2][Pb^{2+}]$	957	S13d
	$[(C_{21}H_{20}N_5O_2)^-][Pb^{2+}]$	582	S13e
4	$[3(C_{26}H_{30}N_5O_2)^-][3Pb^{2+}][2ClO_4^-]$	2154	S14a
	$[2C_{26}H_{31}N_5O_2][(C_{26}H_{30}N_5O_2)^-][2Pb^{2+}][2ClO_4^-]^-$	1948	S14b
	$[2(C_{26}H_{30}N_5O_2)^-][C_{26}H_{31}N_5O_2][2Pb^{2+}][ClO_4^-]$	1847	S14c
	$[2(C_{26}H_{30}N_5O_2)^-][2Pb^{2+}][ClO_4^-]$	1403	S14d
	$[(C_{26}H_{30}N_5O_2)^-][Pb^{2+}]$	652	S14e

* Value corresponding to the peak of the highest intensity in model isotope pattern.

In the FTIR spectrum registered for lead(II) complex of **4** (not shown here), the band corresponding to perchlorate ion is localized at 1104 cm^{-1} suggesting that counter ion is not engaged in complex formation.

On the basis of the above, we propose as probable, but still assumed, a binding model of lead(II) as triple-decker complex for oligoether bearing crowns and for hydrocarbon linked macrocycles (Figure 6).

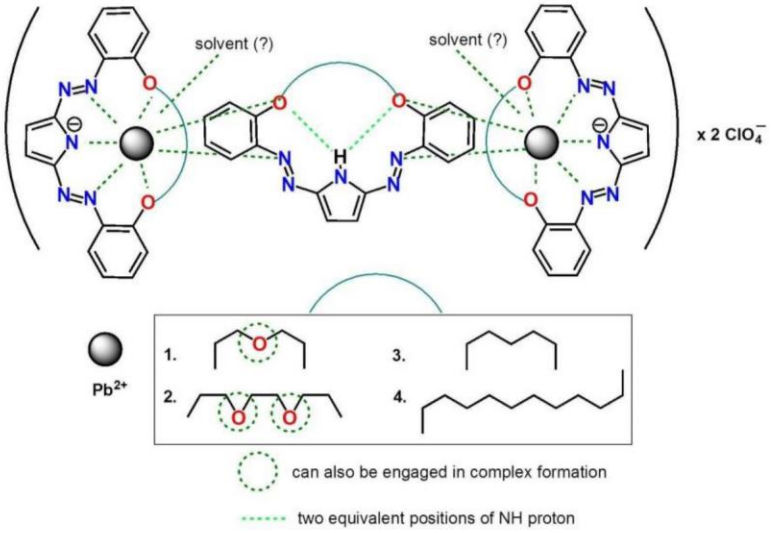

Figure 6. Proposed, simplified model (as triple-decker complex) of lead(II) binding by diazocrowns **1**–**4** bearing pyrrole moiety.

For crown **4,** the presence of nickel(II) and zinc(II) perchlorates in acetonitrile results in the creation of absorption bands of complexes at 567 and 565 nm, respectively. However due to the spectral changes within time (exemplified with titration trace for **4** shown in Figure 7a for nickel(II) and in Figure S5 for zinc (II)), the determination of reliable value of stability constant values of complexes of **4** with zinc(II) and nickel(II) perchlorates was not possible under measurements conditions. For **3** nickel(II) and zinc(II) perchlorates presence causes negligible changes in UV–VIS absorption spectra under titration measurements conditions.

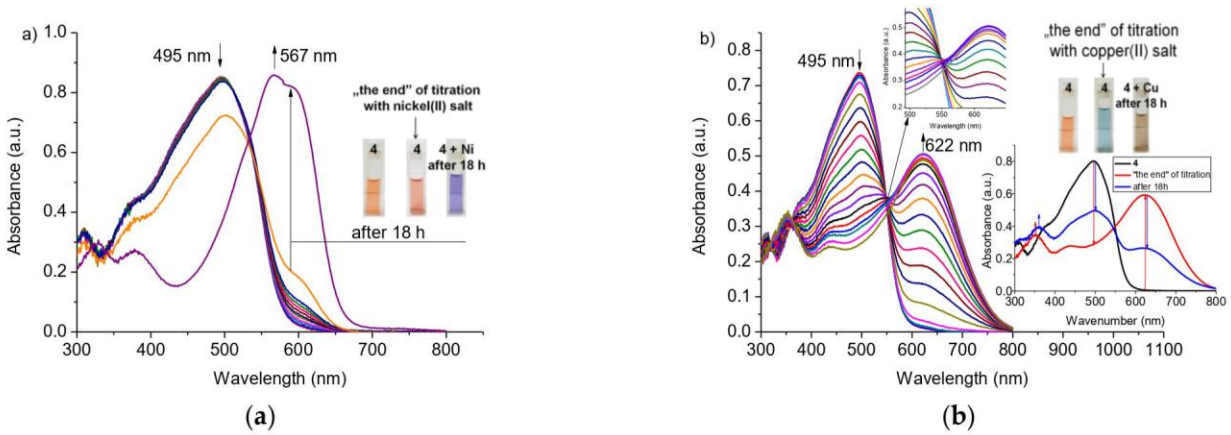

Figure 7. Changes in UV–VIS spectra of **4** upon titration with: (**a**) nickel(II) (c_4 = 3.75 × 10^{-5} M, c_{Ni} = 0–1.35 × 10^{-3} M)—band of the highest absorbance at 567 nm corresponds to absorption spectrum of titrated solution registered after 18 h; (**b**) copper(II) (c_4 = 3.75 × 10^{-5} M, c_{Cu} = 0–4.74 × 10^{-5} M) perchlorates in acetonitrile. Insets: Color change of solutions and change of UV–VIS spectrum for **4**—Cu system after 18 h.

In case of titration with copper(II), perchlorate changes within the time of experiment were observed for **3** and **4**, however, different than for nickel(II) and zinc(II) perchlorates (exemplified with titration trace for **4** in Figure 7b). The clear isosbestic point (550 nm) loses its sharpness (Figure 7b, inset) within the progress of the titration experiment. It can point to the change of complexation equilibrium or the occurrence of other process in the presence of copper(II) perchlorate in acetonitrile. After 18 h, the solution turns to brown, which might be an effect of the changes in the chromophore system resulting from the redox process. The nature, including identification of products of interactions pyrrole bearing diazocrowns with copper(II) in acetonitrile, is under elaboration by our group.

The effect of interfering metal perchlorates on the spectral response of **3** and **4** towards lead(II) in comparison with their oligoether analogs **1** and **2** was investigated. In competing studies, the absorbance of solutions of crowns **1**–**4** in the presence of lead(II) perchlorate (equimolar amount) was measured before (A_0) and just after (A) addition of interfering metal perchlorate in 10-fold excess to lead(II) perchlorate. The influence of tested interfering metal perchlorates on spectrophotometric response towards lead(II), as the relative response RR%, is presented in Figure 8. For most investigated metal cations, the effect of their presence can be treated as negligible, as the RR% value is below 5%.

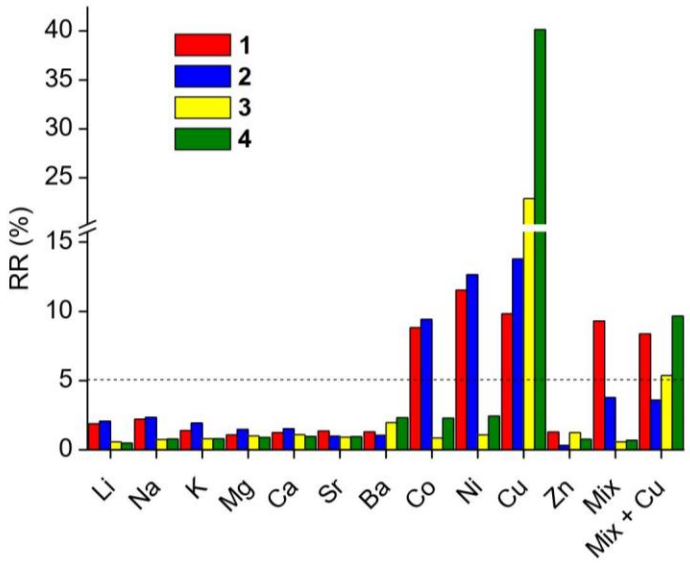

Figure 8. Interferences from several metal perchlorates, used in 10-fold excess, on the spectrophotometric response towards lead(II) for **1** (2.54×10^{-5} M) at 605 nm, **2** (2.73×10^{-5} M) at 610 nm, **3** (2.08×10^{-5} M) at 610 nm and **4** (2.63×10^{-5} M) at 605 nm in acetonitrile (Mix—mixture of metal perchlorates without copper).

The strongest effect on the absorbance of solution crowns **1**–**4** has copper(II) perchlorate and thus soft copper(II) must be considered as the main interfering metal perchlorate in acetonitrile and also as an oxidant. Alkali and alkaline earth metal cations stronger influence the optical response of oligoether bearing crowns **1** and **2**, crowns **3** and **4** bearing hydrocarbon linkage. This can be connected with the hard nature of these cations stronger interaction with the hard oxygen donor atom of the oligoether chain [26]. Moreover, heavy metal cations—cobalt(II) and nickel(II)—affect the spectrophotometric response of crowns **1** and **2** more that in it is observed for macrocycles **3** and **4**. The individual spectral response given as a change of absorbance of each crown in the presence of the equimolar amount of lead(II) perchlorate and the influence of the presence of 10-fold molar excess of interfering metal perchlorates is shown in Figure S6a–d.

The limits of detection (LOD) for lead(II) in acetonitrile determined from UV–VIS measurements were found to be 5.84×10^{-6} M (n = 10) and 6.22×10^{-6} M (n = 20) with linear response range 6.23×10^{-6}–2.26×10^{-5} M for **3** (Figure S7). For 23-membered

crown, **4** LODs were determined as 7.63×10^{-7} M (n = 10) and 9.17×10^{-7} M (n = 20) with a linear response range 1.05×10^{-6}–2.22×10^{-5} M (Figure S8).

3.4. Possible Applications

Promising results obtained in the acetonitrile solution prompted us to check the possibilities of using compound **3** as colorimetric lead(II) sensor in the presence of added water. Spectral changes upon titration of **3** with lead(II) perchlorate in acetonitrile:water solution (9:1, *v/v*) at pH 5 (HCl) are shown in Figure 9a. Under such measurement conditions, the spectral changes are significant (bathochromic shift of 96 nm) with a clear isosbestic point suggesting two species under equilibrium. In the mixed solvent system, at pH 5, the effect of an interfering metal cation, including heavy metal cations, is minor than in the acetonitrile solution (Figure 9b). For the most interfering cation in acetonitrile—copper(II)—the RR% value is below 8%. Interferences from several metal perchlorates, used in 10-fold excess, on the spectrophotometric response (change of absorbance) towards systems containing an equimolar amount of lead(II) perchlorate for **3** (2.13×10^{-5} M) at 608 nm at equimolar (to crown) amount of lead(II) perchlorate in acetonitrile:water (9:1, *v/v*) solution at pH 5 are shown in Figure S6e.

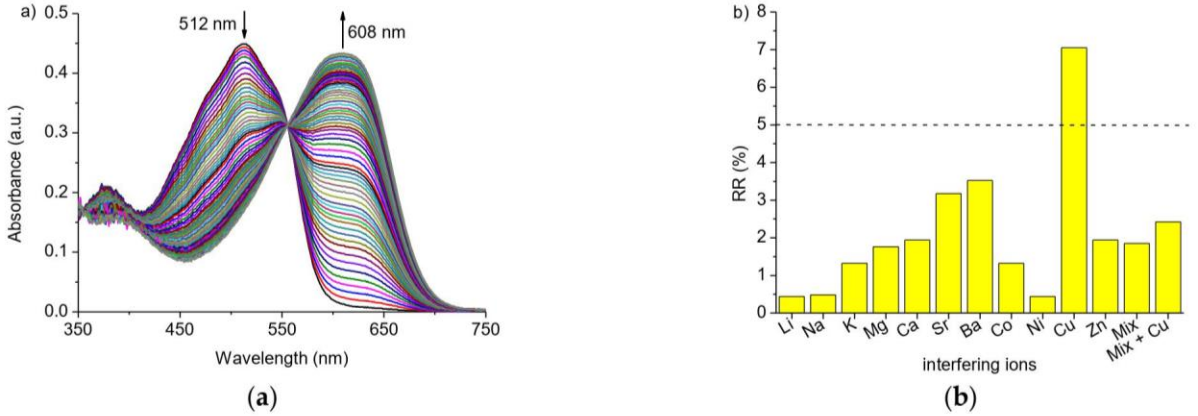

(**a**) (**b**)

Figure 9. (**a**) Changes in the absorption spectrum of crown **3** ($c_3 = 2.13 \times 10^{-5}$ M) upon titration with lead(II) perchlorate (c_{Pb} = 0–4.94×10^{-4} M); (**b**) interferences from several metal perchlorates at 10-fold molar excess on spectrophotometric response of 3 ($c_3 = 2.13 \times 10^{-5}$ M) at 608 nm at equimolar (to crown) amount of lead(II) perchlorate in acetonitrile:water (9:1, *v/v*) solution at pH 5.

The linear response range A = f([Pb(II)]) was determined within 5.00×10^{-7}–1.20×10^{-5} M ($R^2 = 0.9950$) with LOD 2.71×10^{-7} M (Figure S8a). the linear response range can be widened to 5.00×10^{-6}–1.15×10^{-4} M ($R^2 = 0.9995$) using semi the logarithmic scale A = f(log[Pb(II)]), however, with an increase of the limit of detection to 2.97×10^{-6} M (Figure S9). It is worth noting that LODs values are lower in the water containing system than in pure acetonitrile.

For testing the possibility of using **3** as lead(II) sensor, a certain amount of Standard Reference Solution of lead(II) (1000 ppm) was diluted with water and added to acetonitrile solution of crown **3** to maintain 9:1 (*v/v*) solvent mixture at pH 5 (NaOH). The concentration of lead(II) was determined, using calibration curve A = f([Pb(II)]), as 5.06×10^{-7} M showing recovery 102.73% (concentration determined with ICP-OES: 4.93×10^{-7} M). Semilog calibration curve in this case did not allow the determination of lead(II) concentration as it is below LOD. The influence of the sample matrix of drinking water was checked using **3** for lead(II) determination in spiked tap water samples. Recoveries (%), collected in Table 2, are within 97.67–102.42 depending on the type of calibration curve.

Table 2. Determination of lead(II) in spiked tap water samples using crown **3** as colorimetric probe.

Water Sample	Added Pb(II) (mol/dm^3)	Found Pb(II) (mol/dm^3)		Recovery (%)	
		A = f([Pb(II)])	A = f(log [Pb(II)])	A = f([Pb(II)])	A = f(log [Pb(II)])
Tap water 1	no addition	<LOD		-	
	2.00×10^{-6}	1.95×10^{-6}	-	97.68	-
	4.00×10^{-6}	3.94×10^{-6}	-	98.58	-
	8.00×10^{-6}	8.19×10^{-6}	7.81×10^{-6}	102.42	97.67
	2.00×10^{-5}	-	1.97×10^{-5}	-	98.54
	4.00×10^{-5}	-	4.05×10^{-5}	-	101.18
	8.00×10^{-5}	-	8.14×10^{-5}	-	101.77
Tap water 2	no addition	<LOD		-	
	2.00×10^{-6}	2.04×10^{-6}	-	102.19	-
	4.00×10^{-6}	4.03×10^{-6}	-	100.84	-
	8.00×10^{-6}	8.10×10^{-6}	7.89×10^{-6}	101.29	98.68
	2.00×10^{-5}	-	2.01×10^{-5}	-	100.59
	4.00×10^{-5}	-	3.96×10^{-5}	-	99.12
	8.00×10^{-5}	-	8.06×10^{-5}	-	100.73

- out of linear response range.

Newly obtained macrocycles **3** and **4** were also preliminarily tested as components of ion-sensitive optical layers. Test strips bearing crown **4** show color changes in the presence of heavy metal cations nitrates (10^{-2} M) opposite to material obtained with the use of crown **3** (Figure 10).

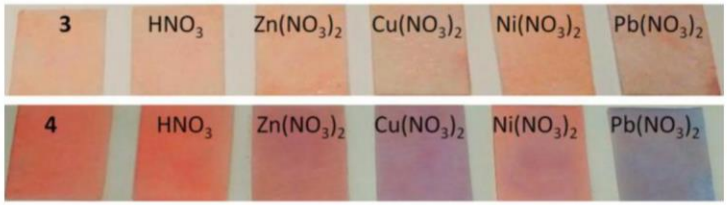

Figure 10. Changes of the color of test strips (glass filter) with adsorbed crowns **3** (2.9×10^{-4} M) and **4** (3.1×10^{-4} M) after immersing them for 15 s in solutions of (from left): deionized water, nitric acid (10^{-1} M) and metal nitrates (10^{-2} M) at pH 5.

Crowns **3** and **4** were also incorporated into PVC-based optodes to test them as potential ionophores for lead(II) detection in water. Results are shown in Figure 11. Sensing material with crown **4** as chromoionophore shows a more distinct color change from red to blue both just after immersing in lead(II) containing solution and after some time.

The preliminary results presented above show that novel lipophilic macrocycles **3** and **4** can be potentially considered as lead(II) receptors in a mixed water containing solvent system and in aqueous solutions. Currently, work in our group is focused on more detailed studies (polymer matrix type, plasticizer, lipophilic salt, and amount of chromoionophore) on the possibilities of immobilization of macrocycles **1**–**4** to obtain lead(II) sensitive optical layers. Results will be published in a specialized analytical chemistry journal.

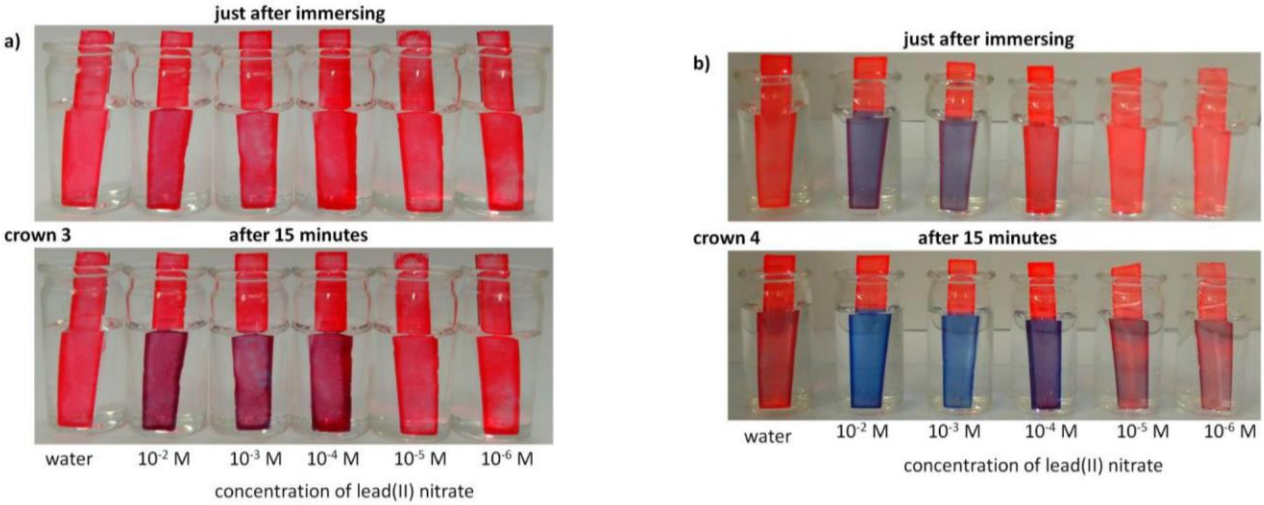

Figure 11. Color change of PVC based optodes bearing crown (**a**) **3** and (**b**) **4** upon immersion in solutions (pH 5) of lead(II) nitrate of different concentrations and, for comparison, in deionized water.

4. Conclusions

Novel 18- and 23-membered diazocrowns with hydrocarbon chain in macrocycle—compounds **3** (C5) and **4** (C10)—were obtained with satisfactory macrocyclization yields in reactions carried out under high dilution technique. For the first time for this class of macrocycles, lipophilicity values were given—important parameter characterizing compounds as candidates for new sensing materials (e.g., optodes). Macrocycles interact with metal cations in acetonitrile showing, analogously to their oligoether analogs, lead(II) selectivity. The introduction of hydrocarbon linkage in compounds **3** and **4** does not affect very strongly the mode and the strength of lead(II) binding comparing oligoether analogs **1** and **2** but makes them more selective in an acetonitrile and mixed acetonitrile-water system. The long, flexible ten carbon atoms linkage probably affects the size of the macrocylic cavity, and thus, lead(II) affinity for 23-membered crown is similar to 18-memered analog **1**. Crown **3** was successfully used as selective and sensitive colorimetric probe for lead(II) determination in organic solvent with the addition of water with limit of detection 2.71×10^{-7} M (56.1 μg/L). The proposed system can be regarded as competing with relatively expensive atomic spectroscopy methods. The obtained results have led the current work in our group to be focused on using crowns **1**–**4** as potential chromoionophores for lead(II) selective optodes, which will be published elsewhere.

Supplementary Materials: The following are available online at https://www.mdpi.com/article/10.3390/ma14237239/s1. 1. Spectra of compounds **3** and **4** and lead(II) complexes: Figure S1a. ^{1}H NMR of **3** (d-chloroform); Figure S1b. ^{13}C NMR of **3** (DMSO-d6); Figure S1c. LRMS (EI) of **3**; Figure S1d. HRMS (EI) of **3**; Figure S1e. Fragmentation pattern for lead(II) complex (ESI—positive ions mode) of **3** and part of mass spectrum presenting isotopic lead(II) peaks with peak of the highest intensity m/z 1636; Figure S2a. ^{1}H NMR of **4** (DMSO-d6); Figure S2b. ^{13}C NMR of **4** (DMSO-d_6); Figure S2c. LRMS (EI) of **4**; Figure S2d. HRMS (EI) of **4**; Figure S2e. Part of ESI-LR (positive ions mode) spectrum of lead(II)complex of **4** comparison of model of isotopic peaks for peak of m/z 1848. 2. Complexation studies—spectroscopic methods: Table S1. Stability constant (log*K*) values of diazocrowns lead(II) complexes **1**–**4** in acetonitrile; Figure S3a. 1H NMR spectrum of **2** (1.6×10^{-2} M) (DMSO-d_6); Figure S3b. Top: ^{1}H NMR spectrum of **2** (1.6×10^{-2}M) in the presence of 10-fold excess of lead(II) perchlorate; bottom: comparison of the spectral pattern of proton signals in free crown **2** and its spectrum in the presence of 10-fold excess lead(II) perchlorate (DMSO-d_6); Figure S3d ^{1}H NMR spectrum of **2** (1.1×10^{-2}M) in the presence of of lead(II) perchlorate, molar ratio of components—crown: lead(II) perchlorate 3:2 (DMSO-d_6); Figure S4a. ^{1}H NMR spectrum of **4** (1.6×10^{-2} M) (DMSO-d_6); Figure S4b. Top: ^{1}H NMR spectrum of **4** (1.6×10^{-2}M) in the presence of 10-fold excess of lead(II) perchlorate; bottom comparison of the spectral pattern of proton signals in free crown 4 and its spectrum in the presence of 10-fold excess lead(II) perchlorate (DMSO-d_6); Figure S5.

UV-Vis titration trace and color change for **4** ($c_4 = 3.14 \times 10^{-5}$ M) and zinc(II) perchlorate (c_{Zn} = 0–1.76×10^{-3} M) in acetonitrile. Bottom: color changes of the solutions; Figure S6. Interferences from several metal perchlorates, used in 10-fold excess, on spectrophotometric response towards systems containing equimolar amount of lead(II) perchlorate for (a) **1** (2.54×10^{-5} M) at 605 nm, (b) **2** (2.73×10^{-5} M) at 610 nm, (c) **3** (2.08×10^{-5} M) at 610 nm and (d) **4** (2.63×10^{-5} M) at 605 nm in acetonitrile (Mix—mixture of metal perchlorates without copper). (e) interferences from several metal perchlorates, used in 10-fold excess, on spectrophotometric response towards systems containing equimolar amount of lead(II) perchlorate for **3** (2.13×10^{-5} M) at 608 nm at equimolar (to crown) amount of lead(II) perchlorate in acetonitrile:water (9:1, *v/v*) solution at pH 5; Figure S7. (a) The relationship A = f([Pb(II)]) at 610 nm and (b) linear range of response towards lead(II) perchlorate for **3** in acetonitrile; Figure S8. (a) The relationship A = f([Pb(II)]) at 605 nm and (b) linear range of response towards lead(II) perchlorate for **4** in acetonitrile; Figure S9. The relationship (a) A = f ([Pb(II)]) with linear range of response 5.00×10^{-7}–1.20×10^{-5} M (b) A = f (log([Pb(II)]) with linear range of response 5.00×10^{-6}–1.15×10^{-4} M for 3 ($c_3 = 2.13 \times 10^{-5}$ M) in acetonitrile:water (9:1, *v/v*) solution at pH 5 at 608 nm; Figure S10. RP18-TLC chromatograms of crowns **1**–**4** and standard substances a–e; **4**. Ionic species detected in ESI mass spectra of lead(II) complex of crown **1**: Figure S11a. Theoretically calculated and experimental isotope pattern of peak m/z 1950 in lead(II) complex of **1**; Figure S11b. Theoretically calculated and experimental isotope pattern of peak m/z 1745 in lead(II) complex of **1**; Figure S11c. Theoretically calculated and experimental isotope pattern of peak m/z 1644 in lead(II) complex of 1; Figure S11d. Theoretically calculated and experimental isotope pattern of peak m/z 1267 in lead(II) complex of 1; Figure S11e. Theoretically calculated and experimental isotope pattern of peak m/z 584 in lead(II) complex of **1**; **4**. Ionic species detected in ESI mass spectra of lead(II) complex of crown **2**: Figure S12a. Theoretically calculated and experimental isotope pattern of peak m/z 2082 in lead(II) complex of 2; Figure S12b. Theoretically calculated and experimental isotope pattern of peak m/z 1876 in lead(II) complex of **2**; Figure S12c. Theoretically calculated and experimental isotope pattern of peak m/z 1776 in lead(II) complex of 2; Figure S12d. Theoretically calculated and experimental isotope pattern of peak m/z 1335 in lead(II) complex of **2**; Figure S12e. Theoretically calculated and experimental isotope pattern of peak m/z 628 in lead(II) complex of **2**; **5**. Ionic species detected in ESI mass spectra of lead (II) complex of crown **3**: Figure S13a. Theoretically calculated and experimental isotope pattern of peak m/z 1944 in lead(II) complex of **3**; Figure S13b. Theoretically calculated and experimental isotope pattern of peak m/z 1636 in lead(II) complex of **3**; Figure S13c. Theoretically calculated and experimental isotope pattern of peak m/z 1263 in lead(II) complex of **3**; Figure S13d. Theoretically calculated and experimental isotope pattern of peak m/z 957 in lead(II) complex of **3**; Figure S13e. Theoretically calculated and experimental isotope pattern of peak m/z 582 in lead(II) complex of **3**; **6**. Ionic species detected in ESI mass spectra of lead (II) complex of crown **4**: Figure S14a. Theoretically calculated and experimental isotope pattern of peak m/z 2154 in lead(II) complex of **4**; Figure S14b. Theoretically calculated and experimental isotope pattern of peak m/z 1948 in lead(II) complex of **4**; Figure S14c. Theoretically calculated and experimental isotope pattern of peak m/z 1848 in lead(II) complex of **4**; Figure S14d. Theoretically calculated and experimental isotope pattern of peak m/z 1403 in lead(II) complex of **4**; Figure S14e. Theoretically calculated and experimental isotope pattern of peak m/z 652 in lead(II) complex of **4**; **7**. X-ray structure of **3**: Crystallographic details; Figure S15. Molecular view of **3** showing atom labeling scheme; Table S2. Crystal data and structure refinement details for **3**; Figure S16. Crystal packing in **3**. Some molecules form stacking layers in parallel, but some pack almost perpendicular to them making complex space-filling pattern. Molecules are coloured by symmetry operation type, hydrogen atoms omitted; Experimental details; Computing details.

Author Contributions: Conceptualization, E.W.-W.; investigation, B.G., J.C. and E.W.-W.; validation, E.W.-W. and E.L.; methodology, B.G., J.C., E.L. and E.W.-W.; formal analysis, E.W.-W. and E.L.; data curation, B.G., J.C. and E.W.-W.; writing—original draft preparation, B.G., J.C. and E.W.-W.; writing—review and editing, E.W.-W., E.L.; visualization, B.G. and E.W.-W.; supervision, E.W.-W.; resources, E.L. All authors have read and agreed to the published version of the manuscript.

Funding: This work was supported by the Faculty of Chemistry, Gdańsk University of Technology, No. 034718 and 035138—an internal grants from statutory funds.

Institutional Review Board Statement: Not applicable.

Informed Consent Statement: Not applicable.

Data Availability Statement: Data sharing is not applicable.

Acknowledgments: Aleksandra Zasada and Ewa Gruba (Mass Spectrometry Laboratory, Laboratory for Analysis of Bioactive Compounds, Institute of Organic Chemistry of Polish Academy of Sciences, Warsaw, Poland) are kindly acknowledged for their engagement and help in registration of mass spectra of complexes.

Conflicts of Interest: The authors declare no conflict of interest.

Appendix A

CCDC 2081633 contains the supplementary crystallographic data for 3. These data can be obtained free of charge via http://www.ccdc.cam.ac.uk/conts/retrieving.html (accessed on 12 October 2021), or from the Cambridge Crystallographic Data Centre, 12 Union Road, Cambridge CB2 1EZ, UK; fax: (+44) 1223-336-033; or e-mail: deposit@ccdc.cam.ac.uk.

References

1. Andreas, A.L.; Browser, S.S. Effects of lead and cadmium exposure on oxygen respiration rates of individual Antarctic foraminifera during agglutinated shell formation. *J. Exp. Mar. Biol. Ecol.* **2021**, *537*, 51514. [CrossRef]
2. Nordberg, G.F.; Fowler, B.A.; Nordberg, M.; Friberg, L. *Handbook on the Toxicology of Metals*; Academic Press: Amsterdam, The Netherlands, 2007.
3. Kumar, A.; Kumar, A.; Cabral-Pinto, M.; Chaturvedi, A.K.; Shabnam, A.A.; Subrahmanyam, G.; Mondal, R.; Gupta, D.K.; Malyan, S.K.; Kumar, S.S.; et al. Lead toxicity: Health hazards, influence on food chain, and sustainable remediation approaches. *Int. J. Environ. Res. Public Health* **2020**, *17*, 2179. [CrossRef] [PubMed]
4. Riva, M.A.; Lafranconi, A.; D'orso, M.I.; Cesana, G. Lead poisoning: Historical aspects of a paradigmatic "occupational and environmental disease". *Saf. Health Work* **2012**, *3*, 11–16. [CrossRef] [PubMed]
5. Montes-Santiago, J. The lead-poisoned genius: Saturnism in famous artists across five centuries. *Prog. Brain Res.* **2013**, *203*, 223–240. [CrossRef]
6. Dongore, R.S. *Lead: Toxicological Profile, Pollution Aspects and Remedial Solutions*; Chooto, P., Ed.; Intech Open: London, UK, 2020; pp. 45–64.
7. Elstrott, B.; Khan, L.; Olson, S.; Raghunathan, V.; DeLoughery, T.; Shatzel, J.J. The role of iron repletion in adult iron deficiency anemia and other diseases. *Eur. J. Haematol.* **2020**, *104*, 153–161. [CrossRef]
8. De Souza, I.D.; De Andrade, A.S.; Dalmolin, R.J.S. Lead-interacting proteins and their implication in lead poisoning. *Crit. Rev. Toxicol.* **2018**, *48*, 375–386. [CrossRef]
9. WHO. Water Sanitation and Health. Available online: https://www.who.int/teams/environment-climate-change-and-health/water-sanitation-and-health/water-safety-and-quality/drinking-water-quality-guidelines (accessed on 3 October 2021).
10. Palisoc, S.T.; Vitto, R.I.M.; Noel, M.G.; Palisoc, K.T.; Natividad, M.T. Highly sensitive determination of heavy metals in water prior to and after remediation using *Citrofortunella Microcarpa*. *Sci. Rep.* **2021**, *11*. [CrossRef]
11. Astolfi, M.L.; Conti, M.E.; Marconi, E.; Massimi, L.; Canepari, S. Effectiveness of different sample treatments for the elemental characterization of bees and beehive products. *Molecules* **2020**, *25*, 4263. [CrossRef]
12. Tang, X.; Wang, P.Y.; Buttcher, G. Ion-selective electrodes for detection of lead (II) in drinking water: A mini-review. *Environments* **2018**, *5*, 95. [CrossRef]
13. Deibler, K.; Basu, P. Continuing issues with lead: Recent advances in detection. *Eur. J. Inorg. Chem.* **2013**, *2013*, 1086–1096. [CrossRef]
14. Cai, Y.; Li, M.; Wang, M.; Li, J.; Zhang, Y.; Zhao, Y. Optical fiber sensors for metal ions detection based on novel fluorescent materials. *Front. Phys.* **2020**, *8*, 598209. [CrossRef]
15. Kassal, P.; Horak, E.; Sigurnjak, M.; Steinberg, M.D.; Steinberg, I.M. Wireless and mobile optical chemical sensors and biosensors. *Rev. Anal. Chem.* **2018**, 20170024. [CrossRef]
16. Du, X.; Xie, X. Ion-Selective optodes: Alternative approaches for simplified fabrication and signaling. *Sens. Actuators B* **2021**, *335*, 129368. [CrossRef]
17. Hosseini, S.; Marandi, F.; Şahin, E.; Musevi, S.J. Synthesis, crystal structure and thermal properties of lead(II) complex with bathophenanthroline and benzoyltrifluoroacetonate ligands. *J. Chem.* **2013**, *2013*. [CrossRef]
18. Paar, J. Some recent coordination chemistry of lead(II). *Polyhedron* **1997**, *16*, 551–566. [CrossRef]
19. Essa, S.M.; Hoidy, W.H. Spectrophotometric determination of cobalt(II) and lead(II) using (1,5-dimethyl-2-phenyl-4-((2,3,4-trihydroxy phenyl)diazenyl)-1H-pyrazol-3(2H)-one) as organic reagent: Using it as antimicrobial and antioxidants. *Nano Biomed. Eng.* **2020**, *12*, 160–166. [CrossRef]
20. Wang, Y.T.; Hu, S.; Zhang, Y.; Gong, H.; Sun, R.; Mao, W.; Wang, D.H.; Chen, Y. A colorimetric Pb2+ chemosensor: Rapid naked-eye detection, high selectivity, theoretical insights, and applications. *J. Photochem. Photobiol. A Chem.* **2018**, *355*, 101–108. [CrossRef]

21. Luboch, E.; Bilewicz, R.; Kowalczyk, M.; Wagner-Wysiecka, E.; Biernat, J.F. Azo Macrocyclic Compounds. *Adv. Supramol. Chem.* **2003**, *9*, 71–162.
22. Wagner-Wysiecka, E.; Łukasik, N.; Biernat, J.F.; Luboch, E. Azo group(s) in selected macrocyclic compounds. *J. Incl. Phenom. Macrocycl. Chem.* **2018**, *90*, 189–257. [CrossRef]
23. Wagner-Wysiecka, E.; Skwierawska, A.; Kravtsov, V.C.; Biernat, J.F. New class of chromogenic proton-dissociable azocrown reagents for alkali metal ions. *J. Supramol. Chem.* **2001**, *1*, 77–85. [CrossRef]
24. Wagner-Wysiecka, E.; Luboch, E.; Kowalczyk, M.; Biernat, J.F. Chromogenic macrocyclic derivatives of azoles-synthesis and properties. *Tetrahedron* **2003**, *59*, 4415–4420. [CrossRef]
25. Luboch, E.; Wagner-Wysiecka, E.; Fainerman-Melnikova, M.; Lindoy, L.F.; Biernat, J.F. Pyrrole azocrown ethers. Synthesis, complexation, selective lead transport and ion-selective membrane electrode studies. *Supramol. Chem.* **2006**, *18*, 593–601. [CrossRef]
26. Wagner-Wysiecka, E.; Rzymowski, T.; Fonari, M.S.; Kulmaczewski, R.; Luboch, E. Pyrrole azocrown ethers-synthesis, crystal structures, and fluorescence properties. *Tetrahedron* **2011**, *67*, 1862–1872. [CrossRef]
27. Wagner-Wysiecka, E.; Luboch, E.; Fonari, M.S. The synthesis, X-ray structure and metal cation complexation properties of colored crown with two heterocyclic residues as a part of macrocycle. *Pol. J. Chem.* **2008**, *82*, 1319–1330.
28. Wagner-Wysiecka, E.; Jamrógiewicz, M.; Fonari, M.S.; Biernat, J.F. Azomacrocyclic derivatives of imidazole: Synthesis, structure, and metal ion complexation properties. *Tetrahedron* **2007**, *63*, 4414–4421. [CrossRef]
29. Luboch, E.; Kravtsov, V.C.; Konitz, A. Reductive cyclization products of 1,2-bis(2-nitrophenoxy)ethanes. X-ray structures of 10-membered azoxycrown ether stereoisomers and the sodium iodide complex of a 20-membered azoazoxycrown. *J. Supramol. Chem.* **2001**, *1*, 101–110. [CrossRef]
30. Jaunin, R.; Holl, R. Macrocycles synthétiques. I. Action du sodium sur les o, o'-polyméthylènedioxy-bis-(benzylidène-anilines). *Helv. Chim. Acta* **1958**, *41*, 1783–1792. [CrossRef]
31. Luboch, E.; Jeszke, M.; Szarmach, M.; Łukasik, N. New bis(azobenzocrown)s with dodecylmethylmalonyl linkers as ionophores for sodium selective potentiometric sensors. *J. Incl. Phenom. Macrocycl. Chem.* **2016**, *86*, 323–335. [CrossRef]
32. Dinten, O.; Spichiger, U.E.; Chaniotakis, N.; Gehrig, P.; Rusterholz, B.; Morf, W.E.; Simon, W. Lifetime of neutral-carrier-based liquid membranes in aqueous samples and blood and the lipophilicity of membrane components. *Anal. Chem.* **1991**, *63*, 596–603. [CrossRef]
33. Dolomanov, O.V.; Bourhis, L.J.; Gildea, R.J.; Howard, J.A.K.; Puschmann, H. OLEX2: A complete structure solution, refinement and analysis program. *J. Appl. Crystallogr.* **2009**, *42*, 339–341. [CrossRef]
34. Sheldrick, G.M. SHELXT—Integrated space-group and crystal-structure determination. *Acta Cryst. A* **2015**, *71*, 3–8. [CrossRef] [PubMed]
35. Kyvala, M.; Lukes, I. Program Package "OPIUM". Available online: https://web.natur.cuni.cz/~{}kyvala/opium.html (accessed on 5 June 2021).
36. Piesch, M.; Dielmann, F.; Reichl, S.; Scheer, M. A general pathway to heterobimetallic triple-decker complexes. *Chem. Eur. J.* **2020**, *26*, 1518–1524. [CrossRef] [PubMed]
37. Babailov, S.P.; Polovkova, M.A.; Kirakosyan, G.A.; Martynov, A.G.; Zapolotsky, E.N.; Gorbunova, Y.G. NMR thermosensing properties on binuclear triple-decker complexes of terbium(III) and dysprosium(III) with 15-crown-5-phthalocyanine. *Sens. Actuators A Phys.* **2021**, *331*, 112933. [CrossRef]
38. Sitzmann, H.; Walter, M.D.; Wolmershäuser, G. A triple-decker sandwich complex of barium. *Angew. Chem. Int. Ed.* **2002**, *41*, 2315–2316. [CrossRef]
39. Scott McIndoe, J.; Vikse, K.L. Assigning the ESI mass spectra of organometallic and coordination compounds. *J. Mass. Spectrom.* **2019**, *54*, 466–479. [CrossRef] [PubMed]

P1 – SUPPLEMENTARY MATERIALS

Novel Diazocrowns with Pyrrole Residue as Lead(II) Colorimetric Probes

Błażej Galiński [1], Elżbieta Luboch [1], Jarosław Chojnacki [2], Ewa Wagner-Wysiecka [1,*]

[1] *Department of Chemistry and Technology of Functional Materials, Faculty of Chemistry, Gdańsk University of Technology, Narutowicza Street 11/12, 80-233 Gdańsk, Poland*

[2] *Department of Inorganic Chemistry, Faculty of Chemistry, Gdańsk University of Technology, Narutowicza Street 11/12, 80-233 Gdańsk, Poland*

* corresponding author: ewa.wagner-wysiecka@pg.edu.pl

1. Spectra of compounds 3 and 4 and lead(II) complexes

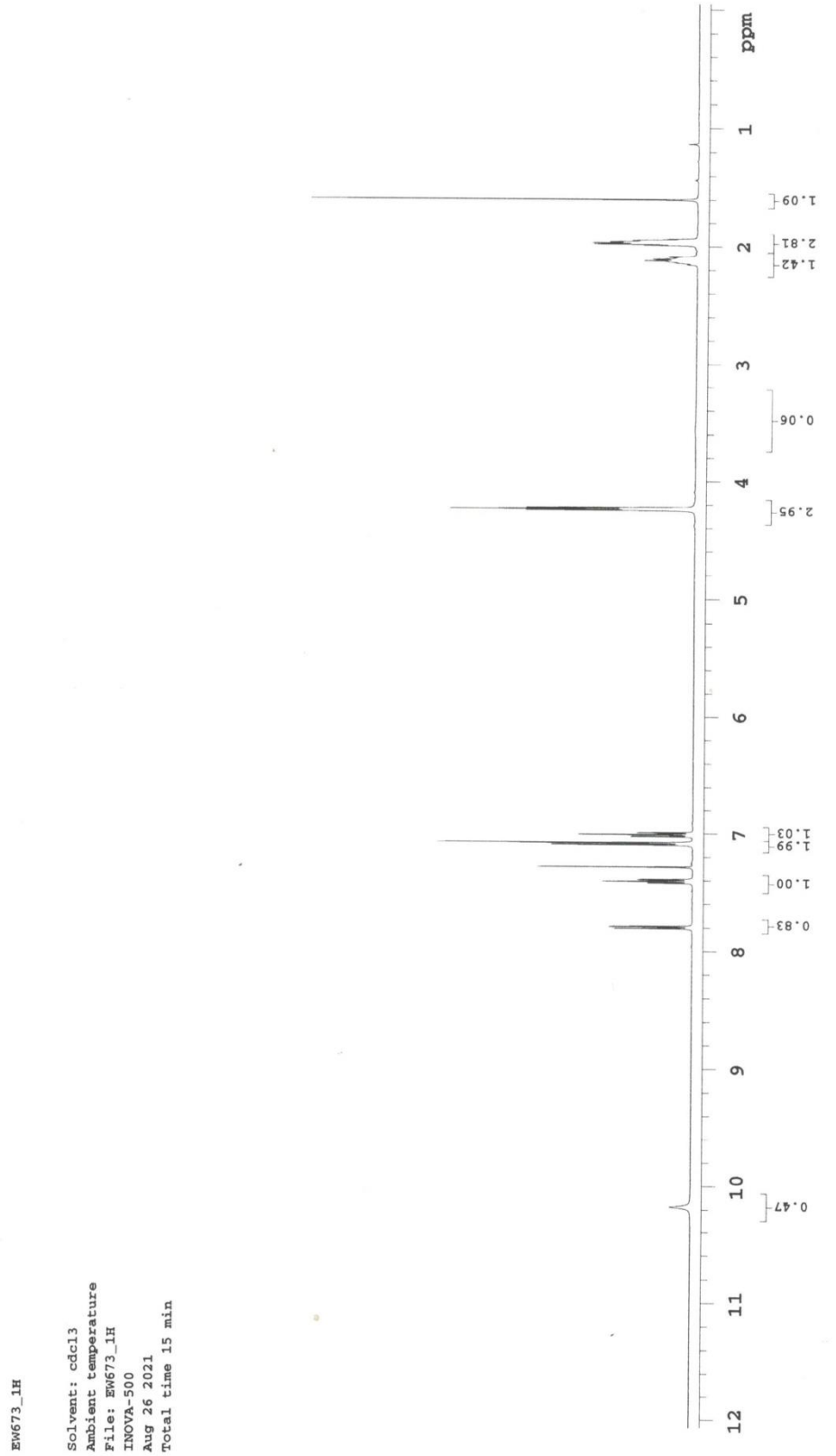

Fig. S1a. ^{1}H NMR of **3** (d-chloroform)

EW532_13Cponiedzialek
temp. 50 deg

Solvent: dmso
Temp. 50.0 C / 323.1 K
INOVA-500
Apr 18 2020
Total time 39 hr, 30 min

INDEX	FREQUENCY	PPM	HEIGHT	INDEX	FREQUENCY	PPM	HEIGHT
1	28509.9	226.857	4.3	21	3865.7	30.760	19.3
2	19770.3	157.315	9.9	22	3008.4	23.939	10.6
3	18432.6	146.671	8.9				
4	17745.1	141.200	8.2				
5	16815.9	133.806	18.4				
6	15214.5	121.064	20.7				
7	14636.3	116.463	18.8				
8	14507.8	115.440	18.1				
9	14421.5	114.754	18.7				
10	8602.8	68.453	18.0				
11	5122.9	40.763	14.6				
12	5112.3	40.679	254.6				
13	5102.7	40.603	40.2				
14	5091.2	40.511	791.9				
15	5081.6	40.435	76.7				
16	5070.1	40.344	1607.2				
17	5049.0	40.176	1902.7				
18	5027.9	40.008	1627.6				
19	5006.8	39.840	815.9				
20	4985.7	39.672	267.9				

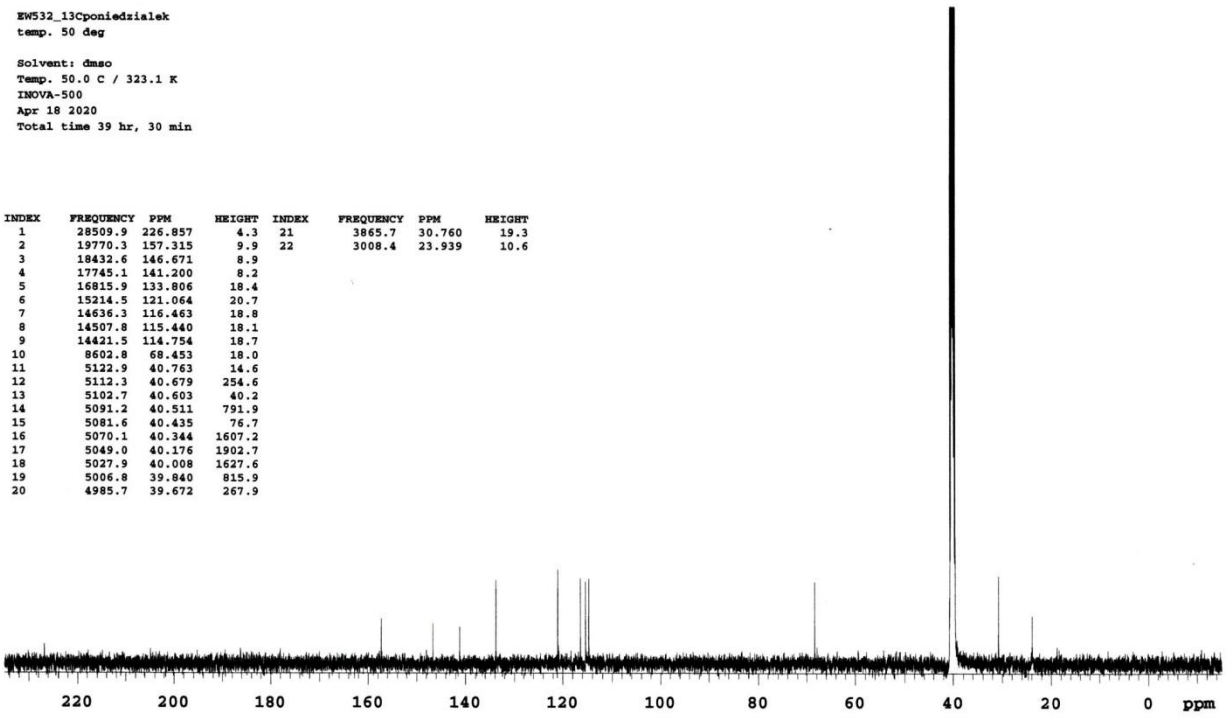

Fig. S1b. 13C NMR of 3 (DMSO-d6)

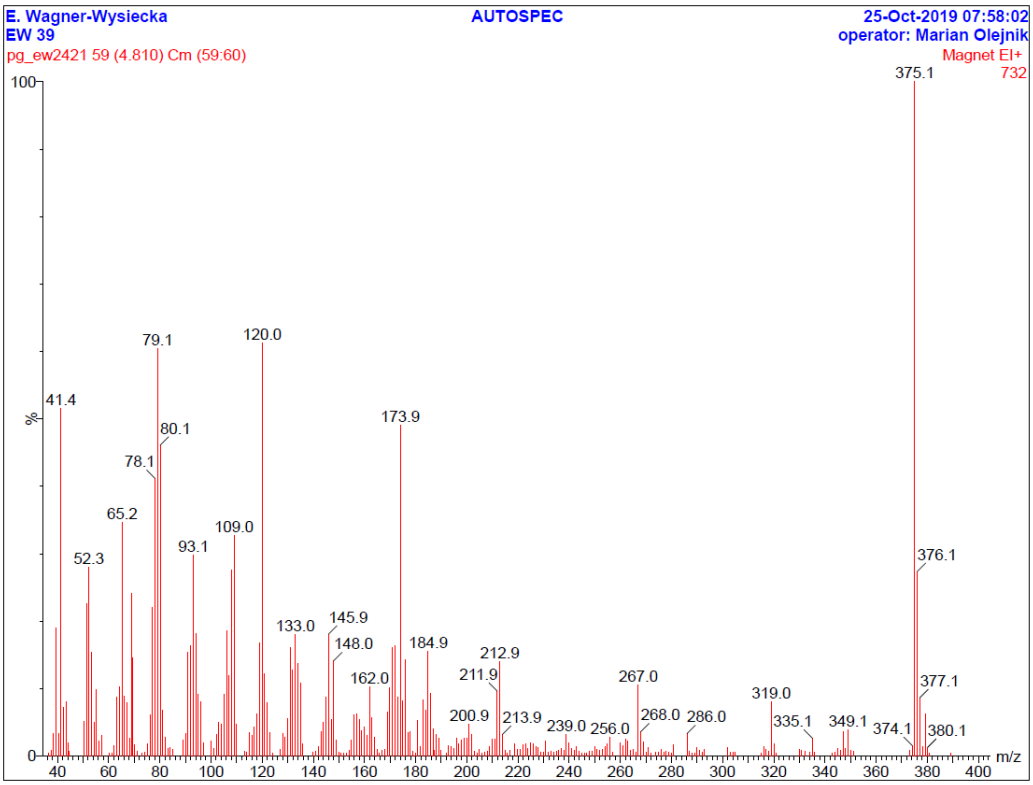

E. Wagner-Wysiecka
EW 39
pg_ew2421 59 (4.810) Cm (59:60)
AUTOSPEC
25-Oct-2019 07:58:02
operator: Marian Olejnik
Magnet EI+

No	Mass	Inten	%BPI	%TIC	No	Mass	Inten	%BPI	%TIC	No	Mass	Inten	%BPI	%TIC	No	Mass	Inten	%BPI	%TIC	No
1:	37.4	6.00e0	0.82	0.05	52:	105.0	6.70e1	9.15	0.58	103:	172.9	6.40e1	8.74	0.56	154:	240.0	1.40e1	1.91	0.12	
2:	38.4	2.40e1	3.28	0.21	53:	106.0	1.36e2	18.58	1.18	104:	173.9	3.59e2	49.04	3.12	155:	241.0	8.00e0	1.09	0.07	
3:	39.4	1.39e2	18.99	1.21	54:	107.0	8.70e1	11.89	0.76	105:	174.9	6.00e1	8.20	0.52	156:	242.0	6.00e0	0.82	0.05	
4:	40.4	2.40e1	3.28	0.21	55:	108.0	2.02e2	27.60	1.76	106:	176.0	1.04e2	14.21	0.90	157:	242.9	1.00e1	1.37	0.09	
5:	41.4	3.77e2	51.50	3.28	56:	109.0	2.39e2	32.65	2.08	107:	177.0	2.50e1	3.42	0.22	158:	250.0	1.00e1	1.37	0.09	
6:	42.4	5.30e1	7.24	0.46	57:	110.0	3.40e1	4.64	0.30	108:	178.0	2.60e1	3.55	0.23	159:	251.0	7.00e0	0.96	0.06	
7:	43.4	5.90e1	8.06	0.51	58:	115.0	2.50e1	3.42	0.22	109:	180.8	3.80e1	5.19	0.33	160:	252.0	6.00e0	0.82	0.05	
8:	44.3	1.40e1	1.91	0.12	59:	116.0	2.20e1	3.01	0.19	110:	181.9	1.00e1	1.37	0.09	161:	253.0	7.00e0	0.96	0.06	
9:	50.3	3.70e1	5.05	0.32	60:	117.0	3.10e1	4.23	0.27	111:	182.9	6.10e1	8.33	0.53	162:	254.0	1.00e1	1.37	0.09	
10:	51.3	1.65e2	22.54	1.43	61:	118.0	4.50e1	6.15	0.39	112:	183.9	4.90e1	6.69	0.43	163:	255.0	1.30e1	1.78	0.11	
11:	52.3	2.05e2	28.01	1.78	62:	119.0	1.23e2	16.80	1.07	113:	184.9	1.13e2	15.44	0.98	164:	256.0	2.00e1	2.73	0.17	
12:	53.3	1.12e2	15.30	0.97	63:	120.0	4.48e2	61.20	3.89	114:	185.9	6.80e1	9.29	0.59	165:	259.9	1.40e1	1.91	0.12	
13:	54.3	3.60e1	4.92	0.31	64:	121.0	8.90e1	12.16	0.77	115:	186.9	2.90e1	3.96	0.25	166:	260.9	1.10e1	1.50	0.10	
14:	55.3	7.20e1	9.84	0.63	65:	122.0	5.80e1	7.92	0.50	116:	187.4	6.00e0	0.82	0.05	167:	262.0	1.80e1	2.46	0.16	
15:	56.3	1.60e1	2.19	0.14	66:	123.0	2.50e1	3.42	0.22	117:	187.9	2.30e1	3.14	0.20	168:	263.0	1.60e1	2.19	0.14	
16:	57.3	2.20e1	3.01	0.19	67:	127.0	7.00e0	0.96	0.06	118:	188.9	1.90e1	2.60	0.17	169:	264.0	6.00e0	0.82	0.05	
17:	62.2	1.10e1	1.50	0.10	68:	128.0	2.40e1	3.28	0.21	119:	189.9	6.00e0	0.82	0.05	170:	265.0	7.00e0	0.96	0.06	
18:	63.2	6.40e1	8.74	0.56	69:	129.0	2.00e1	2.73	0.17	120:	192.9	1.10e1	1.50	0.10	171:	267.0	7.70e1	10.52	0.67	
19:	64.2	7.50e1	10.25	0.65	70:	130.0	4.00e1	5.46	0.35	121:	193.9	1.00e1	1.37	0.09	172:	268.0	2.60e1	3.55	0.23	
20:	65.2	2.53e2	34.56	2.20	71:	130.9	1.17e2	15.98	1.02	122:	194.9	8.00e0	1.09	0.07	173:	269.0	1.50e1	2.05	0.13	
21:	66.2	6.50e1	8.88	0.56	72:	132.0	9.30e1	12.70	0.81	123:	195.9	1.90e1	2.60	0.17	174:	271.0	9.00e0	1.23	0.08	
22:	67.2	5.80e1	7.92	0.50	73:	133.0	1.32e2	18.03	1.15	124:	196.9	1.30e1	1.78	0.11	175:	276.0	7.00e0	0.96	0.06	
23:	68.2	1.90e1	2.60	0.17	74:	134.0	1.00e2	13.66	0.87	125:	197.9	1.70e1	2.32	0.15	176:	280.9	1.20e1	1.64	0.10	
24:	69.1	1.76e2	24.04	1.53	75:	135.0	7.90e1	10.79	0.69	126:	198.9	1.90e1	2.60	0.17	177:	286.0	2.40e1	3.28	0.21	
25:	69.2	1.06e2	14.48	0.92	76:	136.0	1.30e1	1.78	0.11	127:	199.9	1.90e1	2.60	0.17	178:	290.0	9.00e0	1.23	0.08	
26:	70.2	1.20e1	1.64	0.10	77:	141.9	1.00e1	1.37	0.09	128:	200.9	3.40e1	4.64	0.30	179:	291.0	6.00e0	0.82	0.05	
27:	75.1	1.30e1	1.78	0.11	78:	142.9	2.60e1	3.55	0.23	129:	201.9	2.30e1	3.14	0.20	180:	292.9	7.00e0	0.96	0.06	
28:	76.1	4.40e1	6.01	0.38	79:	143.9	3.60e1	4.92	0.31	130:	204.9	7.00e0	0.96	0.06	181:	302.0	9.00e0	1.23	0.08	
29:	77.1	1.61e2	21.99	1.40	80:	144.9	6.40e1	8.74	0.56	131:	208.9	1.00e1	1.37	0.09	182:	316.0	1.00e1	1.37	0.09	
30:	78.1	3.01e2	41.12	2.62	81:	145.9	1.32e2	18.03	1.15	132:	209.9	1.80e1	2.46	0.16	183:	317.0	7.00e0	0.96	0.06	
31:	79.1	4.42e2	60.38	3.84	82:	147.0	3.90e1	5.33	0.34	133:	210.9	1.80e1	2.46	0.16	184:	319.0	5.90e1	8.06	0.51	
32:	80.1	3.37e2	46.04	2.93	83:	148.0	1.03e2	14.07	0.89	134:	211.9	7.00e1	9.56	0.61	185:	320.0	1.30e1	1.78	0.11	
33:	81.1	4.90e1	6.69	0.43	84:	149.0	1.70e1	2.32	0.15	135:	212.9	1.02e2	13.93	0.89	186:	330.0	7.00e0	0.96	0.06	
34:	82.1	2.00e1	2.73	0.17	85:	153.9	6.00e0	0.82	0.05	136:	213.9	2.30e1	3.14	0.20	187:	331.0	6.00e0	0.82	0.05	
35:	83.1	8.00e0	1.09	0.07	86:	154.9	1.70e1	2.32	0.15	137:	214.9	6.00e0	0.82	0.05	188:	335.1	1.90e1	2.60	0.17	
36:	84.1	9.00e0	1.23	0.08	87:	155.9	4.40e1	6.01	0.38	138:	216.9	6.00e0	0.82	0.05	189:	345.1	8.00e0	1.09	0.07	
37:	85.1	7.00e0	0.96	0.06	88:	156.9	4.50e1	6.15	0.39	139:	218.8	1.30e1	1.78	0.11	190:	346.1	6.00e0	0.82	0.05	
38:	89.1	1.70e1	2.32	0.15	89:	157.9	3.90e1	5.33	0.34	140:	219.9	7.00e0	0.96	0.06	191:	347.1	2.60e1	3.55	0.23	
39:	90.1	2.40e1	3.28	0.21	90:	158.9	2.70e1	3.69	0.23	141:	220.9	7.00e0	0.96	0.06	192:	348.1	8.00e0	1.09	0.07	
40:	91.1	1.12e2	15.30	0.97	91:	159.9	3.10e1	4.23	0.27	142:	221.9	1.20e1	1.64	0.10	193:	349.1	2.80e1	3.83	0.24	
41:	92.1	1.19e2	16.26	1.03	92:	161.0	2.20e1	3.01	0.19	143:	222.9	1.30e1	1.78	0.11	194:	350.1	6.00e0	0.82	0.05	
42:	93.1	2.18e2	29.78	1.89	93:	162.0	7.50e1	10.25	0.65	144:	223.9	8.00e0	1.09	0.07	195:	373.1	6.00e0	0.82	0.05	
43:	94.1	1.33e2	18.17	1.16	94:	163.0	4.10e1	5.60	0.36	145:	224.9	1.40e1	1.91	0.12	196:	374.1	1.10e1	1.50	0.10	
44:	95.1	6.70e1	9.15	0.58	95:	164.0	2.00e1	2.73	0.17	146:	225.9	1.30e1	1.78	0.11	197:	375.1	7.32e2	100.00	6.36	
45:	96.1	5.90e1	8.06	0.51	96:	164.9	7.00e0	0.96	0.06	147:	226.9	1.00e1	1.37	0.09	198:	376.1	2.00e2	27.32	1.74	
46:	97.1	1.40e1	1.91	0.12	97:	166.9	6.00e0	0.82	0.05	148:	228.0	9.00e0	1.23	0.08	199:	377.1	6.30e1	8.61	0.55	
47:	100.0	1.60e1	2.19	0.14	98:	167.9	7.00e0	0.96	0.06	149:	230.8	1.60e1	2.19	0.14	200:	378.1	1.00e1	1.37	0.09	
48:	101.0	8.00e0	1.09	0.07	99:	168.9	4.70e1	6.42	0.41	150:	235.9	6.00e0	0.82	0.05	201:	379.1	4.50e1	6.15	0.39	
49:	102.0	2.30e1	3.14	0.20	100:	169.9	7.40e1	10.11	0.64	151:	236.9	8.00e0	1.09	0.07	202:	380.1	9.00e0	1.23	0.08	
50:	103.0	3.60e1	4.92	0.31	101:	170.9	1.17e2	15.98	1.02	152:	237.9	6.00e0	0.82	0.05						
51:	104.0	3.40e1	4.64	0.30	102:	171.9	1.20e2	16.39	1.04	153:	239.0	2.30e1	3.14	0.20						

Fig. S1c. LRMS (EI) of **3**

Elemental Composition Report **Page 1**

Single Mass Analysis
Tolerance = 15.0 PPM / DBE: min = -1.5, max = 50.0
Selected filters: None

Monoisotopic Mass, Odd and Even Electron Ions
23 formula(e) evaluated with 1 results within limits (up to 50 best isotopic matches for each mass)
Elements Used:
C: 0-60 H: 0-100 N: 5-5 O: 0-4

E. Wagner-Wysiecka
EW 39
pg_ew2421h 264 (10.068) Cm (260:282)

AUTOSPEC

28-Oct-2019 12:59:50
Operator: Marian Olejnik
Voltage EI+
1.54e3

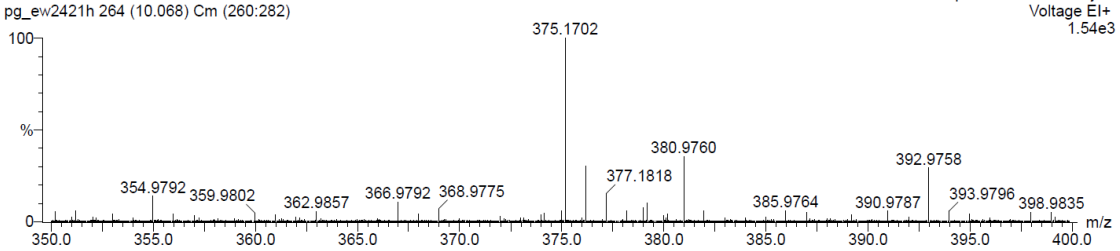

Minimum:				-1.5		
Maximum:		5.0	15.0	50.0		
Mass	Calc. Mass	mDa	PPM	DBE	i-FIT	Formula
375.1702	375.1695	0.7	1.9	14.0	72.2	C21 H21 N5 O2

Fig. S1d. HRMS (EI) of **3**

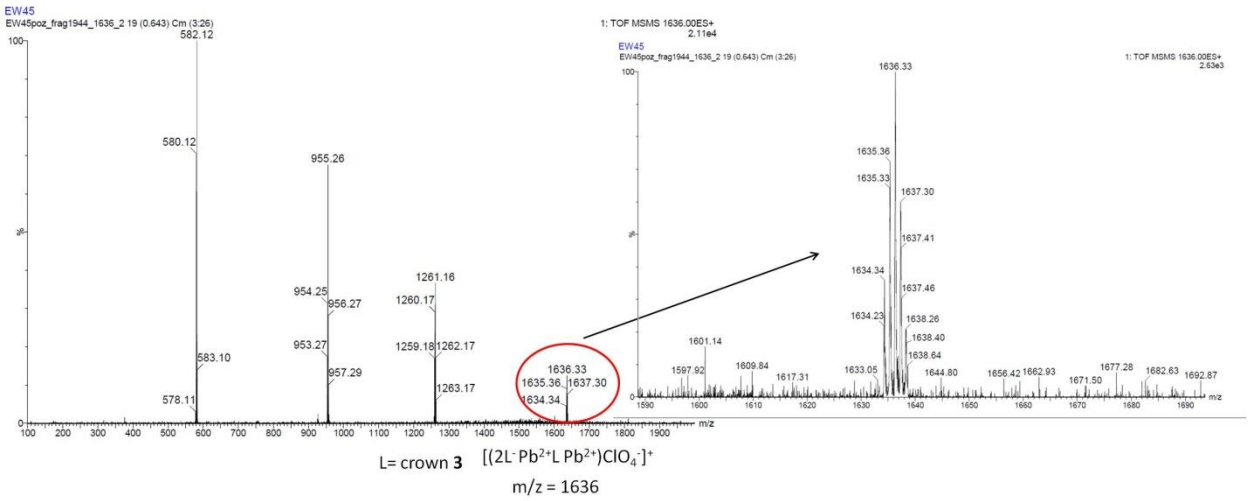

Fig S1e. Fragmentation pattern for lead(II) complex (ESI - positive ions mode) of **3** and part of mass spectrum presenting isotopic lead(II) peaks with peak of the highest intensity m/z 1636.

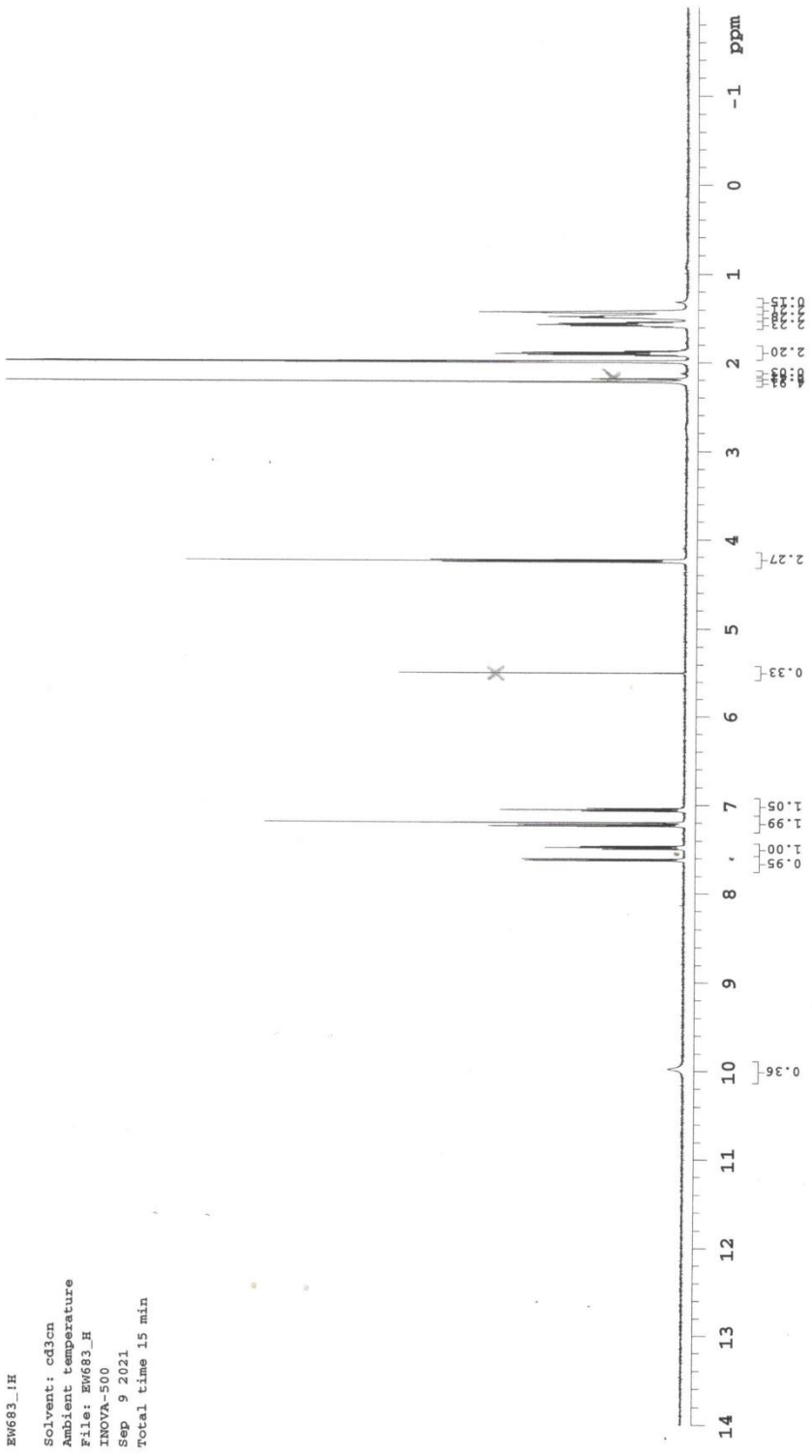

x - solvent residual impurities: 5.45 ppm - dichloromethane, 2.04 - acetone

Fig. S2a. ^{1}H NMR of **4** (acetonitrile-d3)

EW533_13C

INDEX	FREQUENCY	PPM	HEIGHT
1	19553.6	155.591	14.3
2	18497.9	147.190	11.5
3	18073.1	143.810	11.0
4	16634.7	132.364	15.4
5	15228.9	121.178	18.1
6	14814.6	117.882	18.8
7	14665.1	116.692	17.0
8	14470.4	115.143	16.8
9	8739.9	69.545	18.5
10	5086.4	40.473	27.8
11	5065.3	40.305	83.6
12	5055.7	40.229	12.1
13	5045.2	40.145	167.6
14	5024.1	39.977	200.0
15	5003.0	39.809	172.9
16	4981.9	39.642	87.2
17	4960.8	39.474	28.6
18	3620.2	28.807	22.1
19	3563.7	28.356	22.1
20	3516.7	27.983	21.0
21	3185.8	25.350	23.3

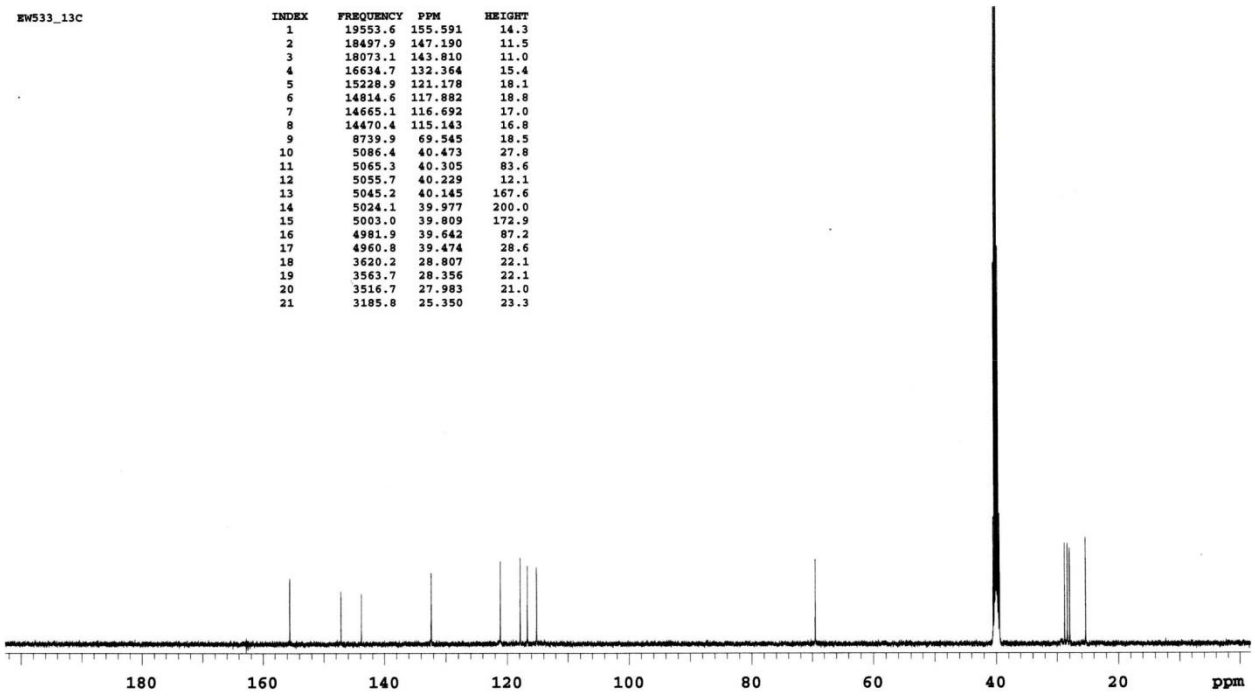

Fig. S2b. ^{13}C NMR of **4** (DMSO-d_6)

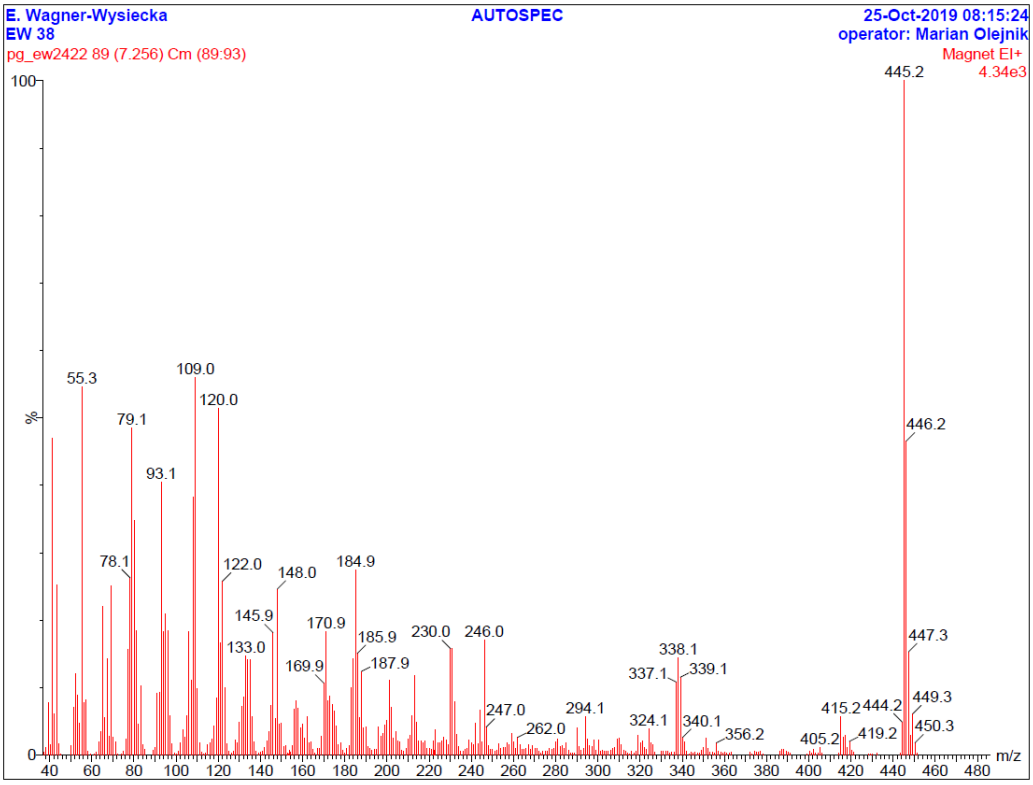

E. Wagner-Wysiecka
EW 38
pg_ew2422 89 (7.256) Cm (89:93)
AUTOSPEC
25-Oct-2019 08:15:24
operator: Marian Olejnik
Magnet EI+

No	Mass	Inten	%BPI	%TIC	No	Mass	Inten	%BPI	%TIC	No	Mass	Inten	%BPI	%TIC	No	Mass	Inten	%BPI	%TIC	No
1:	39.4	3.35e2	7.71	0.44	52:	115.0	6.70e1	1.54	0.09	103:	183.9	6.18e2	14.22	0.80	154:	253.0	6.90e1	1.59	0.09	
2:	40.4	6.30e1	1.45	0.08	53:	116.0	7.40e1	1.70	0.10	104:	184.9	1.19e3	27.41	1.55	155:	257.0	7.40e1	1.70	0.10	
3:	41.4	2.04e3	46.90	2.65	54:	117.0	1.01e2	2.32	0.13	105:	185.9	6.53e2	15.03	0.85	156:	258.0	6.40e1	1.47	0.08	
4:	42.4	2.61e2	6.01	0.34	55:	118.0	1.84e2	4.23	0.24	106:	186.9	2.43e2	5.59	0.32	157:	259.0	1.39e2	3.20	0.18	
5:	43.4	1.10e3	25.22	1.42	56:	119.0	3.67e2	8.45	0.48	107:	187.9	5.37e2	12.36	0.70	158:	260.0	8.30e1	1.91	0.11	
6:	44.4	7.20e1	1.66	0.09	57:	120.0	2.23e3	51.39	2.90	108:	188.9	1.74e2	4.00	0.23	159:	262.0	1.12e2	2.58	0.15	
7:	50.3	5.80e1	1.33	0.08	58:	121.0	7.21e2	16.59	0.94	109:	190.0	1.79e2	4.12	0.23	160:	263.0	6.50e1	1.50	0.08	
8:	51.3	3.05e2	7.02	0.40	59:	122.0	1.12e3	25.75	1.45	110:	191.0	5.60e1	1.29	0.07	161:	267.0	6.40e1	1.47	0.08	
9:	52.3	5.24e2	12.06	0.68	60:	123.0	4.32e2	9.94	0.56	111:	195.9	1.78e2	4.10	0.23	162:	269.0	5.80e1	1.33	0.08	
10:	53.3	3.86e2	8.88	0.50	61:	124.0	7.00e1	1.61	0.09	112:	196.9	1.19e2	2.74	0.15	163:	280.0	8.60e1	1.98	0.11	
11:	54.3	2.02e2	4.65	0.26	62:	128.0	9.40e1	2.16	0.12	113:	197.9	1.38e2	3.18	0.18	164:	281.0	1.04e2	2.39	0.14	
12:	55.3	2.37e3	54.61	3.08	63:	129.0	7.50e1	1.73	0.10	114:	198.9	1.94e2	4.46	0.25	165:	282.0	5.40e1	1.24	0.07	
13:	56.3	3.36e2	7.73	0.44	64:	130.0	2.13e2	4.90	0.28	115:	199.9	2.22e2	5.11	0.29	166:	283.0	5.80e1	1.33	0.08	
14:	57.3	3.56e2	8.19	0.46	65:	131.0	3.13e2	7.20	0.41	116:	200.9	4.81e2	11.07	0.63	167:	285.1	7.50e1	1.73	0.10	
15:	63.2	8.50e1	1.96	0.11	66:	132.0	3.73e2	8.58	0.48	117:	201.9	3.04e2	7.00	0.40	168:	290.0	1.75e2	4.03	0.23	
16:	64.2	1.51e2	3.48	0.20	67:	133.0	6.37e2	14.66	0.83	118:	203.0	1.06e2	2.44	0.14	169:	291.0	5.40e1	1.24	0.07	
17:	65.2	9.54e2	21.96	1.24	68:	134.0	6.13e2	14.11	0.80	119:	204.0	1.50e2	3.45	0.19	170:	294.1	2.47e2	5.68	0.32	
18:	66.2	2.42e2	5.57	0.31	69:	135.0	6.15e2	14.15	0.80	120:	205.0	8.80e1	2.03	0.11	171:	295.1	1.04e2	2.39	0.14	
19:	67.2	6.18e2	14.22	0.80	70:	136.0	2.44e2	5.62	0.32	121:	206.0	8.10e1	1.86	0.11	172:	296.1	6.20e1	1.43	0.08	
20:	68.2	1.22e2	2.81	0.16	71:	137.0	8.20e1	1.89	0.11	122:	209.9	1.04e2	2.39	0.14	173:	297.1	5.60e1	1.29	0.07	
21:	69.1	1.22e2	2.81	0.16	72:	142.9	8.90e1	2.05	0.12	123:	210.9	1.23e2	2.83	0.16	174:	298.1	9.70e1	2.23	0.13	
22:	69.2	1.09e3	25.02	1.41	73:	143.9	1.51e2	3.48	0.20	124:	211.9	2.50e2	5.75	0.32	175:	300.1	9.80e1	2.26	0.13	
23:	70.2	1.16e2	2.67	0.15	74:	145.0	3.16e2	7.27	0.41	125:	212.9	5.13e2	11.81	0.67	176:	309.1	1.00e2	2.30	0.13	
24:	71.2	8.60e1	1.98	0.11	75:	145.9	7.87e2	18.11	1.02	126:	213.9	2.11e2	4.86	0.27	177:	310.1	1.07e2	2.46	0.14	
25:	76.1	1.04e2	2.39	0.14	76:	147.0	2.35e2	5.41	0.31	127:	215.0	8.90e1	2.05	0.12	178:	311.1	6.50e1	1.50	0.08	
26:	77.1	6.78e2	15.60	0.88	77:	148.0	1.07e3	24.56	1.39	128:	216.0	8.90e1	2.05	0.12	179:	319.0	1.28e2	2.95	0.17	
27:	78.1	1.14e3	26.26	1.48	78:	149.0	2.01e2	4.63	0.26	129:	217.0	8.00e1	1.84	0.10	180:	320.0	7.80e1	1.80	0.10	
28:	79.1	2.11e3	48.45	2.74	79:	150.0	2.05e2	4.72	0.27	130:	218.0	9.00e1	2.07	0.12	181:	321.1	9.20e1	2.12	0.12	
29:	80.1	1.51e3	34.71	1.96	80:	152.0	6.20e1	1.43	0.08	131:	221.9	9.10e1	2.09	0.12	182:	324.1	1.70e2	3.91	0.22	
30:	81.1	7.98e2	18.37	1.04	81:	154.9	6.20e1	1.43	0.08	132:	222.9	1.61e2	3.71	0.21	183:	325.1	7.90e1	1.82	0.10	
31:	82.1	1.95e2	4.49	0.25	82:	155.9	2.91e2	6.70	0.38	133:	224.0	7.70e1	1.77	0.10	184:	326.1	6.50e1	1.50	0.08	
32:	83.1	4.47e2	10.29	0.58	83:	156.9	3.46e2	7.96	0.45	134:	224.9	7.60e1	1.75	0.10	185:	337.1	4.68e2	10.77	0.61	
33:	84.1	6.40e1	1.47	0.08	84:	157.9	3.01e2	6.93	0.39	135:	225.9	9.10e1	2.09	0.12	186:	338.1	6.28e2	14.45	0.82	
34:	91.1	3.99e2	9.18	0.52	85:	158.9	1.73e2	3.98	0.22	136:	226.9	1.11e2	2.55	0.14	187:	339.1	5.00e2	11.51	0.65	
35:	92.1	4.04e2	9.30	0.53	86:	159.9	2.01e2	4.63	0.26	137:	228.0	9.80e1	2.26	0.13	188:	340.1	1.11e2	2.55	0.14	
36:	93.1	1.76e3	40.48	2.29	87:	161.0	1.05e2	2.42	0.14	138:	229.0	6.70e1	1.54	0.09	189:	341.2	8.20e1	1.89	0.11	
37:	94.1	7.94e2	18.27	1.03	88:	162.0	2.46e2	5.66	0.32	139:	230.0	6.84e2	15.74	0.89	190:	351.1	1.09e2	2.51	0.14	
38:	95.1	9.09e2	20.92	1.18	89:	163.0	7.60e1	1.75	0.10	140:	231.0	6.83e2	15.72	0.89	191:	356.2	7.70e1	1.77	0.10	
39:	96.1	8.03e2	18.48	1.04	90:	164.0	8.60e1	1.98	0.11	141:	232.0	3.41e2	7.85	0.44	192:	415.2	2.47e2	5.68	0.32	
40:	97.1	2.54e2	5.85	0.33	91:	168.9	1.21e2	2.78	0.16	142:	233.0	1.34e2	3.08	0.17	193:	416.2	1.14e2	2.62	0.15	
41:	98.1	7.10e1	1.63	0.09	92:	169.9	4.62e2	10.63	0.60	143:	234.0	5.50e1	1.27	0.07	194:	417.2	1.25e2	2.88	0.16	
42:	102.0	7.60e1	1.75	0.10	93:	170.9	7.93e2	18.25	1.03	144:	239.0	9.60e1	2.21	0.12	195:	419.2	8.60e1	1.98	0.11	
43:	103.0	1.61e2	3.71	0.21	94:	171.9	3.50e2	8.06	0.45	145:	240.0	7.90e1	1.82	0.10	196:	444.2	2.11e2	4.86	0.27	
44:	104.0	1.16e2	2.67	0.15	95:	172.9	3.76e2	8.65	0.49	146:	241.0	6.60e1	1.52	0.09	197:	445.2	4.34e3	100.00	5.65	
45:	105.0	2.53e2	5.82	0.33	96:	173.9	3.26e2	7.50	0.42	147:	242.0	2.05e2	4.72	0.27	198:	446.2	2.02e3	46.54	2.63	
46:	106.0	7.95e2	18.30	1.03	97:	174.9	2.79e2	6.42	0.36	148:	243.0	7.10e1	1.63	0.09	199:	447.3	6.62e2	15.24	0.86	
47:	107.0	4.82e2	11.09	0.63	98:	176.0	1.86e2	4.28	0.24	149:	244.0	2.90e2	6.67	0.38	200:	448.3	1.26e2	2.90	0.16	
48:	108.0	1.66e3	38.30	2.16	99:	177.0	6.60e1	1.52	0.09	150:	245.0	8.50e1	1.96	0.11	201:	449.3	2.63e2	6.05	0.34	
49:	109.0	2.43e3	55.93	3.16	100:	178.0	7.50e1	1.73	0.10	151:	246.0	7.40e2	17.03	0.96	202:	450.3	7.70e1	1.77	0.10	
50:	110.0	4.28e2	9.85	0.56	101:	181.9	6.00e1	1.38	0.08	152:	247.0	1.78e2	4.10	0.23						
51:	111.0	7.60e1	1.75	0.10	102:	182.9	4.31e2	9.92	0.56	153:	248.0	6.10e1	1.40	0.08						

Fig. S2c. LRMS (EI) of **4**

Elemental Composition Report **Page 1**

Single Mass Analysis
Tolerance = 15.0 PPM / DBE: min = -1.5, max = 50.0
Selected filters: None

Monoisotopic Mass, Odd and Even Electron Ions
28 formula(e) evaluated with 1 results within limits (up to 50 best isotopic matches for each mass)
Elements Used:
C: 0-60 H: 0-100 N: 5-5 O: 0-4

E. Wagner-Wysiecka
EW 38
pg_ew2422h 131 (4.997) Cm (131:146)

AUTOSPEC

28-Oct-2019 13:16:34
Operator: Marian Olejnik
Voltage EI+
3.60e3

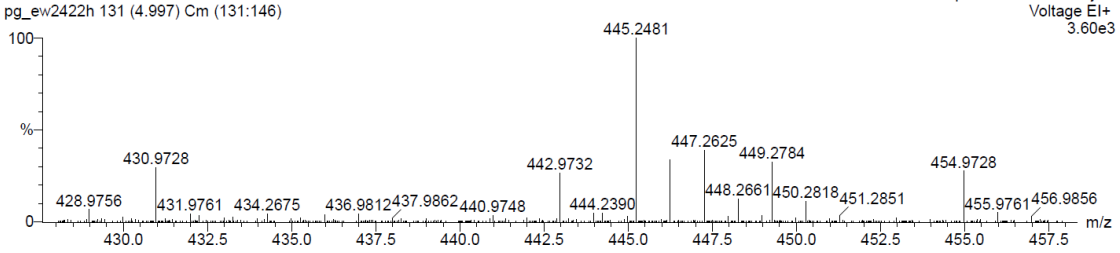

Minimum:				-1.5		
Maximum:		5.0	15.0	50.0		
Mass	Calc. Mass	mDa	PPM	DBE	i-FIT	Formula
445.2481	445.2478	0.3	0.7	14.0	523.4	C26 H31 N5 O2

Fig. S2d. HRMS (EI) of **4**

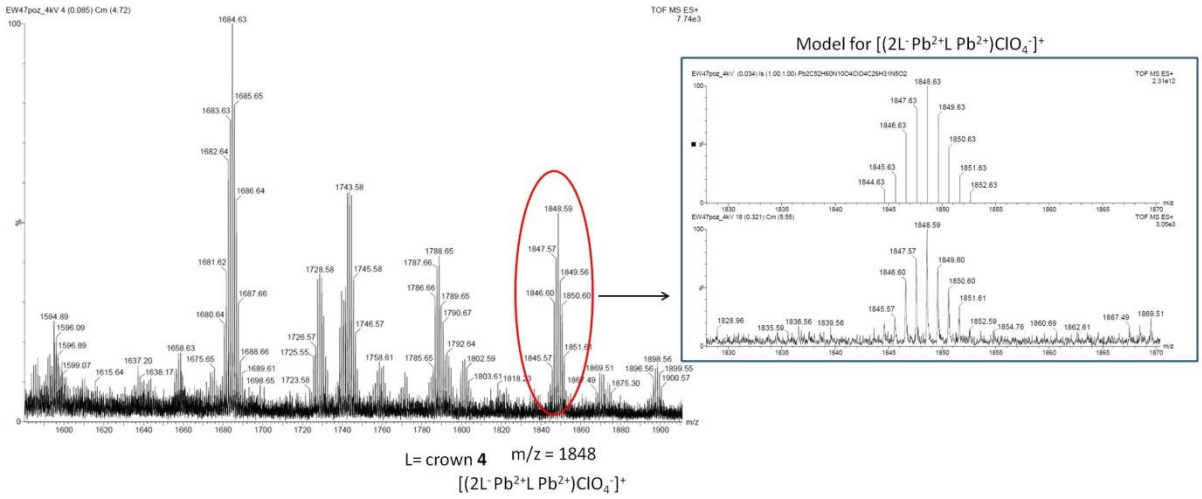

Fig S2e. Part of ESI-LR (positive ions mode) spectrum of lead(II)complex of **4** comparison of model of isotopic peaks for peak of m/z 1848.

2. Complexation studies - spectroscopic methods

Table S1. Stability constant (logK) values of diazocrowns lead(II) complexes **1**-**4** in acetonitrile.

	1[1]	**2**[1]	**3**	**4**
$\log K_{L3Pb2}$	18.10±0.01	21.10±0.09	19.22±0.05	18.37±0.01

1. E. Luboch, E. Wagner-Wysiecka, M. Fainerman-Melnikova, L.F. Lindoy, J.F. Biernat, Pyrrole Azocrown Ethers. Synthesis, Complexation, Selective Lead Transport and Ion-Selective Membrane Electrode Studies, *Supramol. Chem.*, 2006, **18**, 593-601.

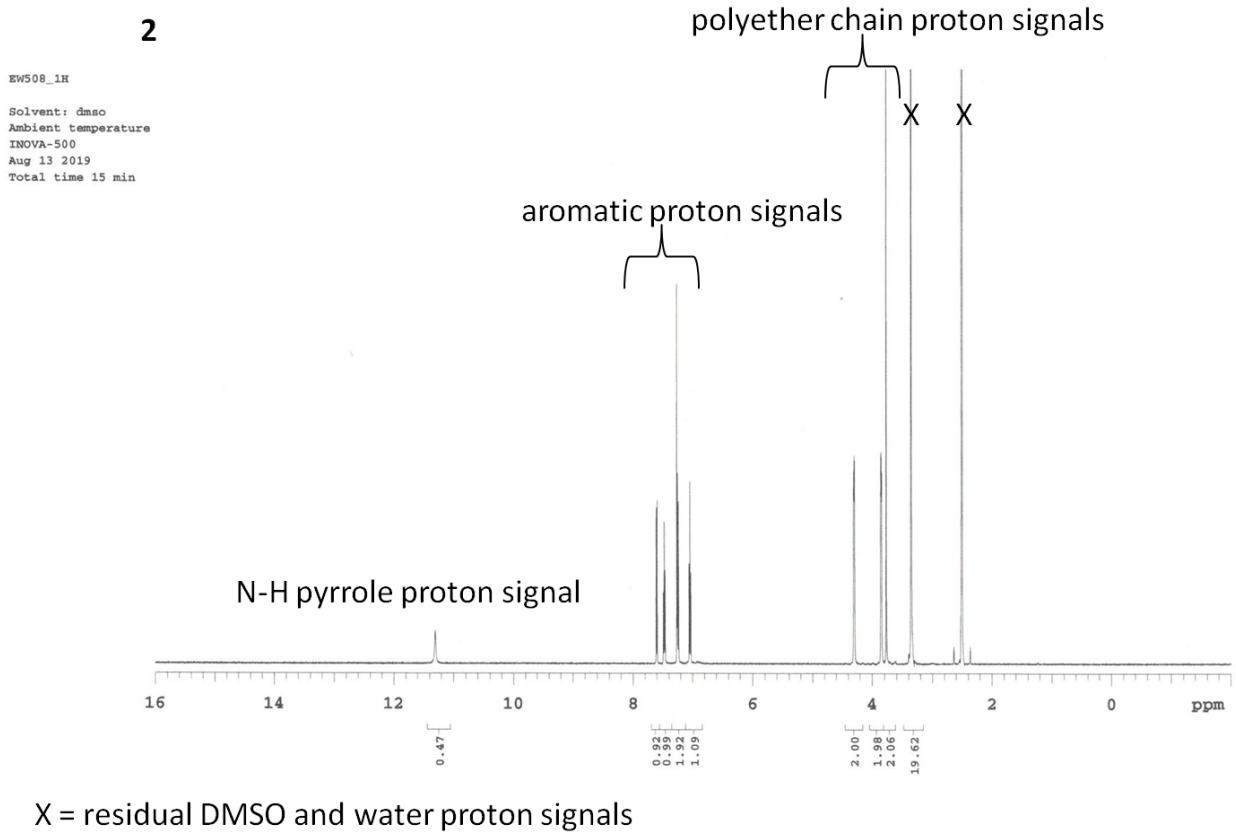

Fig. S3a. ^{1}H NMR spectrum of **2** (1.6×10^{-2}M) (DMSO-d_6)

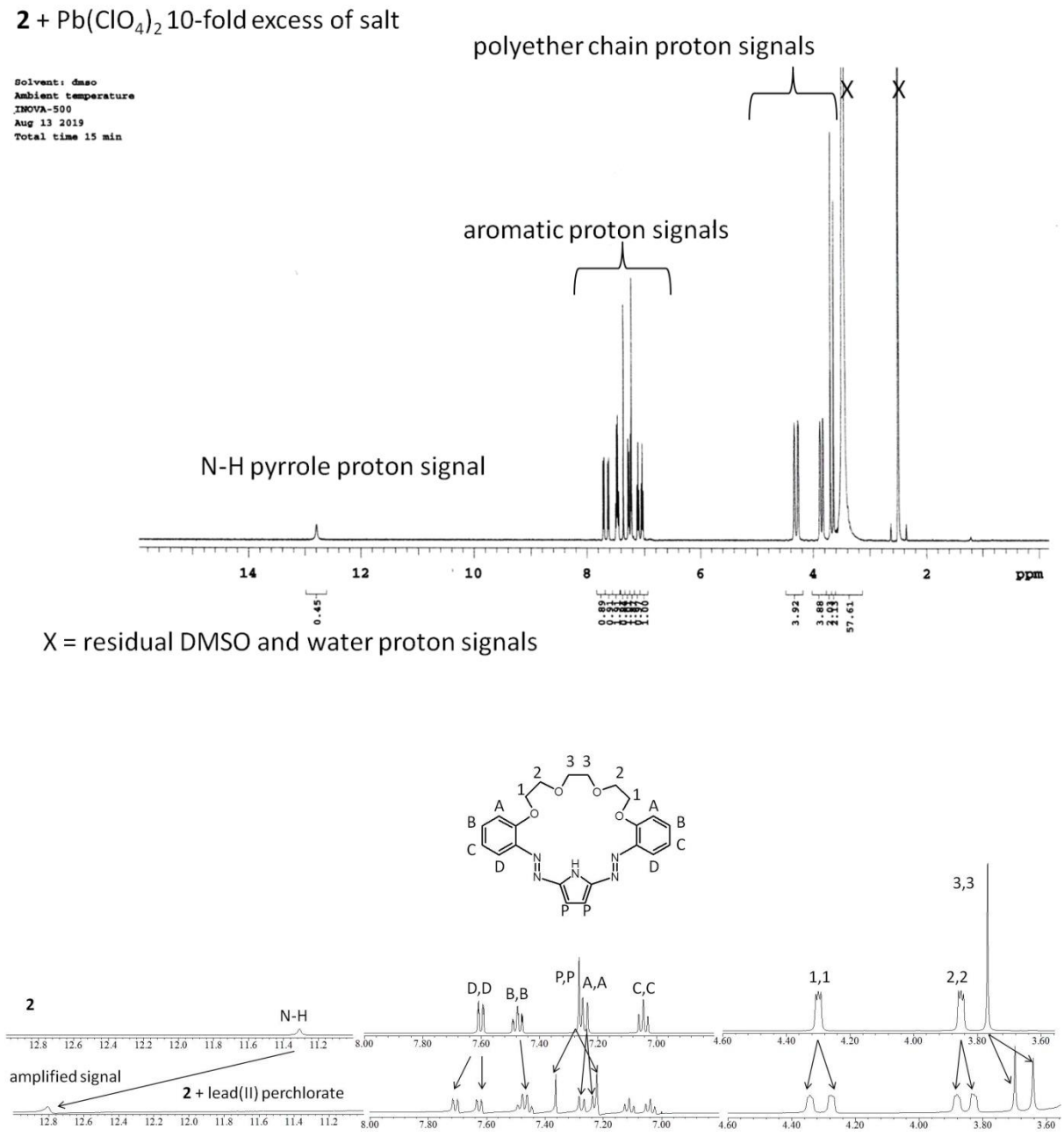

Fig. S3b. Top:^{1}H NMR spectrum of **2** (1.6×10^{-2}M) in the presence of 10-fold excess of lead(II) perchlorate; bottom: comparison of the spectral pattern of proton signals in free crown **2** and its spectrum in the presence of 10-fold excess lead(II) perchlorate (DMSO-d_6)

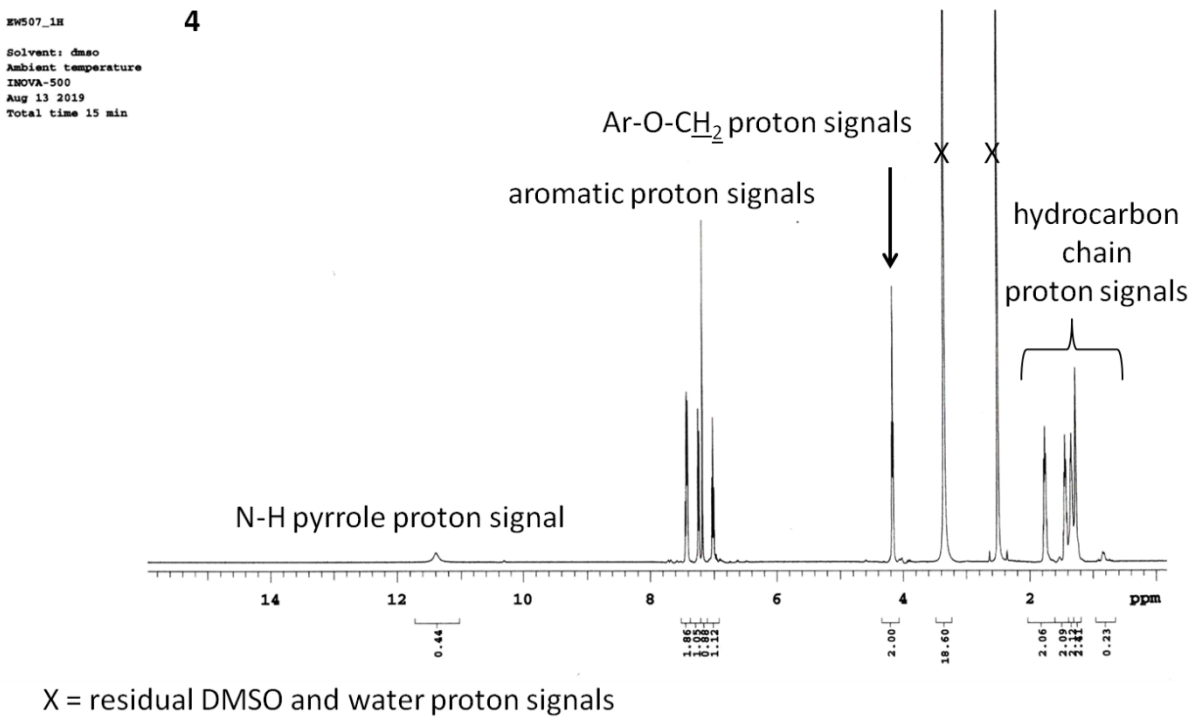

Fig. S4a. ^{1}H NMR spectrum of **4** (1.6×10^{-2}M) (DMSO-d_6)

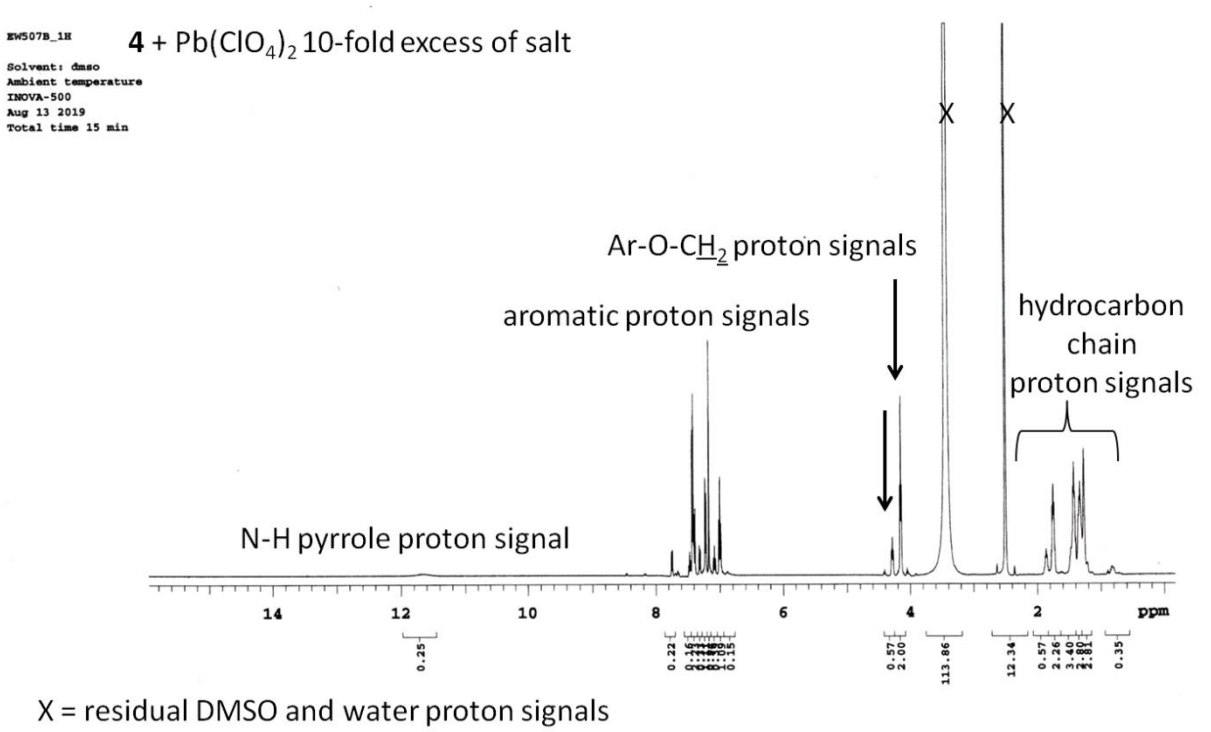

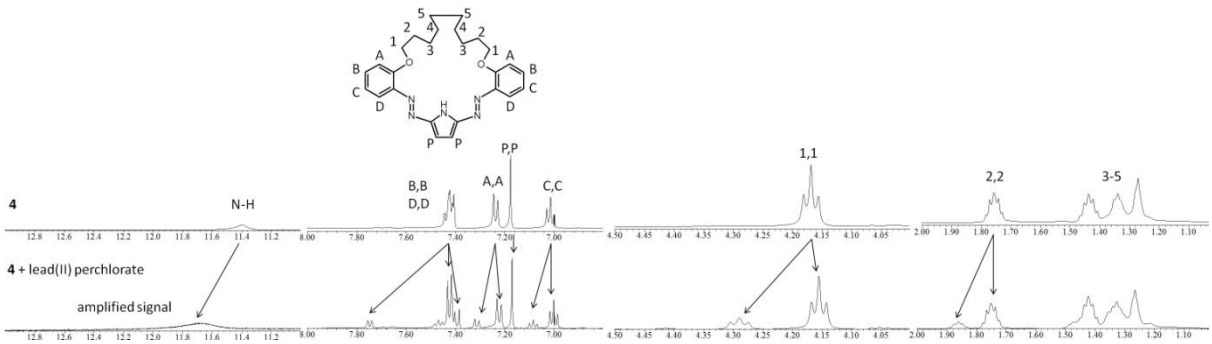

Fig. S4b. Top: ^{1}H NMR spectrum of **4** (1.6×10^{-2}M) in the presence of 10-fold excess of lead(II) perchlorate; bottom comparison of the spectral pattern of proton signals in free crown **4** and its spectrum in the presence of 10-fold excess lead(II) perchlorate (DMSO-d_6)

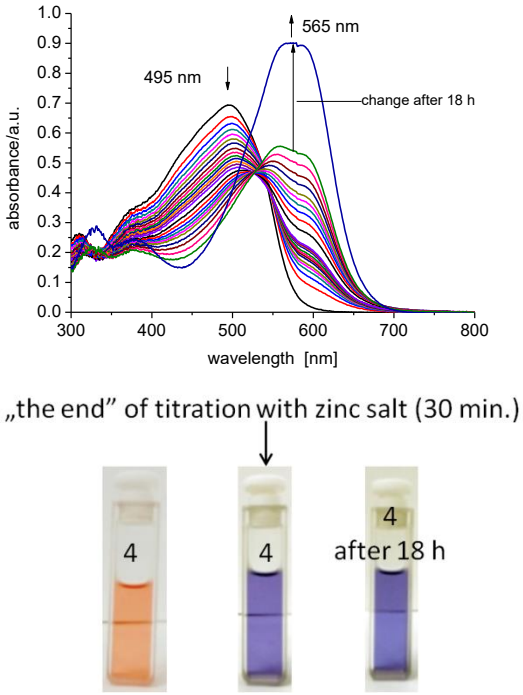

Fig. S5. UV-Vis titration trace and color change for **4** (c_4= 3.14×10^{-5} M) and zinc(II) perchlorate (c_{Zn}= 0-1.76×10^{-3} M) in acetonitrile. Bottom: color changes of the solutions.

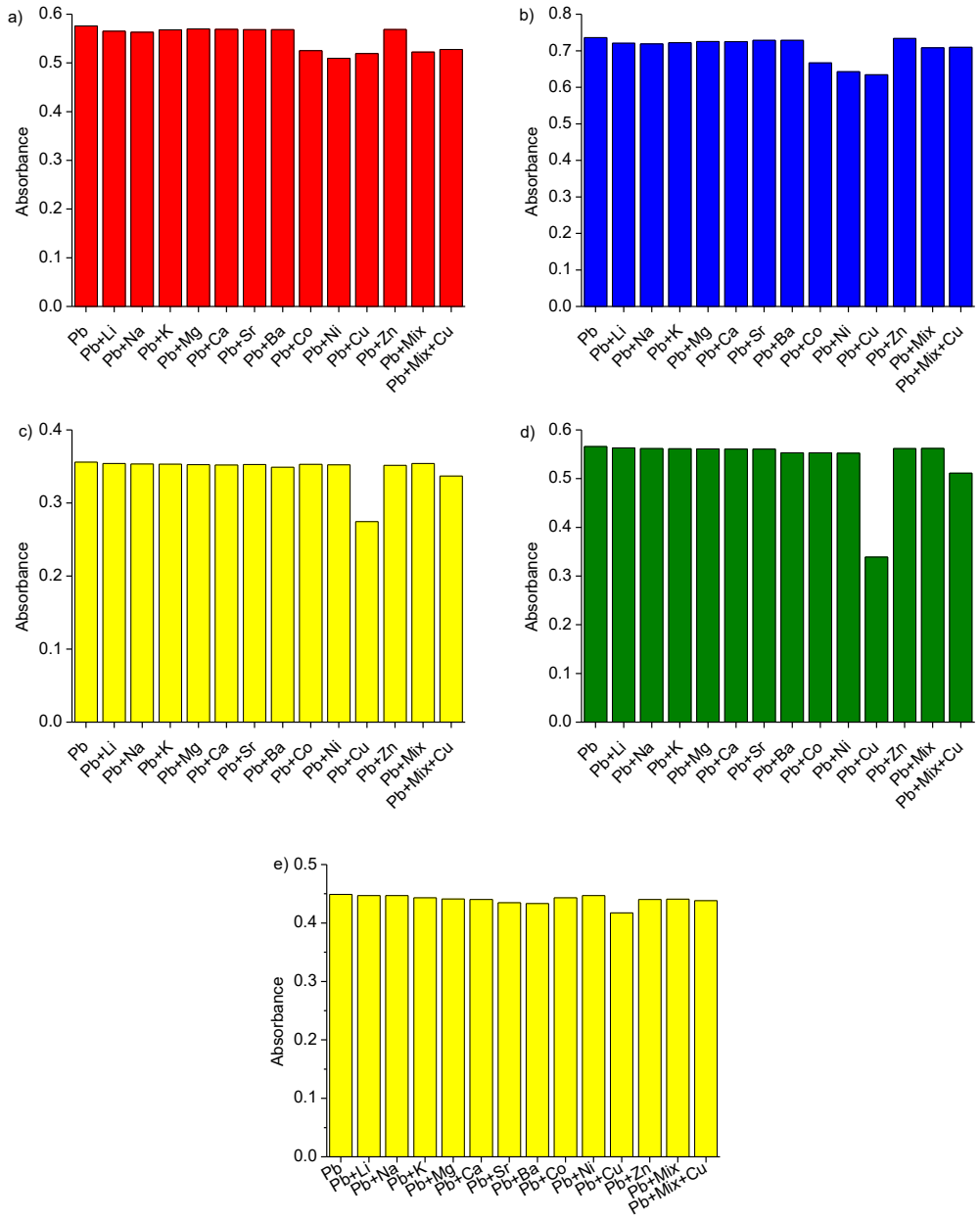

Fig. S6. Interferences from several metal perchlorates, used in 10-fold excess, on spectrophotometric response towards systems containing equimolar amount of lead(II) perchlorate for a) **1** (2.54×10^{-5} M) at 605 nm, b) **2** (2.73×10^{-5} M) at 610 nm, c) **3** (2.08×10^{-5} M) at 610 nm and d) **4** (2.63×10^{-5} M) at 605 nm in acetonitrile (Mix - mixture of metal perchlorates without copper). e) interferences from several metal perchlorates, used in 10-fold excess, on spectrophotometric response towards systems containing equimolar amount of lead(II) perchlorate for **3** (2.13×10^{-5} M) at 608 nm at equimolar (to crown) amount of lead(II) perchlorate in acetonitrile:water (9:1, v/v) solution at pH 5.

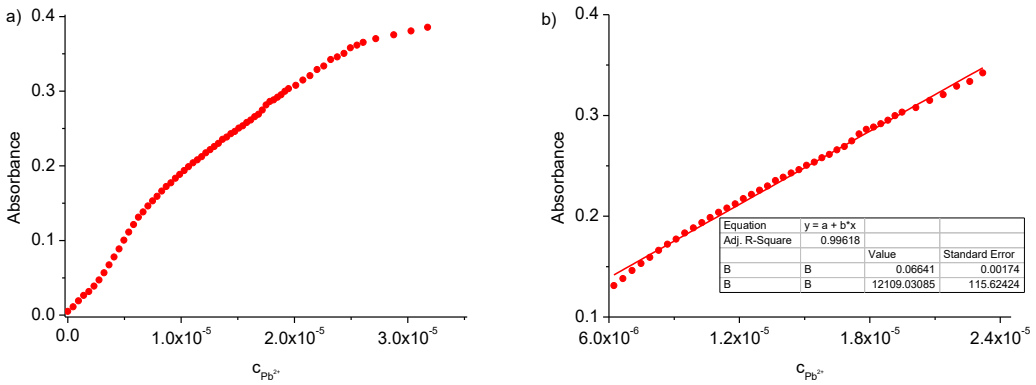

Fig. S7. a) The relationship A = f([Pb(II)]) at 610 nm and b) linear range of response towards lead(II) perchlorate for **3** in acetonitrile.

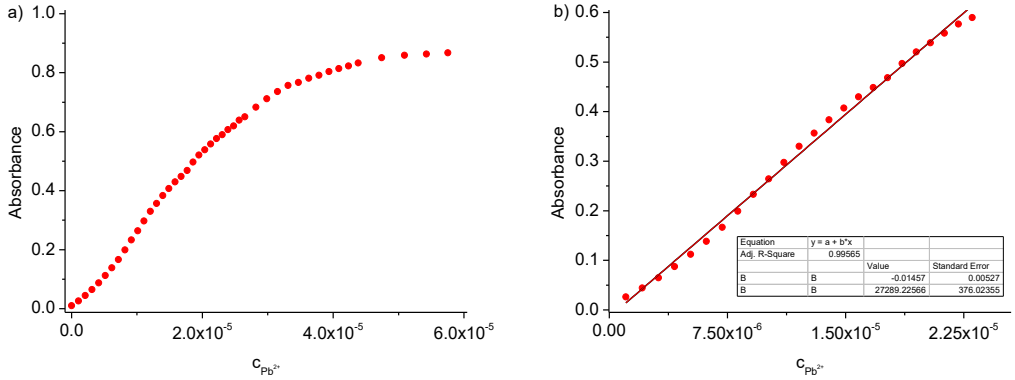

Fig. S8. a) The relationship A = f([Pb(II)]) at 605 nm and b) linear range of response towards lead(II) perchlorate for **4** in acetonitrile.

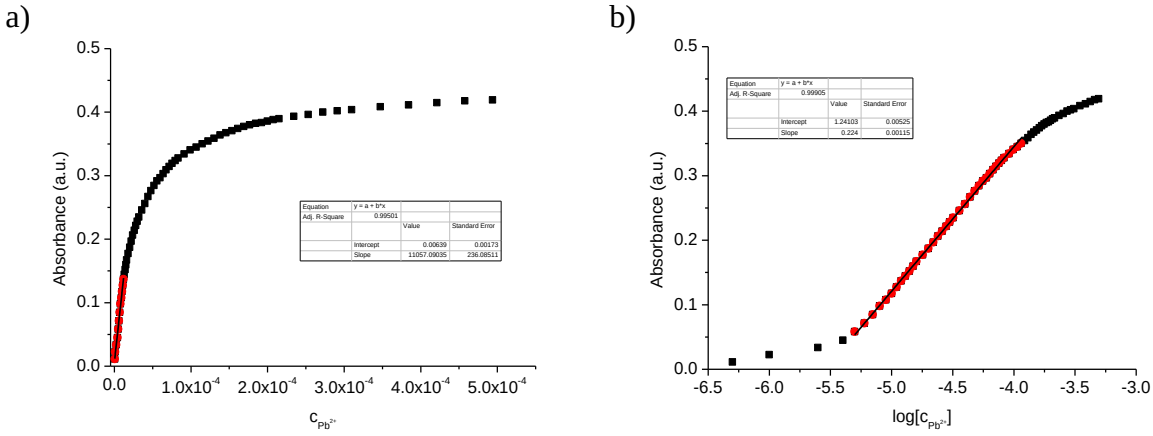

Fig. S9. The relationship a) A = f ([Pb(II)]) with linear range of response 5.00×10^{-7} – 1.20×10^{-5} M b) A = f (log([Pb(II)]) with linear range of response 5.00×10^{-6} – 1.15×10^{-4} M for **3** (c_3= 2.13×10^{-5} M) in acetonitrile:water (9:1, v/v) solution at pH 5 at 608 nm.

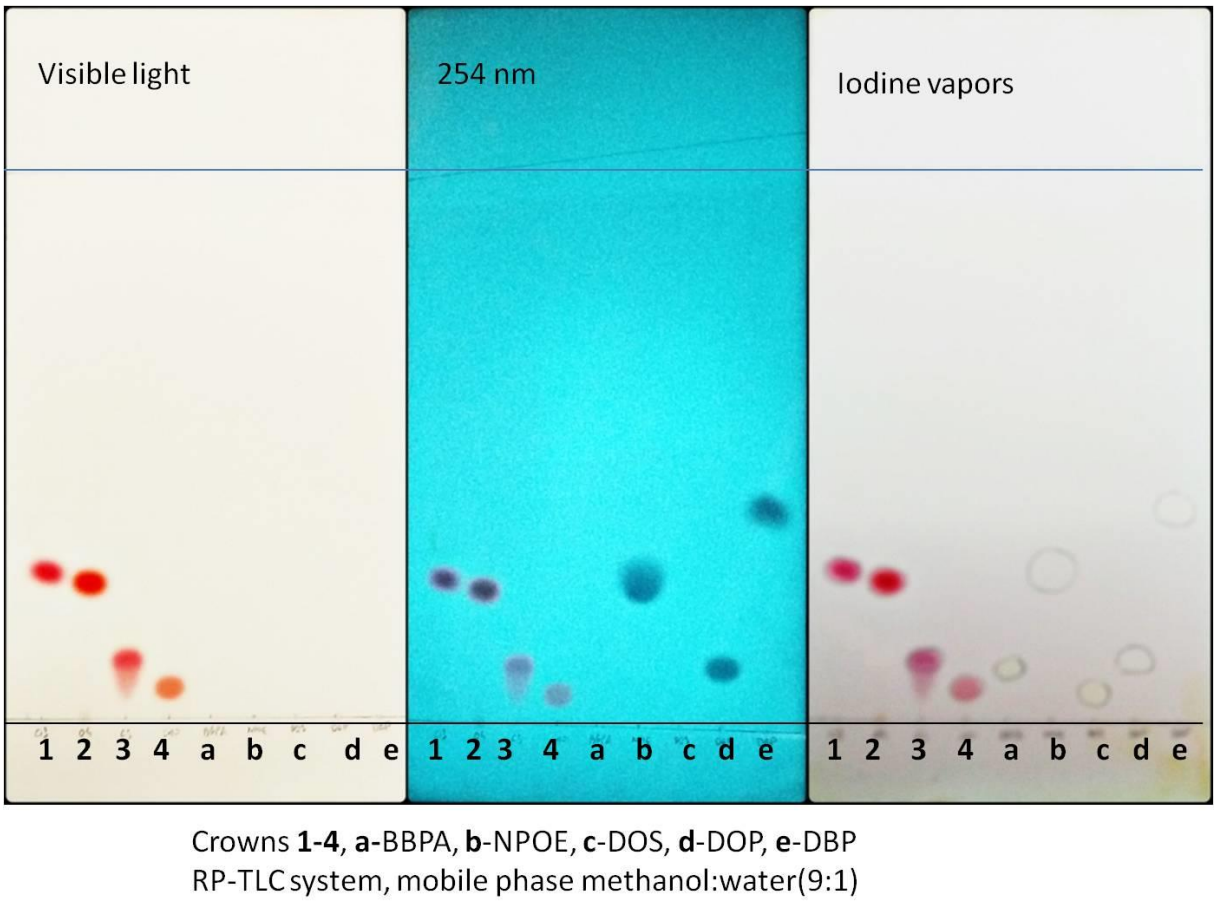

Fig. S10. RP18-TLC chromatograms of crowns **1-4** and standard substances a-e.

On the basis of comparison of R_f values for standards and crowns **1-4** $logP_{TLC}$ values for macrocyles **1-4** were determined as follows: **1**: 5.54±0.05, **2**: 5.67±0.01, **3**: 8.12±0.05 and **4**: 9.42±0.03.

1. O. Dinten, U. E. Spichiger, N. Chaniotakis, P. Gehrig, B. Rusterholz, W. E. Morf, W. Simon, Lifetime of neutral-carrier-based liquid membranes in aqueous samples and blood and the lipophilicity of membrane components, *Anal. Chem.*, 1991, **63**, 596-603.
2. E. Luboch, M. Jeszke, M. Szarmach, N. Łukasik, New bis(azobenzocrown)s with dodecylmethylmalonyl linkers as ionophores for sodium selective potentiometric sensors, *J. Incl. Phenom. Macrocycl. Chem.*, 2016, **86**, 323-335.

3. Ionic species detected in ESI mass spectra of lead(II) complex of crown 1

$$3\bullet(C_{20}H_{18}N_5O_3)^{-}\bullet 3Pb^{2+}\bullet 2ClO_4^{-}$$

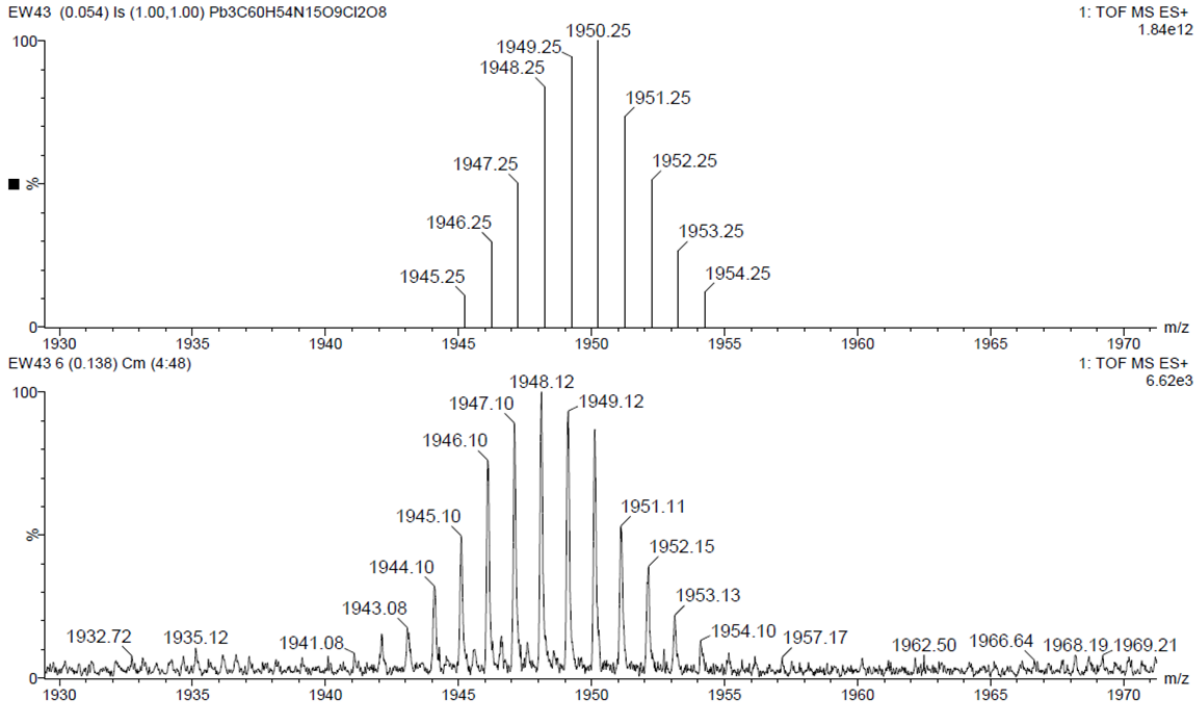

Fig. S11a. Theoretically calculated and experimental isotope pattern of peak m/z 1950 in lead(II) complex of **1**

$$2\bullet C_{20}H_{19}N_5O_3\bullet(C_{20}H_{18}N_5O_3)^{-}\bullet 2Pb^{2+}\bullet 2ClO_4^{-}$$

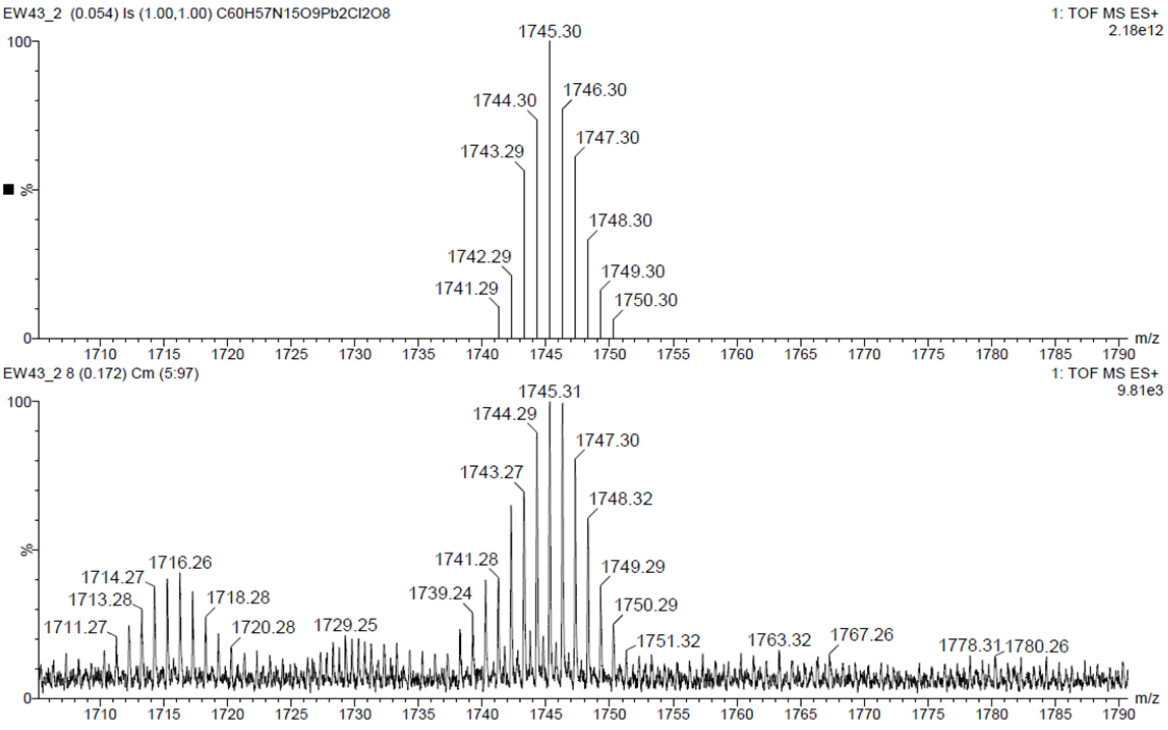

Fig. S11b. Theoretically calculated and experimental isotope pattern of peak m/z 1745 in lead(II) complex of **1**

$2\bullet(C_{20}H_{18}N_5O_3)^{-}\bullet C_{20}H_{19}N_5O_3\bullet 2Pb^{2+}\bullet ClO_4^{-}$

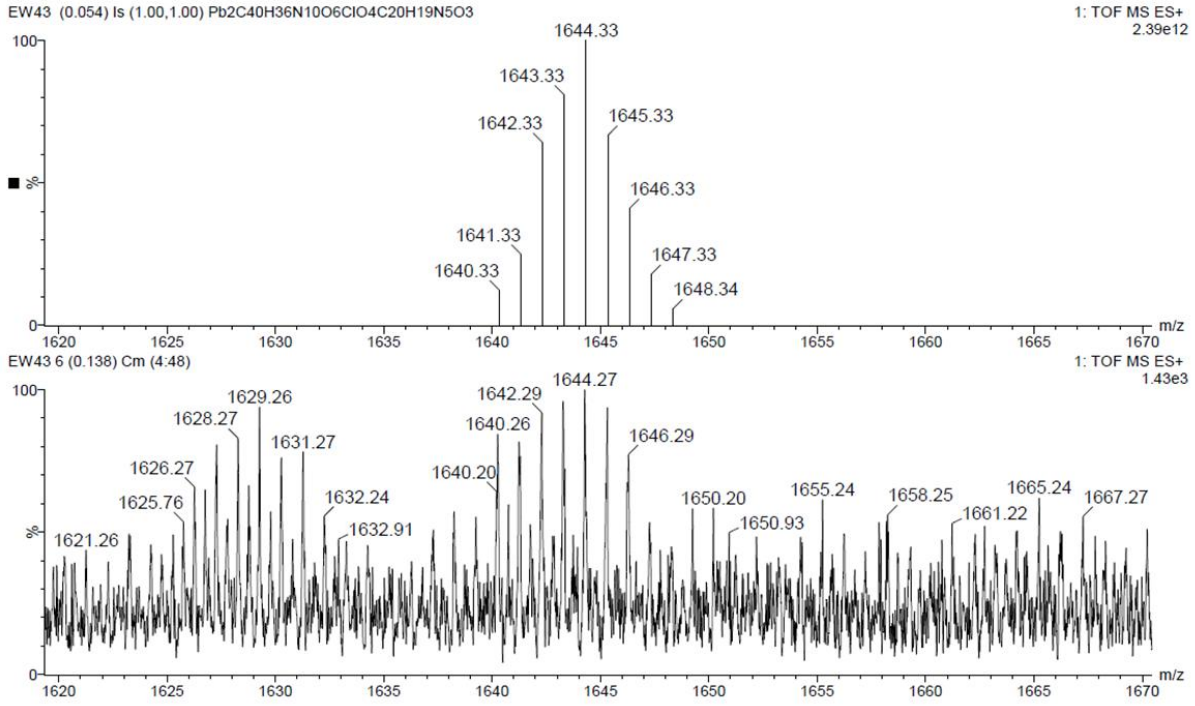

Fig. S11c. Theoretically calculated and experimental isotope pattern of peak m/z 1644 in lead(II) complex of **1**

$2\bullet(C_{20}H_{18}N_5O_3)^{-}\bullet 2Pb^{2+}\bullet ClO_4^{-}$

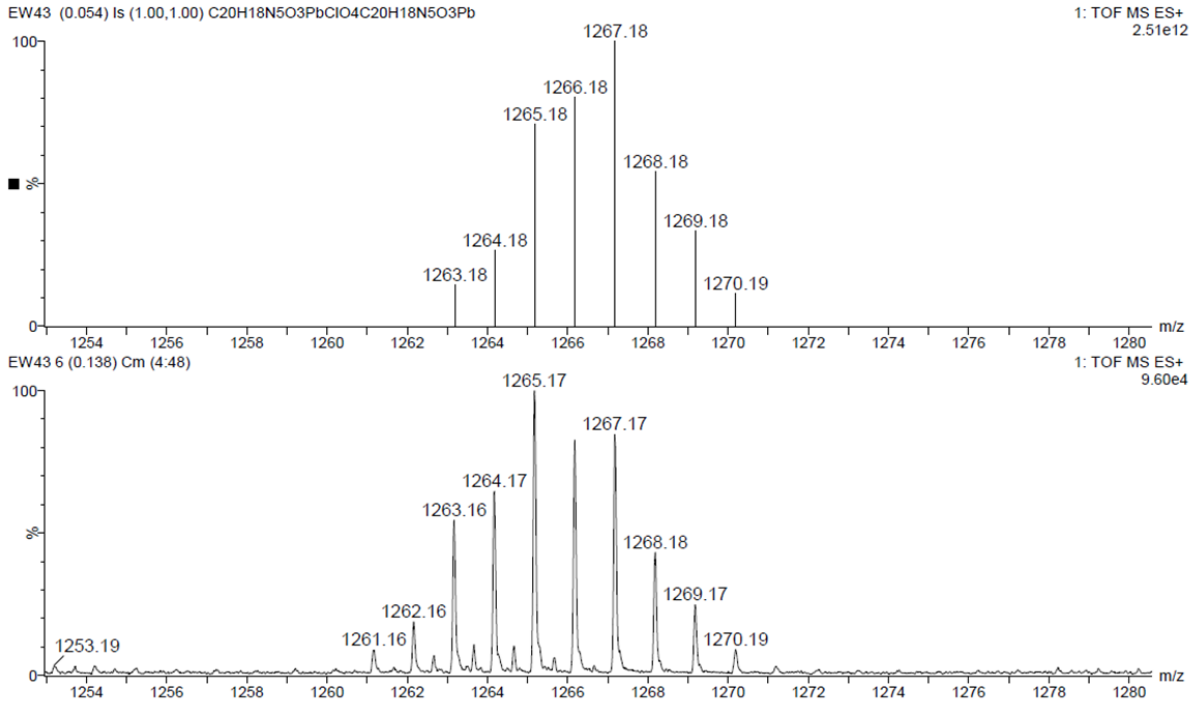

Fig. S11d. Theoretically calculated and experimental isotope pattern of peak m/z 1267 in lead(II) complex of **1**

$(C_{20}H_{18}N_5O_3)^- \bullet Pb^{2+}$

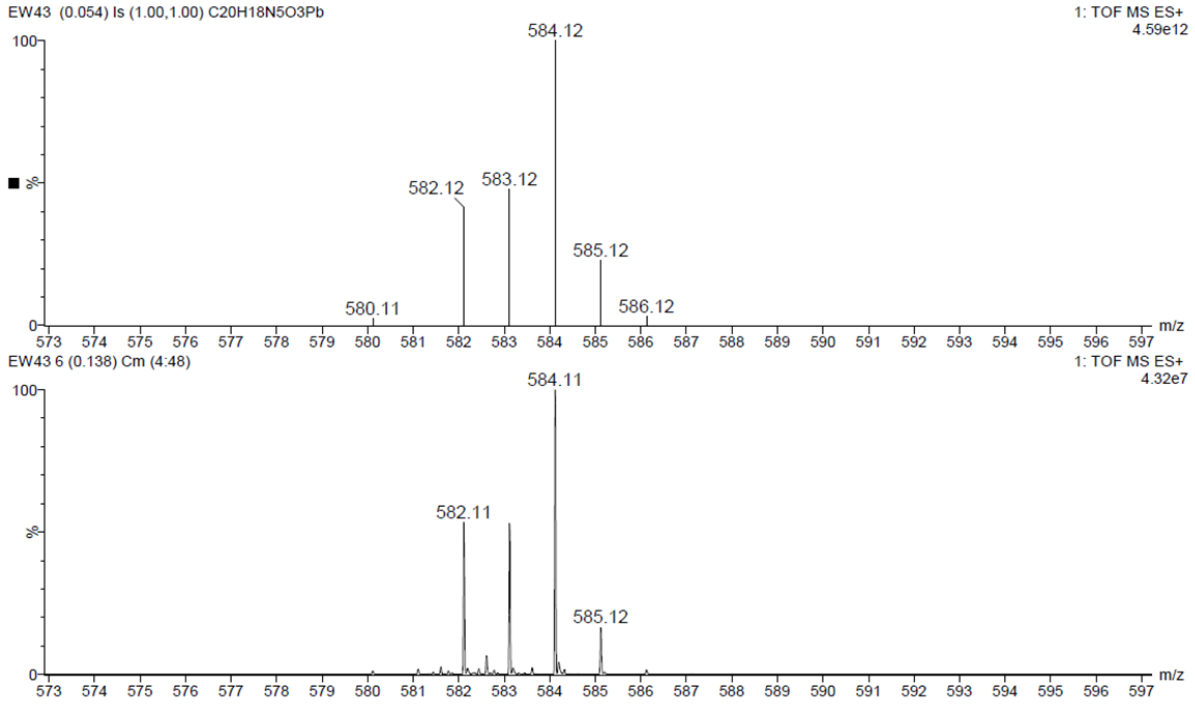

Fig. S11e. Theoretically calculated and experimental isotope pattern of peak m/z 584 in lead(II) complex of **1**

4. Ionic species detected in ESI mass spectra of lead(II) complex of crown 2

$$3\bullet(C_{22}H_{22}N_5O_4)^-\bullet 3Pb^{2+}\bullet 2ClO_4^-$$

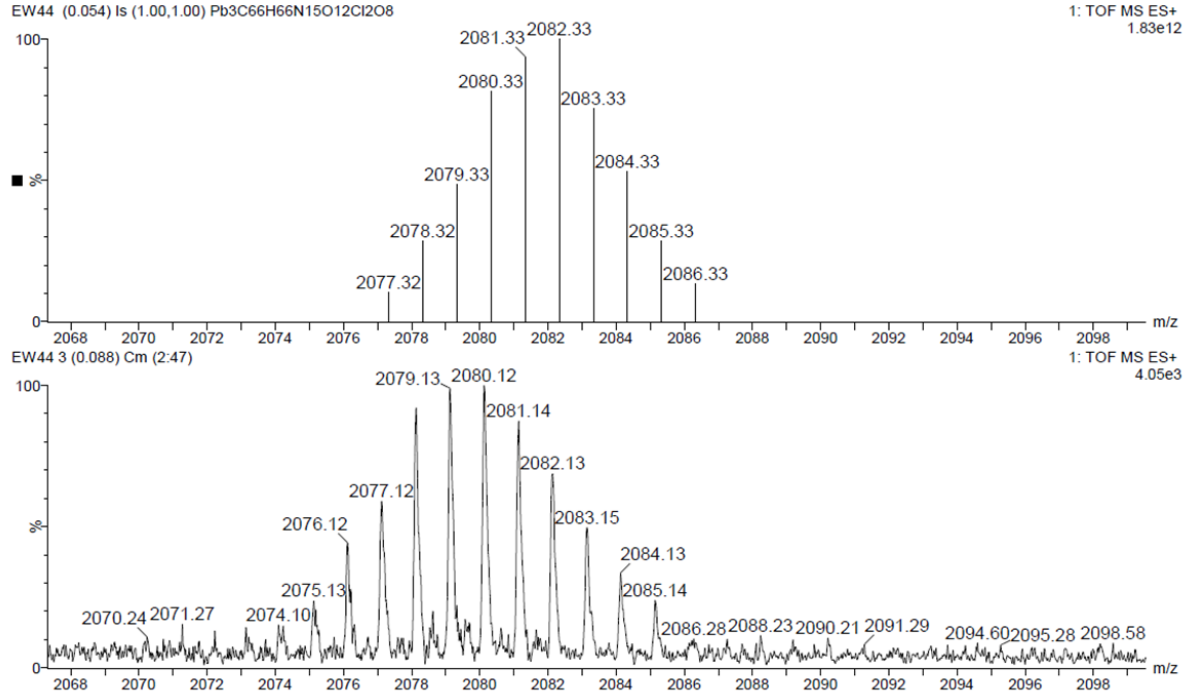

Fig. S12a. Theoretically calculated and experimental isotope pattern of peak m/z 2082 in lead(II) complex of **2**

$$2\bullet C_{22}H_{23}N_5O_4\bullet(C_{22}H_{22}N_5O_4)^-\bullet 2Pb^{2+}\bullet 2ClO_4^-$$

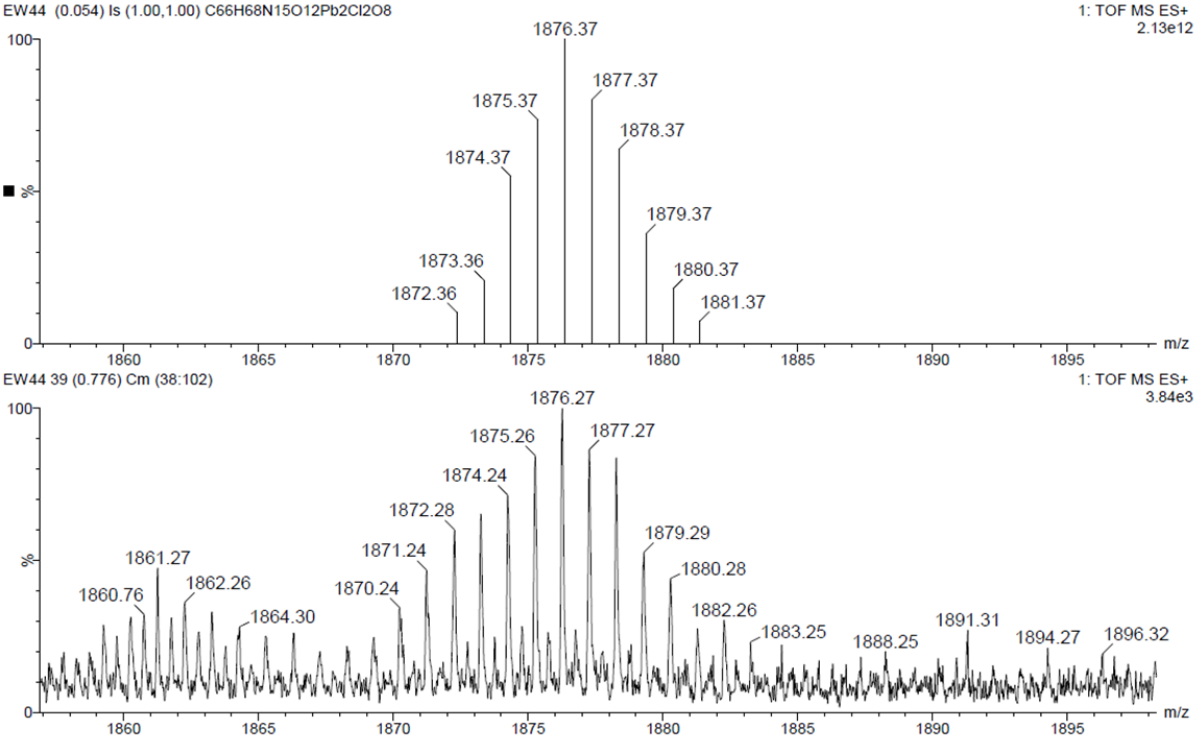

Fig. S12b. Theoretically calculated and experimental isotope pattern of peak m/z 1876 in lead(II) complex of **2**

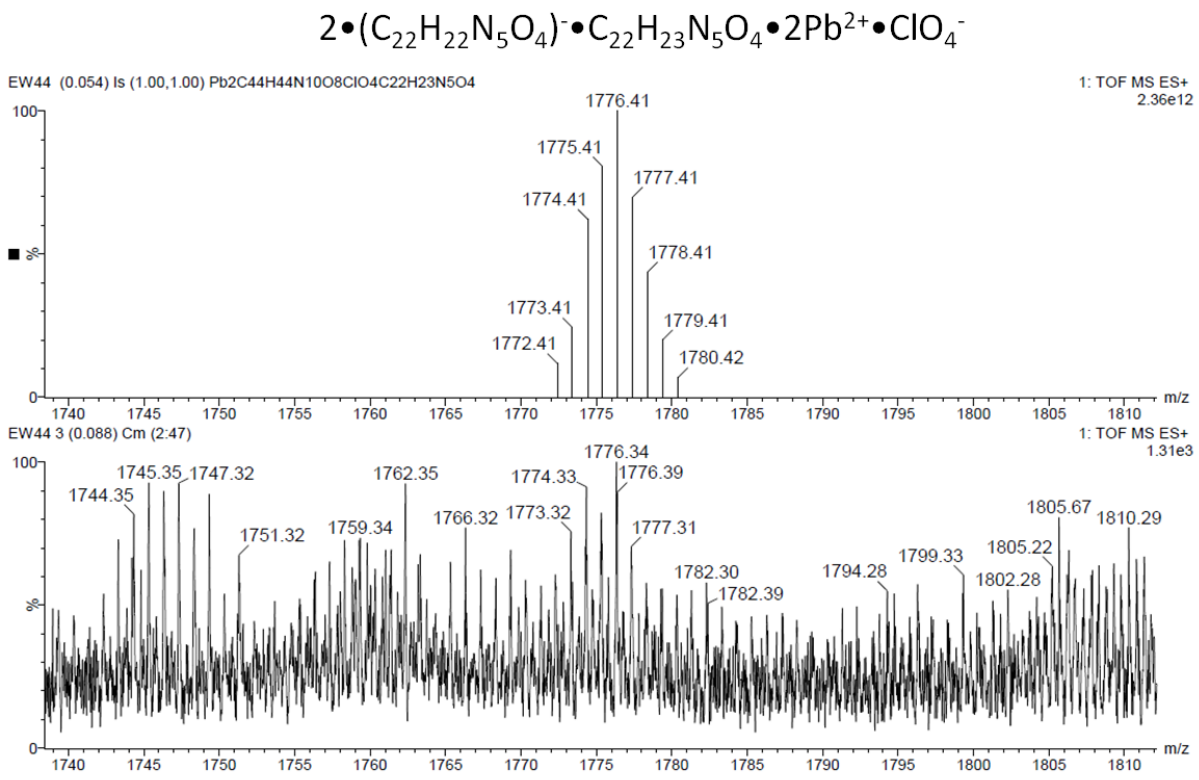

Fig. S12c. Theoretically calculated and experimental isotope pattern of peak m/z 1776 in lead(II) complex of **2**

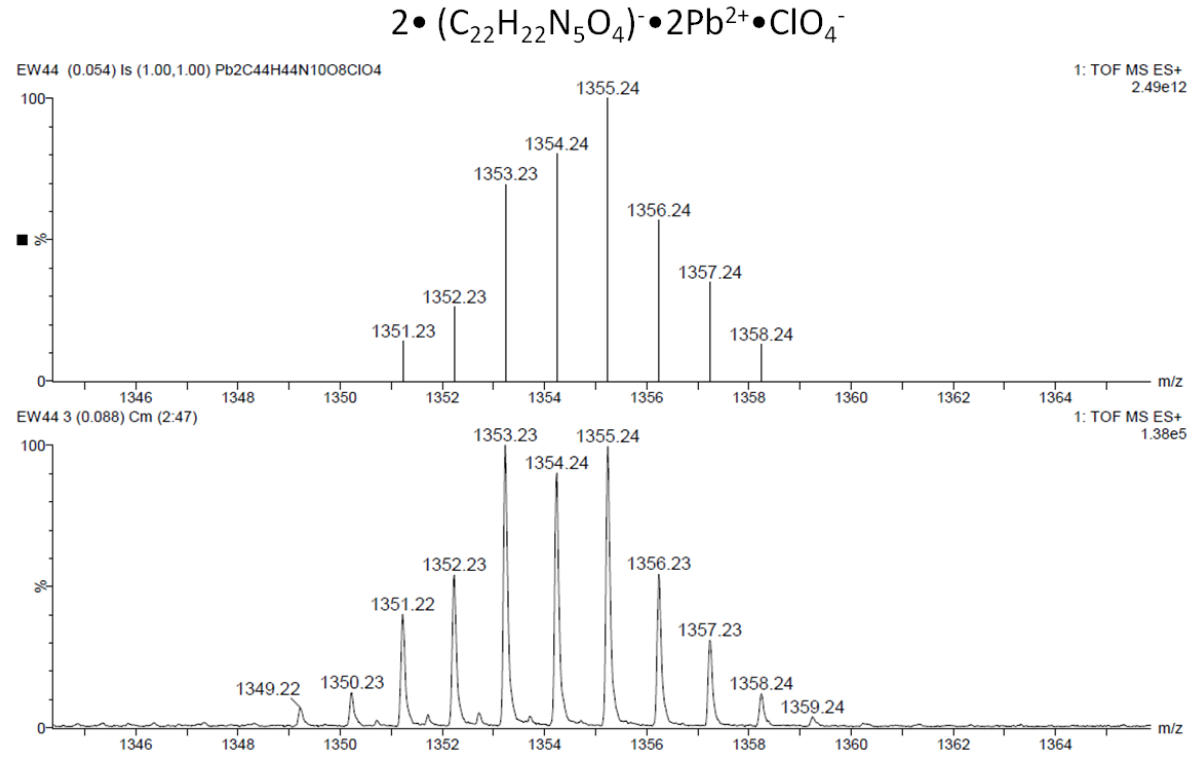

Fig. S12d. Theoretically calculated and experimental isotope pattern of peak m/z 1335 in lead(II) complex of **2**

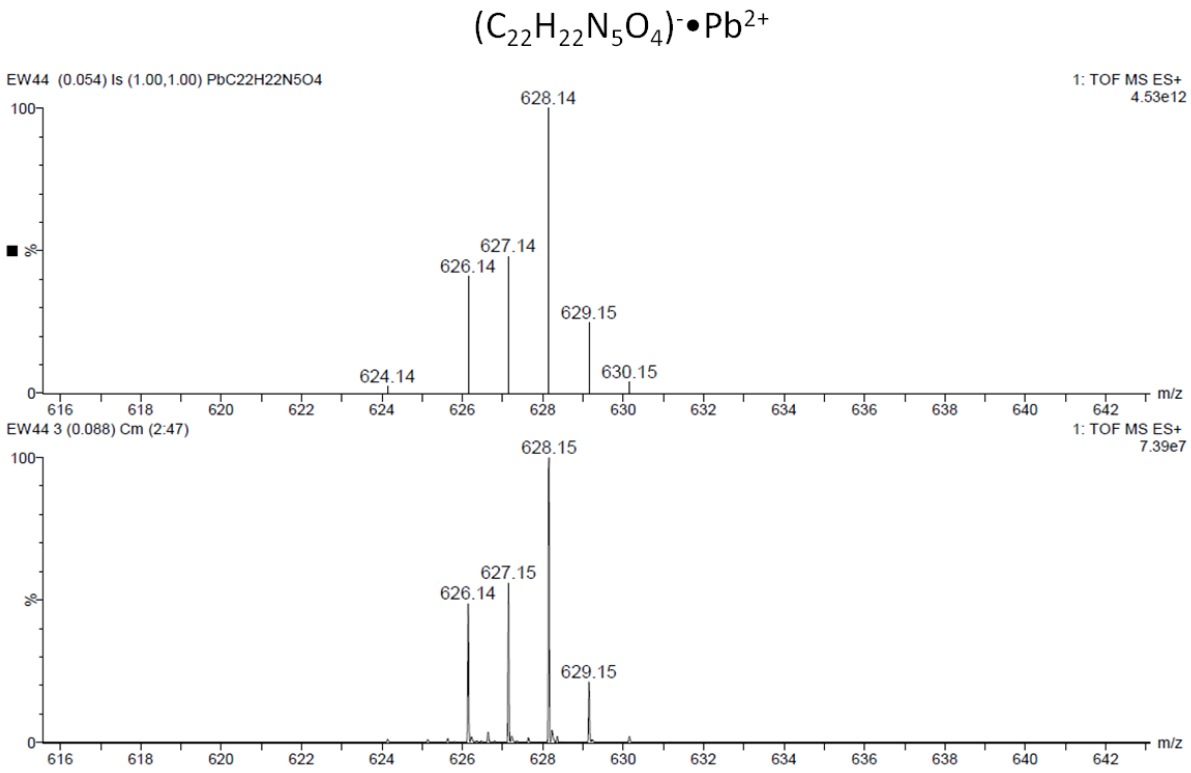

Fig. S12e. Theoretically calculated and experimental isotope pattern of peak m/z 628 in lead(II) complex of **2**

5. Ionic species detected in ESI mass spectra of lead (II) complex of crown 3

$$3\bullet(C_{21}H_{20}N_5O_2)^{-}\bullet 3Pb^{2+}\bullet 2ClO_4^{-}$$

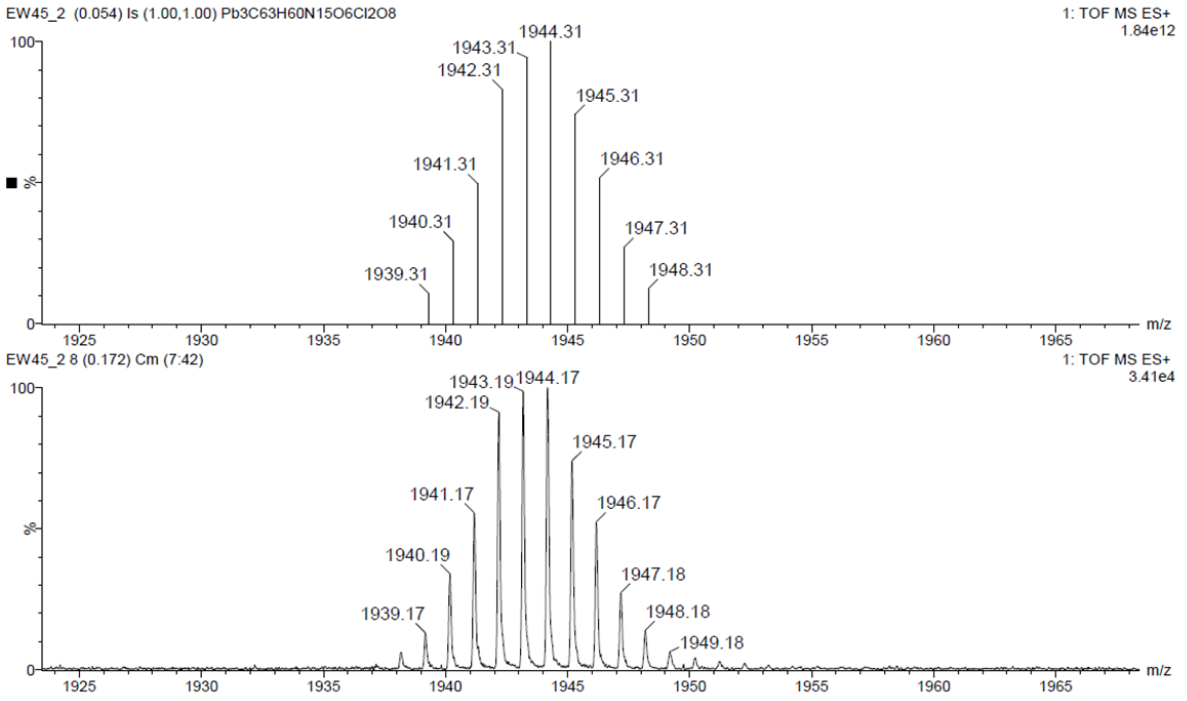

Fig. S13a. Theoretically calculated and experimental isotope pattern of peak m/z 1944 in lead(II) complex of **3**

$$2\bullet(C_{21}H_{20}N_5O_2)^{-}\bullet C_{21}H_{21}N_5O_2\bullet 2Pb^{2+}\bullet ClO_4^{-}$$

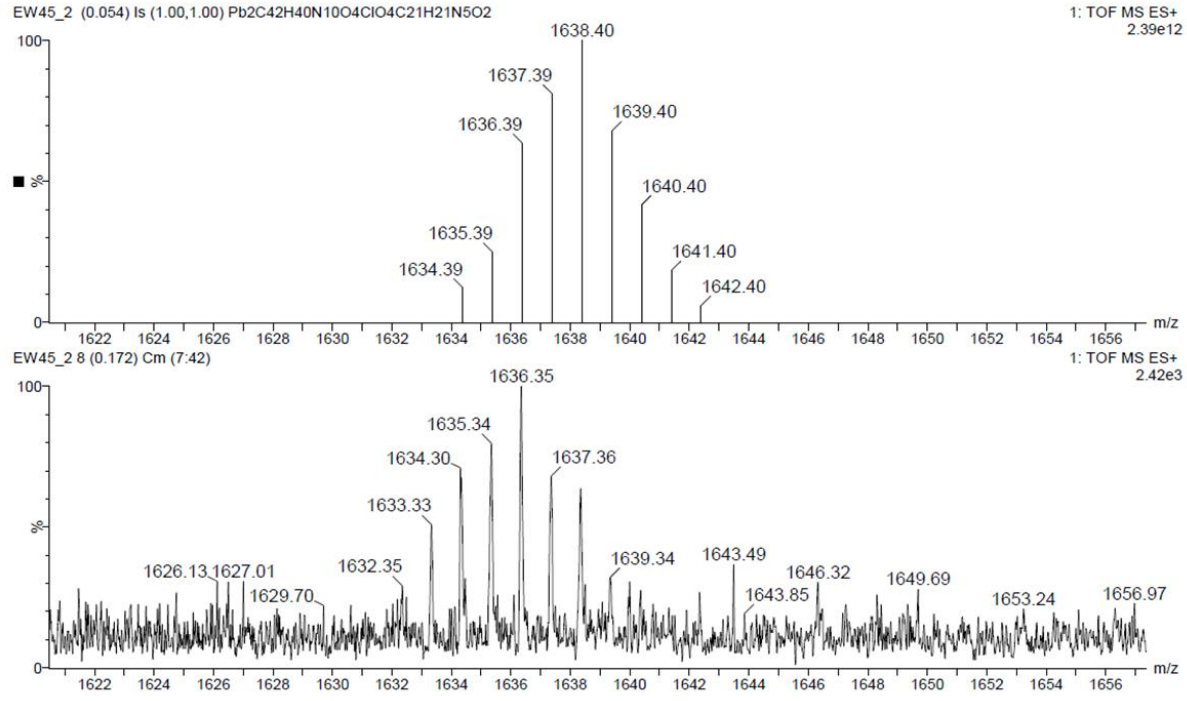

Fig. S13b. Theoretically calculated and experimental isotope pattern of peak m/z 1636 in lead(II) complex of **3**

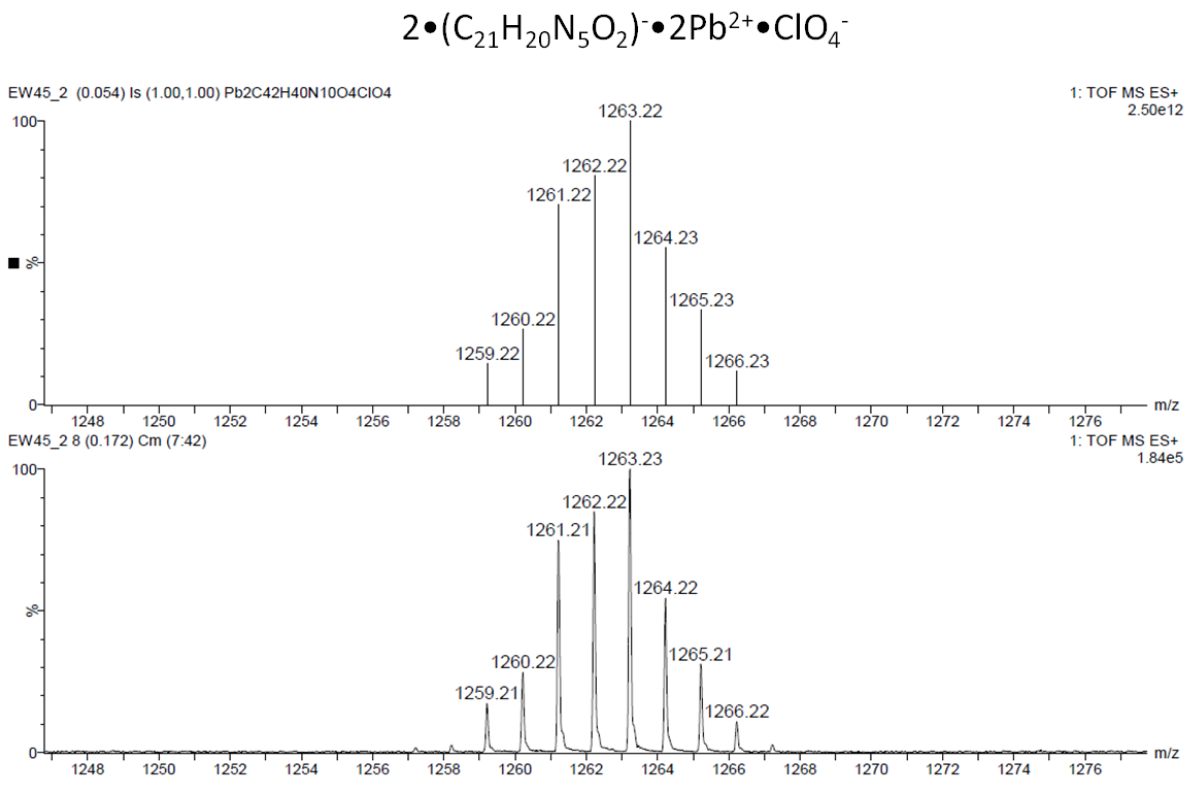

Fig. S13c. Theoretically calculated and experimental isotope pattern of peak m/z 1263 in lead(II) complex of **3**

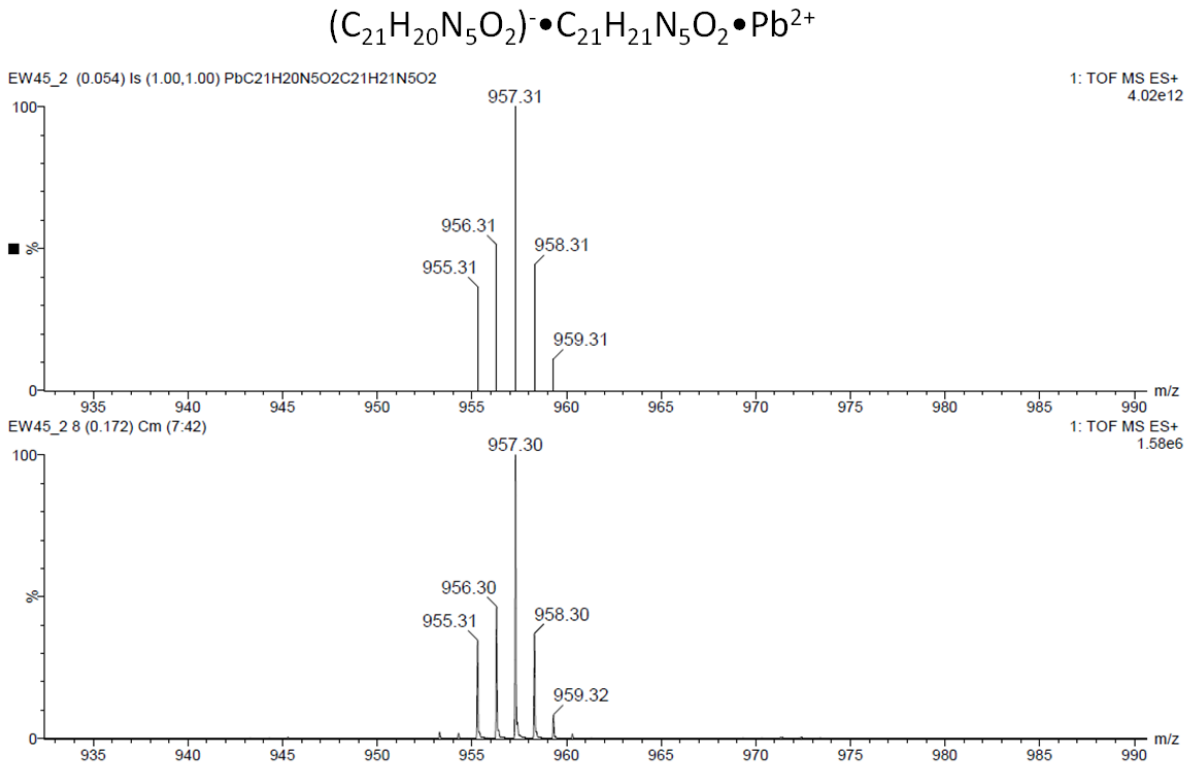

Fig. S13d. Theoretically calculated and experimental isotope pattern of peak m/z 957 in lead(II) complex of **3**

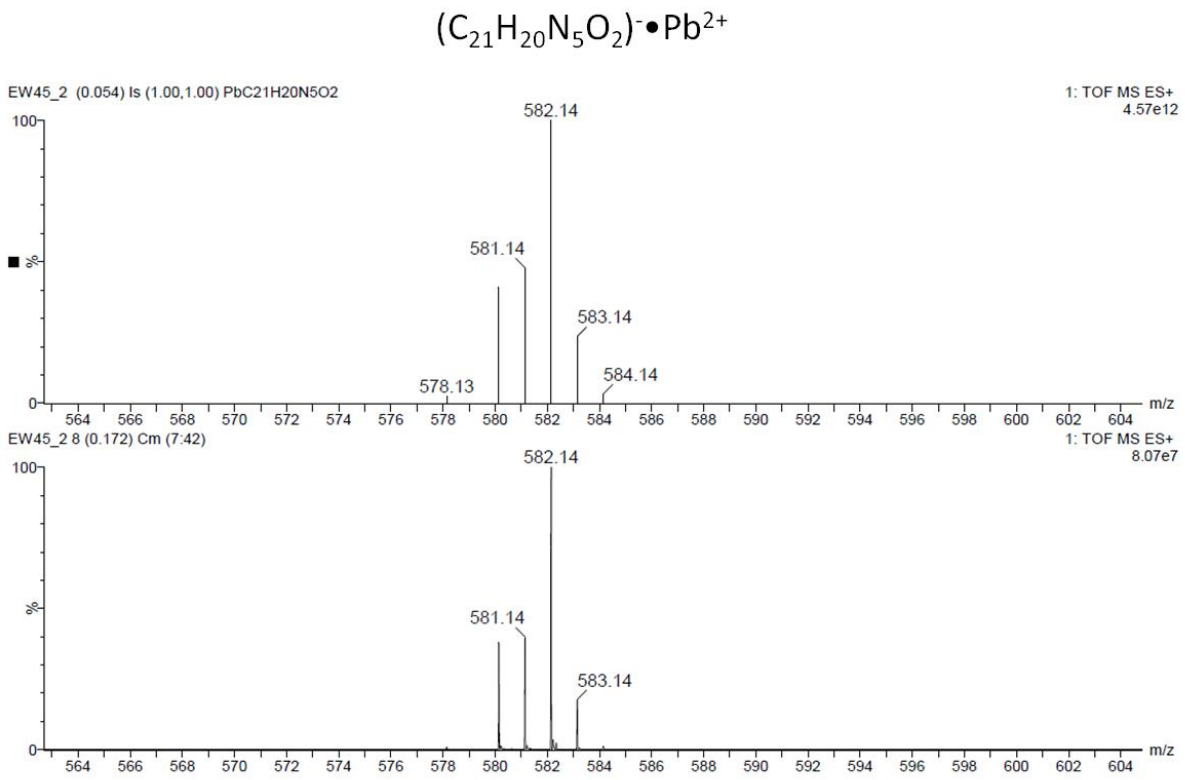

Fig. S13e. Theoretically calculated and experimental isotope pattern of peak m/z 582 in lead(II) complex of **3**

6. Ionic species detected in ESI mass spectra of lead (II) complex of crown 4

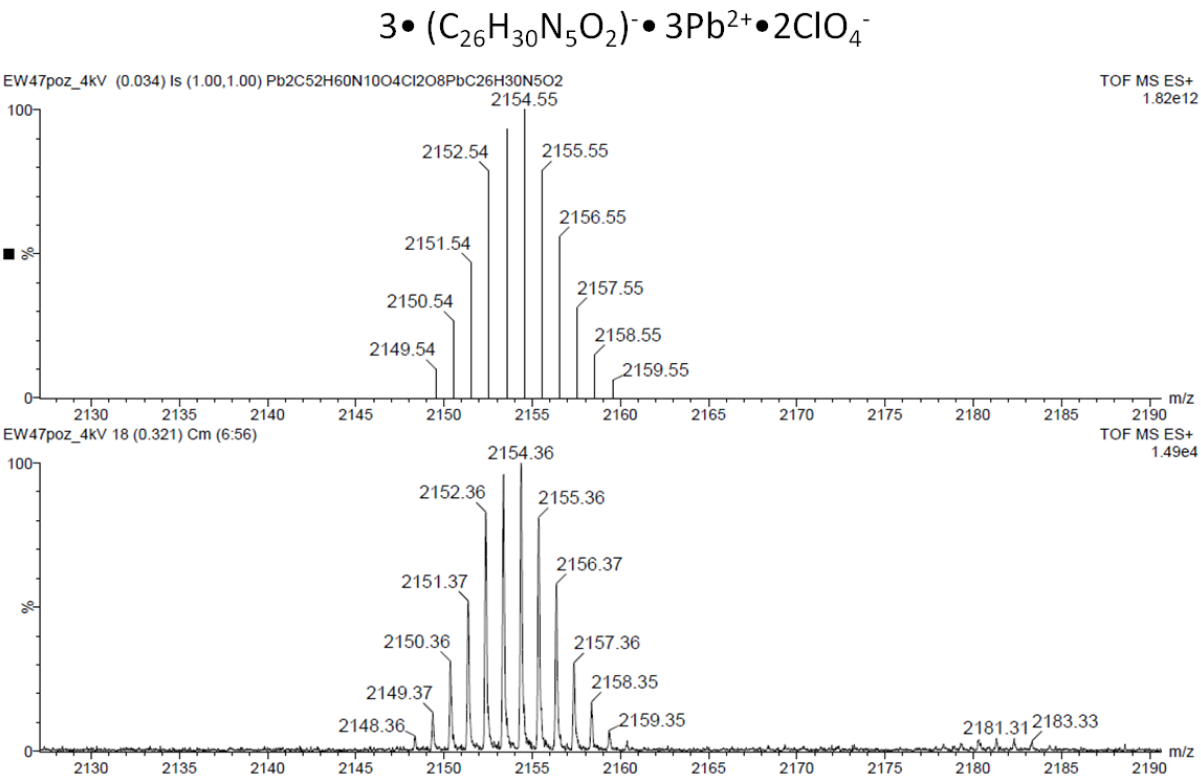

Fig. S14a. Theoretically calculated and experimental isotope pattern of peak m/z 2154 in lead(II) complex of **4**

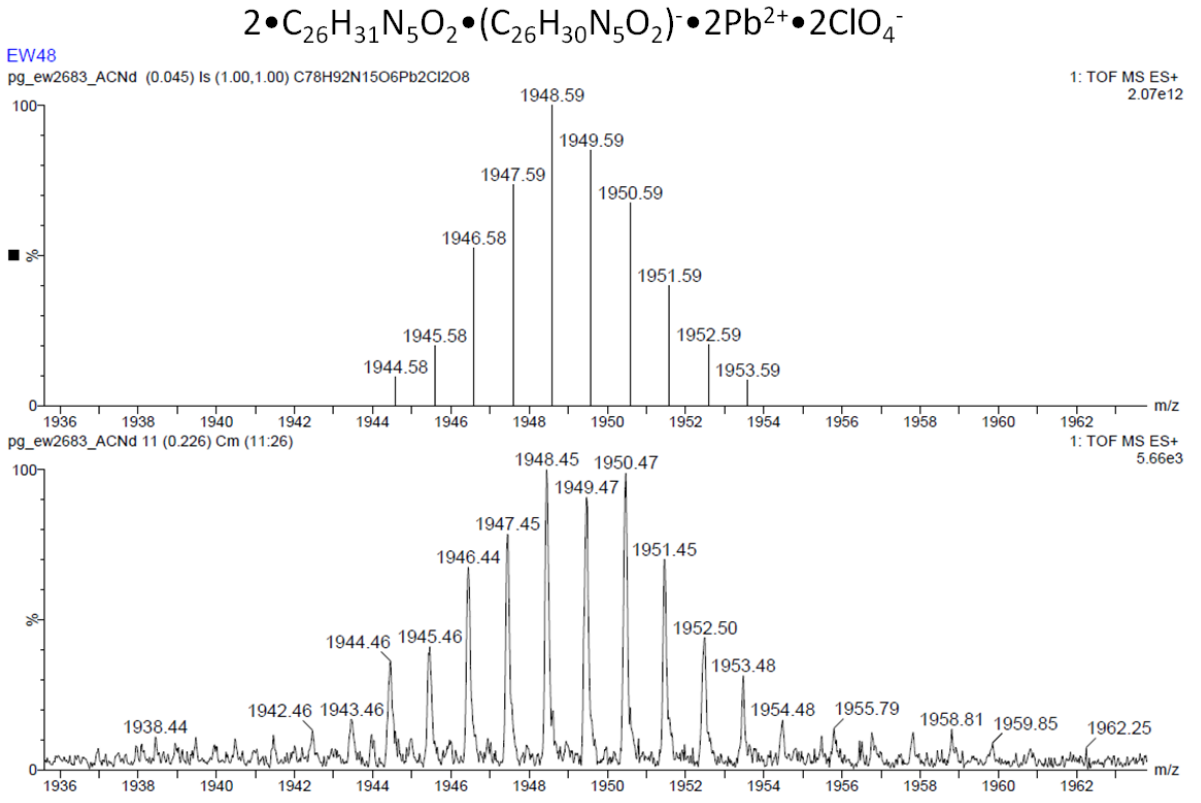

Fig. S14b. Theoretically calculated and experimental isotope pattern of peak m/z 1948 in lead(II) complex of **4**

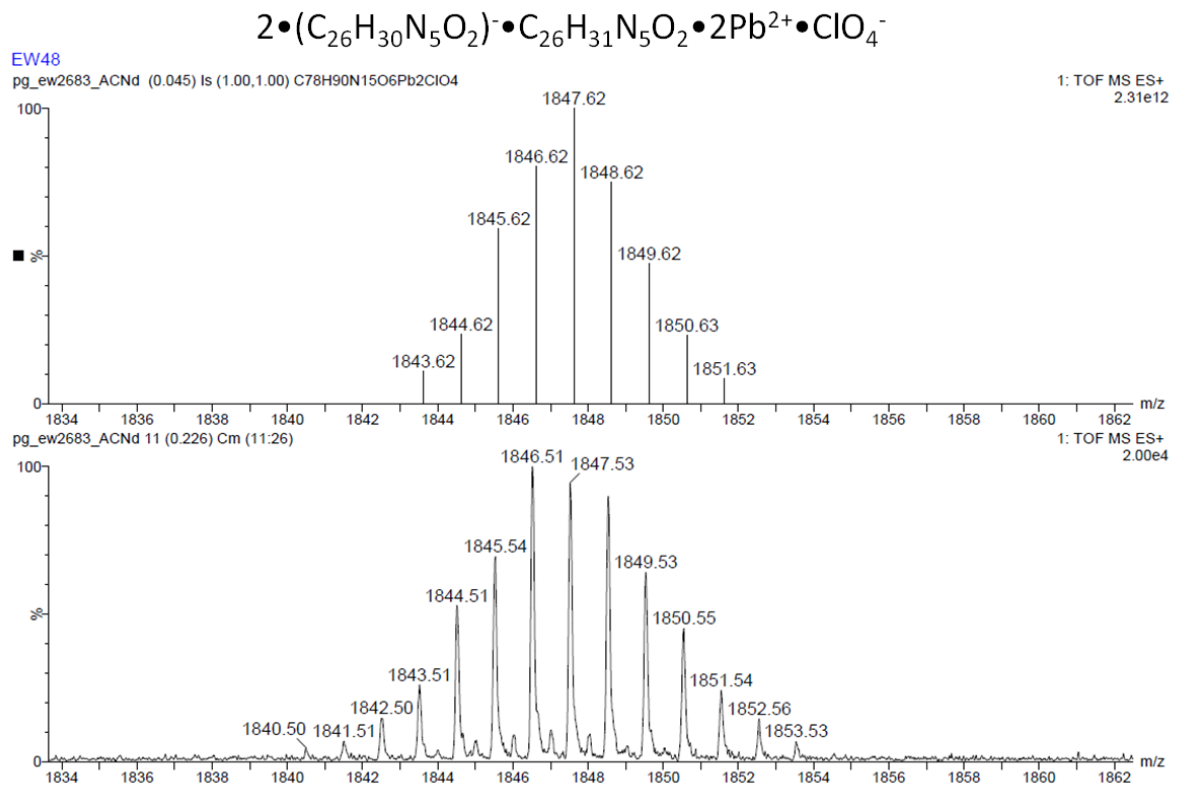

Fig. S14c. Theoretically calculated and experimental isotope pattern of peak m/z 1848 in lead(II) complex of **4**

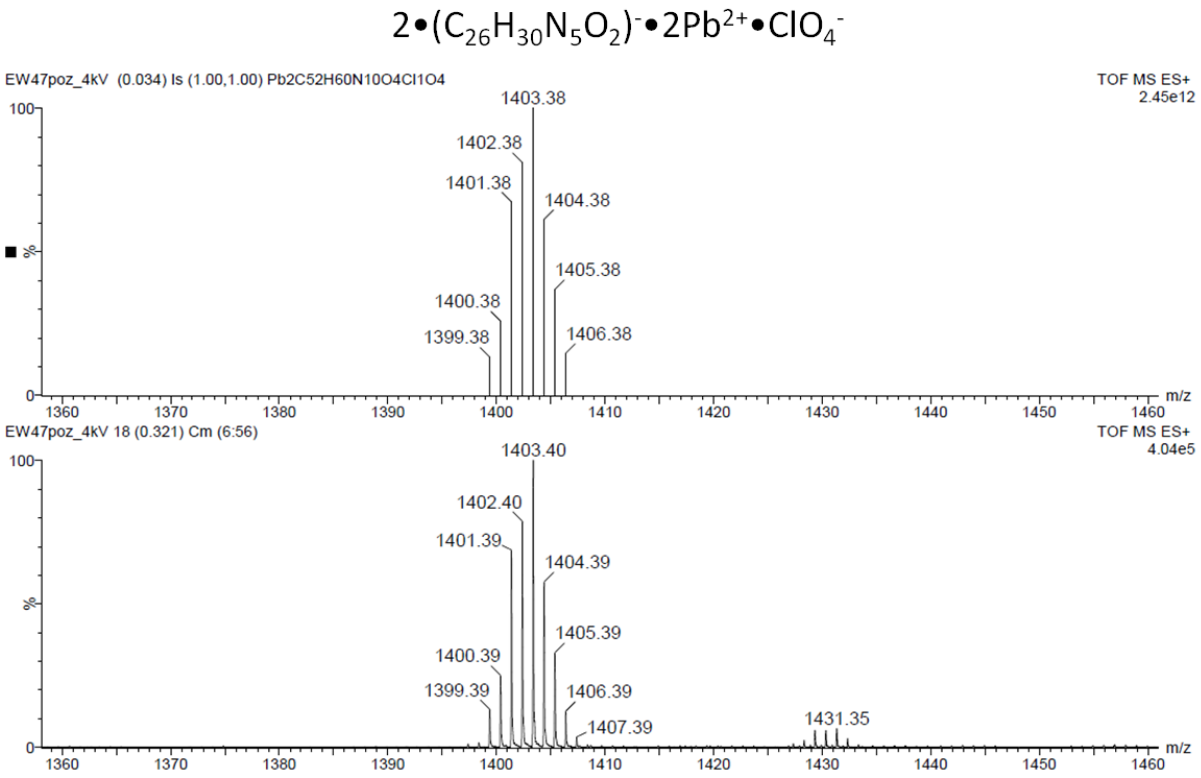

Fig. S14d. Theoretically calculated and experimental isotope pattern of peak m/z 1403 in lead(II) complex of **4**

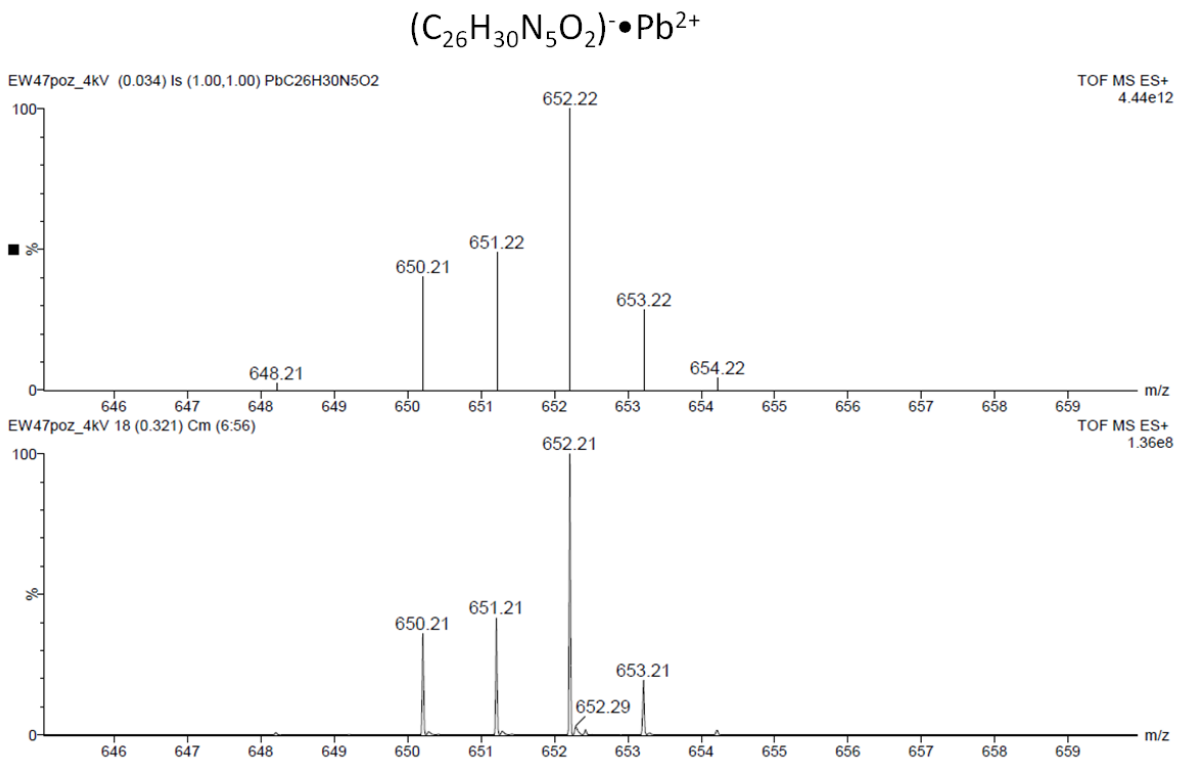

Fig. S14e. Theoretically calculated and experimental isotope pattern of peak m/z 652 in lead(II) complex of **4**

7. X-ray structure of 3

Crystallographic details

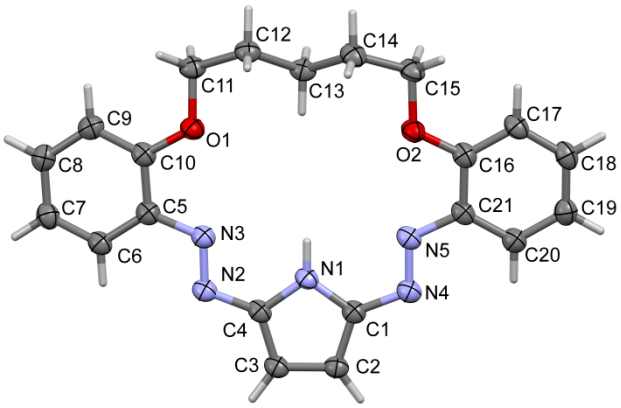

Fig. S15. Molecular view of **3** showing atom labeling scheme. Displacement ellipsoids drawn at 50% probability level. Selected bond lengths (Å) and angles (°): N2-N3 1.278(2), N4-N5 1.281(2), C1-C2 1.391(2), C2-C3 1.398 (3), C3-C4 1.389 (3), O1-C11 1.436 (2), O2-C15 1.438 (2), C12-C13 1.532 (3), C13-C14 1.529 (3); valence angles: C1-N1-C4 108.74 (15), N1-C1-N4 123.38 (16), C1-N4-N5 110.68 (15), N4-N5-C21 114.78 (15), C10-O1-C11 118.38 (14), C15-O2-C16 118.10 (15), C12-C13-C15 109.22 (15); torsions C1-N4N5-C21 -178.64 (14), C4-N2-N5-C5 175.42 (15).

Table S2. Crystal data and structure refinement details for **3**.

	3
CCDC no.	2081633
Empirical formula	$C_{21}H_{21}N_5O_2$
M_r/g mol^{-1}	375.43
Temperature/K	120 K
Crystal system	Orthorhombic
Space group (IT No.)	*Pbca* (61)
a/Å	9.4220 (4)
b/Å	16.9763 (6)
c/Å	22.8215 (7)
α/°	90
β/°	90
γ/°	90
Volume/Å^3	3650.3 (2)
Z	8
ρ_{calc} g/cm^3	1.366
Crystal size/mm^3	0.42 × 0.11 × 0.02
Radiation	Mo Kα (λ = 0.71073)
2Θ range for data collection/°	4.8–58.6
Reflections collected/unique	19075/4927
Completeness to θ_{max} (%)	99.1
Data/restraints/parameters	3615/0/253
Goodness-of-fit on F^2	1.016
Final R indexes [I>=2σ (I)]	R_1 = 0.0595, wR_2 = 0.1451
Final R indexes [all data]	R_1 = 0.0846, wR_2 = 0.1654
Largest diff. peak/hole / e Å^{-3}	0.268/ -0.268

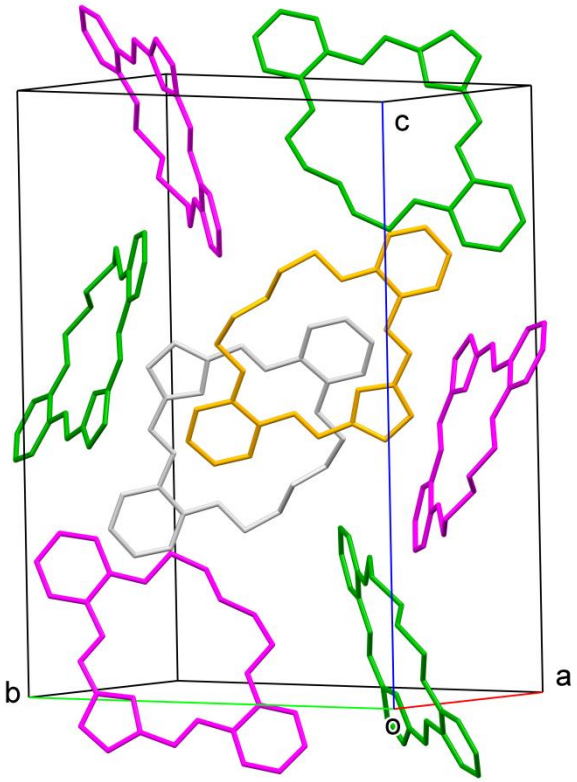

Fig. S16. Crystal packing in **3**. Some molecules form stacking layers in parallel, but some pack almost perpendicular to them making complex space-filling pattern. Molecules are coloured by symmetry operation type, hydrogen atoms omitted.

Experimental details

Crystal data	
Chemical formula	$C_{21}H_{21}N_5O_2$
M_r	375.43
Crystal system, space group	Orthorhombic, *Pbca*
Temperature (K)	120
a, *b*, *c* (Å)	9.4220 (4), 16.9763 (6), 22.8215 (7)
V (Å^3)	3650.3 (2)
Z	8
Radiation type	Mo *K*α
μ (mm^{-1})	0.09
Crystal size (mm)	0.42 × 0.11 × 0.02
Data collection	
Diffractometer	STOE *IPDS* 2T
Absorption correction	–
No. of measured, independent and observed [$I > 2\sigma(I)$] reflections	19075, 4927, 3615
R_{int}	0.046
$(\sin \theta/\lambda)_{max}$ (Å^{-1})	0.688
Refinement	
$R[F^2 > 2\sigma(F^2)]$, $wR(F^2)$, S	0.060, 0.164, 1.02
No. of reflections	4927
No. of parameters	253
H-atom treatment	H-atom parameters constrained
$\Delta\rangle_{max}$, $\Delta\rangle_{min}$ (e Å^{-3})	0.27, -0.27

Computer programs: *X-AREA* WinXpose 2.0.22.0 (STOE, 2016), *X-AREA* Recipe 1.33.0.0 (STOE, 2015), *X-AREA* Integrate 1.72.0.0 (STOE, 2018) *X-AREA X-RED32* 1.63.4.0 (STOE, 2017), ShelXT (Sheldrick, 2015), *SHELXL* (Sheldrick, 2015), Olex2

1 O. V. Dolomanov, L. J. Bourhis, R. J. Gildea, J. A. K. Howard, H. Puschmann, *OLEX2*: a Complete Structure Solution, Refinement And Analysis Program, *J. Appl. Crystallogr.*, 2009, **42**, 339-341.

2 G. M. Sheldrick, *SHELXT* – Integrated Space-Group And Crystal-Structure Determination, *Acta Cryst. A*, 2015, **71**, 3-8.

Computing details

Data collection: *X-AREA* WinXpose 2.0.22.0 (STOE, 2016); cell refinement: *X-AREA* Recipe 1.33.0.0 (STOE, 2015); data reduction: *X-AREA* Integrate 1.72.0.0 (STOE, 2018) *X-AREA X-RED32* 1.63.4.0 (STOE, 2017); program(s) used to solve structure: ShelXT (Sheldrick, 2015); molecular graphics: Olex2 (Dolomanov *et al.*, 2009); software used to prepare material for publication: Olex2 (Dolomanov *et al.*, 2009).

Crystal data	
$C_{21}H_{21}N_5O_2$	D_x = 1.366 Mg m^{-3}
M_r = 375.43	Mo $K\alpha$ radiation, λ = 0.71073 Å
Orthorhombic, *Pbca*	Cell parameters from 18278 reflections
a = 9.4220 (4) Å	θ = 2.4–29.6°
b = 16.9763 (6) Å	μ = 0.09 mm^{-1}
c = 22.8215 (7) Å	T = 120 K
V = 3650.3 (2) Å^3	Plate, red
Z = 8	0.42 × 0.11 × 0.02 mm
F(000) = 1584	
Data collection	
STOE IPDS 2T diffractometer	3615 reflections with $I > 2\sigma(I)$
Radiation source: GeniX Mo, 0.05 x 0.05 mm2 microfocus	R_{int} = 0.046
Detector resolution: 6.67 pixels mm^{-1}	θ_{max} = 29.3°, θ_{min} = 2.4°
rotation method, ω scans	h = -12→12
19075 measured reflections	k = -23→23
4927 independent reflections	l = -31→27
Refinement	
Refinement on F^2	0 restraints
Least-squares matrix: full	Hydrogen site location: inferred from neighbouring sites
$R[F^2 > 2\sigma(F^2)]$ = 0.060	H-atom parameters constrained
$wR(F^2)$ = 0.164	$w = 1/[\sigma^2(F_o^2) + (0.0808P)^2 + 2.2036P]$ where $P = (F_o^2 + 2F_c^2)/3$
S = 1.02	$(\Delta/\sigma)_{max}$ = 0.001
4927 reflections	$\Delta\rangle_{max}$ = 0.27 e Å^{-3}
253 parameters	$\Delta\rangle_{min}$ = -0.27 e Å^{-3}

Special details

Geometry. All esds (except the esd in the dihedral angle between two l.s. planes) are estimated using the full covariance matrix. The cell esds are taken into account individually in the estimation of esds in distances, angles and torsion angles; correlations between esds in cell parameters are only used when they are defined by crystal symmetry. An approximate (isotropic) treatment of cell esds is used for estimating esds involving l.s. planes.

Fractional atomic coordinates and isotropic or equivalent isotropic displacement parameters (Å^2) for ***3***

	x	*Y*	*z*	U_{iso}*/U_{eq}
O1	0.62322 (14)	0.72560 (8)	0.30775 (6)	0.0342 (3)
O2	0.77335 (15)	0.51174 (8)	0.45843 (6)	0.0344 (3)
N1	0.47862 (15)	0.70579 (9)	0.49440 (7)	0.0287 (3)
H1	0.532558	0.683175	0.467790	0.034*
N2	0.39166 (16)	0.81287 (9)	0.43412 (7)	0.0296 (3)
N3	0.46471 (16)	0.78006 (9)	0.39372 (7)	0.0298 (3)
N4	0.51900 (16)	0.61091 (9)	0.57186 (7)	0.0307 (3)
N5	0.59465 (16)	0.57725 (9)	0.53248 (7)	0.0296 (3)
C1	0.45849 (18)	0.67951 (11)	0.55021 (8)	0.0286 (4)
C2	0.36870 (19)	0.73181 (11)	0.57895 (8)	0.0305 (4)
H2	0.337357	0.728078	0.618418	0.037*
C3	0.33319 (19)	0.79092 (11)	0.53887 (8)	0.0305 (4)
H3	0.273675	0.835054	0.546028	0.037*
C4	0.40139 (18)	0.77290 (10)	0.48660 (8)	0.0287 (4)
C5	0.44893 (19)	0.81576 (11)	0.33819 (8)	0.0294 (4)
C6	0.3538 (2)	0.87684 (11)	0.32641 (9)	0.0323 (4)
H6	0.298631	0.898530	0.357286	0.039*
C7	0.3394 (2)	0.90600 (12)	0.27012 (9)	0.0354 (4)
H7	0.274722	0.947658	0.262373	0.042*
C8	0.4201 (2)	0.87402 (12)	0.22485 (9)	0.0341 (4)
H8	0.410254	0.894134	0.186214	0.041*
C9	0.5144 (2)	0.81323 (12)	0.23560 (8)	0.0326 (4)
H9	0.567906	0.791416	0.204263	0.039*
C10	0.53128 (18)	0.78383 (11)	0.29228 (8)	0.0301 (4)
C11	0.69492 (19)	0.68315 (12)	0.26206 (8)	0.0331 (4)
H11A	0.739543	0.720344	0.234190	0.040*
H11B	0.626737	0.649808	0.240283	0.040*
C12	0.80697 (19)	0.63245 (11)	0.29093 (8)	0.0319 (4)
H12A	0.877641	0.667703	0.309448	0.038*
H12B	0.856716	0.602473	0.259899	0.038*
C13	0.75518 (19)	0.57391 (11)	0.33730 (8)	0.0312 (4)
H13A	0.699196	0.601925	0.367522	0.037*
H13B	0.693376	0.533812	0.318834	0.037*
C14	0.8833 (2)	0.53390 (12)	0.36567 (9)	0.0356 (4)
H14A	0.938629	0.507700	0.334345	0.043*
H14B	0.944512	0.575425	0.382682	0.043*
C15	0.8536 (2)	0.47390 (12)	0.41279 (9)	0.0366 (4)
H15A	0.798947	0.429280	0.396337	0.044*
H15B	0.943889	0.453233	0.428795	0.044*
C16	0.75189 (19)	0.47145 (11)	0.50935 (8)	0.0307 (4)
C17	0.8169 (2)	0.39993 (11)	0.52282 (9)	0.0339 (4)
H17	0.880147	0.376149	0.495644	0.041*
C18	0.7891 (2)	0.36368 (11)	0.57596 (9)	0.0354 (4)
H18	0.835126	0.315480	0.585218	0.042*
C19	0.6952 (2)	0.39649 (12)	0.61592 (9)	0.0354 (4)
H19	0.675663	0.370426	0.651864	0.042*
C20	0.6301 (2)	0.46745 (11)	0.60301 (8)	0.0328 (4)
H20	0.566068	0.490189	0.630339	0.039*
C21	0.65790 (18)	0.50607 (11)	0.55005 (8)	0.0291 (4)

Atomic displacement parameters (Å^2) for ***3***

	U^{11}	U^{22}	U^{33}	U^{12}	U^{13}	U^{23}
O1	0.0283 (7)	0.0401 (7)	0.0342 (7)	0.0085 (6)	0.0023 (5)	-0.0009 (6)
O2	0.0307 (7)	0.0331 (7)	0.0395 (7)	0.0051 (5)	0.0070 (6)	0.0020 (6)
N1	0.0208 (7)	0.0314 (7)	0.0339 (7)	0.0031 (6)	0.0026 (6)	-0.0009 (6)
N2	0.0208 (7)	0.0327 (7)	0.0354 (8)	-0.0005 (6)	0.0017 (6)	-0.0012 (6)
N3	0.0231 (7)	0.0319 (7)	0.0342 (8)	-0.0002 (6)	0.0008 (6)	-0.0002 (6)
N4	0.0236 (7)	0.0330 (8)	0.0354 (8)	-0.0001 (6)	-0.0001 (6)	-0.0017 (6)
N5	0.0201 (7)	0.0306 (7)	0.0382 (8)	0.0000 (6)	-0.0010 (6)	-0.0025 (6)
C1	0.0208 (8)	0.0308 (8)	0.0342 (9)	-0.0015 (6)	0.0007 (6)	-0.0001 (7)
C2	0.0245 (8)	0.0334 (9)	0.0337 (9)	0.0001 (7)	0.0022 (7)	-0.0020 (7)
C3	0.0223 (8)	0.0325 (9)	0.0368 (9)	0.0009 (7)	0.0017 (7)	-0.0022 (7)
C4	0.0196 (8)	0.0289 (8)	0.0377 (9)	0.0003 (6)	0.0002 (7)	-0.0006 (7)
C5	0.0217 (8)	0.0317 (8)	0.0350 (9)	-0.0022 (7)	-0.0004 (7)	-0.0001 (7)
C6	0.0257 (8)	0.0328 (9)	0.0384 (9)	0.0011 (7)	0.0001 (7)	-0.0004 (8)
C7	0.0294 (9)	0.0354 (9)	0.0414 (10)	0.0020 (8)	-0.0020 (8)	0.0037 (8)
C8	0.0297 (9)	0.0369 (9)	0.0356 (9)	-0.0042 (8)	-0.0032 (7)	0.0037 (8)
C9	0.0257 (8)	0.0378 (9)	0.0343 (9)	-0.0043 (7)	0.0006 (7)	-0.0015 (8)
C10	0.0205 (8)	0.0325 (8)	0.0373 (9)	-0.0013 (7)	-0.0009 (7)	-0.0003 (7)
C11	0.0238 (8)	0.0411 (10)	0.0343 (9)	0.0008 (7)	0.0034 (7)	-0.0034 (8)
C12	0.0218 (8)	0.0376 (9)	0.0364 (9)	0.0009 (7)	0.0032 (7)	-0.0017 (8)
C13	0.0218 (8)	0.0336 (9)	0.0382 (9)	-0.0020 (7)	0.0037 (7)	-0.0044 (8)
C14	0.0240 (8)	0.0390 (10)	0.0438 (10)	0.0039 (8)	0.0059 (7)	-0.0003 (9)
C15	0.0298 (9)	0.0351 (9)	0.0451 (11)	0.0066 (8)	0.0093 (8)	-0.0009 (8)
C16	0.0207 (8)	0.0313 (8)	0.0400 (9)	-0.0018 (7)	-0.0010 (7)	0.0012 (7)
C17	0.0239 (8)	0.0328 (9)	0.0451 (10)	0.0028 (7)	-0.0001 (7)	-0.0004 (8)
C18	0.0255 (9)	0.0323 (9)	0.0483 (11)	0.0011 (7)	-0.0072 (8)	0.0032 (8)
C19	0.0332 (10)	0.0348 (9)	0.0382 (10)	-0.0013 (8)	-0.0046 (8)	0.0024 (8)
C20	0.0278 (9)	0.0342 (9)	0.0364 (9)	-0.0003 (7)	-0.0013 (7)	-0.0008 (8)
C21	0.0200 (8)	0.0292 (8)	0.0381 (9)	-0.0002 (6)	-0.0025 (7)	-0.0013 (7)

Geometric parameters (Å, º) for ***3***

O1—C10	1.361 (2)	C9—H9	0.9500
O1—C11	1.436 (2)	C9—C10	1.396 (3)
O2—C15	1.438 (2)	C11—H11A	0.9900
O2—C16	1.363 (2)	C11—H11B	0.9900
N1—H1	0.8800	C11—C12	1.513 (3)
N1—C1	1.363 (2)	C12—H12A	0.9900
N1—C4	1.364 (2)	C12—H12B	0.9900
N2—N3	1.278 (2)	C12—C13	1.532 (3)
N2—C4	1.380 (2)	C13—H13A	0.9900
N3—C5	1.412 (2)	C13—H13B	0.9900
N4—N5	1.281 (2)	C13—C14	1.529 (3)
N4—C1	1.388 (2)	C14—H14A	0.9900
N5—C21	1.406 (2)	C14—H14B	0.9900
C1—C2	1.391 (2)	C14—C15	1.507 (3)
C2—H2	0.9500	C15—H15A	0.9900
C2—C3	1.398 (3)	C15—H15B	0.9900
C3—H3	0.9500	C16—C17	1.394 (3)
C3—C4	1.389 (3)	C16—C21	1.411 (3)
C5—C6	1.397 (3)	C17—H17	0.9500
C5—C10	1.412 (3)	C17—C18	1.385 (3)
C6—H6	0.9500	C18—H18	0.9500
C6—C7	1.384 (3)	C18—C19	1.387 (3)
C7—H7	0.9500	C19—H19	0.9500
C7—C8	1.393 (3)	C19—C20	1.383 (3)
C8—H8	0.9500	C20—H20	0.9500
C8—C9	1.384 (3)	C20—C21	1.400 (3)
C10—O1—C11	118.38 (14)	C12—C11—H11B	110.3
C16—O2—C15	118.10 (15)	C11—C12—H12A	108.1
C1—N1—H1	125.6	C11—C12—H12B	108.1
C1—N1—C4	108.74 (15)	C11—C12—C13	116.59 (15)
C4—N1—H1	125.6	H12A—C12—H12B	107.3
N3—N2—C4	112.09 (15)	C13—C12—H12A	108.1
N2—N3—C5	113.80 (15)	C13—C12—H12B	108.1
N5—N4—C1	110.68 (15)	C12—C13—H13A	109.8
N4—N5—C21	114.78 (15)	C12—C13—H13B	109.8
N1—C1—N4	123.38 (16)	H13A—C13—H13B	108.3
N1—C1—C2	108.45 (16)	C14—C13—C12	109.22 (15)
N4—C1—C2	128.16 (17)	C14—C13—H13A	109.8
C1—C2—H2	126.4	C14—C13—H13B	109.8
C1—C2—C3	107.16 (16)	C13—C14—H14A	108.0
C3—C2—H2	126.4	C13—C14—H14B	108.0
C2—C3—H3	126.5	H14A—C14—H14B	107.3
C4—C3—C2	107.04 (16)	C15—C14—C13	117.09 (16)
C4—C3—H3	126.5	C15—C14—H14A	108.0
N1—C4—N2	124.04 (16)	C15—C14—H14B	108.0
N1—C4—C3	108.59 (16)	O2—C15—C14	108.21 (15)
N2—C4—C3	127.33 (16)	O2—C15—H15A	110.1
C6—C5—N3	123.97 (17)	O2—C15—H15B	110.1
C6—C5—C10	119.65 (17)	C14—C15—H15A	110.1
C10—C5—N3	116.31 (16)	C14—C15—H15B	110.1
C5—C6—H6	119.7	H15A—C15—H15B	108.4
C7—C6—C5	120.50 (18)	O2—C16—C17	124.03 (17)
C7—C6—H6	119.7	O2—C16—C21	116.42 (16)

C6—C7—H7	120.1	C17—C16—C21	119.55 (17)
C6—C7—C8	119.71 (18)	C16—C17—H17	120.1
C8—C7—H7	120.1	C18—C17—C16	119.78 (18)
C7—C8—H8	119.7	C18—C17—H17	120.1
C9—C8—C7	120.65 (18)	C17—C18—H18	119.4
C9—C8—H8	119.7	C17—C18—C19	121.20 (18)
C8—C9—H9	119.9	C19—C18—H18	119.4
C8—C9—C10	120.27 (18)	C18—C19—H19	120.3
C10—C9—H9	119.9	C20—C19—C18	119.48 (19)
O1—C10—C5	115.84 (16)	C20—C19—H19	120.3
O1—C10—C9	124.94 (17)	C19—C20—H20	119.7
C9—C10—C5	119.21 (17)	C19—C20—C21	120.60 (18)
O1—C11—H11A	110.3	C21—C20—H20	119.7
O1—C11—H11B	110.3	N5—C21—C16	115.87 (16)
O1—C11—C12	107.31 (15)	C20—C21—N5	124.72 (17)
H11A—C11—H11B	108.5	C20—C21—C16	119.37 (17)
C12—C11—H11A	110.3		
O1—C11—C12—C13	57.5 (2)	C5—C6—C7—C8	0.2 (3)
O2—C16—C17—C18	179.56 (17)	C6—C5—C10—O1	178.75 (16)
O2—C16—C21—N5	1.6 (2)	C6—C5—C10—C9	-1.0 (3)
O2—C16—C21—C20	179.44 (16)	C6—C7—C8—C9	0.1 (3)
N1—C1—C2—C3	0.5 (2)	C7—C8—C9—C10	-0.9 (3)
N2—N3—C5—C6	-5.3 (3)	C8—C9—C10—O1	-178.42 (17)
N2—N3—C5—C10	177.70 (15)	C8—C9—C10—C5	1.3 (3)
N3—N2—C4—N1	-0.6 (2)	C10—O1—C11—C12	170.67 (15)
N3—N2—C4—C3	-178.20 (17)	C10—C5—C6—C7	0.3 (3)
N3—C5—C6—C7	-176.65 (17)	C11—O1—C10—C5	171.24 (15)
N3—C5—C10—O1	-4.1 (2)	C11—O1—C10—C9	-9.0 (3)
N3—C5—C10—C9	176.17 (16)	C11—C12—C13—C14	-174.57 (16)
N4—N5—C21—C16	-174.52 (16)	C12—C13—C14—C15	179.94 (16)
N4—N5—C21—C20	7.7 (3)	C13—C14—C15—O2	-57.9 (2)
N4—C1—C2—C3	-178.70 (17)	C15—O2—C16—C17	8.1 (3)
N5—N4—C1—N1	0.1 (2)	C15—O2—C16—C21	-172.16 (17)
N5—N4—C1—C2	179.18 (18)	C16—O2—C15—C14	-170.87 (16)
C1—N1—C4—N2	-176.54 (16)	C16—C17—C18—C19	1.2 (3)
C1—N1—C4—C3	1.4 (2)	C17—C16—C21—N5	-178.69 (16)
C1—N4—N5—C21	-178.64 (14)	C17—C16—C21—C20	-0.8 (3)
C1—C2—C3—C4	0.4 (2)	C17—C18—C19—C20	-1.3 (3)
C2—C3—C4—N1	-1.1 (2)	C18—C19—C20—C21	0.2 (3)
C2—C3—C4—N2	176.75 (17)	C19—C20—C21—N5	178.45 (17)
C4—N1—C1—N4	178.05 (16)	C19—C20—C21—C16	0.8 (3)
C4—N1—C1—C2	-1.2 (2)	C21—C16—C17—C18	-0.2 (3)
C4—N2—N3—C5	175.42 (15)		

P2 – PYRROLE BEARING DIAZOCROWNS: SELECTIVE CHROMOIONOPHORES FOR LEAD(II) OPTICAL SENSING

Sensors & Actuators: B. Chemical 361 (2022) 131678

Contents lists available at ScienceDirect

Sensors and Actuators: B. Chemical

journal homepage: www.elsevier.com/locate/snb

Pyrrole bearing diazocrowns: Selective chromoionophores for lead(II) optical sensing

Błażej Galiński, Ewa Wagner-Wysiecka *

Department of Chemistry and Technology of Functional Materials, Faculty of Chemistry, Gdańsk University of Technology, Narutowicza 11/12, 80-233 Gdańsk, Poland

ARTICLE INFO

Keywords:
Chromoionophore
Macrocycle
Optode
Cellulose triacetate
Lead(II)

ABSTRACT

Diazocrowns of 18-, 21- and 23-membered rings with pyrrole residue as a part of macrocycle were for the first time used as chromoionophores in lead(II) selective optodes. Sensing properties of optodes depend on the type of macrocycle, namely its size and the type of linker: oligoether or hydrocarbon chain. The best results were obtained for optode bearing 18-membered crown with oligoether linker showing linear response range of 8.05×10^{-8}–2.24×10^{-5} M lead(II) and detection limit of 1.15×10^{-8} M. Membrane, based on cellulose triacetate, is lead(II) selective giving color change from red to different shades of blue (pH 5.5). Results obtained for model and real samples of lead(II) showed that easily accessible and regenerable sensor material can be used for spectrophotometric and colorimetric (Digital Color Analysis) detection and determination of lead(II).

1. Introduction

Common environmental pollutant is lead and its salts. Lead(II) has a negative influence on human's health, but also on animals and plants, which are an integral part of our environment [1–11]. Although lead and its salts were almost eliminated from many areas of life and technologies, the Notre-Dame de Paris fire broke out on 15 April 2019 had risen fears about the potential lead(II) intoxication as a result of melting of 410 tons of lead from roof construction and spire of the cathedral. Harmful lead and its compounds can enter the body directly by respiration or by oral route with water or food. It was a reason for the preventive determination of the level of lead in blood in firefighters as well as its content in natural products such as honey [12–18]. Among others such situations need fast, reliable and importantly - field methods of lead detection and determination of the level of contamination.

Various types of sensors are used nowadays in many fields including control of industrial processes, environmental monitoring, clinical analysis and objects of everyday use, including food quality control [19–22]. Widely used are optical sensors due to their relative simplicity coming along with ensuring the accuracy, precision of indications [23–29] and the possibilities of analysis by digital color sensing - Digital Color Analysis (DCA) [30–33]. Selective optical sensors can be obtained among others by use of a selective (chromo)ionophore [34,35] immobilized in the receptor layer. It allows detection and determination of various chemical species in different types of samples and concentration levels (however, the determination of analytes in highly colored samples can sometimes be difficult). Optical sensors are important analytical tool, e.g. in medical diagnostics, clinical and environmental analysis [36–46]. Good candidates for ionophore-based optical sensors seem macrocyclic azocompounds due to relatively simple synthesis, spectral properties and discrimination of analyte according its size [47].

Our studies [48–50] showed that azomacrocyclic derivatives bearing pyrrole residue are lead(II) selective in acetonitrile and mixture of this solvent with water, but also are good lead(II) ionophores when used as ion-carriers in ion selective electrodes. Since that time other derivatives of this class of compounds were obtained and investigated as chromo (fluoro)ionophores [51,52]. Recently, we have investigated the effect of the exchange of oligoether fragment (18- and 21-membered crowns **1** and **2**, Fig. 1) by hydrocarbon chain in 18- and 23-membered crowns **3** and **4** (Fig. 1) on metal cation complexation [53].

Compounds **1**-**4** (Fig. 1) form stable complexes with lead(II) of 3:2 stoichiometry (crown:Pb) in acetonitrile which has been lastly confirmed by mass spectrometry [53]. Lead(II) complexation in acetonitrile and its mixture with water is related to a large spectral shift in UV–Vis absorption spectra observed as a distinct color change of solution from red-orange to blue. Crown **3** was proposed as a selective lead (II) probe in acetonitrile:water mixture with detection limit 56 μg/L. Preliminary studies showed that macrocycles can serve as chromoionophores in optical sensor layers for lead(II) detection in aqueous solution.

* Corresponding author.
E-mail address: ewa.wagner-wysiecka@pg.edu.pl (E. Wagner-Wysiecka).

https://doi.org/10.1016/j.snb.2022.131678
Received 18 December 2021; Received in revised form 28 February 2022; Accepted 6 March 2022

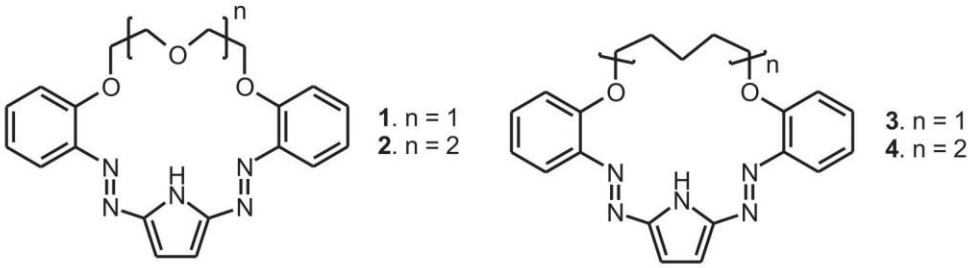

Fig. 1. Diazocrowns 1–4 [48,50,53] with pyrrole moiety in macroring.

In this research, for the first time, four diazobenzocrowns **1**-**4** with pyrrole residue as an integral part of macrocycle were immobilized in a cellulose triacetate (CTA) membrane and were investigated as chromoionophores for lead(II) selective optodes. The spectrophotometric response of prepared optodes towards lead(II) aqueous solution was investigated regarding the influence of membrane composition and pH of solution on the response time, life-time and reversibility of sensor layer, detection limit and linearity of response. Digital Color Analysis (DCA) approach as competing to spectrophotometric measurements was also proposed.

2. Materials and methods

2.1. Chemicals

Chromoionophores **1**-**4** (Fig. 1) were prepared according to the previously reported methods [48,53]. Identity of compounds was confirmed by comparison of spectral and TLC data with data for genuine samples of macrocycles deposited in our lab.

Cellulose triacetate (CTA) was acquired from Acros Organics. Triethylene glycol ≥ 99.0% (TEG) was obtained from Merck (Germany). Bis(1-butylpentyl) adipate ≥ 98.0% (BBPA), dibutyl phthalate ≥ 99.0% (DBP), bis(2-ethylhexyl) phthalate ≥ 99.5% (DOP), bis(2-ethylhexyl) sebacate ≥ 97.0% (DOS) and 2-nitrophenyl octyl ether ≥ 99.0% (NPOE) were purchased from Sigma Aldrich (Selectophore). Potassium tetrakis(4-chlorophenyl)borate ≥ 98.0% (KTClPB) was procured from Fluka (Selectophore). Dichloromethane, chloroform, 2-propanol, acetic acid, hydrochloric acid, disodium ethylenediaminetetraacetate dihydrate (EDTA-Na_2) and ethylenediamine (EDA) were purchased from POCh (Poland).

All aqueous solutions were prepared using ultra-pure water obtained by the reverse osmosis (RO) from Hydrolab Poland station (conductivity <1 μS/cm^{-1}). Nitric acid and sodium hydroxide (p.a.) used for adjusting pH of solutions were purchased from POCh (Poland). Aqueous stock solutions of salts (10^{-2} M) of $NaNO_3$ (≥99.8%), KNO_3 (≥99.8%), $Mg(NO_3)_2 \times 6\ H_2O$ (≥99.0%), $Ca(NO_3)_2 \times 4\ H_2O$ (≥99.0%), $Ni(NO_3)_2 \times 6\ H_2O$ (≥98.0%), $Zn(NO_3)_2 \times 6\ H_2O$ (≥98.0%), $Cd(NO_3)_2 \times 4\ H_2O$ (≥98.0%) from POCh (Poland) and $Cu(NO_3)_2 \times 3\ H_2O$ (≥99.5%) from Merck (Germany) as interfering ions were used. Stock solution (10^{-2} M) of Pb(II) was prepared by dissolving $Pb(NO_3)_2$ (≥99.0%, Alfa Aesar, Massachusetts, USA) (0.0331 g) in nitric acid (1 mL of 10^{-2} M) and diluting it in volumetric flask (10 mL) with deionized water. Working solutions containing Pb(II) were prepared by a serial dilution of the stock solution. For recovery studies Standard Reference Solution of lead (II) 1000 ppm (Merck) was used.

2.2. Instrumentation

All absorbance measurements were carried out using a Unicam UV-300 spectrometer in 1 cm quartz cuvettes (Starna® Brand). pH was monitored using pH-meter CPC-511 with glass electrode EPS-1 (ELMETRON, Poland). The concentration of metal ions in reference sample of real treated industrial wastewater was determined by ICP-OES iCAP 7400 Analyzer.

2.3. Membrane preparation

To obtain the best sensing membrane films in terms of maximum sensitivity towards Pb(II), it was necessary to optimize various experimental conditions. For this purpose four series (A-D), of optodes were prepared, all based on cellulose triacetate (250.0 mg), containing the respective plasticizer and chromoionophores **1, 2, 3** or **4**. Unfortunately membranes with compound **3** can't be obtained, because of crystallization of chromoionophore in the polymer matrix (Fig. S1).

Series A of membranes were based on different types of plasticizers (337.2 mg, d = 1.124 g/mL) and chromoionophore **1**, **2** or **4** (1.0 mg).

Series B of optodes were prepared using triethylene glycol - TEG (337.2 mg) as a plasticizer and different amounts of the respective chromoionophores (0.5–2.0 mg).

Series C of optodes contained varying amounts of TEG (168.6 – 505.8 mg) and the respective amount of chromoionophores from series B.

Series D of membranes consisted of TEG (337.2 mg), 1.0 mg of compounds **1** or **2** or 1.5 mg of compound **4** and different amounts of lipophilic salt KTClPB (0.25–1.00 mg).

The composition of membranes of series A-D with corresponding amounts of all membranes components are shown in Table S1.

All components of each optode from each series were dissolved in dichloromethane (6 mL) with continuous stirring using a magnetic stirrer for 2 h and ultrasonicated for 5 min – to form a clear solution. In the next step, solutions were poured on, prepared in advance (washed with nitric acid, deionized water, acetone and 2-propanol) petri dish (9 cm diameter), covered loosely with a lid and left for solvent evaporation. After 24 h obtained optode films were peeled off from the petri dish and cut into 0.9 × 4.5 cm strips. Blank membranes were prepared in an analogous way using all components besides chromoionophores and lipophilic salt.

2.4. Measurement procedures

2.4.1. Absorbance measurements

Before measurements, membranes were washed three times with deionized water to remove water-soluble additives from the surface. Then the membranes were placed in a quartz cuvette containing nitric acid solution (2.3 mL, 10^{-5} M) in the sample path of the spectrophotometer. Measurements were carried out against blank membranes in the reference path of the spectrophotometer. Then the content of the measurement cell was titrated with a solution of lead(II) nitrate.

In order to avoid the absorbance measurements errors resulting from possible heterogeneity of the optodes prepared in different series, the absorbance value measured at two wavelengths corresponding to the maximum absorbance of the chromoionophore and its complex with lead(II) is given as the spectral response. Then the response is expressed as the difference in absorbance ΔA for two wavelength and calculated using the formula: $\Delta A = (A_{\lambda maxPb}/A_{\lambda max}) - (A_{0\lambda maxPb}/A_{0\lambda max})$, where A_0 is absorbance before and A after contact with lead(II) salt, λ_{max}

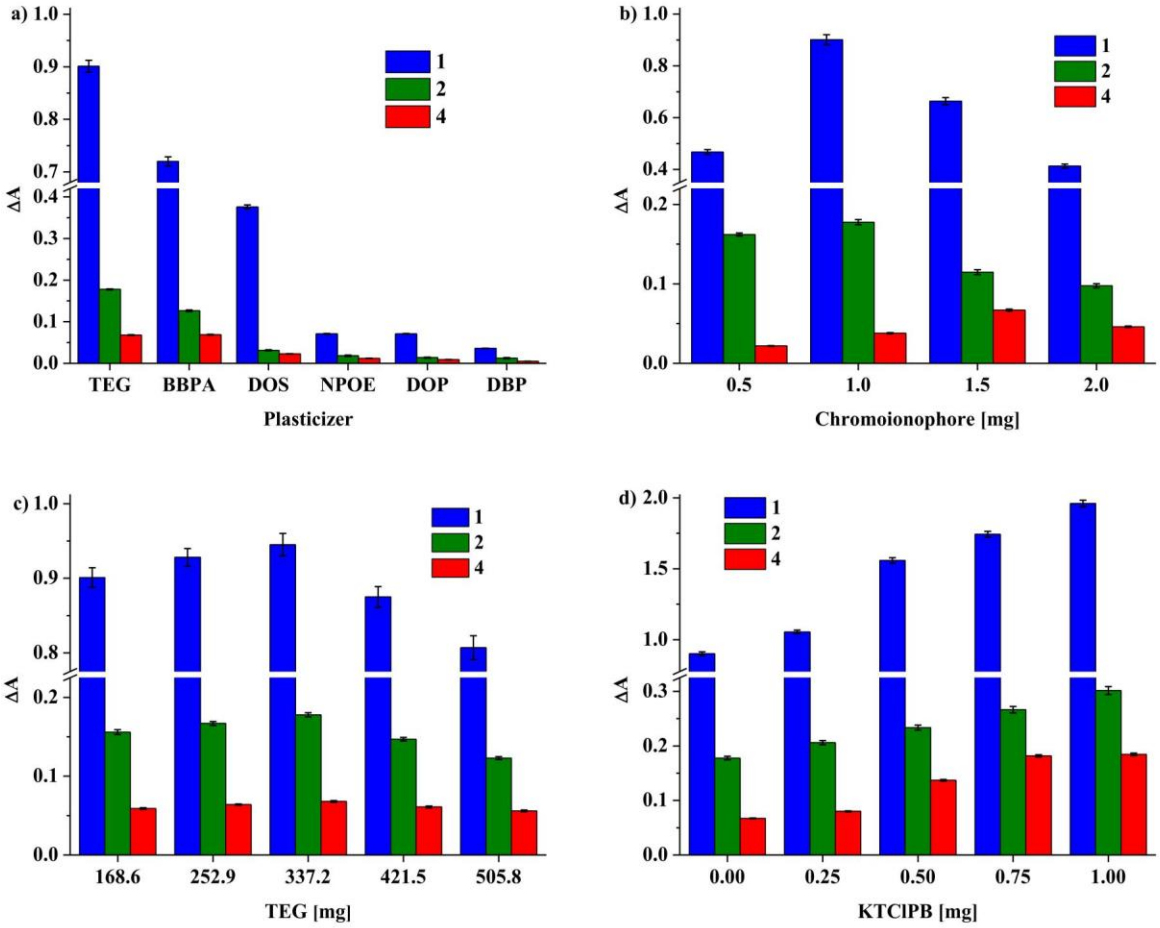

Fig. 2. The effect of a) type of plasticizer, b) amount of chromoionophore [mg], c) amount of TEG [mg] and d) amount of KTClPB [mg] on ΔA value (change of the optical signal, absorbance, in the presence of lead(II) salt) of optodes with chromoionophores **1**, **2** and **4**.

corresponds to maximum absorbance measured for membrane with chromoionophore and λ_{maxPb} is absorbance value at wavelength corresponding to maximum absorbance measured for membrane upon contact with lead(II) salt. Precisely: $A_{\lambda max}$ - the value of absorbance at 518 nm for membranes with azocrown **1** and at 508 nm for optodes with compounds **2** and **4**; $A_{\lambda maxPb}$ - the value of absorbance at 615 nm for membranes with azocrown **1** and at 587 nm for optodes with crowns **2** and **4**.

In competition studies the value of the signal generated by optode in the presence of lead(II) nitrate was recorded before (ΔA_0) and after (ΔA) addition of 10-fold molar excess of interfering metal salt. The influence of interfering ions on spectrophotometric response towards lead(II) was expressed as the absolute value of relative response $RR\% = |[(\Delta A - \Delta A_0)/\Delta A_0]| \times 100\%$.

Limits of detection (LOD) were calculated using expression LOD $= 3\sigma/k$, where σ is the standard deviation of the blank and k is the slope of the linear function $\Delta A = f([Pb(II)])$.

All experiments were carried out in the presence of lead(II) nitrate concentration 10^{-4} M at nitric acid solution (pH 5.50 ± 0.05).

2.4.2. Digital image colorimetry system

Digital images were captured in a photograph lightbox of white sides (20 × 10 × 16 cm) illuminated with 20 LEDs with a color temperature of 6000 K (1.5 W) (Fig. S2). The focusing distance was fixed at 10 cm. Smartphone LG K10 with the Color Analysis application (CA) designed by Roy Leizer [54], was used for capturing digital images. Image data has been processed by cropping to a 260 × 780 pixels rectangular area of the image after immersing the optode in lead(II) nitrate solution. Obtained images were analyzed with a CA application giving the percentage of individual values of red (R), green (G) and blue (B) components of the pixels in the image. These values were saved in an Excel file and sent to a computer to calculate the intensity values of each color. Color change of optode given as ΔE_{RGB} [55–57] was calculated using equation: $\Delta E_{RGB} = [(R_0 - R)^2 + (G_0 - G)^2 + (B_0 - B)^2]^{1/2}$ where R_0, G_0 and B_0 values correspond to membranes dipped in deionized water of pH 5.5 (HNO_3), and R, G and B values correspond to color of membrane after immersing in lead(II) nitrate solution.

3. Results and discussion

3.1. Effect of the individual components of membrane on response value ΔA of the optodes towards lead(II)

Series A of optodes has been investigated in terms of the value of the generated signal depending on the type of plasticizer (Fig. 2a). Optodes were obtained using six most commonly used plasticizers: TEG, BBPA, DOS, NPOE, DOP and DBP. For these screening studies the same amount of each plasticizer i.e. 337.2 mg was used. The highest value of ΔA was obtained for all membranes using TEG. Therefore, this plasticizer was chosen for further studies.

To optimize the amount of chromoionophore, membranes with different quantities (0.5–2.0 mg) of diazocrowns **1**, **2** or **4** were prepared in a series B of membranes. The highest value of ΔA was obtained for optodes with 1.0 mg of compound **1** or **2** and 1.5 mg in the case of chromoionophore **4** (Fig. 2b). More than 1.0 mg of chromoionophore for membranes with crowns **1** or **2** and 1.5 mg for sensor layer with compound **4**, causes the decrease of the observed signal. Worth noting is the highest, among investigated membranes, observed ΔA value for

Table 1
The optimized composition of membranes of optodes with diazobenzocrowns **1**, **2** and **4** as chromoionophores.

Optode	Chromoionophore		KTClPB		TEG		CTA	
	mg	wt%	mg	wt%	mg	wt%	mg	wt%
1	1.00	0.24	0.50	0.12	168.60	40.13	250.00	59.51
2	1.00	0.17	0.50	0.08	337.20	57.28	250.00	42.47
4	1.50	0.25	0.75	0.13	337.20	57.21	250.00	42.41

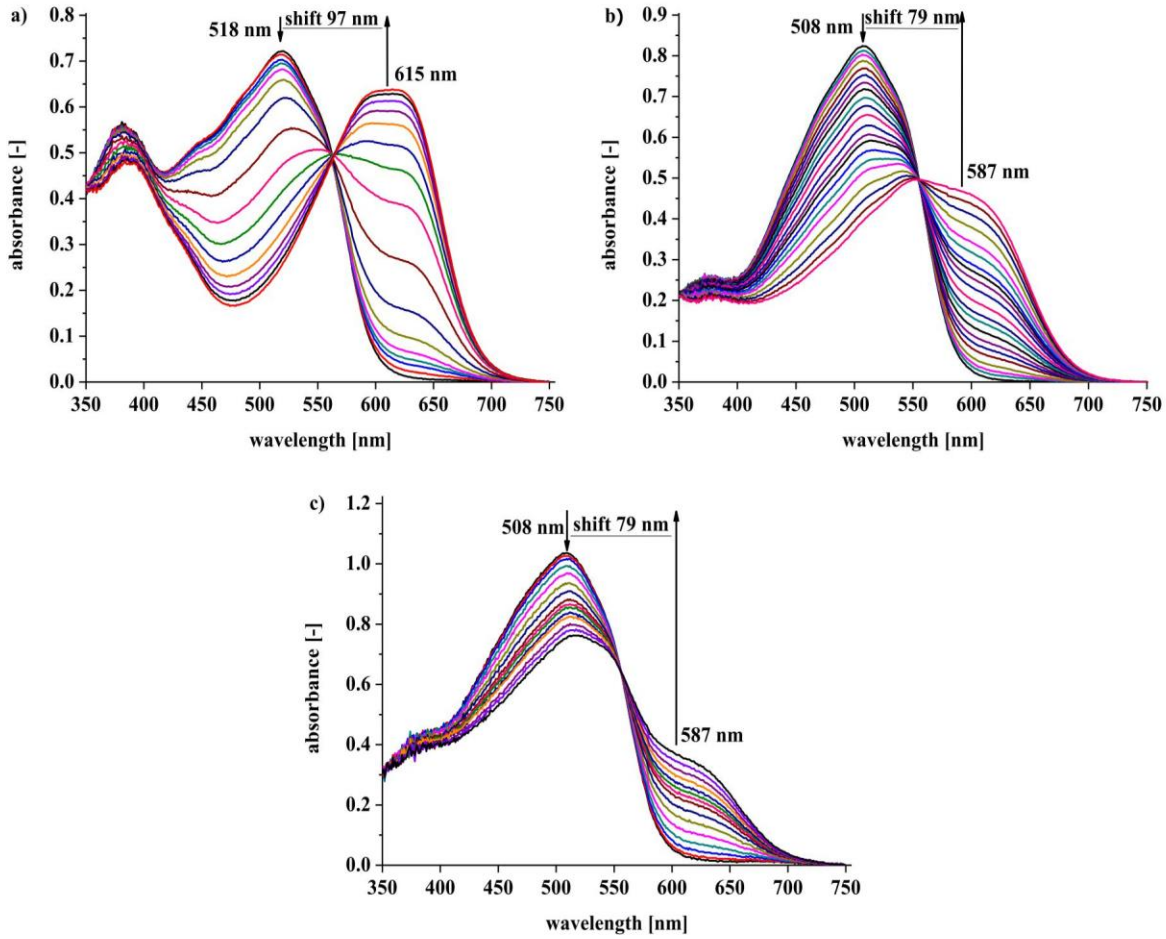

Fig. 3. Changes in UV–Vis spectra of optodes based on diazocrowns: a) **1**, b) **2** and c) **4**, upon titration with aqueous lead(II) nitrate solution in the concentration range of 0–1.25 × 10^{-3} M, 0–2.75 × 10^{-3} M, and 0–1.83 × 10^{-3} M, respectively.

membrane with diazocrown **1** in all cases. Above mentioned quantities of chromoionophores were selected for further research.

The amount of TEG does not significantly affect the response of optodes from series C (Fig. 2c), however, triethylene glycol obviously affects the mechanical properties and membrane durability. For membranes with chromoionophore **1**, maximum amount of TEG is 168.6 mg (150 µl), otherwise the crown eluviation from polymer matrix occurs. For membranes with compounds **2** and **4**, the optimal amount of TEG seems to be 337.2 mg (300 µl). Above this quantity, a slight decrease of response and deterioration of the mechanical properties are noticeable and the membrane ceases to be stiff. The effect of lipophilic salt presence - KTClPB - and its amount (0.25–1.0 mg) on the value of the generated signal ΔA, was checked for the membranes from series B were compared with the optodes from series D. Fig. 2d shows that the highest increase of ΔA signal was obtained for membranes containing 1.0 mg of the KTClPB. For optodes with compound **1** or **2**, the amount of lipophilic salt above 0.5 mg in the membrane, slightly increases the value of the detection limit, however enhances sensitivity (cf. Table S2). The same effect was noticed, when more than 0.75 mg of KTClPB was used in optodes with compound **4**. Having in mind the proposed model of the lead(II) binding by macrocycles **1**-**4** in acetonitrile [53] (realizing that complexation equilibrium can be a different process in pure organic solvent than in membrane) we assume possible functioning mechanism:

$$2Pb^{2+}_{(aq)} + 3LH_{(org)} + 2R^{-}_{(org)} \rightleftarrows (Pb_2L_3H)^{2+}_{(org)} + 2R^{-}_{(org)} + 2H^{+}_{(aq)}$$

where LH is chromoionophore, R^- is the anion of the lipophilic salt and $(Pb_2L_3H)^{2+}$ is a complex. It suggests chromoionophore/lipophilic salt ratio 1.5. On the other hand it was proved that complexes of various stoichiometry can be formed depending on the measurement conditions, e.g. mass spectra registration [53]. Taking all above into account, 0.5 mg of lipophilic salt was selected for further testing of membranes with crowns **1** or **2**, and 0.75 mg for polymer layers with crown **4** as a compromise between detection limit and the sensitivity of the sensing material.

The possible effect of solvent which is used for optode cocktail preparation was also investigated by dissolving all components of membranes in dichloromethane or in chloroform. Interestingly, it was

found that membranes for which dichloromethane was used as solvent characterize larger ΔA values than these for which chloroform was used. All membranes obtained in chloroform showed a lower value of the generated signal (ΔA) than in dichloromethane, regardless of the composition of the receptor layer: type of plasticizer, amount of chromoionophore or amount of additive (Fig. S3a-c). It follows that the use of dichloromethane as a solvent for the preparation of optodes is a better choice (Fig. S4). This can be influenced by the solvent evaporation rate, and perhaps also a tendency to formation of complexes with dichloromethane by azomacrocycles confirmed by the X-ray structure in literature [48].

On the basis of above, for further studies we have chosen as an optimized composition of membranes the composition listed in Table 1.

3.2. UV–Vis spectral characterization of optodes

The response of optodes of composition shown in Table 1 towards lead(II) was investigated spectrophotometrically (Fig. 3). UV–Vis spectra of optodes with crowns **1**, **2** and **4** before contact with lead(II) are similar to spectra of these macrocycles registered in highly apolar solvent - acetonitrile [48,50,53]. Electronic spectra exhibit bands which can be attributed to $\pi \rightarrow \pi^*$ (~390 nm) and $\pi \rightarrow \pi^*$ and/or $n \rightarrow \pi^*$ (~500 nm) electronic transitions typical for chromophore systems with azo group(s) connecting aromatic rings [58]. The spectrophotometric response of optodes in the presence of lead(II) nitrate characterizes with the appearance of a new, bathochromically shifted absorbtion band, which intensity increases with the increasing concentration of lead(II) nitrate (Fig. 3). The maximum of absorption of the optodes with diazocrown **1** is located at 518 nm and for **2** and **4** it is at 508 nm, and is shifted towards 615 (for **1**) and 587 nm (for **2** and **4**) when titrated with aqueous solution of lead(II) nitrate. It is consistent and comparable with spectral and color changes resulting from the formation of complex of 3:2 stoichiometry when titrating acetonitrile solutions of crowns **1**, **2** and **4** with lead(II) perchlorate [50,53]. Thus it can be assumed that the observed spectral pattern for optodes can be a result of the complex formation between macrocyclic chromoionophore entrapped in a polymeric matrix and lead(II) nitrate.

Comparing the obtained results shown in Fig. 3 it is quite well seen that spectral changes - the highest increase of optical signal and the highest spectral shift - are the most pronounced for optodes with crown **1**.

The properties of ion-selective membranes are the result of many factors. The sensing mechanism depends mainly on the properties of ionophore such as its lipophilicity, shape, molar mass and the value of stability constant of complex with target ion. Other membrane components, namely membrane solvent - plasticizer, polymer matrix or ionic additives also affect the characteristics of the sensor layer.

Used by us chromoionophores are macrocyclic compounds of similar structure: two azo groups and pyrrole moiety as parts of macrocycle. The difference is that two of them bear an oligoether chain (**1** and **2**) and in the case of two other (**3** and **4**) ring closure is achieved by introducing hydrocarbon linkage (Fig. 1). Differences in the length of above linkages result in various macrocycle size, namely 18-membered - compounds **1** and **3**, 21- for **2** and 23-membered in case of **4**. The change of linker type obviously affects the lipophilicity of macrocycles (Table S3, Fig. S5). The highest value ($\log P_{TLC}$) 9.42 ± 0.03 was determined for 23-membered crown **4** (ten carbon atoms linkage) and the lowest 5.54 ± 0.05 for 18-membered crown **1** (oligoether moiety).

Macrocycles, as it was reported by us earlier [48,50,53] form in aprotic dipolar solvent - acetonitrile complexes with lead(II) of 3:2 stoichiometry (crown:lead(II)) of relatively high values of stability constants (Table S3, Fig. S5). The highest value of logK 21.10 ± 0.09 was found for complex formed by 21-membered crown **4**, the lowest 18.10 ± 0.01 for 18-membered macrocyle **1**.

Chromogenic crowns **1**, **2** and **4** were successfully incorporated into cellulose triacetate membrane - a polymer matrix of a moderate hydrophobicity [59,60] plasticized with a polar, hydrophilic triethylene glycol. The relative compatibility in hydrophobic/hydrophilic nature between membrane matrix and crown **1** of relatively high, however the lowest, lipophilicity among studied here macrocycles may be one of the reasons for the most promising properties of the obtained sensing layer.

The sensor properties are also dependent on the cation exchange equilibrium between organic (membrane) and aqueous phase, which is on the other hand dependent on the complex formation constant in polymeric matrix [61]. The formation of very stable complexes of relatively high formation constants connected with low dissociation rate usually precludes the use of the particular compound as an effective ionophore in membrane systems. Although given above stability constant values of lead(II) complexes of crowns used here as chromoionophores were determined in acetonitrile, and having in mind that the complex formation unnecessarily must be analogous in polymer membrane, it may be seen that strength of the host-guest interaction correlates with the obtained results for fabricated by us optodes. Namely, more promising in regard to the generated optical signal is optode in which crown **1** of the lowest value of stability constant was used. One more factor connected with the properties of the ionophore and its complex with target ion influencing on optode characteristics, which may be taken under consideration is molar mass. Lower molar mass enables higher mobility in the membrane – which also speaks in favor of using compound **1** as chromoionophore in proposed lead(II) selective optodes.

The effect of the presence of ion-exchange sites as additive components of membranes on the properties of both ion-selective electrodes and optodes was widely discussed in literature as their presence influence the characteristics of sensors [e.g. 62–65]. The positive effect of the use of the lipophilic additives is usually connected among the others with the sensitivity improvement, increasing of the selectivity for divalent over monovalent ions, reduction of the response time, but it was also shown that higher amounts of these components may result in deteriorated detection limit due to increased ion flux across the membranes [66,67]. These and some other reasons discussed in details by Simon and co-workers [62] point, that the components of carrier-based ion-selective electrodes must be chosen very carefully.

The properties of the optodes with crowns **1**, **2** and **4** as chromoionophores are probably the synergistic effect of all mentioned above factors and likely some others, not predicted, connected with the specificity of the investigated system. Thus at this stage, it seems hardly to postulate which of them is dominating. The choice of the membrane of the proposed composition was the compromise among the values of the generated optical signal, linear response range, reversibility and detection limit.

3.2.1. Effect of pH

Aqueous solutions of lead(II) nitrate are undergoing hydrolysis and form hydroxides at pH higher than 5.5 [68–70]. Thus the response of the optodes towards lead(II) obviously can be expected to be influenced by pH. The response of optodes at lead(II) concentration 10^{-4} M in pH range 1–12 (nitric acid/sodium hydroxide) solutions was studied. The response signal (ΔA) increases with the increase of pH in range from 1 to 10 (Fig. S6). Above pH 10 the decrease of signal was observed, which might be connected with the ionization of chromoionophore and its elution from the polymer matrix. Taking all above into account, all further studies were carried out under pH 5.50 ± 0.05.

3.2.2. Response time, reversibility, repeatability and life time

Response time is one of the important factors when considering the applicability of optodes as sensors. To determine the response time, experiments using membranes immersed in solution of lead(II) (10^{-4} M, pH 5.5) with contact time up to 15 min were carried out. ΔA of the optodes as a function of time needed for constant optical signal is shown in Fig. S7. The membranes were found to reach 95% of the final signal (t_{95}) within 7 min for optodes with compound **1**, and 3 min for

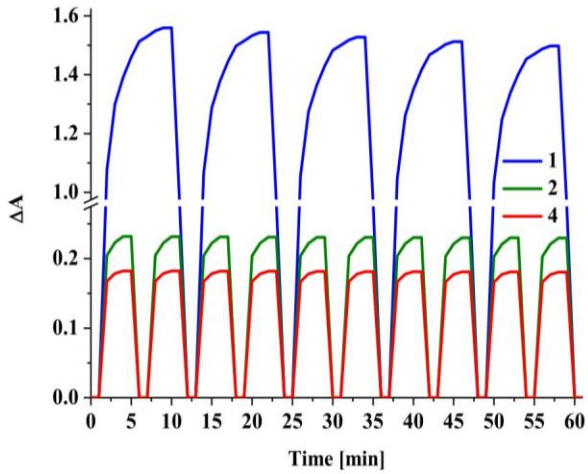

Fig. 4. Regeneration cycles for optodes with crowns **1**, **2** and **4** in 0.1 M HNO_3 solution after contact with lead(II) nitrate solution (10^{-4} M, pH 5.5).

membranes with crowns **2** and **4**. This may be the effect of differences in membrane composition, namely the higher ratio of plasticizer in membranes **2** and **4** comparing membrane **1** affecting the mobility of membrane constituents [63].

The possibility of regeneration of optodes after use - to make them reusable - was checked using as regeneration solutions of HNO_3, HCl, CH_3COOH, EDTA-Na_2 and EDA (10^{-1} and 10^{-2} M). Regeneration time for optodes with compounds **2** and **4**, was 30 s, when using HNO_3 or HCl (10^{-1} M). For membrane with crown **1**, the regeneration time was 2 min. In EDTA-Na_2 and EDA solutions the regeneration time was over 30 min and moreover complete regeneration of membranes was not possible (cf. Fig. S8). Thus 10^{-1} M nitric acid was selected for optodes regeneration. After regeneration, optodes were washed three times with deionized water. In Fig. 4 regeneration of optodes is shown for all prepared membranes. After ten cycles a drift of optical signal was less than 1% for optodes with crows **2** and **4**, and less than 4% after five cycles for membranes with compound **1**.

The reproducibility of optodes was evaluated by comparing the ΔA values of the lead(II) loaded membrane samples obtained in the different series for two concentrations 10^{-5} and 10^{-4} M are shown on Fig. 5. The relative standard deviations for the measured ΔA values for 10^{-5} (n = 10) and 10^{-4} M (n = 10), were 1.1% and 1.5% for optodes with crown **1**, 1.0% and 1.6% for optodes with crown **2**, 1.3% and 1.8% for optodes with crown **4**, respectively.

The life time of all membranes was determined by immersing membranes in nitric acid solution and measuring the value of ΔA over time, i.e. after: 1, 2, 4, 8, 24, 48, 72, 168 (7 days) and 336 h (14 days). No significant loss of signal was found. Membranes were found to be insensitive to sunlight after 14 days. Membranes that were used and left to dry out typically for cellulose triacetate material undergo deformation, losing their mechanical properties (mainly flexibility). Thus between measurements optodes should be kept in solution, preferentially in nitric acid solution. Just prepared optodes and not used for measurements can be stored safely for a period of at least 3 months in a dry and dark place (room conditions) without losing their properties (Fig. S9).

3.2.3. *Effect of interfering ions*

The response of prepared optodes was investigated in the presence of several interfering metal ions: Na^+, K^+, Ca^{2+}, Mg^{2+}, Ni^{2+}, Cu^{2+}, Zn^{2+}, Cd^{2+}. Fig. 6 shows the influence of addition of 10-fold molar excess of interfering ion salt on the generated signal ΔA of optodes immersed in 10^{-4} M solution of lead(II) nitrate (pH 5.5), as RR% value. Only in the presence of copper(II) RR% value exceeds 5%, however just in case of optode with 21-membered crown **2** as chromoionophore this value is higher than 30%. For **1** and **4** the interference from copper is about 6%. The interference from copper(II) is not surprising, taking into account the agreement with results obtained in metal cation complexation studies in solution for crowns **1**, **2** and **4** [53].

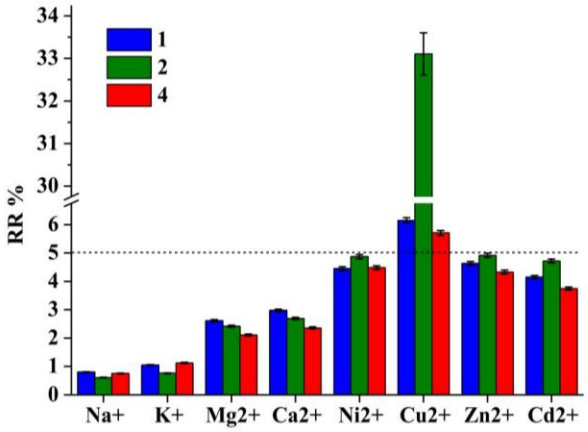

Fig. 6. Interferences of several metal cations (used in 10-fold molar excess), expressed as RR%, to spectral response (ΔA) of optodes with chromoionophores **1** (at 615 nm), **2** (at 587 nm) and **4** (at 587 nm) towards lead(II) nitrate (pH 5.5).

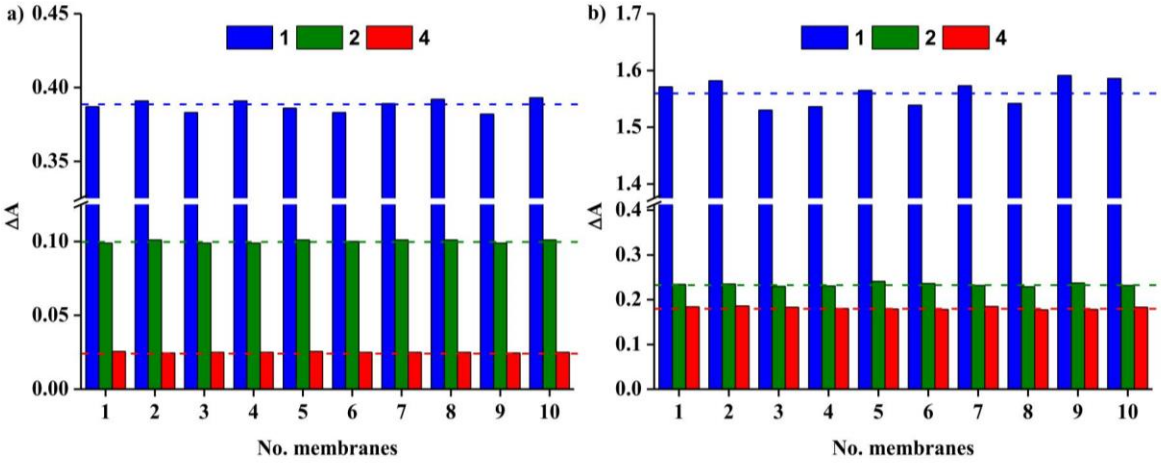

Fig. 5. Reproducibility of optodes with crowns **1**, **2** and **4** after contact with lead(II) nitrate solution a) 10^{-5} M and b) 10^{-4} M (pH 5.5).

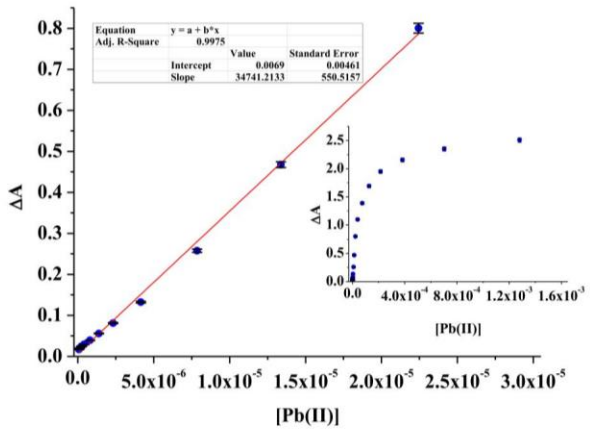

Fig. 7. The optical response ΔA of prepared optodes with chromoionophore **1** to lead(II) concentration. Inset: full range of response.

3.2.4. Linear response range

The optical response ΔA of prepared optodes depending on the used chromoionophore show various ranges of linear responses to lead(II) concentration as it is shown in Figs. 7 and 8. For optode with crown **1** (Fig. 7) linear response was found for lead(II) concentration range of 8.05×10^{-8}–2.24×10^{-5} M with a regression equation of ΔA = 34,741.2133[Pb(II)] + 0.0069 (R^2 = 0.998) and detection limit 1.15×10^{-8} M. At concentration ca. 2.0×10^{-3} M sensor riches saturation with analyte. For optodes with chromoionophores **2** and **4** the linear response range of ΔA vs. lead(II) concentration was found to be relatively narrow. Thus the use of semilogarithmic calibration curves for low concentrations seems to be more convenient (Fig. 8). Then linear response range for optode with compound **1** in semilogarithmic scale covers concentrations 7.86×10^{-6}–3.83×10^{-4} M, for **2** 1.51×10^{-6}–2.02×10^{-4} M and for **4** 4.00×10^{-5}–1.83×10^{-3} M, with regression equations ΔA = 1.1639 log[Pb(II)] + 6.1962 (R^2 = 0.999), ΔA = 0.1248 log[Pb(II)] + 0.7245 (R^2 = 0.996) and ΔA = 0.2071 log[Pb(II)] + 0.9836 (R^2 = 0.995) for **1**, **2** and **4**, respectively. The detection limit of the sensor membranes (n = 10) was found to be 4.79×10^{-6} M, 1.84×10^{-6} M and 2.03×10^{-5} M, for optodes with crowns **1**, **2** and **4**, respectively.

3.3. Comparison of optodes with already existing ones

In Table 2 the properties of lead(II) selective optodes described in literature [71–81] are listed for comparison with the characteristics of membranes obtained in our studies. From this comparison it is quite well seen that optodes obtained by us are, in general, more or less comparable with those proposed by other authors. However, saying that, the optode with 18-membered macrocycle **1** having comparable LOD value and the range of linear response coming along with relatively short response time can compete with most of the optodes listed in Table 2.

3.4. Digital image colorimetry

The colorimetric analysis of the digital images was carried out in parallel with the study of the spectrophotometric response of the optodes. Fig. 9 show color changes of optodes with chromoionophores **1**, **2** and **4** after contact with solutions of different concentrations of lead(II) nitrate at pH 5.5. Photos were taken using a Smartphone camera. The most visible color changes, which can be traced by "the naked eye" were observed in the case of the membrane with compound **1**. In the case of materials with chromoionophores **2** and **4** the observed color changes were not spectacular, especially for membranes with crown **4**. Fig. 9a shows the dependence of color change (ΔE_{RGB}) vs. log[Pb(II)] for optode

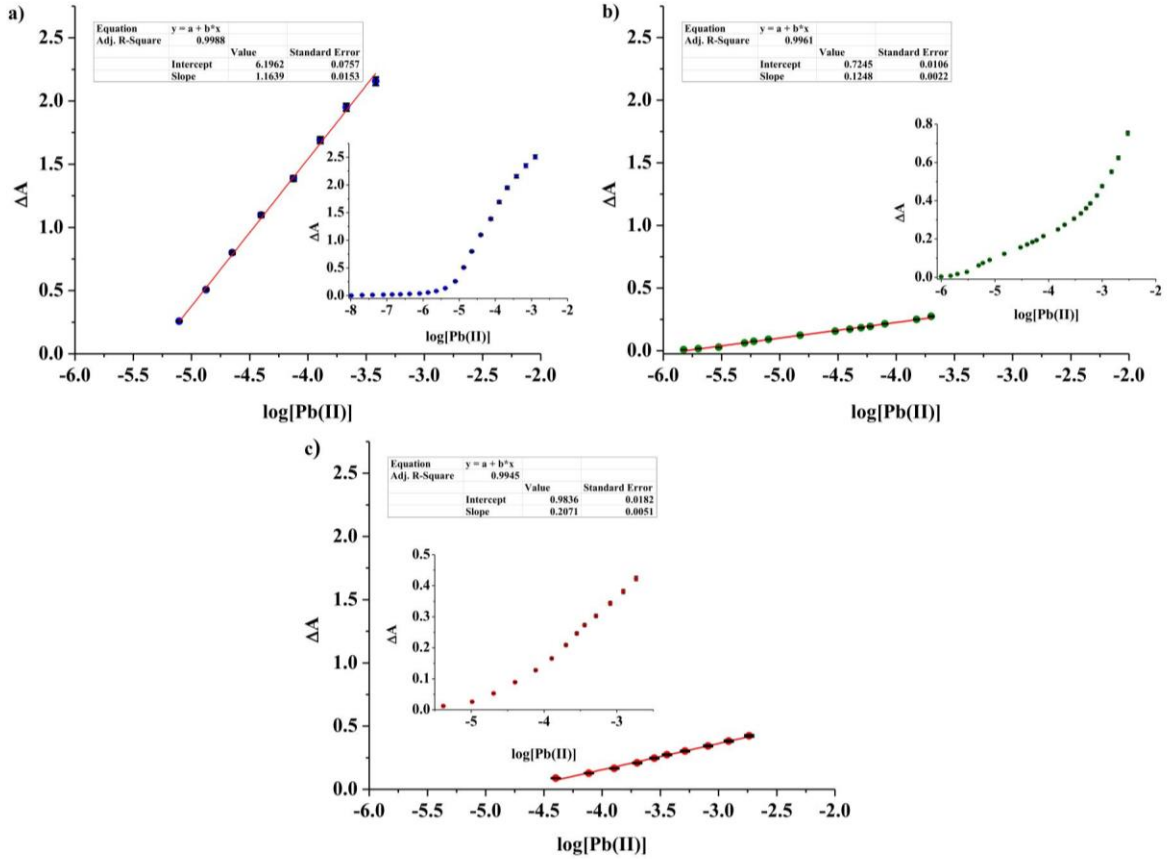

Fig. 8. Calibration curves of optodes with chromoionophores a) **1**, b) **2** and c) **4**. Insets: full range of response.

Table 2
Comparison of obtained optodes with already existing ones.

Sensing material	Support	Dynamic range [Pb (II)]	LOD [Pb (II)]	Response time [min]	Ref.
ETH 5435 + ETH 5418	PVC	5.0×10^{-9}-5.0×10^{-5}	3.2×10^{-12}	order of minutes	[71]
ETH 5493 + ETH 2439	PVC	1.0×10^{-7}-5.0×10^{-2}	N/D	N/D	[72]
PAN + Dibenzodiaza-18-crown-6	PVC	1.0×10^{-8}-5.0×10^{-5}	1.0×10^{-8}	20	[73]
KTBPE[a] + Dibenzo-18-crown-6	PVC	1.0×10^{-5}-1.0×10^{-4}	8.0×10^{-6}	15	[74]
ACAD[b]	CTA	1.0×10^{-6}-5.0×10^{-1}	6.9×10^{-7}	10	[75]
Diphenylcarbazone	PVC	6.9×10^{-6}-1.1×10^{-2}	6.5×10^{-6}	3	[76]
4-hydroxy salophen	CTA	1.0×10^{-7}-1.0×10^{-3}	8.6×10^{-8}	10	[77]
Lead ionophore IV + ETH 5294	PVC	6.2×10^{-8}-5.0×10^{-5}	2.5×10^{-8}	30	[78]
Dithizone	CTA	2.4×10^{-6}-2.7×10^{-5}	7.3×10^{-7}	11–15	[79]
Dithizone	Agarose	1.2×10^{-8}-2.4×10^{-6}	4.0×10^{-9}	28	[80]
Dithizone	Chitosan-Silica	9.7×10^{-7}-5.3×10^{-6}	5.3×10^{-7}	3	[81]
1	CTA	8.1×10^{-8}-2.2×10^{-5}	1.2×10^{-8}	7	This work
2	CTA	1.5×10^{-6}-2.0×10^{-4}	1.8×10^{-6}	3	This work
4	CTA	4.0×10^{-5}-1.8×10^{-3}	2.0×10^{-5}	3	This work

[a] 3′,3′,5′,5′-Tetrabromophenolphthalein ethyl ester potassium salt.
[b] 2-amino-cyclopentene-1-dithiocarboxylic acid.

with compound **1** with the dynamic range covering concentration range 7.79×10^{-7} – 2.07×10^{-4} M and regression equation $\Delta E_{RGB} = 58.44 \log[Pb(II)] + 357.44$ ($R^2 = 0.997$). For membranes with crown **2** (Fig. 9b) the calibration curve in a semilogarithmic scale is linear within 2.37×10^{-5} to 7.10×10^{-4} M of lead(II) salt and calibration curve can be expressed with equation of $\Delta E_{RGB} = 25.39 \log[Pb(II)] + 122.01$ ($R^2 = 0.995$). The response of the optode with compound **4** (Fig. 9c) towards lead(II) can be described by equation $\Delta E_{RGB} = 15.72 \times [Pb(II)] + 75.85$ ($R^2 = 0.997$) with linear range of response in the concentration range of 2.04×10^{-5} – 1.83×10^{-3} M of Pb(II). For detailed data see Tables S4–S6. Comparing slopes of obtained calibration curves, optode **1** characterizes with the highest sensitivity among investigated materials. The detection limits (LOD) are 8.62×10^{-7} M, 2.05×10^{-5} M and 2.33×10^{-5} M for membranes with diazocrowns **1**, **2** and **4**, respectively.

3.5. Analytical performance – determination of Pb(II) in model and real samples

Applications of proposed optodes were tested using different samples: of known lead(II) concentrations – commercial lead(II) standard solution, spiked tap water from different regions of northern Poland, and real industrial sample of treated wastewater of unknown elemental composition. In the last case results were compared with the values obtained by independent analysis using ICP-OES. As a sensor, optode with chromoionophore **1** was chosen, as material of the best properties

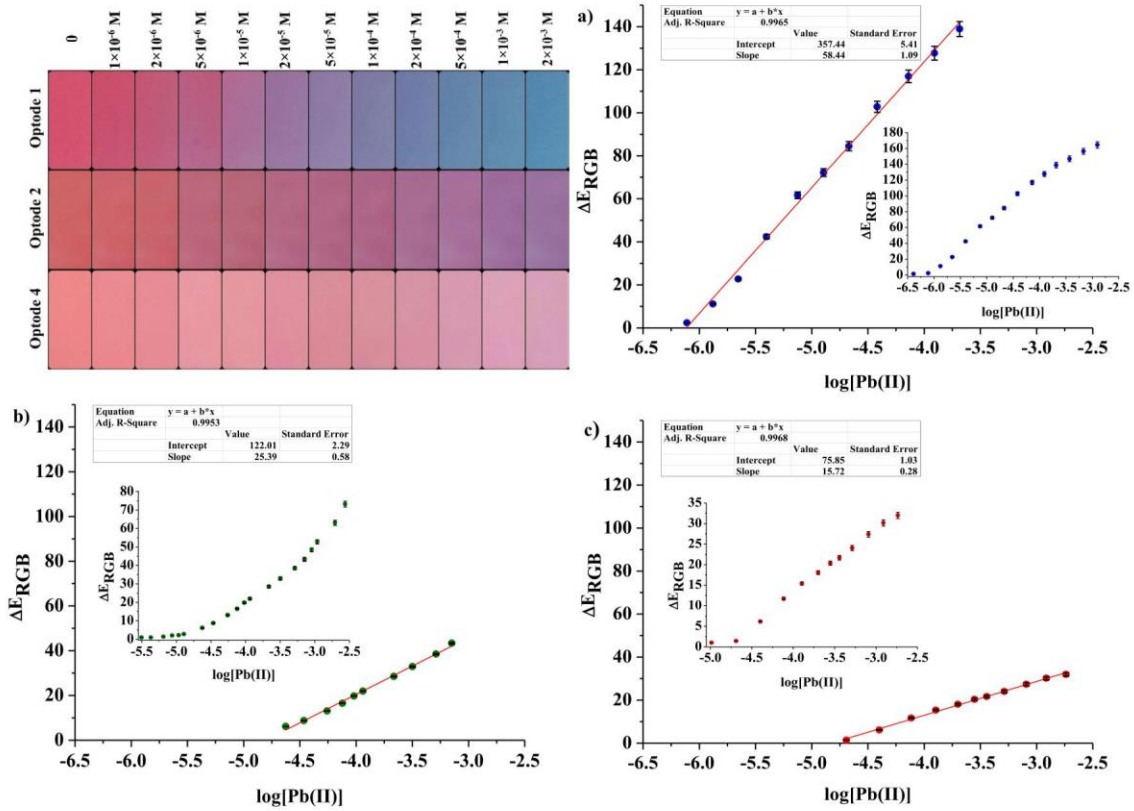

Fig. 9. Left upper corner: Color change of membranes with chromoionophores **1**, **2** and **4** after contact with aqueous lead(II) nitrate at different concentrations (pH 5.5). Calibration curves for membranes with chromoionophores a) **1**, b) **2** and c) **4** as a function of the color change (ΔE_{RGB}) vs. log[Pb(II)] (pH 5.5) Insets: full range response.

Table 3
Determination of lead(II) ions by optode with compound **1** - recovery test for commercial Standard Reference Solution, and in a real sample - spiked tap water.

	Added Pb (II)		Found Pb (II)							
			ΔA		Recovery	RSD	ΔE_{RGB}		Recovery	RSD
	[Pb (II)]	ppb	[Pb (II)]	ppb	%	%	[Pb (II)]	ppb	%	%
Standard Reference Solution of lead(II)	4.76×10^{-8}	9.864	4.84×10^{-8}	10.010	101.59	2.70	<LOD		–	–
	9.94×10^{-8}	20.580	9.90×10^{-8}	20.497	99.60	1.59	<LOD		–	–
	2.43×10^{-7}	50.376	2.45×10^{-7}	50.646	100.82	0.94	<LOD		–	–
	4.86×10^{-7}	100.650	4.81×10^{-7}	99.564	98.97	0.61	<LOD		–	–
Tap water 1	–	–	<LOD		–	–	<LOD		–	–
	4.83×10^{-8}	10.00	4.78×10^{-8}	9.89	98.93	3.26	<LOD		–	–
	4.83×10^{-7}	100.00	4.80×10^{-7}	99.39	99.40	0.34	<LOD		–	–
	4.83×10^{-6}	1000.00	4.85×10^{-6}	1004.58	100.48	0.30	4.89×10^{-6}	1012.32	101.25	0.41
Tap water 2	–	–	<LOD		–	–	<LOD		–	–
	4.83×10^{-8}	10.00	4.89×10^{-8}	10.13	101.31	2.11	<LOD		–	–
	4.83×10^{-7}	100.00	4.84×10^{-7}	100.22	100.22	0.65	<LOD		–	–
	4.83×10^{-6}	1000.00	4.90×10^{-6}	1014.71	101.49	0.45	4.92×10^{-6}	1018.88	101.91	0.57
Tap water 3	–	–	<LOD		–	–	<LOD		–	–
	4.83×10^{-8}	10.00	4.86×10^{-8}	10.07	101.31	2.49	<LOD		–	–
	4.83×10^{-7}	100.00	4.78×10^{-7}	99.03	99.05	0.50	<LOD		–	–
	4.83×10^{-6}	1000.00	4.91×10^{-6}	1016.49	101.67	0.36	4.90×10^{-6}	1014.71	101.49	0.27

Table 4
Determination of lead(II) in treated industrial wastewater using optode with compound **1**.

	ICP-OES		Added Pb (II)		Found Pb (II) ΔA		Recovery	RSD
	[Pb (II)]	ppb	[Pb (II)]	ppb	[Pb (II)]	ppb	%	%
Industrial wastewater	9.51×10^{-8}	19.70	–	–	9.15×10^{-8}	18.95	96.25[a]	3.95
			9.66×10^{-8}	20.00	1.90×10^{-7}	39.33	99.06[b]	1.19
			2.42×10^{-7}	50.00	3.39×10^{-7}	70.13	100.62[b]	0.57

[a] calibration curve.
[b] standard addition method.

among all obtained optodes. All measurements were done at pH 5.5. Both attempts were tested: spectrophotometric (ΔA) and colorimetric (ΔE_{RGB}) detection of lead(II) using a calibration curve method.

Comparison of recovery results obtained for optodes with chromoionophore **1** upon immersion of the sensor layer in a commercial standard lead(II) solution (SRM) of different concentrations are collected in Table 3. The recoveries are at least about 98.97–101.59% (n = 5) for spectrophotometric detection (ΔA) for lead(II) concentrations in range from 4.83×10^{-8} M (10 ppb) to 4.83×10^{-6} M (1000 ppb). Colorimetric determination is possible at concentration 4.83×10^{-6} M (1000 ppb) with recovery 100.96% (n = 5). To evaluate the influence of the sample matrix three different samples of tap water were spiked with known concentration of lead(II) - Table 3. In this case recoveries were within 98.96–101.65% (n = 5) for spectrophotometric detection (ΔA) and 101.24 – 102.28% (n = 5) for Digital Color Analysis attempt (ΔE_{RGB}).

The last probe for testing practical application of the proposed sensor layer was using optode with chromoionophore **1** for spectrophotometric detection of lead(II) in real wastewater sample of the elemental composition shown in Table S7. Trace elements were determined by the ICP-OES method.

In Table 4 results of the recovery test are collected. Recovery when the calibration curve method was used is 96.25% (n = 5), whereas standard addition method was applied the recovery was 99.06–100.62% (n = 5).

Analysis of the recovery test shows successful agreement between our results and the results obtained by both comparison with SRM and obtained by ICP-OES method. It can be concluded that sensing membrane with chromoionophore **1** can be a useful - fast and reliable - analytical tool for detection and determination of lead(II) in aqueous samples.

4. Conclusion

Pyrrole bearing diazocrowns **1**-**4** of different macrocycle size and type of linkers were tested as chromoionophores in optodes based on cellulose triacetate matrix. The best properties: linear response range and detection limit presents sensor material where 18-membered derivative bearing oligoether moiety was used. The obtained optode can be used for the detection and determination of lead(II) in environmental samples, both as a quick qualitative test and for quantitative determination of analyte. Both laboratory applications and also field analyses are worth considering by use of mobile spectrophotometers and using free of charge color application for mobile devices. It might be said that proposed by us, an easy and cheap solution can be considered as at least complementary, if not competitive, for routinely used in environmental analysis methods such as AAS or ICP-OES, which are not only expensive with equipment, but also require well trained staff. To sum up, the proposed optodes can be used for routine analysis of water samples also with portable equipment.

CRediT authorship contribution statement

Błażej Galiński: planning and carrying out of all measurements, data working-up, calculations and visualization, draft interpretation of results, writing draft manuscript. **Ewa Wagner-Wysiecka**: the main conceptual ideas, interpretation and verification of results, writing & editing of the final version, writing - review, supervising project. **Both authors** discussed the results and contributed to the final manuscript.

Declaration of Competing Interest

The authors declare that they have no known competing financial interests or personal relationships that could have appeared to influence the work reported in this paper.

Acknowledgments

This work was supported by the Faculty of Chemistry, Gdańsk University of Technology, Nos. 034718 and 035138 – an internal grants from statutory funds. The authors are grateful to anonymous reviewers for their careful review, which helped us to improve the quality of the above manuscript.

Appendix A. Supplementary material

Supplementary data associated with this article can be found in the online version at doi:10.1016/j.snb.2022.131678.

References

[1] R.S. Boyd, Heavy metal pollutants and chemical ecology: exploring new frontiers, J. Chem. Ecol. 36 (2010) 46–58, https://doi.org/10.1007/s10886-009-9730-5.
[2] K. Jomova, M. Valko, Advances in metal-induced oxidative stress and human disease, Toxicology 283 (2011) 65–87, https://doi.org/10.1016/j.tox.2011.03.001.
[3] P.B. Tchounwou, C.G. Yedjou, A.K. Patlolla, D.J. Sutton, Heavy metal toxicity and the environment, in: A. Luch (Ed.), Molecular, Clinical and Environmental Toxicology, Springer, Basel, 2012, pp. 133–164, https://doi.org/10.1007/978-3-7643-8340-4_6.
[4] S. Squadrone, M. Prearo, P. Brizio, S. Gavinelli, M. Pellegrino, T. Scanzio, S. Guarise, A. Benedetto, M.C. Abete, Heavy metals distribution in muscle, liver, kidney and gill of European catfish (*Silurus glanis*) from Italian rivers, Chemosphere 90 (2013) 358–365, https://doi.org/10.1016/j.chemosphere.2012.07.028.
[5] B.E. Belabed, A. Meddour, B. Samraoui, H. Chenchouni, Modeling seasonal and spatial contamination of surface waters and upper sediments with trace metal elements across industrialized urban areas of the Seybouse watershed in North Africa, Environ. Monit. Assess. 189 (2017) 265, https://doi.org/10.1007/s10661-017-5968-5.
[6] Y. Gan, X. Huang, S. Li, N. Liu, Y.C. Li, A. Freidenreich, W. Wang, R. Wang, J. Dai, Source quantification and potential risk of mercury, cadmium, arsenic, lead, and chromium in farmland soils of Yellow River Delta, J. Clean. Prod. 221 (2019) 98–107, https://doi.org/10.1016/j.jclepro.2019.02.157.
[7] P. Neelam, P. Sumit, M. Anushree, D.K. Singh, Impact assessment of contaminated River Yamuna water irrigation on soil and crop grown in peri-urban area of Delhi-NCR, Environ. Conserv. J. 20 (2019) 99–112, https://doi.org/10.36953/ECJ.2019.20314.
[8] S.C. Obiora, A. Chukwu, T.C. Davies, Contamination of the potable water supply in the lead–Zinc mining communities of Enyigba, Southeastern Nigeria, Mine Water Environ. 38 (2019) 148–157, https://doi.org/10.1007/s10230-018-0550-0.
[9] H. Peng, Y. Chen, L. Weng, J. Ma, Y. Ma, Y. Li, M.S. Islam, Comparisons of heavy metal input inventory in agricultural soils in north and south China: a review, Sci. Total Environ. 660 (2019) 776–786, https://doi.org/10.1016/j.scitotenv.2019.01.066.
[10] H. Can, I.I. Ozyigit, M. Can, A. Hocaoglu-Ozyigit, I.E. Yalcin, Environment-based impairment in mineral nutrient status and heavy metal contents of commonly consumed leafy vegetables marketed in Kyrgyzstan: a case study for health risk assessment, Biol. Trace Elem. Res. 199 (2020) 1123–1144, https://doi.org/10.1007/s12011-020-02208-6.
[11] C. Ma, F. Liu, P. Xie, K. Zhang, J. Yang, J. Zhao, H. Zhang, Mechanism of Pb absorption in wheat grains, J. Hazard. Mater. 415 (2021), 125618, https://doi.org/10.1016/j.jhazmat.2021.125618.
[12] G. Le Roux, F. De Vleeschouwer, D. Weiss, O. Masson, E. Pinelli, W. Shotyk, Learning from the past: fires, architecture, and environmental lead emissions, Environ. Sci. Technol. 53 (2019) 8482–8484, https://doi.org/10.1021/acs.est.9b03869.
[13] K.E. Smith, D. Weis, C. Chauvel, S. Moulin, Honey maps the Pb Fallout from the 2019 fire at Notre-Dame Cathedral, Paris: a geochemical perspective, Environ. Sci. Technol. Lett. 7 (2020) 753–759, https://doi.org/10.1021/acs.estlett.0c00485.
[14] A. van Geen, Y. Yao, T. Ellis, A. Gelman, Fallout of lead over Paris from the 2019 Notre-Dame Cathedral Fire, GeoHealth 4 (2020), https://doi.org/10.1029/2020GH000279 e2020GH000279.
[15] N. Date, A. Sato, K. Takeuchi, T. Mori, K. Yokosuka, Y. Ito, K. Shima, K. Suzuki, H. Taguchi, T. Chiyozaki, K. Yanagawa, T.K. Giles, T. Akitsu, Fire at Notre Dame Cathedral and lead materials in the environment, Fire Sci. Technol. 39 (2020) 17–37, https://doi.org/10.3210/fst.39.17.
[16] P. Glorennec, A. Azema, S. Durand, S. Ayrault, B. Le Bot, The isotopic signature of lead emanations during the fire at Notre Dame Cathedral in Paris, France, Int. J. Environ. Res. Public Health 18 (2021) 5420, https://doi.org/10.3390/ijerph18105420.
[17] A. Vallée, E. Sorbets, H. Lelong, J. Langrand, J. Blacher, The lead story of the fire at the Notre-Dame cathedral of Paris, Environ. Pollut. 269 (2021), 116140 https://doi.org/.1016/j.envpol.2020.116140.
[18] A. Allonneau, S. Mercier, O. Maurin, F. Robardet, A. Menguy-Fleuriot, S.-C. Luu, C. Louyot, N. Jacques, R. Jouffroy, B. Prunet, Lead contamination among Paris Fire Brigade firefighters who fought the Notre Dame Cathedral fire in Paris, Int. J. Hyg. Environ. Health 233 (2021), 113707, https://doi.org/10.1016/j.ijheh.2021.113707.
[19] I. Yaroshenko, D. Kirsanov, M. Marjanovic, P.A. Lieberzeit, O. Korostynska, A. Mason, I. Frau, A. Legin, Real-time water quality monitoring with chemical sensors, Sensors 20 (2020) 3432, https://doi.org/10.3390/s20123432.
[20] J. Tan, J. Xie, Applications of electronic nose (e-nose) and electronic tongue (e-tongue) in food quality-related properties determination: a review, Artif. Intell. Agric. 4 (2020) 104–115, https://doi.org/10.1016/j.aiia.2020.06.003.
[21] J. Saini, M. Dutta, G. Marques, Sensors for indoor air quality monitoring and assessment through internet of things: a systematic review, Environ. Monit. Assess. 193 (2021) 66, https://doi.org/10.1007/s10661-020-08781-6.
[22] J. Perumal, Y. Wang, A. Binte Ebrahim Attia, U.S. Dinish, M. Olivo, Towards a point-of-care SERS sensor for biomedical and agri-food analysis applications: a review of recent advancements, Nanoscale 13 (2021) 553–580, https://doi.org/10.1039/D0NR06832B.
[23] C. McDonagh, C.S. Burke, B.D. MacCraith, Optical chemical sensors, Chem. Rev. 108 (2008) 400–422, https://doi.org/10.1021/cr068102g.
[24] A. Lobnik, M. Turel, S.K. Urek, Optical chemical sensors: design and applications, in: W. Wang (Ed.), Advances in Chemical Sensors, InTech, 2012, pp. 3–28, https://doi.org/10.5772/31534.
[25] G. Mistlberger, G.A. Crespo, E. Bakker, Ionophore-based optical sensors, Annu. Rev. Anal. Chem. 7 (2014) 483–512, https://doi.org/10.1146/annurev-anchem-071213-020307.
[26] X. Xie, E. Bakker, Ion selective optodes: from the bulk to the nanoscale, Anal. Bioanal. Chem. 407 (2015) 3899–3910, https://doi.org/10.1007/s00216-014-8413-4.
[27] K.N. Mikhelson, M.A. Peshkova, Advances and trends in ionophore-based chemical sensors, Russ. Chem. Rev. 84 (2015) 555–578, https://doi.org/10.1070/RCR4506.
[28] I.I. Ebralidze, N.O. Laschuk, J. Poisson, O.V. Zenkina, Colorimetric sensors and sensor arrays, in: O.V. Zenkina (Ed.), Nanomaterials Design for Sensing Applications, Elsevier, 2019, pp. 1–39, https://doi.org/10.1016/B978-0-12-814505-0.00001-1.
[29] X. Du, X. Xie, Ion-Selective optodes: alternative approaches for simplified fabrication and signaling, Sens. Actuators B Chem. 335 (2021), 129368, https://doi.org/10.1016/j.snb.2020.129368.
[30] X. Du, X. Xie, Non-equilibrium diffusion controlled ion-selective optical sensor for blood potassium determination, ACS Sens. 2 (2017) 1410–1414, https://doi.org/10.1021/acssensors.7b00614.
[31] A. Kalinichev, M. Peshkova, N. Pokhvishcheva, K. Mikhelson, Ion-selective optical sensors: a new look at well-established techniques of signal acquisition, Proceedings 2 (2018) 825, https://doi.org/10.3390/proceedings2130825.
[32] G. Albizu, A. Bordagaray, S. Dávila, R. Garcia-Arrona, M. Ostra, M. Vidal, Analytical control of nickel coating baths by digital image analysis, Microchem. J. 154 (2020), 104600, https://doi.org/10.1016/j.microc.2020.104600.
[33] N.Yu Tiuftiakov, A.V. Kalinichev, N.V. Pokhvishcheva, M.A. Peshakova, Digital color analysis for colorimetric signal processing: towards an analytically justified choice of acquisition technique and color space, Sens. Actuators B 344 (2021), 130274, https://doi.org/10.1016/j.snb.2021.130274.
[34] S. Upadhyay, A. Singh, R. Sinha, S. Omer, K. Negi, Colorimetric chemosensors for d-metal ions: a review in the past, present and future prospect, J. Mol. Struct. 1193 (2019) 89–102, https://doi.org/10.1016/j.molstruc.2019.05.007.
[35] G. Fukuhara, Analytical supramolecular chemistry: colorimetric and fluorimetric chemosensors, J. Photochem. Photobiol. C 42 (2020), 100340, https://doi.org/10.1016/j.jphotochemrev.2020.100340.
[36] U.E. Spichiger, D. Freiner, E. Bakker, T. Rosatzin, W. Simon, Optodes in clinical chemistry: potential and limitations, Sens. Actuators B Chem. 11 (1993) 263–271, https://doi.org/10.1016/0925-4005(93)85264-B.
[37] H.N. Kim, W.X. Ren, J.S. Kim, J. Yoon, Fluorescent and colorimetric sensors for detection of lead, cadmium, and mercury ions, Chem. Soc. Rev. 41 (2012) 3210–3244, https://doi.org/10.1039/C1CS15245A.
[38] K.L. Diehl, E.V. Anslyn, Array sensing using optical methods for detection of chemical and biological hazards, Chem. Soc. Rev. 42 (2013) 8596–8611, https://doi.org/10.1039/C3CS60136F.
[39] L. You, D. Zha, E.V. Anslyn, Recent advances in supramolecular analytical chemistry using optical sensing, Chem. Rev. 115 (2015) 7840–7892, https://doi.org/10.1021/cr5005524.
[40] H. Sharma, N. Kaur, A. Singh, A. Kuwar, N. Singh, Optical chemosensors for water sample analysis, J. Mater. Chem. C 4 (2016) 5154–5194, https://doi.org/10.1039/C6TC00605A.
[41] P.V.S. Ajay, J. Printo, D.S.C.G. Kiruba, L. Susithra, K. Takatoshi, M. Sivakumar, Colorimetric sensors for rapid detection of various analytes, Mater. Sci. Eng. C 78 (2017) 1231–1245, https://doi.org/10.1016/j.msec.2017.05.018.
[42] M.J. Kangas, R.M. Burks, J. Atwater, R.M. Lukowicz, P. Williams, A.E. Holmes, Colorimetric sensor arrays for the detection and identification of chemical weapons and explosives, Crit. Rev. Anal. Chem. 47 (2017) 138–153, https://doi.org/10.1080/10408347.2016.1233805.
[43] Y. Ma, Y. Li, K. Ma, Z. Wang, Optical colorimetric sensor arrays for chemical and biological analysis, Sci. China Chem. 61 (2018) 643–655, https://doi.org/10.1007/s11426-017-9224-3.
[44] K. Koren, S.E. Zieger, Optode based chemical imaging-possibilities, challenges, and new avenues in multidimensional optical sensing, ACS Sens. 6 (2021) 1671–1680, https://doi.org/10.1021/acssensors.1c00480.
[45] S. Kumar, R. Singh, Recent optical sensing technologies for the detection of various biomolecules: review, Opt. Laser Technol. 134 (2021), 106620, https://doi.org/10.1016/j.optlastec.2020.106620.
[46] T. Minami, Design of supramolecular sensors and their applications to optical chips and organic devices, Bull. Chem. Soc. Jpn. 94 (2021) 24–33, https://doi.org/10.1246/bcsj.20200233.

[47] E. Wagner-Wysiecka, N. Łukasik, J.F. Biernat, E. Luboch, Azo group(s) in selected macrocyclic compounds, J. Incl. Phenom. Macrocycl. Chem. 90 (2018) 189–257, https://doi.org/10.1007/s10847-017-0779-4.
[48] E. Wagner-Wysiecka, E. Luboch, M. Kowalczyk, J.F. Biernat, Chromogenic macrocyclic derivatives of azoles - synthesis and properties, Tetrahedron 59 (2003) 4415–4420, https://doi.org/10.1016/S0040-4020(03)00618-5.
[49] E. Wagner-Wysiecka, E. Luboch, M. Janrógiewicz, J. Szczygelska-Tao, J.F. Biernat, Metallochromic azole azomacrocyclic reagents, Ann. Pol. Chem. Soc. 4 (2005) 11–14.
[50] E. Luboch, E. Wagner-Wysiecka, M. Fainerman-Melnikova, L.F. Lindoy, J. F. Biernat, Pyrrole azocrown ethers. Synthesis, complexation, selective lead transport and ion-selective membrane electrode studies, Supramol. Chem. 18 (2006) 593–601, https://doi.org/10.1080/10610270600879068.
[51] E. Wagner-Wysiecka, E. Luboch, M. Fonari, The synthesis, X-ray structure and metal cation complexation properties of colored crown with two heterocyclic residues as a part of macrocycle, Pol. J. Chem. 82 (2008) 1319–1330.
[52] E. Luboch, E. Wagner-Wysiecka, T. Rzymowski, M. Fonari, R. Kulmaczewski, Pyrrole azocrown ethers - synthesis, crystal structures, and fluorescence properties, Tetrahedron 67 (2011) 1862–1872, https://doi.org/10.1016/j.tet.2011.01.027.
[53] B. Galiński, E. Luboch, J. Chojnacki, E. Wagner-Wysiecka, Novel diazocrowns with pyrrole residue as lead(II) colorimetric probes, Materials 14 (2021) 7239, https://doi.org/10.3390/ma14237239.
[54] ⟨https://play.google.com/store/apps/details?id=com.leizersoft.coloranalysis&hl=pl&gl=US⟩.
[55] N.A. Gavrilenko, S.V. Muravyov, S.V. Silushkin, A.S. Spiridonovab, Polymethacrylate optodes: a potential for chemical digital color analysis, Measurement 51 (2014) 464–469, https://doi.org/10.1016/j.measurement.2013.11.027.
[56] S.V. Muravyov, A.S. Spiridonova, N.A. Gavrilenko, P.V. Baranov, L. I. Khudonogovo, A digital colorimetric analyzer for chemical measurements on the basis of polymeric optodes, Instrum. Exp. Tech. 59 (2016) 592–600, https://doi.org/10.1134/S0020441216030210.
[57] S.V. Muravyov, N.A. Gavrilenko, N.V. Saranchina, P.V. Baranov, Polymethacrylate sensors for rapid digital colorimetric analysis of toxicants in natural and anthropogenic objects, IEEE Sens. J. 19 (2019) 4765–4772, https://doi.org/10.1109/JSEN.2019.2903314.
[58] M.A.D. Rabbani, B. Khalili, H. Saeidian, Novel edaravone-based azo dyes: efficient synthesis, characterization, antibacterial activity, DFT calculations and comprehensive investigation of the solvent effect on the absorption spectra, RSC Adv. 10 (2020) 35729, https://doi.org/10.1039/d0ra06934e.
[59] Y. Peng, Y. Sui, Compatibility research on PVC/PVB blended membranes, Desalination 196 (2006) 13–21, https://doi.org/10.1016/j.desal.2005.07.053.
[60] G.E. Chen, W.G. Sun, Q. Wu, Y.F. Kong, Z.L. Xu, S.J. Xu, X.P. Zheng, Effect of cellulose triacetate membrane thickness on forward-osmosis performance and application for spent electroless nickel plating baths, J. Appl. Polym. Sci. 38 (2017) 148–157, https://doi.org/10.1007/s10230-018-0550-0.
[61] E. Bakker, M. Willer, M. Lerchi, K. Seller, E. Pretsch, Determination of complex formation constants of neutral cation-selective ionophores in solvent polymeric membranes, Anal. Chem. 66 (1994) 516–521, https://doi.org/10.1021/ac00076a016.
[62] P.C. Meier, W.E. Morf, M. Läubli, W. Simon, Evaluation of the optimum composition of neutral-carrier membrane electrodes with incorporated cation-exchanger sites, Anal. Chim. Acta 156 (1984) 1–8, https://doi.org/10.1016/S0003-2670(00)85531-2.
[63] E. Bakker, P. Bühlmann, E. Pretsch, Carrier-based ion-selective electrodes and bulk optodes. 1. General characteristics, Chem. Rev. 97 (1997) 3083–3132, https://doi.org/10.1021/cr940394a.
[64] O.M. Petrukhin, A.B. Kharitonov, E.V. Frakiisky, Y.I. Urusov, A.F. Zhukov, A. N. Shipway, V.E. Baulin, Effect of lipophilic anionic additives on detection limits of ion-selective electrodes based on ionophores with phosphoryl complexing groups, Sens. Actuators B Chem. 76 (2001) 653–659, https://doi.org/10.1016/S0925-4005(01)00662-1.
[65] D.I. Dekina, A.V. Kalinichev, N.V. Pokhvishcheva, M.A. Peshkova, K.N. Mikhelson, Effects of quantitative composition of the sensing phase in the response of ionophore-based optical sensors, Sens. Actuators B Chem. 277 (2018) 535–543, https://doi.org/10.1016/j.snb.2018.09.018.
[66] S.L.R. Barker, M.R. Shortreed, R. Kopelman, Utilization of lipophilic ionic additives in liquid polymer film optodes for selective anion activity measurements, Anal. Chem. 69 (1997) 990–995, https://doi.org/10.1021/ac960700f.
[67] L. Li, P. Du, Y. Zhang, Y. Qian, P. Zhan, Q. Guo, Intramolecularly hydrogen-bonded cavity containing macrocyclic/acyclic aromatic pyridone foldarands as modularly tunable ionophores for selective potentiometric sensing of metal ions, Sens. Actuators B Chem. 331 (2021), 129385, https://doi.org/10.1016/j.snb.2020.129385.
[68] C.F. Baes, R.S. Mesmer, The Hydrolysis of Cations, John Wiley & Sons, New York, 1976.
[69] R.N. Sylva, P.L. Brown, The hydrolysis of metal ions. Part 3. Lead(II), J. Chem. Soc. Dalton Trans. 9 (1980) 1577–1581, https://doi.org/10.1039/DT9800001577.
[70] J.J. Cruywagen, R.F. van de Water, The hydrolysis of lead(II). A potentiometric and enthalpimetric study, Talanta 40 (1993) 1091–1095, https://doi.org/10.1016/0039-9140(93)80171-M.
[71] M. Lerchi, E. Bakker, B. Rusterholz, W. Simon, Lead-selective bulk optode based on neutral ionophores with subnanomolar detection limits, Anal. Chem. 64 (1992) 1534–1540, https://doi.org/10.1021/ac00038a007.
[72] E. Anticó, M. Lerchi, B. Rusterholz, N. Achermann, M. Badertscher, M. Valiente, E. Pretsch, Monitoring Pb^{2+} with optical sensing films, Anal. Chim. Acta 388 (1999) 327–338, https://doi.org/10.1016/S0003-2670(99)00085-9.
[73] N. Alizadeh, A. Moemeni, M. Shamsipur, Poly(vinyl chloride)-membrane ion-selective bulk optode based on 1,10-dibenzyl-1,10-diaza-18-crown-6 and 1-(2-pyridylazo)-2-naphthol for Cu^{2+} and Pb^{2+} ions, Anal. Chim. Acta 464 (2002) 187–196, https://doi.org/10.1016/S0003-2670(02)00477-4.
[74] Y. Takahashi, T. Hayashita, T.M. Suzuki, Test strips for lead(II) based on a unique color change of PVC-film containing O-donor macrocycles and an anionic dye, Anal. Sci. 23 (2007) 147–150, https://doi.org/10.2116/analsci.23.147.
[75] A.A. Ensafi, Z.N. Isfahani, Determination of lead ions by an optical sensor based on 2-amino-cyclopentene-1-dithiocarboxylic acid, IEEE Sens. J. 7 (2007) 1112–1117, https://doi.org/10.1109/JSEN.2007.897942.
[76] A.A. Ensafi, M. Fouladgar, Development a simple PVC membrane bulk optode for determination of lead ions in water samples, Sens. Lett. 7 (2009) 177–184, https://doi.org/10.1166/sl.2009.1029.
[77] A.A. Asnafi, A. Katiraei Far, S. Meghdadi, Highly selective optical-sensing film for lead(II) determination in water samples, J. Hazard. Mater. 172 (2009) 1069–1075, https://doi.org/10.1016/j.jhazmat.2009.07.112.
[78] C. Bualoma, W. Ngeontaeb, S. Nitiyanontakita, P. Ngamukota, A. Imyima, T. Tuntulania, W. Aeungmaitrepirom, Bulk optode sensors for batch and flow-through determinations of lead ion in water samples, Talanta 82 (2010) 660–667, https://doi.org/10.1016/j.talanta.2010.05.028.
[79] H. Tavallali, L. Dorostghoal, Design and evaluation of a lead (II) optical sensor based on immobilization of dithizone on triacetylcellulose membrane, Int. J. ChemTech Res. 6 (2014) 3179–3186.
[80] K. Zargoosh, F.F. Babadi, Highly selective and sensitive optical sensor for determination of Pb(II) and Hg^{2+} ions based on the covalent immobilization of dithizone on agarose membrane, Spectrochim. Acta A Mol. Biomol. Spectrosc. 137 (2015) 105–110, https://doi.org/10.1016/j.saa.2014.08.043.
[81] Y. Nur, E. Rohaeti, L.K. Darusman, Optical sensor for the determination of Pb(II) based on immobilization of dithizone onto chitosan-silica membrane, Indones. J. Chem. 17 (2017) 7–14, https://doi.org/10.22146/ijc.23560.

Błażej Galiński (1994) is Ph.D. student at Faculty of Chemistry of Gdańsk University of Technology – M.Sc. in 2018. His scientific interest covers supramolecular chemistry, mainly chromoionophores and their applications in optical sensing.

Ewa Wagner-Wysiecka obtained her Ph.D. (2002) and D.Sc. (2013) in Chemistry from Gdańsk University of Technology (Poland), where now is working as associate professor. The main topic of her research is supramolecular chemistry (organic synthesis, spectroscopic methods, colorimetric receptors and sensors).

P2 – SUPPLEMENTARY MATERIALS

Pyrrole bearing diazocrowns: selective chromoionophores for lead(II) optical sensing

Błażej Galiński, Ewa Wagner-Wysiecka *

Department of Chemistry and Technology of Functional Materials, *Faculty of Chemistry, Gdańsk University of Technology, Narutowicza Street 11/12, 80-233 Gdańsk, Poland*

* corresponding author: ewa.wagner-wysiecka@pg.edu.pl

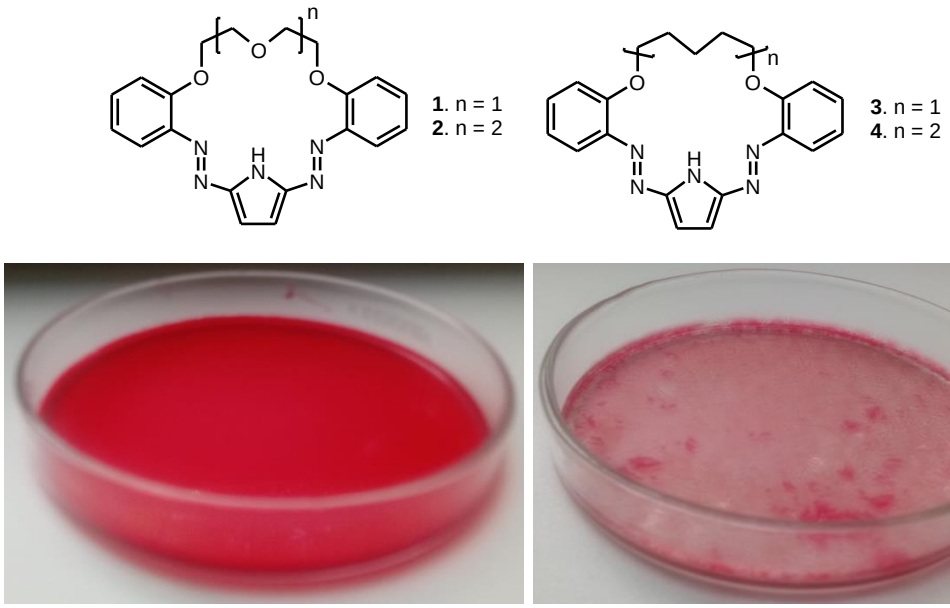

Fig. S1. Exemplary photos of the optodes with compound **1** (left) and **3** (right) - showing its crystallization in the membrane.

Fig. S2. Photographs of colorimetric measurement set-up.

As solvents used for dissolution of all components of membranes dichloromethane (DCM) and chloroform (TCM) were tested. All membranes for preparation of which chloroform was used show a lower value of the generated signal (ΔA) than in dichloromethane, regardless of the composition of the receptor layer: the type of plasticizer, the amount of chromoionophore or the amount of the lipophilic salt KTClPB. Results are exemplified with membranes with crown **2** as chromoionophore in Figure S3 a-c.

It follows that the use of dichloromethane as a solvent is a better choice. It may be influenced by the rate of solvent evaporation.

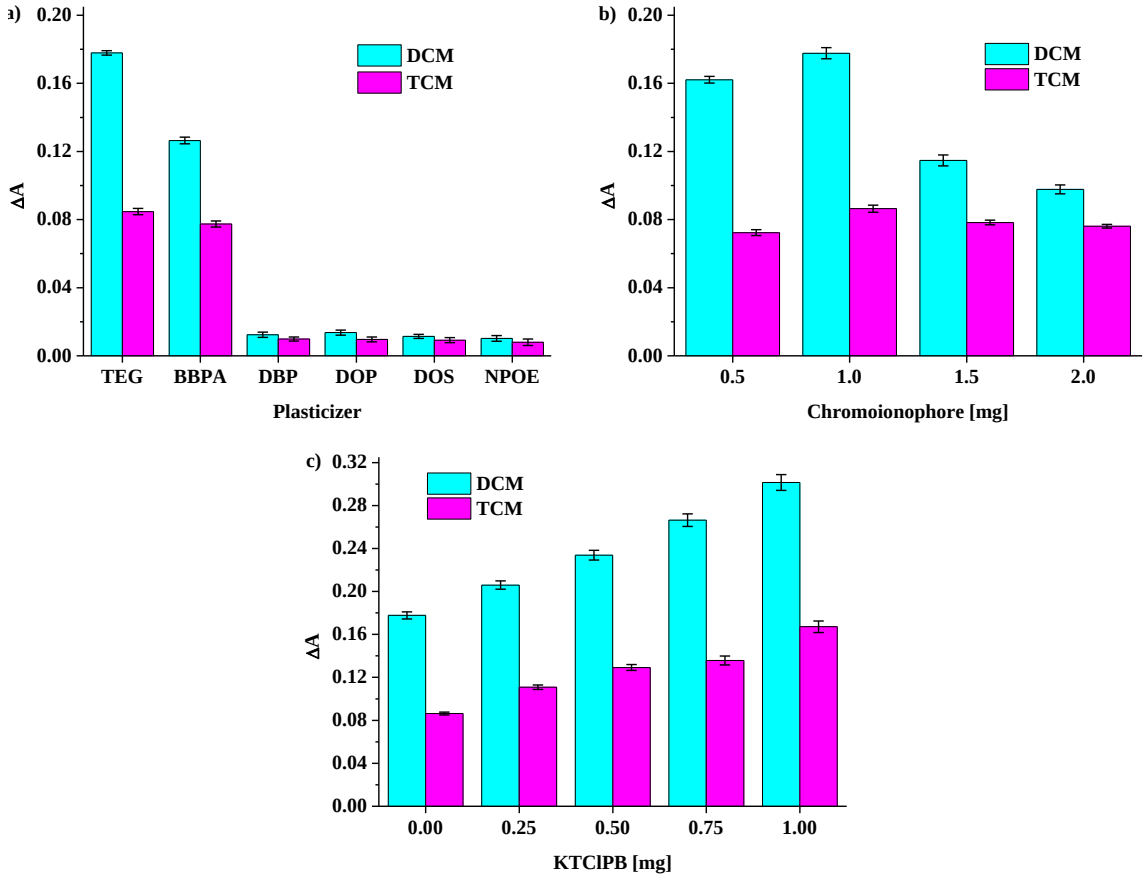

Fig. S3. Effect of the solvent type on the optode with compound **2** response signal (ΔA) depending on a) type of plasticizer, b) amount of chromoionophore and c) amount of KTClPB.

The comparison of the optode signal response ΔA of optodes with chromoionophores **1**, **2** and **4** depending on the type of solvent used for membrane preparation is shown in Figure S4.

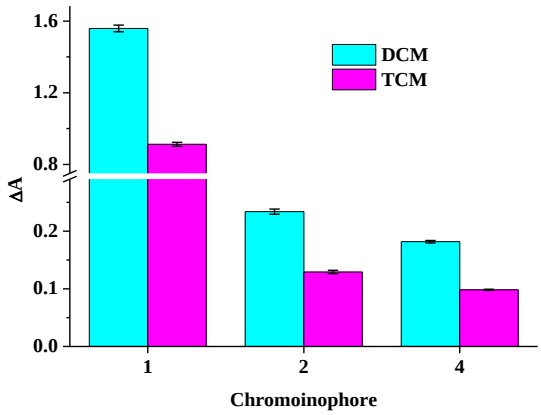

Fig. S4. Effect of solvent type on the optodes with chromoionophores **1**, **2** and **4** response signal (ΔA) towards lead(II) at concentration 10^{-4} M at pH 5.5.

Table S1. Membranes composition.

Series	TCA [mg]	Chromoinophore [mg]		Plasticizer [mg]		KTClPB [mg]
A	250.0	**1**, **2**, **3**, **4**	1.00	TEG	337.2	-
	250.0	**1**, **2**, **3**, **4**	1.00	BBPA	337.2	-
	250.0	**1**, **2**, **3**, **4**	1.00	DOS	337.2	-
	250.0	**1**, **2**, **3**, **4**	1.00	NPOE	337.2	-
	250.0	**1**, **2**, **3**, **4**	1.00	DOP	337.2	-
	250.0	**1**, **2**, **3**, **4**	1.00	DBP	337.2	-
B	250.0	**1**, **2**, **4**	0.50	TEG	337.2	-
	250.0	**1**, **2**, **4**	0.75	TEG	337.2	-
	250.0	**1**, **2**, **4**	1.00	TEG	337.2	-
	250.0	**1**, **2**, **4**	1.50	TEG	337.2	-
C	250.0	**1**, **2**	1.00	TEG	168.6	-
	250.0	**1**, **2**	1.00	TEG	252.9	-
	250.0	**1**, **2**	1.00	TEG	337.2	-
	250.0	**1**, **2**	1.00	TEG	421.5	-
	250.0	**1**, **2**	1.00	TEG	505.8	-
	250.0	**4**	1.50	TEG	168.6	-
	250.0	**4**	1.50	TEG	252.9	-
	250.0	**4**	1.50	TEG	337.2	-
	250.0	**4**	1.50	TEG	421.5	-
	250.0	**4**	1.50	TEG	505.8	-
D	250.0	**1**	1.00	TEG	168.6	0.25
	250.0	**1**	1.00	TEG	168.6	0.50
	250.0	**1**	1.00	TEG	168.6	0.75
	250.0	**1**	1.00	TEG	168.6	1.00
	250.0	**2**	1.00	TEG	337.2	0.25
	250.0	**2**	1.00	TEG	337.2	0.50
	250.0	**2**	1.00	TEG	337.2	0.75
	250.0	**2**	1.00	TEG	337.2	1.00
	250.0	**4**	1.50	TEG	337.2	0.25
	250.0	**4**	1.50	TEG	337.2	0.50
	250.0	**4**	1.50	TEG	337.2	0.75
	250.0	**4**	1.50	TEG	337.2	1.00

Table S2. The effect of the amount of the lipophilic salt on the properties of optodes with crowns **1**, **2** and **4** (exemplified on the single set of results).

Optode	KTClPB [mg]	Dynamic range [Pb(II)]	Equation	R^2	LOD [Pb(II)]
1	0.00	1.34×10^{-5}-1.28×10^{-3}	$\Delta A = 0.6111\log[Pb(II)] + 3.0262$	0.995	1.12×10^{-5}
	0.25	1.34×10^{-5}-1.28×10^{-3}	$\Delta A = 0.7488\log[Pb(II)] + 3.8393$	0.998	7.47×10^{-6}
	0.50	1.34×10^{-5}-3.83×10^{-4}	$\Delta A = 1.1351\log[Pb(II)] + 6.0694$	0.997	4.50×10^{-6}
	0.75	1.34×10^{-5}-3.83×10^{-4}	$\Delta A = 1.3301\log[Pb(II)] + 7.0388$	0.998	5.11×10^{-6}
	1.00	1.34×10^{-5}-3.83×10^{-4}	$\Delta A = 1.4929\log[Pb(II)] + 7.8849$	0.997	5.23×10^{-6}
2	0.00	3.00×10^{-6}-6.00×10^{-4}	$\Delta A = 0.1064\log[Pb(II)] + 0.6041$	0.996	2.55×10^{-6}
	0.25	3.00×10^{-6}-3.00×10^{-4}	$\Delta A = 0.1184\log[Pb(II)] + 0.6765$	0.997	2.30×10^{-6}
	0.50	3.00×10^{-6}-1.50×10^{-4}	$\Delta A = 0.1289\log[Pb(II)] + 0.7425$	0.996	1.85×10^{-6}
	0.75	3.00×10^{-6}-1.50×10^{-4}	$\Delta A = 0.1534\log[Pb(II)] + 0.8756$	0.996	2.24×10^{-6}
	1.00	3.00×10^{-6}-1.50×10^{-4}	$\Delta A = 0.1770\log[Pb(II)] + 1.0066$	0.995	2.31×10^{-6}
4	0.00	1.27×10^{-4}-1.22×10^{-3}	$\Delta A = 0.0742\log[Pb(II)] + 0.3535$	0.997	3.46×10^{-5}
	0.25	1.27×10^{-4}-1.22×10^{-3}	$\Delta A = 0.0897\log[Pb(II)] + 0.4259$	0.998	3.18×10^{-5}
	0.50	4.00×10^{-5}-1.22×10^{-3}	$\Delta A = 0.1478\log[Pb(II)] + 0.7098$	0.998	2.24×10^{-5}
	0.75	4.00×10^{-5}-1.22×10^{-3}	$\Delta A = 0.1991\log[Pb(II)] + 0.9564$	0.996	2.04×10^{-5}
	1.00	4.00×10^{-5}-1.22×10^{-3}	$\Delta A = 0.2035\log[Pb(II)] + 0.9755$	0.997	2.07×10^{-5}

Results for series D of membranes: TEG (337.2 mg), 1.0 mg of compounds **1** or **2** or 1.5 mg of compound **4** and different amounts of lipophilic salt KTClPB (0.25 – 1.00 mg).

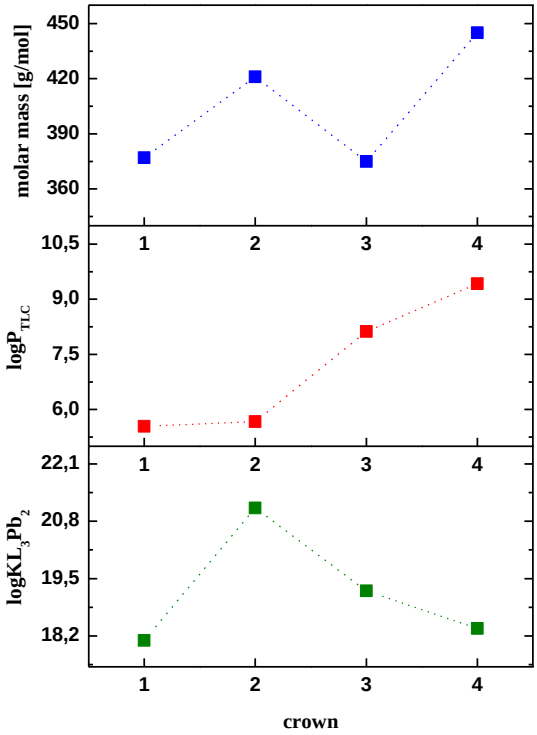

Fig. S5. Comparison (from bottom) of the: values of stability constants of lead(II) complexes ($logK_{L2Pb3}$) in acetonitrile, $logP_{TLC}$ and molar masses of chromogenic crowns **1**-**4** [1-3].

Table S3. Stability constant (logK) values of diazocrowns lead(II) (3:2, crown:Pb) complexes **1**-**4** in acetonitrile [1-3] and comparison of the lipophilicity values of macrocycles [3].

	1	**2**	**3**	**4**
$logK_{L3Pb2}$	18.10±0.01	21.10±0.09	19.22±0.05	18.37±0.01
$logP_{TLC}$	5.54±0.05	5.67±0.01	8.12±0.05	9.42±0.03
molar mass [g/mol]	377	421	375	445

1. E. Wagner-Wysiecka, E. Luboch, M. Kowalczyk, J.F. Biernat, Chromogenic macrocyclic derivatives of azoles - synthesis and properties, Tetrahedron 59 (2003) 4415-4420.
2. E. Luboch, E. Wagner-Wysiecka, M. Fainerman-Melnikova, L.F. Lindoy, J.F. Biernat, Pyrrole Azocrown Ethers. Synthesis, Complexation, Selective Lead Transport and Ion-Selective Membrane Electrode Studies, Supramol. Chem., **18** (2006) 593-601.
3. B. Galiński, E. Luboch, J. Chojnacki, E. Wagner-Wysiecka, Novel Diazocrowns with Pyrrole Residue as Lead(II)Colorimetric Probes. Materials 14 (2021) 7239.

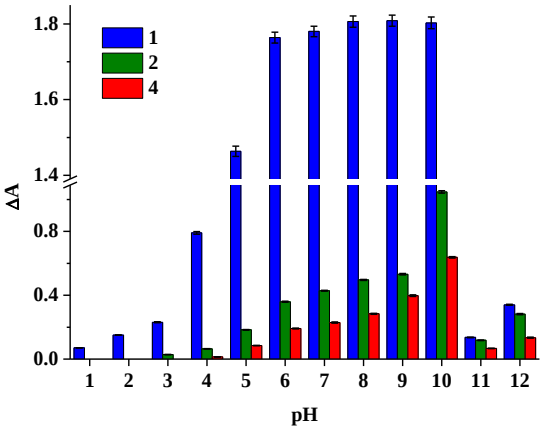

Fig. S6. Effect of pH on the response (ΔA) of optodes with chromoionophores **1**, **2** and **4** at lead(II) salt concentration 10^{-4} M.

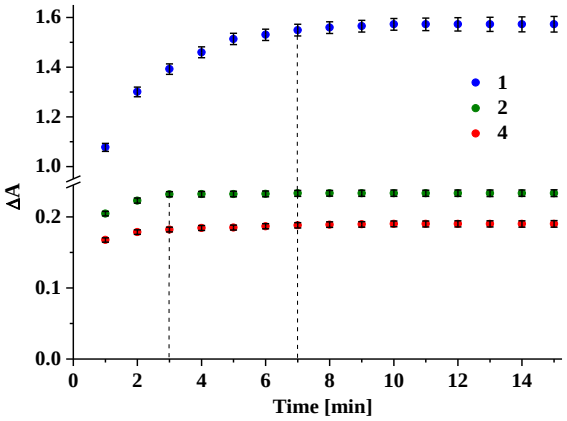

Fig. S7. The change of signal (ΔA) of optodes with crowns **1**, **2** and **4** upon immersion in lead(II) solution (10^{-4} M, pH 5.5) over time.

The possibility of regenerating the optodes was tested in the following solutions: hydrochloric acid, nitric acid, acetic acid (AcOH), ethylenediaminetetraacetic acid disodium salt (EDTA-Na_2) and ethylenediamine (EDA) of a concentrations of 10^{-2} and 10^{-1} M. All solutions can be used for the regeneration of the optode, but they differ in the time required for the regeneration of the optode, which is illustrated by the example of the optode with crown **2** - Fig. S4. The shortest regeneration time for a concentration of 10^{-4} M of lead(II) was obtained when using a solution of hydrochloric acid and nitric acid with a concentration of 10^{-1} M - 2 min for optode with chromoionophore **1** and 30 s for optode with macrocycle **2** or **4**. The EDTA-Na_2 and the EDA solutions change the pH, which results in an initial significant increase in the optode response. A regeneration time of more than 20 min with EDTA-Na_2 and more than 30 min with EDA indicates that the use of an acid solution as a regeneration system is the better choice.

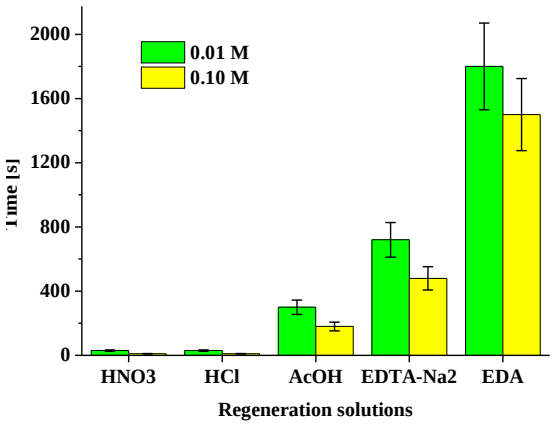

Fig. S8. Regeneration time of the optode with compound **2** depending on the type of regeneration solution, after being immersed in a solution containing lead(II) 10^{-4} M.

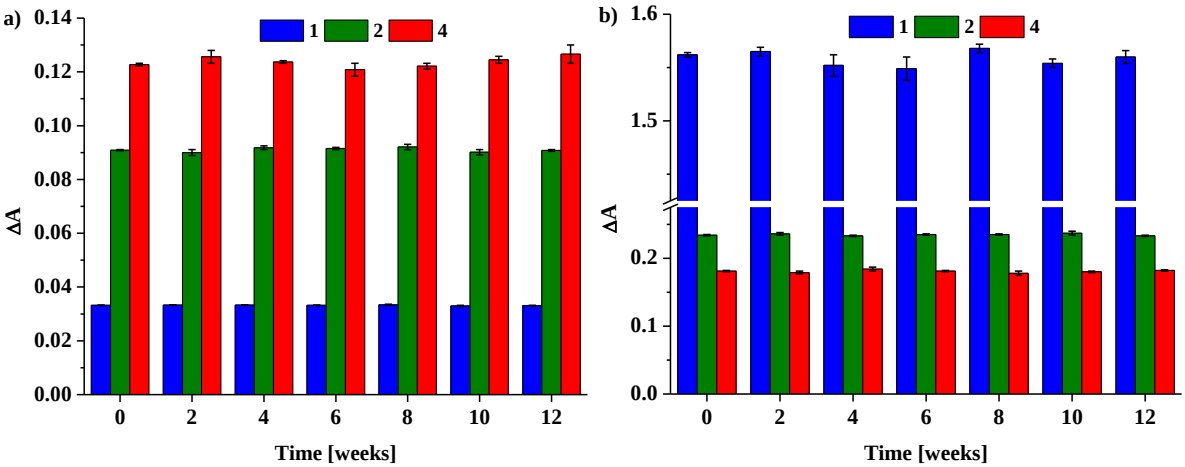

Fig. S9. Response of optodes a) before and b) after contact with lead(II) salt (10^{-4} M), storage in a dry and dark place for different time (weeks, 0 – optodes checked after obtained), pH 5.5.

Table S4. Summary of RGB values optode with compound **1** for a given lead(II) concentration.

[Pb(II)]	log[Pb(II)]	R	G	B
0	-	208	83	112
4.11×10^{-7}	-6.39	207	83	113
7.79×10^{-7}	-6.11	206	84	113
1.32×10^{-6}	-5.88	197	86	114
2.22×10^{-6}	-5.65	189	89	123
3.97×10^{-6}	-5.40	180	104	136
7.51×10^{-6}	-5.12	166	108	149
1.28×10^{-6}	-4.89	153	109	151
2.14×10^{-5}	-4.67	144	112	159
3.83×10^{-5}	-4.42	121	116	156
7.25×10^{-5}	-4.14	114	127	167
1.23×10^{-4}	-3.91	104	133	167
2.07×10^{-4}	-3.68	84	124	160
3.70×10^{-4}	-3.43	85	134	174
6.81×10^{-4}	-3.17	81	142	182
1.25×10^{-3}	-2.90	75	152	180

Table S5. Summary of RGB values optode with compound **2** for a given lead(II) concentration.

[Pb(II)]	log[Pb(II)]	R	G	B
0	-	201	103	101
3.15×10^{-6}	-5.50	202	103	101
4.29×10^{-6}	-5.37	202	103	101
6.52×10^{-6}	-5.19	202	104	101
8.70×10^{-6}	-5.06	203	104	101
1.08×10^{-5}	-4.97	203	104	102
1.29×10^{-5}	-4.89	203	105	102
2.39×10^{-5}	-4.63	200	105	107
3.43×10^{-5}	-4.46	198	105	109
5.53×10^{-5}	-4.26	192	106	110
7.57×10^{-5}	-4.12	190	106	113
9.57×10^{-5}	-4.02	188	106	115
1.15×10^{-4}	-3.94	186	106	117
2.17×10^{-4}	-3.66	183	106	123
3.18×10^{-4}	-3.50	181	107	127
5.16×10^{-4}	-3.29	176	107	130
7.10×10^{-4}	-3.15	170	107	131
9.00×10^{-4}	-3.05	170	107	138
1.09×10^{-3}	-2.96	168	107	142
1.96×10^{-3}	-2.71	158	108	148
2.75×10^{-3}	-2.56	152	109	155

Table S6. Summary of RGB values optode with compound **4** for a given lead(II) concentration.

[Pb(II)]	log[Pb(II)]	R	G	B
0	-	216	161	164
4.15×10^{-6}	-5.38	216	161	164
1.03×10^{-5}	-4.99	215	161	164
2.04×10^{-5}	-4.69	215	161	165
4.00×10^{-5}	-4.40	213	163	169
7.69×10^{-5}	-4.11	208	164	172
1.27×10^{-4}	-3.90	205	165	174
2.00×10^{-4}	-3.70	203	167	175
2.81×10^{-4}	-3.55	202	168	177
3.61×10^{-4}	-3.44	201	168	178
5.16×10^{-4}	-3.29	201	169	181
8.13×10^{-4}	-3.09	199	171	183
1.22×10^{-3}	-2.91	198	173	185
1.83×10^{-3}	-2.74	198	174	187

Table S7. Elemental composition of real sample of treated industrial wastewater - determination method ICP-OES.

	As	Cd	Cr	Cu	Ni	Pb	Zn
M	3.74×10^{-8}	4.89×10^{-7}	1.15×10^{-7}	4.09×10^{-8}	5.11×10^{-8}	9.51×10^{-8}	6.07×10^{-7}
ppb	2.8±0.8	55.0±0.4	6.0±0.1	2.6±0.4	3.0±0.3	19.7±0.8	39.7±0.4

P3 – SIMPLE COLORIMETRIC COPPER(II) SENSOR – SPECTRAL CHARACTERIZATION AND POSSIBLE APPLICATIONS

Contents lists available at ScienceDirect

Spectrochimica Acta Part A:
Molecular and Biomolecular Spectroscopy

journal homepage: www.journals.elsevier.com/spectrochimica-acta-part-a-molecular-and-biomolecular-spectroscopy

Simple colorimetric copper(II) sensor – Spectral characterization and possible applications

Błażej Galiński [a], Jarosław Chojnacki [b], Ewa Wagner-Wysiecka [a,c,*]

[a] Department of Chemistry and Technology of Functional Materials, Faculty of Chemistry, Gdańsk University of Technology, Narutowicza Street 11/12, 80-233 Gdańsk, Poland
[b] Department of Inorganic Chemistry, Faculty of Chemistry, Gdańsk University of Technology, Narutowicza Street 11/12, 80-233 Gdańsk, Poland
[c] Advanced Materials Center, Faculty of Chemistry, Gdańsk University of Technology, Narutowicza Street 11/12, 80-233 Gdańsk, Poland

HIGHLIGHTS

- New *o*-hydroxyazocompound **L** has been obtained.
- **L** was investigated as spectrophotometric colorimetric chemosensor for copper(II).
- **L**-based test strips and cotton swabs can colorimetrically detect copper(II) in water.
- **L**-based copper(II) selective optodes were proposed.

GRAPHICAL ABSTRACT

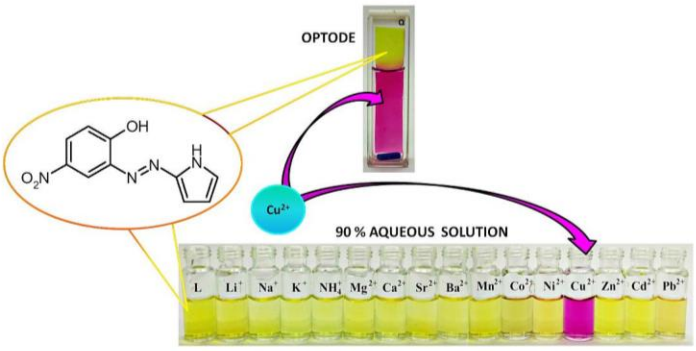

ARTICLE INFO

Keywords:
Copper(II)
Optical sensing
Chromoionophore
Azocompound
Pyrrole

ABSTRACT

New *o*-hydroxyazocompound **L** bearing pyrrole residue was obtained in the simple synthetic protocol. The structure of **L** was confirmed and analyzed by X-ray diffraction. It was found that new chemosensor can be successfully used as copper(II) selective spectrophotometric regent in solution and can be also applied for the preparation of sensing materials generating selective color signal upon interaction with copper(II). Selective colorimetric response towards copper(II) is manifested by a distinct color change from yellow to pink. Proposed systems were effectively used for copper(II) determination at concentration level 10^{-8} M in model and real samples of water.

1. Introduction

Copper(II) is an essential and third most abundant transition metal ion in human body and plays a unique physiological role in animals and plants [1–4]. However, an excess as well as a deficiency of copper with respect to a critical level may cause many disorders in human body like for example Alzheimer's, Menkes and Wilson diseases [5–10] and also can be poisoning for animals and plants [11–13]. Because of toxic nature of copper(II) above a certain level of concentration, WHO has set maximum permissible limit of copper(II) in drinking water as 2.0 mg/L

* Corresponding author.
E-mail address: ewa.wagner-wysiecka@pg.edu.pl (E. Wagner-Wysiecka).

https://doi.org/10.1016/j.saa.2023.122472
Received 28 October 2022; Received in revised form 28 January 2023; Accepted 4 February 2023

(3.15×10^{-5} M) [14]. Therefore, the detection of copper(II) in the various type of samples, e.g. environmental, biological, like body fluids, is important and essential. Various spectroscopic and electrochemical methods can be used for the detection and determination of metal ions in aqueous samples [15–20]. An elegant and comprehensive review on chemical, polymer and nanoparticle copper(II) colorimetric and/or fluorimetric sensors has been recently published [21]. The choice of the method depends on many factors such as for example the type of the sample, the concentration level of analyte. Often also the economic criterion is taken into consideration. Thus, besides the selectivity and sensitivity of sensor, also the price of the instrumentation and overall costs of the analysis are important. In this respect chemical sensors, including optical ones, can compete with most of the instrumental analytical methods. The operation of sensors can be based on different mechanisms of the generation of the analytical signal. One of them is chemical recognition of the analyte taking place in the receptor layer of the sensor. The process of chemical recognition relies on the affinity of the particular receptor towards analyte according to the rules of host-guest chemistry – one of the research area of supramolecular chemistry, where the design and synthesis of ion receptors for analytical purposes is one of the goals [22–32]. Important analytes include heavy metal cations [33–39], which have a significant impact on human health and the environment. Properly designed receptors of chromoionophoric properties can be components of sensing optical materials for the detection and determination of these ions in an aqueous medium [40–44]. Azo compounds due to their relatively simple synthesis, spectral and complexing properties constitute a promising group of such chromoionophores [45–47]. Essential receptors of heavy metal cations are often compounds bearing heterocyclic moieties [21]. Due to the various reactivity and photophysical properties, heterocyclic receptors containing nitrogen atoms are described as one of the best systems for the detection and determination of heavy metal ions [48,49]. The interaction of heavy metal ions with the receptor can generate an optical signal that is measurable using spectrophotometric methods [50], but also solutions where the use of mobile detection systems e.g. Smartphone-based detection devices [51–54] that use digital color analysis [55–62].

Here we present a facile synthesis and spectral characterization of simple *o*-hydroxyazocompound **L** bearing pyrrole residue. Newly obtained compound was characterized with the use of spectroscopic methods and investigated as a copper(II) receptor in organic solvents, mixtures of these solvents with water and in systems of complex ionic matrix, namely artificial body fluid and artificial urine. It has also been tested as a component of optical sensing materials for selectivity, sensitivity, regenerability, pH effect, limit of detection, interfering ions effect and lifetime. Tests were carried out to assess the possibility of using the prepared materials for the detection and determination of copper(II) in model and real samples of water.

2. Experimental

2.1. Reagents and materials

All chemicals of the highest available purity were purchased from commercial sources and used without further purification. Lithium perchlorate, sodium perchlorate monohydrate, bis(2-ethylhexyl) phthalate (DOP) and dibutyl phthalate (DBP) were obtained from Fluka. Potassium perchlorate, barium perchlorate, cobalt(II) perchlorate hexahydrate, nickel(II) perchlorate hexahydrate, copper(II) perchlorate hexahydrate, zinc perchlorate hexahydrate, lead(II) perchlorate trihydrate, tetrabutylammonium hydroxide 30-hydrate (TBAOH), *p*-toluenesulfonic acid monohydrate (TsOH), uric acid, creatinine, bis(1-butylpentyl) adipate (BBPA), 2-nitrophenyl octyl ether (NPOE), bis(2-ethylhexyl) sebacate (DOS), cellulose triacetate (CTA), triethylene glycol (TEG), potassium tetrakis(4-chlorophenyl)borate (KTClPB), acetonitrile (ACN), dichloromethane (DCM) and methanol (MeOH) were acquired from Sigma Aldrich. Magnesium perchlorate, calcium perchlorate hydrate, strontium perchlorate trihydrate and cadmium perchlorate hexahydrate were purchased from Alfa Aesar. All inorganic salts, hydrochloric acid, nitric acid, sodium hydroxide, disodium ethylenediaminetetraacetate dihydrate (EDTA), sodium citrate dehydrate, dipotassium oxalate monohydrate, urea, tris(hydroxymethyl) aminomethane, dimethyl sulfoxide (DMSO), acetone, 2-propanol, and filter papers were obtained from POCh. Glass microfiber filter Whatman GF/C was acquired from Schleicher & Schuell. TLC glass plates 60 RP-18 F_{254} and silica gel 60 (0.063–0.200 mm) for column chromatography were purchased from Merck. For measurements performed in mixed, water containing systems, deionized water (conductivity < 1 $\mu S \cdot cm^{-1}$, Hydrolab) was used. For recovery studies Standard Reference Solution of copper(II) 1000 ppm (Merck) and Qnova calibration solution were used. Copper(II) concentration for comparative studies was determined using the ICP-OES method with iCAP 7400 Analyzer. Mineral water samples were commercial bottled ones purchased from regular stores. Tap water samples were taken from local domestic sources of Pomerania (sample 1) and Warmian-Masurian (sample 2 and 3) Voivodeships (Poland).

2.2. Apparatus

^1H and ^{13}C spectra were recorded on Varian INOVA 500 spectrometer at 500 MHz and 125 MHz, respectively. Chemical shifts are reported as δ [ppm] values in relation to TMS. HR MS mass spectrum was recorded on an AutoSpec Premier (Waters) instrument. FTIR spectra (KBr) were taken on a Nicolet iS10 apparatus. For UV–Vis measurements an UNICAM UV 300 series apparatus was used. Fluorescence spectra were recorded on a luminescence spectrometer (AMINCO Bowman Series 2 spectrofluorometer) using the flash xenon lamp. The bandpass of excitation and emission monochromators was 16 nm. Spectroscopic measurements were carried out in 1 cm quartz cuvettes in solvents of the highest available purity. The solution pH was measured by an pH-meter CPC-511 with glass electrode EPS-1 (ELMETRON), standardized with buffer solutions. Portable LED light box (23 × 23 × 23 cm) was used to guarantee the reproducibility of the photos (PULUZ, Photography Light Box, Shenzhen Puluz Technology Limited). Pictures were taken by a Smartphone LG *K*10.

2.3. Synthesis of L

Compound **L** was obtained by diazocoupling reaction of diazonium salt with pyrrole, giving the product as orange solid with satisfactory 73 % yield. The procedure of the synthesis and structural characterization of **L** in given in Supplementary Material.

2.4. Lipophilicity (logP)

The lipophilicity values ($logP_{TLC}$) of ligand was estimated by TLC method using reverse phase chromatography (RP18) with a mixture of methanol:water (9:1, v/v) as mobile phase. As standards BBPA, NPOE, DOS, DOP and DBP were used. On the basis of comparison of R_f values for standards and ligand $logP_{TLC}$ values was determined [63–65].

2.5. X-ray structure

Diffraction intensity data for **L** were collected on an IPDS 2T dual beam diffractometer (STOE & Cie GmbH, Darmstadt, Germany) at 120.0 (2) K with MoKa radiation of a microfocus X-ray source (GeniX 3D Mo High Flux, Xenocs, Sassenage, 50 kV, 1.0 mA, and $\lambda = 0.71069$ Å). Investigated crystals were thermostated under a nitrogen stream at 120 K using the CryoStream-800 device (Oxford CryoSystem, UK) during the entire experiment. Data collection and data reduction were controlled by using the X-Area 1.75 program (STOE, 2015). Due to low absorption coefficient no absorption correction was performed. The structure was

solved using intrinsic phasing implemented in SHELXT and refined anisotropically using the program packages Olex2 [66] and SHELX-2015 [67]. Positions of the C–H hydrogen atoms were calculated geometrically taking into account isotropic temperature factors. All hydrocarbonic H-atoms were refined as riding on their parent atoms with the usual restraints. Both OH and NH atoms were found in the Fourier electron density map and refined without constraines. Structure of **L** was refined with no special treatment.

2.6. Complexation studies

Metal cation complexation studies were carried out using UV–Vis titration in acetonitrile, dichloromethane, methanol, DMSO and the mixture of DMSO with water. A series of solutions of pH values ranging from 2 to 12 was prepared by mixing sodium hydroxide solution (0.1 M) and hydrochloric acid (0.1 M). Simulated body fluid (SBF), phosphate buffer saline (PBS) and artificial urine (AU) samples were prepared according described procedures [68–70]. The stock solutions of **L** ($\sim 10^{-3}$ M), metal perchlorates ($\sim 10^{-2}$ M), TsOH ($\sim 10^{-2}$ M), TBAOH ($\sim 10^{-2}$ M) and chlorides ($\sim 10^{-2}$ M), were prepared by weighting the respective quantities of them and dissolving in the respective solvent system in volumetric flasks. The values of binding constant (logK) were calculated with the use of OPIUM [71] program on the basis of titration experiment data. Limits of detection (LOD) for copper(II) were calculated DL = 3σ/k, where σ is the standard deviation of the blank and k is the slope of the linear function A = f(molar concentration of analyte). The spectral response towards copper(II) was expressed as $\Delta A = A_{Cu} - A_0$, where A_0 stands for absorbance of solution of **L** (or optode) and A_{Cu} absorbance value of **L** (or optode) in the presence of copper(II) salt. The influence of interfering ions on spectrophotometric response towards copper(II) was expressed as the absolute value of relative response $RR\% = |[(A - A_{Cu})/A_{Cu}]| \times 100\%$, where A_{Cu} stands for absorbance of solution of **L** in the presence of copper(II) chloride (equimolar to ligand amount) and A is absorbance value measured just after addition of interfering metal chloride in the same quantity, 10-fold and 100-fold molar excess in relation to copper(II) chloride [65,72].

2.7. 7. Digital color analysis

Pictures were analyzed using free software ImageJ [73,74]. The change of optode color given as ΔE_{RGB} [75] was calculated using the equation: $\Delta E_{RGB} = [(R_0\text{- } R)^2 + (G_0\text{- } G)^2 + (B_0\text{-}B)^2]^{1/2}$ where R_0, G_0 and B_0 values correspond to color of solution (or optode) in the absence of copper(II) salt, and R, G and B values correspond to color of solution (or optode) in the presence of copper(II). The value of the intensity of green color I_G was calculated using the equation: $I_G = -\log(G/G_0)$.

2.8. Test strips

Solutions of **L** ($\sim 10^{-3}$ M or $\sim 10^{-4}$ M) in dichloromethane were poured into a chromatographic chamber, into which a strip of glass microfiber filter or filter paper was placed. After 5 min. strips were taken out and solvent was evaporated in a stream of hot air.

2.9. Cotton swabs

Cotton swabs [76] were soaked with the 100.0 μL of **L** solution ($\sim 10^{-3}$ M or $\sim 10^{-4}$ M) in dichloromethane and left for solvent evaporation.

2.10. Membrane preparation

CTA optodes were prepared according to previously described procedures [72]. Membranes contained 250.0 mg of CTA, 1.0 mg of **L**, 168.6 mg (150.0 μL) of TEG and 0.5 mg of KTClPB. All components of optodes were dissolved in dichloromethane (6 mL) with continuous stirring using a magnetic stirrer for 2 h and were sonicated for ca. 15 min. – until a clear solution is formed. In the next step, solutions were poured on, prepared in advance (washed with nitric acid, deionized water, acetone and 2-propanol) Petri dish (9 cm diameter), covered loosely with a lid and left for solvent evaporation. After 24 h obtained optode films were peeled off from the Petri dish and cut into 0.9 × 4.5 cm strips. Blank membranes were prepared in an analogous way using all components besides chromoionophore **L**.

3. Results and discussion

3.1. Synthesis and characterization of L

New compound **L** was obtained with satisfactory yield (73%) in a simple diazocoupling reaction of diazonium salt (1a) of 4-amino-4-nitrophenol (1) with pyrrole (2) in aqueous solution of pH ~ 10 (NaOH) (Fig. 1). Crystallization from dichloromethane preceded by column chromatography isolation gave a pure compound in the form of long orange needles. Spectral data (^{1}H and ^{13}C NMR, HRMS and IR) confirming the structure of newly obtained azopyrrole dye **L** are included in Supplementary Information (Fig. S1). As an additional parameter characterizing new compound **L** its lipophilicity logP 3.40 ± 0.02 was determined using TLC method.

3.2. Structure of L in solution

Hydroxyazocompounds are known to undergo prototropic tautomerism resulting in azophenol ⇄ quinone-hydrazone equilibrium [77–79]. Tautomeric equilibrium depends on several factors, both structural (e.g. type and location of substituents, macrocyclic/acyclic structure) and those resulting from the chemical environment of molecule like solvent and its properties, the presence of ionic species [80–83]. From the other hand, azo compounds bearing pyrrole moiety can be also considered as systems of possible prototropic tautomeric equilibrium proceeding with the engagement of N–H pyrrole proton [84]. Taking all of this into account for investigated here **L** tautomeric equilibrium shown in Fig. 2 can be considered.

Tautomeric equilibrium of **L** was investigated in solution using NMR spectroscopy. ^{1}H NMR spectra were registered in acetonitrile-d_3, DMSO-d_6, methanol-d_4 (Fig. 3). Signals of protons of pyrrole moiety are observable as multiplets at ~6.5, 7.1 and 7.4 ppm. Signals of benzene protons are seen as well shaped signals characteristic for 1,2,4-substituted benzene at ~8.5 (d, J ~ 2 Hz), 8.2 (dd, J1 ~ 2 Hz, J ~ 9 Hz) and doublet 7.3 (d, J ~ 9 Hz). Signals of protons of OH and NH groups seen as singlets at above 10.0 ppm (acetonitrile-d_3, DMSO-d_6) provide the evidence for hydrogen bonded system. Comparing with acetonitrile, in highly dipolar DMSO stronger hydrogen bonding between solvent acting as proton acceptor and **L** as hydrogen bond donor is expected, which correlates with the observed position of NH and OH proton signals at 10.93 and 11.92 ppm respectively. Signals of aromatic protons are shielded comparing to acetontrile. Analyzing the observed spectral pattern in ^{1}H NMR spectra it can be concluded that in all investigated solvents **L** exists in azophenol (AZ) form.

UV–Vis spectra of **L**, where lower than in NMR experiments concentrations of solute are used, were also registered in different solvents (Fig. 4(a)). In all cases, namely acetonitrile, DMSO, methanol and dichloromethane two absorption bands are observed in spectrum of **L**. The first one, of lower value of molar absorption coefficient, at ~310 nm and the second one of higher intensity at ~420 nm in acetonitrile and dichloromethane. The last mentioned absorption band in methanol is broaden and right side asymmetric. In DMSO, broader than in acetonitrile and dichloromethane absorption peak is additionally coming along with a band of low intensity on the red side of absorption, within 500 and 575 nm. The differences in spectral pattern in DMSO and methanol are manifested by deeper yellow color of solution of **L** in these solvents (Fig. 4(b)), what can suggest the solvation effect [85]. The relative

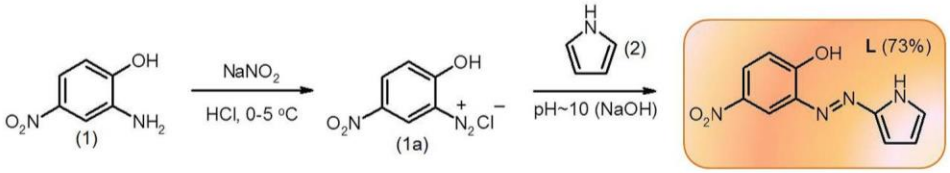

Fig. 1. Synthetic route for **L**.

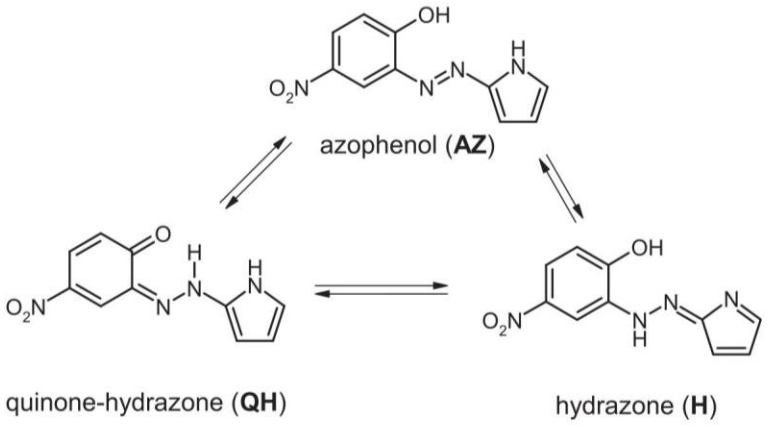

Fig. 2. Proposed tautomeric equilibrium of **L**.

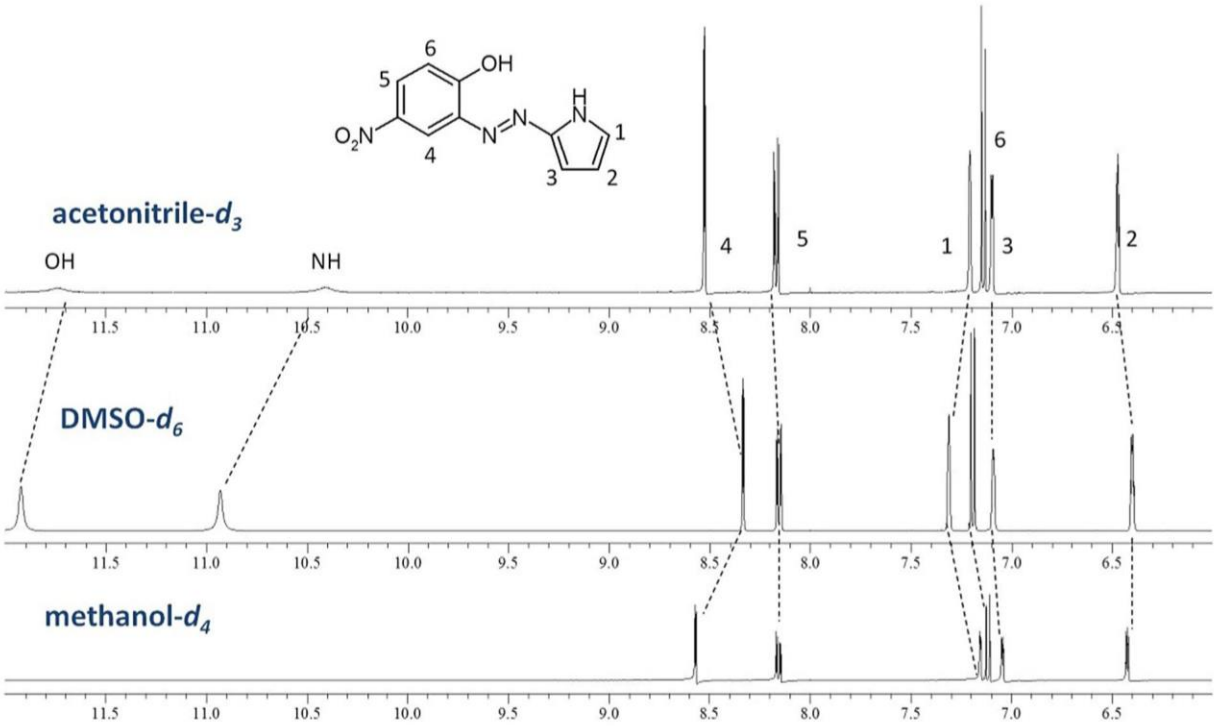

Fig. 3. ^{1}H NMR spectra of **L** in various solvents.

intensity of band at ~520 nm in spectrum of **L** registered in DMSO depends on **L** concentration (Fig. 4(c)). Also the relative intensity of bands at 420 and 520 nm is concentration dependent and the value of the molar absorption coefficient (515 nm) is decreasing with the increase of the concentration (Fig. 4(d)). It can be associated with the presence of various forms of dye or can be an effect of dye-dye interactions in solution - self-organization. UV–Vis spectroscopy is one of the useful tools for investigation of aggregation process [86] and as it is reported by other authors the spectral pattern observed in case of **L** might point out the formation of different types of aggregates [87,88]. Moreover, in fluorescence spectra of solutions of **L** of the same concentrations in above mentioned solvents emission bands are detectable in dichloromethane, acetonitrile and methanol (Fig. 4(e)). In DMSO under the same measurement conditions fluorescence is too weak to register emission spectrum. It can be connected with well-known aggregation-caused quenching (ACQ) effect due to π-π stacking interactions. Such interactions for **L** were confirmed in solid state (*vide infra*).

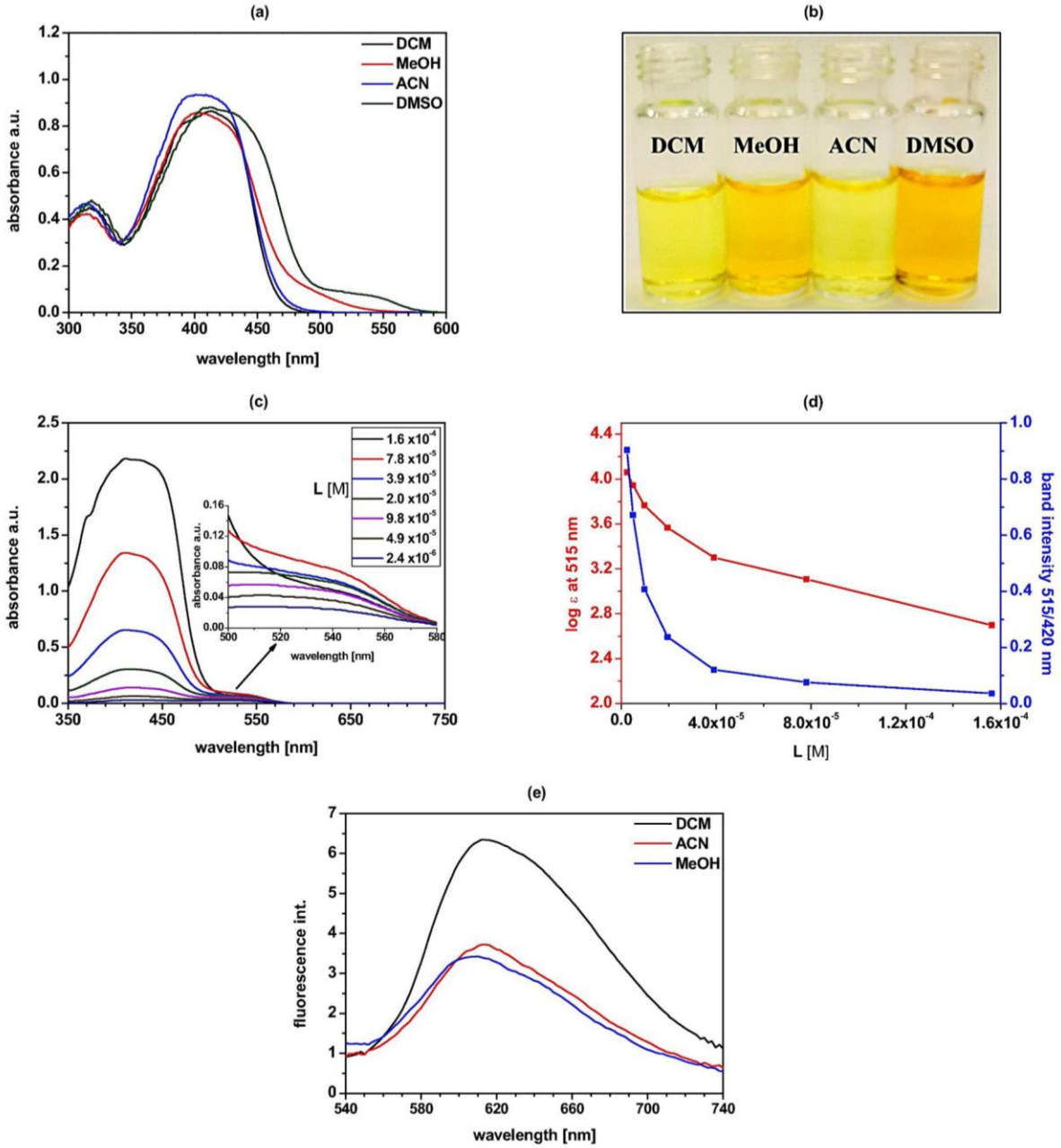

Fig. 4. (a) UV–Vis absorption spectra of **L** (4.05×10^{-5} M) in different solvents; (b) Solutions of **L** (1.02×10^{-4} M) in different solvents; (c) UV–Vis absorption spectra registered for solutions of different concentration of **L** in DMSO; (d) Correlation of relative intensity of bands and the molar absorption coefficient with the concentration of **L** in DMSO; (e) Emission spectra of **L** (1.02×10^{-4} M) registered in different solvents (λ_{ex} 600 nm, λ_{em} 618 (dichloromethane - DCM); 614 (acetonitrile - ACN and methanol - MeOH).

3.3. *Structure of L in solid state*

Single crystals of **L** suitable for X-ray analysis were obtained by crystallization from dichloromethane. Molecular view of **L** is shown in Fig. 5. Crystal data and structure refinement details are collected in Table 1. Compound **L** forms needle, red crystals, with symmetry of the monoclinic system, the space group $P2_1/n$ (no. 14). Asymmetric unit contains one molecule and the whole unit cell is built from four molecules, Z = 4. Most of the bond lengths and angles are in the expected ranges (see Fig. 5). Based on short interatomic distances one may assume mostly double character of N1-N2 bonds and aromatic character of the pyrrolic ring. The molecule is essentially flat. Dihedral angle between the phenyl ring and NO_2 group plane is ca −5°. Hydroxyl group forms internal H-bond with N2 atom, while the N-H hydrogen bond donor forms intermolecular interaction with O2 atom from neighbor molecule nitro group (Fig. 6, left). For details, see Table 2.

Crystal packing (Fig. 6) is dictated by hydrogen bonding and stacking interactions between the aromatic rings of the same nature. Actually the centroid distance between both planes, 3.741(8) Å, is equal to the *b* parameter of the unit cell, and is a pure lattice translation, so the dihedral angle between the planes α is equal to zero.

3.4. *Acid-base properties of L*

Azocompounds - weak bases - are protonated at one of two azo N-atoms forming non symmetric π-complex [89]. Protonation of azobenzenes usually leads to red shift of absorption band observed as a significant color change. However, the introduction of heterocyclic

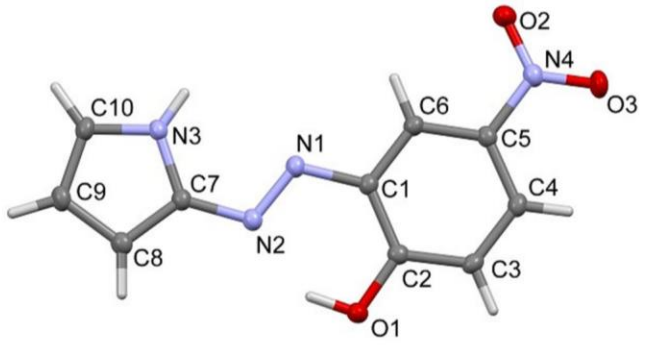

Fig. 5. Molecular view of **L** showing atom labeling scheme. Displacement ellipsoids drawn at 50% probability level. Selected bond lengths (Å) and angles (°): N1-N21.2842(13), N1-C1 1.4033(13), N2-C7 1.3722(13), N3-C7 1.3738 (14), C2-O1 1.3433(13), N4-O2 1.2340(13), N4-O3 1.2276(12), N4-C5 1.4547 (14); valence angles: N2-N1-C1 115.55(9), N1-N2-C7 113.24(9), C10-N3-C7 108.79(9), O3-N4-O2 122.90(10), O1-C2-C1 122.16(9); torsions O3-N4-C5-C4 −5.5(2), O2-N4 C5 C6 −4.8(2) C2-C1-N1-N2 0.0(2).

Table 1
Crystal data and structure refinement details for **L**.

	L
CCDC no.	2190550
Empirical formula	$C_{10}H_8N_4O_3$
M_r/g mol^{-1}	232.20
Temperature/K	120 K
Crystal system	Monoclinic
Space group (IT No.)	*P* $2_1/n$ (14)
a/Å	11.6673 (15)
b/Å	3.7411 (5)
c/Å	22.581 (3)
α/°	90
β/°	92.829(11)
γ/°	90
Volume/Å^3	984.4 (2)
Z	4
ρ_{calc} g/cm^3	1.567
Crystal size/mm^3	0.52 × 0.12 × 0.05
Radiation	Mo Kα (λ = 0.71073)
2Θ range for data collection/°	3.2–58.4
Reflections collected/unique	8887/2631
Completeness to θ_{max} (%)	99.8
Data/restraints/parameters	3631/0/162
Goodness-of-fit on F^2	1.07
Final R indexes [I>=2σ (I)]	R_1 = 0.0398, wR_2 = 0.1121
Final R indexes [all data]	R_1 = 0.0463, wR_2 = 0.1164
Largest diff. peak/hole / e Å^{-3}	0.37/ −0.23

moiety instead of one of benzene ring can significantly change the properties of azocompound including acid-base properties [46]. In case of **L**, ionization of molecule can be also an effect of the deprotonation of hydroxy group, which typically for ionized dye molecules causes the color change resulting from the appearance of the red shifted absorption band of deionized form.

Quantitative colorimetric probes of the acid-base properties of **L** in different solvents are shown in Fig. 7 (top). The presence of *p*-toluenesulfonic acid (TsOH) slightly influences the color of the solutions what is in agreement with very small changes in absorption spectra. Titration trace of **L** with TsOH in methanol and DMSO is exemplified in Fig. 7(a) and (b).

Upon titration with TsOH the only observed change in UV–Vis spectra is the decrease of the band in a region of 500–575 nm. This can support the thesis drawn above as this band comes from the dye-dye interactions in solution. The presence of acid can destroy the hydrogen bonded self-organized structure of **L** in solution (UV–Vis titration in dichloromethane was not carried out due to low solubility of TsOH in this solvent). This is evidenced in ^{1}H NMR spectra (Fig. 8) registered for **L** in the presence of equimolar and 5-fold excess of TsOH. The most significant change in spectra is the broadening and lowering of the intensity and finally the disappearance of the N–H proton signal at 10.93 ppm. Signals of protons of benzene rings are not changed both in the position and shape (for full range spectra and the values of chemical shift see Fig. S2 and Table S1), whereas signals of protons of pyrrole ring are slightly shielded and changed in shape. It means that N–H proton also in solution (similarly as in a solid state) can be engaged in the formation of hydrogen bond, probably intermolecular H-bonding with the nitro group of neighboring molecule of **L**.

Titration of **L** with tetra-n-butylammonium hydroxide (TBAOH) results with the appearance of new bathochromically shifted absorption band with maxima at 468, 502 and 512 nm in methanol, acetonitrile and DMSO respectively (Fig. 9(a)-(c)). The values of equilibrium constants logK (**L**:TBAOH, 1:1) are comparable in methanol and acetonitrile 4.45 ± 0.01 and 4.59 ± 0.03, whereas the higher value was obtained in DMSO 5.45 ± 0.03. The logK values correlate with the value of the spectral shift between bands of neutral and ionized form in absorption spectra: the largest in DMSO, and the lowest in methanol (Fig. 9(d)).

In the ^{1}H NMR spectrum of **L** registered in equimolar amount of TBAOH (DMSO-d_6) (Fig. S3) its deprotonation as one might expected is seen as disappearance of OH and NH proton signals and shielding of all signals of aromatic protons.

3.5. Complexation of metal cations in solution

The presence of azo moiety, with one of the nitrogen acting as a donor atom, in connection with the *o*-hydroxyl group and heterocyclic residue makes the structure of **L** similar to well-known metallochromic reagents. Metal cation complexation for **L** was investigated with the use of spectroscopic methods.

Quantitative colorimetric probes of metal cation complexation, realized in practice as an addition of the excess of metal perchlorate to solution of **L** (Fig. 10(a)), showed that the most significant, specific color change from yellow to purple is observed only for copper(II) perchlorate in methanol and DMSO. Some changes in color of the solution of **L** in methanol and DMSO are observed also in the presence of the excess of nickel(II), zinc(II) and lead(II) perchlorates. The excess of these salts, added to solutions of **L** as solid salts, cause the formation of the spectral bands falling in a spectral region of copper(II) complex absorption (Fig. S4). It means that these salts in extremely high concentrations can influence the detection and determination of copper(II).

The change of color in the presence of copper(II) perchlorate is a result of the formation of new absorption bands at 540 and 556 nm respectively in UV–Vis spectra (Fig. 10(b) and (c)). The values of stability constants logK 5.21 ± 0.02 (methanol) and 5.42 ± 0.06 (DMSO) of 1:1 complexes (Job's plots) were calculated from titration data using OPIUM software. The titration trace and Job's plots (insets) in methanol and DMSO are shown in Fig. 10(b) and (c). The presence of metal perchlorates does not affect the color of solution in dichloromethane.

Complex formation is probably connected with the change of the arrangement of the hydrogen bonding system in solution (at the beginning of titration experiment in methanol and DMSO the intensity of absorption band in a region of 500–575 nm decreases upon addition of copper(II) perchlorate). Sharp isosbestic points at 460 nm and at 474 nm for methanol and DMSO providing the presence of two absorbing species under equilibrium are observed only upon addition of a certain amount of copper(II) salt (Fig. 11). ^{1}H NMR spectrum of **L** in the presence of 10-fold excess of copper(II) perchlorate was registered (having in mind paramagnetic properties of copper(II)). In the registered spectrum, as can be expected broad - all shielded - signals are observed (Fig. S5). The presence of OH and NH proton signals suggests that the interaction with copper(II) ions in DMSO does not cause deprotonation of the ligand. The upfield shift can point out the change of the hydrogen

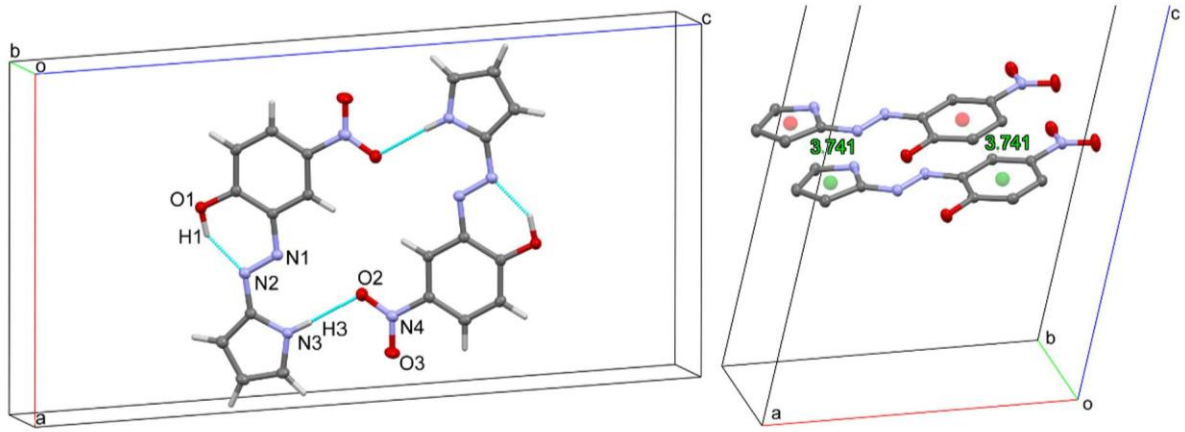

Fig. 6. Left: Hydrogen bonding in compound **L**, selected atom labels shown, cyan dashed lines show direction of bonding. Both molecules are related by the inversion centre at (½ 0 ½). Right: Stacking interactions in **L**. Centroids for pyrrole rings and phenyl rings have equal distance of one another (3.741(9) and 3.741(8) Å for pyrrolic and phenyl rings, respectively). (For interpretation of the references to color in this figure legend, the reader is referred to the web version of this article.)

Table 2
Hydrogen-bond geometry (Å, °) for **L**.

D—H···*A*	*D*—H	H···*A*	*D*···*A*	*D*—H···*A*
N3—H3···O2^{i}	0.859 (19)	2.142 (19)	2.9988 (13)	175.2 (17)
O1—H1···N1	0.93 (2)	2.45 (2)	2.9635 (13)	114.9 (15)
O1—H1···N2	0.93 (2)	1.79 (2)	2.6121 (13)	145.3 (18)

Symmetry code: (i) -*x* + 1, -*y*, -*z* + 1.

bonding system upon copper(II) complexation [90].

In acetonitrile at the beginning of titration the formation of a new, broad band at ~ 500 nm is observed. Higher amounts of copper(II) perchlorate causes the decrease of the absorbance in (Fig. S6) resulting in decolorization of solution. Due to possible side reactions of **L** with copper(II) perchlorate in acetonitrile this solvent was not considered for practical applications here. The nature of interactions of copper(II) - azo compounds (possible redox process) in acetonitrile is under investigation in our group.

From a practical, namely analytical point of view a selective response towards analyte in pure organic solvent has less importance than selective recognition in aqueous or mixed water-organic solvent systems. We found that the stability constant of the copper(II) complex of **L** has the highest value in DMSO. This hygroscopic solvent is well miscible with water and less toxic contrary to methanol. However saying that, the last studies have shown that DMSO is not so inert as it was considered for many years [91]. We carried out the spectrophotometric titration of **L** in mixed solvent system: DMSO with various water content (v/v) using in experiments both copper(II) perchlorate (Fig. S7) and chloride (Fig. S8), as the last is one of the most ubiquitous anions in natural systems. In all mixed solvent system molar ratio plots shows 1:1 (**L**:Cu) stoichiometry of complex (Fig. S9 and S10).

The presence of a defined amount of water in a titrated system

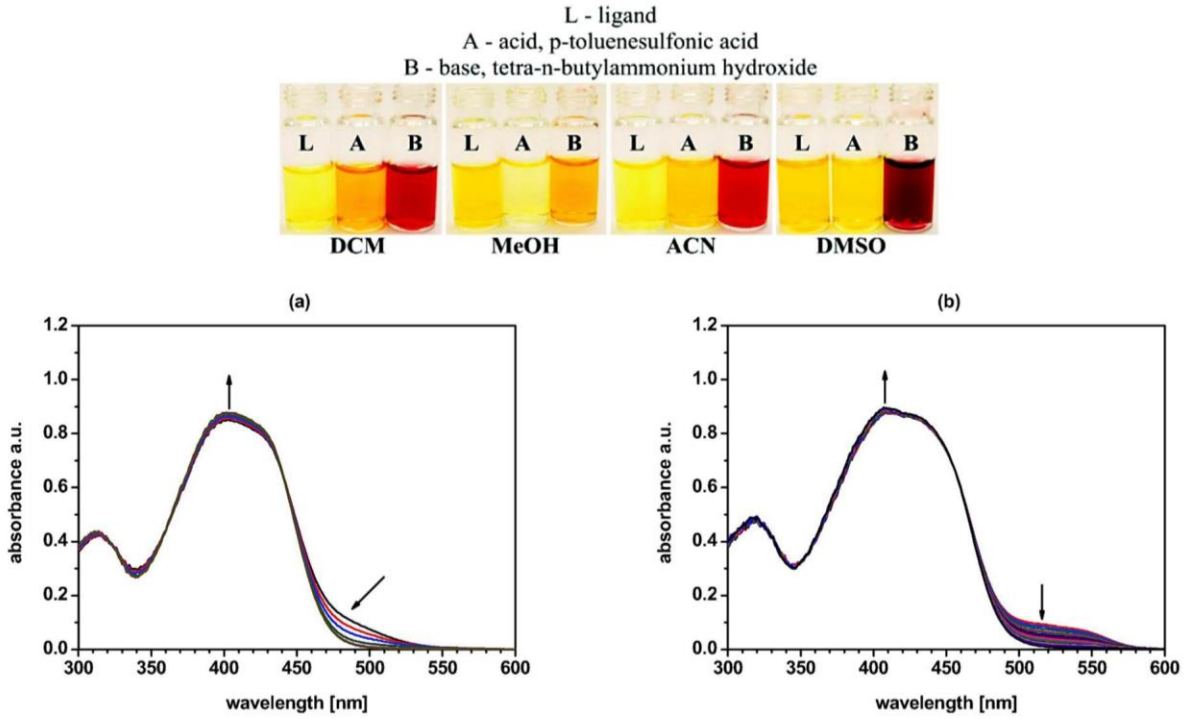

Fig. 7. Top: solutions of **L** (1.02×10^{-4} M) in different solvents with acid or base. Bottom: spectral changes upon titration of **L** ($c_L = 4.05 \times 10^{-5}$ M) with TsOH in (a) methanol ($c_{TsOH} = 0–2.03 \times 10^{-5}$ M) and (b) DMSO ($c_{TsOH} = 0–2.05 \times 10^{-5}$ M).

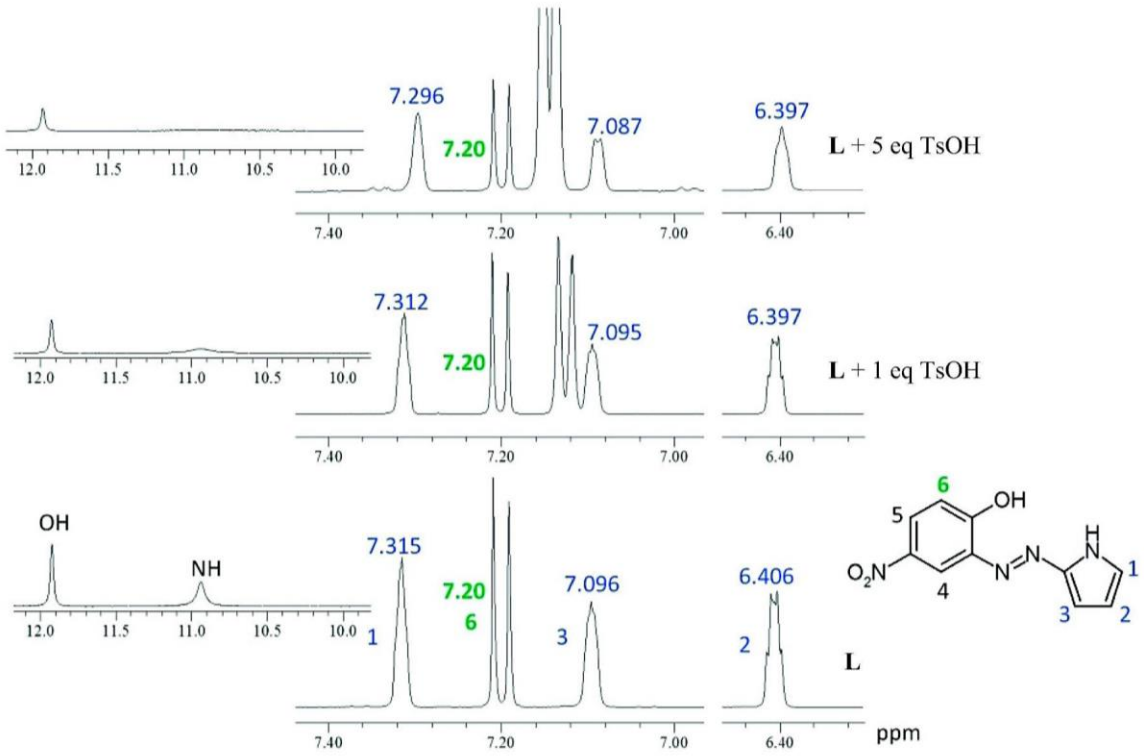

Fig. 8. Partial ^{1}H NMR spectra of **L** 1.42×10^{-2} M (bottom), **L** in the presence of equimolar (middle) and 5-fold excess (top) of TsOH in DMSO-d_6.

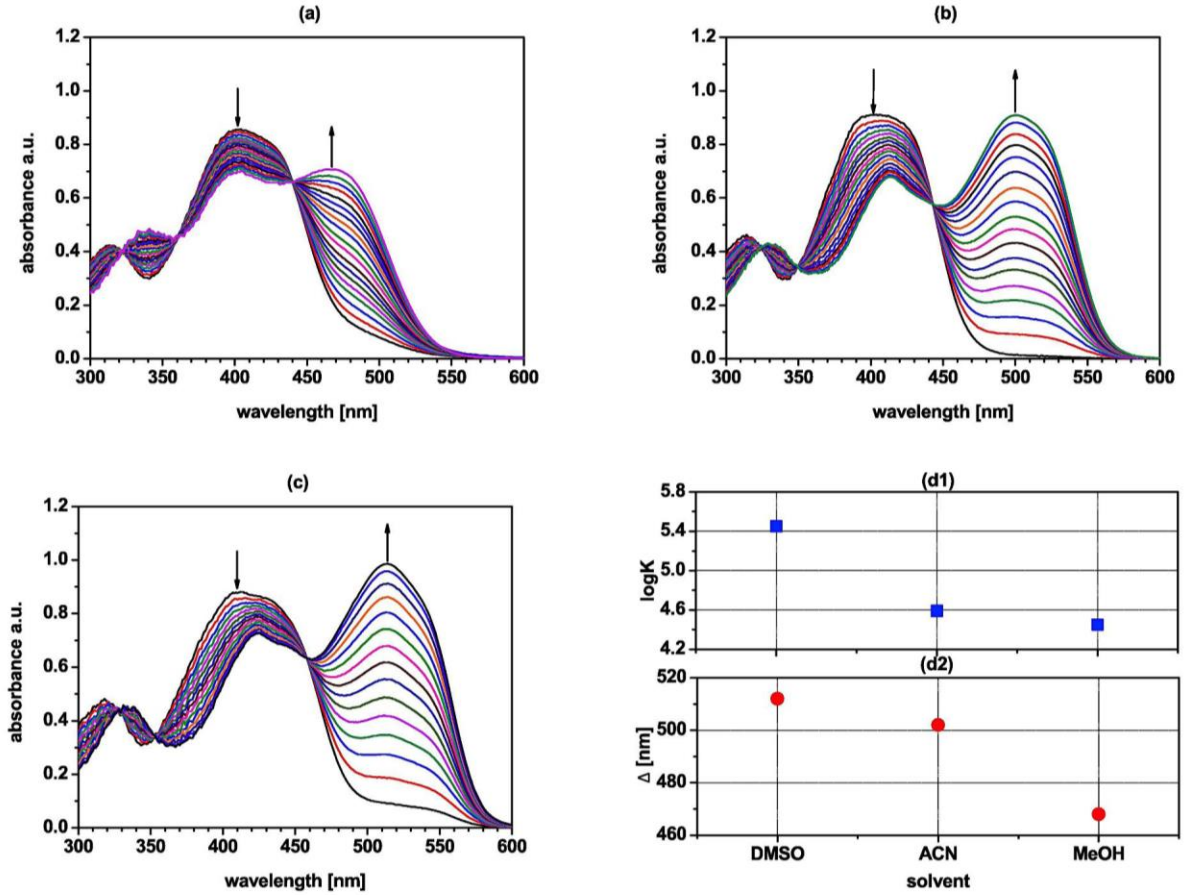

Fig. 9. Spectral changes upon titration of **L** ($c_L = 4.05 \times 10^{-5}$ M) with TBAOH in (a) methanol (c_{TBAOH} = 0–4.20×10^{-5} M), (b) acetonitrile (c_{TBAOH} = 0–8.26×10^{-5} M) and (c) DMSO (c_{TBAOH} = 0–4.34×10^{-5} M). (d) The relationship between logK value and the spectral shift Δ [nm] in dependence of the type of solvent.

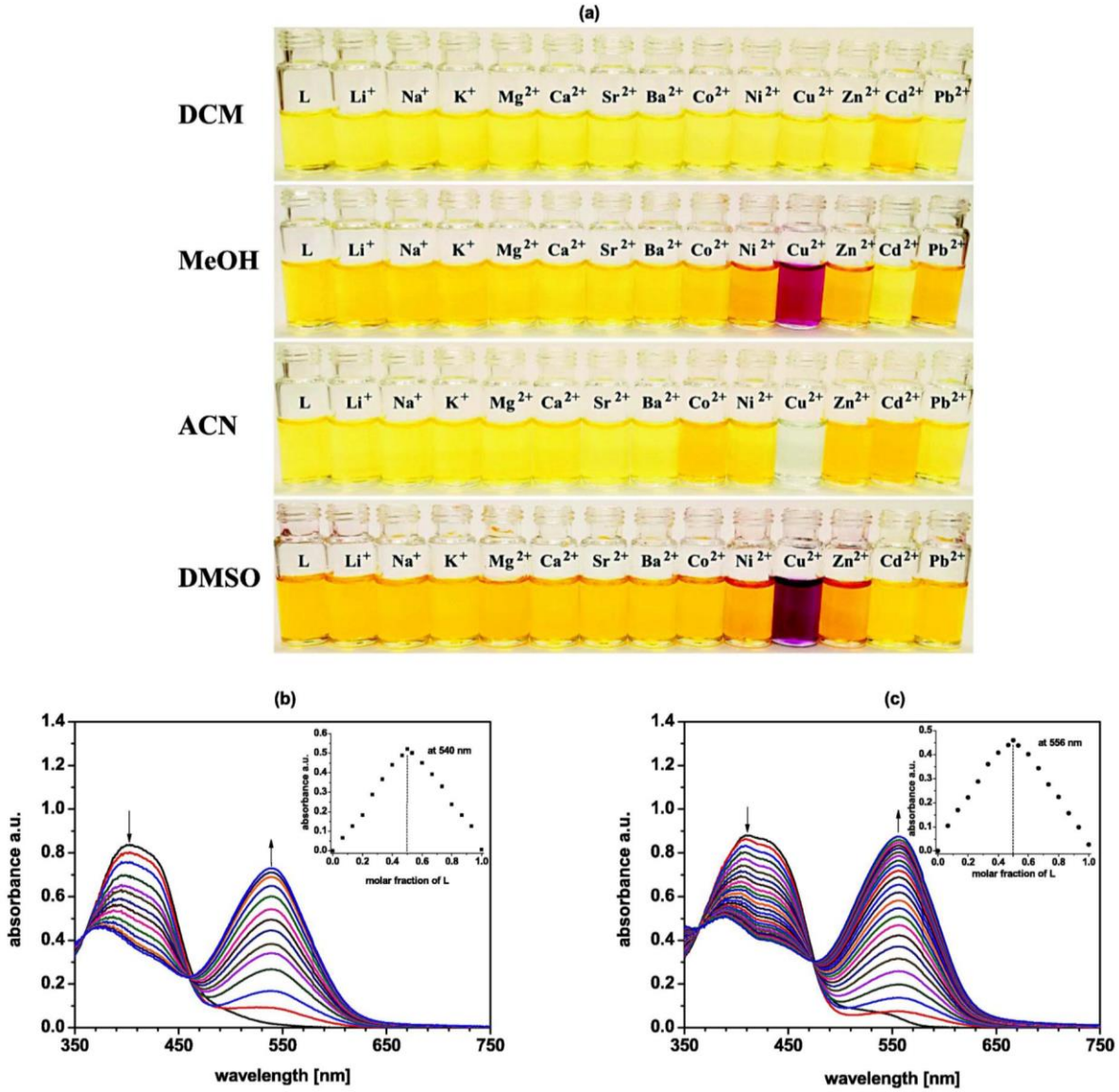

Fig. 10. (a) The change of the color of **L** ($c_L = 1.02 \times 10^{-4}$ M) in the presence of the excess of metal perchlorates in various solvents; from the top: dichloromethane (DCM), methanol (MeOH), acetonitrile (ACN) and DMSO; changes in UV–Vis absorption spectra of **L** ($c_L = 4.05 \times 10^{-5}$ M) upon titration with copper(II) perchlorate in (b) methanol ($c_{Cu} = 0$–1.19×10^{-4} M) and (c) DMSO ($c_{Cu} = 0$–8.26×10^{-5} M). Insets: Job's plots.

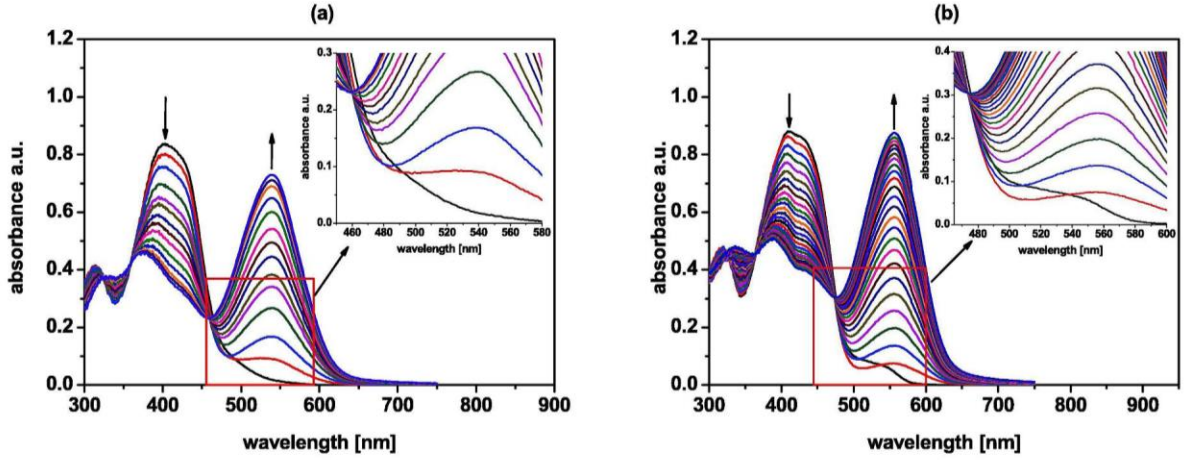

Fig. 11. UV–Vis titration trace of **L** ($c_L = 4.05 \times 10^{-5}$ M) for copper(II) perchlorate in (a) methanol ($c_{Cu} = 0$–1.19×10^{-4} M) and (b) DMSO ($c_{Cu} = 0$–8.26×10^{-5} M). Insets: spectral changes in region of isosbestic points and changes in a range 500–575 nm.

influences the value of spectral shift between free **L** and its copper(II) complex (color change is shown in Fig. S11), which is visualized schematically in Fig. 12(a). The largest value is observed in pure DMSO and systems with 10% of water, 144 nm. When water is present in 90% spectral shift is still over 100 nm, i.e. 122 nm (Fig. 12(b)). The benefit of the addition of water is the decrease of the intensity of the band of ligand in the region of 500–575 nm, where copper(II) complex absorbs. The counter ion has negligible effect on the difference between spectral shift of **L** and its copper(II) complex, however it affects the value of stability constant logK of copper(II) complex (1:1) (Fig. 12(c)). The stability constant values, at the same solvent composition, are higher when copper(II) chloride is used as a salt.

Investigating the selectivity of colorimetric response of **L** towards metal cations (quantitative probes) it was found that color change of **L** from yellow to purple in solvent mixture water-DMSO (9:1) is observed only in the presence of copper(II) chloride (Fig. 13). Slight changes of color to orange in the case of high concentrations of nickel(II) and lead (II) salts are observable and these ions may be considered as the main interfering ions.

3.6. Effect of pH

The effect of pH on spectral changes of **L** in water-DMSO (9:1, v/v) solution is shown in Fig. 14(a). With increasing pH the increase of absorption band at 470 nm is observed what can be connected with the deprotonation of **L**. It confirms the titration trace of **L** with sodium hydroxide (Fig. 14(b)) with clear isosbestic points suggesting two species under equilibrium. The spectral response ΔA towards copper(II) chloride (Fig. 14(c)) is constant in pH range 5.0–9.0 with linear response range $6.68 \times 10^{-8} - 1.67 \times 10^{-5}$M (Fig. 14(d)) and detection limit 5.00×10^{-8} M. Spectral changes upon titration of **L** with copper(II) chloride at pH 5.0, 7.0 and 9.0 in solvent mixture water-DMSO (9:1, v/v) are shown in Fig. S12. Only at pH 5 clear isosbestic point is observed, however it does not strongly influence the linear spectrophotometric response towards copper(II) presence (Fig. S13). Titration of **L** with copper(II) chloride in an alkaline environment (NaOH) gives linear response in a range of $6.68 \times 10^{-8} - 2.19 \times 10^{-5}$M (Fig. S14) and detection limit 6.19×10^{-8} M.

3.7. Regeneration

Regeneration cycles of **L** with 0.01 M EDTA solution after addition of copper(II) chloride are shown in Fig. S15. **L** can be regenerated at least 10 times without losing properties.

3.8. Interfering cations

The response of **L** was investigated in the presence of several interfering cations: Li^+, Na^+, K^+, NH_4^+, Mg^{2+}, Ca^{2+}, Sr^{2+}, Ca^{2+}, Ba^{2+}, Mn^{2+}, Co^{2+}, Ni^{2+}, Zn^{2+}, Cd^{2+}, Pb^{2+} and their mixture. Fig. 15 shows the influence of addition of equimolar, 10-fold and 100-fold molar excess of interfering ammonium and metal chlorides on the spectrophotometric response of **L** at equimolar (to **L**) amounts of copper(II) chloride. The effect of interfering ions is given as RR% value, in water-DMSO (9:1, v/v) solvent mixture at pH 7.0. RR% value does not exceed 5% even in 100-fold molar excess of interfering ions and their mixture.

3.9. Studies in multi-component solutions

The possibility of application of **L** for the detection of copper(II) was

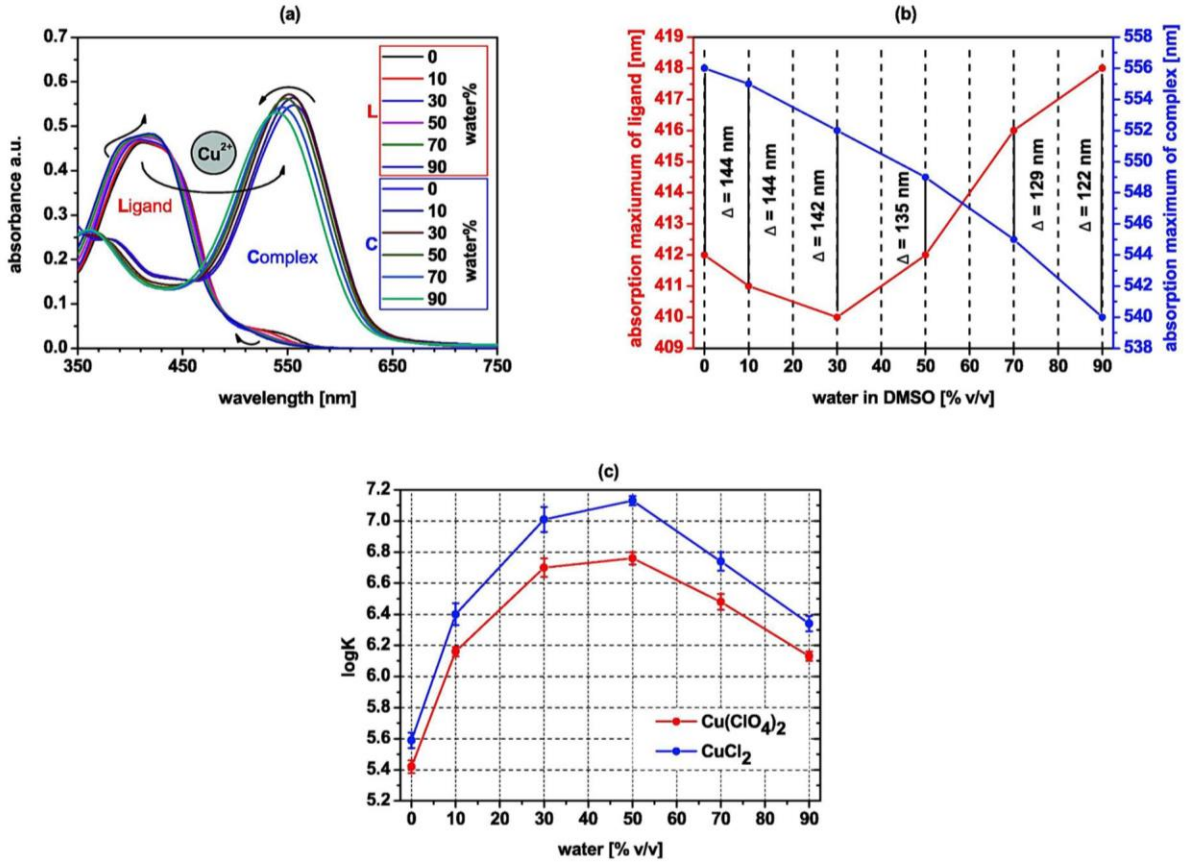

Fig. 12. (a) The influence of water content (%, v/v) in DMSO on spectral changes of **L** (2.16×10^{-5} M) and its copper(II) complex **C** (limiting spectra from copper(II) perchlorate titration experiments are shown); (b) the relationship between the position of the absorption maxima of **L** [nm] and its copper(II) complex [nm] and water content [%] in DMSO; (c) the comparison of the values of stability constants of copper(II) complexes (1:1) with **L** in dependence on counter ion.

Fig. 13. Color change of ligand ($c_L = 2.16 \times 10^{-5}$ M) in water-DMSO solution (9:1, v/v) in the presence of ammonium and metal chlorides (pH 6.0).

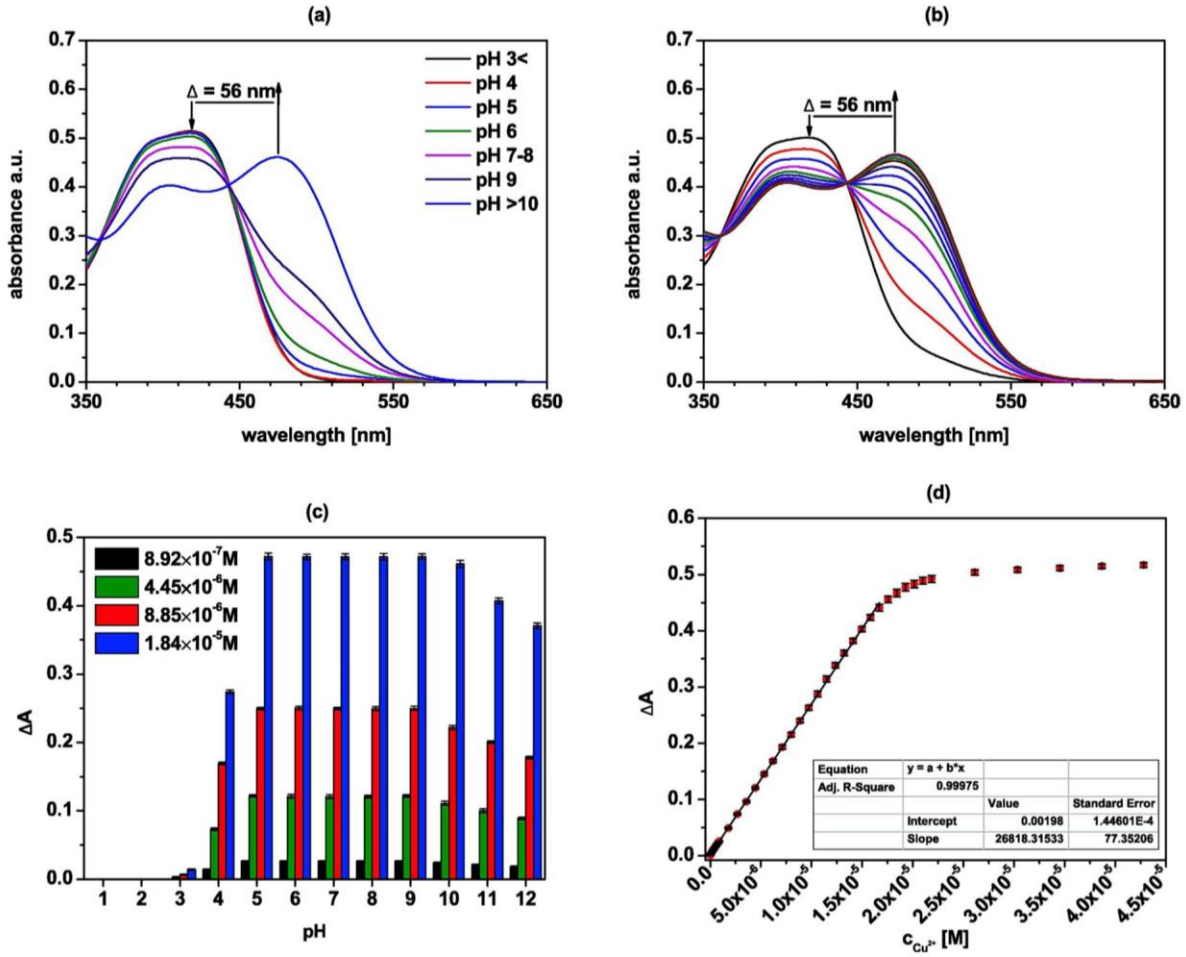

Fig. 14. The change of UV–Vis spectrum of **L** ($c_L = 2.16 \times 10^{-5}$ M) (a) with increasing pH and (b) upon titration with sodium hydroxide ($c_{NaOH} = 0–1.08 \times 10^{-5}$ M) in water-DMSO (9:1, v/v) from pH 6; (c) spectral response towards copper(II) chloride of **L** ($c_L = 2.16 \times 10^{-5}$ M) depending on pH ($\lambda = 540$ nm); (d) spectral response ΔA towards copper(II) chloride presence of **L** ($c_L = 2.16 \times 10^{-5}$ M) in pH range 5.0–9.0.

checked in mixtures of DMSO with multicomponent aqueous solutions, namely artificial urine (AU), simulated body fluid (SBF) and phosphate buffer saline (PBS) (9:1,v/v). Spectral changes upon titration of **L** with copper(II) chloride in AU (pH 6.0), SBF (pH 7.4) and PBS (pH 7.4) are shown in Fig. 16. In multi-component solutions the presence of ionic species significantly affects the spectral properties of **L**, which is manifested by the presence of two absorption bands at 405 and 474 nm in UV–Vis spectrum, but it does not significantly affect the range of the linear response (Fig. 17) and the limits of detection (Table S2) for copper (II). The UV–Vis spectrum of **L** in AU and SBF indicates partial ligand deprotonation, while in PBS compound **L** is in deprotonated form. Stability constant values (logK) of copper(II) complexes (1:1) calculated in AU, SBF and PBS are 6.31 ± 0.04, 6.32 ± 0.02 and 6.40 ± 0.05, respectively.

3.10. Digital color analysis

Fig. 18 shows color changes of **L** in solutions with increasing concentration of copper(II) chloride in solvents of different composition. Photos were taken using a Smartphone camera. Observable color changes, which can be traced by "the naked eye", were visible above the 10^{-7} M copper(II) chloride.

Using digital color analysis we combined different color dependences with concentration of copper(II) chloride. Fig. 19 shows these correlations in SBF:DMSO (9:1, v/v) solution. The largest range of the linear response $8.92 \times 10^{-7} – 2.18 \times 10^{-5}$ M was obtained for color ratio B/G with detection limit 1.07×10^{-7} M. However the lowest LOD = 8.66×10^{-8} M was obtained for color change ΔE_{RGB} with linear response $8.92 \times 10^{-7} – 1.32 \times 10^{-5}$ M. All color dependences with concentration of copper(II) chloride (Fig. S16-S19) at different pH are collected in Table S3.

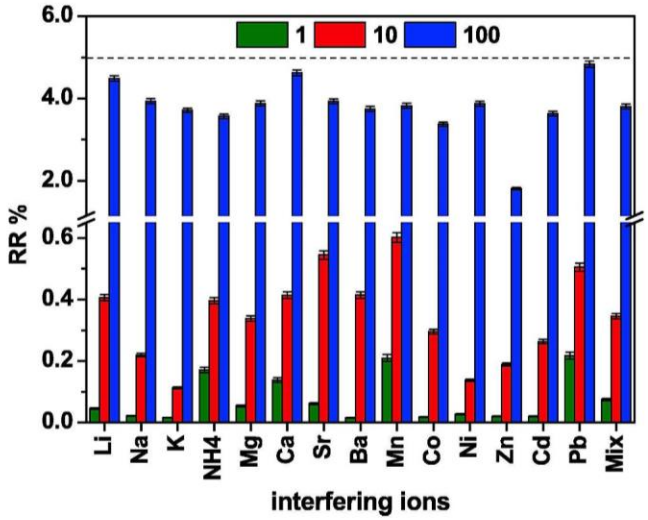

Fig. 15. Interferences of ammonium and several metal chlorides used in equimolar, 10-fold and 100-fold molar excess, on the spectrophotometric response of **L** ($c_L = 2.16 \times 10^{-5}$ M) (540 nm) at equimolar (to **L**) amount of copper(II) chloride in water-DMSO (9:1, v/v) solvent mixture, pH 7.0.

3.11. Comparison of chemosensor L with the other reported chemosensors.

In Table 3 we compared compound **L** with other reported chemosensors that use Smartphone camera detection for the determination of copper(II) [92–95]. The synthesized chemosensor **L** has many advantages over the other reported chemosensors such as: simple preparation, use of inexpensive reagents and lower detection limits than the other chemosensors.

3.12. Tests strips and cotton swabs

Test strips and cotton swabs were used for fast and qualitative detection of copper(II) ions in water solutions. In Fig. 20 color changes of prepared sensors after immersion in solutions of different copper(II) chloride concentration are shown. Detection of copper(II) by naked-eye is possible above 1.0×10^{-5} M and 1.0×10^{-7} of copper(II) chloride for sensors where **L** was used in concentration of 1.04×10^{-3} M and 1.04×10^{-4} M, respectively.

3.13. Optodes

The response of cellulose triacetate (CTA) optode towards copper(II) was investigated spectrophotometrically (Fig. 21(a)). UV–Vis spectra of optodes before contact with copper(II) are similar to spectra of **L** registered in dichloromethane, acetonitrile and water-DMSO (9:1, v/v) below pH 5.0. The spectrophotometric response of optode in the presence of copper(II) chloride characterizes with the appearance of a new, bathochromically shifted absorption band, which intensity increases with the increasing concentration of copper(II) chloride. The maximum of absorption of the optode based on **L** is located at 412 nm and is shifted towards 540 nm, when titrated with an aqueous solution of copper(II) chloride. It is consistent and comparable with spectral and color changes resulting from the formation of a complex of 1:1 stoichiometry, when titrating organic and water mixture solutions of **L** with copper(II) perchlorate and chloride. Thus it can be assumed that the observed spectral pattern for optodes can be a result of the complex formation between chromoionophore entrapped in a polymeric matrix and copper

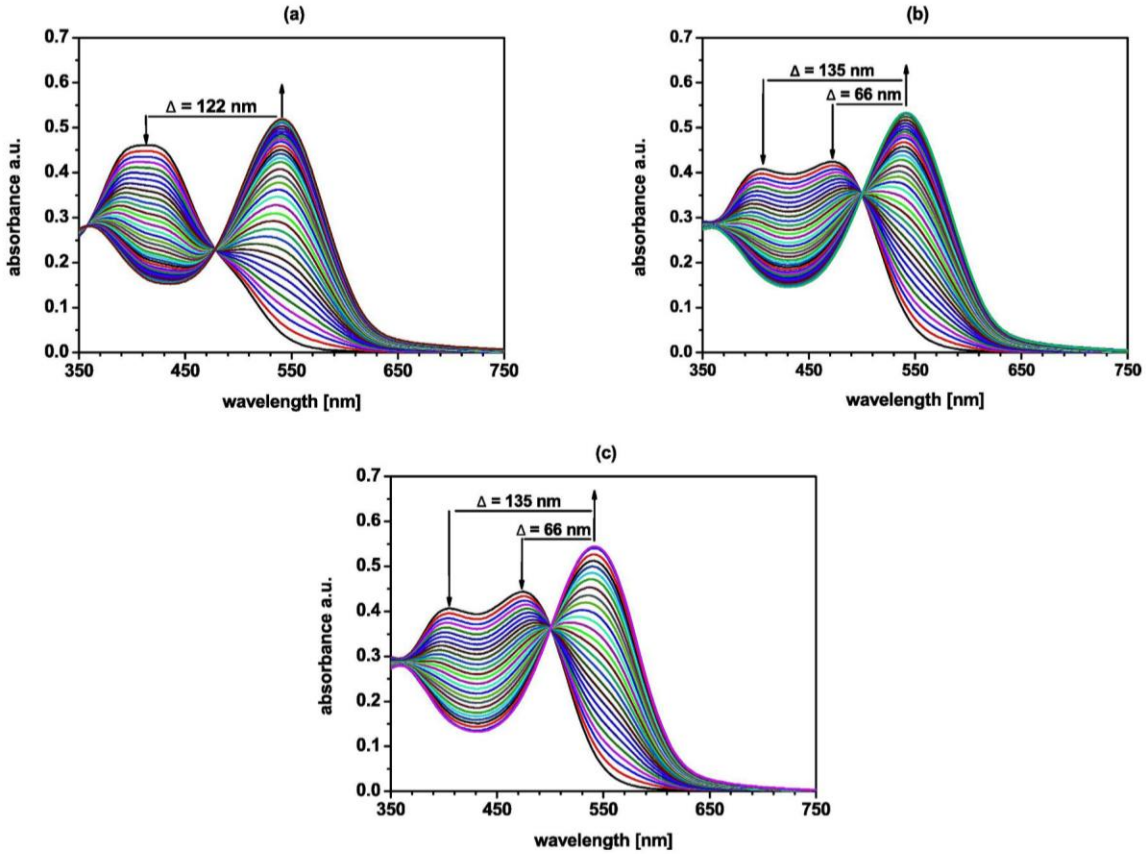

Fig. 16. The change of UV–Vis spectrum of **L** ($c_L = 2.16 \times 10^{-5}$ M) upon titration with copper(II) chloride ($c_{Cu} = 0$–4.28×10^{-5} M) in (9:1, v/v) solvent mixtures: (a) AU:DMSO (pH 6.0); (b) SBF:DMSO (pH 7.4) and (c) PBS: DMSO (pH 7.4).

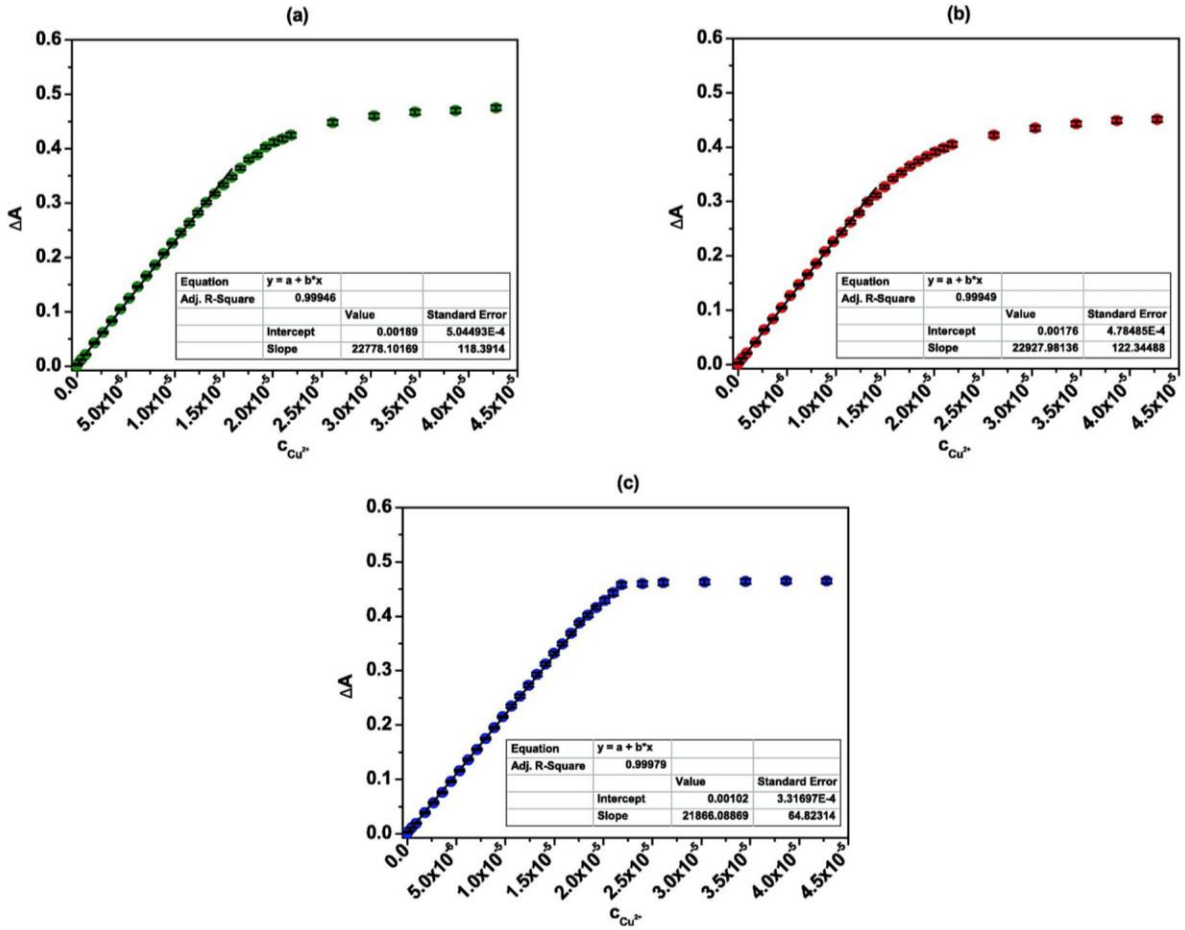

Fig. 17. Linear responses of **L** ($c_L = 2.16 \times 10^{-5}$ M) upon titration with copper(II) chloride (c_{Cu} = 0–4.28×10^{-5} M) in (9:1, v/v) solvent mixtures: (a) AU:DMSO (pH 6.0); (b) SBF:DMSO (pH 7.4) and (c) PBS: DMSO (pH 7.4).

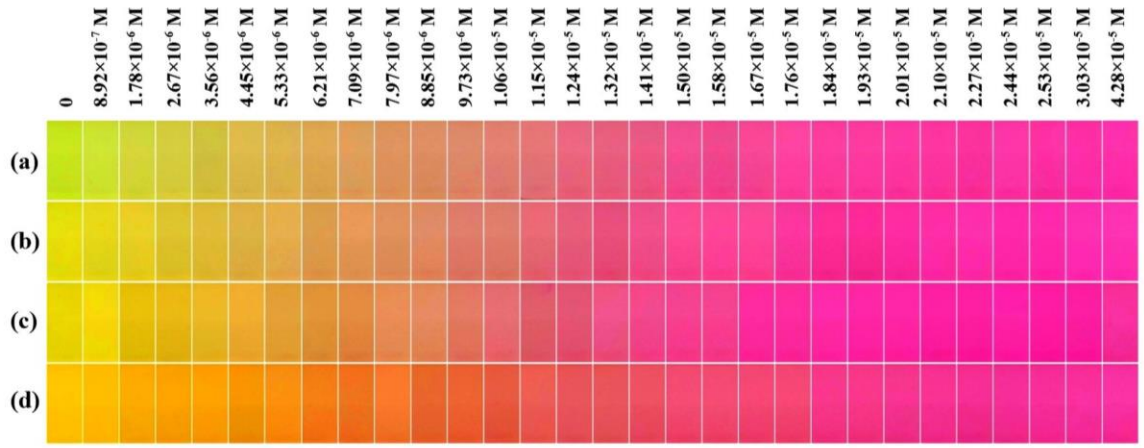

Fig. 18. Color changes of **L** ($c_L = 2.16 \times 10^{-5}$ M) upon titration with copper(II) chloride (c_{Cu} = 0–4.28×10^{-5} M) in water-DMSO (9:1, v/v) solvent mixture at pH: (a) 5.0; (b) 7.0; (c) 9.0 and (d) SBF:DMSO (9:1, v/v) at pH 7.4.

(II) chloride.

Linear response for optode with **L** (Fig. 21(b)) was found for copper (II) concentration range of 5.41×10^{-8} – 2.48×10^{-5} M with a regression equation of $\Delta A = 22769.9221 \times c_{Cu(II)} + 0.0011$ (R^2 = 0.9971) and detection limit 7.22×10^{-8} M. At concentration ca. 4.00×10^{-4} M sensor riches saturation with analyte.

To determine the response time, experiments using membranes immersed in two solutions of copper(II) chloride 1.0×10^{-5} M and 1.0×10^{-6} M, with contact time up to 15 min. were carried out. ΔA of the optodes as a function of time needed for reaching a constant optical signal is shown in Fig. S20. The optode was found to reach 95% of the final signal (t_{95}) within 2 min and 4 min for copper(II) concentration 1.0×10^{-5} M and 1.0×10^{-6} M, respectively.

The reproducibility of optodes was evaluated by comparing the ΔA values of the copper(II) loaded membrane samples obtained in the different series for two concentrations 1.0×10^{-6} M and 1.0×10^{-5} M

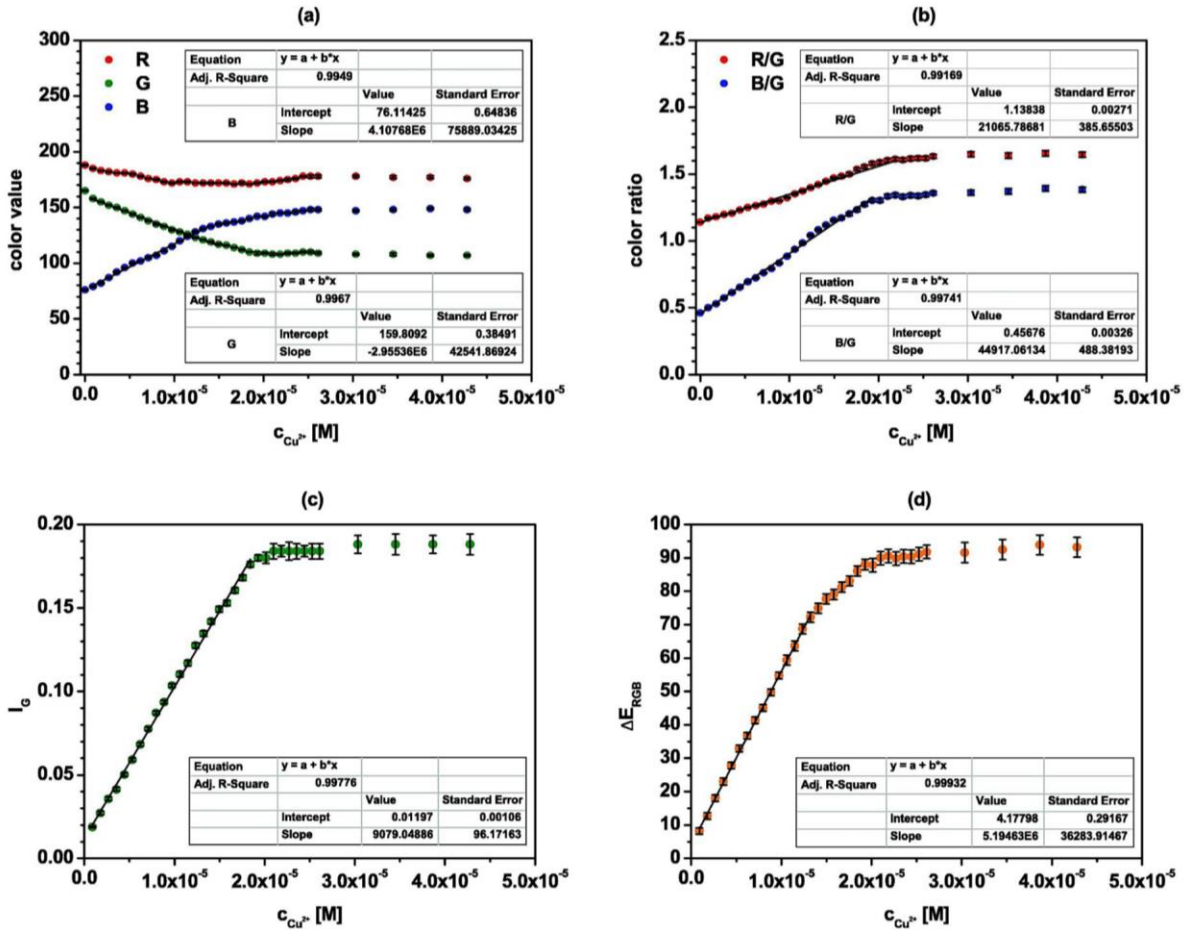

Fig. 19. Dependence of (a) color value, (b) color ratio (R/G, B/G), (c) color intensity (I_G) and (d) color change (ΔE_{RGB}) of **L** ($c_L = 2.16 \times 10^{-5}$ M) upon titration with copper(II) chloride (c_{Cu} = 0–4.28 × 10^{-5} M) in SBF:DMSO (9:1, v/v) at pH 7.4.

Table 3
Comparison of chemosensor **L** with the other reported copper(II) chemosensors with Smartphone detection.

Chemosensor	Method	Medium	Linear response [M]	LOD [M]	Reference
Naphthalimide-based Schiff base	UV–Vis	DMSO	$2.0 \times 10^{-5} - 2.0 \times 10^{-4}$	1.60×10^{-6}	[92]
	Smartphone	EtOAc:H_2O (1:1, v/v, pH 4.8)	$0.0 - 1.0 \times 10^{-3}$	4.80×10^{-5}	
NBD[a]-benzimidazole based dyad	UV–Vis	MeOH:H_2O (1:1, v/v)	$0.0–1.5 \times 10^{-6}$	1.23×10^{-7}	[93]
	Smartphone	MeOH:H_2O (1:1, v/v)	$5.0 \times 10^{-7} - 3.5 \times 10^{-6}$	3.80×10^{-6}	
Red beet pigment	Smartphone	H_2O (pH 9.0)	$4.0 \times 10^{-6} - 2.0 \times 10^{-5}$	8.40×10^{-7}	[94]
Tri-imidazolium salt	Smartphone	DCM:DMSO (49:1, v/v)	$0.0–3.6 \times 10^{-5}$	5.10×10^{-7}	[95]
L	UV–Vis	H_2O:DMSO (9:1, v/v, pH 5.0–9.0)SBF:DMSO (9:1, v/v, pH 7.4)	$6.68 \times 10^{-8} - 1.67 \times 10^{-5}$ $6.68 \times 10^{-8} - 1.41 \times 10^{-5}$	5.00×10^{-8} 5.85×10^{-8}	This work
	Smartphone	H_2O:DMSO (9:1, v/v, pH 5.0) H_2O:DMSO (9:1, v/v, pH 7.0) H_2O:DMSO (9:1, v/v, pH 9.0)SBF:DMSO (9:1, v/v, pH 7.4)	$8.92 \times 10^{-8} - 1.58 \times 10^{-5}$ $8.92 \times 10^{-8} - 1.76 \times 10^{-5}$ $8.92 \times 10^{-8} - 2.10 \times 10^{-5}$ $8.92 \times 10^{-8} - 1.32 \times 10^{-5}$	8.33×10^{-8} 7.72×10^{-8} 6.37×10^{-8} 8.66×10^{-8}	

[a] 4-choloro-7-nitrobenzafuran.

(Fig. 22(a)). The relative standard deviations for the measured ΔA values for 1.0×10^{-6} M and 1.0×10^{-5} M were 1.68% and 0.96%, respectively. The possibility of regeneration of optode after use - to make them reusable - was checked using a regeneration solution of 0.1 M HCl. Regeneration time for optode was less than 30 sec. After regeneration, optodes were washed three times with deionized water. In Fig. S21 regeneration of optodes is shown after contact with 1.08×10^{-5} M copper(II) chloride solution. After ten cycles the drift of the optical signal was less than 1.27%. However in the same time some leaching of **L** from the polymer matrix was observed - the solution turned purple in color. This effect was investigated qualitatively using two concentrations of copper(II) salt chloride: 1.0×10^{-6} M and 1.0×10^{-5} M (Fig. S22). After ten cycles leaching of **L** from optodes for 1.0×10^{-6} M and 1.0×10^{-5} M were 12.9 ± 0.1 and 29.4 ± 0.3, respectively. Despite the leaching of the compound from the membrane, it is possible to use optode at least 10 times. Membranes that were used and left to dry out typically for cellulose triacetate material undergo deformation, losing their mechanical properties (mainly flexibility). Thus between measurements optodes should be kept in solution, preferentially in regeneration solution. Just prepared optodes and not used for measurements can be stored safely for a period of at least 3 months in a dry and dark place (room conditions) without losing their properties. Fig. 22b shows the influence of addition of equimolar, 10-fold and 100-fold molar excess of interfering ions salt on the spectral response of optodes

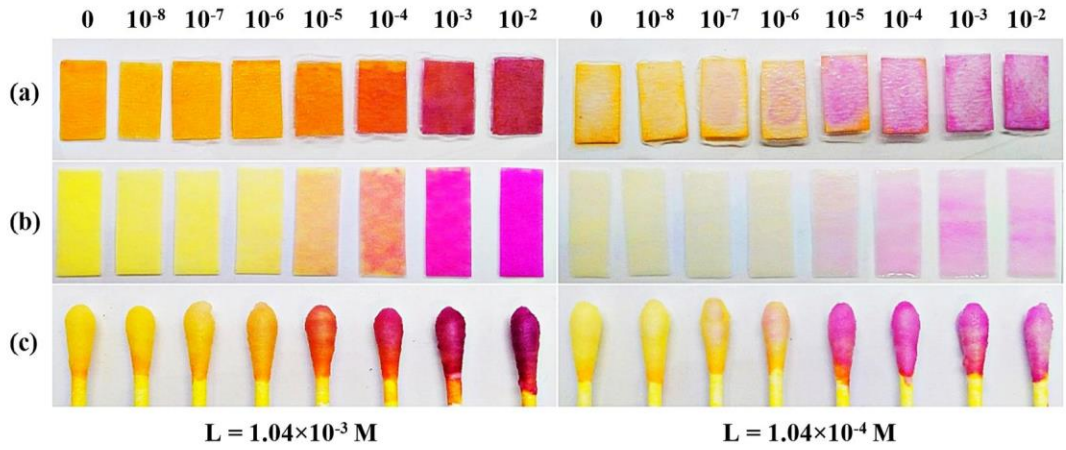

Fig. 20. Color changes of test strips (a) glass microfiber filter and (b) filter paper; (c) cotton swabs.

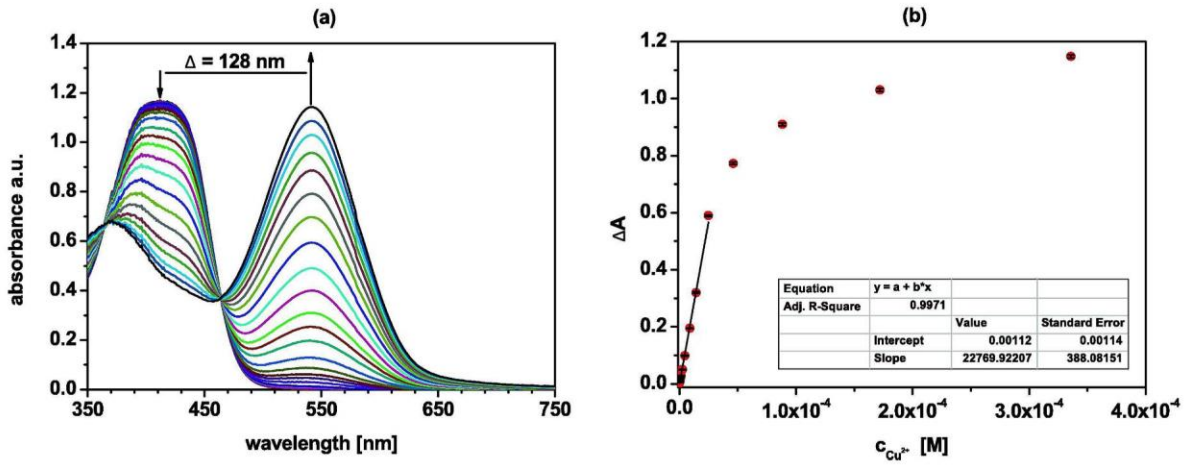

Fig. 21. (a) Changes in UV–Vis spectrum and (b) optical response of optode with **L** upon titration copper(II) chloride (c_{Cu} = 0–3.36 × 10^{-4} M) in aqueous solution (pH 5.0).

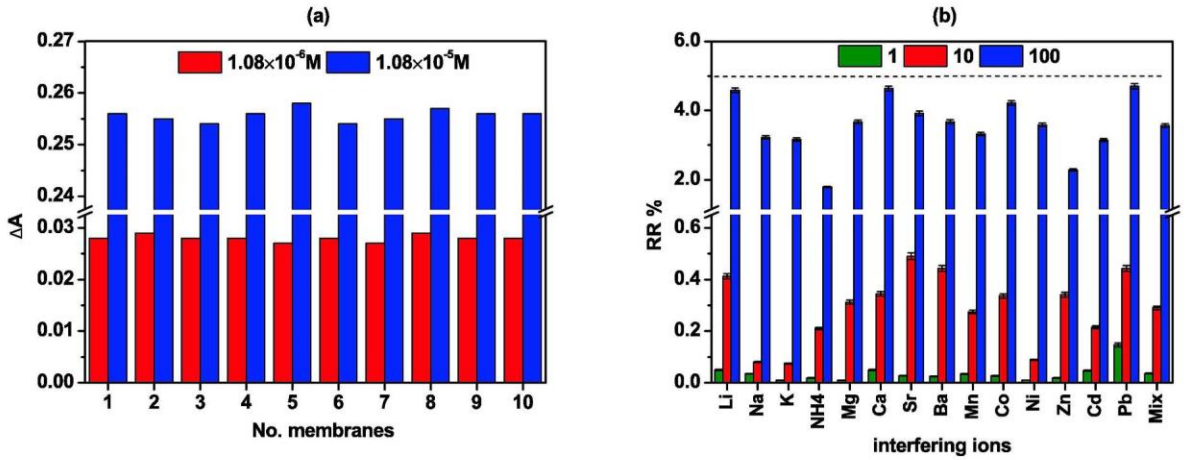

Fig. 22. (a) Reproducibility of optode after contact with copper(II) chloride solution (pH 5.0) and (b) interferences of several metal chlorides used at equimolar, 10-fold and 100-fold molar excess, expressed as RR%, to spectral response (ΔA) of optodes (at 540 nm) towards copper(II) chloride (pH 5.0).

immersed in 10^{-5} M solution of copper(II) chloride. RR% value does not exceed 5% even in 100-fold molar excess of interfering ions and their mixture.

Fig. 23 shows color changes of optodes with **L** after contact with increasing concentration of copper(II) chloride at pH 5.0. Naked-eye color changes were observed above 10^{-6} M of copper(II) chloride.

The colorimetric analysis of the digital images was carried out in parallel with the studies of the spectrophotometric response of the optodes. Fig. 24 shows these correlations in DMSO:SBF 1:9 (v/v) solution. The widest range of the linear response 2.16 × 10^{-7} –1.72 × 10^{-4}

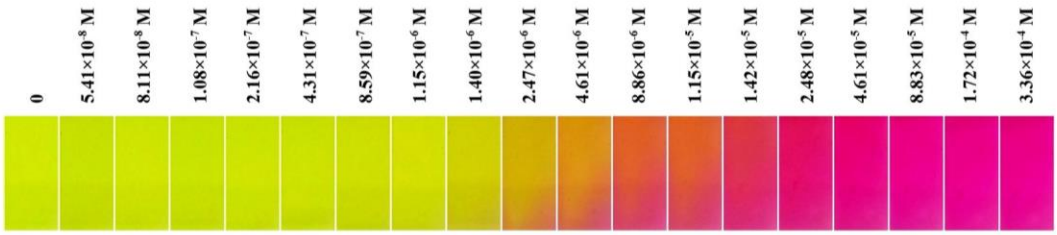

Fig. 23. Color changes of optode upon titration with copper(II) chloride (c_{Cu} = 0–3.36 × 10^{-4} M) at pH 5.0.

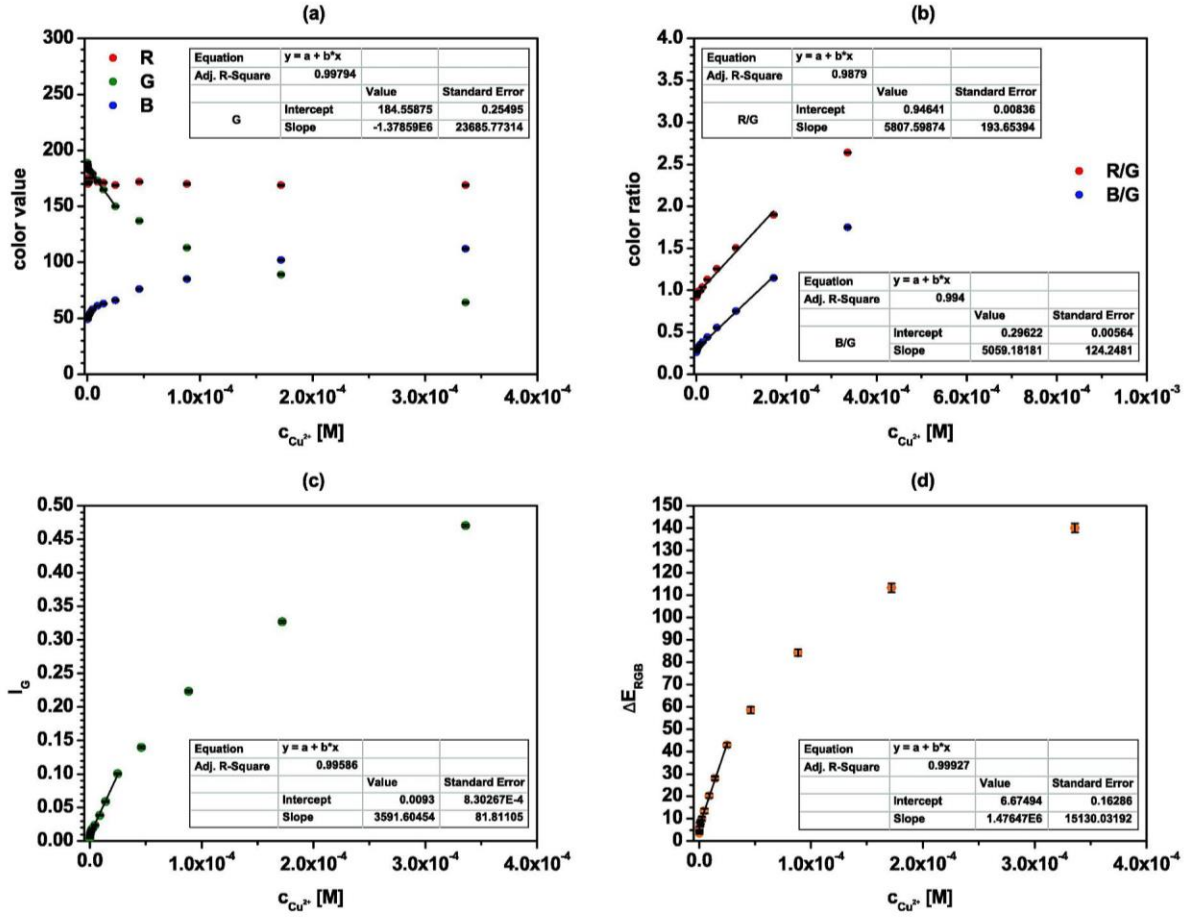

Fig. 24. Dependence of (a) color value; (b) color ratio (R/G, B/G); (c) color intensity (I_G) and (d) color change (ΔE_{RGB}) of optode with **L** upon titration with copper (II) chloride (c_{Cu} = 0–4.28 × 10^{-5} M) at pH 5.0.

M (R^2 = 0.9879) was obtained for R/G color ratio with detection limit 8.27 × 10^{-7} M, but the lowest LOD 4.06 × 10^{-7} M was obtained for color change ΔE_{RGB} with linear response 4.31 × 10^{-7} – 2.48 × 10^{-5} M (R^2 = 0.9993). All investigated color dependences for discussed optodes with concentration of copper(II) chloride are collected in Table S4.

In Table 4 the properties of copper(II) selective optodes obtained in recent years and described in literature [96–99] are listed for comparison with the characteristics of optode with **L**. From this comparison it is quite well seen that optode obtained by us is, in general, more or less comparable with those proposed by other authors. The advantage is the use of a biodegradable polymer matrix that does not require additional support in the form of glass and the possibility of colorimetric determination of copper(II) ions using a Smartphone.

3.14. *Determination of copper(II) in model and real samples*

Possible application of proposed chemosensor **L** and optode were tested using different samples: of known copper(II) concentrations – commercial copper(II) standard solution, spiked tap water from different regions of northern Poland, commercial drinking water samples and Qnova calibration solution. In the last case results were compared with the values obtained by independent analysis using ICP-OES. All measurements were done at pH 5.0. Both attempts were tested: spectrophotometric and colorimetric detection of copper(II).

Comparison of recovery results obtained for chemosensor **L** in solution and optodes upon immersion of the sensor layer in a commercial standard reference solution of copper(II) for different concentrations in range from 4.46 × 10^{-7} to 1.32 × 10^{-5} M are collected in Table 5. The recoveries are at least about 98.96–99.96 % and 95.56–100.18 % for spectrophotometric detection (ΔA) for **L** and optode, respectively.

To evaluate the influence of the sample matrix three different samples of tap water and three samples of drinking water were spiked with known concentration of copper(II) - Table 6. In this case ΔA recoveries were within 98.58 – 101.92 % and 97.05 – 101.35 % for solution of **L**

Table 4
Comparison of obtained optode with already existing ones.

Sensing material	Support	pH	Response time	Linear response [M]	LOD [M]	Reference
EBSI [a]	PVC	4.0	3 min	$1.57 \times 10^{-7} - 5.04 \times 10^{-4}$	1.26×10^{-7}	[96]
HIBIN	Sol-gel	5.0	2 min	$9.10 \times 10^{-8} - 1.12 \times 10^{-5}$	1.80×10^{-8}	[97]
Schiff base	Sol-gel	5.5	2 min	$8.54 \times 10^{-8} - 1.00 \times 10^{-5}$	1.53×10^{-8}	[98]
Schiff base	PVA/TEOS	5.0	1.5 min	$9.34 \times 10^{-8} - 1.15 \times 10^{-5}$	1.27×10^{-8}	[99]
L	CTA	5.0	2–4 min	$5.41 \times 10^{-8} - 2.48 \times 10^{-5}$	7.22×10^{-8}	This work
				$4.31 \times 10^{-7} - 2.48 \times 10^{-5}$	4.06×10^{-7} [b]	

[a] N,N'-(4,40-ethylene biphenyl)bis(3-methoxy salicylidineimine).
[b] Smartphone detection.

Table 5
Determination of copper(II) ions - recovery test for commercial standard solution.

Standard reference solution of copper(II) [M]	L		Optode	
	Found copper(II) [M]	Recovery [%]	Found copper(II) [M]	Recovery [%]
4.46×10^{-7}	$4.38 \times 10^{-7} \pm 3.11 \times 10^{-8}$	98.21 ± 6.97	$4.26 \times 10^{-7} \pm 3.68 \times 10^{-8}$	95.56 ± 8.25
8.92×10^{-7}	$8.92 \times 10^{-7} \pm 3.10 \times 10^{-8}$	99.96 ± 2.93	$8.85 \times 10^{-7} \pm 3.26 \times 10^{-8}$	99.19 ± 3.66
2.67×10^{-6}	$2.66 \times 10^{-6} \pm 3.08 \times 10^{-8}$	99.63 ± 1.15	$2.67 \times 10^{-6} \pm 3.19 \times 10^{-8}$	100.07 ± 1.20
4.45×10^{-6}	$4.42 \times 10^{-6} \pm 3.83 \times 10^{-8}$	99.37 ± 0.86	$4.44 \times 10^{-6} \pm 6.48 \times 10^{-8}$	99.82 ± 1.45
8.85×10^{-6}	$8.80 \times 10^{-6} \pm 7.66 \times 10^{-8}$	99.41 ± 0.87	$8.87 \times 10^{-6} \pm 8.08 \times 10^{-8}$	100.18 ± 0.91
1.32×10^{-5}	$1.31 \times 10^{-5} \pm 8.94 \times 10^{-8}$	99.55 ± 0.68	$1.32 \times 10^{-5} \pm 1.10 \times 10^{-7}$	99.85 ± 0.83

Table 6
Determination of copper(II) ions in a real sample - spiked tap water and drinking water.

Real sample	Added copper(II) [M]	L		Optode	
		Found copper(II) [M]	Recovery [%]	Found copper(II) [M]	Recovery [%]
Tap water 1	0	$4.12 \times 10^{-7} \pm 3.11 \times 10^{-8}$	–	$3.91 \times 10^{-7} \pm 7.07 \times 10^{-8}$	–
	4.46×10^{-7}	$8.21 \times 10^{-7} \pm 3.65 \times 10^{-8}$	99.32 ± 4.44	$8.12 \times 10^{-7} \pm 5.56 \times 10^{-8}$	97.05 ± 6.85
	4.45×10^{-6}	$4.85 \times 10^{-6} \pm 3.40 \times 10^{-8}$	100.59 ± 0.70	$4.80 \times 10^{-6} \pm 7.28 \times 10^{-8}$	99.24 ± 1.52
	1.10×10^{-5}	$1.15 \times 10^{-5} \pm 2.76 \times 10^{-8}$	100.31 ± 0.24	$1.14 \times 10^{-5} \pm 5.70 \times 10^{-8}$	100.14 ± 0.50
Tap water 2	0	$1.33 \times 10^{-6} \pm 3.32 \times 10^{-8}$	–	$1.29 \times 10^{-6} \pm 1.67 \times 10^{-7}$	–
	4.46×10^{-7}	$1.79 \times 10^{-6} \pm 7.09 \times 10^{-8}$	101.40 ± 3.96	$1.71 \times 10^{-6} \pm 6.75 \times 10^{-8}$	98.57 ± 3.95
	4.45×10^{-6}	$5.79 \times 10^{-6} \pm 3.42 \times 10^{-8}$	100.36 ± 0.59	$5.78 \times 10^{-6} \pm 7.29 \times 10^{-8}$	100.74 ± 1.26
	1.10×10^{-5}	$1.24 \times 10^{-5} \pm 3.60 \times 10^{-8}$	99.91 ± 0.29	$1.23 \times 10^{-5} \pm 7.19 \times 10^{-8}$	99.98 ± 0.58
Tap water 3	0	$1.01 \times 10^{-6} \pm 2.63 \times 10^{-8}$	–	$1.02 \times 10^{-6} \pm 1.34 \times 10^{-7}$	–
	4.46×10^{-7}	$1.45 \times 10^{-6} \pm 5.63 \times 10^{-8}$	100.05 ± 3.88	$1.45 \times 10^{-6} \pm 6.98 \times 10^{-8}$	98.92 ± 4.80
	4.45×10^{-6}	$5.45 \times 10^{-6} \pm 3.54 \times 10^{-8}$	100.00 ± 0.65	$5.42 \times 10^{-6} \pm 7.28 \times 10^{-8}$	99.17 ± 1.34
	1.10×10^{-5}	$1.21 \times 10^{-5} \pm 3.39 \times 10^{-8}$	100.09 ± 0.28	$1.22 \times 10^{-5} \pm 5.87 \times 10^{-8}$	100.93 ± 0.48
Drinking water 1	0	<LOD	–	<LOD	–
	4.46×10^{-7}	$4.47 \times 10^{-7} \pm 2.26 \times 10^{-8}$	100.25 ± 5.05	$4.52 \times 10^{-7} \pm 2.17 \times 10^{-8}$	101.35 ± 4.80
	4.45×10^{-6}	$4.43 \times 10^{-6} \pm 4.02 \times 10^{-8}$	99.64 ± 0.91	$4.47 \times 10^{-6} \pm 4.76 \times 10^{-8}$	100.46 ± 1.07
	1.10×10^{-5}	$1.11 \times 10^{-5} \pm 5.49 \times 10^{-8}$	100.69 ± 0.49	$1.11 \times 10^{-5} \pm 7.82 \times 10^{-8}$	100.90 ± 0.70
Drinking water 2	0	<LOD	–	<LOD	–
	4.46×10^{-7}	$4.40 \times 10^{-7} \pm 2.67 \times 10^{-8}$	98.58 ± 6.06	$4.35 \times 10^{-7} \pm 2.79 \times 10^{-8}$	97.41 ± 6.43
	4.45×10^{-6}	$4.43 \times 10^{-6} \pm 6.14 \times 10^{-8}$	99.30 ± 1.39	$4.46 \times 10^{-6} \pm 5.83 \times 10^{-8}$	100.26 ± 1.31
	1.10×10^{-5}	$1.11 \times 10^{-5} \pm 7.22 \times 10^{-8}$	100.42 ± 0.65	$1.11 \times 10^{-5} \pm 9.58 \times 10^{-8}$	100.82 ± 0.86
Drinking water 3	0	<LOD	–	<LOD	–
	4.46×10^{-7}	$4.55 \times 10^{-7} \pm 2.68 \times 10^{-8}$	101.92 ± 5.89	$4.44 \times 10^{-7} \pm 1.77 \times 10^{-8}$	99.38 ± 3.99
	4.45×10^{-6}	$4.45 \times 10^{-6} \pm 4.92 \times 10^{-8}$	100.14 ± 1.11	$4.48 \times 10^{-6} \pm 4.34 \times 10^{-8}$	100.66 ± 0.97
	1.10×10^{-5}	$1.11 \times 10^{-5} \pm 6.93 \times 10^{-8}$	100.96 ± 0.62	$1.11 \times 10^{-5} \pm 6.91 \times 10^{-8}$	100.58 ± 0.62

Table 7
Spectrophotometric determination of copper(II) ions in Qnova calibration solution.

	ICP-OES	Added copper(II) [M]	L		Optode	
			Found copper(II) [M]	Recovery [%]	Found copper(II) [M]	Recovery [%]
Qnova calibration solution	$2.36 \times 10^{-7} \pm 1.18 \times 10^{-8}$	0	$2.30 \times 10^{-7} \pm 1.65 \times 10^{-8}$	97.63 ± 7.01	$2.24 \times 10^{-7} \pm 1.97 \times 10^{-8}$	94.83 ± 8.34
		4.46×10^{-7}	$6.75 \times 10^{-7} \pm 4.05 \times 10^{-8}$	99.03 ± 5.94	$6.63 \times 10^{-7} \pm 3.68 \times 10^{-8}$	97.18 ± 5.40
		4.45×10^{-6}	$4.65 \times 10^{-6} \pm 4.38 \times 10^{-8}$	99.19 ± 0.93	$4.64 \times 10^{-6} \pm 9.78 \times 10^{-8}$	99.06 ± 2.09
		1.10×10^{-5}	$1.12 \times 10^{-5} \pm 8.37 \times 10^{-8}$	99.50 ± 0.74	$1.12 \times 10^{-5} \pm 1.14 \times 10^{-7}$	99.32 ± 1.01

and optode, respectively. Elemental composition of drinking water samples was included in the Table S5.

The last probe for testing practical application of the proposed chemosensor and sensor layer for spectrophotometric detection of copper (II) in a complex matrix was carried out using Qnova calibration solution. The elemental composition of the Qnova calibration solution is shown in Table S6. Trace elements were determined by the ICP-OES method. In Table 7 results of the recovery test are collected. The spectrophotometric (ΔA) recoveries were 97.63–99.50 % and 94.83–99.32 % for **L** in solution and optode, respectively.

4. Conclusion

New *o*-hydroxyazocompound **L** bearing pyrrole moiety was obtained in a facile procedure. It was found that this simple compound has interesting properties in solution and in a solid state. Detailed studies of metal cation complexation by **L** allow to conclude that this easily available compound can serve as an effective spectrophotometric reagent for detection and determination of copper(II) in samples of various compositions. On the other hand, simple sensing materials based on **L** selectively generate colorimetric signal in the presence of copper(II), which can be used for non-instrumental detection of this important metal cation. The second option is using a mobile device camera as a detector. The characteristics of the above systems such as linear response range, limit of detection, possibility of regeneration etc. make them useful for wireless routine analysis of environmental and biological samples in laboratories and field analysis.

CRediT authorship contribution statement

Błażej Galiński: Conceptualization, Data curation, Formal analysis, Investigation, Methodology, Project administration, Validation, Visualization, Writing – original draft, Writing – review & editing. **Jarosław Chojnacki:** Data curation, Investigation, Methodology, Visualization, Writing – original draft. **Ewa Wagner-Wysiecka:** Conceptualization, Data curation, Supervision, Validation, Visualization, Writing – original draft, Writing – review & editing.

Declaration of Competing Interest

The authors declare that they have no known competing financial interests or personal relationships that could have appeared to influence the work reported in this paper.

Data availability

Data will be made available on request.

Acknowledgments

This work was supported by the Faculty of Chemistry, Gdańsk University of Technology, No. 035376 - an internal grant from statutory funds. Financial support of these studies from Gdańsk University of Technology by the DEC-**2/2021/IDUB/V.6/Si** grant under the **SILICIUM SUPPORTING CORE R&D FACILITIES** - "Excellence Initiative - Research University" program is gratefully acknowledged.

Appendix A. Supplementary data

Crystallographic data for all structures reported in this paper have been deposited with the Cambridge Crystallographic Data Centre as supplementary publication No. CCDC 2190550. The data can be obtained free of charge from The Cambridge Crystallographic Data Centre via www.ccdc.cam.ac.uk/structures. Supplementary data to this article can be found online at https://doi.org/10.1016/j.saa.2023.122472.

References

[1] H. Tapiero, D.M. Townsend, K.D. Tew, Trace elements in human physiology and pathology. Copper, Biomed. Pharmacother. 57 (2003) 386–398.
[2] B.-E. Kim, T. Nevitt, D.J. Thiele, Mechanisms for copper acquisition, distribution and regulation, Nat. Chem. Biol. 4 (2008) 176–185.
[3] R.A. Festa, D.J. Thiele, Copper: An essential metal in biology, Curr. Biol. 21 (2011) 877–883.
[4] T. Tsang, C.I. Davis, D.C. Brady, Copper biology, Curr. Biol. 31 (2021) 421–427.
[5] O. Bandmann, K.H. Weiss, S.G. Kaler, Wilson's disease and other neurological copper disorders, Lancet Neurol. 14 (2015) 103–113.
[6] A. Członkowska, T. Litwin, P. Dusek, P. Ferenci, S. Lutsenko, V. Medici, J. K. Rybakowski, K.H. Weiss, M.L. Schilsky, Wilson disease, Nat. Rev. Dis. Prim. 4 (2018) 21.
[7] T. Fukai, M. Ushio-Fukai, J.H. Kaplan, Copper transporters and copper chaperones: Roles in cardiovascular physiology and disease, Am. J. Physiol. Cell Physiol. 315 (2018) 186–201.
[8] M. Siotto, R. Squitti, Copper imbalance in Alzheimer's disease: Overview of the exchangeable copper component in plasma and the intriguing role albumin plays, Coord. Chem. Rev. 371 (2018) 86–95.
[9] T.J. Huat, J. Camats-Perna, E.A. Newcombe, N. Valmas, M. Kitazawa, R. Medeiros, Metal toxicity links to Alzheimer's disease and neuroinflammation, J. Mol. Biol. 431 (2019) 1843–1868.
[10] M. Altarelli, N. Ben-Hamouda, A. Schneider, M.M. Berger, Copper deficiency: Causes, manifestations, and treatment, Nutr. Clin. Pract. 34 (2019) 504–513.
[11] M. Rehman, L. Liu, Q. Wang, M.H. Saleem, S. Bashir, S. Ullah, D. Peng, Copper environmental toxicology, recent advances, and future outlook: A review, Environ. Sci. Pollut. Res. 26 (2019) 18003–18016.
[12] M.I. El Sabry, F.K.R. Stino, W.A.A. El-Ghany, Copper: benefits and risks for poultry, livestock, and fish production, Trop. Anim. Health Prod. 53 (2021) 487.
[13] V. Kumar, S. Pandita, G.P. Singh Sidhu, A. Sharma, K. Khanna, P. Kaur, A.S. Bali, R. Setia, Copper bioavailability, uptake, toxicity and tolerance in plants: A comprehensive review, Chemosphere 262 (2021), 127810.
[14] World Health Organization. Guidelines for drinking-water quality: fourth edition incorporating the first and second addenda. Geneva, 2022.
[15] S. Carter, A. Fisher, B. Gibson, J. Marshall, B. Russelle, I. Whitesidef, Atomic spectrometry update: Review of advances in the analysis of metals, chemicals and materials, J. Anal. At. Spectrom. 32 (2017) 2068–2117.
[16] Y. Lu, X. Liang, C. Niyungeko, J. Zhou, J. Xu, G. Tian, A review of the identification and detection of heavy metal ions in the environment by voltammetry, Talanta 178 (2018) 324–338.
[17] S.-H. Chen, Y.-X. Li, P.-H. Li, X.-Y. Xiao, M. Jiang, S.-S. Li, W.-Y. Zhou, M. Yang, X.-J. Huang, W.-Q. Liu, Electrochemical spectral methods for trace detection of heavy metals: a review, Trends Anal. Chem. 106 (2018) 139–150.
[18] J. Dalmieda, P. Kruse, Metal cation detection in drinking water, Sensors 19 (2019) 5134.
[19] Q. Ding, C. Li, H. Wang, C. Xu, H. Kuang, Electrochemical detection of heavy metal ions in water, Chem. Commun. 57 (2021) 7215–7231.
[20] S. Sharma, K.S. Ghosh, Recent advances (2017–20) in the detection of copper ion by using fluorescence sensors working through transfer of photo-induced electron (PET), excited-state intramolecular proton (ESIPT) and Forster resonance energy (FRET), Spectrochim. Acta A Mol. Biomol. Spectrosc. 254 (2021), 119610.
[21] T. Chopra, S. Sasan, L. Devi, R. Parkesh, K.K. Kapoor, A comprehensive review on recent advances in copper sensors, Coord. Chem. Rev. 140 (2022), 214704.
[22] M. Saleema, K.H. Lee, Optical sensor: a promising strategy for environmental and biomedical monitoring of ionic species, RSC Adv. 5 (2015) 72150–72287.
[23] L. You, D. Zha, E.V. Anslyn, Recent advances in supramolecular analytical chemistry using optical sensing, Chem. Rev. 115 (2015) 7840–7892.
[24] J. Wu, B. Kwon, W. Liu, E.V. Anslyn, P. Wang, J.S. Kim, Chromogenic/Fluorogenic ensemble chemosensing systems, Chem. Rev. 115 (2015) 7893–7943.
[25] H. Sharma, N. Kaur, A. Singh, A. Kuwar, N. Singh, Optical chemosensors for water sample analysis, J. Mater. Chem. C 4 (2016) 5154–5194.
[26] P.V.S. Ajay, J. Printo, D.S.C.G. Kiruba, L. Susithra, K. Takatoshi, M., Sivakumar Colorimetric sensors for rapid detection of various analytes, Mater. Sci. Eng. C 78 (2017) 1231–1245.
[27] I.V. Kolesnichenko, E.V. Anslyn, Practical applications of supramolecular chemistry, Chem. Soc. Rev. 46 (2017) 2385–2390.
[28] Y. Ma, Y. Li, K. Ma, Z. Wang, Optical colorimetric sensor arrays for chemical and biological analysis, Sci. China Chem. 61 (2018) 643–655.
[29] I.I. Ebralidze, N.O. Laschuk, J. Poisson, O.V. Zenkina, Colorimetric sensors and sensor arrays, in: O.V. Zenkina (Ed.), Nanomaterials Design for Sensing Applications, Elsevier, 2019, pp. 1–39.
[30] G. Fukuhara, Analytical supramolecular chemistry: Colorimetric and fluorimetric chemosensors, J. Photochem. Photobiol. C: Photochem. Rev. 42 (2020), 100340.
[31] P.R. Dongare, A.H. Gore, Recent advances in colorimetric and fluorescent chemosensors for ionic species: design, principle and optical signalling mechanism, ChemistrySelect 6 (2021) 5657–5669.
[32] J. Kramer, R. Kang, L.M. Grimm, L. De Cola, P. Picchetti, F. Biedermann, Molecular probes, chemosensors, and nanosensors for optical detection of biorelevant molecules and ions in aqueous media and biofluids, Chem. Rev. 122 (2022) 3459–3636.
[33] H.N. Kim, W.X. Ren, J.S. Kim, J. Yoon, Fluorescent and colorimetric sensors for detection of lead, cadmium, and mercury ions, Chem. Soc. Rev. 41 (2012) 3210–3244.

[34] D. Udhayakumari, S. Nahaa, S. Velmathi, Colorimetric and fluorescent chemosensors for Cu2+. A comprehensive review from the years 2013–15, Anal. Methods 9 (2017) 552–578.

[35] B. Kaur, N. Kaur, S. Kumar, Colorimetric metal ion sensors – A comprehensive review of the years 2011–2016, Coord. Chem. Rev. 358 (2018) 13–69.

[36] A. Patil, S. Salunke-Gawali, Overview of the chemosensor ligands used for selective detection of anions and metal ions (Zn^{2+}, Cu^{2+}, Ni^{2+}, Co^{2+}, Fe^{2+}, Hg^{2+}), Inorg. Chim. Acta 482 (2018) 99–112.

[37] S. Upadhyay, A. Singh, R. Sinha, S. Omer, K. Negi, Colorimetric chemosensors for d-metal ions: A review in the past, present and future prospect, J. Mol. Struct. 1193 (2019) 89–102.

[38] S. Chakraborty, V. Ravindran, P.V. Nidheesh, S. Rayalu, Optical sensing of copper and its removal by different environmental technologies, ChemistrySelect 5 (2020) 10432–10474.

[39] A. Roy, M. Nandi, P. Roy, Dual chemosensors for metal ions: A comprehensive review, Trends Anal. Chem. 138 (2021), 116204.

[40] A. Lobnik, M. Turel, S.K. Urek, Optical chemical sensors: design and applications, in: W. Wang (Ed.), Advances in Chemical Sensors, InTech, 2012, pp. 3–28.

[41] G. Mistlberger, G.A. Crespo, E. Bakker, Ionophore-based optical sensors, Annu. Rev. Anal. Chem. 7 (2014) 483–512.

[42] X. Xie, E. Bakker, Ion selective optodes: From the bulk to the nanoscale, Anal. Bioanal. Chem. 407 (2015) 3899–3910.

[43] K.N. Mikhelson, M.A. Peshkova, Advances and trends in ionophore-based chemical sensors, Russ. Chem. Rev. 84 (2015) 555–578.

[44] X. Du, X. Xie, Ion-Selective optodes: Alternative approaches for simplified fabrication and signaling, Sens. Actuators B Chem. 335 (2021), 129368.

[45] E. Wagner-Wysiecka, N. Łukasik, J.F. Biernat, E. Luboch, Azo group(s) in selected macrocyclic compounds, J. Incl. Phenom. Macrocycl. Chem. 90 (2018) 189–257.

[46] H. Chen, W. Chen, Y. Lin, Y. Xie, S.H. Liu, J. Yin, Visible and near-infrared light activated azo dyes, Chin. Chem. Lett. 32 (2021) 2359–2368.

[47] R.I. Alsantali, Q.A. Raja, A.Y.A. Alzahrani, A. Sadiq, N. Naeem, E.U. Mughal, M. M. Al-Rooqi, N. El Guesmi, Z. Moussa, S.A. Ahmed, Miscellaneous azo dyes: A comprehensive review on recent advancements in biological and industrial applications, Dyes Pigm. 199 (2022), 110050.

[48] R. Nagarajan, C. Varadaraju, K.H. Lee, Recent advancements in the role of N-Heterocyclic receptors on heavy metal ion sensing, Dyes Pigm. 91 (2021), 109331.

[49] F. Ahmed, H. Xiong, Recent developments in 1,2,3-triazole-based chemosensors, Dyes Pigm. 185 (2021), 108905.

[50] X. Wang, C. Shen, C. Zhou, Y. Bu, X. Yan, Methods, principles and applications of optical detection of metal Ios, Chem. Eng. J. 417 (2021), 129125.

[51] K.E. McCrackena, J.-Y. Yoon, Recent approaches for optical smartphone sensing in resource-limited settings: a brief review, Anal. Methods 8 (2016) 6591–6601.

[52] M. Rezazadeh, S. Seidi, M. Lid, S. Pedersen-Bjergaard, Y. Yamini, The modern role of smartphones in analytical chemistry, Trends Anal. Chem. 118 (2019) 548–555.

[53] S. Di Nonno, R. Ulber, Smartphone-based optical analysis systems, Analyst 146 (2021) 2749–2768.

[54] R. Sivakumar, N.Y. Lee, Recent progress in smartphone-based techniques for food safety and the detection of heavy metal ions in environmental water, Chemosphere 275 (2021), 130096.

[55] L.F. Capitán-Vallvey, N. López-Ruiz, A. Martínez-Olmos, M.M. Erenas, A.J. Palma, Recent developments in computer vision-based analytical chemistry: A tutorial review, Anal. Chim. Acta 899 (2015) 23–56.

[56] D. Yusufu, A. Mills, Spectrophotometric and digital colour colourimetric (DCC) analysis of colour-based indicators, Sensor. Actuators B Chem. 273 (2018) 1187–1194.

[57] A.V. Kalinichev, N.V. Pokhvishcheva, M.A. Peshkova, Novel color standards for digital color analysis of optochemical sensor arrays, Talanta 197 (2019) 638–644.

[58] G.M. Fernandes, W.R. Silva, D.N. Barreto, R.S. Lamarca, P.C.F. Lima Gomes, J.F.D. S. Petruci, A.D. Batista, Novel approaches for colorimetric measurements in analytical chemistry – A review, Anal. Chim. Acta (2020, 1135,) 187–203.

[59] R. Jain, A. Thakur, P. Kaur, K.-H. Kim, P. Devi, Advances in imaging-assisted sensing techniques for heavy metals in water: Trends, challenges, and opportunities, Trends Anal. Chem. 123 (2020), 115758.

[60] N.Y. Tiuftiakov, A.V. Kalinichev, N.V. Pokhvishcheva, M.A. Peshkova, Digital color analysis for colorimetric signal processing: Towards an analytically justified choice of acquisition technique and color space, Sens. Actuators B Chem. 344 (2021), 130274.

[61] K. Koren, S.E. Zieger, Optode based chemical imaging—Possibilities, challenges, and new avenues in multidimensional optical sensing, ACS Sens. 6 (2021) 1671–1680.

[62] Y. Fan, J. Li, Y. Guo, L. Xie, G. Zhang, Digital image colorimetry on smartphone for chemical analysis: A review, Measurement 171 (2021) 108829.

[63] O. Dinten, U.E. Spichiger, N. Chaniotakis, P. Gehrig, B. Rusterholz, W.E. Morf, W. Simon, Lifetime of neutral-carrier-based liquid membranes in aqueous samples and blood and the lipophilicity of membrane components, Anal. Chem. 63 (1991) 596–603.

[64] E. Luboch, M. Jeszke, M. Szarmach, N. Łukasik, New bis(azobenzocrown)s with dodecylmethylmalonyl linkers as ionophores for sodium selective potentiometric sensors, J. Incl. Phenom. Macrocycl. Chem. 86 (2016) 323–335.

[65] B. Galiński, E. Luboch, J. Chojnacki, E. Wagner-Wysiecka, Novel diazocrowns with pyrrole residue as lead(II) colorimetric probes, Materials 14 (2021) 7239.

[66] O.V. Dolomanov, L.J. Bourhis, R.J. Gildea, J.A.K. Howard, H.J. Puschmann, OLEX2: a complete structure solution, refinement and analysis program, Appl. Crystallogr. 42 (2009) 339–341.

[67] G.M. Sheldrick, Crystal structure refinement with SHELXL, Acta Cryst. A 71 (2015) 3–8.

[68] T. Kokubo, H. Kushitani, S. Sakka, T. Kitsugi, T. Yamamuro, Solutions able to reproduce in vivo surface-structure changes in bioactive glass-ceramic A-W, J. Biomed. Mater. Res. 24 (1990) 721–734.

[69] Cold Spring Harbor Laboratory Press. Phosphate-buffered saline (PBS). Available online: http://cshprotocols.cshlp.org/content/2006/1/pdb.rec8247 (accessed on 16 August 2022).

[70] N. Sarigul, F. Korkmaz, I. Kurultak, A new artificial urine protocol to better imitate human urine, Sci. Rep. 9 (2019) 20159.

[71] M. Kyvala, I. Lukes, Program Package "OPIUM". Available online: https://web.natur.cuni.cz/~kyvala/opium.html (accessed on 16 August 2022).

[72] B. Galiński, E. Wagner-Wysiecka, Pyrrole bearing diazocrowns: Selective chromoionophores for lead(II) optical sensing, Sens. Actuators B Chem. 361 (2022), 131678.

[73] M.D. Abramoff, P.J. Magalhaes, S.J. Ram, Image processing with ImageJ, Biophotonics Int. 11 (2004) 36–42.

[74] C.A. Schneider, W.S. Rasband, K.W. Eliceiri, NIH Image to ImageJ: 25 years of image analysis, Nat. Methods 9 (2012) 671–675.

[75] N.A. Gavrilenko, S.V. Muravyov, S.V. Silushkin, A.S. Spiridonovab, Polymethacrylate optodes: A potential for chemical digital color analysis, Measurement 51 (2014) 464–469.

[76] S. Erdemir, O. Kocyigit, S. Malkondu, Optical and quantitative detection of Ca^{2+} ion by an calix[4] arene-isophorone incorporated fluorometric and colorimetric probe, J. Photochem. Photobiol. A Chem. 425 (2022), 113713.

[77] S. Millefori, F. Zuccarello, A. Millefori, F. Guerrera, Tautomerism in arylazonaphthols by dipole moment analysis, Tetrahedron 30 (1974) 735–738.

[78] P. Ball, C.H. Nicholls, Azo-hydrazone tautomerism of hydroxyazo compounds—A review, Dyes Pigm. 3 (1982) 5–26.

[79] M.A. Rauf, S. Hisaindee, N. Saleh, Spectroscopic studies of keto–enol tautomeric equilibrium of azo dye, RSC Adv. 5 (2015) 18097–18110.

[80] R.L. Reeves, R.S. Kaiser, Selective solvation of hydrophobic ions in structured solvents. Azo-hydrazone tautomerism of azo dyes in aqueous organic solvents, J. Org. Chem. 35 (1970) 3670–3675.

[81] X.-C. Chen, T. Tao, Y.-G. Wang, Y.-X. Peng, W. Huang, H.-F. Qian, Azo-hydrazone tautomerism observed from UV-vis spectra by pH control and metal-ion complexation for two heterocyclic disperse yellow dyes, Dalton Trans. 41 (2012) 11107–11115.

[82] L. Antonov, Tautomerism: methods and theories, Wiley-VCH, Weinheim, 2014.

[83] L. Antonov, Tautomerism: Concepts and Applications in Science and Technology, Wiley-VCH, Weinheim, 2016.

[84] Y. Li, B.O. Patrick, D. Dolphin, Near-Infrared absorbing azo dyes: Synthesis and X-ray crystallographic and spectral characterization of monoazopyrroles, bisazopyrroles, and a boron−azopyrrole complex, J. Org. Chem. 74 (2009) 5237–5243.

[85] A. Ghanadzadeh Gilani, V. Taghvaei, E. Moradi Rufchahi, M. Mirzaei, Tautomerism, solvatochromism, preferential solvation, and density functional study of some heteroarylazo dyes, J. Mol. Liq. 273 (2019) 392–407.

[86] D. Bialas, E. Kirchner, M.I.S. Röhr, F. Würthner, Perspectives in dye chemistry: A rational approach toward functional materials by understanding the aggregate state, J. Am. Chem. Soc. 143 (2021) 4500–4518.

[87] S.G. Muntean, G.M. Sinu, L. Kurunczi, Z. Szabadai, investigation of the aggregation of three disazo direct dyes by Uv-Vis spectroscopy and mathematical analysis, Rev. Chim. (Bucureşti) 60 (2009) 152–155.

[88] J.A. Balam-Villarreal, B.J. López-Mayorga, D. Gallardo-Rosas, R.A. Toscano, M. P. Carreón-Castro, V.A. Basiuk, F. Cortés-Guzmán, J.G. López-Cortés, M.C. Ortega-Alfaro, π-Extended push-pull azo-pyrrole photoswitches: synthesis, solvatochromism and optical band gap, Org. Biomol. Chem. 18 (2020) 1657–1670.

[89] E. Haselbach, Electronenstruktur und physikalisch-chemische Eigenschaften von Azo-Verbindungen, Teil XV. Über die Struktur der protonierten Azobrücke in Azobenzolderivaten, Helv. Chim. Acta 53 (1970) 1526–1543.

[90] B. Bernet, A., Vasella ^{1}H-NMR analysis of intra- and intermolecular H-bonds of alcohols in DMSO: chemical shift of hydroxy groups and aspects of conformational analysis of selected monosaccharides, inositols, and ginkgolides, Helv. Chim. Acta 83 (2000) 995–1021.

[91] M. Verheijen, M. Lienhard, Y. Schrooders, O. Clayton, R. Nudischer, S. Boerno, B. Timmermann, N. Selevsek, R. Schlapbach, H. Gmuender, S. Gotta, J. Geraedts, R. Herwig, J. Kleinjans, F. Caiment, DMSO induces drastic changes in human cellular processes and epigenetic landscape in vitro, Sci. Rep. 9 (2019) 4641.

[92] I.J. Chang, M.G. Choi, Y.A. Jeong, S.H. Lee, S.-H. Chang, Colorimetric determination of Cu^{2+} in simulated wastewater using naphthalimide-based Schiff base, Tetrahedron Lett. 58 (2017) 474–477.

[93] T. Anand, S.K. Sahoo, Cost-effective approach to detect Cu(II) and Hg(II) by integrating a smartphone with the colorimetric response from a NBD-benzimidazole based dyad, Phys. Chem. Chem. Phys. 21 (2019) 11839–11845.

[94] Y. Cao, Y. Liu, F. Li, S. Guo, Y. Shui, H. Xue, L. Wang, Portable colorimetric detection of copper ion in drinking water via red beet pigment and smartphone, Microchem. J. 15 (2019), 104176.

[95] Z.-H. Zhao, Z.-L. Hu, X.-T. Zhang, Q.-X. Liu, A new tridentate fluorescent-colorimetric chemosensor for copper(II) ion, Tetrahedron 75 (2019), 130675.

[96] Z. Lashkari, M. Arvand, Sensitive and selective detection of trace copper in standard alloys, food and biological samples using a bulk optode based on N, N0-(4,40-ethylene biphenyl) bis(3-methoxy salicylidine imine) as neutral carrier, Spectrochim. Acta A Mol. Biomol. Spectrosc. 107 (2013) 280–288.

[97] S.A. Shahamirifard, M. Ghaedi, M. Montazerozohori, Design a sensitive optical thin film sensor based on incorporation of isonicotinohydrazide derivative in sol–gel matrix for determination of trace amounts of copper (II) in fruit juice: Effect of

sonication time on immobilization approach, Ultrason. Sonochem. 42 (2018) 723–730.
[98] Z. Parsaeea, N. Karachi, R. Razavi, Ultrasound assisted fabrication of a novel optode base on a triazine based Schiff base immobilized on TEOS for copper detection, Ultrason. Sonochem. 47 (2018) 36–46.
[99] W. Gao, P. Haratipour, M.R.R. Kahkha, A. Tahvili, Ultrasound-electrospinning-assisted fabrication and sensing evaluation of a novel membrane as ultrasensitive sensor for copper (II) ions detection in aqueous environment, Ultrason. Sonochem. 44 (2018) 152–161.

P3 – SUPPLEMENTARY MATERIALS

Simple colorimetric copper(II) sensor – spectral characterization and possible applications

Błażej Galiński [1], Jarosław Chojnacki [2] and Ewa Wagner-Wysiecka [1,3*]

[1] *Department of Chemistry and Technology of Functional Materials, Faculty of Chemistry, Gdańsk University of Technology, Narutowicza Street 11/12, 80-233 Gdańsk, Poland*

[2] *Department of Inorganic Chemistry, Faculty of Chemistry, Gdańsk University of Technology, Narutowicza Street 11/12, 80-233 Gdańsk, Poland*

[3] *Advanced Materials Center, Faculty of Chemistry, Gdańsk University of Technology, Narutowicza Street 11/12, 80-233 Gdańsk, Poland*

* corresponding author: ewa.wagner-wysiecka@pg.edu.pl

Synthesis of L

In ice bath three solutions were placed:

A: 2-amino-4-nitrophenol (1.54 g, 10.2 mmol) in water (20 mL) acidified with conc. hydrochloric acid (2 mL)

B: sodium nitrite (0.72 g, 10.5 mmol) in water (30 mL)

C: pyrrole (0.67 g, 0.69 mL, 10 mmol) in alkalized with NaOH (2.00 g, 50 mmol) in water (30 mL).

Diazonium salt of 2-amino-4-nitrophenol was obtained by adding solution B to A in portions keeping mixture stirred. After 30 min. obtained diazonium salt and solution C were added in portions to alkalized pH ~10 water (300 mL) placed in an ice bath within 30 minutes keeping vigorous stirring of reaction mixture. After 2 h in an ice bath reaction was left for night at room temperature under stirring. The obtained solid was filtered off under reduced pressure and dried on the air. Azocompound was isolated using column chromatography with dichloromethane and next dichloromethane:acetone (10:1, v/v) mixture as eluents. 1.7 g (73%) of pure **L**, crystallizing as orange needles from dichloromethane, was obtained. mp. 179-180 °C (with decomposition); TLC: $R_f = 0.62$ (chloroform), $R_f = 0.73$ (dichloromethane); ^{1}H NMR (metanol-d_4): $\delta = 6.42$ (1H, m, ArH), 7.04 - 7.05 (1H, m, ArH), 7.12 (1H, d, $J = 9.4$ Hz, ArH), 7.14 - 7.16 (1H, m, ArH), 8.16 (1H, dd, $J = 9.3$ Hz, $J = 2.7$ Hz, ArH), 8.57 (1H, d, $J = 2.8$ Hz, ArH) ppm; ^{1}H NMR (acetone-d_6): $\delta = 6.47$ - 6.48 (1H, m ArH), 7.14 - 7.15 (1H, m ArH), 7.20 (1H, d, $J =$ 8.8 Hz, ArH), 7.30 (1H, s, ArH), 8.20 (1H, dd, $J = 9.4$ Hz, $J = 2.8$ Hz, ArH), 8.52 (1H, d, $J =$ 2.8 Hz, ArH), 11.48 (~0.2 H, s, OH) ppm; ^{1}H NMR (acetonitrile-d_3): $\delta = 6.47$ - 6.48 (1H, m, ArH), 7.09 - 7.11 (1H, m, ArH), 7.14 (1H, d, $J = 9.4$ Hz, ArH), 7.21 (1H, s, ArH), 8.17 (1H, dd, $J = 9.3$ Hz, $J = 2.7$ Hz, ArH), 8.52 (1H, d, $J = 2.8$ Hz, ArH), 10.40 (~0.3H, s, NH), 11.73 (~0.3H, s, OH) ppm; ^{1}H NMR (DMSO-d_6): $\delta = 6.39$ - 6.41 (1H, m, ArH), 7.08 - 7.09 (1H, m, ArH), 7.19 (1H, d, $J = 9.1$ Hz, ArH), 7.31 (1H, d, $J = 1.2$ Hz, ArH), 8.16 (1H, dd, $J = 9.1$ Hz, $J = 2.7$ Hz, ArH), 8.33 (1H, d, $J = 3.0$ Hz, ArH), 10.93 (1H, s, NH), 11.92 (1H, s, OH) ppm; ^{13}C NMR (DMSO-d_6): δ = 111.6, 112.5, 118.2, 125.8, 126.3, 138.5, 140.7, 147.0, 160.7 ppm; IR (crystalline film): $\nu = 3320$, 2921, 2852, 1575, 1539, 1480, 1343, 1285, 1084, 903, 794, 743, 729, 591 cm^{-1}; HR MS (EI) $[M]^+$: calc. 232.0596 for $C_{10}H_8N_4O_3$, found: 232.0598; UV-vis (DCM): λ_{max} (ε) 312 (10965), 412 (26915); UV-vis (MeOH): 314 (12023), 402 (23988), ~ 492 nm (broad, 2884); UV-vis (ACN): 316 (12023), 402 (23988); UV-vis (DMSO): 318 (12022), 412 (21878), ~ 526 (broad, 1995); Emission spectra: λ_{ex}, λ_{em} (DCM) 400, 618; (MeOH): 400, 614; (ACN): 400, 614.

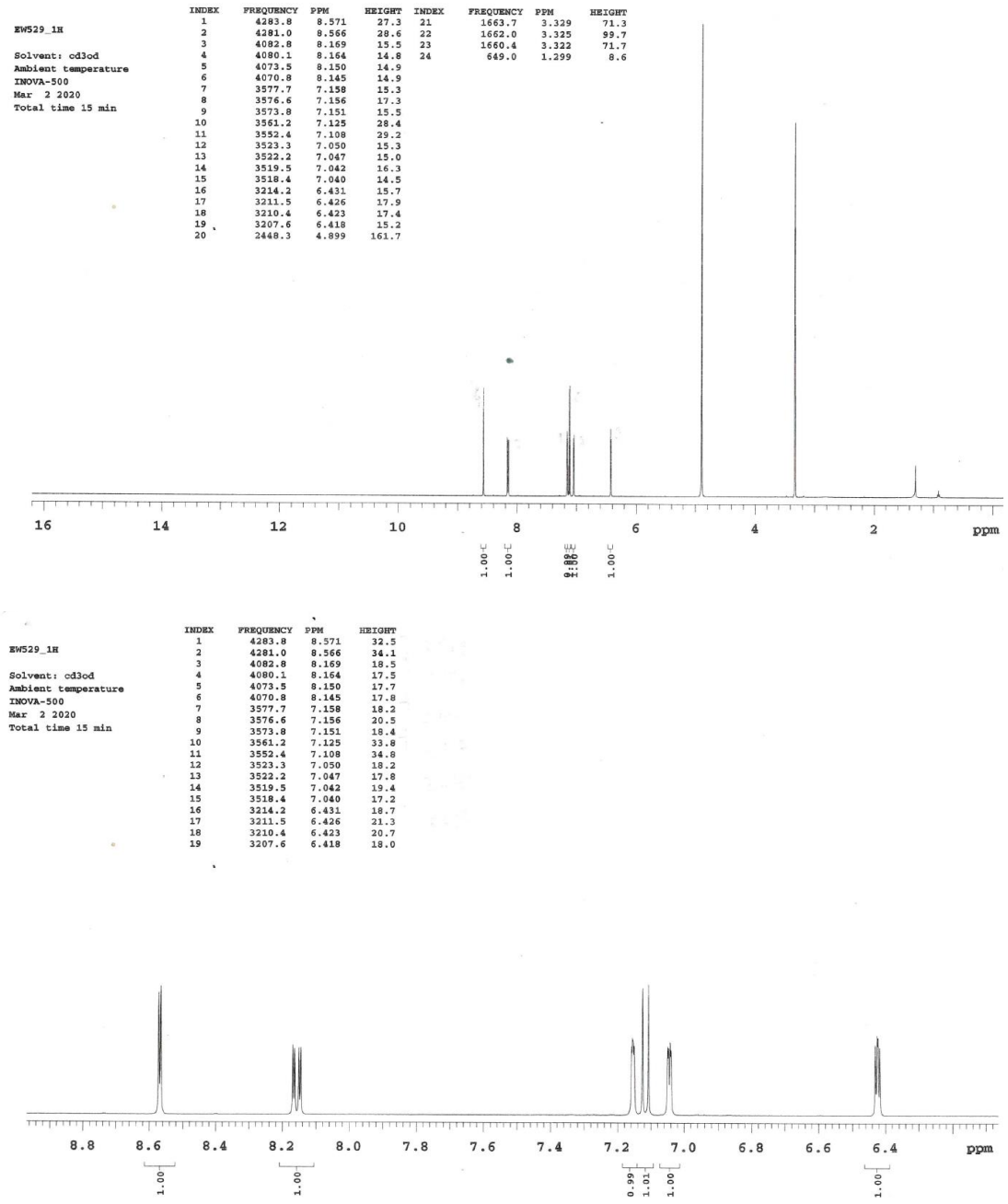

Fig. S1a. ^{1}H NMR spectrum of **L** (methanol-d_4).

EW530_1H

Solvent: acetone
Ambient temperature
INOVA-500
Mar 2 2020
Total time 15 min

INDEX	FREQUENCY	PPM	HEIGHT	INDEX	FREQUENCY	PPM	HEIGHT
1	4259.7	8.523	37.2	21	1096.0	2.193	3.1
2	4256.9	8.517	38.9	22	1046.6	2.094	20.9
3	4105.4	8.214	18.7	23	1044.4	2.090	25.5
4	4102.7	8.209	17.1	24	1040.5	2.082	282.2
5	4096.1	8.195	20.8	25	1038.3	2.078	552.6
6	4093.3	8.190	20.2	26	1036.1	2.073	792.8
7	3651.9	7.307	22.0	27	1033.9	2.069	543.2
8	3650.8	7.305	22.0	28	1031.7	2.064	271.4
9	3602.5	7.208	36.9	29	974.6	1.950	2.7
10	3593.7	7.190	37.5	30	972.4	1.946	3.8
11	3574.5	7.152	17.1	31	970.3	1.941	2.6
12	3573.4	7.150	17.4	32	648.5	1.298	2.9
13	3570.6	7.144	18.1				
14	3238.4	6.480	18.6				
15	3235.7	6.474	22.0				
16	3234.6	6.472	21.4				
17	3231.8	6.466	17.2				
18	1483.6	2.968	17.2				
19	1100.4	2.202	3.1				
20	1098.2	2.197	4.4				

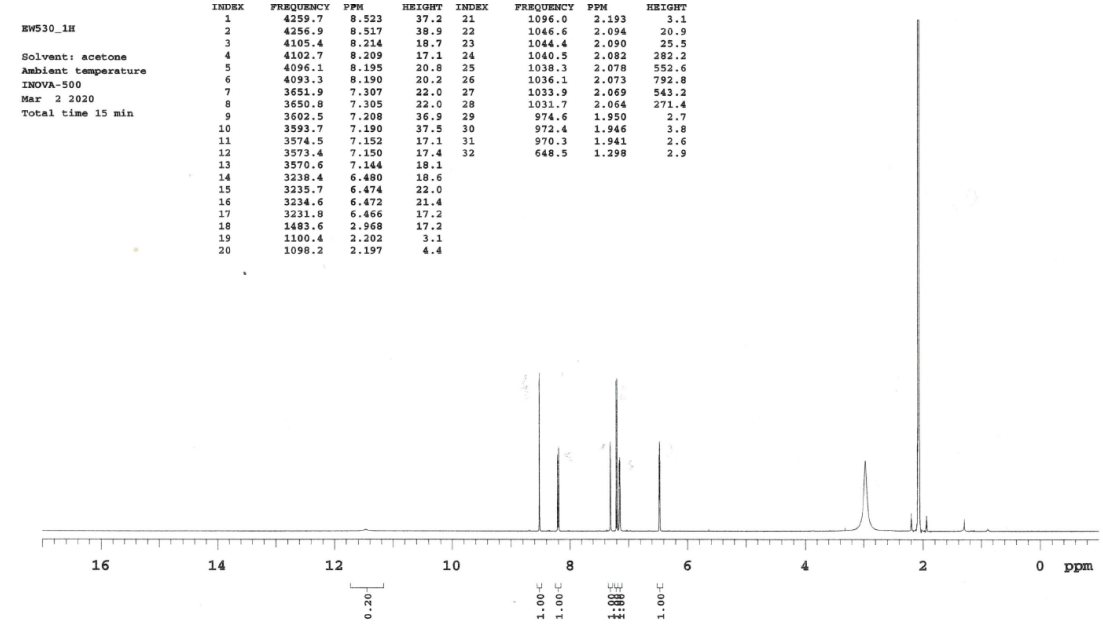

EW530_1H

Solvent: acetone
Ambient temperature
INOVA-500
Mar 2 2020
Total time 15 min

INDEX	FREQUENCY	PPM	HEIGHT
1	4259.7	8.523	37.2
2	4256.9	8.517	38.9
3	4105.4	8.214	18.7
4	4102.7	8.209	17.1
5	4096.1	8.195	20.8
6	4093.3	8.190	20.2
7	3651.9	7.307	22.0
8	3650.8	7.305	22.0
9	3602.5	7.208	36.9
10	3593.7	7.190	37.5
11	3574.5	7.152	17.1
12	3573.4	7.150	17.4
13	3570.6	7.144	18.1
14	3238.4	6.480	18.6
15	3235.7	6.474	22.0
16	3234.6	6.472	21.4
17	3231.8	6.466	17.2

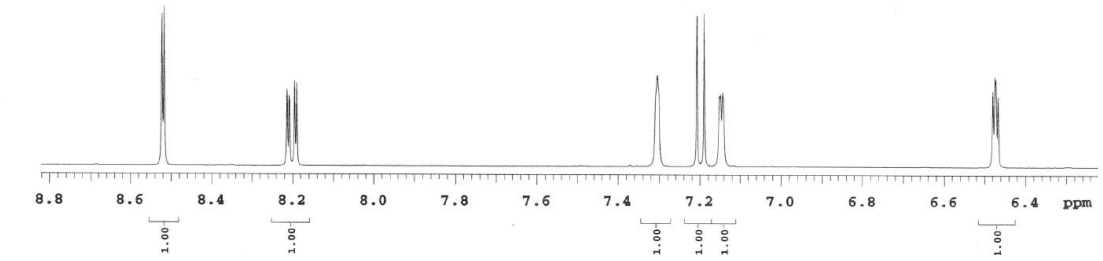

Fig. S1b. ^{1}H NMR spectrum of **L** (acetone-d_6).

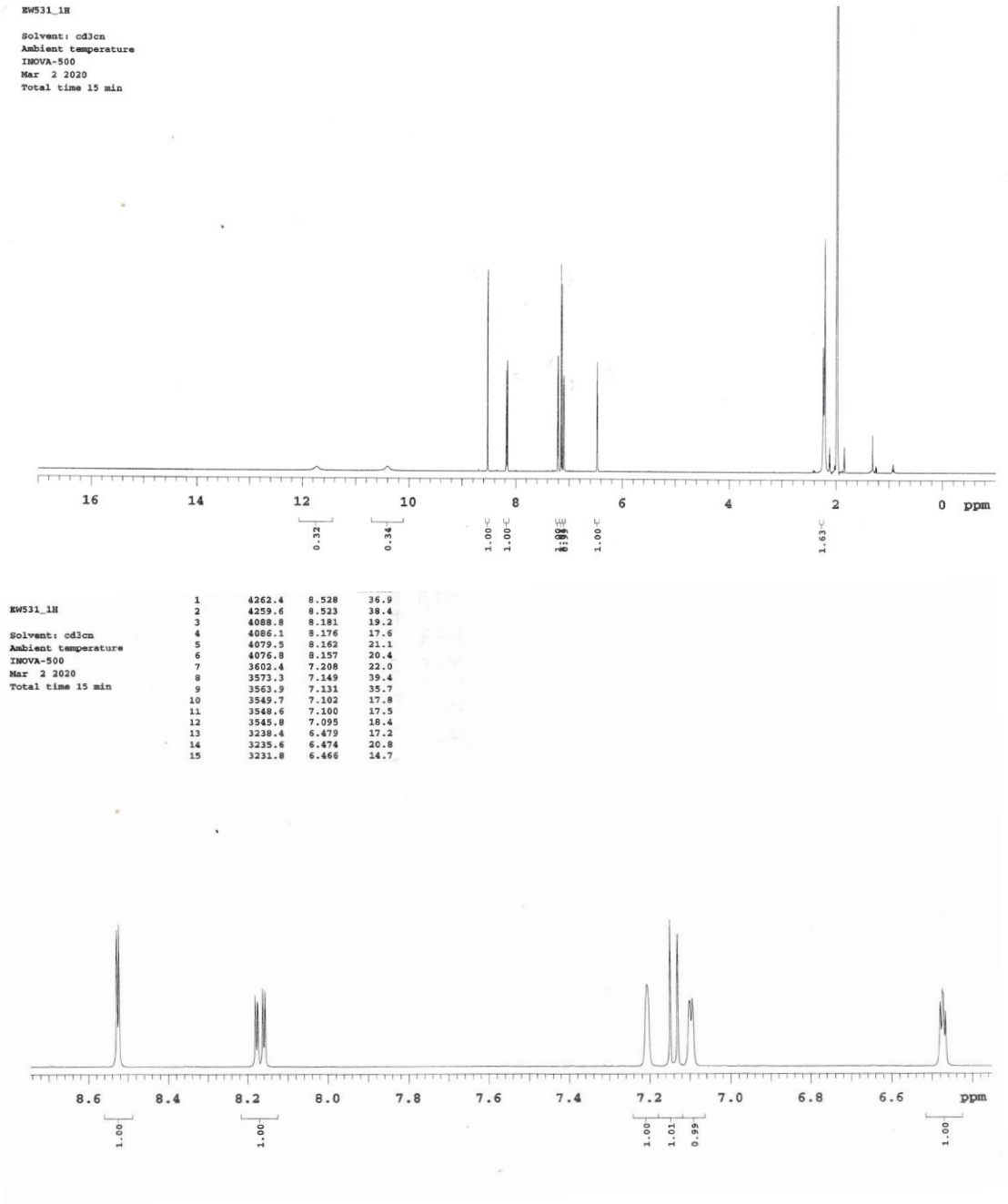

Fig. S1c. ^{1}H NMR spectrum of **L** (acetonitrile-d_3).

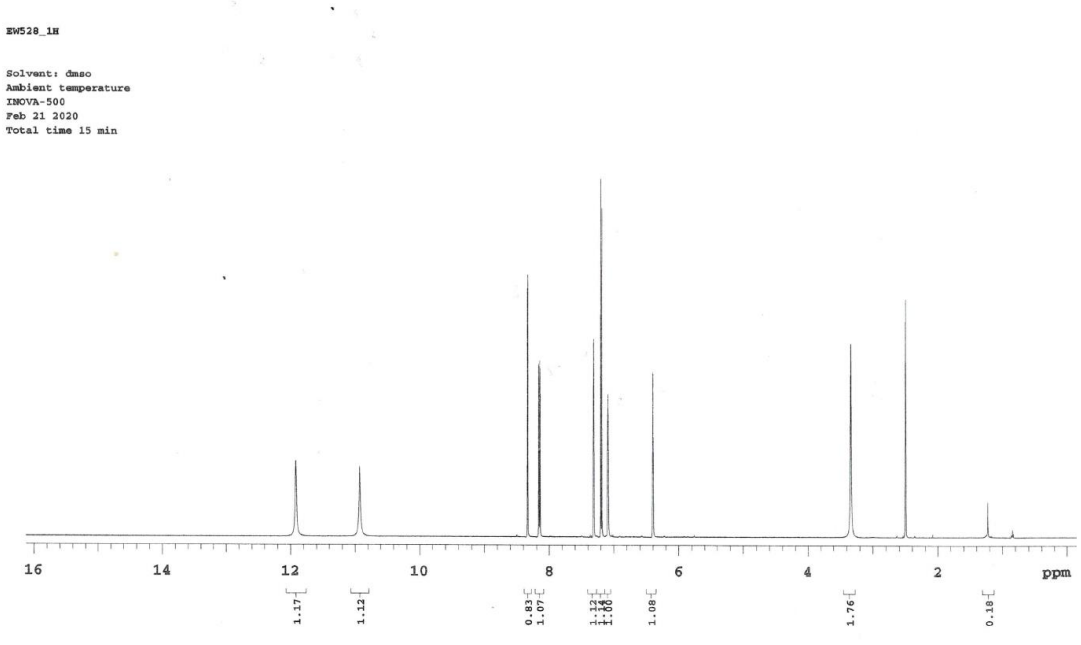

Fig. S1d. ^{1}H NMR spectrum of **L** (DMSO-d_6).

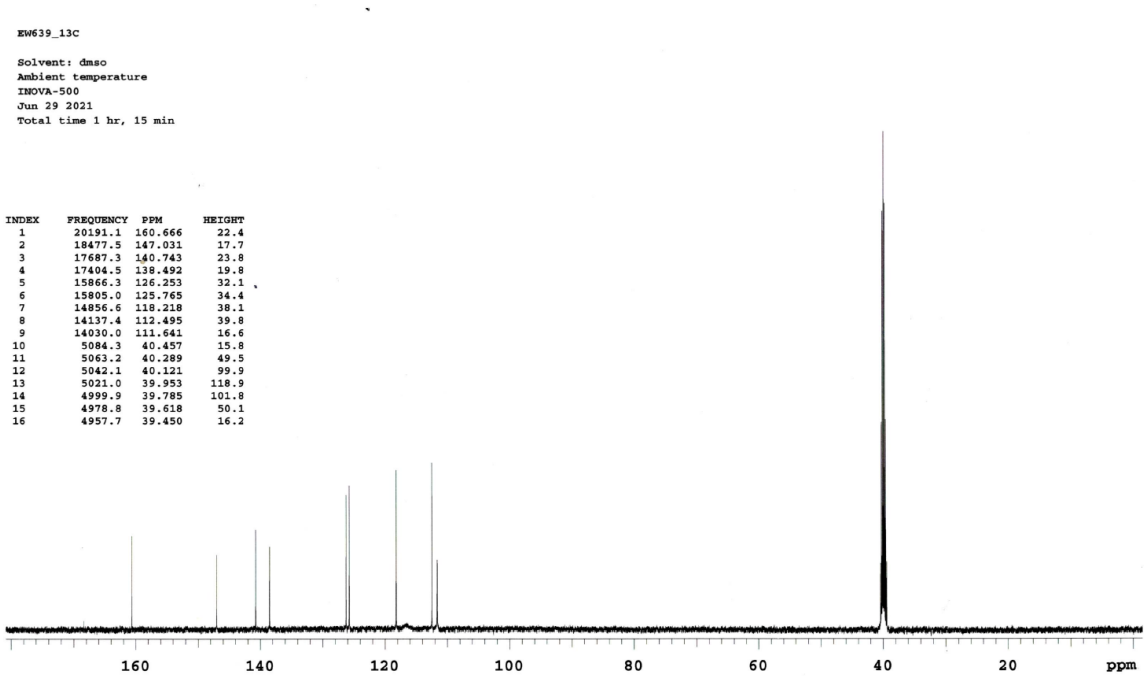

Fig. S1e. ^{13}C NMR spectrum of **L** (DMSO-d_6).

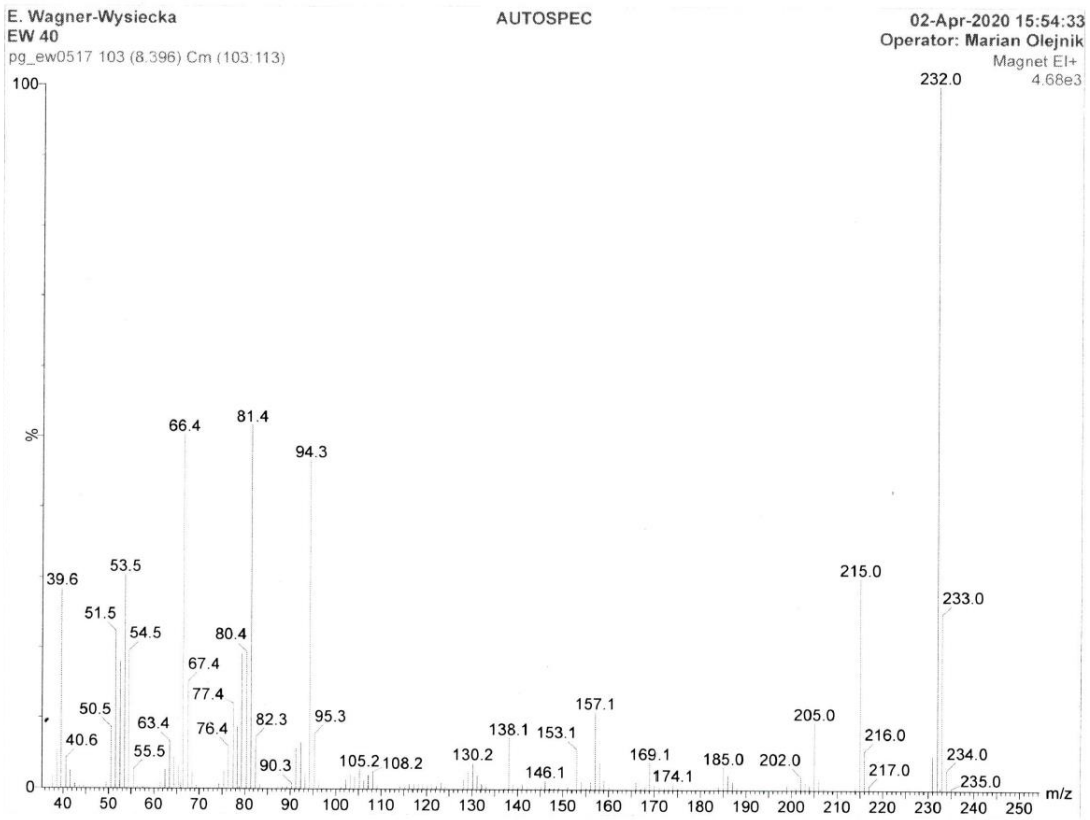

Elemental Composition Report Page 1

Single Mass Analysis
Tolerance = 20.0 PPM / DBE: min = -1.5, max = 50.0
Selected filters: None

Monoisotopic Mass, Odd and Even Electron Ions
91 formula(e) evaluated with 4 results within limits (up to 50 best isotopic matches for each mass)
Elements Used:
C: 0-70 H: 0-100 N: 0-5 O: 0-4

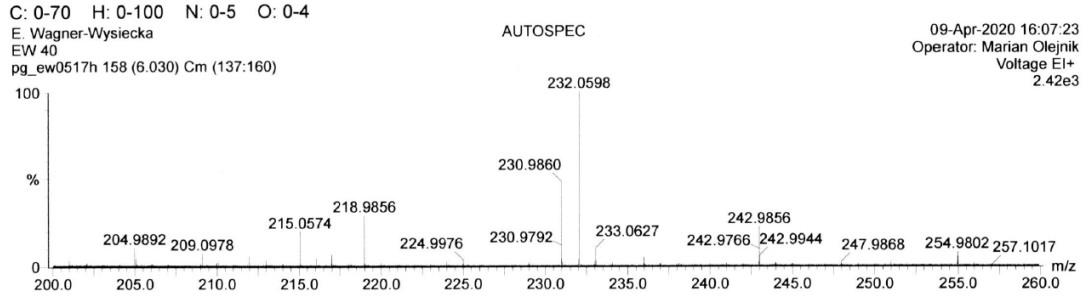

Minimum:				-1.5		
Maximum:		5.0	20.0	50.0		
Mass	Calc. Mass	mDa	PPM	DBE	i-FIT	Formula
232.0598	232.0596	0.2	0.9	9.0	10.5	C10 H8 N4 O3
	232.0610	-1.2	-5.2	8.5	15.1	C12 H10 N O4
	232.0623	-2.5	-10.8	13.5	32.5	C13 H6 N5
	232.0637	-3.9	-16.8	13.0	48.1	C15 H8 N2 O

Fig. S1f. HRMS (EI) spectrum of **L**.

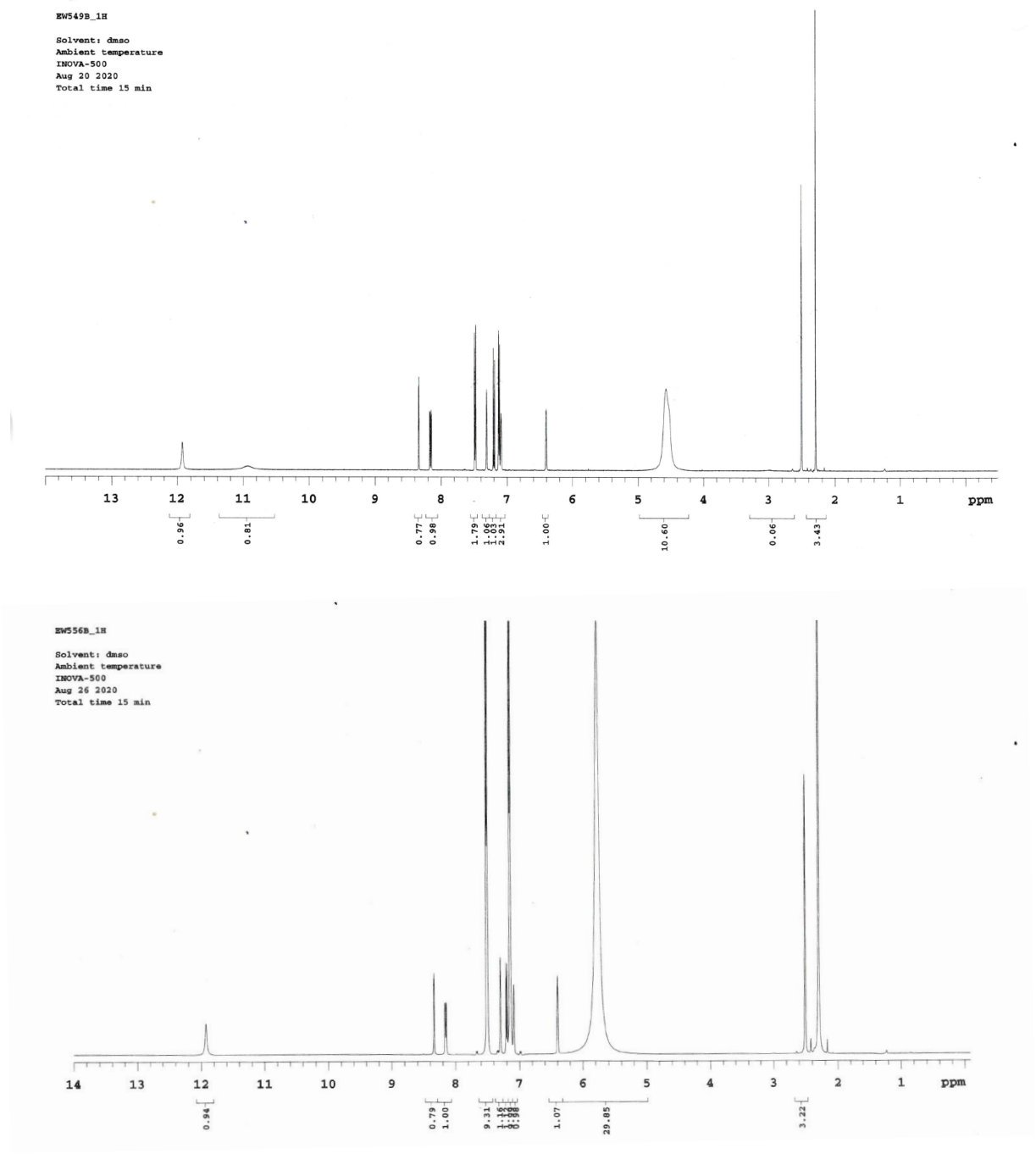

Fig. S2. ^{1}H NMR spectra of **L** (1.42×10^{-2} M) in the presence of equimolar (top) and 5-fold excess (bottom) of TsOH in DMSO-d_6.

Table S1. The position of signals of aromatic protons of **L** and their shift in spectra registered in the presence of *p*-toulenesulfonic acid (DMSO-d_6).

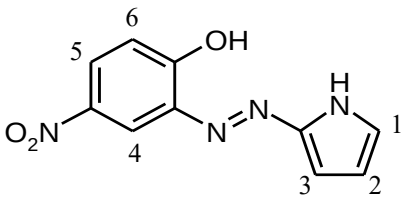

	1	2	3	4	5	6	NH	OH
L	7.315	6.406	7.096	8.334	8.156	7.20	10.937	11.923
L + 1 eq TsOH	7.312	6.397	7.095	8.340	8.162	7.20	10.933 (broaden)	11.925
L + 5 eq TsOH	7.296	6.397	7.087	8.340	8.155	7.20	not detectable	11.929

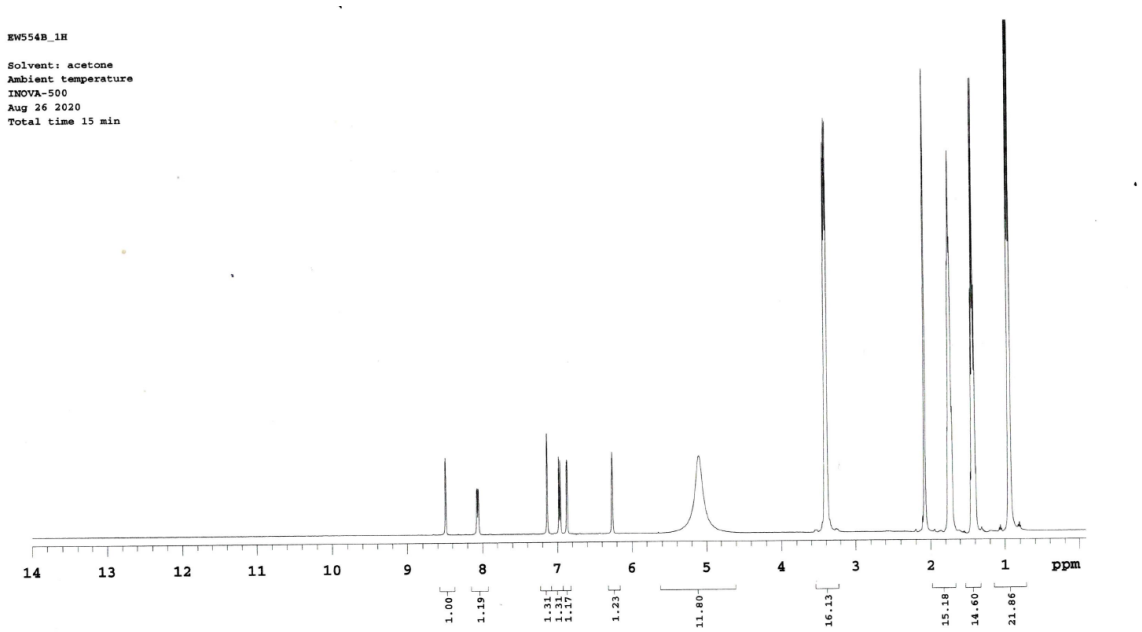

Fig. S3. ^{1}H NMR spectrum of **L** (1.42×10^{-2} M) registered in equimolar amount of TBAOH (DMSO-d_6).

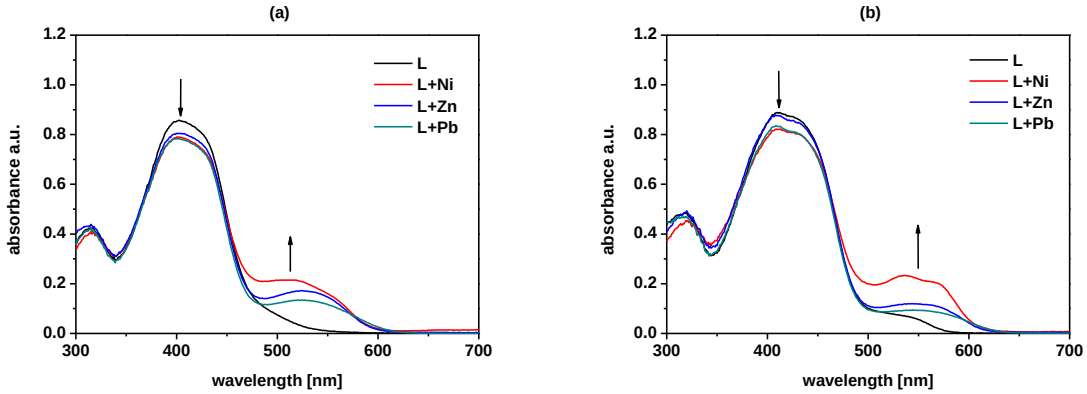

Fig. S4. Changes in UV-vis absorption spectra of **L** (4.05×10^{-5} M) in the presence of the excess of metal perchlorates (added as solid salts) in (a) methanol (b) DMSO.

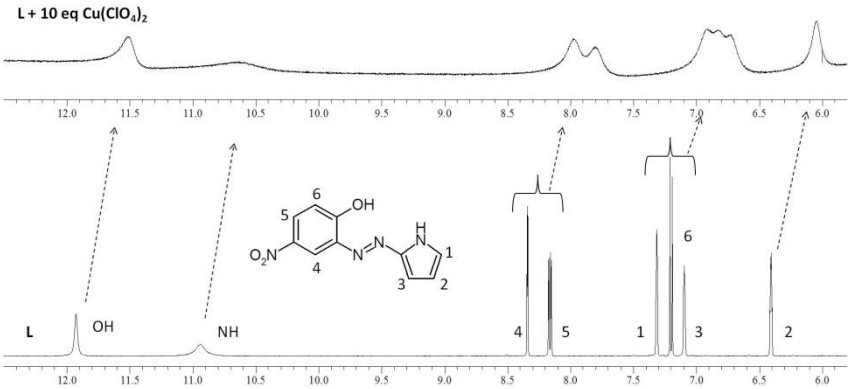

Fig. S5. ^{1}H NMR spectrum of **L** ($c_L = 1.42\times10^{-2}$ M) and its spectrum registered in 10-fold excess of copper(II) perchlorate in DMSO-d_6.

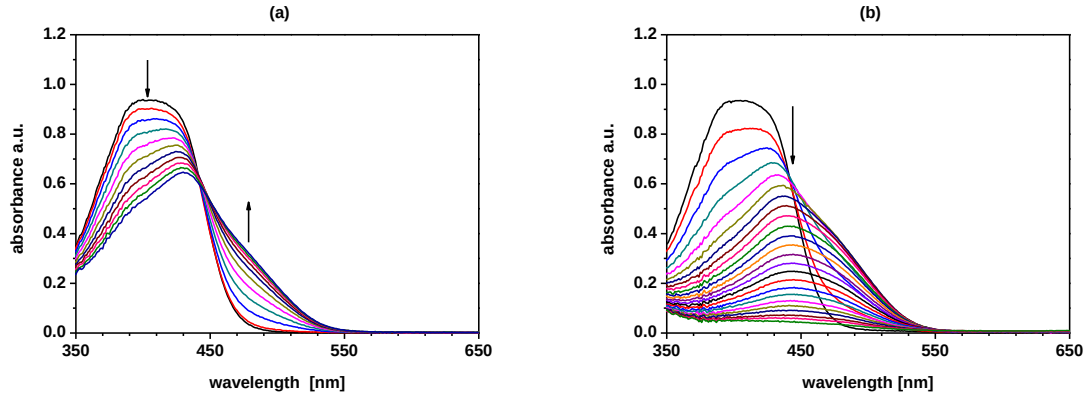

Fig. S6. UV-vis titration trace of **L** ($c_L = 4.05\times10^{-5}$ M) with copper(II) perchlorate in ACN (a) (c_{Cu} = 0-1.22×10^{-4} M) and (b) (c_{Cu} = 0-6.53×10^{-4} M). Absorbance is decreasing after crossing the molar ratio 1:3 (**L**:Cu).

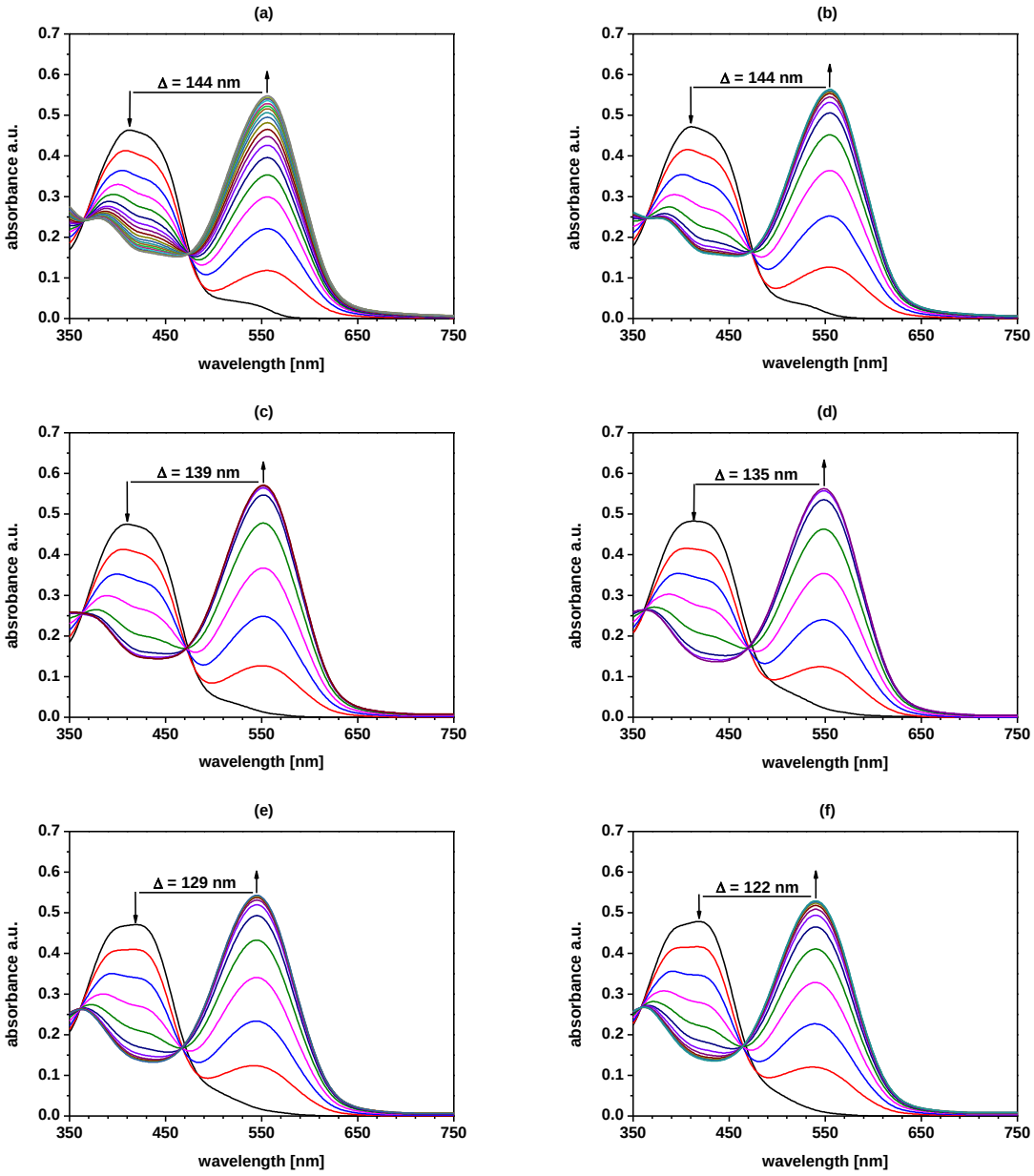

Fig. S7. Changes in UV-vis spectra of **L** (2.16×10^{-5} M) upon titration with copper(II) perchlorate in DMSO of different content of water: (a) 0% (c_{Cu} = 0-7.43×10^{-5} M), (b) 10% (c_{Cu} = 0-4.67×10^{-5} M), (c) 30% (c_{Cu} = 0-3.85×10^{-5} M), (d) 50% (c_{Cu} = 0-3.02×10^{-5} M), (e) 70% (c_{Cu} = 0-4.26×10^{-5} M) and (f) 90% (c_{Cu} = 0-5.07×10^{-5} M).

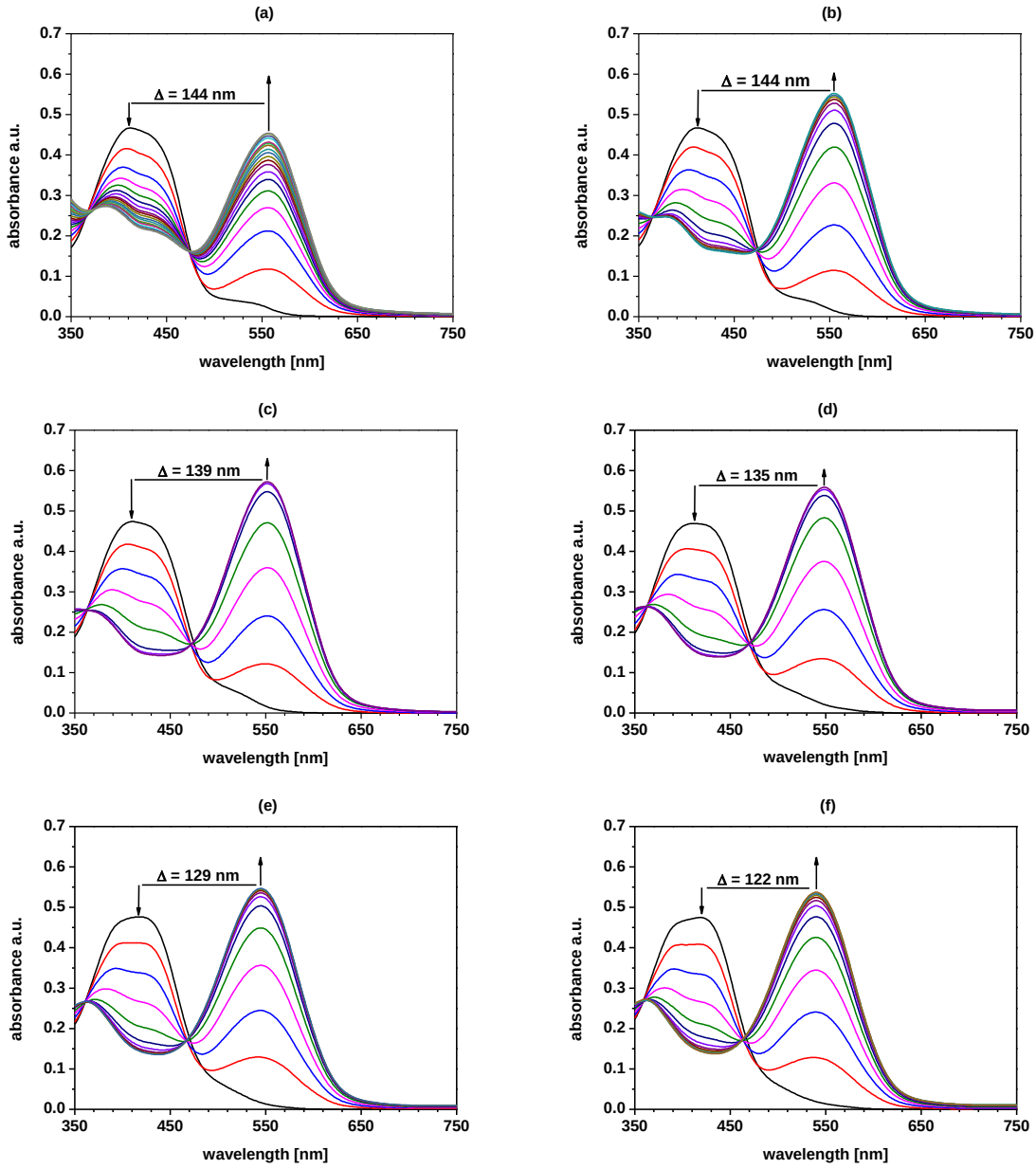

Fig. S8. Changes in UV-vis spectra of **L** (2.16×10^{-5} M) upon titration with copper(II) chloride in DMSO with various content of water: (a) 0% (c_{Cu} = 0-7.45×10^{-5} M), (b) 10% (c_{Cu} = 0-4.69×10^{-5} M), (c) 30% (c_{Cu} = 0-3.45×10^{-5} M), (d) 50% (c_{Cu} = 0-3.03×10^{-5} M), (e) 70% (c_{Cu} = 0-4.28×10^{-5} M) and (f) 90% (c_{Cu} = 0-5.09×10^{-5} M).

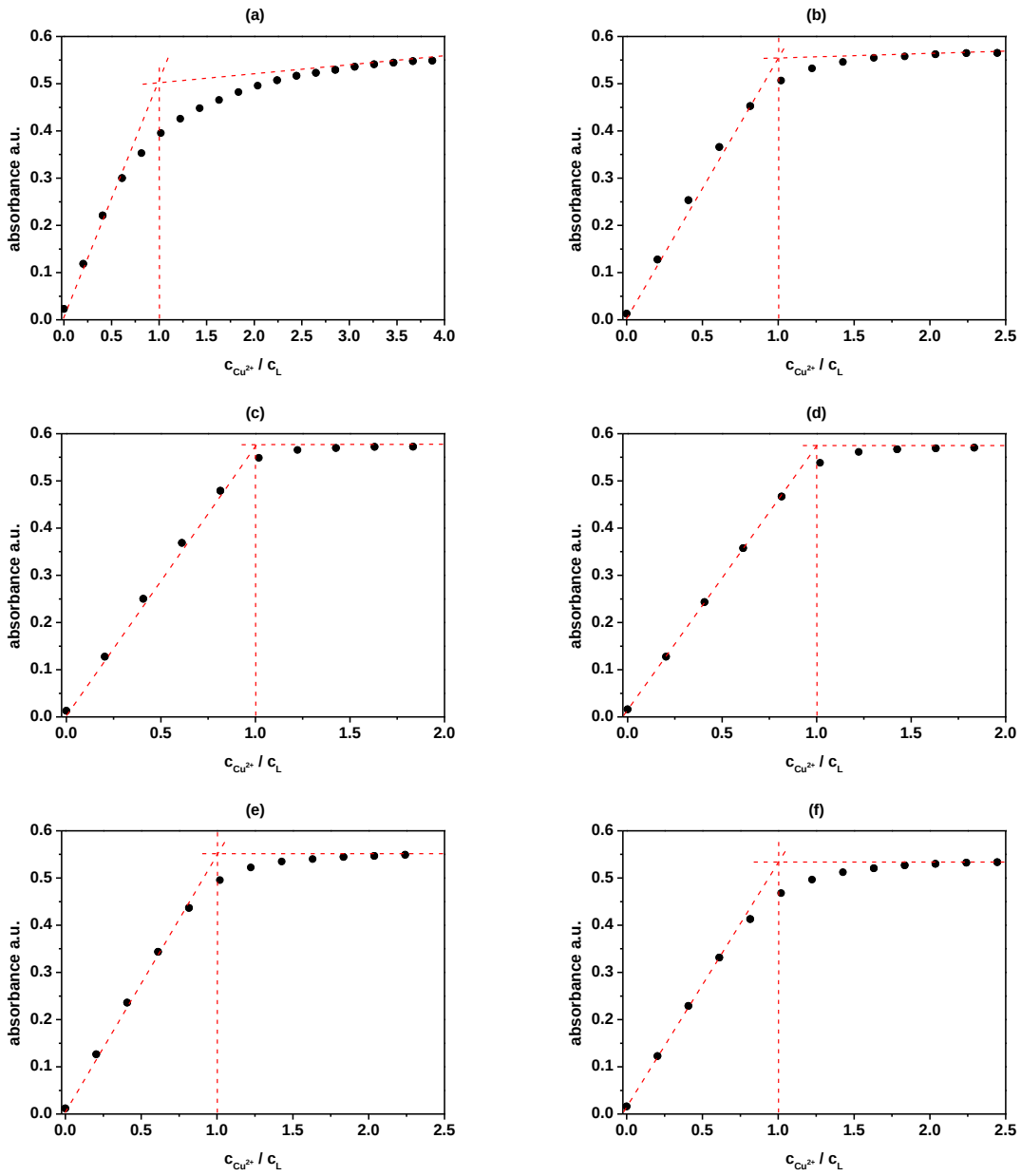

Fig. S9. Molar ratio of **L** (2.16×10^{-5} M) with copper(II) perchlorate in DMSO with various content of water [%]: (a) 0% (c_{Cu} = 0-7.45×10^{-5} M), (b) 10% (c_{Cu} = 0-4.69×10^{-5} M), (c) 30% (c_{Cu} = 0-3.45×10^{-5} M), (d) 50% (c_{Cu} = 0-3.03×10^{-5} M), (e) 70% (c_{Cu} = 0-4.28×10^{-5} M) and (f) 90% (c_{Cu} = 0-5.09×10^{-5} M).

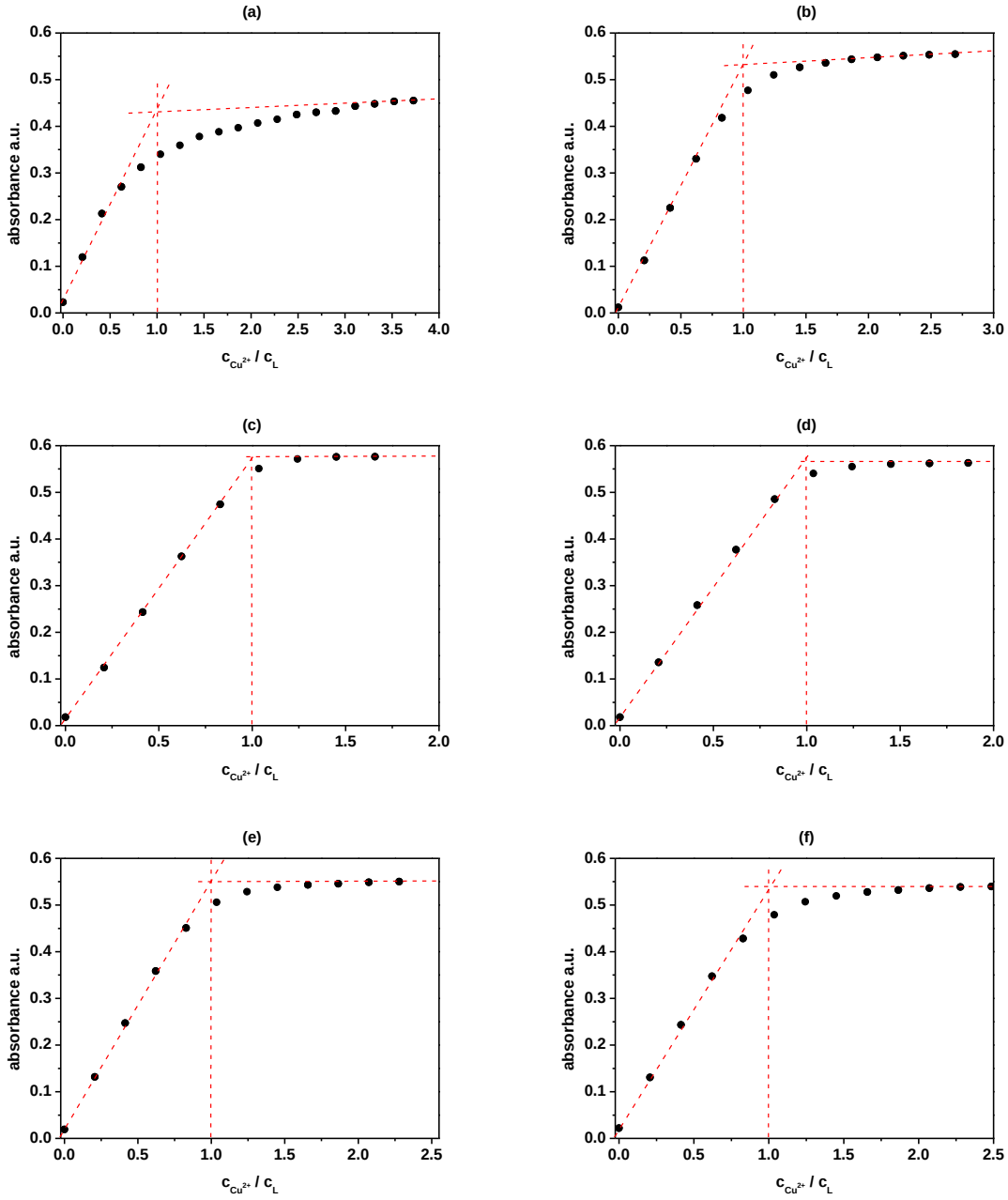

Fig. S10. Molar ratio of **L** (2.16×10^{-5} M) with copper(II) chloride in DMSO with various content of water [%]: (a) 0% (c_{Cu} = 0-7.45×10^{-5} M), (b) 10% (c_{Cu} = 0-4.69×10^{-5} M), (c) 30% (c_{Cu} = 0-3.45×10^{-5} M), (d) 50% (c_{Cu} = 0-3.03×10^{-5} M), (e) 70% (c_{Cu} = 0-4.28×10^{-5} M) and (f) 90% (c_{Cu} = 0-5.09×10^{-5} M).

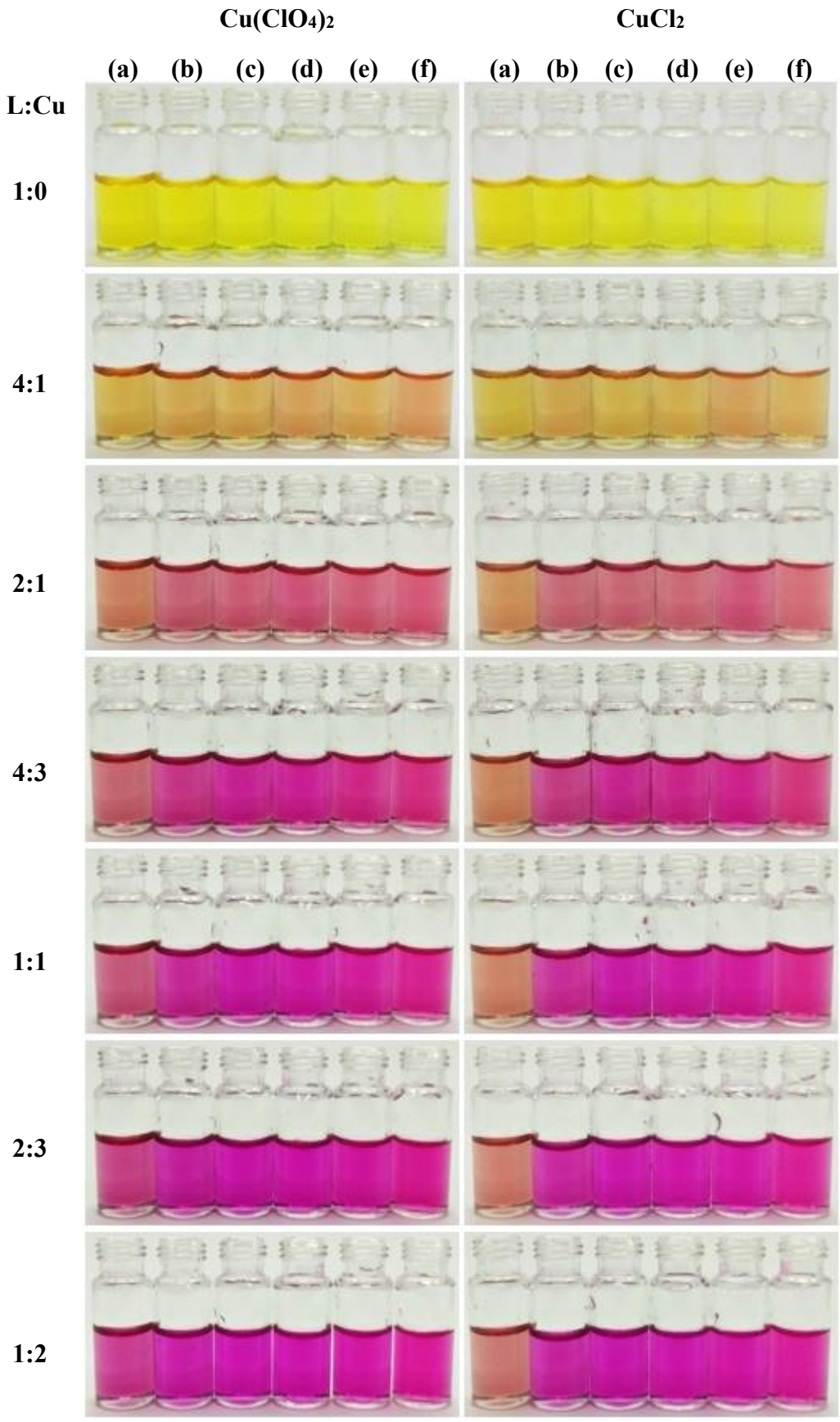

Fig. S11. Color change of **L** ($c_L = 2.16\times10^{-5}$ M) upon addition of copper(II) perchlorate/chloride (molar ratio **L**:Cu) in DMSO with various content of water: (a) 0%, (b) 10%, (c) 30%, (d) 50%, (e) 70% and (f) 90%.

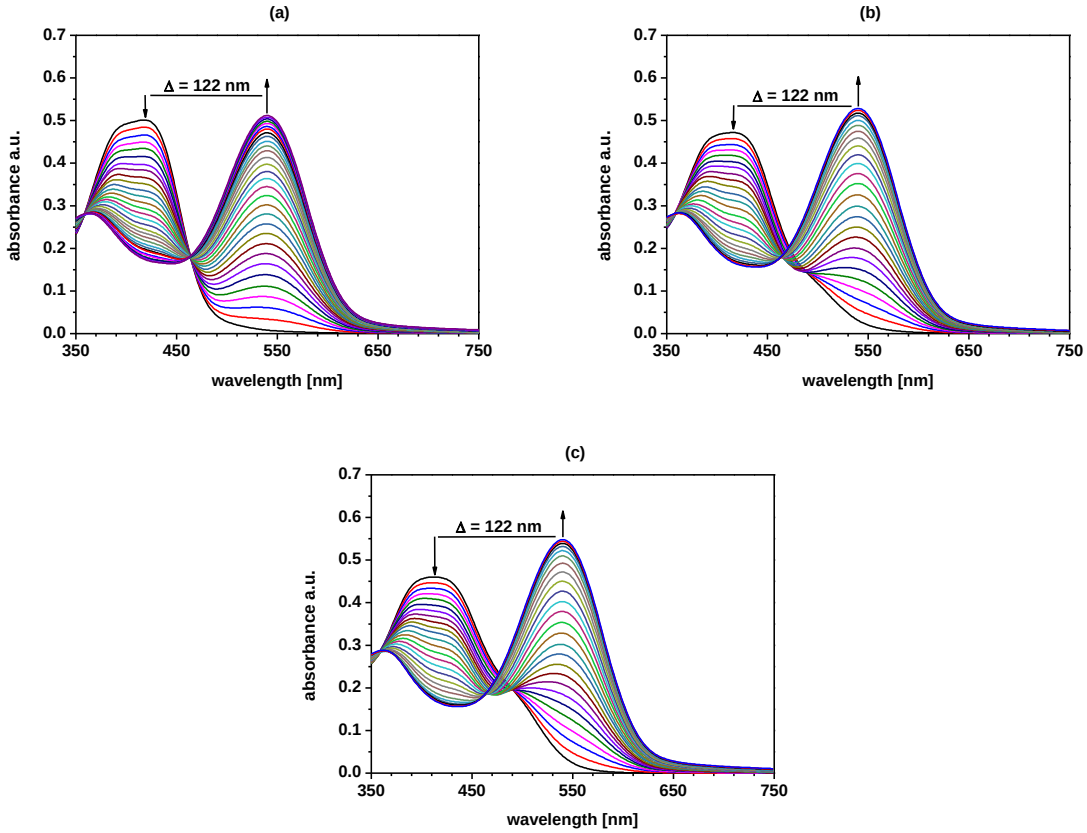

Fig. S12. The change of UV-Vis spectrum of **L** ($c_L = 2.16\times10^{-5}$ M) upon titration with copper(II) chloride (c_{Cu} = 0-4.28×10^{-5} M) in water-DMSO (9:1, v/v) solvent mixture at pH: (a) 5.0, (b) 7.0 and (c) 9.0.

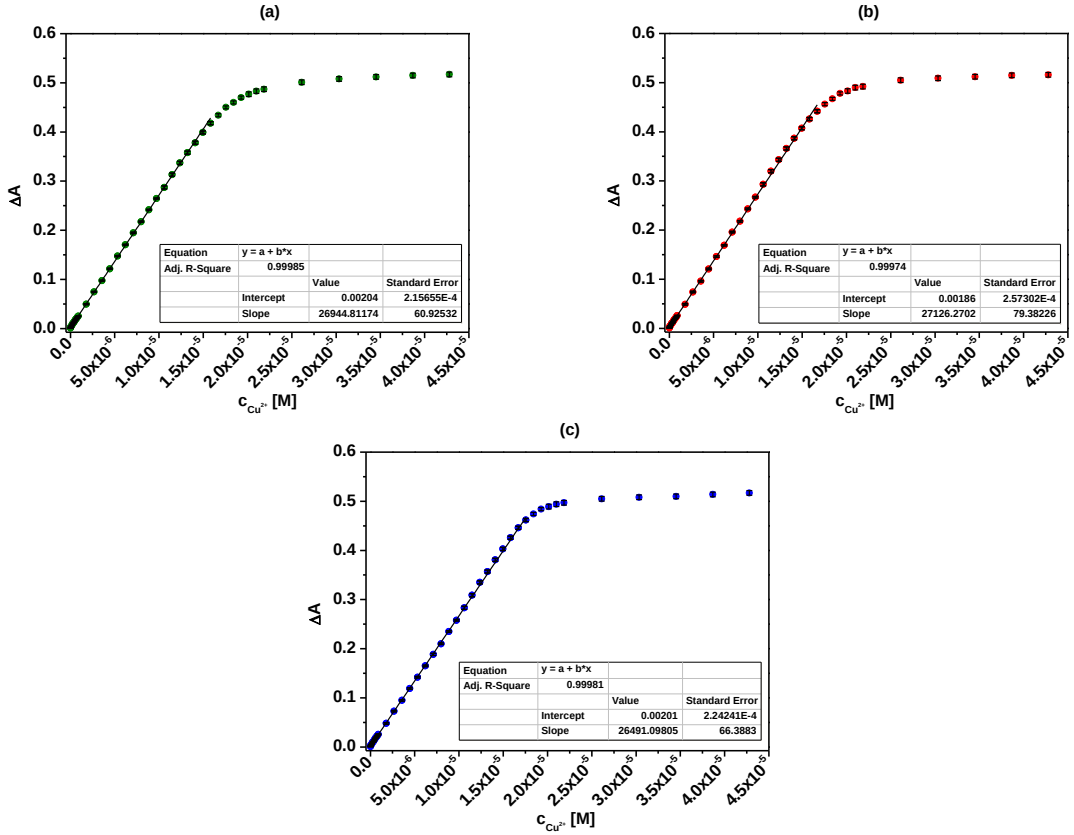

Fig. S13. Linear responses of **L** ($c_L = 2.16\times10^{-5}$ M) upon titration with copper(II) chloride (c_{Cu} = 0-4.28×10^{-5} M) in water-DMSO (9:1, v/v) solvent mixture at pH: (a) 5.0, (b) 7.0 and (c) 9.0.

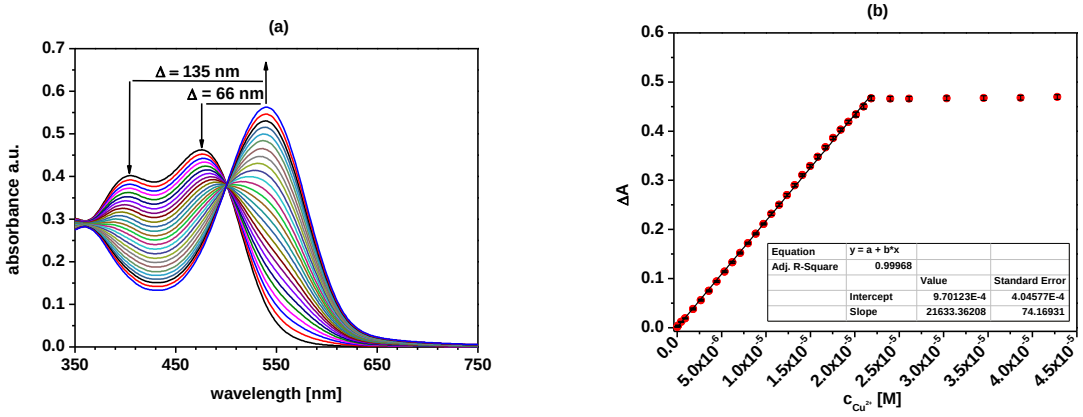

Fig. S14. (a) The change of UV-vis spectrum of **L** ($c_L = 2.16\times10^{-5}$ M) upon titration with copper(II) chloride (c_{Cu} = 0-2.61×10^{-5} M) in the presence of sodium hydroxide ($c_{NaOH} = 1.08\times10^{-5}$ M) in water-DMSO (9:1, v/v) and (b) spectral response (ΔA) towards copper(II) chloride.

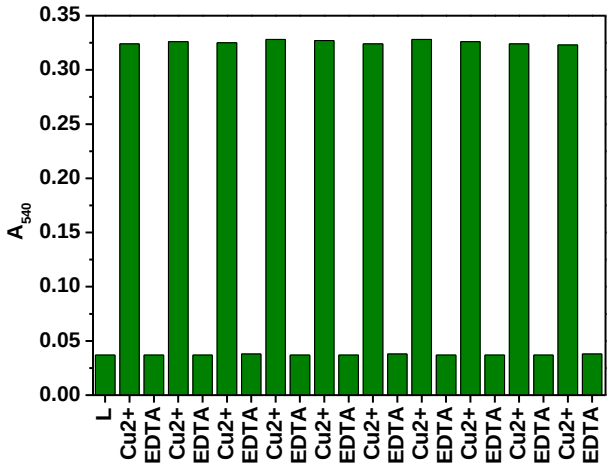

Fig. S15. Regeneration cycles of **L** ($c_L = 2.16\times10^{-5}$ M) with 0.01 M EDTA solution after addition of copper(II) chloride ($c_{Cu} = 1.08\times10^{-5}$ M) in water-DMSO (9:1, v/v) at pH 5.0.

Table S2. Spectrophotometric linear responses and limits of detection of **L** ($c_L = 2.16\times10^{-5}$ M) upon titration with copper(II) chloride in different solvent mixtures-DMSO (9:1, v/v).

	Linear range [M]	Equation	R^2	LOD [M]
pH 5.0	$6.68\times10^{-8} – 1.58\times10^{-5}$	$y = 26944.8117 \cdot c_{Cu^{2+}} + 0.0020$	0.9999	4.98×10^{-8}
pH 7.0	$6.68\times10^{-8} – 1.67\times10^{-5}$	$y = 27126.2702 \cdot c_{Cu^{2+}} + 0.0019$	0.9997	4.95×10^{-8}
pH 9.0	$6.68\times10^{-8} – 1.76\times10^{-5}$	$y = 26491.0981 \cdot c_{Cu^{2+}} + 0.0020$	0.9998	5.06×10^{-8}
pH 5.0-9.0	$6.68\times10^{-8} – 1.67\times10^{-5}$	$y = 26818.3153 \cdot c_{Cu^{2+}} + 0.0020$	0.9998	5.00×10^{-8}
NaOH	$6.68\times10^{-8} – 2.19\times10^{-5}$	$y = 21633.3621 \cdot c_{Cu^{2+}} + 0.0010$	0.9997	6.19×10^{-8}
AU	$6.68\times10^{-8} – 1.58\times10^{-5}$	$y = 22778.1017 \cdot c_{Cu^{2+}} + 0.0019$	0.9995	5.89×10^{-8}
SBF	$6.68\times10^{-8} – 1.41\times10^{-5}$	$y = 22927.9814 \cdot c_{Cu^{2+}} + 0.0018$	0.9995	5.85×10^{-8}
PBS	$6.68\times10^{-8} – 1.93\times10^{-5}$	$y = 21866.0887 \cdot c_{Cu^{2+}} + 0.0010$	0.9998	6.14×10^{-8}

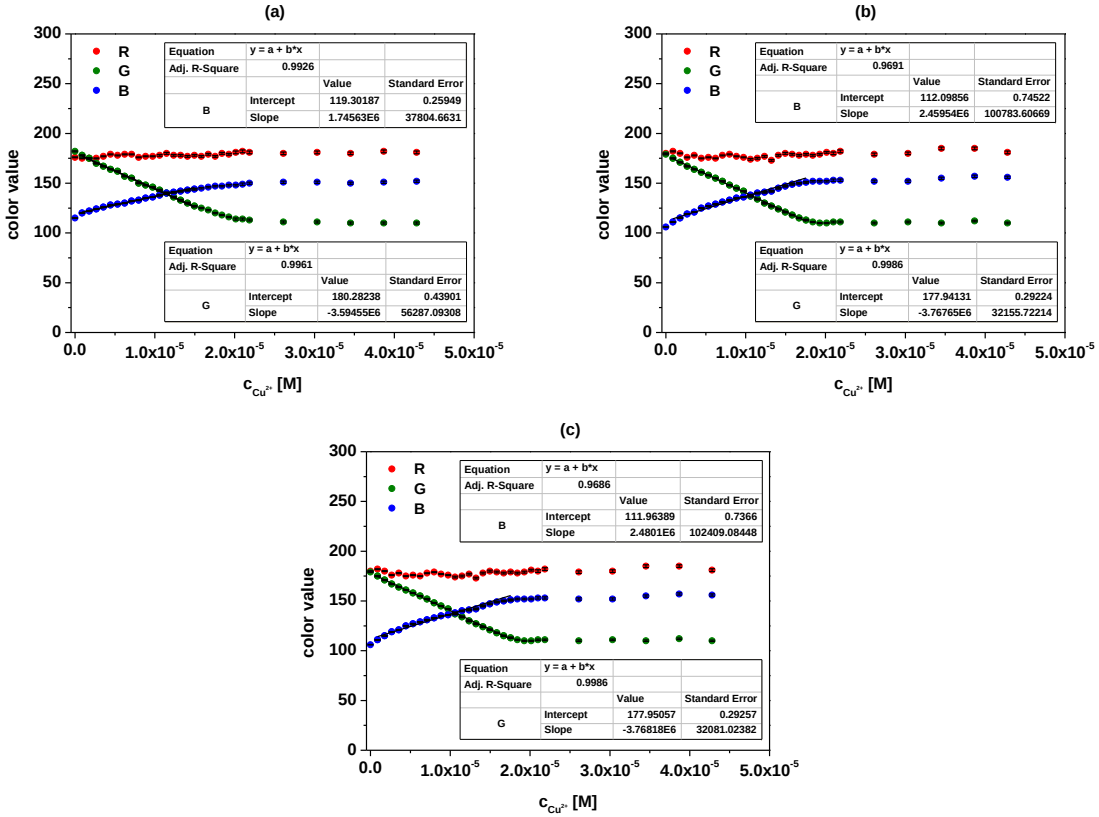

Fig. S16. Dependences of color value of **L** ($c_L = 2.16\times10^{-5}$ M) upon titration with copper(II) chloride (c_{Cu} = 0-4.28×10^{-5} M) in water-DMSO (9:1, v/v) solvent mixture at pH: (a) 5.0, (b) 7.0 and (c) 9.0.

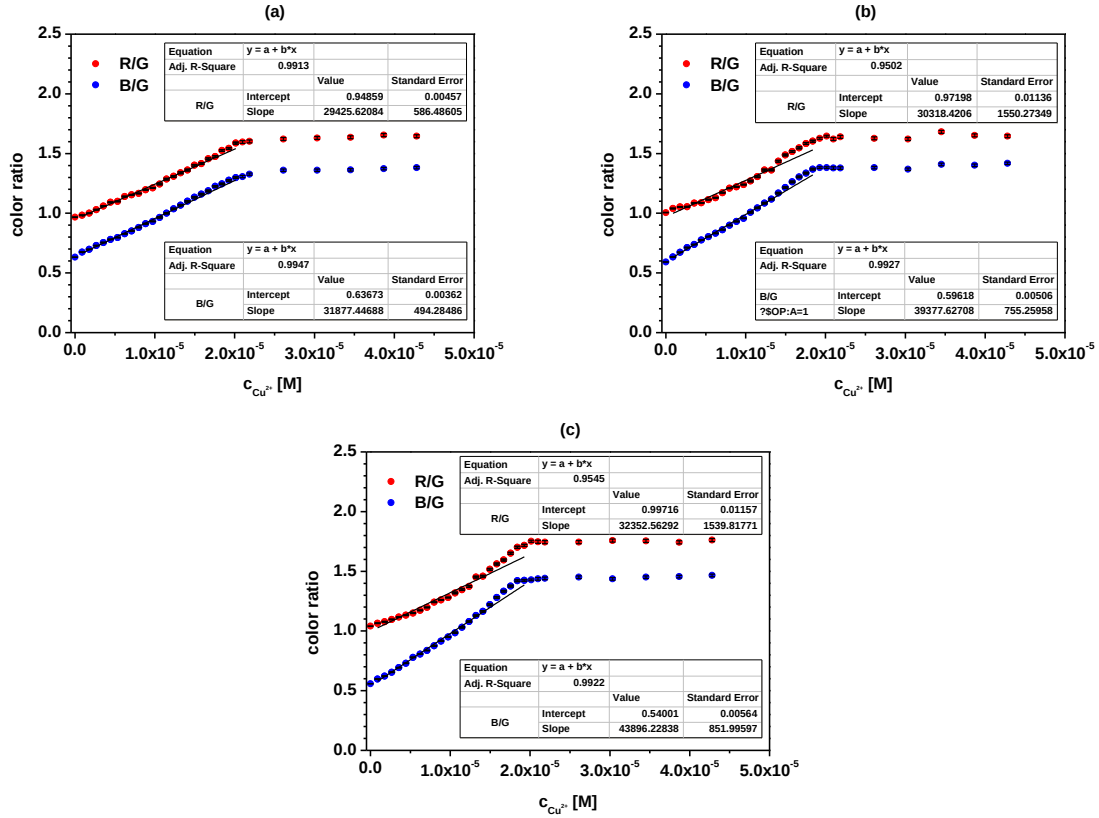

Fig. S17. Dependence of color ratio (R/G and B/G) of **L** ($c_L = 2.16\times10^{-5}$ M) upon titration with copper(II) chloride (c_{Cu} = 0-4.28×10^{-5} M) in water-DMSO (9:1, v/v) solvent mixture at pH: (a) 5.0, (b) 7.0 and (c) 9.0.

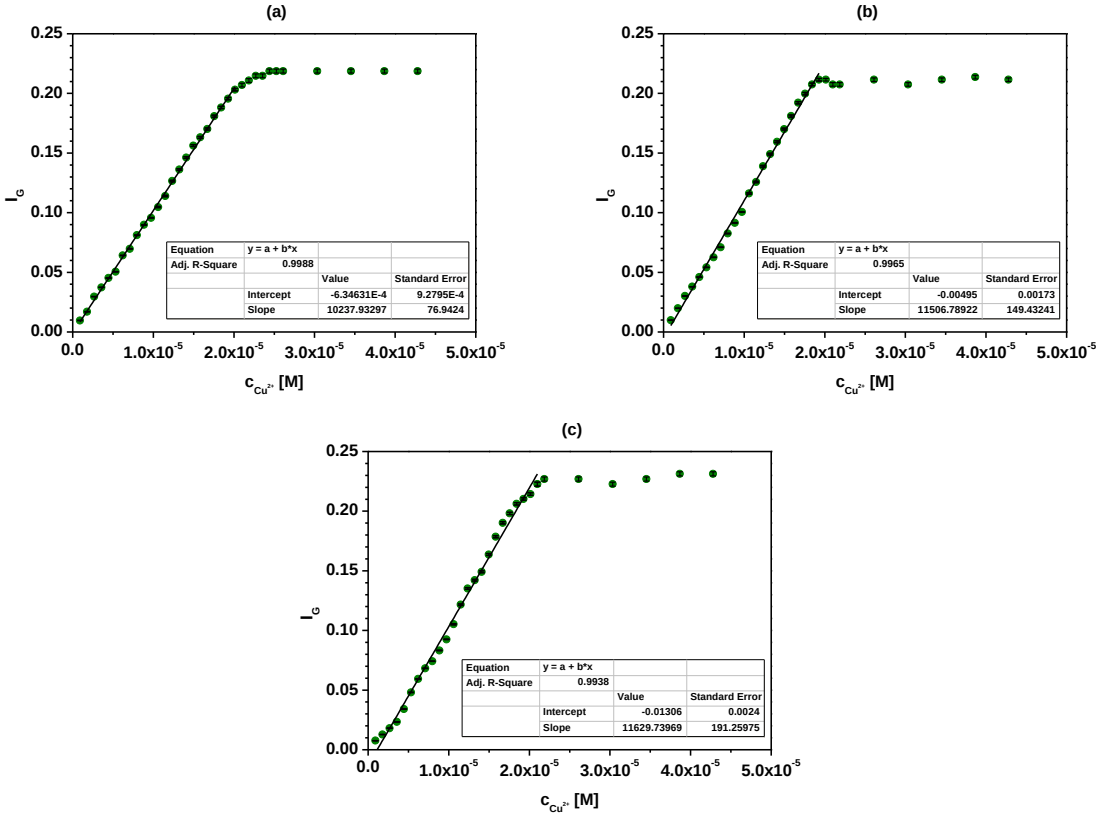

Fig. S18. Dependence of color intensity (I_G) of **L** ($c_L = 2.16\times10^{-5}$ M) upon titration with copper(II) chloride (c_{Cu} = 0-4.28×10^{-5} M) in water-DMSO (9:1, v/v) solvent mixture at pH: (a) 5.0, (b) 7.0 and (c) 9.0.

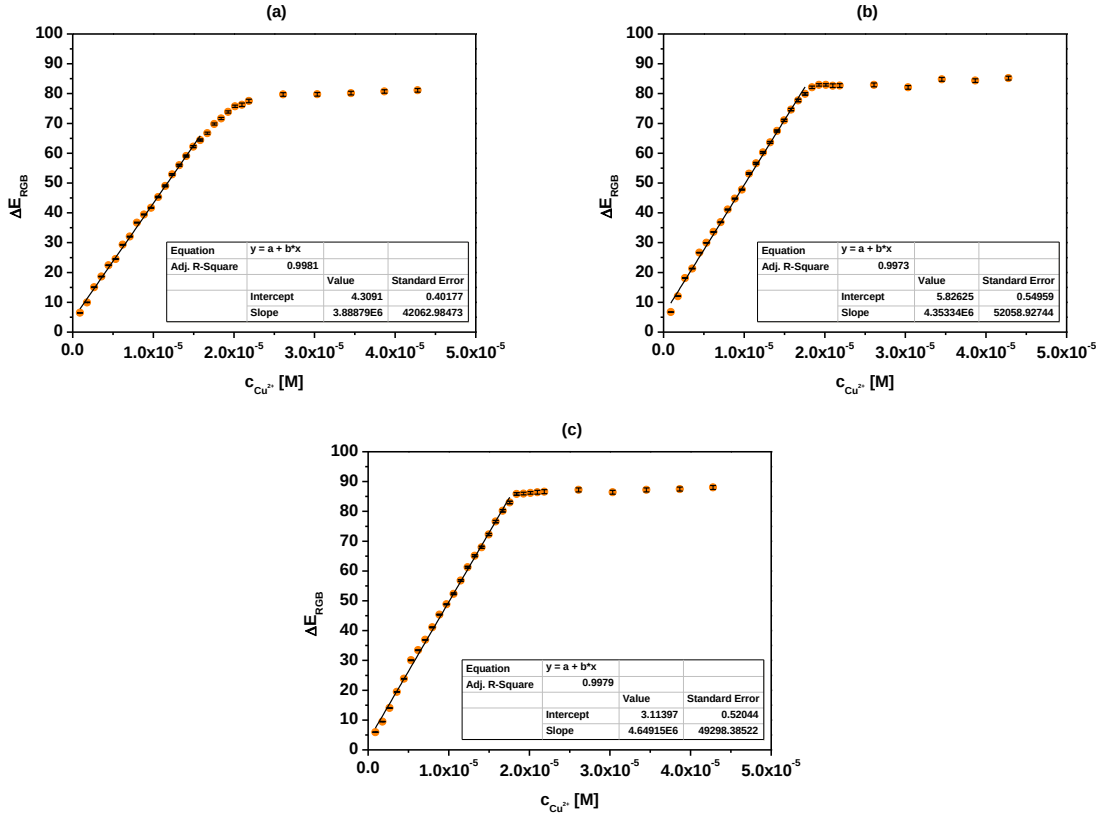

Fig. S19. Dependence of color change (ΔE_{RGB}) of **L** ($c_L = 2.16\times10^{-5}$ M) upon titration with copper(II) chloride (c_{Cu} = 0-4.28×10^{-5} M) in water-DMSO (9:1, v/v) solvent mixture at pH: (a) 5.0, (b) 7.0 and (c) 9.0.

Table S3. Colorimetric linear responses and limits of detection of **L** (c_L = 2.16×10^{-5} M) upon titration with copper(II) chloride in different solvent mixtures water-DMSO (9:1, v/v).

	Method	Linear range [M]	Equation	R^2	LOD [M]
pH 5	G	8.92×10^{-8} – 1.50×10^{-5}	$y = -3626600.00 \cdot c_{Cu^{2+}} + 180.49$	0.9957	1.25×10^{-7}
	B	8.92×10^{-8} – 1.50×10^{-5}	$y = 1745630.00 \cdot c_{Cu^{2+}} + 119.30$	0.9926	1.65×10^{-7}
	R/G	8.92×10^{-8} – 2.01×10^{-5}	$y = 29425.6208 \cdot c_{Cu^{2+}} + 0.9486$	0.9913	2.47×10^{-7}
	B/G	8.92×10^{-8} – 2.01×10^{-5}	$y = 31877.4469 \cdot c_{Cu^{2+}} + 0.6367$	0.9947	1.49×10^{-7}
	I_G	8.92×10^{-8} – 2.01×10^{-5}	$y = 10237.933 \cdot c_{Cu^{2+}} - 6{,}3463$	0.9988	1.41×10^{-7}
	ΔE_{RGB}	8.92×10^{-8} – 1.58×10^{-5}	$y = 3888790.00 \cdot c_{Cu^{2+}} + 4.31$	0.9981	8.33×10^{-8}
pH 7	G	8.92×10^{-8} – 1.76×10^{-5}	$y = -3767650.00 \cdot c_{Cu^{2+}} + 177.94$	0.9986	1.19×10^{-7}
	B	8.92×10^{-8} – 1.76×10^{-5}	$y = 2459540.00 \cdot c_{Cu^{2+}} + 112.10$	0.9691	1.08×10^{-7}
	R/G	8.92×10^{-8} – 1.84×10^{-5}	$y = 30318.4206 \cdot c_{Cu^{2+}} + 0.9720$	0.9502	2.48×10^{-7}
	B/G	8.92×10^{-8} – 1.84×10^{-5}	$y = 39377.6271 \cdot c_{Cu^{2+}} + 0.5962$	0.9927	1.13×10^{-7}
	I_G	8.92×10^{-8} – 1.93×10^{-5}	$y = 11506{,}789 \cdot c_{Cu^{2+}} - 0.005$	0.9965	1.28×10^{-7}
	ΔE_{RGB}	8.92×10^{-8} – 1.76×10^{-5}	$y = 4353340.00 \cdot c_{Cu^{2+}} + 5.83$	0.9973	7.72×10^{-8}
pH 9	G	8.92×10^{-8} – 1.76×10^{-5}	$y = -3768180.00 \cdot c_{Cu^{2+}} + 177.95$	0.9986	1.14×10^{-7}
	B	8.92×10^{-8} – 1.76×10^{-5}	$y = 2480100.00 \cdot c_{Cu^{2+}} + 111.96$	0.9686	9.68×10^{-8}
	R/G	8.92×10^{-8} – 1.93×10^{-5}	$y = 32352.5629 \cdot c_{Cu^{2+}} + 0.9972$	0.9545	2.41×10^{-7}
	B/G	8.92×10^{-8} – 1.93×10^{-5}	$y = 43896.2284 \cdot c_{Cu^{2+}} + 0.5400$	0.9922	9.57×10^{-8}
	I_G	8.92×10^{-8} – 2.10×10^{-5}	$y = 11629{,}740 \cdot c_{Cu^{2+}} - 0.013$	0.9938	1.91×10^{-7}
	ΔE_{RGB}	8.92×10^{-8} – 1.84×10^{-5}	$y = 4649150.00 \cdot c_{Cu^{2+}} + 3.11$	0.9979	6.37×10^{-8}
SBF	G	8.92×10^{-8} – 1.50×10^{-5}	$y = -2955360.00 \cdot c_{Cu^{2+}} + 159.81$	0.9967	1.52×10^{-7}
	B	8.92×10^{-8} – 1.41×10^{-5}	$y = 4107680.00 \cdot c_{Cu^{2+}} + 76.11$	0.9949	1.10×10^{-7}
	R/G	8.92×10^{-8} – 1.93×10^{-5}	$y = 21065.7868 \cdot c_{Cu^{2+}} + 1.1384$	0.9917	2.28×10^{-7}
	B/G	8.92×10^{-8} – 2.18×10^{-5}	$y = 44917.0613 \cdot c_{Cu^{2+}} + 0.4568$	0.9974	1.07×10^{-7}
	I_G	8.92×10^{-8} – 1.84×10^{-5}	$y = 9079.049 \cdot c_{Cu^{2+}} + 0.012$	0.9978	1.65×10^{-7}
	ΔE_{RGB}	8.92×10^{-8} – 1.32×10^{-5}	$y = 5194630.00 \cdot c_{Cu^{2+}} + 4.18$	0.9993	8.66×10^{-8}

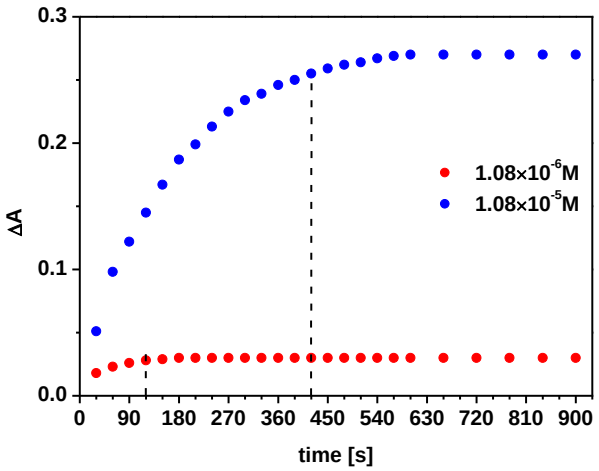

Fig. S20. Response time of optode with **L** upon immersion in copper(II) solution in pH 5.0.

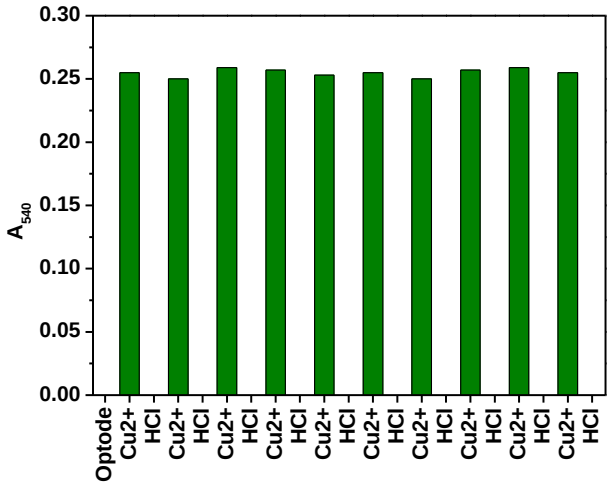

Fig. S21. Regeneration cycles for optodes in 0.1 M HCl solution after contact with copper(II) chloride solution (c_{Cu} = 1.08×10^{-5} M) at pH 5.0.

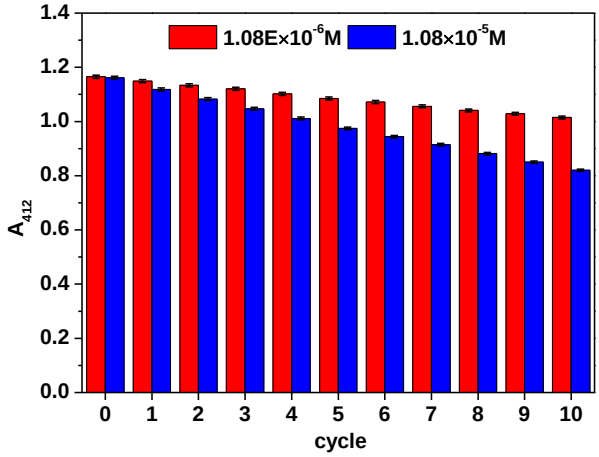

Fig. S22. Dependence of the change of absorbance at wavelength corresponding to the optode maximum (A_{412}) on the subsequent uses of membrane after contact with solutions with different concentration of copper(II) ions.

Table S4. Colorimetric linear responses and limits of detection of optode upon titration with copper(II) chloride at pH 5.0.

Method	Linear range [M]	Equation	R^2	LOD [M]
G	$4.31\times10^{-7} - 2.48\times10^{-5}$	$y = 1378590.00 \cdot c_{Cu^{2+}} + 184.56$	0.9979	9.72×10^{-7}
R/G	$2.16\times10^{-7} - 1.72\times10^{-4}$	$y = 5807.5987 \cdot c_{Cu^{2+}} + 0.9464$	0.9879	8.27×10^{-7}
B/G	$4.31\times10^{-7} - 1.72\times10^{-4}$	$y = 5059.1818 \cdot c_{Cu^{2+}} + 0.2962$	0.9940	9.49×10^{-7}
I_G	$2.16\times10^{-7} - 2.48\times10^{-5}$	$y = 3591.6045 \cdot c_{Cu^{2+}} + 0.0093$	0.9959	4.57×10^{-7}
ΔE_{RGB}	$4.31\times10^{-7} - 2.48\times10^{-5}$	$y = 1476470.00 \cdot c_{Cu^{2+}} + 6.67$	0.9993	4.06×10^{-7}

Table S5. Elemental composition of drinking water samples.

mg/L	Drinking water		
	1	2	3
Na^+	11.00	91.50	33.17
K^+	5.00	7.50	3.73
Mg^{2+}	21.90	103.50	61.62
Ca^{2+}	130.30	228.60	325.80
HCO_3^-	539.10	1479.90	1314.00
SO_4^{2-}	1.00	16.30	16.50
Cl^-	5.00	17.70	8.93
F^-	0.50	0.05	0.11
H_2SiO_4	-	35.00	-
SiO_2	22.10	-	-
CO_2	-	<1500.00	<1500.00

Table S6. Elemental composition of Qnova calibration solution.

	Qnova calibration solution [µg/L]
Be^{2+}	35.00±1.75
Zn^{2+}	20.00±1.00
Cu^{2+}, Ni^{2+}	15.00±0.75
Al^{3+}, Ga^{3+}, Mg^{2+}	10.00±0.50
Co^{2+}, Li^+, Sc^{2+}	8.00±0.40
Ag^+, Mn^{2+}	6.00±0.30
Sr^{2+}	5.00±0.25
Ba^{2+}, Tl^{3+}	4.00±0.20
Bi^{3+}, Ce^{2+}, Cs^+, Ho^{3+}, In^{3+}, Rh^{3+}, Ta^{5+}, $Tb3^+$, UO_2^{2+}, Y^{3+}	3.00±0.15

P4 – CHROMOGENIC AZOMACROCYCLES WITH IMIDAZOLE RESIDUE: STRUCTURE VS. PROPERTIES

Dyes and Pigments 219 (2023) 111610

Contents lists available at ScienceDirect

Dyes and Pigments

journal homepage: www.elsevier.com/locate/dyepig

Chromogenic azomacrocycles with imidazole residue: Structure vs. properties

Błażej Galiński [a], Jarosław Chojnacki [b], Katarzyna Szwarc-Karabyka [c], Adrian Małkowski [a,1], Diana Sopel [a,1], Agnieszka Zwolińska [a,1], Ewa Wagner-Wysiecka [a,d,*]

[a] Department of Chemistry and Technology of Functional Materials, Faculty of Chemistry, Gdańsk University of Technology, Narutowicza Street 11/12, 80-233, Gdańsk, Poland
[b] Department of Inorganic Chemistry, Faculty of Chemistry, Gdańsk University of Technology, Narutowicza Street 11/12, 80-233, Gdańsk, Poland
[c] Nuclear Magnetic Resonance Laboratory, Faculty of Chemistry, Gdańsk University of Technology, Narutowicza Street 11/12, 80-233, Gdańsk, Poland
[d] Advanced Materials Center, Faculty of Chemistry, Gdańsk University of Technology, Narutowicza Street 11/12, 80-233, Gdańsk, Poland

ARTICLE INFO

Keywords:
Azocompound
X-ray analysis
Colorimetric sensor
Porous glass
Smartphone

ABSTRACT

New diazo macrocycles linked by hydrocarbon chain bearing imidazole or 4-methylimidazole residue have been synthetized with satisfactory yield (24–55%). The structure of macrocycles was confirmed by X-ray analysis and spectroscopic methods (^{1}H NMR, MS, FTIR). Metal cation complexation studies were carried out in acetonitrile and acetonitrile-water system. It was found that azomacrocyles form triple-decker complexes with lead(II). The highest values of stability constant were found for lead(II) complexes of 21-membered derivatives. For the first time azomacrocycles bearing imidazole residue were immobilized on a porous glass. Obtained materials can act as lead(II) or copper(II) colorimetric optical sensors with color digital analysis as detection using simple portable devices.

1. Introduction

The presence of harmful compounds including heavy metals in food, such as fish, vegetables and fruit, associated with increasing environmental pollution is an ever-growing global problem [1–3]. Water is an essential nutrient and the most important solvent for living organisms. Its availability is decreasing and its pollution is increasing [4]. Pollution of water, soil [5–8] and air [9–12], causes accumulation of hazardous metals in aqueous systems [13], and animal [14] and plant organisms [15]. Consumption of contaminated food is associated with frequent poisoning as well as dangerous diseases caused by the accumulation of heavy metals in the human body [16–21]. Some heavy metals such as chromium, manganese, nickel, zinc, iron or copper are key elements necessary for the proper functioning of the human body, however, also their elevated levels are dangerous for health and life [22,23]. On the other hand, heavy metals such as lead, cadmium, mercury or arsenic pose a serious ecological threat and are toxic to living organisms and their accumulation may result in kidney dysfunction, brain tumors and metabolic disorders [24]. Early and rapid detection of elevated levels of heavy metals and other harmful compounds in biological and environmental samples is of great importance and crucial in maintaining health [25]. Valuable analytical tools which can be used for this purpose are optical sensors which serve fast and reliable detection/determination of analytes of different nature [26–33]. Constantly popular are chemical optical sensors, including optodes, due to their simplicity and possibility of non-instrumental detection, i.e. detection and determination with the naked eye, as well as low hardware requirements [34–37]. Receptor layers of optical sensors are characterized by relatively high sensitivity and selectivity, relatively simple and low cost preparation and relatively fast response time [38–41]. Optical sensors allow determination of many chemical species of different properties and chemical nature, depending on the receptor layers used. Among various solutions of preparation of optical sensor layers porous glasses can be used for the immobilization chromo(fluoro)ionophores. Comparing, for example polymeric matrix often used in classical optodes, such materials offer the photochemical and thermal stability, which is limited by the duration of the chromoionophore and the rest of the components (plasticizer, ionic additives etc.) of the layer [42]. Among the others, colorimetric and fluorescent

* Corresponding author.Department of Chemistry and Technology of Functional Materials, Faculty of Chemistry, Gdańsk University of Technology, Narutowicza Street 11/12, 80-233, Gdańsk, Poland.
E-mail address: ewa.wagner-wysiecka@pg.edu.pl (E. Wagner-Wysiecka).
[1] authors of the same degree of contribution given in alphabetical order.

https://doi.org/10.1016/j.dyepig.2023.111610
Received 25 June 2023; Received in revised form 1 August 2023; Accepted 7 August 2023
Available online 8 August 2023

pH sensors using covalently immobilized pH indicators onto porous glasses were obtained [43–46]. Porous matrix materials were also interest as optical sensing of gaseous oxygen [47]. The advantage is the longer life time of sensing material comparing materials where physical immobilization is used. However the weak point is the preparation of the sensing layer, which usually needs a multi step preparation protocol.

Large group of the optical sensors is based on supramolecular approach, where in the sensor matrix selective towards a particular analyte (guest) host molecule is immobilized. Among such solutions interesting are those which use chromogenic receptors. It differs from traditional optodes for which the most often solution is using ionophore responsible for analyte recognition and chromophore (usually acid-base indicator) thanks to which the optical signal is generated. One of the advantages of such an approach is the limitation of the chemical components of the sensing layer. Among colored metal ion receptors large group of effective chromionophores constitute azo compounds [48,49] and among them macrocylic azo derivatives [50,51]. Application of well-designed macrocylic receptors discriminating metal ions according to their size can significantly improve selectivity of optical sensors. However the synthesis of the macrocyclic compounds is often laborious and challenging [52–54]. Among chromogenic macrocyclic compounds an interesting group of are molecules with two azo groups and heterocyclic moiety constituting a part of macroring. Compounds of this type have been obtained in our group in relatively facile synthetic protocols with satisfactory yields [55–61]. The high selectivity towards metal cations enabled using macrocyclic pyrrole derivatives as ionophores in lead(II) selective ion-selective electrodes [56] and optodes [61]. Macrocyclic derivatives bearing imidazole moiety as a part of macrocycle have been also investigated as ionophores in membrane ion-selective electrodes [59]. Some macrocyclic imidazole derivatives were encapsulated in silica xerogel matrices and proposed as optical chemical recognition elements [62].

Promising results obtained for optodes based on macrocyclic pyrrole derivatives [61] have encouraged us to study the influence of the type of heterocyclic moiety on selectivity of the chromogenic receptor layers towards metal ions. Therefore, the aim of the work is to investigate the properties of macrocyclic imidazole derivatives as chromoionphores and to determine their possible use in the receptor layers of optical sensors. New macrocyclic derivatives of imidazole and 4-methylimidazole besides previously obtained were also synthetized for the purposes of this study. Moreover, the goal of this paper is the assessment of the application of the porous glass as solid support for chromoionophore immobilization – as easy and non-labor and non-time consuming user friendly optical sensors with digital color analysis used as detection mode.

2. Experimental

2.1. Materials

All chemicals of the highest available purity were purchased from commercial sources and used without further purification. For metal cation complexation, lithium perchlorate (99.9%, Sigma Aldrich), sodium perchlorate monohydrate (>99.0%, Fluka), potassium perchlorate (>99.0%, Sigma Aldrich), magnesium perchlorate (≤100%, Alfa Aesar), calcium perchlorate tetrahydrate (99.0%, Alfa Aesar), strontium perchlorate trihydrate (≤100%, Alfa Aesar), barium perchlorate (97.0%, Sigma Aldrich), cobalt(II) perchlorate hexahydrate (98.0%, Sigma Aldrich), nickel(II) perchlorate hexahydrate (≥98.5%, Sigma Aldrich), copper(II) perchlorate hexahydrate (98.0%, Sigma Aldrich), zinc perchlorate hexahydrate (Sigma Aldrich), cadmium perchlorate hexahydrate (Alfa Aesar) and lead(II) perchlorate trihydrate (≥99.0%, Sigma Aldrich). For acid-base properties studies *p*-toluenesulfonic acid monohydrate (pure, POCH, Gliwice, Poland), tetra-*n*-butylammonium hydroxide 30-hydrate (98%, Sigma-Aldrich, Steinhaim, Germany) were used. Metal nitrates: sodium nitrate (≥99.8%, POCH), potassium nitrate (≥99.8%, POCH), magnesium nitrate hexahydrate (≥99.0%, POCH), calcium nitrate tetrahydrate (≥99.0%, POCH), strontium nitrate (≥99.0%, POCH), barium nitrate (≥99.0%, POCH), cobalt(II) nitrate hexahydrate (≥98.0%, POCH), nickel(II) nitrate hexahydrate (≥98.0%, POCH), copper(II) nitrate trihydrate (≥99.5%, Merck), zinc nitrate hexahydrate (≥98.0%, POCH), cadmium nitrate tetrahydrate (≥98.0%, POCH) and lead(II) nitrate (≥99.0%, Alfa Aesar). Porous glass (polystyrene modified, particle size 0.075–0.125 mm, $M_w \sim 120000$ Corning) was used for preparation of sensing layers. UV–Vis measurements were carried out in acetonitrile (spectroscopic-grade, Merck). All aqueous solutions were prepared using ultra-pure water obtained by the reverse osmosis (RO) from Hydrolab Poland station (conductivity <1 μS/cm^{-1}). For preparation of sensing layers dichloromethane (p.a. POCh) was used as a solvent. In synthetic protocols p.a. solvents were used. TLC plates 60 RP-18 F_{254} for lipophilicity determination, TLC plates 60 F_{254} for reaction progress tracing and determination of R_f parameters and silica gel 60 (0.063–0.200 mm) for column chromatography were purchased from Merck.

2.2. Instrumentation

^{1}H and ^{13}C NMR spectra were recorded on a Varian INOVA 500 spectrometer at 500 and at 125 MHz, respectively. Chemical shifts are reported in δ (ppm) units. FTIR spectra (ATR) were taken on the Nicolet iS10 apparatus. Mass spectra (LR and HRMS EI) were taken on a Autospec Premier (Waters) spectrometer. UV–Vis measurements were carried out in 1 cm quartz cuvettes with the use of an UNICAM UV 300 series spectrometer. The solution pH was measured by an pH-meter CPC-511 with glass electrode EPS-1 (ELMETRON), standardized with buffer solutions. Portable LED light box (23 × 23 × 23 cm) was used to guarantee the reproducibility of the photos (PULUZ, Photography Light Box, Shenzhen Puluz Technology Limited). The phone which camera was used for the photos was the Apple iPhone 7 Plus.

2.3. Synthesis of macrocycles 1–4

Macrocycles **1**–**4** were obtained by diazocoupling of diazonium salt with imidazole or 4-methylimidazole using synthetic protocols elaborated on our group [55–60]. The procedure of the synthesis and structural characterization of newly obtained macrocycles are given in Electronic Supplementary Information (ESI).

2.4. X-ray structure determination

Diffraction intensity data for **1**, **3**, **4** and **6** were collected on an IPDS 2T dual beam diffractometer (STOE & Cie GmbH, Darmstadt, Germany) at 120.0(2) K with MoKα radiation of a microfocus X-ray source (GeniX 3D Mo High Flux, Xenocs, Sassenage, 50 kV, 1.0 mA, and $\lambda = 0.71069$ Å). Investigated crystals were thermostated under a nitrogen stream at 120 K using the CryoStream-800 device (Oxford CryoSystem, UK) during the entire experiment.

Data collection and data reduction were controlled by using the X-Area 1.75 program (STOE, 2015). Due to low absorption coefficient no absorption correction was performed. The structures were solved using intrinsic phasing implemented in SHELXT and refined anisotropically using the program packages Olex2 [63] and SHELX-2015 [64]. Positions of the C–H hydrogen atoms were calculated geometrically taking into account isotropic temperature factors. All hydrocarbonic H-atoms were refined as riding on their parent atoms with the usual restraints. All NH atoms were found in the Fourier electron density map and refined with N–H bond length constrained to 0.86(2) Å.

Structure of **1** was solved in the space group $P2_1/c$ and refined without any special treatment. Structure **3** was refined with the assumption the electron density in the mean unit cell has higher symmetry than actual molecules. The mean electron density is an average of the molecule and its mirror reflection. Thus, the asymmetric unit, being

half of the molecule, contains N3–H3 and (C11–H11 and N4) and C9, H9A, H9B atoms with occupation factor equal to ½. It is worthy to add, that initially the solution was found in polar space group $Pna2_1$, but PLATON finds additional symmetry, leading to the reported solution in space group *Pnma*. In order to maintain numerical stability restrains of equal ellipsoids were applied to (half occupied) atoms N4 and C11, sharing the same positions.

Structure of **4** was solved in the space group $P2_1/c$ and refined without any special treatment.

Compound **5** crystallizes in the space group *I2/m* (No. 12, cell choice 3 of *C2/m*). Cell parameters: (*a, b, c* (Å); *α, β, γ* (°) = 7.7187 (17), 31.861 (9), 29.749 (6); 90, 94.805 (17), 90). The structure was solved, but not refined to a satisfactory quality and therefore it was not deposited in the Cambridge Database. Raw results indicate the asymmetric unit contains one regular macrocycle molecule and two halves of the two other, chemically identical, macrocycles, both having a mirror *m* symmetry. Each macrocyclic molecule is accompanied with a water molecule forming hydrogen bonding with an imidazole N-atom directed to the ring centre.

Structure of compound **6** was solved in the space group $P2_12_12_1$ and refined without any special treatment, but the absolute structure is uncertain since no heavy atom is present. Crystal data and structure refinement details for all crystal determined structures are collected in Table 1.

2.5. Structure determination in solution

The NMR spectra of **4** and **6** were recorded using a Varian INOVA 500 Spectrometer operating at 499.795 MHz in DMSO-d_6 solutions in ambient temperature. Chemical shifts are reported in δ (ppm) units using ^{1}H (residual) from DMSO-d_6 (2.49 ppm) as internal standard. 1D ^{1}H NMR spectra were collected with standard parameters (45° pulse length 3.9 μs and the delay time 1s). The 2D NMR spectra of **4** and **6** were recorded in ambient temperature. The ROESY spectrum was collected in the phase-sensitive mode with a spectral width of 5856 Hz and a mix time of 300 ms in a 4100 × 280 matrix with 16 accumulations per increment in a 4K × 1K matrix. The gHSQC and gHMBC experiments of all samples were performed with pulse field gradients. The gHSQC spectra were acquired in the phase-sensitive mode with ^{1}J(CH) set to 146 Hz. The spectral windows for ^{1}H and ^{13}C of axes were 5856 Hz and 20111 Hz, respectively. The data were collected with 64 accumulations per increment in a 1610 × 170 matrix and processed in a 2K × 2K matrix. The gHMBC spectra were acquired in absolute value mode with ^{n}J(CH) set to 8 Hz. The spectral windows for ^{1}H and ^{13}C of axes were 5856 Hz and 23881 Hz, respectively. The data were collected with 112 accumulations per increment in a 2620 × 170 matrix and processed in a 2K × 2K matrix.

2.6. Lipophilicity ($logP_{TLC}$)

The lipophilicity values of chromoionophores were determined by TLC method [48,60,66] using reversed phase RP18-TLC chromatography and mixture methanol:water (9:1, v/v) as a mobile phase. As standards BBPA, DBP, DOP, DOS and NPOE were used. $LogP_{TLC}$ values were determined by comparison of R_f values for standards and macrocycles.

Table 1
Crystal data and structure refinement details for all crystal structures determined.

Deposition No.	1	3	4	6
	2256005	2256006	2256007	2256008
Crystal data				
Chemical formula	$C_{19}H_{18}N_6O_2$	$C_{20}H_{20}N_6O_2$	$C_{21}H_{22}N_6O_2$	$C_{20}H_{20}N_6O_3$
M_r	362.39	376.42	390.44	392.42
Crystal system, space group	Monoclinic, $P2_1/c$	Orthorhombic, *Pnma*	Monoclinic, $P2_1/c$	Orthorhombic, $P2_12_12_1$
Temperature (K)	120	120	120	120
a, b, c (Å)	10.8716 (11), 7.0094 (4), 22.680 (2)	6.9729 (18), 15.911 (6), 16.167 (5)	15.677 (3), 11.0103 (16), 11.4065 (19)	4.0512 (3), 16.296 (2), 27.797 (3)
α, β, γ (°)	90, 91.818 (8), 90	90, 90, 90	90, 103.907 (13), 90	90, 90, 90
V (Å^3)	1727.4 (3)	1793.7 (10)	1911.2 (5)	1835.1 (4)
Z	4	4	4	4
Radiation type	Mo *Kα*	Mo *Kα*	Mo *Kα*	Mo *Kα*
μ (mm^{-1})	0.10	0.10	0.09	0.10
Crystal size (mm)	0.21 × 0.18 × 0.02	0.21 × 0.11 × 0.02	0.38 × 0.07 × 0.05	0.28 × 0.08 × 0.03
Data collection				
Diffractometer	STOE *IPDS* 2T	STOE *IPDS* 2T	STOE *IPDS* 2T	STOE *IPDS* 2T
Absorption correction	Multi-scan[a]	Multi-scan[a]	–	–
T_{min}, T_{max}	0.267, 0.997	0.444, 0.997	–	–
No. of measured, independent and observed [$I > 2\sigma(I)$] reflections	13715, 3050, 2007	12590, 2506, 2008	17724, 4175, 3395	7259, 2994, 1924
R_{int}	0.087	0.035	0.080	0.100
$(\sin\theta/\lambda)_{max}$ (Å^{-1})	0.595	0.691	0.639	0.580
Refinement				
$R[F^2 > 2\sigma(F^2)]$, $wR(F^2)$, *S*	0.073, 0.194, 1.13	0.039, 0.104, 1.01	0.068, 0.195, 1.03	0.107, 0.277, 1.16
No. of reflections	3050	2506	4175	2994
No. of parameters	248	130	266	264
No. of restraints	1	0	1	1
H-atom treatment	H atoms treated by a mixture of independent and constrained refinement	H-atom parameters constrained	H atoms treated by a mixture of independent and constrained refinement	H-atom parameters constrained
$\Delta\rho_{max}$, $\Delta\rho_{min}$ (e Å^{-3})	0.30, −0.38	0.28, −0.20	0.31, −0.35	0.34, −0.33
Absolute structure	–	–	–	Refined as an inversion twin.
Absolute structure parameter	–	–	–	0 (7)

[a] Multi-scan: STOE LANA, absorption correction by scaling of reflection intensities Afterwards a spherical absorption correction was performed within STOE LANA [65].

2.7. Metal cation complexation

Metal cation complexation studies were carried out using UV–Vis titration in acetonitrile and the mixture of acetonitrile with water. The stock solutions of macrocycles ($\sim 10^{-3}$ M), metal perchlorates ($\sim 10^{-2}$ M), TsOH ($\sim 10^{-2}$ M), TBAOH ($\sim 10^{-2}$ M) nitrates ($\sim 10^{-2}$ M), were prepared by weighting the respective quantities of them and dissolving in the respective solvent system in volumetric flasks. The values of binding constant (logK) were calculated with the use of OPIUM [67] program on the basis of titration experiment data.

2.8. Sensing layers preparation

Sensing materials based on porous glass (PG-PS) with different chromoionophore content (mg of chromoionophore per g of porous glass) were prepared using as working solutions of chromoionophores at a concentration of 0.1 mg/mL. Then 1.25, 2.5, 3.75 and 5 mL of solution was diluted to 10 mL with dichloromethane and next added to 500 mg of PG-PS to obtain sensing materials of 0.25, 0.5, 0.75 and 1 mg/g chromoionophore content per g of solid material. The mixture was stirred for 10 min and after that the mixture was transferred onto the Petri dish to evaporate solvent. The properties of the receptor layers were studied after immobilization using double-sided tape of the prepared material on 0.9 × 4.5 cm glass plates.

2.9. Measurement procedures-digital color analysis

Pictures of sensor layers were analyzed using free software ImageJ [68,69]. The change of optode color given as ΔE_{RGB} [48,61,70] was calculated using the equation: $\Delta E_{RGB} = [(R_0 - R)^2 + (G_0 - G)^2 + (B_0 - B)^2]^{1/2}$ where R_0, G_0 and B_0 values correspond to color of layer in the absence of metal salt, and R, G and B values correspond to color of layer in the presence of metal salt. Limits of detection (LOD) for copper (II) and lead(II) were calculated $DL = 10^{[(3\sigma - b)/a]}$, where σ is the standard deviation of the blank, b is intercept and a is the slope of the linear function ΔE_{RGB} = f(logarithm of molar concentration of analyte).

3. Results and discussion

3.1. Synthesis and characterization of macrocycles

New azomacrocycles **1**–**4** (Scheme 1) were obtained in analogous way as their oligoether analogs **5**–**8** [55,59]. The respective diazonium salt obtained from diamine **12** (or **13**) was diazocoupled with imidazole or 4-methylimidazole under high dilution conditions. In this way new 17- and 18-membered crowns **1**,**2** and **3**,**4** respectively were obtained.

It can be noted that macrocyclization yield for **1**–**4** is slightly higher for reactions where 4-methylimidazole was used as a substrate. Yields of compounds **1**–**4** linked by hydrocarbon chain are in general lower than for oligoether analogs **5**–**8**. Interestingly for oligoether linked compounds **5** and **7** bearing imidazole residue yields are higher than for macrocycles bearing 4-methylimidazole moiety. Yield of macrocyclization for compounds **1**–**8** is compared in Fig. 1. It can be stated that macrocyles with imidazole/4-methylimidazole rings are compounds obtained in relatively facile way with satisfactory (when regarding macrocyclization reactions) 24–55% yields. It makes above macrocycles promising potential metal cation complexing reagents in analytical chemistry providing that presenting satisfactory selectivity.

The structure of all new compounds was confirmed by spectroscopic methods: ^{1}H and ^{13}C NMR, HRMS and FTIR spectra (ESI Fig. S1-S16). The structure of macrocycles crystalizing in a form suitable for X-ray analysis was confirmed in a solid state. The structure of selected macrocycles was also investigated in solution using NMR spectroscopy (vide infra).

3.2. Description of X-ray structures

Compound **1** forms red, needle – like crystals with monoclinic symmetry. Structure of **1** was solved in the space group $P2_1/c$ and refined without any special treatment. Crystallographic details are listed in Table 1. The asymmetric unit contains one macrocyclic molecule. Atom labeling scheme is shown in Fig. 2.

Imidazolic N–H group is directed to the center of the macrocycle and does not form any hydrogen bonding in the crystalline state. The whole molecule is twisted, which manifests in a dihedral angle between the phenyl rings C4–C9 and C14–C19 equal to 20.2(2). The imidazole ring is almost coplanar with phenyl C14–C19, perhaps due to stacking interactions. Such an interaction with 3.858(2) Å inter-centroid distance is indeed formed between the imidazole ring and C14–C19 phenyl ring from a neighbour molecule, generated by inversion symmetry (1-*x*, 2-*y*,1-*z*).

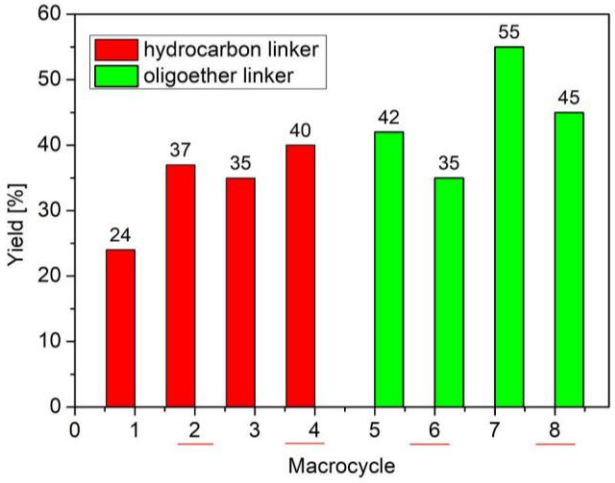

Fig. 1. The comparison of macrocyclization yield for compounds **1**–**8**. (No. of 4-methylimidazole derivatives are red underlined).

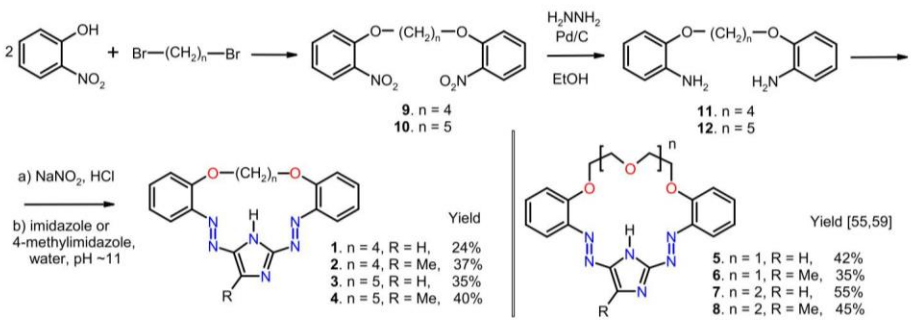

Scheme 1. Synthesis of macrocyclic compounds **1**–**4** with hydrocarbon linker and formulas of macrocycles bearing oligoether moiety **5**–**8**.

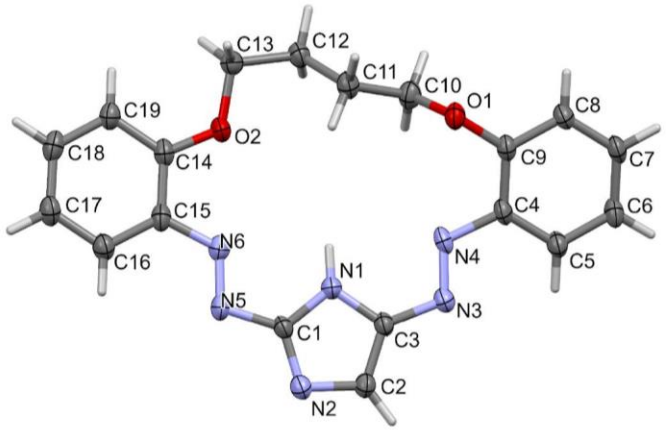

Fig. 2. Molecular view of **1**, showing atom labeling scheme. Displacement ellipsoids drawn at 50% probability level. Selected bond lengths (Å) and angles (°): N3–N4 1.267(4), N5–N6 1.268(4), N1–C1 1.347(5), N1–C3 1.360(5), N2–C1 1.323(5), N2–C2 1.381(5), C2–C3 1.373(5), N5–C1 1.408(5), N3–C3 1.392(5); valence angles: C9–O1–C10 116.1(3), C14–O2–C13 120.6(3), C1–N1–C3 106.5(3), C1–N2–C2 104.2(3), C3–C2–N2 109.7(3), N4–N3–C3 111.0(3), N3–N4–C4 114.9(3); torsions C8–C9–O1–C10 104.3(4), C9–O1–C10–C11 158.2(3), O1–C10–C11–C12 173.0(3), C10–C11–C12–C13 161.4(3), C11–C12–C13–O2 -62.6(4), C12–C13–O2–C14–179.3(3), C13–O2–C14–C19 13.6(6).

Compound **3** forms red crystals of needle habit. Its structure was solved and refined in the orthorhombic system, space group *Pnma* with four molecules in the unit cell. Structure **3** was refined making an assumption that the electron density in the mean unit cell has higher symmetry than actual molecules. The mean electron density is an average of the molecule and its mirror plane reflection. Thus, the asymmetric unit, being half of the molecule, contains N3–H3 and (C11–H11 and N4) and C9, H9A, H9B atoms with occupation factor equal to ½ (see Fig. 3). Dihedral angle between ring C1–C6 and its symmetry related counterpart (by mirror plane with symmcode: (x, 3/2 -y, z)) is equal to 43.20(4)°.

Structure of **4** was solved in the space group $P2_1/c$ and refined without any special treatment. The asymmetric unit contains one molecule and the unit cell four (Z = 4). Atom numbering scheme is shown in Fig. 4.

Again the imidazolic NH group is not engaged in hydrogen bonding. Bond lengths and valence angles are rather typical. The rings in the molecule are not coplanar. Dihedral angle between rings C5–C10 and C16–C21 equals to 26.72(12)°. Imidazole ring forms dihedral angles of 15.51(13)° with C5–C10 and 17.75(13)° with C16–C21 ring. Stacking interactions seems to play a secondary role in crystal packing due to large slippage of all the rings.

Compound **5** crystallizes in the space group *I2/m* (No. 12, cell choice 3 of *C2/m*). Cell parameters: (*a*, *b*, *c* (Å); *α*, *β*, *γ* (°) = 7.7187 (17), 31.861 (9), 29.749 (6); 90, 94.805 (17), 90). The structure was solved, but not refined to a satisfactory quality and therefore it was not deposited in the Cambridge Database. Raw results indicate the asymmetric unit contains one regular macrocycle molecule and two halves of the two other, chemically identical, macrocycles, both having mirror *m* symmetry. Each macrocyclic molecule is accompanied with a water molecule forming hydrogen bonding with an imidazole N-atom directed to the ring centre.

Compound **6** also forms red needle crystals. Structure of **6** was solved in the space group $P2_12_12_1$ and refined as the 2-component inversion twin (basf refined to meaningless −0.04537+-7.2). Atom labeling scheme is shown inFig. 5. Bond lengths and valence angles are not unusual. The imidazole N–H group is directed to the centre of the macrocycle but no hydrogen bonding is formed.

Etheric O2 atom is placed ca. 1 Å above the common molecular plane. The imidazole ring and C15–C20 phenyl ring are almost coplanar (1.7(7)°) and the other C5–C10 phenyl ring is only slightly twisted forming a dihedral angle equal to 11.2(7) ° to the imidazole ring. Stacking interactions play a marginal role in the crystal packing since the shortest ring inter-centroid distances are greater than 4 Å (based on PLATON results).

3.3. Structure in solution

The structure of 18-membered derivatives bearing 4-methylimidazole, namely compounds **4** and **6**, was investigated in solution using

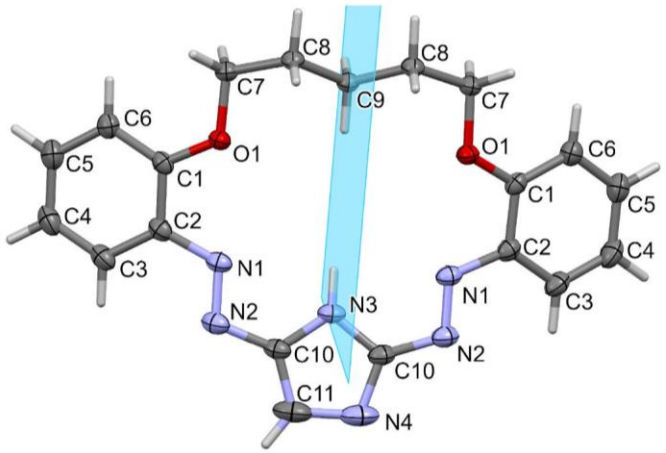

Fig. 3. Molecular view of **3** showing atom labeling scheme of the asymmetric unit and the molecule. Displacement ellipsoids drawn at 50% probability level. Atoms with repeated labels are related by the mirror symmetry (*x*, 3/2 - *y*, *z*). Selected bond lengths (Å) and angles (°): N1–N2 1.2700(14), O1–C1 1.3574 (13), O1–C7 1.4382(13), N1–C2 1.4031(16), N2–C10 1.3918(17), N3–C10 1.3627(14), N4–C10 1.3409(17), N4–C11 1.404(17); valence angles: C1–O1–C7 118.16(9), O1–C7–C8 106.93(9), N2–N1–C2 116.02(10), N1–N2–C10 109.86 (10), N3–C10–N2 123.99(10), N4–C10–N2 126.74(12), N4–C10–N3 109.14 (12); torsions C6–C1–O1–C7 -5.90(16), C1–O1–C7–C8 177.71(9), O1–C7–C8–C9 61.59(13), C7 C8 C9 C8#1 178.46(8).

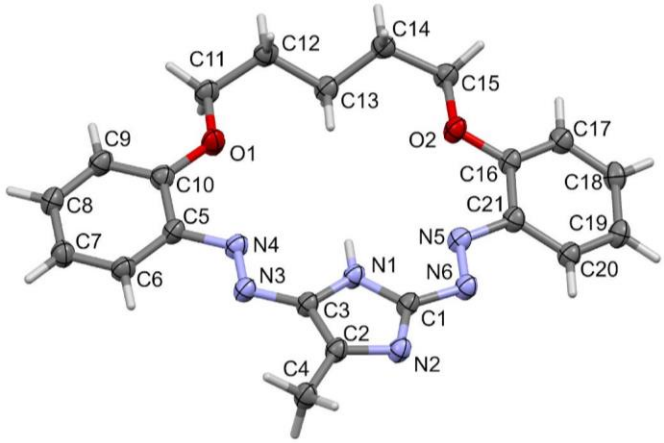

Fig. 4. Molecular view of **4** showing atom labeling scheme. Displacement ellipsoids drawn at 50% probability level. Selected bond lengths (Å) and angles (°): N3–N4 1.278(3), N5–N6 1.273(3), O1–C10 1.352(3), O1–C11 1.440(3), N1–C1 1.345(3), N1–C3 1.365(3), N2–C1 1.331(3), N2–C2 1.371(3), C2–C3 1.386(3), C2–C4 1.491(3), N3–C3 1.374(3), N4–C5 1.403(3); valence angles: C10–O1–C11 118.68(18), C16–O2–C15 117.78(16), C1–N1–C3 106.87(18), C1–N2–C2 104.58(18), N2–C1–N1 112.70(19), N2–C2–C3 109.84(19), N1–C3–C2 105.99(18); torsions: C5–C10–O1–C11 169.6(2), C10–O1–C11–C12 169.5(2), O1–C11–C12–C13 61.8(3), C11–C12–C13–C14 –175.1(2), C12–C13–C14–C15 –178.85(19), C13–C14–C15–O2 -60.5(3), C16–O2–C15–C14 –177.98(19).

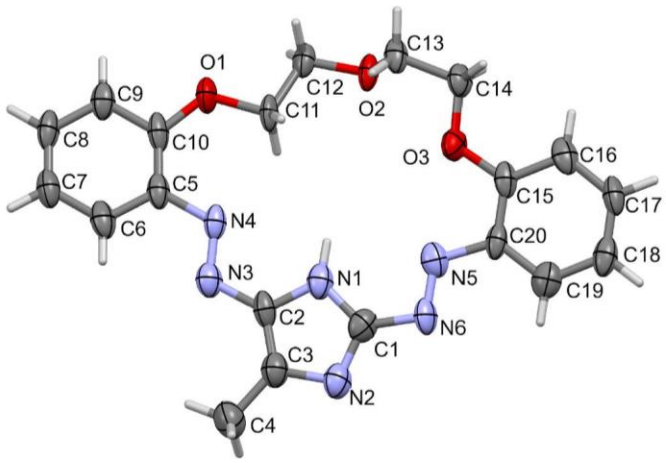

Fig. 5. Molecular view of **6** showing atom labeling scheme. Displacement ellipsoids drawn at 50% probability level. Selected bond lengths (Å) and angles (°): N3–N4 1.290(13), N5–N6 1.269(14), N1–C1 1.363(15), N1–C2 1.372(14), C2–C3 1.367(17), C3–C4 1.491(17), O1–C10 1.385(14), O1–C11 1.430(12), O2–C12 1.435(12), O2–C13 1.437(12); valence angles: C10–O1–C11 124.2 (10), C12–O2–C13 111.9(8), C15–O3–C14 119.5(8), N2–C1–N1 112.2(11), C1–N2–C3 104.5(10), C2–C3–N2 109.4(11), C3–C2–N1 107.8(11), C1–N1–C2 106.0(11); torsions: C5–C10–O1–C11 –2.4(19), C10–O1–C11–C12n 175.6(9), O1–C11–C12–O2 -178.6(8), C11–C12–O2–C13 –85.4(11), C12–O2–C13–C14 169.2(10), O2–C13–C14–O3 -69.1(12), C13–C14–O3–C15 –175.5(9), C14–O3–C15–C16 –4.4(16).

NMR spectroscopy to find out if the linker type affects the position of N–H imidazole proton. The ROESY spectrum of the **4** clearly indicates that the aromatic proton is bound to the nitrogen N1(cf. crystal structure Fig. 6) of imidazole, setting the N–H proton inside the molecule's macrocyclic ring. The proton exhibits the ROE effect to the methylene group of the aliphatic chain. If the proton was bound to the second imidazole nitrogen (N2), then a strong cross-space correlation to the methyl group should be observed in the ROESY spectrum.

The ROESY spectrum of **6** (Fig. S16a) does not show diagnostic effects, which could define the position of the aromatic N–H proton. Only on the basis of the lack of interaction with the methyl group can it be suggested that the discussed proton is also bound to the same nitrogen of imidazole ring, like in the case **4**.

3.4. Lipophilicity

The lipophilicity of newly obtained compounds **1**–**4** and oligoether analogs **5**–**8** with imidazole and 4-methylimidazole residues were determined to link this parameter with their chromoionophoric properties when studied in solution and incorporated in the receptor layer. The lipophilicity of these compounds has not been determined before. The lipophilicity ($logP_{TLC}$) parameters determined using reverse phase thin layer chromatography method [48,60,66] for macrocycles **1**–**8** are presented in Fig. 7 and collected in Table S1.

As expected, the $logP_{TLC}$ values obtained for compounds (**1**–**4**) with a hydrocarbon chain are greater than those received for macrocyles (**5**–**8**) with an oligoether linkage. However, the exception is compound **6**, which, despite having a shorter chain, has a higher lipophilicity value than the rest of the oxygen analogs. In addition, the type of substituent in the imidazole structure also affects the $logP_{TLC}$ value - 4-methylimidazole derivatives are more lipophilic than macrocyles (**1**, **3**, **5** and **7**) bearing unsubstituted imidazole.

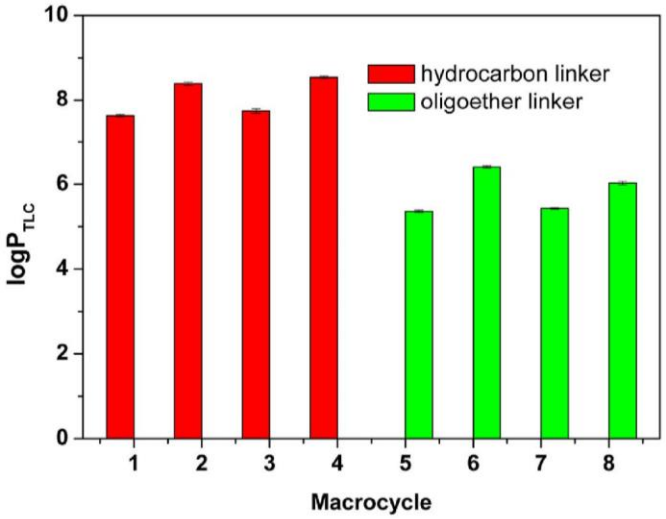

Fig. 7. Comparison of lipophilicity parameter ($logP_{TLC}$) for macrocycles **1**–**8**.

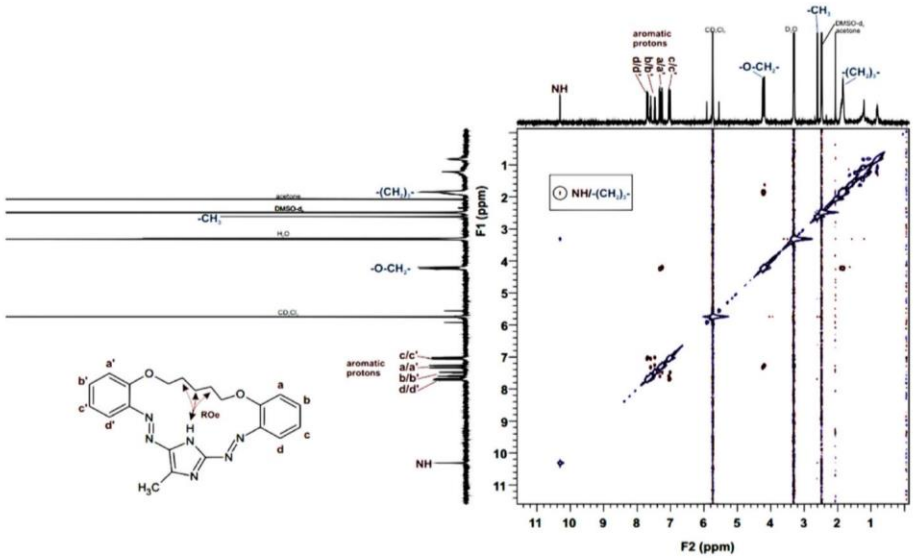

Fig. 6. ROESY spectrum of **4** in DMSO-d_6.

3.5. Acid base-properties of novel macrocycles 1-4

Color properties of macrocyclic compound **1**–**8** are affected by the presence of the methyl group in the imidazole ring. In general 4-methylimidazole derivatives have deeper colors both in acetonitrile and its mixture with water.

The acid-base properties of the newly obtained compounds **1**–**4** were tested in acetonitrile and in a mixture of acetonitrile:water (9:1, v/v). In all cases, more or less intense changes in the color of solutions are observable, both in the presence of *p*-toluenesulfonic acid (TsOH) and tetra-*n*-butylammonium hydroxide (TBAOH) (Fig. S17). In the case of compounds **2**–**4**, the addition of water to acetonitrile causes a partial or complete color withdrawal to the color corresponding to macrocyclic compounds in acetonitrile. Only for compound **1** a color change from orange to yellow is maintained in the presence of *p*-toluenesulfonic acid in a solution of acetonitrile:water 9:1 (v/v). Color changes caused by the pH alteration are relatively more distinct for oligoether bearing macrocycles **5**–**8**. The observed color changes can be explained by the course of absorption spectra registered in the presence of *p*-toluenesulfonic acid. It is exemplified by absorption spectra registered for spectrophotometric titration of compounds **1**–**4** with TsOH in acetonitrile (Fig. S18). The presence of acid is manifested by the increase of the intensity of the absorption bands below 450 nm. The main absorption band corresponding to protonated form is slightly red shifted, however it largely overlaps the main absorption band. In Fig. S19 spectral changes upon titration of compounds **1**–**4** with TBAOH in acetonitrile are presented. Bands corresponding to deprotonated forms of macrocycles are observed at ~510 nm (for **1** and **3**) and ~540 nm (for **2** and **4**). It explains more significant color changes of solutions from orange to purple of compounds **2** and **4** and only a deepening of the color in the case of solutions of compounds **1** and **3**. In Table S2 UV–Vis spectral characterization of compounds **1**–**4** in acetonitrile is presented.

Color properties of macrocyclic compound **1**–**8** are affected by the presence of the methyl group in the imidazole ring. In general 4-methylimidazole derivatives have deeper colors both in acetonitrile and its mixture with water than imidazole bearing macrocycles. When comparing the position of the longwave absorption maximum (Fig. 8) in acetonitrile for 4-methylimidazole derivatives and imidazole ones it is well seen that the last absorbs at lower wavelengths. Comparing the position of absorption bands it can be concluded that excitation energy for 4-methylimidazole derivatives is lower. The electronic effect of the methyl group can contribute to this phenomena. However one of the factors which affect the absorption of light is geometry of the molecule. If a molecule is planar then the energy of excitation is lower and as a result the absorption maximum is bathochromically shifted when comparing molecules of similar type, but of disordered planarity. This can find confirmation in comparison of crystal structures of molecules **3** and **4** (having in mind that the direct comparison cannot be done, because of the different chemical environment of the molecule in a solid state and in solution). Molecule of compound **4** is more planar than the molecule of macrocycle **3**. And probably thus 4-metyhlimidazole macrocyclic azoderivatives have deeper colors.

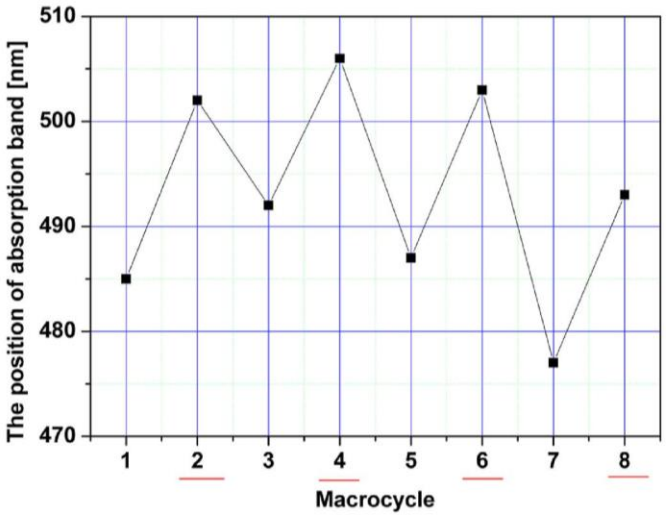

Fig. 8. Comparison of the position of the longwave absorption bands of macrocycles **1**–**4** in acetonitrile (No. of 4-methylimidazole derivatives are red underlined).

3.6. Metal cation complexation of in solution

The first step of the study of chromoionophic properties of compounds **1**–**8** included the investigation of color changes of solutions in the presence of metal salts. In Fig. S20 color of the solutions of compounds **1**–**4** (qualitative tests carried out as an addition to the solution of the macrocyclic compound of excess salt in solid form) in the presence of alkali and alkaline earth metal perchlorates. The presence of the above metal perchlorates has no significant effect on the color of solutions of compounds **1**–**4** with hydrocarbon linker in acetonitrile and acetonitrile: water (9:1, v/v) solvent system. On the other hand, the color of solutions of oligoether derivatives **5**–**8** is affected by the presence of alkali and alkaline earth metal perchlorates. Color changes from orange to yellow. The different affinity of compounds **1**–**4** and **5**–**8** to alkali and alkaline earth metal cations can be explained on the basis of the hard and soft acid and bases theory. Alkali and alkaline earth metal cations are hard acids interacting with hard bases. Oxygen atoms act as hard donor centers in oligoether moiety. Macrocycles **5**–**8** are richer in coordination oxygen atoms, thus their affinity towards hard metal cations is higher. The presence of water - acting as a competitive ligand - causes a partial or complete return to the color corresponding to the original color of the macrocycle solution, which is an effect of high hydratation energies of alkali and alkaline earth metal cations in water.

Besides oxygen coordination centers in investigated macrocycles nitrogen atom(s) of azo group(s) and imidazole residue can also serve as donor atoms in metal complexation. Nitrogen is softer than oxygen donor thus the complex formation with softer metal cation can be obviously expected. The results of quantitative tests for selected heavy metal perchlorates are presented in Fig. 9. The presence of heavy metal perchlorates affects the color of solutions of both groups of investigated macrocycles: hydrocarbon **1**–**4** and oligoether linked **5**–**8**. Solutions of **1**–**4** change color from orange/red to red/purple in the presence of lead (II) perchlorate. The presence of water causes an increase of color intensity in the presence of copper(II) and lead(II) perchlorates and a color withdrawal to the initial color of the solution in the presence of zinc(II) and cadmium(II) ions. The exception is the solution of **1**, for which color changes from orange to yellow in the presence of cadmium(II) in acetonitrile and its mixture with water. Unfortunately this selective color change is observable only when a high excess of cadmium(II) perchlorate is used. This limits the potential applications of macrocycle **1** as cadmium selective probe in real e.g. environmental samples.

Among oligoether derivatives **5**–**8** a solution of **5** shows the less distinct color changes caused by the presence of heavy metal perchlorates. Only a slight color change is observed in the presence of zinc(II) and lead(II) perchlorates in acetonitrile:water mixture (9:1, v/v). The solutions of compounds **6** and **8** change color from orange to purple in the presence of copper(II) and lead(II) perchlorates in acetonitrile and for **6** color change is still observable in water containing the solvent system. Solution of compound **7** changes color in the presence of copper (II) salt from orange to red in acetonitrile and to purple in a mixture of acetonitrile:water (9:1, v/v). In the mixture with water, a change in color is observed in the presence of nickel(II) and zinc(II) perchlorates for solutions of compounds **7** and **8**.

On the basis of the qualitative research, it can be assumed that the compounds **1**–**4** with a hydrocarbon chain present promising heavy

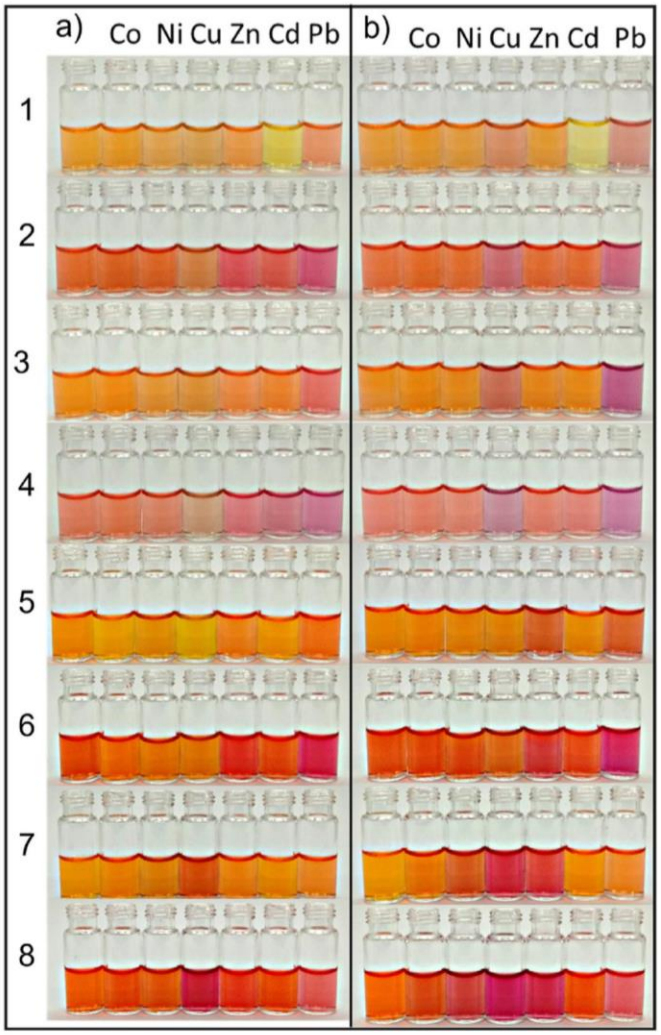

Fig. 9. Color changes of macrocyclic compounds **1–8** in the presence of selected heavy metal perchlorates in a) acetonitrile and b) acetonitrile:water (9:1,v/v) solutions.

metal receptors in water containing solvent system. The greater selectivity towards heavy metal ions compared to oligoether analogs **5–8** can be explained by the reduction in the number of hard coordination centers in the molecule.

3.6.1. Lead(II) complexes

Observing the color changes in qualitative tests for macrocycles **1–8** heavy metal cation complexation was investigated by UV–Vis absorption spectrophotometry in acetonitrile and acetonitrile:water (9:1, v/v) solvent system. Changes in the absorption spectra of solutions of compounds **1–4** and **5–8** during titration with lead(II) perchlorate in acetonitrile are shown in Fig. S21 and Fig. S22 respectively. Complex formation with lead(II) is connected with formation of a new absorption band. However, absorption bands of macrocycles and their complexes are poorly separated, thus only a slight change in color upon complexation is observable. Spectral changes are more distinct for **1–4** than for **5–8** titration experiments. In a mixed solvent system - acetonitrile:water (9:1, v/v) – band separation for **3** and **4** and their complexes is ca. 50 nm (Fig. 10). In case of compounds **1** and **2** upon spectrophotometric titration a wide band of the complex is formed in the range of 530–650 nm and 560–690 nm, respectively.

Spectral changes upon UV–Vis titration of **5–8** with lead(II) perchlorate in acetonitrile:water (9:1, v/v) are shown in Fig. 11. Spectral shift between the absorption band of macrocycle and its complex with lead(II) is ca. 50 nm for **5** and **6**. Complex band is well pronounced. For **7** and **8** spectral shifts are also observed, however the complex absorption bands are less developed.

On the basis of Job's plots [71], it can be concluded that complex of 3:2 (ligand:cation) stoichiometry is formed in the systems **1**-Pb(II), **2**-Pb(II), **3**-Pb(II) and **4**-Pb(II), both in acetonitrile and in the mixture with water (Fig. S23 and Fig. S24, respectively). Stoichiometry of 3:2 (crown:Pb(II)) in acetonitrile was earlier confirmed for pyrrole bearing macrocycles [60], so a similar mode, namely triple-decker sandwich type complex, can be also proposed for imidazole derivatives. Stability constant values (logK) of the complexes of **1–8** with lead(II), calculated from titration data using the OPIUM program [67] are presented in Fig. 12 and summarized in Table S3.

In acetonitrile, the highest values of stability constant (logK) have lead(II) complexes of 21-membered crowns **7–8**, 19.66 ± 0.10 and 20.16 ± 0.12, respectively. Macrocycles of 17- and 18-membered rings form complexes of lower and comparable values of stability constants (log K ~18), independent of the type of linker (hydrocarbon/oligoether). However, the lowest value, 17.24 was found for the lead(II) complex of macrocycle **5**. The value of the stability constant of lead(II) complexes is influenced by the size of the macroring, which defines the size of the molecular cavity. 21-membered crowns form stronger complexes with lead(II) than 17- and-18 membered macrocycles. Similar trend in stability constant values was found for pyrrole bearing macrocycles [60]. Moreover, lead(II) complexes formed by macrocyclic compounds bearing 4-methylimidazole residue (**2**, **4**, **6** and **8**) are characterized by higher values of stability constants compared to their imidazole analogs. It can be another confirmation of the effect of the methyl substituent in heterocyclic ring on the geometry of the molecule. When a molecule is more planar the accessibility of binding sites is better and ion is bound more efficiently. The trend of stability constant values of lead(II) complexes is similar in acetonitrile:water (9:1,v/v). Not surprisingly in mixed solvent system stability constant values are lower than in acetonitrile.

3.6.2. Copper(II) recognition in solution

Due to color changes observed during qualitative tests in the presence of copper(II) perchlorate, for compounds **1–4** spectroscopic titration with copper(II) perchlorate was carried out in acetonitrile and the mixture of this solvent with water (Fig. S25 and Fig. S26). The registered spectra are characterized with an increase of band intensity in the 310–450 nm wavelength range and the formation of a broad bathochromically shifted band λ = 550–650 nm. The changes, similar to the spectral changes observed in the presence of TsOH, are not spectacular. On the basis of titration experiments the determination of a reliable value of stability constant for copper(II) complexes was not possible.

3.7. Metal ion recognition in receptor layers

3.7.1. Preliminary studies

Macrocycles **1–8** were tested as lead(II) and copper(II) receptors upon immobilization in a solid matrix. For current studies porous glass (PG-PS) was used. In preliminary studies the content of chromoionophore in solid material was established as 0.5 mg per g of porous glass.

Materials with compounds **1** and **2** have shown no color change in the presence of copper(II) and lead(II) nitrates. In Fig. 13 color changes (photos were taken using Smartphone camera) of sensors with chromoionophores **3–8** after contact with solutions of different concentrations of copper(II) or lead(II) nitrate are presented. Observable color changes, which can be traced by "the naked eye" were found to more or less degree for all sensors. However, in the case of materials with chromoionophores **4**, **6** and **8** the observed color changes were more distinct than for sensors with compounds **3**, **5** and **7**. Color changes were from the orange/red to violet/blue depending on the macrocycle and the metal nitrate. More significant color change was observed for lead(II) nitrate then for copper(II).

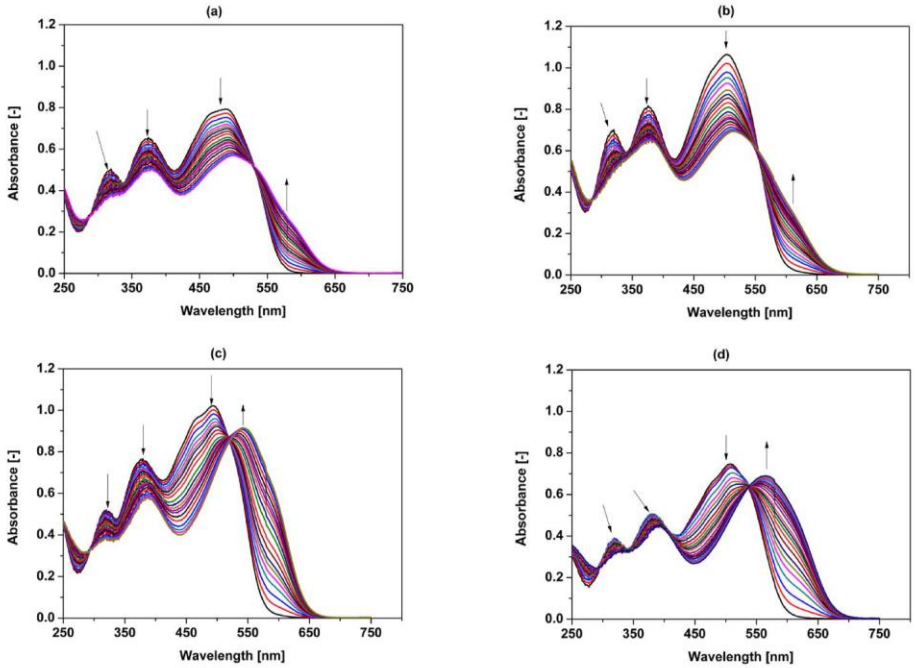

Fig. 10. Changes in absorption spectra of **1**–**4** during spectrophotometric titration with lead(II) perchlorate in acetonitrile:water (9:1, v/v) mixture: a) **1** ($c_1 = 4.97 \times 10^{-5}$ M) ($c_{Pb} = 0$–6.97×10^{-5} M); b) **2** ($c_2 = 4.96 \times 10^{-5}$ M) ($c_{Pb} = 0$–8.03×10^{-5} M); c) **3** ($c_3 = 5.09 \times 10^{-5}$ M) ($c_{Pb} = 0$–1.97×10^{-4} M); d) **4** ($c_4 = 4.91 \times 10^{-5}$ M) ($c_{Pb} = 0$–2.43×10^{-4} M).

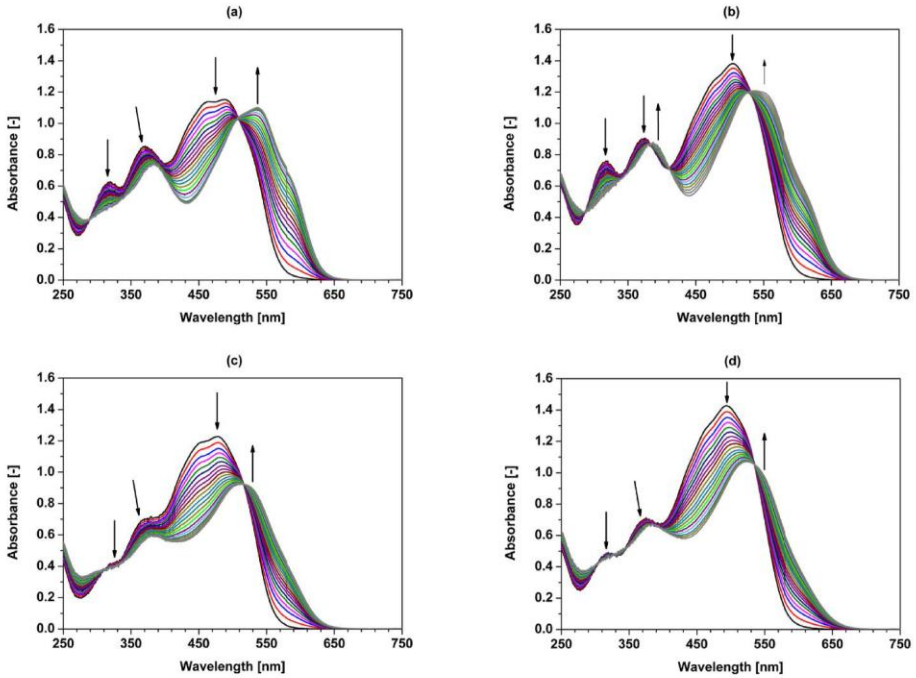

Fig. 11. Changes in absorption spectra of **5**–**8** during spectrophotometric titration with lead(II) perchlorate in acetonitrile:water (9:1, v/v) mixture: a) **5** ($c_5 = 4.97 \times 10^{-5}$ M) ($c_{Pb} = 0$–7.11×10^{-5} M); b) **6** ($c_6 = 4.99 \times 10^{-5}$ M) ($c_{Pb} = 0$–7.58×10^{-5} M); c) **7** ($c_7 = 4.90 \times 10^{-5}$ M) ($c_{Pb} = 0$–9.46×10^{-5} M); d) **8** ($c_8 = 5.00 \times 10^{-5}$ M) ($c_{Pb} = 0$–8.52×10^{-5} M).

3.7.2. PG-PS sensor layers – the effect of amount of chromoionophore

The amount of chromoionophore can affect the color response towards analytes. Thus to optimize the amount of chromoionophore, sensor materials with different quantities (0.25, 0.50, 0.75 and 1.00 mg/g) of macrocycles **3**–**8** were prepared. The color response towards the presence of copper(II) and lead(II) nitrates is shown in Fig. 14 taking the material with immobilized macrocycle **6** as an example. The lowest amount of chromoionophore, namely 0.25 mg/g, seems to be not sufficient to observe significant color changes. This can be an effect of the insufficient amount of chromoionophore for complex formation. On the other hand, the use of higher amounts, 0.75 and 1.00 mg/g, results in material which gives no color change - red sensor material changes the hue of the color in the presence of copper(II) and lead(II) nitrates. The higher concentration of chromoionophore can affect its organization in

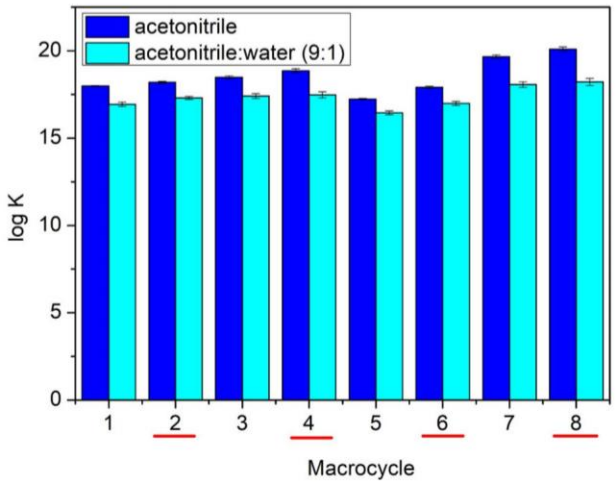

Fig. 12. Comparison of stability constants (logK) of 3:2 (crown:Pb(II)) complexes of macrocycles **1**–**8** (4-methylimidazole derivatives are red underlined) in acetonitrile and acetonitrile:water (9:1, v/v) solvent system.

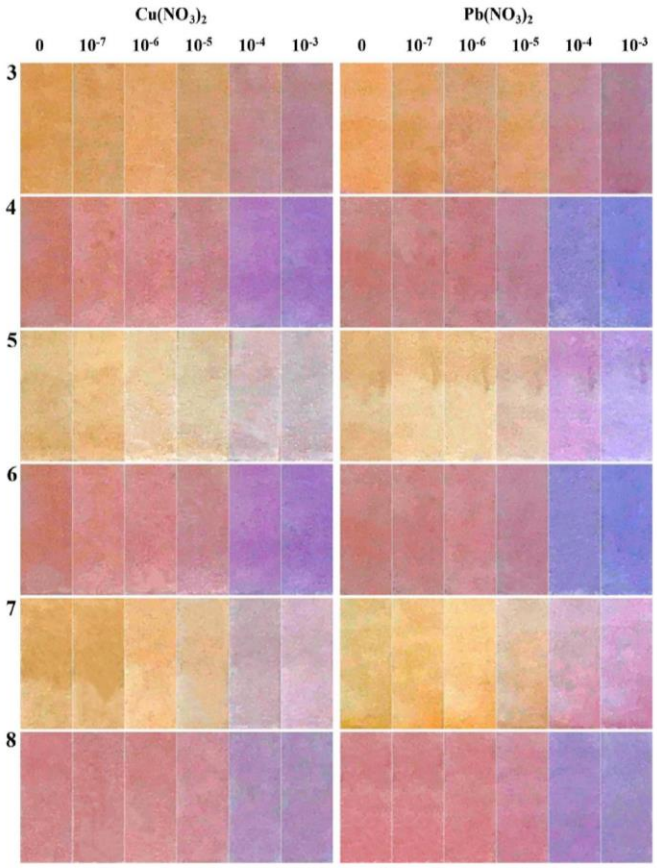

Fig. 13. Color changes of sensor layers with compounds **3**–**8** (0.5 mg/g) in solutions of different concentrations [M] of copper(II) or lead(II) nitrate.

solid material which makes complex formation not fully effective. On the basis of above, the amount of 0.5 mg/g seems to be optimal when considering the color response of sensing material. Thus materials containing this amount of chromoionophores were used in further studies.

3.7.3. Response time

Response time is one of the important factors when considering the

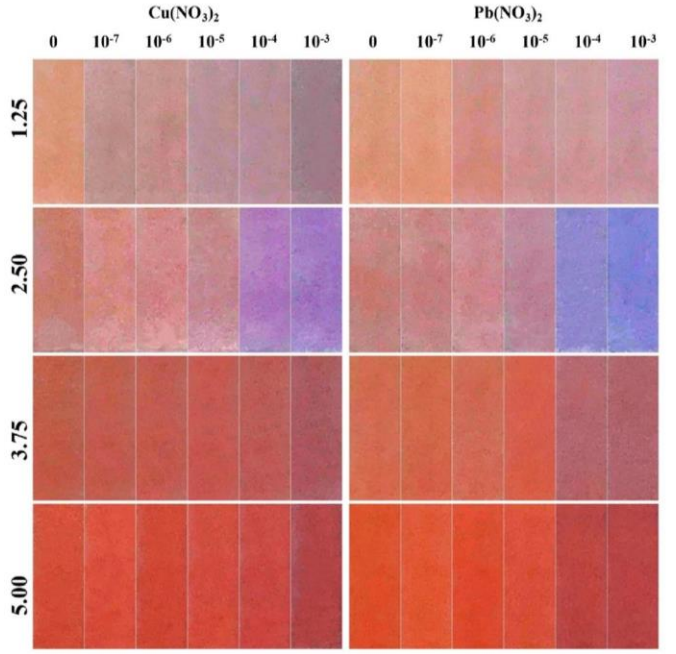

Fig. 14. Color changes of sensor layers with compound **6** - used in different amounts (mg/g) - after contact with solutions of different concentrations [M] of copper(II) or lead(II) nitrates.

applicability of receptor layers as sensor material. To determine the response time, experiments where sensor layers were immersed in solution copper(II) of lead(II) nitrate (10^{-4} M or 10^{-5} M) with contact time up to 10 min were carried out. As a response, the change of the ΔE_{RGB} parameter as a function of time needed for constant optical signal setting up was taken. The sensors were found to reach 95% of the final signal (t_{95}) within 3 min for materials with compound **3**–**6** and 4 min for with macrocyles **7** and **8** (Fig. 15)

3.7.4. Interfering ions

The response of prepared sensor layers towards copper(II)/lead(II) was investigated in the presence of several interfering metal nitrates: sodium, potassium, calcium, magnesium, strontium, barium, nickel(II), copper(II), zinc(II) and lead(II) at fixed pH 6. In Fig. 16 the influence of addition of 10-fold molar excess of interfering ion salt on the color change ΔE_{RGB} of sensor material immersed in 10^{-4} M solution of copper (II) or lead(II) nitrate is shown. From Fig. 16 it can be concluded that during the detection/determination of lead(II), significant color changes are observed for copper(II), and when copper(II) is the main analyte, lead(II) must be considered as the most interfering cation.

3.7.5. Linear response

Linear response range, defined as the change of ΔE_{RGB} vs. copper(II) or lead(II) concentration was determined for sensor layers with macrocycles **3**–**8**. In Fig. S27 the dependence of color change (ΔE_{RGB}) vs. concentration of copper(II) for materials with compounds **3**–**8** is shown. The linear response of sensor layers (Table S4) with compounds **4**–**8** toward copper(II) are in range $1.0 \times 10^{-6} - 1.0 \times 10^{-3}$ M, only for sensor with chromoionophore **3** have narrower range $1.0 \times 10^{-5} - 1.0 \times 10^{-3}$ M. The lowest LOD 4.09×10^{-7} M was obtained for a sensor with compound **7**.

All linear response ranges for lead(II) for materials with macrocycles **3**–**8** are collected in Table S5 and curves are shown in Fig. S28. The narrower range of linear response $1.0 \times 10^{-5} - 1.0 \times 10^{-3}$ M was obtained for sensor material with compound **3**. The rest of investigated materials are characterized by a linear response range within $1.0 \times 10^{-6} - 1.0 \times 10^{-3}$ M with the lowest LOD = 2.84×10^{-7} M for optical sensor

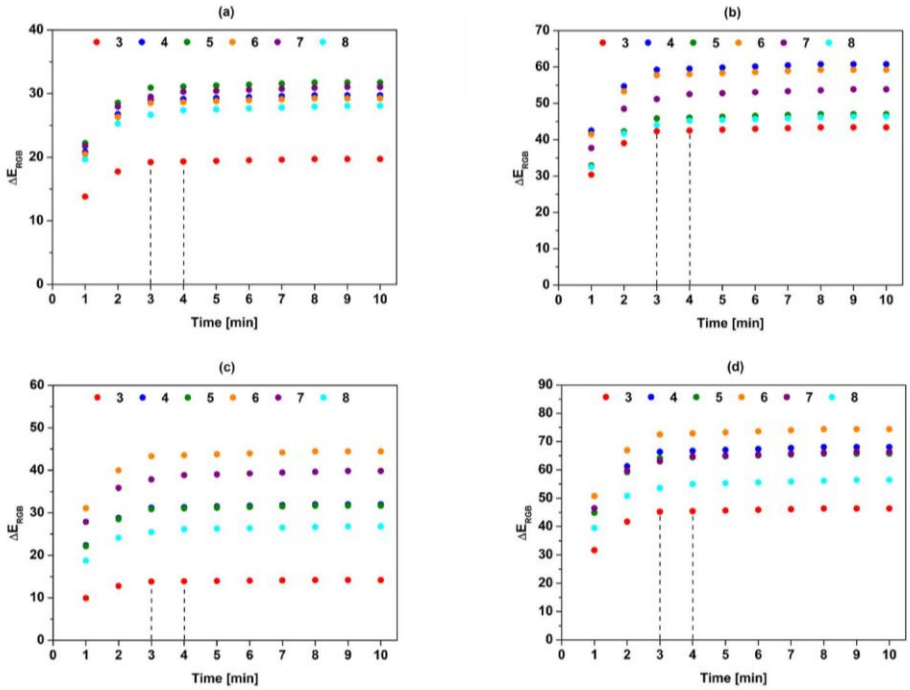

Fig. 15. The color change (ΔE_{RGB}) of sensor layers with chromoionophores **3–8** upon immersion in metal nitrates: a) copper(II) 10^{-4} M, b) copper(II) 10^{-5} M, c) lead (II) 10^{-4} M and d) lead(II) 10^{-5} M over time.

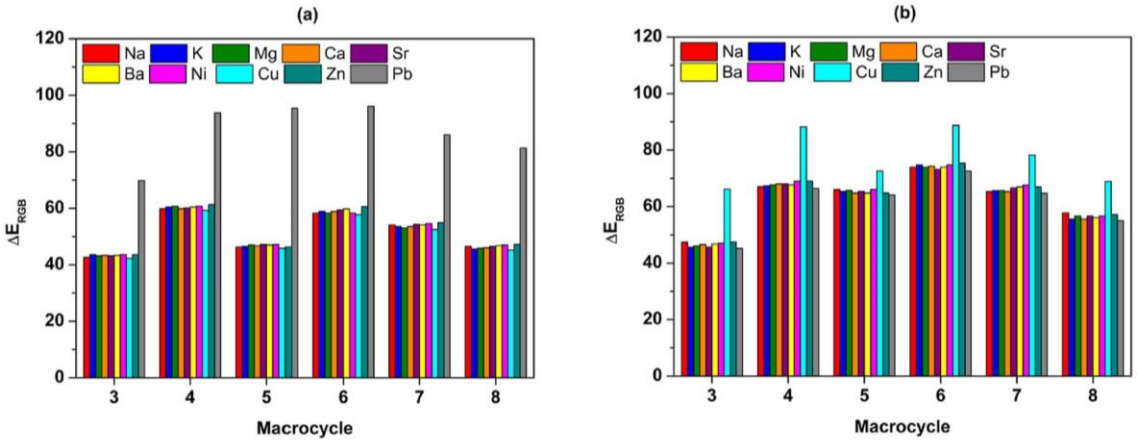

Fig. 16. Interferences of several metal cations (used in 10-fold molar excess), to color change (ΔE_{RGB}) of sensing layers with chromoionophores (0.5 mg/g) **3–8** towards: a) copper(II) and b) lead(II) nitrate at pH 6.

containing crown **6**.

The weaker point of the proposed optical sensors is their inability to be regenerated. While the color of the sensor used to detect copper(II) or lead(II) returns to its original color after immersion in an acid solution (0.1 M nitric acid), repeated placement in a salt solution does not generate a color change. Therefore, these sensors should be considered as single-use materials.

3.7.6. Applications for real samples analysis

The possibility of application of the proposed sensor layers was assessed on three samples of spiked tap water from different regions of northern Poland. All measurements were done at pH 6.0. Comparison of the recovery results obtained for materials with chromoionophores **3–8** upon immersion of the sensor layer in samples with added copper(II) solution of different concentrations is collected in Table S6. The recoveries are at least about 97.13–104.40% (n = 3) for colorimetric detection (ΔE_{RGB}) for copper(II) concentrations in range from 1.0×10^{-6} M to 1.0×10^{-4} M. Analogous tests were carried out for lead(II) at the same concentration range. In this case recoveries were within 97.81–103.95% (n = 3) – Table S7.

3.7.7. Comparison with the other reported sensing materials

In Table 2 the properties of selected lead(II) and copper(II) selective sensing materials obtained in recent years and described in literature are listed for comparison with the materials obtained in this work.

From Table 2 it can be concluded that materials based on commercial porous glass obtained by us have more or less comparable properties to solutions described in literature. In comparison with other sensors which are based on silica materials, which use mostly covalently bonded sensing molecules, the main advantage of proposed materials is their facile preparation. Compared with classical optodes the proposed materials are prepared with a limited number of components. Thus the usage of chemicals in such an approach is minimized. The application of colorimetric detection with widely used mobile devices makes the

Table 2
Comparison of obtained sensing materials with already existing ones.

Copper (II) sensing materials						
Chromoionophore	Support	Method	Response time [min]	Linear response [M]	LOD [M]	Reference
HIBIN[a]	Sol-gel	Absorbance	2	$9.1 \times 10^{-8} - 1.1 \times 10^{-5}$	1.8×10^{-8}	[72]
Schiff base	Sol-gel	Absorbance	2	$8.5 \times 10^{-8} - 1.0 \times 10^{-5}$	1.5×10^{-8}	[73]
HQDB[b]	Hybrid Monolith	Absorbance	2	$4.7 \times 10^{-9} - 1.6 \times 10^{-6}$	7.1×10^{-9}	[74]
TPDP[c]	Mesoporous Silica	Absorbance	60–300	$3.2 \times 10^{-8} - 1.6 \times 10^{-6}$	4.4×10^{-9}	[75]
Hydroxyazocompound	CTA	Absorbance	3	$5.4 \times 10^{-8} - 2.5 \times 10^{-5}$	7.2×10^{-8}	[48]
		Colorimetric		$4.3 \times 10^{-7} - 2.5 \times 10^{-5}$	4.1×10^{-7}	
7	PG-PS	Colorimetric	4	$1.0 \times 10^{-6} - 1.0 \times 10^{-3}$	4.1×10^{-7}	This work
Lead(II) sensing materials						
Chromoionophore	Support	Method	Response time [min]	Linear response [M]	LOD [M]	Reference
DPDB[d]	Mesoporous Silica	Absorbance	40–180	$1.5 \times 10^{-11} - 7.8 \times 10^{-7}$	8.7×10^{-10}	[76]
DPAP[e]	Mesoporous Silica	Absorbance	5–15	$2.4 \times 10^{-8} - 9.7 \times 10^{-7}$	5.0×10^{-9}	[77]
Dithizone	Chitosan-Silica	Absorbance	3	$9.7 \times 10^{-7} - 5.3 \times 10^{-6}$	5.3×10^{-7}	[78]
HMBA[f]	Silica Monolith	Absorbance	30–180	$9.7 \times 10^{-12} - 7.8 \times 10^{-7}$	2.0×10^{-9}	[79]
Diazocrown	CTA	Absorbance	7	$8.1 \times 10^{-8} - 2.2 \times 10^{-5}$	1.2×10^{-8}	[61]
		Colorimetric		$7.8 \times 10^{-7} - 2.1 \times 10^{-4}$	8.6×10^{-7}	
6	PG-PS	Colorimetric	3	$1.0 \times 10^{-6} - 1.0 \times 10^{-3}$	2.8×10^{-7}	This work

[a] N′-(2-hydroxy-5-iodobenzylidene)isonicotinohydrazide
[b] 4-hexyl-6-(quinolin-8-yldiazenyl)benzene-1,3-diol.
[c] 4-*tert*-octyl-4-((phenyl)diazenyl)phenol.
[d] 4-dodecyl-6-((4-(hexyloxy)phenyl)diazenyl)benzene-1,3-diol.
[e] 4-dodecyl-6-(2-pyridylazo)-phenol.
[f] 6-((2-(2-hydroxy-1-naphthoyl)hydrazono)methyl)benzoic acid.

sophisticated measurement equipment almost no needed.

4. Conclusions

New chromogenic macrocycles containing a hydrocarbon linker and imidazole or 4-methylimidazole were obtained. Synthetic protocol enables the preparation of the macrocycles with satisfactory yields. The properties of the newly obtained macrocycles were compared with macrocycles linked via an oligoether bond. The effect of the type of heterocyclic residue and the type of linker is seen in color properties (deeper colors of 4-methylimidazole derivatives) and in metal cation affinity. The last is affected by the chemical environment, namely acetonitrile or acetonitrile:water mixture or hydrophilic solid support – porous glass. After physical immobilization of the macrocycles on porous glass, a selective color change was observed as an analytical response to the presence of heavy metal cations, namely lead(II) and copper(II). Promising properties, among investigated materials, have sensors based on crowns with oligoether moiety. Among them are an 18-membered crown with 4-methylimidazole (**6**) as lead(II) and 21-membered crown (**7**) with imidazole residue as copper(II) chromoionophore.

The optical sensors obtained by us, compared to many solutions proposed in the literature, are materials with an extremely simple composition: only chromophore and porous glass - which is one of the advantages of the proposed solution. And in conjunction with the fact that macrocyclic chromoionophores are relatively easy to prepare, our proposed approach, although imperfect, seems promising for further research and development of optical sensors. Another possible application of the proposed system, which is out of scope of this article, is the possibility of usage of the materials for detection and capturing of heavy metals from wastewater.

CRediT authorship contribution statement

Błażej Galiński: Conceptualization, Data curation, Formal analysis, Investigation, Methodology, Validation, Visualization, Writing – original draft, Writing – review & editing. **Jarosław Chojnacki:** Data curation, Investigation, Methodology, Visualization, Writing – original draft, Writing – review & editing. **Katarzyna Szwarc-Karabyka:** Data curation, Investigation, Writing – original draft. **Adrian Małkowski:** Data curation, Investigation. **Diana Sopel:** Data curation, Investigation. **Agnieszka Zwolińska:** Data curation, Investigation. **Ewa Wagner-Wysiecka:** Conceptualization, Data curation, Supervision, Validation, Visualization, Writing – original draft, Writing – review & editing.

Declaration of competing interest

The authors declare that they have no known competing financial interests or personal relationships that could have appeared to influence the work reported in this paper.

Data availability

Data will be made available on request.

Acknowledgments

This work was supported by the Faculty of Chemistry, Gdańsk University of Technology, No. 035376 and 036276 — internal grants from statutory funds. The financial support to maintenance of research facilities used in these studies from Gdańsk University of Technology by the DEC-2/2021/IDUB/V.6/Si grant under the SILICIUM SUPPORTING CORE R&D FACILITIES – "Excellence Initiative - Research University" program is gratefully acknowledged.

Appendix A. Supplementary data

Supplementary data to this article can be found online at https://doi.org/10.1016/j.dyepig.2023.111610.

References

[1] Tchounwou PB, Yedjou CG, Patlolla AK, Sutton DJ. Heavy metal toxicity and the environment. In: Luch A, editor. Molecular, Clinical and Environmental Toxicology, 101. Basel: Springer; 2012. p. 133–64. https://doi.org/10.1007/978-3-7643-8340-4_6.
[2] Rehman M, Liu L, Wang Q, Saleem MH, Bashir S, Ullah S, Peng D. Copper environmental toxicology, recent advances, and future outlook: a review. Environ Sci Pollut Res 2019;26:18003–16. https://doi.org/10.1007/s11356-019-05073-6.

[3] Buzea C, Pacheco I. Heavy metals: definition, toxicity, and uptake in plants. In: Faisal M, Saquib Q, Alatar AA, Al-Khedhairy AA, editors. Cellular and molecular Phytotoxicity of heavy metals, Nanotechnology in the life Sciences. Cham: Springer; 2020. https://doi.org/10.1007/978-3-030-45975-8_1.
[4] Belabed BE, Meddour A, Samraoui B, Chenchouni H. Modeling seasonal and spatial contamination of surface waters and upper sediments with trace metal elements across industrialized urban areas of the Seybouse watershed in North Africa. Environ Monit Assess 2017;189. https://doi.org/10.1007/s10661-017-5968-5.
[5] Gan Y, Huang X, Li S, Liu N, Li YC, Freidenreich A, Wang W, Wang R, Dai J. Source quantification and potential risk of mercury, cadmium, arsenic, lead, and chromium in farmland soils of Yellow River Delta. J Clean Prod 2019;221:98–107. https://doi.org/10.1016/j.jclepro.2019.02.157.
[6] Peng H, Chen Y, Weng L, Ma J, Ma Y, Li Y, Islam MS. Comparisons of heavy metal input inventory in agricultural soils in north and south China: a review. Sci Total Environ 2019;660:776–86. https://doi.org/10.1016/j.scitotenv.2019.01.066.
[7] Nassiri O, Rhoujjati A, Moreno-Jimenez E, Hachimi MLEL. Environmental and geochemical characteristics of heavy metals in soils around the former mining area of Zeïda (High Moulouya, Morocco). Water Air Soil Pollut 2023;234. https://doi.org/10.1007/s11270-023-06103-3.
[8] Kannan G, Roy PD, Sundar S, Usha T, Gowranppan M, Kishore PV, Periyasamy R, Johnatan MP, Chokkalingam L. Pollution assessment with respect to five heavy metals in urban soils of the Greater Chennai Region, Southeast Coast of India. Water Air Soil Pollut 2023;234. https://doi.org/10.1007/s11270-022-06031-8.
[9] Yu P, Han Y, Wang M, Zhu Z, Tong Z, Shao XY, Peng J, Hamid Y, Yang X, Deng Y, Huang Y. Heavy metal content and health risk assessment of atmospheric particles in China: a meta-analysis. Sci Total Environ 2023;867. https://doi.org/10.1016/j.scitotenv.2023.161556.
[10] Rivero CI-D, Fry KL, Gillings MM, Barlow CF, Aelion CM, Taylor MP. Sources, pathways and concentrations of potentially toxic trace metals in home environments. Environ Res 2023;220. https://doi.org/10.1016/j.envres.2022.115173.
[11] Rizo OD, Diaz AOC, Ramos AGT, Lopez DR. Heavy metals concentration, pollution indexes, and health risk assessment of urban road dust in the historical center of Havana, Cuba. Environ Monit Assess 2023;195. https://doi.org/10.1007/s10661-022-10875-2.
[12] Wang M, Lv Y, Lv X, Wang Q, Li Y, Lu P, Yu H, Wei P, Cao Z, An T. Distribution, sources and health risks of heavy metals in indoor dust across China. Chemosphere 2022;313. https://doi.org/10.1016/j.chemosphere.2022.137595.
[13] Obiora SC, Chukwu A, Davies TC. Contamination of the potable water supply in the lead – zinc mining communities of Enyigba, Southeastern Nigeria. Mine Water Environ 2019;38:148–57. https://doi.org/10.1007/s10230-018-0550-0.
[14] Andreas AL, Browser SS. Effects of lead and cadmium exposure on oxygen respiration rates of individual Antarctic foraminifera during agglutinated shell formation. J Exp Mar Biol Ecol 2021;537. https://doi.org/10.1016/j.jembe.2021.151514.
[15] Kumar V, Pandita S, Sidhu GPS, Sharma A, Khanna K, Kaur P, Bali AS, Setia R. Copper bioavailability, uptake, toxicity and tolerance in plants: a comprehensive review. Chemosphere 2021;262. https://doi.org/10.1016/j.chemosphere.2020.127810.
[16] Kumar A, Kumar A, Cabral-Pinto M, Chaturvedi AK, Shabnam AA, Subrahmanyam G, Mondal R, Gupta DK, Malyan SK, Kumar SS, Khan SA, Yadav KK. Lead toxicity: health hazards, influence on food chain, and sustainable remediation approaches. Int J Environ Res Publ Health 2020;17. https://doi.org/10.3390/ijerph17072179.
[17] Can H, Ozyigit II, Can M, Hocaoglu-Ozyigit A, Yalcin IE. Environment-based impairment in mineral nutrient status and heavy metal contents of commonly consumed leafy vegetables marketed in Kyrgyzstan: a case study for health risk assessment. Biol Trace Elem Res 2020;199:1123–44. https://doi.org/10.1007/s12011-020-02208-6.
[18] Sabry MIE, Stino FKR, El-Ghany WAA. Copper: benefits and risks for poultry, livestock, and fish production. Trop Anim Health Prod 2021;53. https://doi.org/10.1007/s11250-021-02915-9.
[19] Ma C, Liu F, Xie P, Zhang K, Yang J, Zhao J, Zhang H. Mechanism of Pb absorption in wheat grains. J Hazard Mater 2021;415. https://doi.org/10.1016/j.jhazmat.2021.125618.
[20] Aalami AH, Hoseinzadeh M, Manesh PH, Sharahi AJ, Aliabadi EK. Carcinogenic effects of heavy metals by inducing dysregulation of microRNAs: a review. Mol Biol Rep 2022;49:12227–38. https://doi.org/10.1007/s11033-022-07897-x.
[21] Wang C-C, Zhang Q-C, Kang S-G, Li M-Y, Zhang M-Y, Xu W-M, Xiang P, Ma LQ. Heavy metal(loid)s in agricultural soil from main grain production regions of China: bioaccessibility and health risks to humans. Sci Total Environ 2023;858. https://doi.org/10.1016/j.scitotenv.2022.159819.
[22] Elstrott B, Khan L, Olson S, Raghunathan V, DeLoughery T, Shatzel JJ. The role of iron repletion in adult iron deficiency anemia and other diseases. Eur J Haematol 2020;104:153–61. https://doi.org/10.1111/ejh.13345.
[23] Tsang T, Davis CI, Brady DC. Copper biology. Curr Biol 2021;31:421–7. https://doi.org/10.1016/j.cub.2021.03.054.
[24] De Souza ID, De Andrade AS, Dalmolin RJS. Lead-interacting proteins and their implication in lead poisoning. Crit Rev Toxicol 2018;48:375–86. https://doi.org/10.1080/10408444.2018.1429387.
[25] Wang X, Shen C, Zhou C, Bu Y, Yan X. Methods, principles and applications of optical detection of metal ions. Chem Eng J 2021;417. https://doi.org/10.1016/j.cej.2021.129125.
[26] Saleema M, Lee KH. Optical sensor: a promising strategy for environmental and biomedical monitoring of ionic species. RSC Adv 2015;5:72150–287. https://doi.org/10.1039/C5RA11388A.
[27] You L, Zha D, Anslyn EV. Recent advances in supramolecular analytical chemistry using optical sensing. Chem Rev 2015;115:7840–92. https://doi.org/10.1021/cr5005524.
[28] Wu J, Kwon B, Liu W, Anslyn EV, Wang P, Kim JS. Chromogenic/Fluorogenic ensemble chemosensing systems. Chem Rev 2015;115:7893–943. https://doi.org/10.1021/cr500553d.
[29] Sharma H, Kaur N, Singh A, Kuwar A, Singh N. Optical chemosensors for water sample analysis. J Mater Chem C 2016;4:5154–94. https://doi.org/10.1039/C6TC00605A.
[30] Ajay PVS, Printo J, Kiruba DSCG, Susithra L, Takatoshi K, Sivakumar M. Colorimetric sensors for rapid detection of various analytes. Mater Sci Eng C 2017;78:1231–45. https://doi.org/10.1016/j.msec.2017.05.018.
[31] Dongare PR, Gore AH. Recent advances in colorimetric and fluorescent chemosensors for ionic species: design, principle and optical signaling mechanism. ChemistrySelect 2021;6:5657–69. https://doi.org/10.1002/slct.202101090.
[32] Kramer J, Kang R, Grimm LM, De Cola L, Picchetti P, Biedermann F. Molecular probes, chemosensors, and nanosensors for optical detection of biorelevant molecules and ions in aqueous media and biofluids. Chem Rev 2022;122:3459–636. https://doi.org/10.1021/acs.chemrev.1c00746.
[33] Chen Z, Zhang Z, Qi J, You J, Ma J, Chen L. Colorimetric detection of heavy metal ions with various chromogenic materials: strategies and applications. J Hazard Mater 2023;441. https://doi.org/10.1016/j.jhazmat.2022.129889.
[34] McCrackena KE, Yoon J-Y. Recent approaches for optical smartphone sensing in resource-limited settings: a brief review. Anal Methods 2016;8:6591–601. https://doi.org/10.1039/C6AY01575A.
[35] Rezazadeh M, Seidi S, Lid M, Pedersen-Bjergaard S, Yamini Y. The modern role of smartphones in analytical chemistry. Trends Anal Chem 2019;118:548–55. https://doi.org/10.1016/j.trac.2019.06.019.
[36] Di Nonno S, Ulber R. Smartphone-based optical analysis systems. Analyst 2021;146:2749–68. https://doi.org/10.1039/D1AN00025J.
[37] Sivakumar R, Lee NY. Recent progress in smartphone-based techniques for food safety and the detection of heavy metal ions in environmental water. Chemosphere 2021;275. https://doi.org/10.1016/j.chemosphere.2021.130096.
[38] Mistlberger G, Crespo GA, Bakker E. Ionophore-based optical sensors. Annu Rev Anal Chem 2014;7:483–512. https://doi.org/10.1146/annurev-anchem-071213-020307.
[39] Xie X, Bakker E. Ion selective optodes: from the bulk to the nanoscale. Anal Bioanal Chem 2015;407:3899–910. https://doi.org/10.1007/s00216-014-8413-4.
[40] Mikhelson KN, Peshkova MA. Advances and trends in ionophore-based chemical sensors. Russ Chem Rev 2015;84:555–78. https://doi.org/10.1070/RCR4506.
[41] Du X, Xie X. Ion-Selective optodes: alternative approaches for simplified fabrication and signaling. Sensor Actuator B Chem 2021;335. https://doi.org/10.1016/j.snb.2020.129368.
[42] Oehme I, Wolfbeis OS. Optical sensors for determination of heavy metal ions. Microchim Acta 1997;126:177–92. https://doi.org/10.1007/BF01242319.
[43] Baldini F, Falai A. Characterization of an optical fibre pH sensor with methyl red as optical indicator. In: Martellucci S, Chester AN, Mignani AG, editors. Optical Sensors and Microsystems: New Concepts, Materials, Technologies. New York: Kluwer Academic Publishers; 2000. p. 53–60. https://doi.org/10.1007/0-306-47099-3_5.
[44] Enke D, Janowski F, Schwieger W. Porous glasses in the 21st century—a short review. Microporous Mesoporous Mater 2003;60:19–30. https://doi.org/10.1016/S1387-1811(03)00329-9.
[45] Ma QJ, Li HP, Yang F, Zhang J, Wu XF, Bai Y, Li XF. A fluorescent sensor for low pH values based on a covalently immobilized rhodamine–napthalimide conjugate. Sensor Actuator B Chem 2012;166–7:68–74. https://doi.org/10.1016/j.snb.2011.12.025.
[46] Muller R, Anders N, Titus J, Enke D. Ultra-thin porous glass membranes — an innovative material for the immobilization of active species for optical chemosensors. Talanta 2013;107:255–62. https://doi.org/10.1016/j.talanta.2012.12.038.
[47] Dalfen I, Borisov SM. Porous matrix materials in optical sensing of gaseous oxygen. Anal Bioanal Chem 2022;414:4311–30. https://doi.org/10.1007/s00216-022-04014-6.
[48] Galiński B, Chojnacki J, Wagner-Wysiecka E. Simple colorimetric copper(II) sensor – spectral characterization and possible applications. Spectrochim Acta Mol Biomol Spectrosc 2023;293. https://doi.org/10.1016/j.saa.2023.122472.
[49] Ghorbanian M, Asghari S, Tajbakhsh M. A new benzothiazole azo dye colorimetric chemosensor for detecting Pb^{2+} ion. Spectrochim Acta Mol Biomol Spectrosc 2023;296. https://doi.org/10.1016/j.saa.2023.122652.
[50] Luboch E, Bilewicz R, Kowalczyk M, Wagner-Wysiecka E, Biernat JF. Azo macrocyclic compounds. Adv Supramol Chem 2003;9:71–162.
[51] Wagner-Wysiecka E, Łukasik N, Biernat JF, Luboch E. Azo group(s) in selected macrocyclic compounds. J Inclusion Phenom Macrocycl Chem 2018;90:189–257. https://doi.org/10.1007/s10847-017-0779-4.
[52] Mortensen KT, Osberger TJ, King TA, Sore HF, Spring DR. Strategies for the diversity - oriented synthesis of macrocycles. Chem Rev 2019;119:10288–317. https://pubs.acs.org/doi/10.1021/acs.chemrev.9b00084.
[53] Amrhein JA, Knapp S, Hanke T. Synthetic opportunities and challenges for macrocyclic kinase inhibitors. J Med Chem 2021;64:7991–8009. https://doi.org/10.1021/acs.jmedchem.1c00217.
[54] Zhang X, Lin L, Li J, Duan S, Long Y, Li J. Recent progress in the synthesis of medium-sized ring and macrocyclic compounds. Chin J Org Chem 2021;41:1878–87. https://doi.org/10.6023/cjoc202010026.

[55] Wagner-Wysiecka E, Luboch E, Kowalczyk M, Biernat JF. Chromogenic macrocyclic derivatives of azoles-synthesis and properties. Tetrahedron 2003;59:4415–20. https://doi.org/10.1016/S0040-4020(03)00618-5.
[56] Luboch E, Wagner-Wysiecka E, Fainerman-Melnikova M, Lindoy LF, Biernat JF. Pyrrole azocrown ethers. Synthesis, complexation, selective lead transport and ion-selective membrane electrode studies. Supramol Chem 2006;18:593–601. https://doi.org/10.1080/10610270600879068.
[57] Wagner-Wysiecka E, Rzymowski T, Fonari MS, Kulmaczewski R, Luboch E. Pyrrole azocrown ethers-synthesis, crystal structures, and fluorescence properties. Tetrahedron 2011;67:1862–72. https://doi.org/10.1016/j.tet.2011.01.027.
[58] Wagner-Wysiecka E, Luboch E, Fonari MS. The synthesis, X-ray structure and metal cation complexation properties of colored crown with two heterocyclic residues as a part of macrocycle. Pol J Chem 2008;82:1319–30.
[59] Wagner-Wysiecka E, Jamrógiewicz M, Fonari MS, Biernat JF. Azomacrocyclic derivatives of imidazole: synthesis, structure, and metal ion complexation properties. Tetrahedron 2007;63:4414–21. https://doi.org/10.1016/j.tet.2007.03.095.
[60] Galiński B, Luboch E, Chojnacki J, Wagner-Wysiecka E. Novel diazocrowns with pyrrole residue as lead(II) colorimetric probes. Materials 2021;14. https://doi.org/10.3390/ma14237239.
[61] Galiński B, Wagner-Wysiecka E. Pyrrole bearing diazocrowns: selective chromoionophores for lead(II) optical sensing. Sensor Actuator B Chem 2022;361. https://doi.org/10.1016/j.snb.2022.131678.
[62] Jamrógiewicz M, Kledzik K, Gwiazda M, Wagner-Wysiecka E, Jezierska J, Biernat JF, Kłonkowski A. Optical recognition elements: macrocyclic imidazole chromoionophores entrapped in silica xerogel. Mater Sci-Pol 2007;25:1044–51.
[63] Dolomanov OV, Bourhis LJ, Gildea RJ, Howard JAK, Puschmann H. OLEX2: a complete structure solution, refinement and analysis program. J Appl Crystallogr 2009;42:339–41. https://doi.org/10.1107/S0021889808042726.
[64] Sheldrick GM. Shelxt - integrated space-group and crystal-structure determination. Acta Crystallogr A 2015;71:3–8. https://doi.org/10.1107/S2053273314026370.
[65] Koziskova J, Hahn F, Richter J, Kozisek J. Comparison of different absorption corrections on the model structure of tetrakis(m_2-acetato)-diaqua-di-copper(II). Acta Chim Slovaca 2016;9:136–40. https://doi.org/10.1515/acs-2016-0023.
[66] Dinten O, Spichiger UE, Chaniotakis N, Gehrig P, Rusterholz B, Morf WE, Simon W. Lifetime of neutral-carrier-based liquid membranes in aqueous samples and blood and the lipophilicity of membrane components. Anal Chem 1991;63:596–603. https://doi.org/10.1021/ac00006a009.
[67] Kyvala M, Lukes I. Program package "OPIUM" (free access) at, https://web.natur.cuni.cz/~kyvala/opium.html.
[68] Abramoff MD, Magalhaes PJ, Ram SJ. Image processing with ImageJ. Biophot Int 2004;11:36–42.
[69] Schneider CA, Rasband WS, Eliceiri KW. NIH Image to ImageJ: 25 years of image analysis. Nat Methods 2012;9:671–5. https://doi.org/10.1038/nmeth.2089.
[70] Gavrilenko NA, Muravyov SV, Silushkin SV, Spiridonovab AS. Polymethacrylate optodes: a potential for chemical digital color analysis. Measurement 2014;51:464–9. https://doi.org/10.1016/j.measurement.2013.11.027.
[71] Job P. Formation and stability of inorganic complexes in solution. Ann Chim 1928;9:113–203.
[72] Shahamirifard SA, Ghaedi M, Montazerozohori M. Design a sensitive optical thin film sensor based on incorporation of isonicotinohydrazide derivative in sol–gel matrix for determination of trace amounts of copper (II) in fruit juice: effect of sonication time on immobilization approach. Ultrason Sonochem 2018;42:723–30. https://doi.org/10.1016/j.ultsonch.2017.12.043.
[73] Parsaeea Z, Karachi N, Razavi R. Ultrasound assisted fabrication of a novel optode base on a triazine based Schiff base immobilized on TEOS for copper detection. Ultrason Sonochem 2018;47:36–46. https://doi.org/10.1016/j.ultsonch.2018.04.007.
[74] Kumar SK, Mohan AM. Porous inorganic/organic hybrid monolith-based solid sensor for the colorimetric analysis of Cu^{2+} ions. J Nanoparticle Res 2021;23. https://doi.org/10.1007/s11051-021-05316-z.
[75] Salman S, Hasan N, Hasan M, Kubra KT, Sheikh C, Rehan AI, Waliullah RM, Rasee AI, Awua E, Hossain MS, Alsukaibi AKD, Alshammari HM, Awual R. Improving copper(II) ion detection and adsorption from wastewater by the ligand-functionalized composite adsorbent. J Mol Struct 2023:1282. https://doi.org/10.1016/j.molstruc.2023.135259.
[76] Awual R, Hasan M. Novel conjugate adsorbent for visual detection and removal of toxic lead(II) ions from water. Microporous Mesoporous Mater 2014;196:261–9. https://doi.org/10.1016/j.micromeso.2014.05.021.
[77] Prabhakaran D, Subashini C, Maheswari MA. Synthesis of mesoporous silica monoliths — a novel approach towards fabrication of solid-state optical sensors for environmental applications. Int J Nanosci 2016;15. https://doi.org/10.1142/S0219581X16600140.
[78] Nur Y, Rohaeti E, Darusman LK. Optical sensor for the determination of Pb(II) based on immobilization of dithizone onto chitosan-silica membrane. Indones J Chem 2017;17:7–14. https://doi.org/10.22146/ijc.23560.
[79] Awual R. Mesoporous composite material for efficient lead(II) detection and removal from aqueous media. J Environ Chem Eng 2019;7. https://doi.org/10.1016/j.jece.2019.103124.

P4 – SUPPLEMENTARY MATERIALS

Chromogenic azomacrocycles with imidazole residue: Structure vs. properties

Błażej Galiński [1], Jarosław Chojnacki [2], Katarzyna Szwarc-Karabyka [3], Adrian Małkowski [1#], Diana Sopel [1#], Agnieszka Zwolińska [1#], Ewa Wagner-Wysiecka [*,1,4]

[1]Department of Chemistry and Technology of Functional Materials, Faculty of Chemistry, Gdańsk University of Technology, Narutowicza Street 11/12, 80-233 Gdańsk, Poland

[2]Department of Inorganic Chemistry, Faculty of Chemistry, Gdańsk University of Technology, Narutowicza Street 11/12, 80-233 Gdańsk, Poland

[3]Nuclear Magnetic Resonance Laboratory, Faculty of Chemistry, Gdańsk University of Technology, Narutowicza Street 11/12, 80-233 Gdańsk, Poland

[4]Advanced Materials Center, Faculty of Chemistry, Gdańsk University of Technology, Narutowicza Street 11/12, 80-233 Gdańsk, Poland

*corresponding author: ewa.wagner-wysiecka@pg.edu.pl

authors of the same degree of contribution given in alphabetical order

Synthesis

*Synthesis of crowns **1-4***

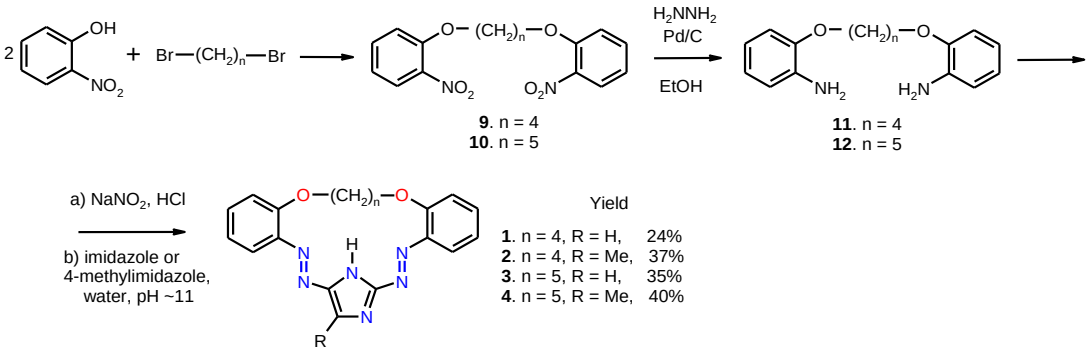

Scheme. Synthesis of macrocyclic compounds **1**-**4** with hydrocarbon linker.

*1,4-bis(2-nitrophenoxy)butane (**9**) and 1,5-bis(2-nitrophenoxy)pentane (**10**)*

Compounds **9** and **10** were prepared analogously as described in the literature [1, 2]. A mixture of 2-nitrophenol (16 mmol), 1,4-dibromobutane (9 mmol) or 1,5-dibromopentane (9 mmol) and anhydrous potassium carbonate (16 mmol) in dry dimethylformamide (6 mL) were stirred and heated at 140 °C for 2 h. The mixture was diluted with cooled water (120 mL) to precipitate crude dinitro derivatives **9** or **10**. Pure compounds **9** and **10** were obtained after crystallization from propan-2-ol (20 mL). **9**: yield 90%, light beige solid, mp 123 – 124 °C (lit. mp 124 °C) [3]; **10**: yield 80%, light beige solid, mp 82 – 83 °C. (lit. mp 83 °C) [3].

*1,4-bis(2-aminophenoxy)butane (**11**) and 1,5-bis(2-aminophenoxy)pentane (**12**)*

Compounds **11** and **12** were obtained using protocols described in the literature [2, 4-8]. The reaction mixture containing compound **9** (5.5 mmol) or **10** (5.5 mmol) and propan-2-ol (50 mL) together with a Pd/C catalyst was magnetically stirred and heated in an oil bath at 58 °C. Aqueous hydrazine solution (80%) was added to the reaction mixture in 4 portions (0.5 mL each). Five hours after the last portion of hydrazine was added, the solution was filtered off to separate the catalyst. The solvent was evaporated under the reduced pressure. Amines were crystallized from propan-2-ol. **11**: yield 90%, white flakes, mp 108 – 109 °C (lit. mp 108 – 110 °C) [3]; **12**: yield 87%, white flakes, mp 60 – 61 °C. (lit. mp 61 – 62 °C) [3].

*Preparation of new diazocrowns **1-4***

The synthesis of diazocrown **1-4** was based on a high dilution approach [2, 4-8]. Three solutions were prepared:

I: Diaminopodand **11** or **12** (1 mmol) and concentrated hydrochloric acid (0.5 mL) in water (20 mL) (DMF or THF in needed amount can be added to increase solubility of amines);

II: Sodium nitrite (2 mmol) in water (30 mL);

III: Imidazole (1 mmol) or 4-methylimidazole (1 mmol) and sodium hydroxide (5 mmol) in water (30 mL).

All solutions were cooled in an ice bath to 0 – 5 °C. Solution II was added portionwise to solution I to obtain the bisdiazonium salt. The combined solutions were left for 30 min in an ice bath. After this time, solutions I-II (bisdiazonium salt) and III were added dropwise to deionized water (300 mL) at pH ~10 (NaOH), within 30 min, ensuring intensive stirring of the reaction system. The pH was controlled during the addition of solutions to the reaction container. After 2 h, the ice bath was removed, and the mixture was left for 24 h at room temperature. The precipitate was filtered off under reduced pressure. Products were isolated by column chromatography using initially dichloromethane and finally dichloromethane:acetone (10:1, v/v) as eluent.

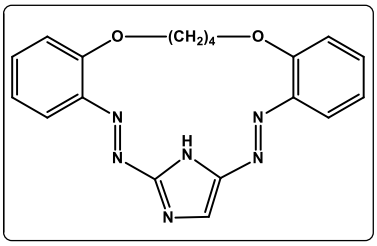

Compound **1**: yield 24%; red solid; mp 204 – 206 °C (with decomposition); R_f = 0.40 (dichloromethane:acetone 20:1); ^{1}H NMR (chloroform-d, 500MHz, δ [ppm]): 2.17 – 2.52 (4H, m), 4.26 – 4.30 (4H, m), 7.09 – 7.15 (2H, m), 7.28 – 7.31 (2H, m), 7.55 (1H, td, J_1 = 1.7 Hz, J_2 = 7.1 Hz), 7.64 (1H, td , J_1 = 1.6 Hz, J_2 = 7.1 Hz), 7.78 (1H, dd, J_1 = 1.6 Hz, J_2 = 7.6 Hz), 7.82 (1H, dd, J_1 = 1.6 Hz, J_2 = 7.6 Hz), 7.96 (1H, s), 10.81 (1H, bs, NH); ^{13}C NMR (chloroform, 125 MHz, δ [ppm]): 159.2, 158.4, 153.2, 145.9, 140.4, 140.3, 136.5, 134.6, 121.4, 121.3, 115.6, 115.3, 115.0, 114.9, 69.5, 69.3, 27.5, 27.3; FTIR (ATR, cm^{-1}): 3436, 3123, 3069, 2956, 2909, 2869, 1587, 1567, 1531, 1485, 1463, 1401, 1380, 1358, 1289, 1306, 1262, 1244, 1224, 1208, 1149, 1111, 1099, 1063, 1031, 990, 968, 938, 905, 858, 840, 769, 741, 727, 670, 641, 604, 556, 534, 507, 482, 458, 439, 417; UV-Vis (acetonitrile): $\lambda_1(\varepsilon_1)$ = 317 (9.36×10^3), $\lambda_2(\varepsilon_2)$ = 373 (1.26×10^4), $\lambda_3(\varepsilon_3)$ = 485 (1.57×10^4); UV-Vis (acetonitrile:water 9:1): $\lambda_1(\varepsilon_1)$ = 318 (1.00×10^4), $\lambda_2(\varepsilon_2)$ = 375 (1.31×10^4), $\lambda_3(\varepsilon_3)$ = 487 (1.60×10^4); HRMS [EI]: 362.1496 calculated for: $C_{19}H_{18}N_6O_2$ 362.1491.

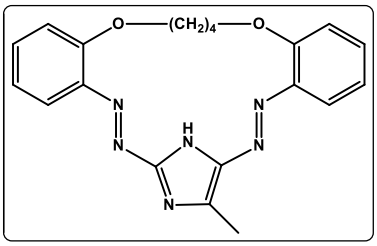

Compound **2**: yield 37%; red solid; mp 276 – 280 °C (with decomposition); R_f = 0.44 (dichloromethane:aceton 20:1); ^{1}H NMR (acetone-d_6, 500MHz, δ [ppm]): 2.13 – 2.19 (4H, m), 2.64 (3H, s), 4.25 (2H, t, J = 4.4 Hz), 4.29 (2H, t, J = 4.7 Hz), 7.08 – 7.14 (2H, m), 7.23 (1H, dd, J_1 = 1.1 Hz, J_2 = 8.2 Hz), 7.29 (1H, dd, J_1 = 1.1 Hz, J_2 = 8.2 Hz), 7.49 – 7.52 (1H, m), 7.61 – 7.64 (1H, m), 7.78 – 7.81 (2H, m), 10.64 (1H, bs, NH); ^{13}C NMR (chloroform-d, 125 MHz, δ [ppm]: 159.4, 158.2, 140.5, 140.3, 136.8, 134.1, 121.4, 121.4, 115.7, 115.0, 110.0, 69.7, 69.4, 27.5, 27.3; FTIR (ATR, cm^{-1}): 3426, 3061, 2909, 2859, 1589, 1574, 1542, 1485, 1456, 1377, 1338, 1304, 1285, 1259, 1231, 1152, 1126, 1105, 1066, 1033, 978, 939, 919, 861, 754, 739, 716, 661, 628, 592, 575, 552, 478, 444, 418; UV-Vis (acetonitrile): $\lambda_1(\varepsilon_1)$ = 317 (1.35×10^4), $\lambda_2(\varepsilon_2)$ = 373 (1.60×10^4), $\lambda_3(\varepsilon^3)$ = 502 (2.18×10^4); UV-Vis (acetonitrile:water 9:1): $\lambda_1(\varepsilon_1)$ = 318 (1.39×10^4), $\lambda_2(\varepsilon_2)$ = 375 (1.63×10^4), $\lambda_3(\varepsilon_3)$ = 504 (2.23×10^4); HRMS [EI]: 376.1655 calculated for: $C_{20}H_{20}N_6O_2$ 376.1648.

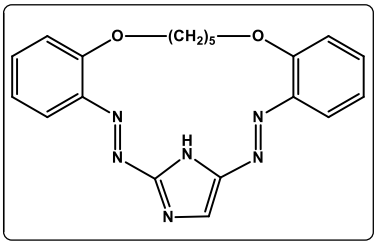

Compound **3**: yield 35%; red solid; mp 172 – 176 °C (with decomposition); R_f = 0.53 (chloroform:acetone 100:1); ^{1}H NMR (acetone-d_6, 500MHz, δ [ppm]): 1.92 – 1.98 (4H, m), 2.04 – 2.18 (2H, m, under residual acetone-d_6 signal), 4.30 (2H, t, J = 4.9 Hz), 4.33 (2H, t, J = 4.9 Hz), 7.03 – 7.10 (2H, m), 7.28 (1H, d, J = 8.2 Hz), 7.33 (1H, d, J = 8.3 Hz), 7.51 – 7.54 (1H, m), 7.60 – 7.63 (1H, m), 7.76 (1H, dd, J_1 = 1.6 Hz, J_2 = 8.2 Hz), 7.83 (1H, dd, J_1 = 1.7 Hz, J_2 = 7.6 Hz), 8.04 (1H, s) 10.51 (1H, bs, NH); ^{13}C NMR (chloroform-d, 125 MHz): 158.2, 157.4, 145.5, 140.9, 140.8, 135.5, 133.7, 132.7, 120.8, 120.7, 116.3, 115.7, 113.4, 68.0, 67.9, 30.9, 24.0; FTIR (ATR, cm^{-1}): 3439, 3063, 2949, 2931, 2887, 2863, 1588, 1576, 1528, 1485, 1459, 1388, 1310, 1280, 1268, 1233, 1201, 1156, 1143, 1115, 1054, 1036, 981, 947, 904, 858, 840, 824, 757, 739, 665, 642, 605, 579, 556, 539, 500, 483, 426; UV-Vis (acetonitrile): $\lambda_1(\varepsilon_1)$ = 319 (9.82×10^3), $\lambda_2(\varepsilon_2)$ = 377 (1.46×10^4), $\lambda_3(\varepsilon_3)$ = 492 (2.01×10^4); UV-Vis (acetonitrile:water 9:1): $\lambda_1(\varepsilon_1)$ = 320 (1.02×10^4), $\lambda_2(\varepsilon_2)$ = 379 (1.50×10^4), $\lambda_3(\varepsilon_3)$ = 494 (2.20×10^4); HRMS [EI]: 376.1654 calculated for: $C_{20}H_{20}N_6O_2$ 376.1648.

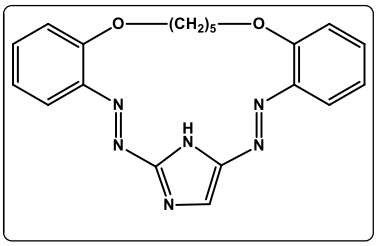

Compound **4**: yield 40%; red solid; mp 182 – 184 °C (with decomposition); R_f = 0.60 (chloroform:acetone 100:1); ^{1}H NMR (acetone-d_6, 500MHz, δ [ppm]): 1.92-1.97 (4H, m), 2.04 – 2.18 (2H, m, under residual acetone-d_6 signal), 2.66 (3H, s), 4.28 (2H, t, *J* = 4.9 Hz), 4.36 (2H, t, *J* = 4.9 Hz), 7.02 – 7.10 (2H, m), 7.26 (1H, d, *J* = 8.2 Hz), 7.32 (1H, d, *J* = 8.8 Hz), 7.47 – 7.50 (1H, m), 7.58 – 7.67 (1H, m), 7.75 – 7.83 (2H, m), 10.38 (1H, bs, NH); Due to low solubility of 4 instead of standard ^{13}C NMR spectra, heterocorrelation spectra gHSQC and gHMBC were recorded; FTIR (ATR, cm^{-1}): 3647, 3433, 3079, 2938, 2907, 2869, 2838, 1589, 1578, 1544, 1488, 1470, 1454, 1429, 1399, 1383, 1353, 1308, 1281, 1263, 1254, 1230, 1218, 1177, 1159, 1132, 1114, 1073, 1053, 1041, 1030, 980, 939, 879, 856, 823, 759, 749, 722, 711, 688, 679, 643, 625, 605, 591, 574, 555, 543, 509, 479, 447, 418; UV-Vis (acetonitrile): $\lambda_1(\varepsilon_1)$ = 319 (7.15×10^3), $\lambda_2(\varepsilon_2)$ = 377 (9.80×10^3), $\lambda_3(\varepsilon_3)$ = 506 (1.52×10^4); UV-Vis (acetonitrile:water 9:1): $\lambda_1(\varepsilon_1)$ = 320 (7.70×10^3), $\lambda_2(\varepsilon_2)$ = 379 (1.02×10^4), $\lambda_3(\varepsilon_3)$ = 508 (1.60×10^4); HRMS [EI]: 390.1796 calculated for: $C_{21}H_{22}N_6O_2$ 390.1804.

^{1}H, ^{13}C NMR, LR and HRMS, FT-IR (ATR) spectra of newly obtained compounds **1-4** are shown in Supplementary Materials (Figures S1-S16).

Compounds **5-8** were synthesized analogously to previous protocol [5, 7] and the identity of material was confirmed by comparison of TLC and spectral properties with original samples of crowns deposited in our lab.

1. E. Luboch, V.C. Kravtsov, A. Konitz, Reductive cyclization products of 1,2-bis(2-nitrophenoxy)ethanes. X-ray structures of 10-membered azoxycrown ether stereoisomers and the sodium iodide complex of a 20-membered azoazoxycrown, *J. Supramol. Chem.*, 2001, **1**, 101–110.
2. B. Galiński, E. Luboch, J. Chojnacki, E. Wagner-Wysiecka, Novel diazocrowns with pyrrole residue as lead(II) colorimetric probes, *Materials*, 2021, **14**, 7239.
3. R. Jaunin, R. Holl, Macrocycles synthétiques. I. Action du sodium sur les o, o'-polyméthylènedioxy-bis-(benzylidène-anilines), *Helv. Chim. Acta*, 1958, **41**, 1783–1792.
4. E. Wagner-Wysiecka, E. Luboch, M. Kowalczyk, J.F. Biernat, Chromogenic macrocyclic derivatives of azoles-synthesis and properties, *Tetrahedron*, 2003, **59**, 4415–4420.
5. E. Luboch, E. Wagner-Wysiecka, M. Fainerman-Melnikova, L.F. Lindoy, J.F. Biernat, Pyrrole azocrown ethers. Synthesis, complexation, selective lead transport and ion-selective membrane electrode studies, *Supramol. Chem.*, 2006, **18**, 593–601.
6. E. Wagner-Wysiecka, M. Jamrógiewicz, M.S. J.F. Fonari, Biernat, Azomacrocyclic derivatives of imidazole: Synthesis, structure, and metal ion complexation properties, *Tetrahedron*, 2007, **63**, 4414–4421.
7. E. Wagner-Wysiecka, E. Luboch, M.S. Fonari, The synthesis, X-ray structure and metal cation complexation properties of colored crown with two heterocyclic residues as a part of macrocycle, *Pol. J. Chem.*, 2008, **82**, 1319–1330.
8. E. Wagner-Wysiecka, T. Rzymowski, M.S. Fonari, R. Kulmaczewski, E. Luboch, Pyrrole azocrown ethers-synthesis, crystal structures, and fluorescence properties, *Tetrahedron*, 2011, **67**, 1862–1872.

Spectra

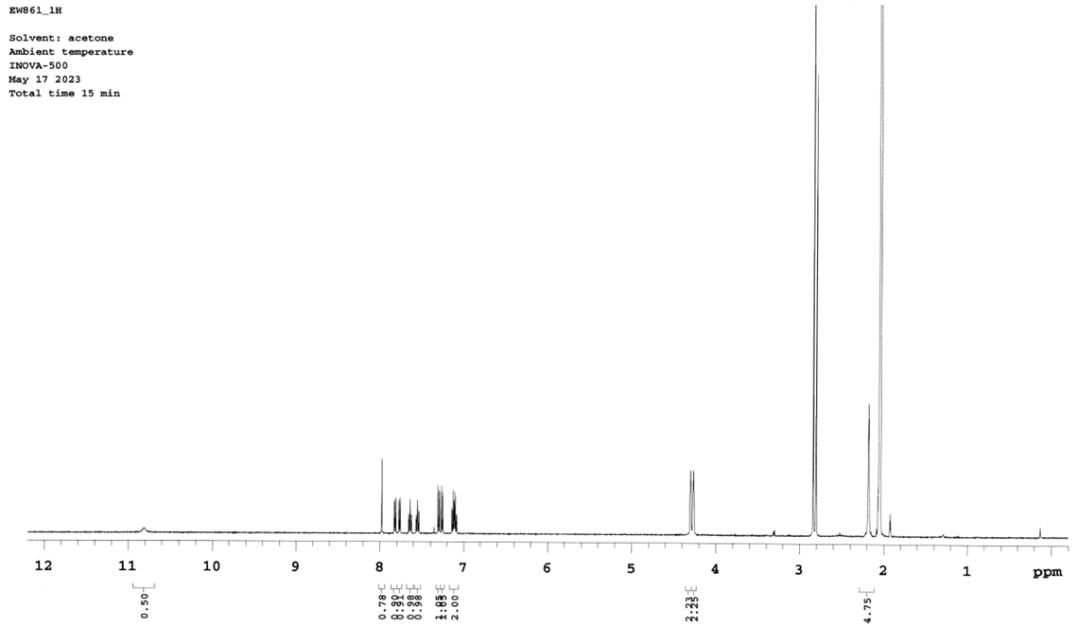

INDEX	FREQUENCY	PPM	HEIGHT	INDEX	FREQUENCY	PPM	HEIGHT
1	5402.8	10.810	10.5	38	1651.6	3.305	11.7
2	3985.6	7.975	176.8	39	1648.8	3.299	12.6
3	3913.1	7.830	73.6	40	1421.0	2.843	3036.3
4	3911.5	7.827	80.9	41	1403.9	2.809	1097.3
5	3905.5	7.814	72.3	42	1261.2	2.523	10.2
6	3903.8	7.811	84.2	43	1094.3	2.190	241.1
7	3886.2	7.776	75.3	44	1092.1	2.185	316.3
8	3884.6	7.773	81.2	45	1089.9	2.181	279.7
9	3878.6	7.761	72.2	46	1083.8	2.169	34.1
10	3876.9	7.757	85.7	47	1076.1	2.153	9.8
11	3828.0	7.660	44.7	48	1044.3	2.090	20.4
12	3826.4	7.656	47.8	49	1036.6	2.074	96.5
13	3819.3	7.642	82.2	50	1034.4	2.070	119.6
14	3818.2	7.640	65.4	51	1030.0	2.061	2702.0
15	3812.1	7.628	43.2	52	1028.4	2.058	5964.1
16	3810.5	7.624	44.7	53	1026.2	2.053	8258.0
17	3783.6	7.571	41.8	54	1024.0	2.049	5983.1
18	3781.9	7.567	44.4	55	1021.8	2.044	3148.4
19	3774.8	7.553	78.7	56	966.3	1.934	18.5
20	3773.7	7.551	65.6	57	964.1	1.929	35.7
21	3768.2	7.540	51.4	58	961.9	1.925	54.5
22	3766.5	7.536	53.8	59	959.7	1.920	38.9
23	3676.5	7.356	15.7	60	957.5	1.916	19.4
24	3652.9	7.309	114.0	61	65.3	0.131	22.3
25	3644.7	7.293	101.6				
26	3633.1	7.270	113.7				
27	3624.9	7.253	98.9				
28	3572.2	7.148	54.8				
29	3571.1	7.145	61.4				
30	3563.9	7.131	103.6				
31	3557.4	7.118	76.6				
32	3555.7	7.115	62.4				
33	3550.2	7.104	98.5				
34	3542.0	7.087	47.8				
35	2148.5	4.299	154.5				
36	2132.5	4.267	154.8				
37	1657.1	3.316	10.6				

Fig. S1. ^{1}H NMR spectrum of **1** (acetone-d_6).

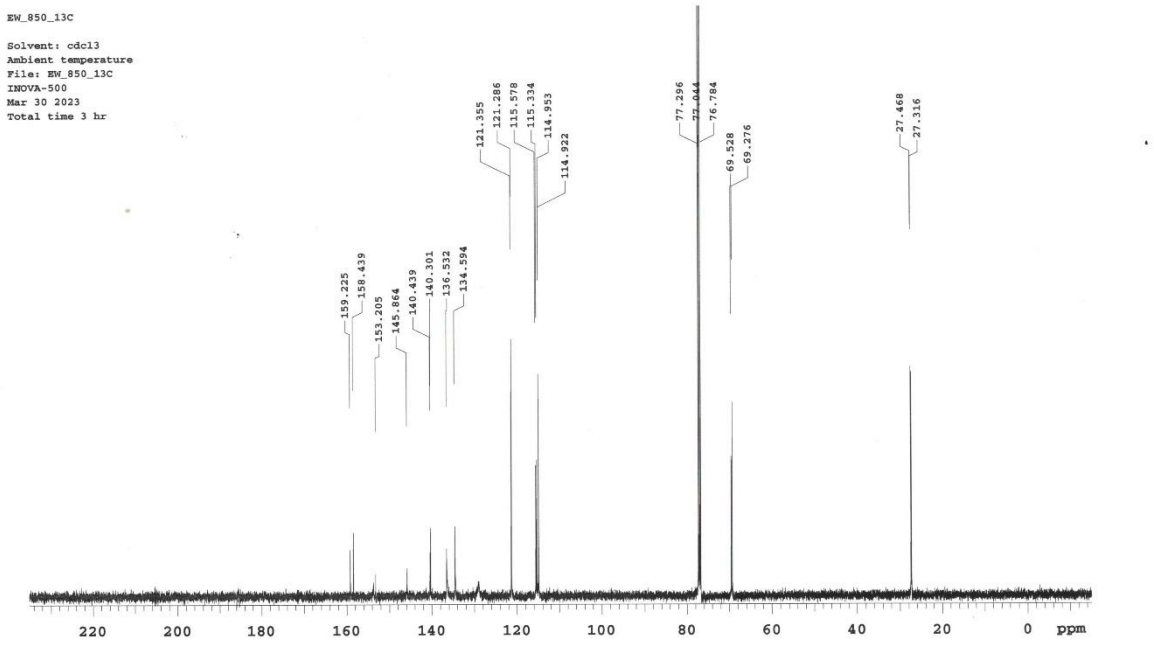

Fig. S2. ^{13}C NMR spectrum of **1** (chloroform-d).

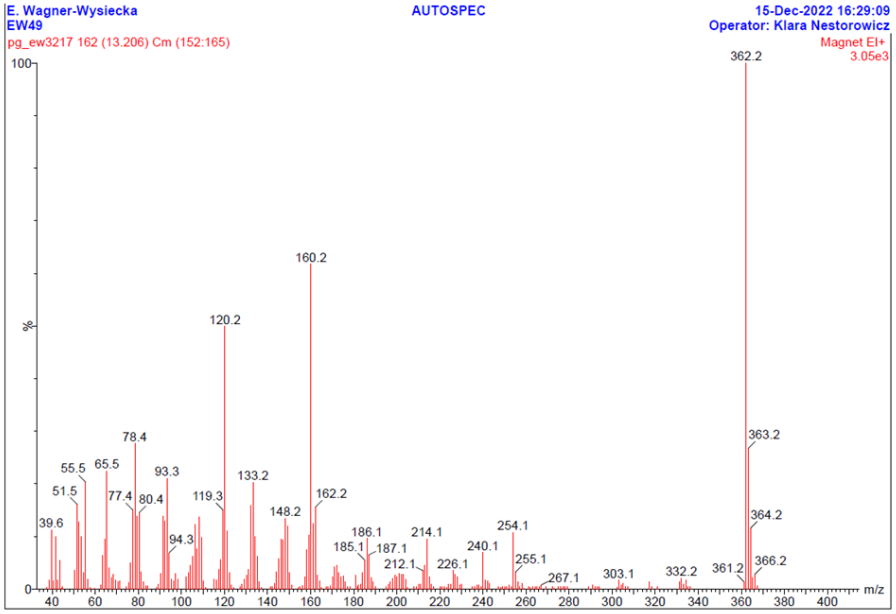

Elemental Composition Report **Page 1**

Single Mass Analysis
Tolerance = 20.0 PPM / DBE: min = -1.5, max = 150.0
Selected filters: None

Monoisotopic Mass, Odd and Even Electron Ions
103 formula(e) evaluated with 3 results within limits (up to 50 best isotopic matches for each mass)
Elements Used:
C: 0-100 H: 0-200 N: 0-6 O: 0-2

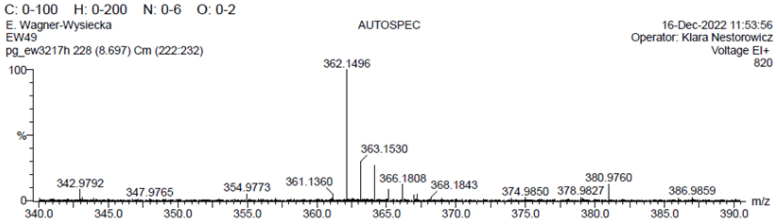

Minimum:				-1.5		
Maximum:		5.0	20.0	150.0		
Mass	Calc. Mass	mDa	PPM	DBE	i-FIT	Formula
362.1496	362.1491	0.5	1.4	14.0	90.5	C19 H18 N6 O2
	362.1531	-3.5	-9.7	18.0	80.9	C24 H18 N4
	362.1545	-4.9	-13.5	17.5	77.3	C26 H20 N O

Fig. S3. EI mass spectra LR (top) and HR (bottom) of **1**.

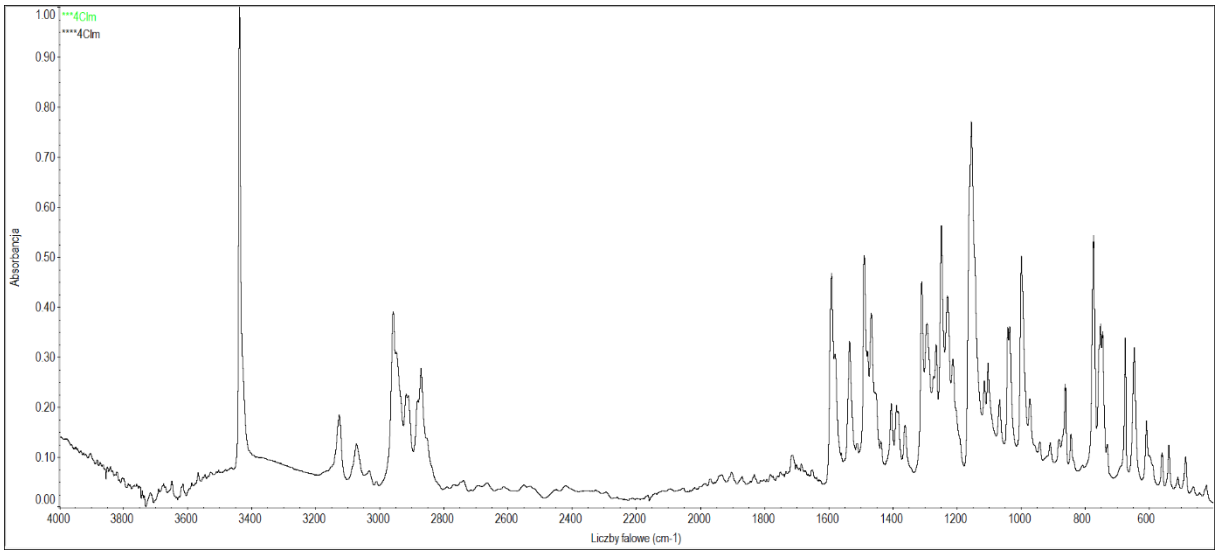

Fig. S4. FTIR (ATR) spectrum of **1**.

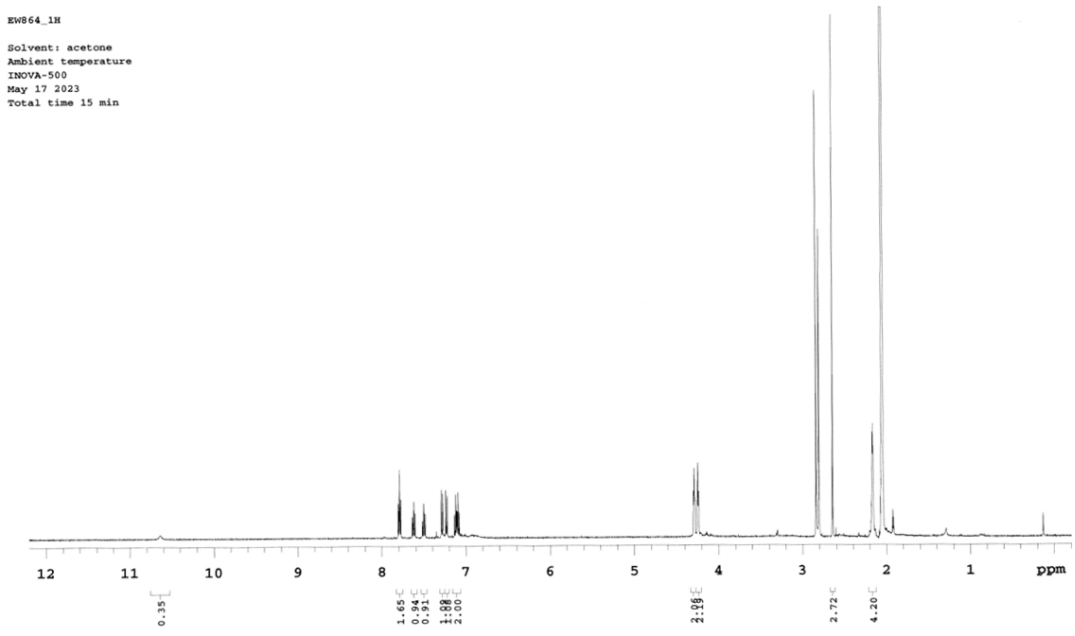

EW864_1H

Solvent: acetone
Ambient temperature
INOVA-500
May 17 2023
Total time 15 min

INDEX	FREQUENCY	PPM	HEIGHT	INDEX	FREQUENCY	PPM	HEIGHT	INDEX	FREQUENCY	PPM	HEIGHT
1	5317.7	10.640	2.9	38	2147.9	4.298	32.6	75	964.1	1.929	13.6
2	3902.7	7.809	24.0	39	2143.0	4.288	48.6	76	961.9	1.925	19.2
3	3901.1	7.806	24.5	40	2139.1	4.280	28.2	77	959.7	1.920	13.5
4	3894.5	7.792	48.5	41	2126.0	4.254	26.8	78	957.5	1.916	7.4
5	3893.4	7.790	33.6	42	2121.6	4.245	52.5	79	645.1	1.291	5.6
6	3887.9	7.779	27.5	43	2116.6	4.235	32.6	80	65.9	0.132	16.5
7	3886.2	7.776	26.9	44	2106.2	4.214	3.2				
8	3819.8	7.643	14.8	45	2072.7	4.147	3.2				
9	3818.2	7.640	14.8	46	2066.7	4.135	2.8				
10	3812.7	7.629	19.8	47	1649.4	3.300	4.7				
11	3811.6	7.627	26.0	48	1419.9	2.841	316.5				
12	3809.9	7.623	19.8	49	1402.8	2.807	218.0				
13	3804.4	7.612	18.0	50	1322.7	2.647	370.3				
14	3802.8	7.609	17.2	51	1302.4	2.606	6.4				
15	3760.0	7.523	12.1	52	1166.7	2.335	2.9				
16	3758.3	7.520	12.0	53	1101.4	2.204	3.9				
17	3751.7	7.507	24.5	54	1098.7	2.198	4.0				
18	3744.6	7.493	17.4	55	1095.9	2.193	4.2				
19	3742.9	7.489	16.9	56	1092.6	2.186	11.4				
20	3676.5	7.356	4.9	57	1089.9	2.181	23.9				
21	3647.4	7.298	33.4	58	1087.7	2.176	47.6				
22	3646.3	7.296	34.3	59	1085.5	2.172	74.2				
23	3639.2	7.282	31.2	60	1083.3	2.168	80.3				
24	3638.1	7.279	31.5	61	1081.1	2.163	64.7				
25	3620.5	7.244	34.0	62	1070.7	2.142	5.1				
26	3612.3	7.228	30.2	63	1065.7	2.132	4.8				
27	3611.2	7.226	29.1	64	1043.7	2.088	4.7				
28	3566.7	7.137	15.8	65	1036.1	2.073	29.0				
29	3567.8	7.139	16.1	66	1033.9	2.069	41.4				
30	3559.6	7.122	30.5	67	1030.0	2.061	897.0				
31	3555.2	7.114	19.2	68	1027.8	2.057	1763.2				
32	3554.1	7.111	19.0	69	1025.6	2.052	2538.1				
33	3553.0	7.109	19.0	70	1023.4	2.048	1747.3				
34	3546.9	7.097	32.3	71	1021.2	2.043	881.8				
35	3539.8	7.083	18.5	72	1005.9	2.013	5.6				
36	3538.7	7.081	17.3	73	998.7	1.998	5.4				
37	3531.6	7.066	3.3	74	966.3	1.934	7.4				

Fig. S5. ^{1}H NMR spectrum of **2** (acetone-d_6).

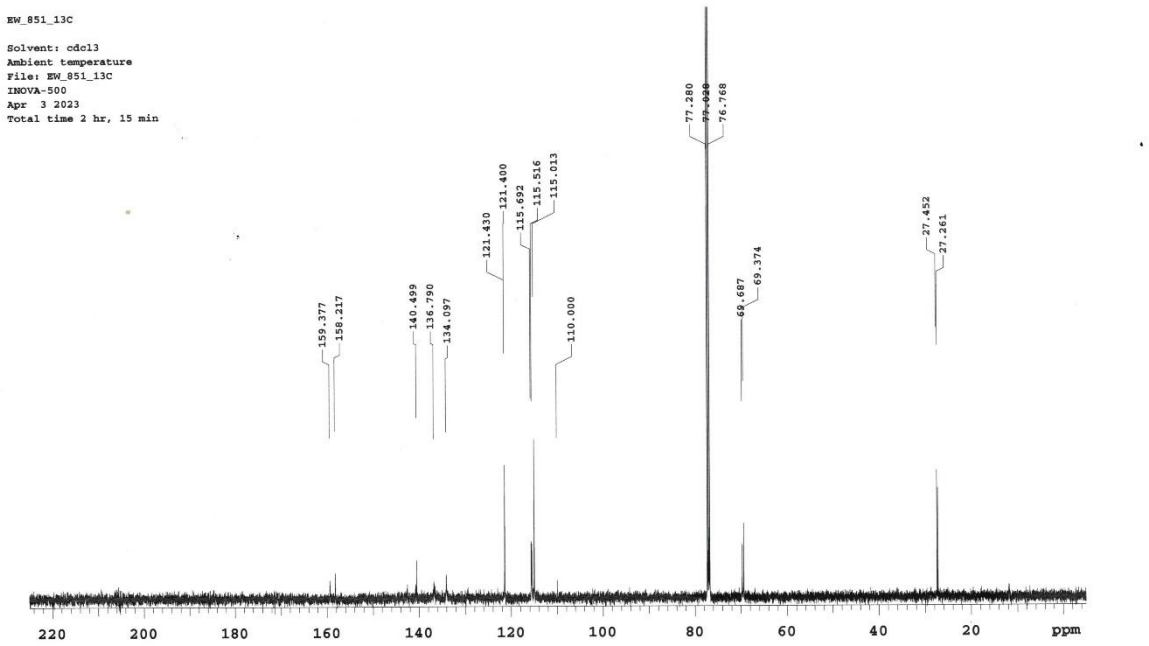

Fig. S6. ^{13}C NMR spectrum of **2** (chloroform-d).

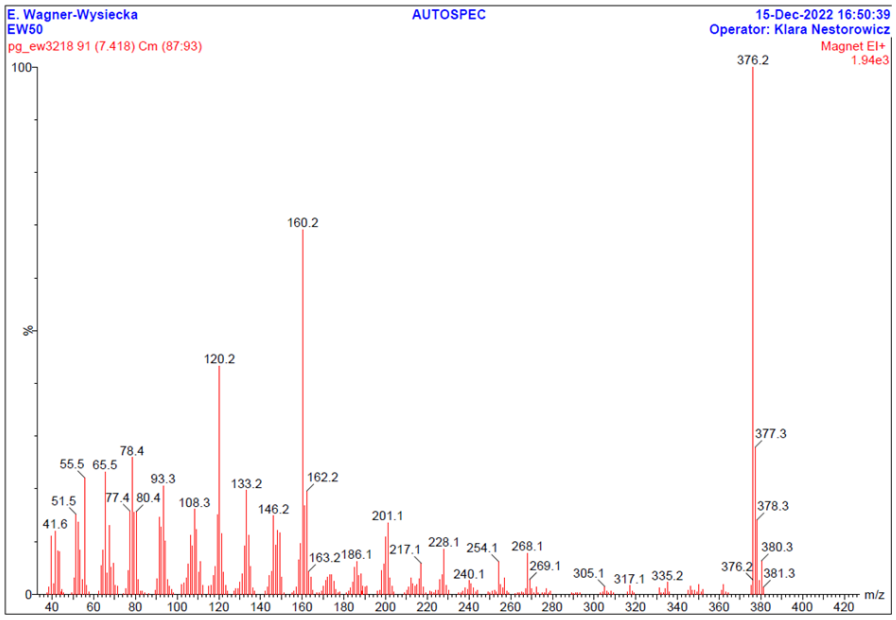

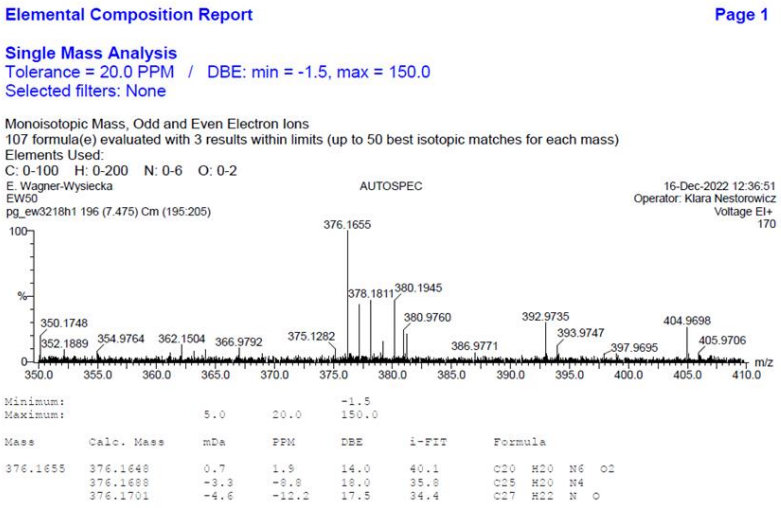

Fig. S7. EI mass spectra LR (top) and HR (bottom) of **2**.

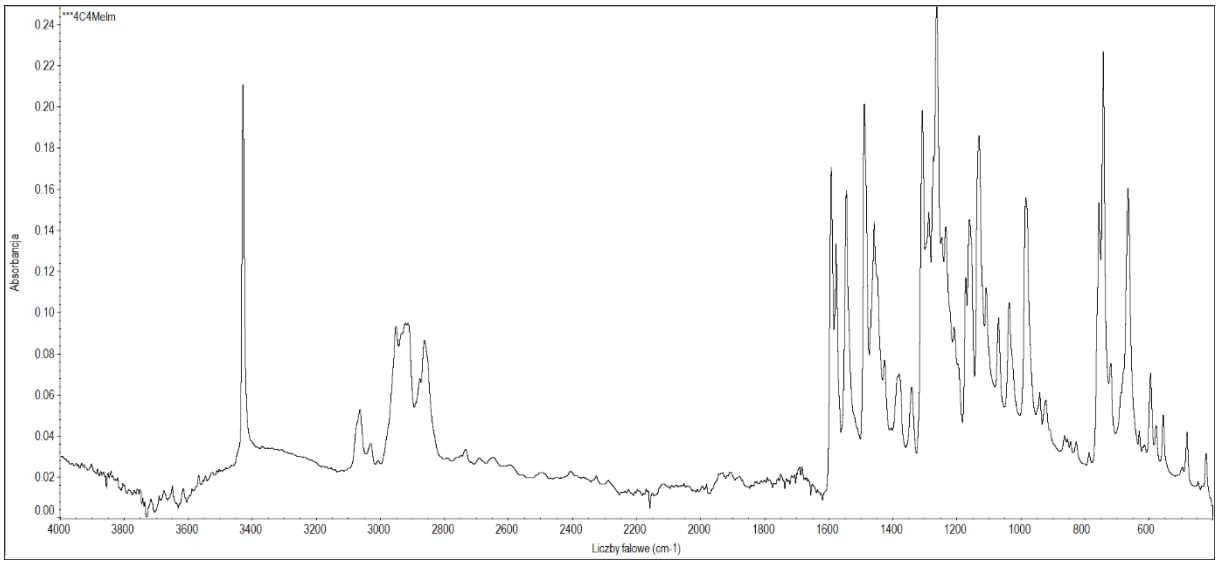

Fig. S8. FTIR (ATR) spectrum of **2**.

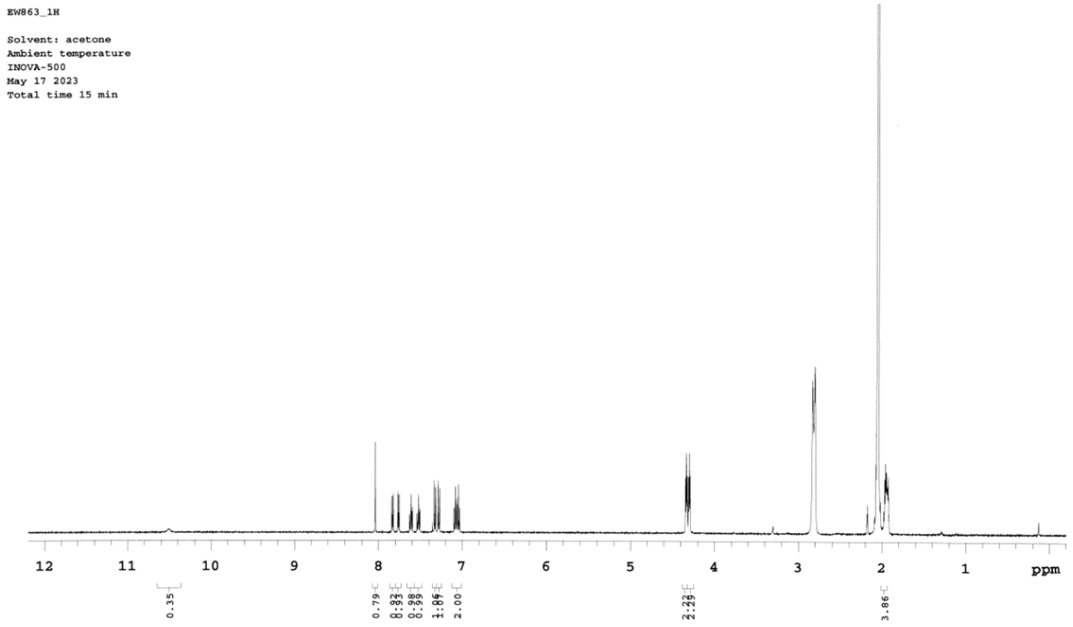

EW863_1H

Solvent: acetone
Ambient temperature
INOVA-500
May 17 2023
Total time 15 min

INDEX	FREQUENCY	PPM	HEIGHT	INDEX	FREQUENCY	PPM	HEIGHT
1	5251.8	10.508	7.0	38	2147.9	4.298	160.4
2	4018.0	8.040	181.1	39	2143.0	4.288	114.8
3	3919.2	7.842	71.4	40	1649.9	3.301	15.4
4	3917.5	7.839	74.0	41	1417.7	2.837	306.8
5	3911.5	7.827	70.9	42	1403.9	2.809	335.1
6	3909.9	7.823	77.9	43	1092.6	2.186	19.8
7	3884.0	7.772	76.2	44	1090.4	2.182	40.4
8	3882.4	7.768	80.9	45	1088.2	2.177	58.8
9	3875.8	7.755	74.6	46	1086.0	2.173	41.6
10	3874.2	7.752	76.8	47	1083.8	2.169	22.0
11	3813.8	7.631	34.5	48	1044.3	2.090	35.8
12	3812.1	7.628	36.6	49	1036.6	2.074	139.7
13	3805.0	7.613	77.4	50	1033.9	2.069	202.1
14	3803.3	7.610	57.3	51	1030.0	2.061	3407.1
15	3797.8	7.599	50.4	52	1027.8	2.057	6691.7
16	3796.2	7.596	50.5	53	1025.6	2.052	9600.3
17	3769.3	7.542	37.7	54	1024.0	2.049	6757.5
18	3767.6	7.539	38.3	55	1021.8	2.044	3523.2
19	3760.5	7.524	76.0	56	1008.6	2.018	64.8
20	3753.4	7.510	46.6	57	988.3	1.977	46.3
21	3751.7	7.507	48.6	58	982.8	1.966	109.6
22	3676.5	7.356	21.5	59	977.9	1.957	141.5
23	3666.1	7.335	104.1	60	972.9	1.947	124.2
24	3657.8	7.319	89.7	61	966.3	1.934	95.4
25	3643.0	7.289	103.4	62	964.1	1.929	92.0
26	3634.8	7.273	87.0	63	961.9	1.925	115.2
27	3545.8	7.095	49.5	64	959.7	1.920	73.7
28	3538.7	7.081	92.2	65	957.5	1.916	39.4
29	3529.9	7.063	69.3	66	644.0	1.289	6.8
30	3528.8	7.061	58.7	67	65.3	0.131	25.8
31	3521.7	7.046	96.7				
32	3514.5	7.032	49.4				
33	3513.4	7.030	49.9				
34	2170.4	4.343	111.3				
35	2165.5	4.333	161.0				
36	2160.5	4.323	114.5				
37	2152.9	4.308	112.2				

Fig. S9. ^{1}H NMR spectrum of **3** (acetone-d_6).

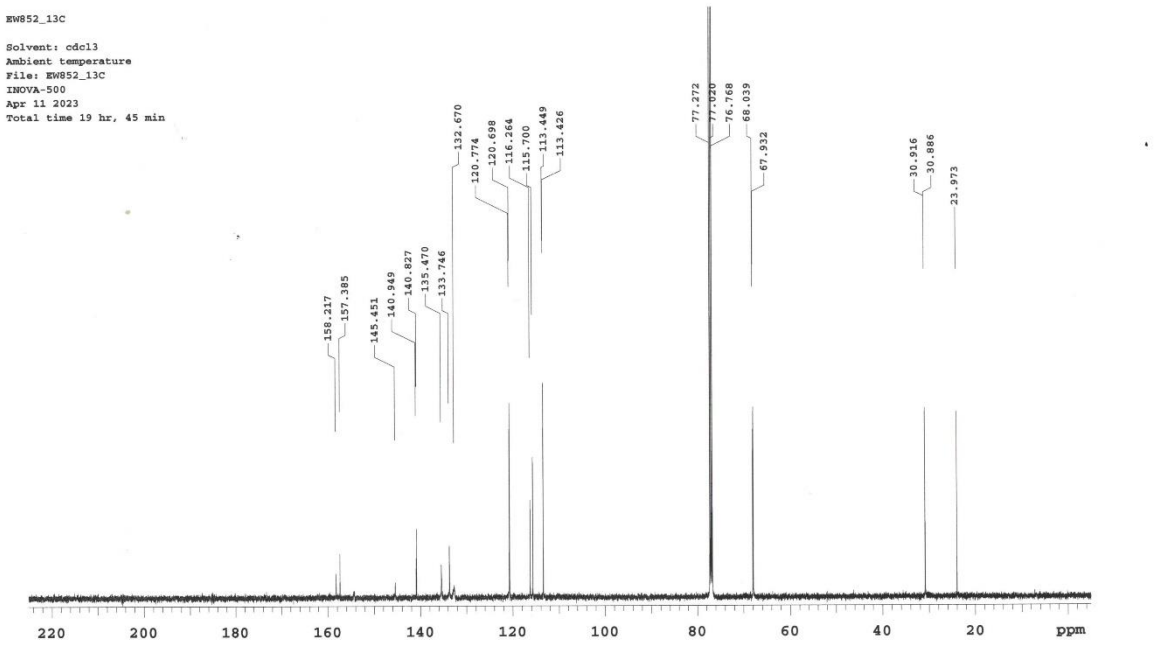

Fig. S10. ^{13}C NMR spectrum of **3** (chloroform-d).

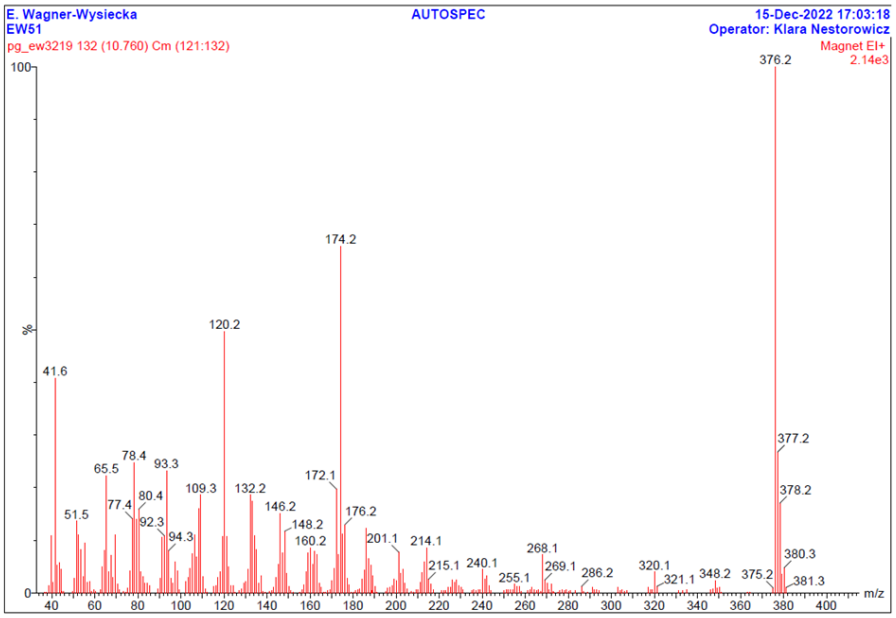

Elemental Composition Report Page 1

Single Mass Analysis
Tolerance = 20.0 PPM / DBE: min = -1.5, max = 150.0
Selected filters: None

Monoisotopic Mass, Odd and Even Electron Ions
107 formula(e) evaluated with 3 results within limits (up to 50 best isotopic matches for each mass)
Elements Used:
C: 0-100 H: 0-200 N: 0-6 O: 0-2

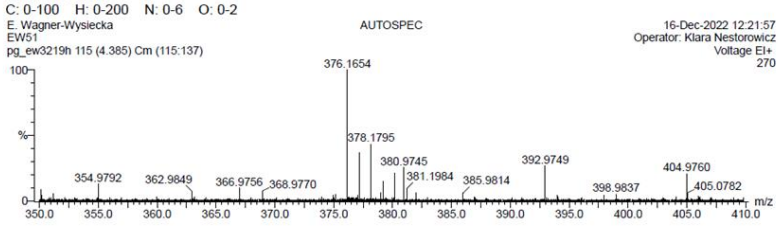

Minimum:		5.0	20.0	-1.5		
Maximum:				150.0		
Mass	Calc. Mass	mDa	PPM	DBE	i-FIT	Formula
376.1654	376.1648	0.6	1.6	14.0	53.7	C20 H20 N6 O2
	376.1688	-3.4	-9.0	18.0	48.6	C25 H20 N4
	376.1701	-4.7	-12.5	17.5	46.9	C27 H22 N O

Fig. S11. EI mass spectra LR (top) and HR (bottom) of **3**.

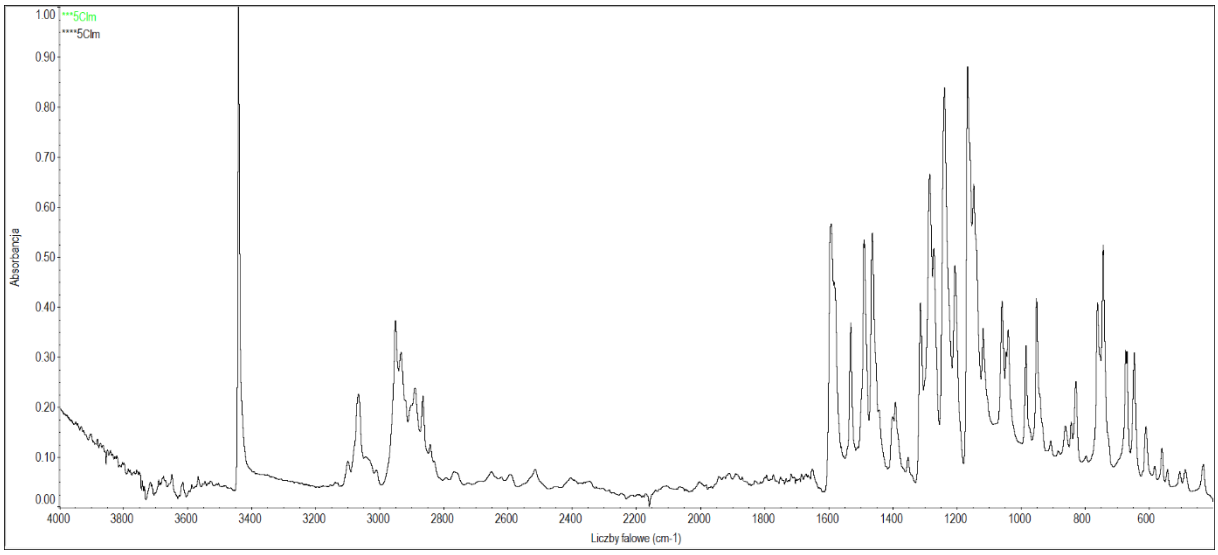

Fig. S12. FTIR (ATR) spectrum of **3**.

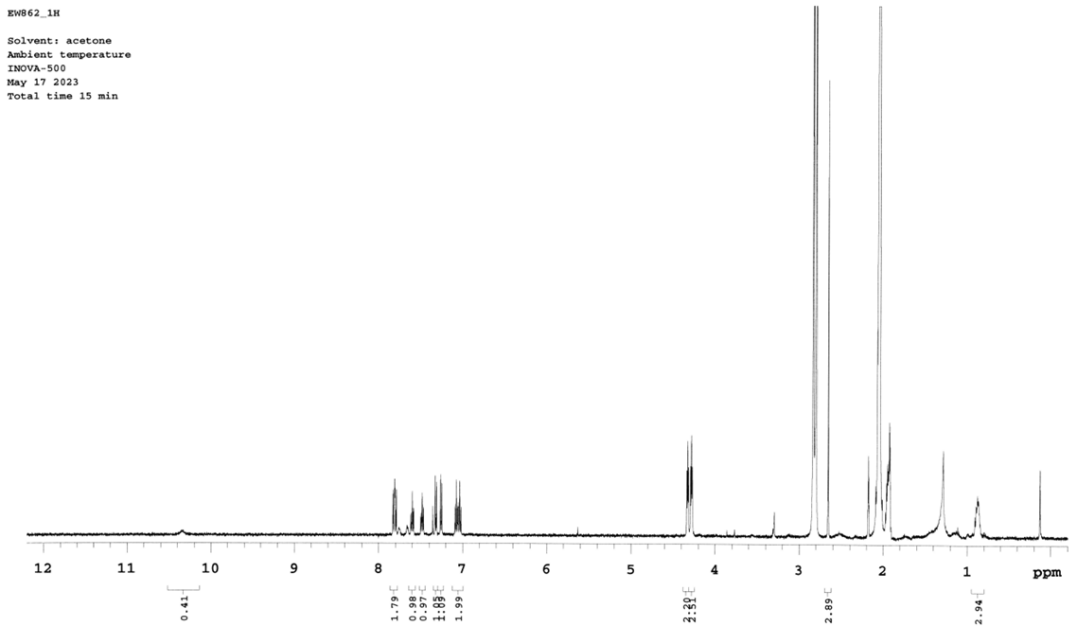

INDEX	FREQUENCY	PPM	HEIGHT	INDEX	FREQUENCY	PPM	HEIGHT	INDEX	FREQUENCY	PPM	HEIGHT
1	3913.1	7.830	48.5	38	1929.9	3.862	6.4	75	438.7	0.878	49.0
2	3911.5	7.827	53.7	39	1884.4	3.770	7.9	76	433.7	0.868	43.4
3	3904.9	7.813	50.1	40	1657.1	3.316	9.1	77	405.7	0.812	5.9
4	3902.7	7.809	66.4	41	1648.8	3.299	29.1	78	399.1	0.799	6.9
5	3900.5	7.805	55.5	42	1418.8	2.839	1459.2	79	65.3	0.131	80.7
6	3893.9	7.791	45.5	43	1402.3	2.806	1460.7				
7	3892.8	7.789	54.0	44	1329.8	2.661	543.0				
8	3876.4	7.756	8.7	45	1263.9	2.529	5.8				
9	3830.8	7.665	11.5	46	1092.6	2.186	32.8				
10	3807.2	7.618	23.1	47	1090.4	2.182	66.2				
11	3805.5	7.614	25.0	48	1088.2	2.177	96.4				
12	3798.9	7.601	52.1	49	1086.0	2.173	71.6				
13	3791.8	7.587	30.6	50	1083.8	2.169	37.9				
14	3790.2	7.584	31.9	51	1044.3	2.090	60.4				
15	3748.4	7.500	22.7	52	1036.1	2.073	248.0				
16	3747.3	7.498	25.0	53	1030.0	2.061	5717.9				
17	3740.2	7.484	50.1	54	1028.4	2.058	11256.9				
18	3733.1	7.469	30.8	55	1026.2	2.053	16487.0				
19	3731.4	7.466	33.0	56	1024.0	2.049	12108.9				
20	3676.5	7.356	34.4	57	1021.8	2.044	6426.6				
21	3662.8	7.329	70.6	58	1005.3	2.012	44.1				
22	3654.0	7.311	63.0	59	985.5	1.972	29.5				
23	3630.9	7.265	71.9	60	979.5	1.960	64.4				
24	3622.7	7.249	62.0	61	974.6	1.950	86.9				
25	3543.1	7.089	36.9	62	969.1	1.939	78.4				
26	3535.9	7.075	66.0	63	966.3	1.934	90.2				
27	3527.7	7.059	33.8	64	964.1	1.929	124.3				
28	3523.9	7.051	38.9	65	961.9	1.925	136.2				
29	3516.7	7.037	64.3	66	959.7	1.920	106.8				
30	3508.5	7.020	33.3	67	957.5	1.916	61.7				
31	2813.4	5.629	10.3	68	644.6	1.290	102.9				
32	2167.1	4.336	77.8	69	565.5	1.132	8.6				
33	2161.6	4.325	112.8	70	558.4	1.117	11.9				
34	2156.7	4.315	81.7	71	551.8	1.104	8.1				
35	2144.6	4.291	83.0	72	469.4	0.939	6.0				
36	2139.7	4.281	119.7	73	455.2	0.911	24.6				
37	2134.7	4.271	82.4	74	448.6	0.898	37.3				

Fig. S13. ^{1}H NMR spectrum of **4** (acetone-d_6).

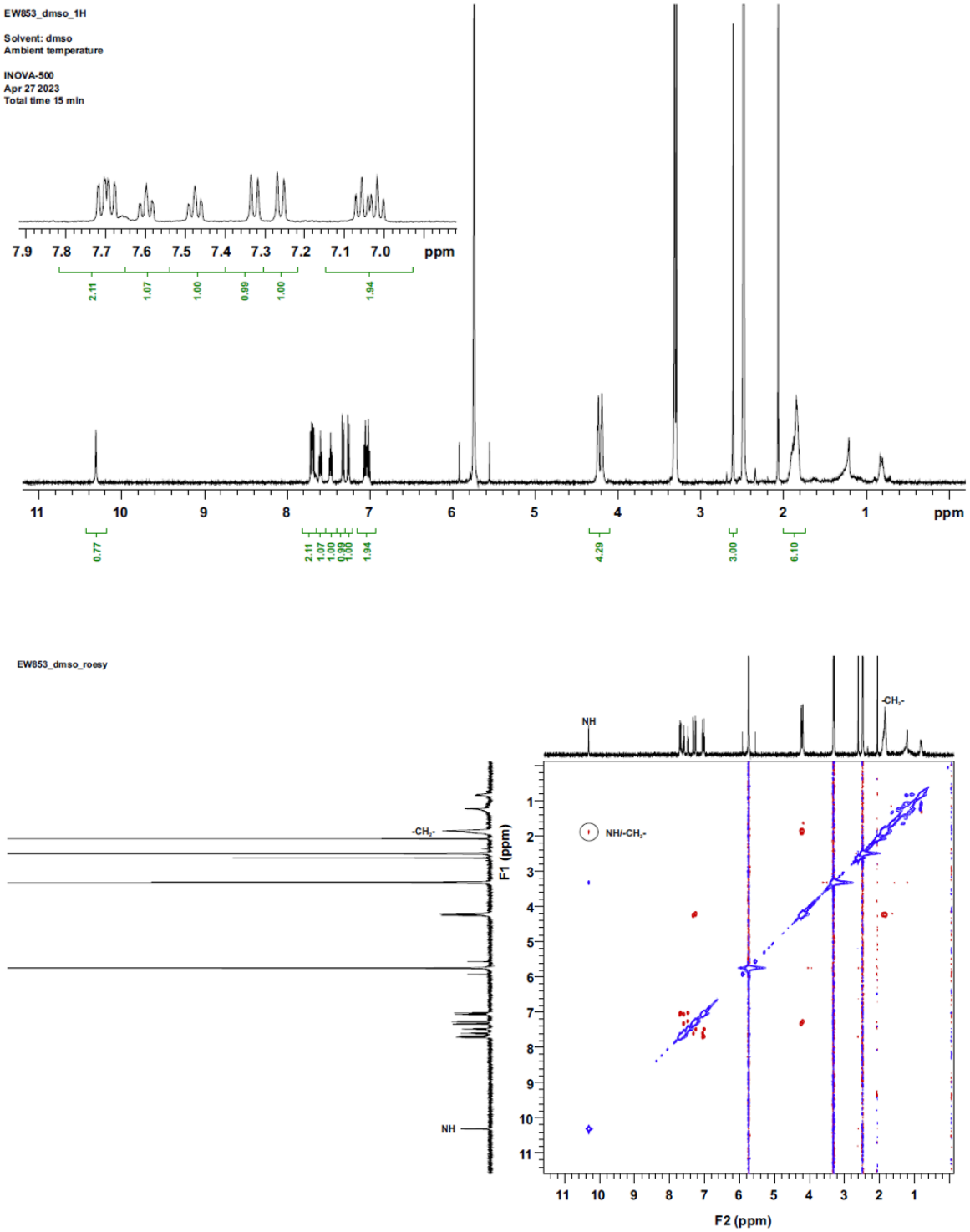

Fig. 14. Top: ^{1}H NMR spectrum of **4** (DMSO-d_6); bottom: ROESY spectrum of **4** (DMSO-d_6).

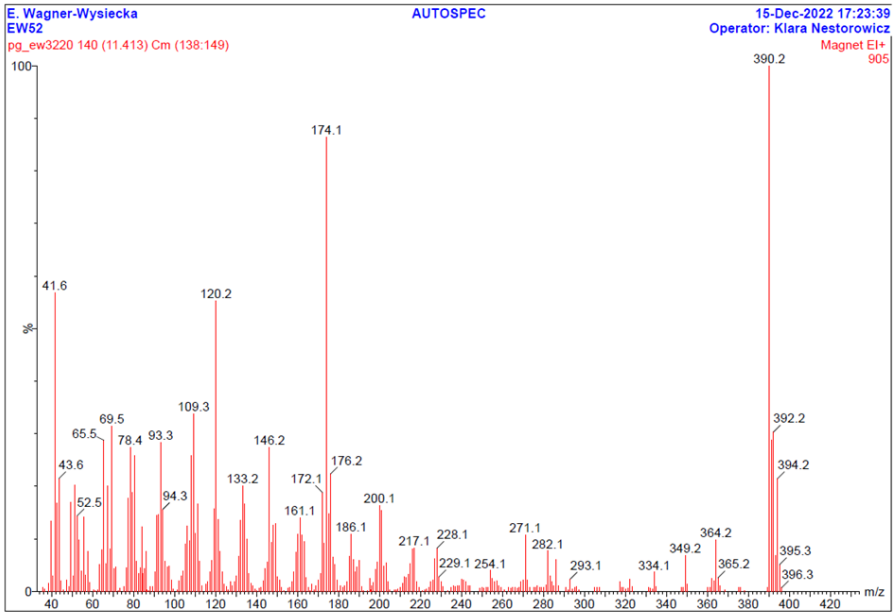

Elemental Composition Report **Page 1**

Single Mass Analysis
Tolerance = 20.0 PPM / DBE: min = -1.5, max = 150.0
Selected filters: None

Monoisotopic Mass, Odd and Even Electron Ions
110 formula(e) evaluated with 5 results within limits (up to 50 best isotopic matches for each mass)
Elements Used:
C: 0-100 H: 0-200 N: 0-6 O: 0-2

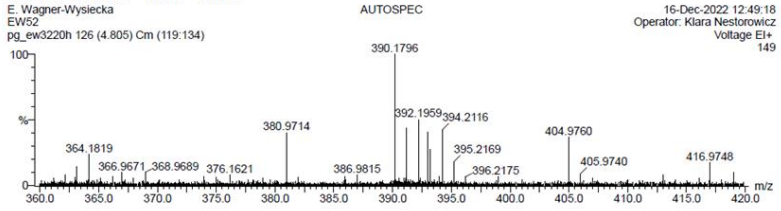

Minimum:				-1.5		
Maximum:		5.0	20.0	150.0		
Mass	Calc. Mass	mDa	PPM	DBE	i-FIT	Formula
390.1796	390.1804	-0.8	-2.1	14.0	36.5	C21 H22 N6 O2
	390.1719	7.7	19.7	18.5	4.0	C25 H20 N5
	390.1844	-4.8	-12.3	18.0	32.9	C26 H22 N4
	390.1732	6.4	16.4	18.0	3.1	C27 H22 N2 O
	390.1858	-6.2	-15.9	17.5	31.7	C28 H24 N O

Fig. S15. EI mass spectra LR (top) and HR (bottom) of **4**.

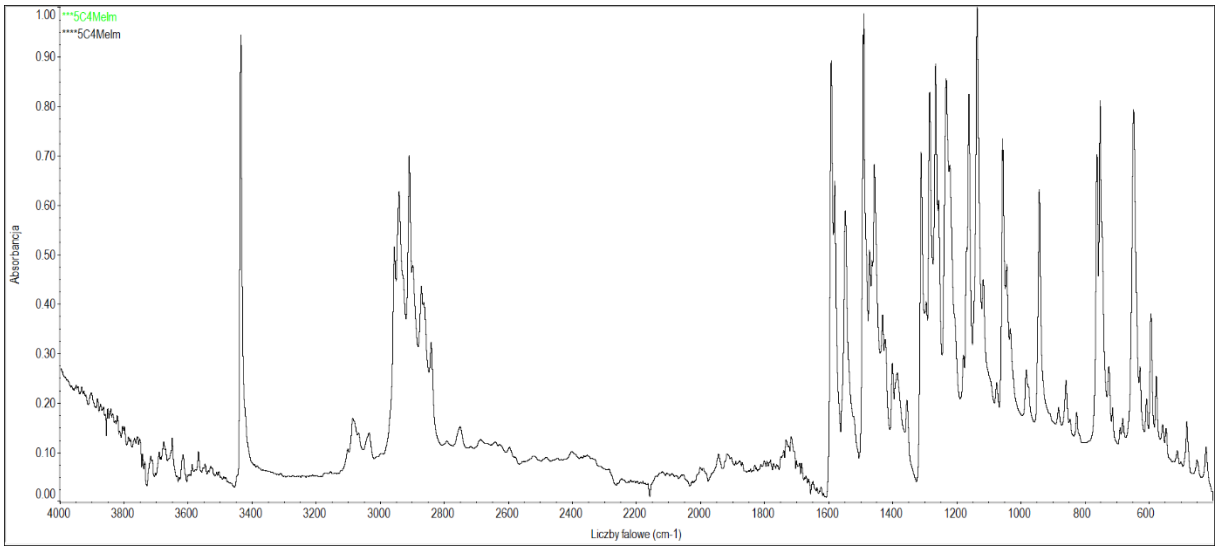

Fig. S16. FTIR (ATR) spectrum of **4**.

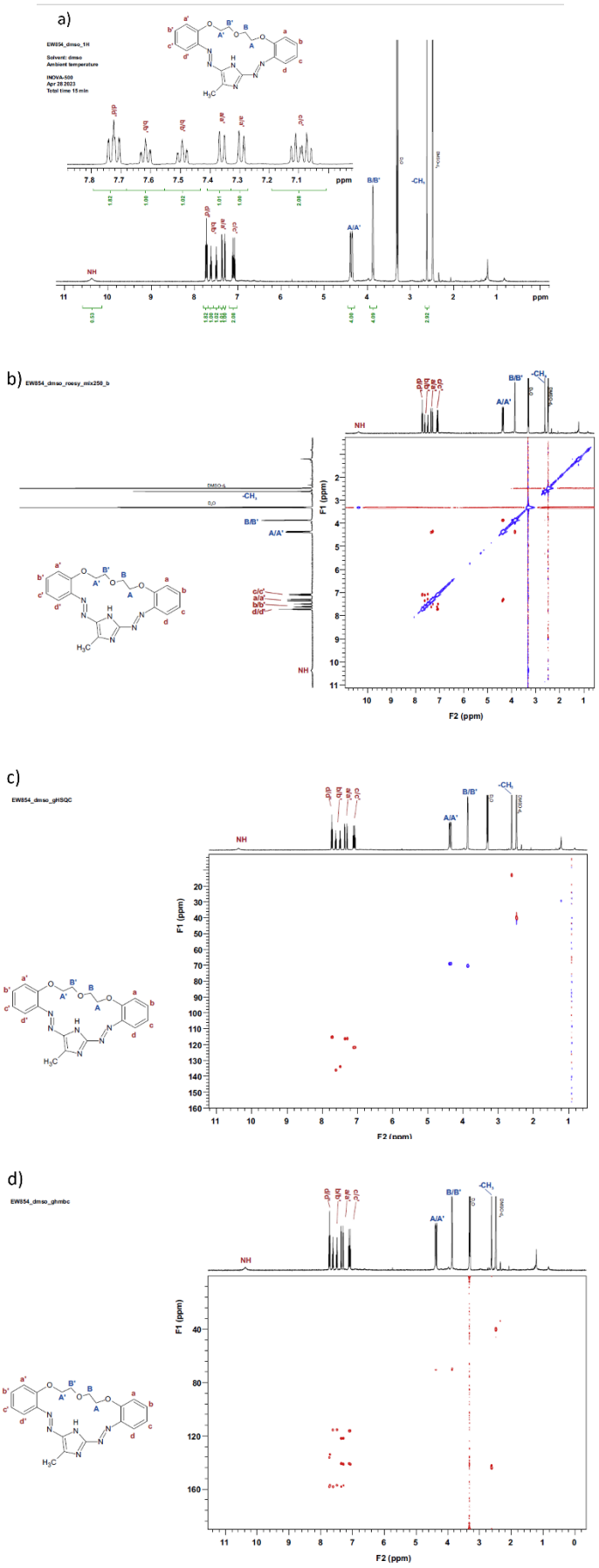

Fig. S16a. NMR spectra of **6**: a) ^{1}H b) ROESY c) gHSQC d) ghmbc (DMSO-d_6).

Other Supplementary data

Table S1. Determined values of lipophilicity ($logP_{TLC}$) of macrocyclic chromoionophores **1**-**8**.

	1	**2**	**3**	**4**	**5**	**6**	**7**	**8**
$logP_{TLC}$	7.62±0.03	8.39±0.04	7.73±0.05	8.54±0.03	5.36±0.03	6.41±0.03	5.43±0.02	6.03±0.04

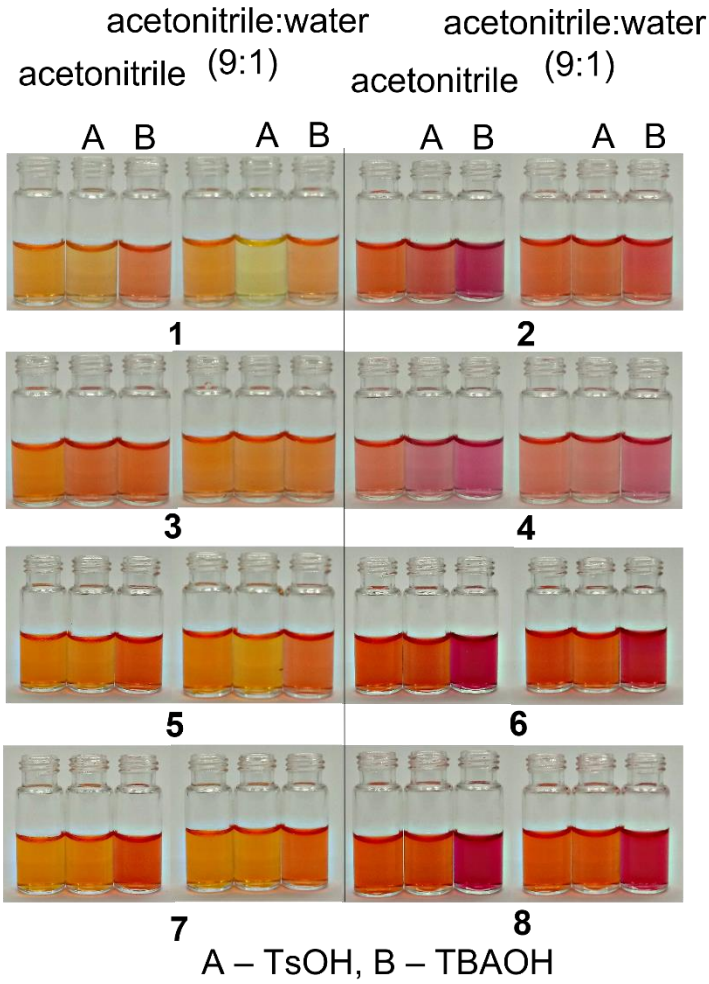

Fig. S17. Color changes of macrocyclic compounds **1**-**8** (c ~ 5.0×10^{-5} mol/dm^3) in the presence of TsOH and TBAOH in acetonitrile and acetonitrile:water 9:1(v/v). In the pictures, in series of three, from left to right: respective macrocycle, and its solution in the presence of TsOH and next TBAOH.

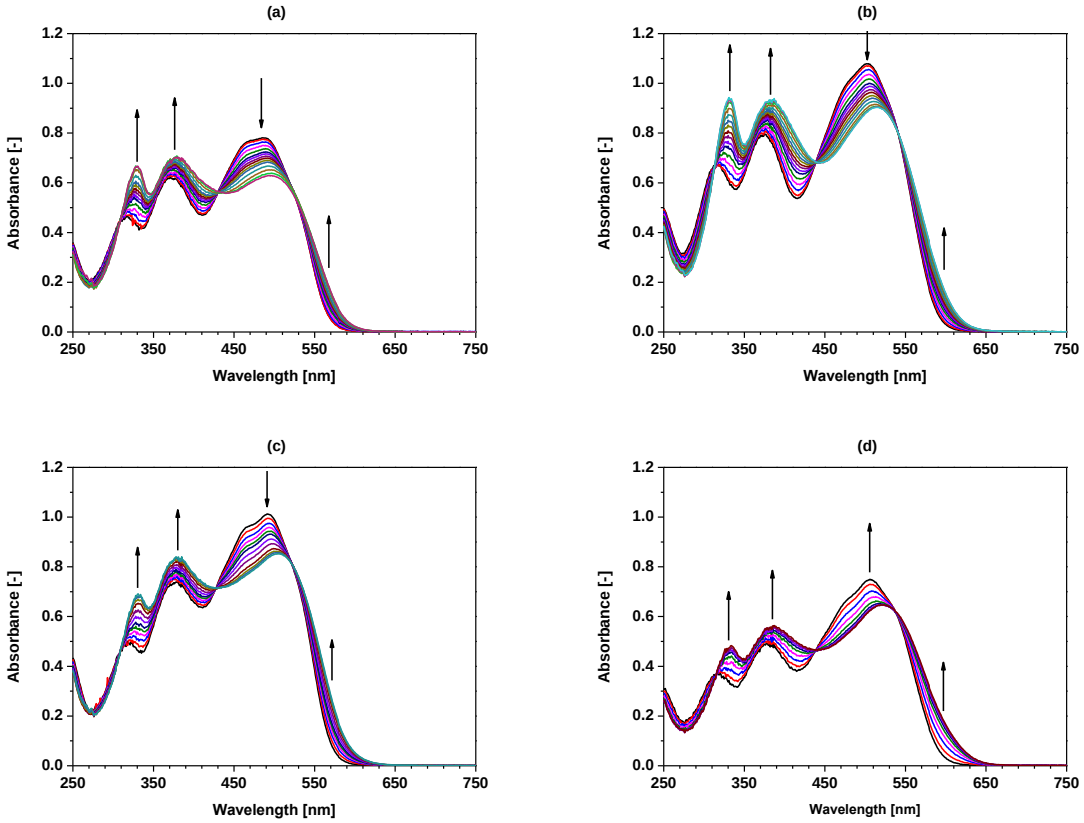

Fig. S18. Changes in absorption spectra of macrocyclic compounds **1**-**4** during spectrophotometric titration with TsOH solution in acetonitrile: a) **1** ($c_1 = 4.97\times10^{-5}$ M) ($c_{TsOH} = 0\text{-}6.40\times10^{-5}$ M); b) **2** ($c_2 = 4.96\times10^{-5}$ M) ($c_{TsOH} = 0\text{-}7.70\times10^{-5}$ M); c) **3** ($c_3 = 5.09\times10^{-5}$ M) ($c_{TsOH} = 0\text{-}5.13\times10^{-5}$ M); d) **4** ($c_4 = 4.91\times10^{-5}$ M) ($c_{TsOH} = 0\text{-}6.57\times10^{-5}$ M).

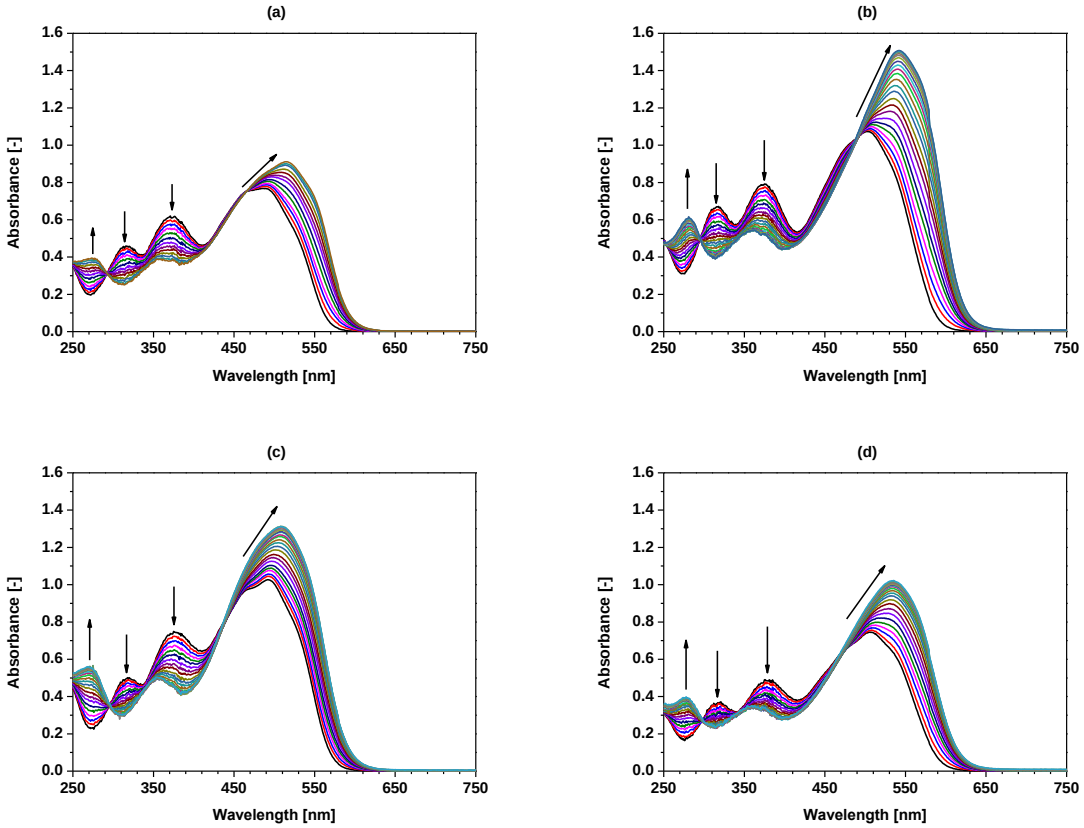

Fig. S19. Changes in absorption spectra of macrocyclic compounds **1**-**4** during spectrophotometric titration with TBAOH solution in acetonitrile: a) **1** ($c_1 = 4.97\times10^{-5}$ M) ($c_{TBAOH} = 0\text{-}5.48\times10^{-5}$ M); b) **2** ($c_2 = 4.96\times10^{-5}$ M) ($c_{TBAOH} = 0\text{-}1.01\times10^{-4}$ M); c) **3** ($c_3 = 5.09\times10^{-5}$ M)($c_{TBAOH} = 0\text{-}5.59\times10^{-5}$ M); d) **4** ($c_4 = 4.91\times10^{-5}$ M) ($c_{TBAOH} = 0\text{-}6.05\times10^{-4}$ M).

Table S2. Wavelengths corresponding to the maxima of **1**-**4** in the presence of TsOH (A) and TBAOH (B) and the equilibrium constants (logK) in the macrocyclic compound:acid/base system.

	1	**2**	**3**	**4**
λ [nm]	485	502	492	506
λ_{L+A} [nm]	530-610	540-630	520-620	540-650
λ_{L+B} [nm]	515	542	510	534

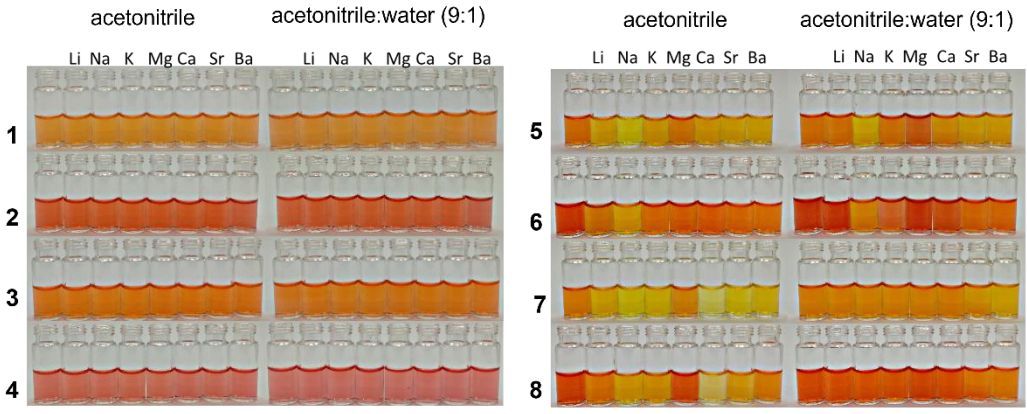

Fig. S20. Color changes of macrocyclic compounds **1**-**4** (left) and **5**-**8** (right) in the presence alkali and alkaline earth metal perchlorates, in the acetonitrile and acetonitrile:water (9:1,v/v) solution.

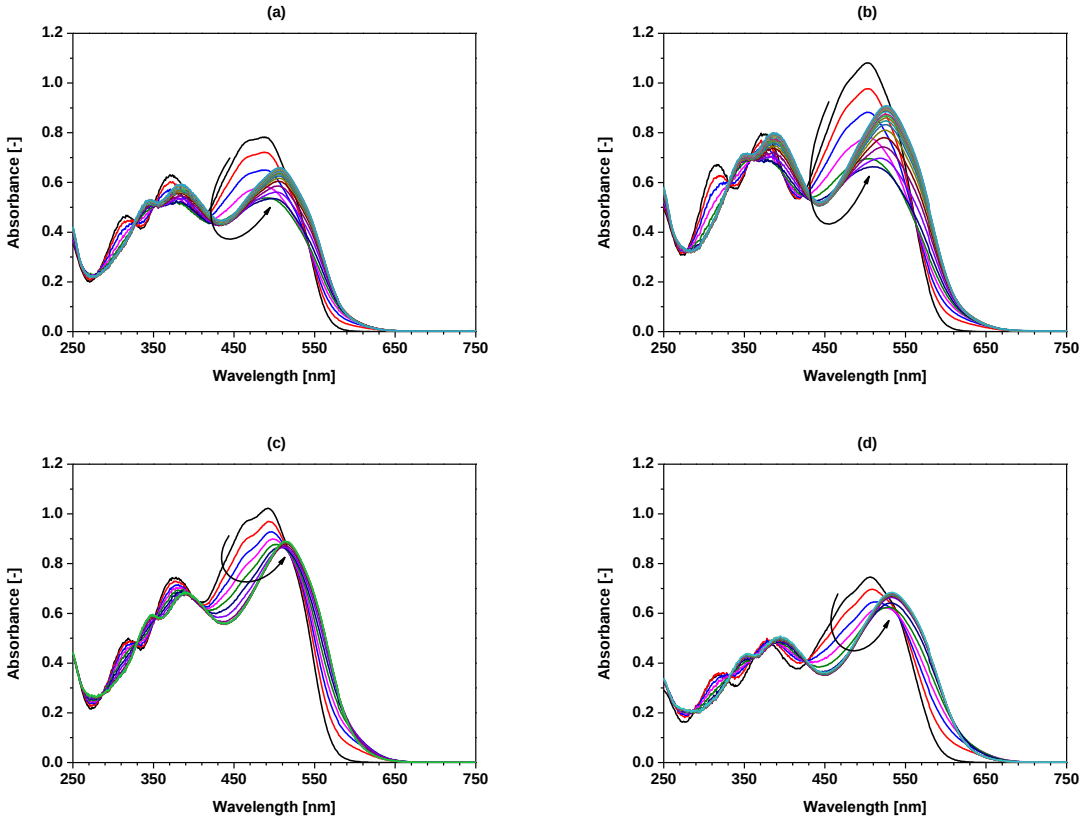

Fig. S21. Changes in absorption spectra of **1**-**4** during spectrophotometric titration with lead(II) perchlorate in acetonitrile: a) **1** ($c_1 = 4.97\times10^{-5}$ M) ($c_{Pb} = 0\text{-}9.46\times10^{-5}$ M); b) **2** ($c_2 = 4.96\times10^{-5}$ M) ($c_{Pb} = 0\text{-}9.93\times10^{-5}$ M); c) **3** ($c_3 = 5.09\times10^{-5}$ M) ($c_{Pb} = 0\text{-}6.17\times10^{-5}$ M); d) **4** ($c_4 = 4.91\times10^{-5}$ M) ($c_{Pb} = 0\text{-}7.11\times10^{-5}$ M).

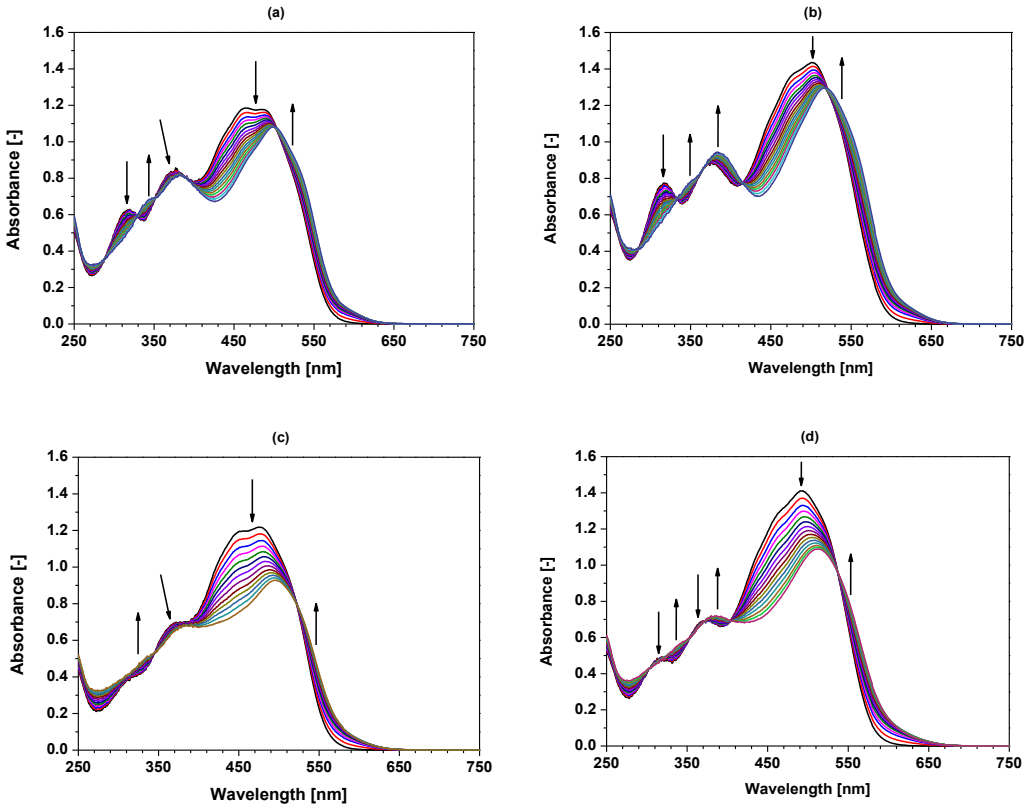

Fig. S22. Changes in absorption spectra of **5**-**8** during spectrophotometric titration with lead(II) perchlorate in acetonitrile a) **5** (c_5 = 4.97×10^{-5} M) (c_{Pb} = 0-5.54×10^{-5} M); b) **6** (c_6 = 4.99×10^{-5} M) (c_{Pb} = 0-5.97×10^{-5} M); c) **7** (c_7 = 4.90×10^{-5} M) (c_{Pb} = 0-5.12×10^{-5} M); d) **8** (c_8 = 5.00×10^{-5} M) (c_{Pb}= 0-5.97×10^{-5} M).

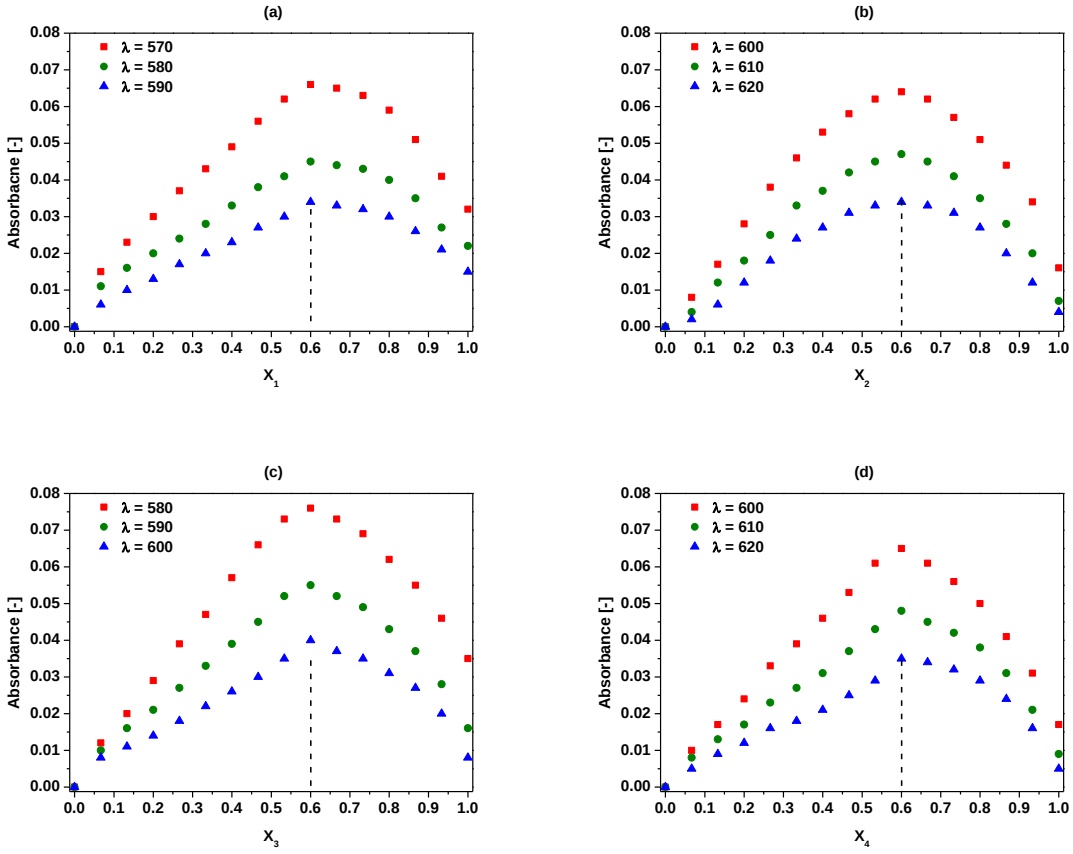

Fig. 23. Job's plots for complexes of **1**-**4** with lead(II) perchlorate: a) **1** ($c_1 = 2.49\times10^{-5}$ M), b) **2** ($c_2 = 2.48\times10^{-5}$ M), c) **3** ($c_3 = 2.55\times10^{-5}$ M) and d) **4** ($c_4 = 2.46\times10^{-5}$ M) in acetonitrile.

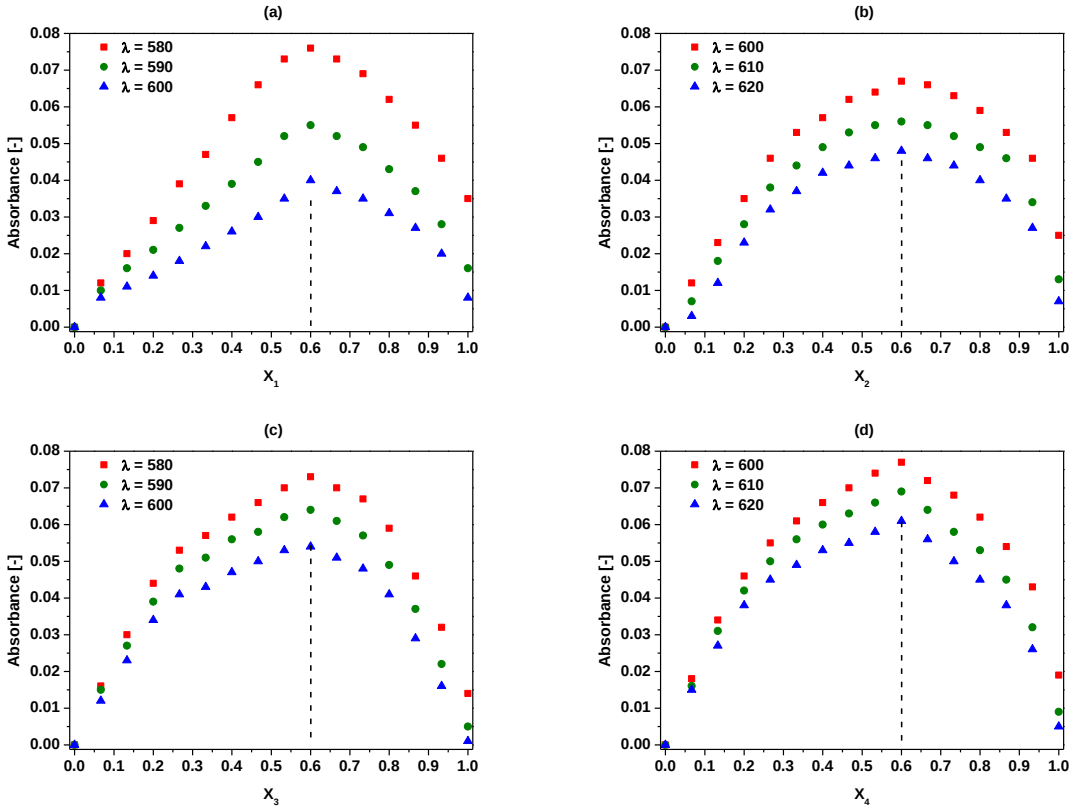

Fig. 24. Job's plots for complexes of **1**-**4** with lead(II) perchlorate: a) **1** ($c_1 = 2.49\times10^{-5}$ M), b) **2** ($c_2 = 2.48\times10^{-5}$ M), c) **3** ($c_3 = 2.55\times10^{-5}$ M) and d) **4** ($c_4 = 2.46\times10^{-5}$ M) in acetonitrile:water (9:1, v/v).

Table S3. Stability constants (log K) of complexes (3:2, crown:Pb(II)) of macrocycles **1**-**8** with lead(II) in acetonitrile and acetonitrile:water (9:1, v/v).

	1	**2**	**3**	**4**	**5**	**6**	**7**	**8**
acetonitrle	17.99±0.03	18.20±0.05	18.49±0.08	18.86±0.11	17.24±0.03	17.91±0.06	19.66±0.10	20.18±0.12
acetonitrile:water (9:1 v/v)	16.94±0.12	17.30±0.09	17.41±0.14	17.48±0.18	16.45±0.11	16.99±0.12	18.07±0.16	18.22±0.20

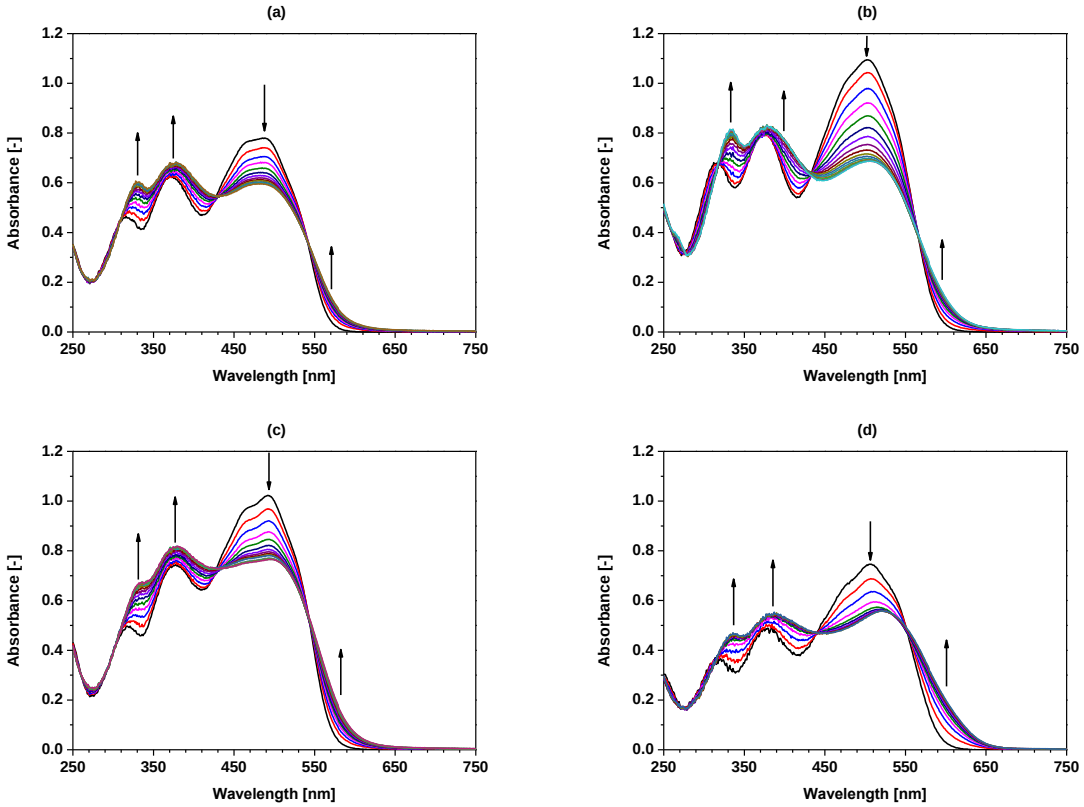

Fig. 25. Changes in the absorption spectra of compounds **1**-**4** during spectrophotometric titration with copper(II) perchlorate solution in acetonitrile: a) **1** ($c_1 = 4.97\times10^{-5}$ M) ($c_{Cu} = 0\text{-}6.97\times10^{-5}$ M); b) **2** ($c_2 = 4.96\times10^{-5}$ M) ($c_{Cu} = 0\text{-}8.03\times10^{-5}$ M); c) **3** ($c_3 = 5.09\times10^{-5}$ M) ($c_{Cu} = 0\text{-}7.50\times10^{-5}$ M); d) **4** ($c_4 = 4.91\times10^{-5}$ M) ($c_{Cu} = 0\text{-}6.92\times10^{-5}$ M).

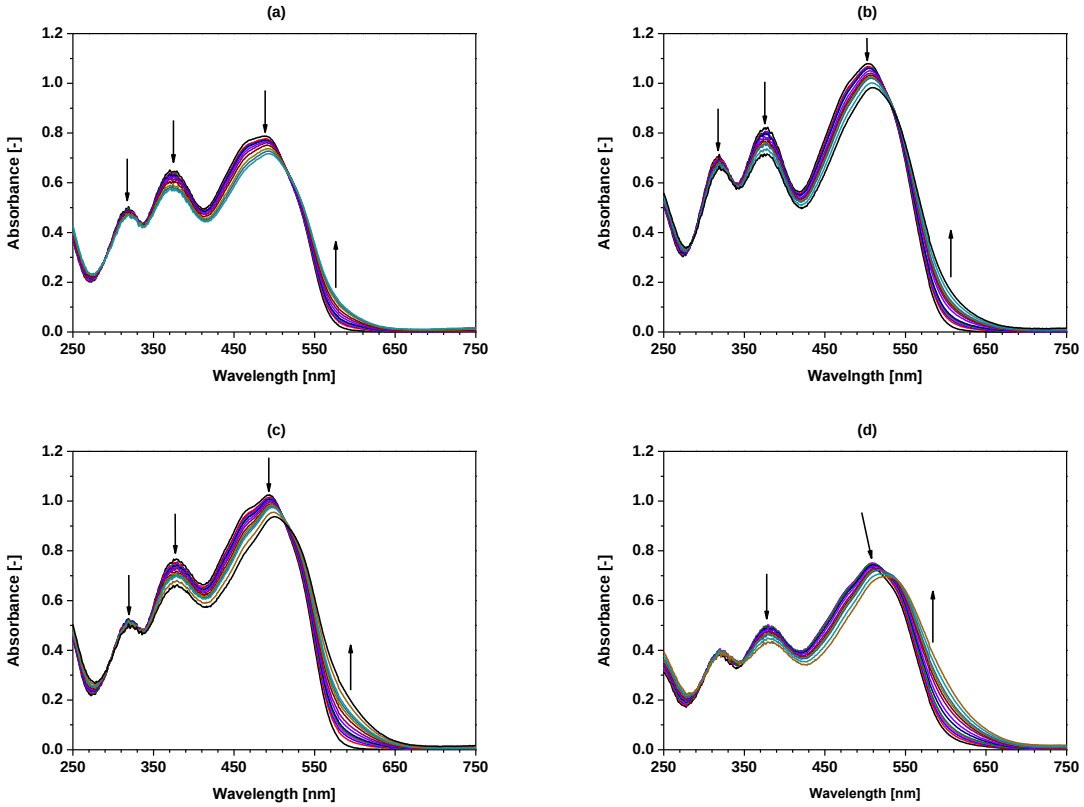

Fig. 26. Changes in the absorption spectra of compounds 1-4 during spectrophotometric titration with copper(II) perchlorate solution in acetonitrile:water (9:1, v/v) mixture: a) **1** ($c_1 = 4.97\times10^{-5}$ M) (c_{Cu} = 0-4.42×10^{-4} M); b) **2** ($c_2 = 4.96\times10^{-5}$ M) (c_{Cu} = 0-3.41×10^{-4} M); c) **3** ($c_3 = 5.09\times10^{-5}$ M) (c_{Cu} = 0-4.17×10^{-4} M); d) **4** ($c_4 = 4.91\times10^{-5}$ M) (c_{Cu}= 0-5.36×10^{-4} M).

Table S4. Linear response range and detection limits for copper(II) determined for sensor materials with chromoionophores **3**-**8**.

Material with…	Equation	R^2	Linear response Cu(II) [M]	LOD [M]
3	$y = 21.99 + 129.47$	0.9970	$1.0\times10^{-5} – 1.0\times10^{-3}$	1.49×10^{-6}
4	$y = 25.39 + 159.20$	0.9946	$1.0\times10^{-6} – 1.0\times10^{-3}$	6.23×10^{-7}
5	$y = 20.63 + 133.05$	0.9962	$1.0\times10^{-6} – 1.0\times10^{-3}$	4.17×10^{-7}
6	$y = 25.28 + 157.06$	0.9942	$1.0\times10^{-6} – 1.0\times10^{-3}$	7.02×10^{-7}
7	$y = 20.81 + 134.48$	0.9984	$1.0\times10^{-6} – 1.0\times10^{-3}$	4.09×10^{-7}
8	$y = 18.86 + 121.17$	0.9993	$1.0\times10^{-6} – 1.0\times10^{-3}$	4.45×10^{-7}

Table S5. Linear response range and detection limits for lead(II) determined for materials with chromoionophores **3**-**8**.

Material with…	Equation	R^2	Linear response Pb(II) [M]	LOD [M]
3	$y = 28.40 + 156.28$	0.9929	$1.0\times10^{-5} – 1.0\times10^{-3}$	3.51×10^{-6}
4	$y = 30.49 + 185.70$	0.9978	$1.0\times10^{-6} – 1.0\times10^{-3}$	9.20×10^{-7}
5	$y = 29.54 + 180.25$	0.9913	$1.0\times10^{-6} – 1.0\times10^{-3}$	8.85×10^{-7}
6	$y = 27.37 + 180.67$	0.9992	$1.0\times10^{-6} – 1.0\times10^{-3}$	2.84×10^{-7}
7	$y = 24.71 + 161.65$	0.9978	$1.0\times10^{-6} – 1.0\times10^{-3}$	3.31×10^{-7}
8	$y = 26.31 + 159.44$	0.9956	$1.0\times10^{-6} – 1.0\times10^{-3}$	9.83×10^{-7}

P5 – MACROCYCLIC DERIVATIVES OF IMIDAZOLE AS CHROMOIONOPHORES FOR BISMUTH(III)/LEAD(II) PAIR

Sensors & Actuators: B. Chemical 399 (2024) 134798

Contents lists available at ScienceDirect

Sensors and Actuators: B. Chemical

journal homepage: www.elsevier.com/locate/snb

Macrocyclic derivatives of imidazole as chromoionophores for bismuth (III)/lead(II) pair

Błażej Galiński [a], Ewa Wagner-Wysiecka [a,b,*]

[a] Department of Chemistry and Technology of Functional Materials, Faculty of Chemistry, Gdańsk University of Technology, Narutowicza Street 11/12, 80–233 Gdańsk, Poland

[b] Advanced Materials Center, Faculty of Chemistry, Gdańsk University of Technology, Narutowicza Street 11/12, 80–233 Gdańsk, Poland

ARTICLE INFO

Keywords:
Chromoionophore
Macrocycle
Imidazole
Optode
Cellulose triacetate
Bismuth(III)
Lead(II)

ABSTRACT

18-membered diazomacrocycles with imidazole or 4-methylimidazole residue as a part of macrocycle were used as chromoionophores in bismuth(III) and lead(II) dual selective optodes for the first time. Cellulose triacetate membranes doped with macrocyclic chromoionophores are bismuth(III) and lead(II) selective with color change from orange/red to different shades of blue and violet, respectively. Results obtained for model and real samples of bismuth(III) and lead(II) showed that easily accessible and regenerable sensor materials can be used for spectrophotometric and colorimetric detection and determination of bismuth(III) and lead(II). The obtained LOD values for bismuth(III) are 1.63×10^{-7} M and 3.03×10^{-7} M with spectrophotometric and colorimetric detection, respectively, when using optode with imidazole residue. For sensing material with 4-methylimidazole in macroring the lowest detection limits were obtained for lead(II): 2.14×10^{-7} M and 3.99×10^{-7} M with spectrophotometric and digital color analysis detection mode, respectively.

1. Introduction

Bismuth(III) is a heavy metal with a relatively low toxicity and has been used by man in various areas of his activity since ancient times, although being confused with other metals, e.g. lead or tin [1,2]. Currently it is used in medicine, electronics or nuclear industry [3–11]. Bismuth(III) is used as a leading non-toxic substitute for lead(II) in brass hydraulic devices, fishing weights, free machining steel and solder, and as a metallurgical additive in casting. Bismuth applications also cover ceramic glazes, pearl pigments, lubricants and crystal products. The lack of toxicity associated with some bismuth salts has led to a growing number of reports exploring their potential applications in synthetic chemistry [12–15]. Interesting and important seems to be the potential of a photocatalytic process based on bismuth(III) catalyst for the ammonia production [16]. It can be an environmentally friendly alternative for energy consuming Haber-Bosch process. Bismuth(III) complexes also show antibacterial activity. However, it has been shown that under certain conditions it can be toxic to the human body [17].

The above is causing a growing interest in finding reliable, but also convenient for the analyst, methods of determining bismuth(III) which can be alternatives to the currently used methods. Most current methods for the determination of bismuth(III) are instrumental techniques [18–23] including atomic absorption spectroscopy (AAS), X-ray fluorescence spectroscopy (XRF) and others. These methods require significant economic outlays, taking into account the costs of both equipment and the properly qualified personnel. Optical sensors, that can also be used in field analysis, can be an alternative or complementary to many analytical methods that are used in research laboratories [24–36].

The expanding interest in the coordination chemistry of lead(II) and bismuth(III) is connected, among the others, with the potential applications of the radioisotopes of these metal cations as radiopharmaceuticals. Bismuth-212 and bismuth-213 have relatively short half-lives (61 and 46 min respectively). Therefore the usage of longer-lived radionuclides such as ^{212}Pb (half-life 10.6 h) can be proposed as an in situ generator of ^{212}Bi. Thanks to this, the half-life of radioactive bismuth-212 can be extended to about 11 h [37,38]. Therefore the eventual chelators should have high affinity towards both lead(II) and bismuth (III). Acyclic azo derivative was found to form hypervalent bismuth(III) compound in which a nitrogen of azo group and oxygen atoms were engaged in coordination [15]. Authors reported that the binding constant must be very low in the case of this acyclic derivative of azobenzene thus was not given. Macrocyclic compounds, providing the

* Corresponding author at: Department of Chemistry and Technology of Functional Materials, Faculty of Chemistry, Gdańsk University of Technology, Narutowicza Street 11/12, 80–233 Gdańsk, Poland.
E-mail address: ewa.wagner-wysiecka@pg.edu.pl (E. Wagner-Wysiecka).

https://doi.org/10.1016/j.snb.2023.134798
Received 18 July 2023; Received in revised form 14 October 2023; Accepted 15 October 2023
Available online 17 October 2023

selectivity of the molecular recognition, are well known host molecules for the metal cations. Suitably designed compounds, in terms of the type and number of donor sites, can also be used for quantitative determination of metal ions through colorimetric detection. Among macrocyclic ligands forming complexes with bismuth(III) and lead(II) a series of ligands was investigated, such as cyclens and others [39–41] acting as N, O donor ligands. An excellent selectivity towards bismuth(III) was also found for tetra-substituted benzimidazole zinc(II) phthalocyanine [42]. Several ideas of the application of optical sensors (Table 1 and Table 2) for bismuth(III) [43–47] and/or lead(II) [48–59] determination were also proposed. Various approaches can be used to achieve selective materials. The most popular and longest-used optode design uses an ionophore/chromophore system, as for example in the case of lead(II) optical sensors with an acyclic [48,49] or a macrocyclic ionophore such as crown ether [50,51] or calix[4]arene [55]. Reducing the number of components in the detection layers is achieved by using a selective chromogenic complexing reagents of the metallochromic indicator type. Such solutions can be found for both lead(II) [56–58] and bismuth(III) [46,47] optodes. Some attempts include the use of chromogenic macrocycles as a more selective complexing reagents [59], but these are few examples. Another option in metal cation optical sensor design is to change the material used to immobilize the components of the sensing layer. It is relatively common to use PVC [43,48–51,53,55], CTA [44–46,52,54,56,59] or others such as agarose [57] or, for example, chitosan-silica matrix [58]. Porous glass in combination with macrocyclic chromoionophore was proposed as aluminum sensitive optical sensor [60].

In this article we describe azo macrocyclic compounds acting as O,N effective colorimetric receptors for borderline Lewis acids: lead(II) and bismuth(III). The possible application of macrocycles for determination of bismuth(III) and lead(II) in water samples is also proposed.

2. Materials and methods

2.1. Chemicals

Diazomacrocycles **1** and **2** (Fig. 1) were prepared according to the previously reported by us method [61,62]. The identity of chromoionophores was confirmed by the comparison of NMR and FT-IR spectra and TLC data with data for genuine samples of these compounds deposited in our lab.

All chemicals of the highest available purity were purchased from commercial sources and used without further purification. The complexation of metal cations was studied using appropriate nitrates: $NaNO_3$ (≥99.8 %), KNO_3 (≥99.8 %), $Mg(NO_3)_2 \times 6\ H_2O$ (≥99.0 %), $Ca(NO_3)_2 \times 4\ H_2O$ (≥99.0 %), $Ni(NO_3)_2 \times 6\ H_2O$ (≥98.0 %), $Zn(NO_3)_2 \times 6\ H_2O$ (≥98.0 %), $Al(NO_3)_3 \times 9\ H_2O$ (≥98.0 %), $Cr(NO_3)_3 \times 9\ H_2O$ (≥99.0 %), $Fe(NO_3)_3 \times 9\ H_2O$ (≥98.0 %) from POCh, $Cu(NO_3)_2 \times 3\ H_2O$ (≥99.5 %) from Merck, $Pb(NO_3)_2$ (≥99.0 %) from Alfa Aesar and $Bi(NO_3)_3 \times 5\ H_2O$ (≥98.0 %) from Sigma Aldrich. Dimethyl sulfoxide (DMSO), dichloromethane, acetone, 2-propanol, nitric acid, sodium hydroxide and disodium ethylenediaminetetraacetate dihydrate (EDTA) were purchased from POCh. All aqueous solutions were prepared using ultra-pure water obtained by the reverse osmosis (RO) from Hydrolab Poland station (conductivity <1 μS/cm^{-1}). For recovery studies Standard Reference Solution of bismuth(III) 1000 ppm and lead (II) 1000 ppm from Merck was used.

For the preparation of the receptor layers of optical sensors cellulose triacetate (CTA), triethylene glycol ≥ 99.0 % (TEG) and potassium tetrakis(4-chlorophenyl)borate ≥ 98.0 % (KTClPB) from Sigma Aldrich were used.

Table 1
Spectrophotometric linear response with equations, LOD and LOQ for optode **1** and **2** for bismuth(III) or lead(II).

Optode	Ion	Equation	R^2	Dynamic range [M]	LOD [M]	LOQ [M]
1	Bi (III)	$y = 32{,}530.50 \times x + 0.0030$	0.9995	7.13×10^{-7} – 1.50×10^{-5}	1.63×10^{-7}	5.38×10^{-7}
	Pb (II)	$y = 22{,}902.52 \times x - 0.0017$	0.9990	8.91×10^{-7} – 1.70×10^{-5}	2.31×10^{-7}	7.62×10^{-7}
2	Bi (III)	$y = 27{,}465.62 \times x + 0.0053$	0.9992	7.13×10^{-7} – 1.76×10^{-5}	1.71×10^{-7}	5.64×10^{-7}
	Pb (II)	$y = 21{,}954.11 \times x + 0.0138$	0.9987	8.91×10^{-7} – 2.02×10^{-5}	2.14×10^{-7}	7.06×10^{-7}

Table 2
Colorimetric linear response with equations, LOD and LOQ values for optode **1** and **2** for bismuth(III) or lead(II).

Optode	Ion	Equation	R^2	Dynamic range [M]	LOD [M]	LOQ [M]
1	Bi (III)	$y = 8{,}402{,}510 \times x + 2.9592$	0.9957	7.13×10^{-7} – 1.50×10^{-5}	3.03×10^{-7}	1.00×10^{-6}
	Pb (II)	$y = 5{,}777{,}870 \times x + 2.3911$	0.9972	8.91×10^{-7} – 1.70×10^{-5}	4.41×10^{-7}	1.46×10^{-6}
2	Bi (III)	$y = 7{,}304{,}100 \times x + 0.0053$	0.9982	7.13×10^{-7} – 1.76×10^{-5}	3.22×10^{-7}	1.06×10^{-6}
	Pb (II)	$y = 5{,}895{,}590 \times x - 1.0959$	0.9975	8.91×10^{-7} – 2.02×10^{-5}	3.99×10^{-7}	1.32×10^{-6}

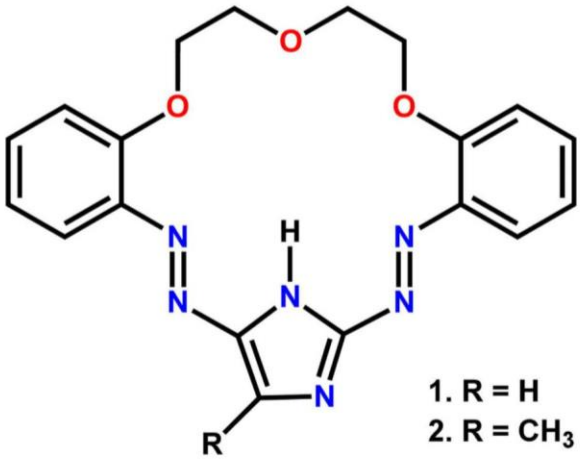

Fig. 1. Chromoionophores **1** and **2** [61,62].

2.2. Instrumentation

All UV-Vis absorption spectra were registered in 1 cm quartz cuvettes (Starna® Brand) using a Unicam UV-300 spectrometer. pH was monitored using pH-meter CPC-511 with glass electrode EPS-1 (ELMETRON), standardized with buffer solutions. Portable LED light box (23 × 23 × 23 cm) was used to guarantee the reproducibility of the photos (PULUZ, Photography Light Box, Shenzhen Puluz Technology Limited). Pictures were taken by a Smartphone Vivo Y11s.

2.3. Complexation studies

Considering the possible application of macrocycles for the determination of metal ions in aqueous media, we have chosen a mixture of polar and protic solvent - water - with polar DMSO mixing freely with water as solvent. The 1:1 (v/v) ratio of these solvents ensures the

solubility of macrocyclic compounds, which are insoluble in water. The use of a mixture of organic solvent and water also ensures the solubility of bismuth salts. That's why metal cation complexation studies were carried out using UV-Vis titration in DMSO:water (v/v, 1:1) mixture. A series of solutions of pH values ranging from 1 to 10 was fixed by addition of small amounts of sodium hydroxide solution (0.1 M) or nitric acid (0.1 M). The stock solutions of chromoionophores ($\sim 10^{-4}$ M) and metal nitrates ($\sim 10^{-4}$ M) were prepared by weighting the respective quantities of them and dissolving in the solvent system in volumetric flasks. The values of binding constant (logK) were calculated with the use of OPIUM [63] program on the basis of titration experiment data. The stoichiometry of complexes was confirmed by Job's method [64].

2.4. Membrane preparation

CTA optodes were prepared according to previously described procedures [59,65]. Membranes contained 250.0 mg of CTA, 1.0 mg of chromoionophore **1** or **2**, 168.6 mg (150.0 μL) of TEG and 1.5 mg of KTClPB. All components of optodes were dissolved in dichloromethane (6 mL) with continuous stirring using a magnetic stirrer for 2 h and were sonicated for ca. 15 min – until a clear solution is formed. In the next step, solutions were poured on, prepared in advance (washed with nitric acid, deionized water, acetone and 2-propanol) Petri dish (9 cm diameter), covered loosely with a lid and left for solvent evaporation. After 24 h obtained optode films were peeled off from the Petri dish and cut into 0.9 × 4.5 cm strips. Blank membranes were prepared in an analogous way using all components besides chromoionophores and a lipophilic salt.

2.5. Absorbance measurements

Before measurements, membranes were washed three times with deionized water to remove water-soluble additives from the surface. Then membranes were placed in a quartz cuvette containing water (2.4 mL) in the sample path of the spectrophotometer. Measurements were carried out against blank membranes in the reference path of the spectrophotometer. Then the content of the measurement cell was titrated with a solution of bismuth(III) or lead(II) nitrate.

Limits of detection (LOD) for bismuth(III) and lead(II) were calculated using relationship: LOD = 3σ/k, where σ is the standard deviation of the blank and k is the slope of the linear function A = f(molar concentration of analyte). Limits of quantitation (LOQ) were approximated by multiplying the LOD by 3.3. The spectral response towards bismuth (III) and lead(II) was expressed as $\Delta A = A_{Bi/Pb} - A_0$, where A_0 stands for absorbance of optode with compound **1** or **2** and $A_{Bi/Pb}$ absorbance value of optode in the presence of bismuth(III) or lead(II) salt. The influence of interfering ions on spectrophotometric response towards bismuth(III) or lead(II) was expressed as the absolute value of relative response $RR\% = |[(A - A_{Bi/Pb})/A_{Bi/Pb}]| \times 100$ %, where $A_{Bi/Pb}$ stands for absorbance of optode with diazocrowns in the presence of bismuth(III) or lead(II) nitrate and *A* is absorbance value of optode measured just after addition of interfering metal nitrate in the 10-fold molar excess in relation to bismuth(III) or lead(II) nitrate [59,65,66].

2.6. Digital color analysis

Pictures were analyzed using free software ImageJ [67–69]. The change of optode color given as ΔE_{RGB} [59,65,70–72] was calculated using the equation: $\Delta E_{RGB} = [(R_0 - R)^2 + (G_0 - G)^2 + (B_0 - B)^2]^{1/2}$ where R_0, G_0 and B_0 values correspond to color of optode in the absence of bismuth(III) or lead(II) salt, and R, G and B values correspond to color of optode in the presence of bismuth(III) or lead(II) ions.

3. Results and discussion

3.1. Investigation of the complexing properties in solution

In order to determine the ion complexing ability and the effect of the presence of metal ions on the spectroscopic characteristics of compounds **1** and **2**, a series of spectrophotometric titrations were carried out in a DMSO:water (v/v, 1:1) mixture. Changes in the absorption spectra of solutions of compounds **1** and **2** during titration with a solution of bismuth(III) and lead(II) nitrate in a mixture of DMSO:water (1:1, v/v) are shown in Fig. 2. The absorption maxima for **1** and **2** are located at 502 nm and 516 nm, respectively. In both cases, the presence of bismuth(III) or lead(II) salts results in a appearance of new, redshifted of 80 or 46 nm for **1** and 96 or 58 nm for **2**, band respectively for the complex with bismuth(III) or lead(II). The presence of a well-defined isosbestic point indicates the existence of one equilibrium under the conditions of spectrophotometric titration.

^{1}H NMR spectra of **2** (Fig. 3 and full range spectra Fig. S1-S3) registered in DMSO-d_6 indicate that the formation of the complex with bismuth(III), as expected, involves the coordination of metal ion by oxygen atoms of the oligoether chain which is manifested by downfield shift of signals labeled as a,a′ and b,b′. When spectrum is registered for 1:1 molar ratio of complex components, a double set of oligoether proton signals is observed pointing out that under measurement conditions complex of higher stoichiometry can be formed. The position of most signals of aromatic protons is unchanged, however an additional signal of low intensity at ~8 ppm is present. Single set of signals (with residual double set) is observed when the 10-fold excess of bismuth(III) nitrate was used in experiment. The signal of methyl group protons shifts + 0.26 ppm in complex, which points to the engagement of the nitrogen of the imidazole ring in complex formation (see Fig. S1-S3).

This can correlate with the results obtained from the analysis of the molar ratio curves obtained during the spectrophotometric titration (Fig. S4) and Job's plots (Fig. S5) on the basis of which a triple-decker complex (double sandwich complex 3:2 crown:bismuth(III)) can be proposed. The formation of the complex is accompanied by a change in the equivalence of the protons of the oligoether chain, which indicates the symmetry of the forming system. The spectrum recorded in the presence of a 10-fold excess of salt indicates that the formation of the complex may be accompanied by deprotonation of the imidazole ring. However, it cannot be ruled out that the signal of the N-H proton observed in the spectrum of compound **2** at 11.99 ppm (in the presence of an equimolar salt, a weakly visible signal in this region of the spectrum) is not visible in the spectrum of the complex due to the significant share of water in the analyzed sample derived from the hydrated salt.

The stability constants of the complexes were calculated using the OPIUM [63] software and titration data. For the assumed 3:2 crown: metal cation complexation model, stability constant values (logK) for bismuth(III) complexes of **1** and **2** are 17.51 ± 0.08 and 16.67 ± 0.06, respectively.

Molar ratio curves with lead(II) nitrate and Job's plot (Fig. S6 and Fig. S7) also allow to assume the formation of a triple-decker complex. This similar complexation model that was found for pyrrole bearing macrocyles [66]. The stability constants values (logK) of the complexes of compounds **1** and **2** with lead(II) are 17.10 ± 0.04 and 17.46 ± 0.03, respectively. Comparison of the stability constant values of the above complexes (Fig. 4) shows that both macrocycles form complexes with bismuth(III) and lead(II) of comparable stability. However for macrocycle **1** the binding constant for bismuth(III) is slightly higher than for **2**. On the other hand **2** binds lead(II) stronger than macrocycle **1**.

Complexation of bismuth(III) by chromogenic macrocyclic azo compounds is to our knowledge reported for the first time.

3.2. UV-Vis spectral characterization of optodes

The spectral properties of the prepared sensing materials (optodes)

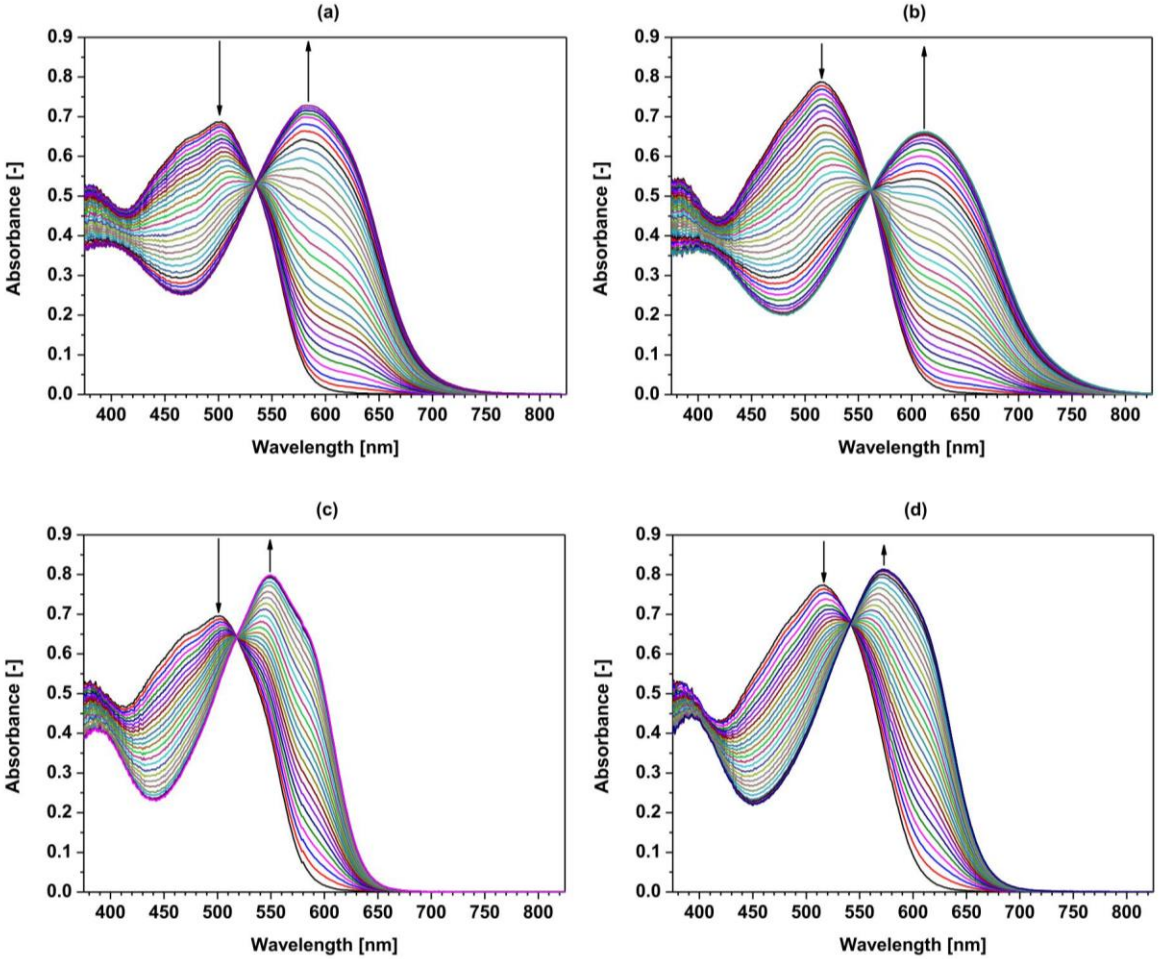

Fig. 2. Changes in the absorption spectra of chromoionophores during spectrophotometric titration with a solution of bismuth(III) nitrate: a) **1** ($c_1 = 4.10 \times 10^{-5}$ M) ($c_{Bi(III)} = 0 - 6.29 \times 10^{-5}$ M), b) **2** ($c_2 = 4.11 \times 10^{-5}$ M) ($c_{Bi(III)} = 0 - 7.91 \times 10^{-5}$ M); and with solution of lead(II) nitrate c) **1** ($c_1 = 4.10 \times 10^{-5}$ M) ($c_{Pb(II)} = 0 - 7.35 \times 10^{-5}$ M) and d) **2** ($c_2 = 4.11 \times 10^{-5}$ M) ($c_{Pb(II)} = 0 - 7.83 \times 10^{-5}$ M) in DMSO:water (1:1, v/v).

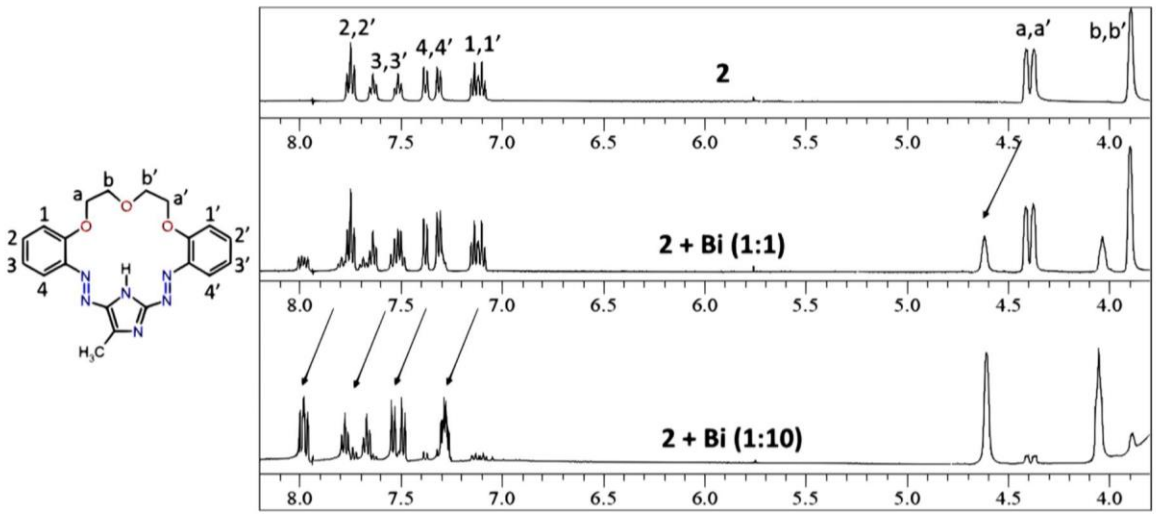

Fig. 3. ^{1}H NMR spectrum of **2** ($c_2 = 3.64 \times 10^{-3}$ M) and its spectra recorded in the equimolar amount and ten-fold excess of bismuth(III) nitrate in DMSO-d_6.

based on the macrocycles **1** or **2** and cellulose triacetate as polymer matrix have been studied. For preliminary studies the membranes were obtained without the addition of the lipophilic salt. In Fig. 5 changes in the absorption spectra of optodes in the presence of bismuth(III) and lead(II) nitrates in water are shown. The maximum of absorption for optode with macrocycle **1** is located at 472 nm and for **2** at 502 nm. It shifts towards 587 (for **1**, Δ +115 nm) and 604 nm (for **2**, Δ +102 nm), when titrated with aqueous solution of bismuth(III) nitrate. Upon titration with aqueous solution of lead(II) nitrate the absorption bands are located at 550 (for **1**, Δ +78 nm) and 572 nm (for **2**, Δ +70 nm). The

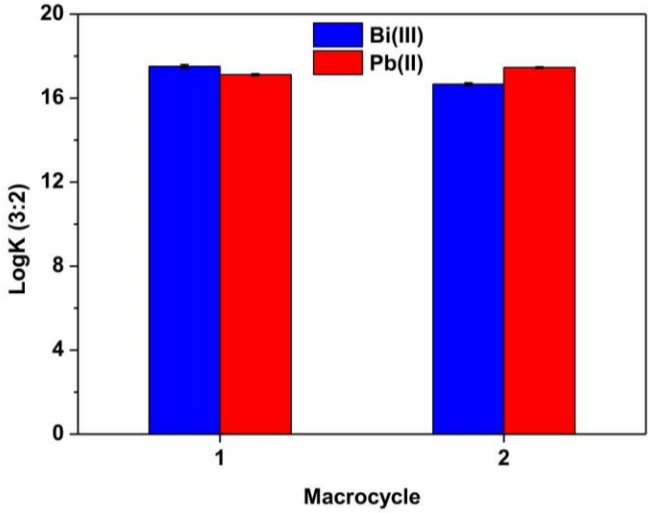

Fig. 4. Comparison of the values of stability constants (logK) of bismuth(III) and lead(II) complexes (3:2) of macrocycles **1** and **2** in DMSO:water (1:1, v/v) solvent system.

nature of spectral changes for macrocycles entrapped in a polymeric matrix is similar to those which are observed for the corresponding systems in solution (Fig. 2), however it is worth to noting that the spectral bathochromic shifts observed upon metal cation complexation are higher for system entrapped in cellulose triacetate polymeric matrix than in DMSO:water solvent mixture. It can be connected with the competing interactions with the chemical environment, namely the polarity and hydrogen bonding affinity of the components. It can be assumed that the spectral changes observed for the optodes are the result of the formation by bismuth(III)/lead(II) complexes with chromoionophores **1** or **2** immobilized in the membranes.

3.2.1. The effect of lipophilic salt

The effect of the lipophilic salt - KTClPB - and its amount (0.5 – 3.0 mg) on parameters like: the value of the generated signal ΔA, time of response and the percentage of leaching of chromoinonophores from membranes (after ten times usage) was investigated. As a model system, optodes with macrocycle **1** were taken. Fig. S8a shows that the highest increase of optical signal, defined as ΔA, is obtained for membranes containing 2.0 mg of the KTClPB. The lipophilic salt content also affects the response time of optodes (Fig. S8b). In general, the response time is lower for bismuth(III) than for lead(II). The response time increases depending on the amount of lipophilic salt from 3 to 6 min for bismuth (III) and from 10 to 16 min for lead(II). The presence of lipophilic salt has also an effect on the stability of membranes regarding as leaching out of chromoionophore from the membrane. If the content of lipophilic salt is 1.5 or 2.0 mg the leaching percentage of chromoionophore from membranes is less than 2 % (Fig. S8c) after 10 regeneration cycles. Having in mind the previously proposed model of the lead(II) binding by pyrrole macrocycles entrapped CTA membranes [59] we assume the possible functioning mechanism of optodes for bismuth(III) (Eq.1) and

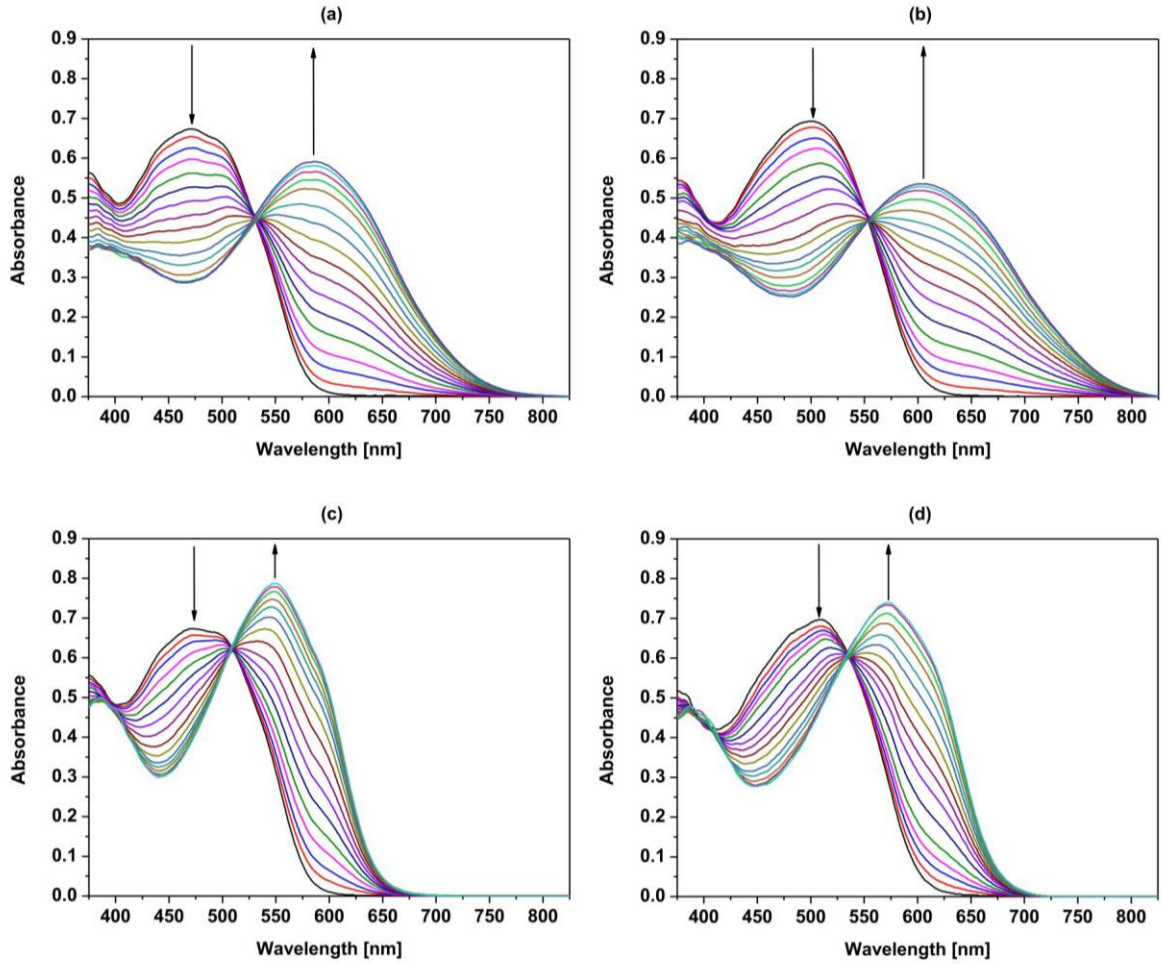

Fig. 5. Change of absorption spectra for optodes with macrocyclic derivatives **1** or **2** as chromoionophores upon titration with bismuth(III): a) **1** ($c_{Bi(III)} = 0 - 2.02 \times 10^{-5}$ M) and b) **2** ($c_{Bi(III)} = 0 - 2.14 \times 10^{-5}$ M); lead(II): c) **1** ($c_{Pb(II)} = 0 - 2.33 \times 10^{-5}$ M) and d) **2** ($c_{Pb(II)} = 0 - 2.33 \times 10^{-5}$ M).

lead(II) (Eq.2):

$$2Bi^{3+}_{(aq)} + 3LH_{(org)} + 3R^{-}_{(org)} \rightleftarrows (Bi_2L_3)^{3+}_{(org)} + 3R^{-}_{(org)} + 3H^{+}_{(aq)} \quad (1)$$

$$2Pb^{2+}_{(aq)} + 3LH_{(org)} + 2R^{-}_{(org)} \rightleftarrows (Pb_2L_3H)^{2+}_{(org)} + 2R^{-}_{(org)} + 2H^{+}_{(aq)} \quad (2)$$

It suggests chromoionophore (L)/lipophilic salt (R) ratio 1.0 and 1.5 with bismuth(III) and lead(II), respectively. Taking all above into account, 1.5 mg of lipophilic salt was selected for further testing of optodes. Membranes of such composition were investigated as described in the next sections.

3.2.2. Effect of pH

The influence of pH on the response of the optodes was tested by immersing the membranes in previously prepared solutions of lead(II) or bismuth(III) nitrates (1.05×10^{-5} M) of fixed pH, which were obtained by diluting with small amounts of solution of nitric acid (1.0 M) or sodium hydroxide (0.1 M). The constant response of the optodes in the pH 5 – 9 range and pH 6 – 9, respectively for bismuth(III) and lead(II) (Fig. 6)was found, thus pH 6 was chosen for further research. However, it is worth mentioning that it is possible to detect and determine bismuth (III) in the presence of lead(II) in an acidic environment (below pH 1) in which no spectral response for lead(II) is observed.

3.2.3. Response time of optodes

The response time t_{95} of the optodes was determined as the change of the generated signal (ΔA) over time (Fig. S9). The response time t_{95} for the optodes with compounds **1** and **2** at the bismuth(III) nitrate concentration of 1.05×10^{-5} M is 5 min. Longer response time 15 min was determined for optodes **1** and **2** after contact with solution of lead(II) nitrate. Response time of 5 min was taken for further testing of bismuth (III) ions and 15 min for lead(II).

3.2.4. Reversibility

The possibility of regeneration of optodes after use - to make them reusable - was checked using EDTA and HNO_3 (0.1 M) as regeneration solutions after contact with bismuth(III) or lead(II) salts (1.05×10^{-5} M) at pH 6, respectively. Regeneration time for optodes with compounds **1** and **2** was 2 min, when using EDTA and 1 min when for regeneration HNO_3 was used. After regeneration, optodes were washed three times with deionized water. In Fig. S10 regeneration of optodes is shown. After ten cycles of immersion in bismuth(III) nitrate a drift of optical signal was less than 1.5 % and 1.2 %, for optodes with macrocycles **1** and **2**, respectively, and less than 1.9 % and 1.4 % after ten cycles with lead(II) salt for membranes with compound **1** and **2**, respectively. It means that optodes can be used without a loss of their properties at least ten times.

3.2.5. Repeatability and lifetime

The reproducibility of optodes was evaluated by comparing the ΔA values of the bismuth(III) and lead(II) loaded membrane samples obtained in the different series for concentration 1.05×10^{-5} M (Fig. S11). The relative standard deviations for the measured ΔA (n = 10) values, were 1.0 % and 1.4 % for optodes with crown **1**, 1.2 % and 1.5 % for optodes with crown **2**, after contact with bismuth(III) and lead(II) nitrates respectively.

The lifetime of all membranes was determined by immersing membranes in water solution and measuring the value of ΔA over time, i.e. after: 1, 2, 3, 7, 14, 21 and 28 days. No significant loss of signal was found. Membranes were found to be insensitive to sunlight after 28 days. Just prepared optodes and not used for measurements can be stored safely for a period of at least 3 months in a dry and dark place (room conditions) without losing their properties (Fig. S12).

3.2.6. Effect of interfering ions

The response of prepared optodes was investigated in the presence of several interfering metal ions: Na(I), K(I), Ca(II), Mg(II), Ni(II), Cu(II), Zn(II), Pb(II), Al(III), Cr(III), Fe(III), Bi(III). The influence of other ions on the generation of optical signal was expressed as RR% value and was realized as addition of 10-fold molar excess of interfering salt to a solution of bismuth(III) or lead(II) nitrates (1.05×10^{-5} M) in which the sensing material was immersed (Fig. 7). The effect of solution composition was measured as a generated signal given as ΔA. For bismuth(III) only in the presence of lead(II) RR% value exceeds 5 % for both optodes (RR% = 10.8 – 13.3 %). For lead(II) the most interfering ion was iron(III) (RR% = 53.2 – 72.6 %) and bismuth(III) (RR% = 96.8 – 208.3 %), but the first one can be masked by sodium fluoride.

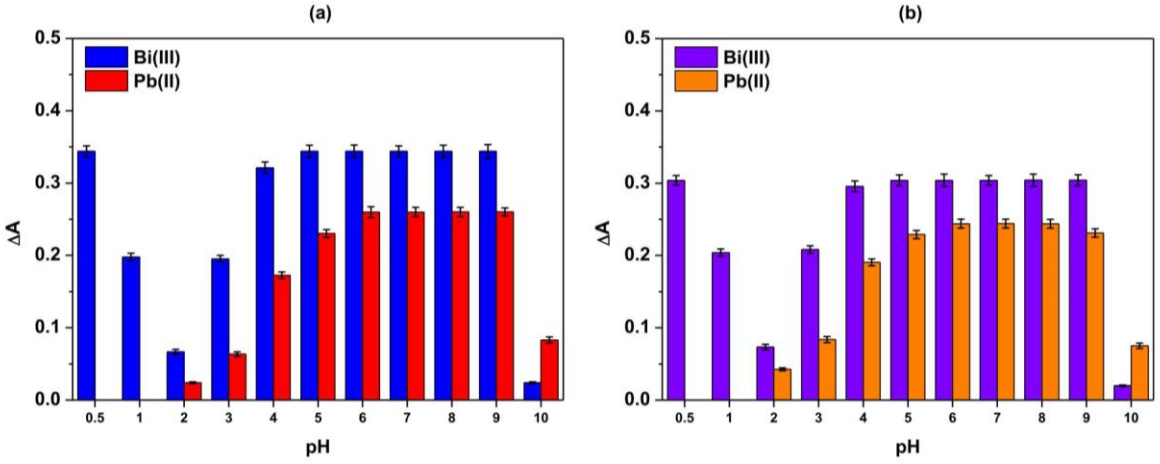

Fig. 6. Influence of pH on the response of the optodes with chromoionophores: a) **1** and b) **2**; towards bismuth(III) nitrate (1.05×10^{-5} M) and lead(II) nitrate (1.05×10^{-5} M) presence.

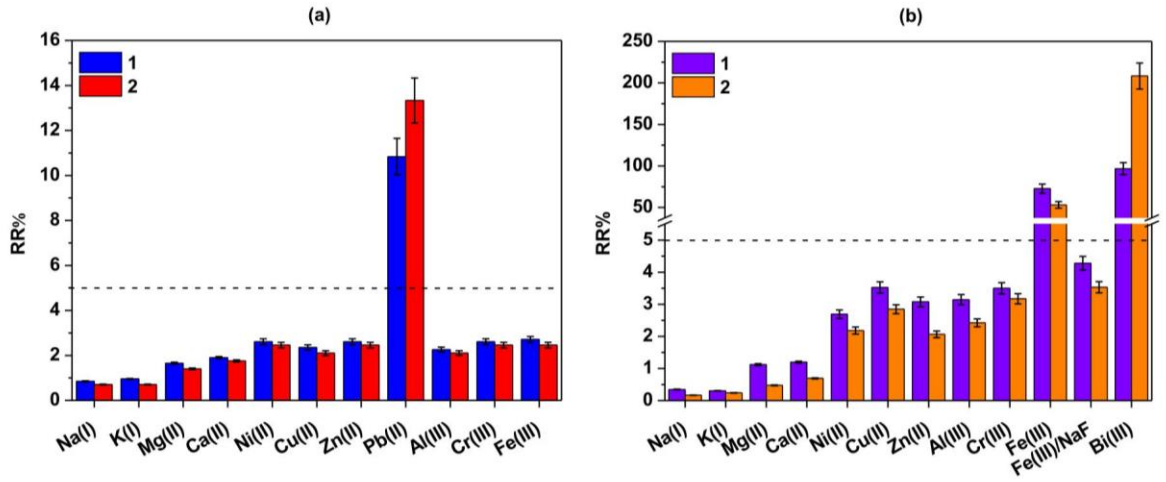

Fig. 7. Interferences from several metal cations (used in 10-fold molar excess), expressed as RR%, to spectral response (ΔA) of optodes with chromoionophores **1** and **2** towards: a) bismuth(III) and b) lead(II) nitrates.

3.3. Linear response range of membranes

The relationship: the value of the generated signal ΔA vs. the concentration of bismuth(III) or lead(II) for the membrane with compound **1** is presented in Fig. S13a and Fig. S13c. Fig. S13b and Fig. S13d show the change of the generated signal with the change of the concentration of bismuth(III) or lead(II) nitrates for membranes with macrocycle **2**. In Table 1 spectrophotometric linear response with equations, LOD and LOQ of optode **1** and **2** for bismuth(III) or lead(II) are collected.

3.4. Digital image colorimetry

Simultaneously with the studies of the spectral linear response of the optodes, the colorimetric analysis of the digital image was carried out. In Fig. 8 photos (taken using Smartphone) showing the color changes of the optodes after contact with aqueous bismuth(III) and lead(II) solutions (pH 6) are presented. In both cases, for both optodes, changes in the color of the membranes are well visible to the naked eye.

The dynamic range of the optodes, tested above spectrophotometrically, was determined as the dependence of the color change (ΔE_{RGB}) vs. concentration of bismuth(III) and lead(II) nitrates. The obtained relationships are shown in Fig. S14 and summarized in Table 2. It is worth noting that with the comparable range of linear response and similar LOD values, the optode with compound **1** characterizes with more significant color change than the optode with compound **2**, which translates into greater sensitivity of the membrane for bismuth(III) (Table 2). The opposite situation takes place in the presence of lead(II) ions, because in this case the optode with compound **2** generates a higher color change value, which indicates a higher selectivity.

3.5. Dual detection

Additional tests were carried out to check the possibility of the simultaneous detection and determination of bismuth(III) and lead(II). For this purpose, spectrophotometric titration was carried out with a solution containing both bismuth(III) and lead(II) in a molar ratio of 1:1 (total concentration 1.13×10^{-5} M). Changes in the absorption spectra of solutions of macrocycles **1** and **2** upon the titration with the mixture Bi(III)/Pb(II) in the DMSO:water (1:1) mixture are shown in Fig. 9.

The spectral trace is in correlation with the changes of spectra obtained for sensing materials with chromoionophores **1** and **2** (Fig. 10). The obtained values of stability constants of complexes with bismuth

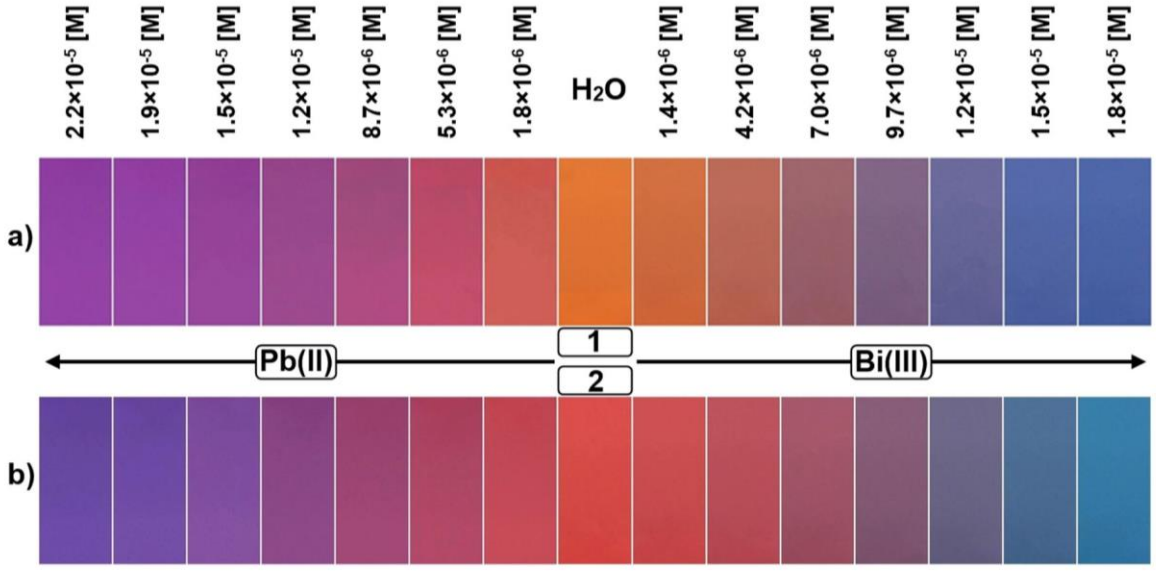

Fig. 8. Color change of the optodes with the compound: a) **1** and b) **2**; after contact with bismuth(III) and lead(II) nitrates of different concentrations in water.

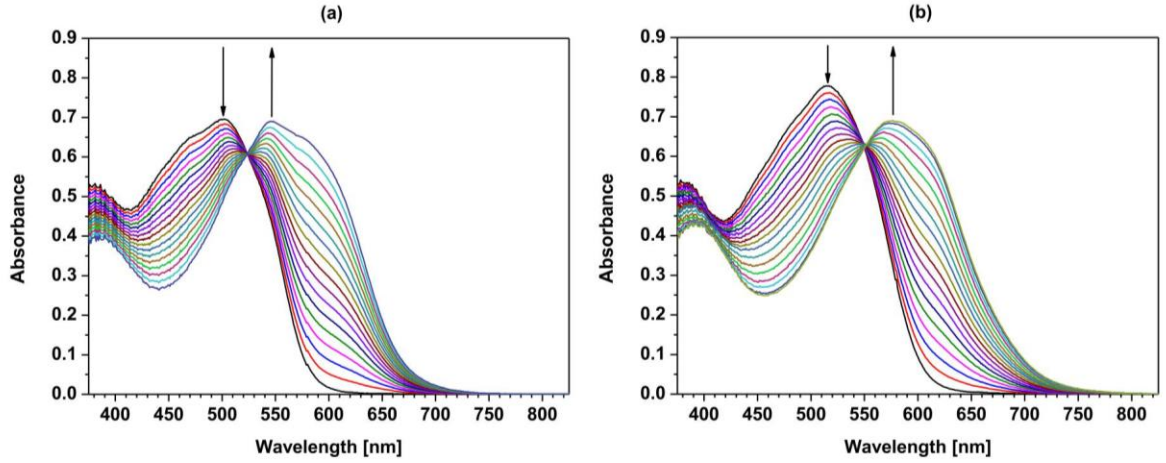

Fig. 9. Changes in the absorption spectra during spectrophotometric titration of **1** and **2** with bismuth(III) and lead(II) mixture: a) **1** ($c_1 = 4.10 \times 10^{-5}$ M) ($c_{Bi(III)/Pb(II)} = 0 - 1.71 \times 10^{-5}$ M) and b) **2** ($c_2 = 4.11 \times 10^{-5}$ M) ($c_{Bi(III)/Pb(II)} = 0 - 1.97 \times 10^{-5}$ M) in DMSO:water (1:1) mixture.

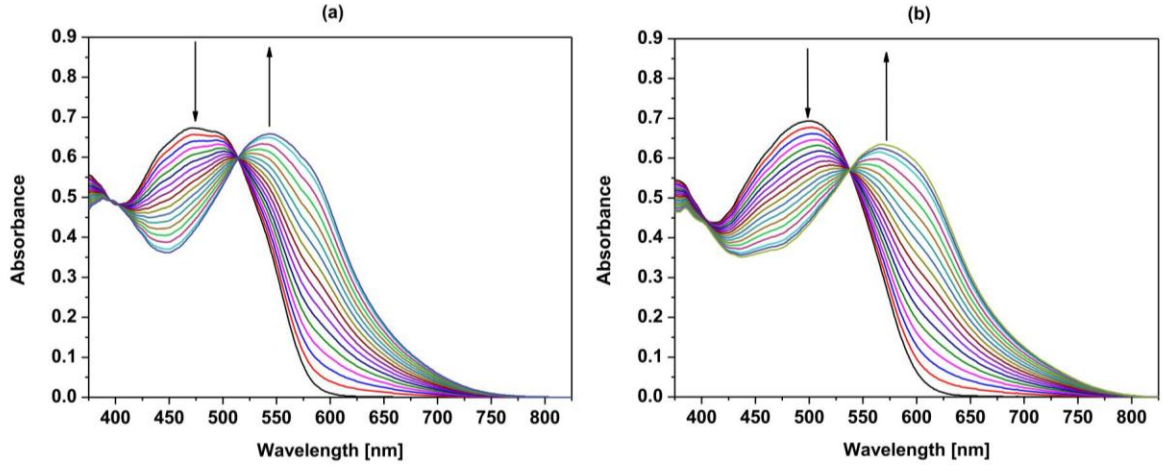

Fig. 10. Change of absorption spectra for optodes: a) **1** and b) **2**, in the presence of bismuth(III) and lead(II) ($c_{Bi(III)/Pb(II)} = 0 - 1.09 \times 10^{-5}$ M).

(III) and lead(II) are comparable, which means that both ions can effectively compete for binding sites of chromoionophores. During the titration, a new bathochromically shifted band is formed, the maximum of which is located at the wavelength corresponding to the maximum of lead(II) complex. However, the absorption band covers a broader spectral range - above 690 nm - which can correspond to the formation of a complex with bismuth(III) in the presence of lead(II). Therefore it can be assumed that the proposed system can be potentially regarded for

Table 3
Spectrophotometric linear response with equations, LOD and LOQ for optode **1** and **2** for dual detection of bismuth(III) and lead(II).

Optode	Ion	Equation	R^2	Dynamic range [M]	LOD [M]	LOQ [M]
1	Bi(III)	y = 10,574.87 ×x – 5.8280	0.9993	$7.13 \times 10^{-7} - 1.50 \times 10^{-5}$	5.00×10^{-7}	1.65×10^{-6}
	Pb(II)	y = 15,248.56 ×x + 8.1053	0.9982	$8.91 \times 10^{-7} - 1.70 \times 10^{-5}$	3.47×10^{-7}	1.15×10^{-6}
2	Bi(III)	y = 9604.91 ×x – 1.1736	0.9991	$7.13 \times 10^{-7} - 1.76 \times 10^{-5}$	4.88×10^{-7}	1.61×10^{-6}
	Pb(II)	y = 15,998.31 ×x – 5.1136	0.9981	$8.91 \times 10^{-7} - 2.02 \times 10^{-5}$	2.93×10^{-7}	9.67×10^{-7}

Table 4
Comparison of obtained optodes selective to bismuth(III) with already existing ones.

Sensing material	Support	Method	Dynamic range [M]	LOD [M]	LOQ [M]	Response time [min]	Reference
(2*E*,4*E*)– 5-(2,4-dinitrophenylamino)penta-2,4-dienal	PVC	Absorbance	$9.6 \times 10^{-7} - 2.9 \times 10^{-4}$	4.5×10^{-7}	1.5×10^{-6}	0.3	[43]
Methyltrioctylammonium chloride	CTA	Absorbance	$3.4 \times 10^{-6} - 4.8 \times 10^{-5}$	1.0×10^{-6}	3.3×10^{-6}	7	[44]
4-(4-nitrophenyl)– 1-naphthol	CTA	Absorbance	$1.9 \times 10^{-6} - 1.7 \times 10^{-5}$	6.7×10^{-7}	2.2×10^{-6}	0.5	[45]
Pyrocatechol violet	CTA	Absorbance	$5.0 \times 10^{-6} - 4.8 \times 10^{-5}$	8.5×10^{-7}	2.8×10^{-6}	10	[46]
Methyl thymol blue	Cellulose	Colorimetric	$2.4 \times 10^{-5} - 2.4 \times 10^{-4}$	1.4×10^{-5}	4.6×10^{-5}	10	[47]
1	CTA	Absorbance	$7.1 \times 10^{-7} - 1.5 \times 10^{-5}$	1.6×10^{-7}	5.3×10^{-7}	5	This work
		Colorimetric		3.0×10^{-7}	1.0×10^{-6}		
2	CTA	Absorbance	$7.1 \times 10^{-7} - 1.8 \times 10^{-5}$	1.7×10^{-7}	5.6×10^{-7}	5	This work
		Colorimetric		3.2×10^{-7}	1.1×10^{-6}		

dual detection bismuth(III) and lead(II) using the concentration dependence at two different analytical wavelengths values. One wavelength corresponds to the isosbestic point of the complex formed with bismuth(III). At this wavelength there is an increase in absorbance only in the presence of lead(II), namely at 532 and 554 nm, while the second one is 692 and 710 nm characteristic for bismuth(III) complex in the range where two bands do not overlap, for optode with compound **1** and **2**, respectively.

In Fig. S15 the range of linear response and comparison with the change of absorbance during spectrophotometric titration with individual ion salts at the wavelengths described above for a mixture of bismuth(III) and lead(II) is shown. These ranges overlap, which allows to determine the ranges of linear response for the concentrations of both analytes at the same time. Unfortunately, using colorimetric analysis, it was not possible to quantify bismuth(III) and lead(II) side by side. The dual sensing ranges of the linear response coincide with the ranges for single analytes, however, due to the smaller slopes of the characteristics, higher values of the detection limit are obtained (Table 3).

3.6. Comparison of optodes with other sensing materials

In Table 4 and Table 5 the properties of bismuth(III) and lead(II) selective optodes described in literature [43–59] are listed for comparison with the characteristics of membranes obtained in our studies. From this comparison it is quite well seen that optodes obtained by us are, in general, more or less comparable with those proposed by other authors.

3.7. Determination of bismuth(III) and lead(II) in model and real samples

Applications of the proposed optodes were tested using different samples: of known bismuth(III) and lead(II) concentrations – commercial bismuth(III) and lead(II) standard solution, and next spiked tap water from different regions of Northern Poland (3 series of 5 samples each). All measurements were done at pH 6. Both attempts were tested: spectrophotometric (ΔA) and colorimetric (ΔE_{RGB}) detection of bismuth (III) and lead(II), and ΔA for dual sensing of bismuth(III) with lead(II).

Comparison of recovery results obtained for optodes with chromoionophore **1** upon immersion of the sensor layer in Standard Reference Solution of bismuth(III) of different concentrations is collected in Table S1 and for optode with compound **2** in Table 6. The recoveries are at least about 98.92 – 101.56% for spectrophotometric detection (ΔA) for bismuth(III) in concentration range from 4.78×10^{-7} M to 9.57×10^{-6} M. Colorimetric determination is possible at the same concentration range with recovery 98.85 – 102.01 %. To evaluate the influence of the sample matrix three different samples of tap water were spiked with known concentration of bismuth(III). In this case recoveries are within 98.61 – 100.75 % for spectrophotometric detection (ΔA) and 98.80 – 101.02 % for colorimetric attempt (ΔE_{RGB}).

In Table S2 recovery results for obtained optodes with compound **1** after immersion in lead(II) solutions are presented and in Table 7 for optodes with chromionophore **2**. The recoveries in Standard Reference Solution of lead(II) are at least about 98.96 – 101.90% for ΔA and 98.18 – 100.85 % for ΔE_{RGB}. For samples of tap water spiked with lead(II) recoveries are 98.37 – 101.64 % for spectrophotometric detection and 99.05 – 101.74% for colorimetric detection.

Dual detection of bismuth(III) and lead(II) was possible only by using the spectrophotometric method. Comparison of recovery results are compiled in Table S3 an Table 8, respectively for optode **1** and **2**.

4. Conclusion

Easily available on non-complicated synthetic protocols, 18-membered chromogenic macrocycles bearing imidazole (**1**) or 4-methylimidazole (**2**) residues were investigated as bismuth(III) and lead(II) receptors in solution and after immobilization them in polymeric matrix (CTA). Investigated macrocycles are to our best knowledge the first

Table 5
Comparison of obtained optodes selective to lead(II) with already existing ones.

Sensing material	Support	Method	Dynamic range [M]	LOD [M]	LOQ [M]	Response time [min]	Reference
ETH 5435 + ETH 5418	PVC	Absorbance	$5.0 \times 10^{-9} - 5.0 \times 10^{-5}$	3.2×10^{-12}	1.1×10^{-11}	order of minutes	[48]
ETH 5493 + ETH 2439	PVC	Absorbance	$1.0 \times 10^{-7} - 5.0 \times 10^{-2}$	N/D	N/D	N/D	[49]
PAN + Dibenzodiaza-18-crown-6	PVC	Absorbance	$1.0 \times 10^{-8} - 5.0 \times 10^{-5}$	1.0×10^{-8}	3.3×10^{-8}	20	[50]
3′,3′,5′,5′-Tetrabromophenolphthalein ethyl ester potassium salt + Dibenzo-18-crown-6	PVC	Absorbance	$1.0 \times 10^{-5} - 1.0 \times 10^{-4}$	8.0×10^{-6}	2.6×10^{-5}	15	[51]
2-amino-cyclopentene-1-dithiocarboxylic acid	CTA	Absorbance	$1.0 \times 10^{-6} - 5.0 \times 10^{-1}$	6.9×10^{-7}	3.8×10^{-6}	10	[52]
Diphenylcarbazone	PVC	Absorbance	$6.9 \times 10^{-6} - 1.1 \times 10^{-2}$	6.5×10^{-6}	2.1×10^{-5}	3	[53]
4-hydroxy salophen	CTA	Absorbance	$1.0 \times 10^{-7} - 1.0 \times 10^{-3}$	8.6×10^{-8}	2.4×10^{-7}	10	[54]
Lead ionophore IV + ETH 5294	PVC	Absorbance	$6.2 \times 10^{-8} - 5.0 \times 10^{-5}$	2.5×10^{-8}	8.3×10^{-8}	30	[55]
Dithizone	CTA	Absorbance	$2.4 \times 10^{-6} - 2.7 \times 10^{-5}$	7.3×10^{-7}	2.4×10^{-6}	11–15	[56]
Dithizone	Agarose	Absorbance	$1.2 \times 10^{-8} - 2.4 \times 10^{-6}$	4.0×10^{-9}	1.3×10^{-8}	28	[57]
Dithizone	Chitosan-Silica	Absorbance	$9.7 \times 10^{-7} - 5.3 \times 10^{-6}$	5.3×10^{-7}	1.7×10^{-6}	3	[58]
18-membered diazocrown with pyrrole residue	CTA	Absorbance	$8.1 \times 10^{-8} - 2.2 \times 10^{-5}$	1.2×10^{-8}	4.0×10^{-8}	7	[59]
		Colorimetric	$7.8 \times 10^{-7} - 2.1 \times 10^{-4}$	8.6×10^{-7}	2.8×10^{-6}		
1	CTA	Absorbance	$8.9 \times 10^{-7} - 1.7 \times 10^{-5}$	2.3×10^{-7}	7.6×10^{-7}	15	This work
		Colorimetric		4.4×10^{-7}	1.5×10^{-6}		
2	CTA	Absorbance	$8.9 \times 10^{-7} - 2.0 \times 10^{-5}$	2.1×10^{-7}	6.9×10^{-7}	15	This work
		Colorimetric		4.0×10^{-7}	1.3×10^{-6}		

Table 6
Determination of bismuth(III) by optodes with chromoionophore **2** in real samples and for commercial standard reference solution.

	Added Bi (III) [M]	Found Bi (III)					
		ΔA Bi (III) [M]	Recovery %	RSD %	ΔE_{RGB} Bi (III) [M]	Recovery %	RSD %
Standard Reference Solution of bismuth(III)	4.78×10^{-7}	4.85×10^{-7}	101.56	4.40	4.88×10^{-7}	102.01	6.61
	9.57×10^{-7}	9.47×10^{-7}	98.92	3.80	9.58×10^{-7}	100.07	2.86
	4.78×10^{-6}	4.77×10^{-6}	99.78	1.58	4.78×10^{-6}	99.95	2.15
	9.57×10^{-6}	9.58×10^{-6}	100.06	0.76	9.46×10^{-6}	98.85	1.72
Tap water 1	0	< LOD	-	-	< LOD	-	-
	4.78×10^{-7}	4.73×10^{-7}	99.02	7.62	4.78×10^{-7}	100.10	8.59
	9.57×10^{-7}	9.59×10^{-7}	100.19	4.39	9.67×10^{-7}	101.02	3.30
	4.78×10^{-6}	4.79×10^{-6}	100.29	1.76	4.80×10^{-6}	100.33	2.32
	9.57×10^{-6}	9.60×10^{-6}	100.31	0.88	9.48×10^{-6}	99.04	1.66
Tap water 2	0	< LOD	-	-	< LOD	-	-
	4.78×10^{-7}	4.61×10^{-7}	96.48	4.40	4.74×10^{-7}	99.15	5.38
	9.57×10^{-7}	9.35×10^{-7}	97.65	2.20	9.53×10^{-7}	99.59	4.19
	4.78×10^{-6}	4.76×10^{-6}	99.53	1.16	4.77×10^{-6}	99.85	2.01
	9.57×10^{-6}	9.56×10^{-6}	99.93	0.58	9.46×10^{-6}	98.80	1.57
Tap water 3	0	< LOD	-	-	< LOD	-	-
	4.78×10^{-7}	4.73×10^{-7}	99.02	7.62	4.78×10^{-7}	100.10	7.73
	9.57×10^{-7}	9.47×10^{-7}	98.92	6.59	9.58×10^{-7}	100.07	6.29
	4.78×10^{-6}	4.77×10^{-6}	99.78	2.75	4.78×10^{-6}	99.95	3.43
	9.57×10^{-6}	9.58×10^{-6}	100.06	1.32	9.46×10^{-6}	98.85	2.50

Table 7
Determination of lead(II) by optodes with chromoionophore **2** in real samples and for commercial Standard Reference Solution.

	Added Pb (II) [M]	Found Pb (II)					
		ΔA Pb (II) [M]	Recovery %	RSD %	ΔE_{RGB} Pb (II) [M]	Recovery %	RSD %
Standard Reference Solution of lead(II)	4.78×10^{-7}	4.71×10^{-7}	98.47	5.50	4.69×10^{-7}	98.18	5.42
	9.57×10^{-7}	9.41×10^{-7}	98.37	2.75	9.44×10^{-7}	98.66	3.71
	4.78×10^{-6}	4.78×10^{-6}	100.06	1.91	4.78×10^{-6}	100.07	2.42
	9.57×10^{-6}	9.58×10^{-6}	100.11	0.73	9.57×10^{-6}	99.96	1.34
Tap water 1	0	< LOD	-	-	< LOD	-	-
	4.78×10^{-7}	4.78×10^{-7}	100.06	8.25	4.75×10^{-7}	99.36	7.10
	9.57×10^{-7}	9.57×10^{-7}	99.95	4.47	9.50×10^{-7}	99.25	5.32
	4.78×10^{-6}	4.80×10^{-6}	100.37	1.88	4.81×10^{-6}	100.54	2.64
	9.57×10^{-6}	9.60×10^{-6}	100.27	1.10	9.58×10^{-6}	100.08	1.54
Tap water 2	0	< LOD	-	-	< LOD	-	-
	4.78×10^{-7}	4.86×10^{-7}	101.64	4.40	4.86×10^{-7}	101.72	4.10
	9.57×10^{-7}	9.72×10^{-7}	101.54	2.75	9.67×10^{-7}	101.03	3.07
	4.78×10^{-6}	4.75×10^{-6}	99.42	2.20	4.77×10^{-6}	99.83	2.43
	9.57×10^{-6}	9.50×10^{-6}	99.32	1.45	9.52×10^{-6}	99.49	1.41
Tap water 3	0	< LOD	-	-	< LOD	-	-
	4.78×10^{-7}	4.86×10^{-7}	101.64	5.50	4.81×10^{-7}	100.54	5.42
	9.57×10^{-7}	9.57×10^{-7}	99.59	4.76	9.56×10^{-7}	99.84	4.69
	4.78×10^{-6}	4.80×10^{-6}	100.37	1.46	4.78×10^{-6}	99.95	2.25
	9.57×10^{-6}	9.61×10^{-6}	100.43	0.48	9.59×10^{-6}	100.20	1.82

Table 8
Dual determination of bismuth(III) and lead(II) by optodes with chromoionophore **2** in real samples and for commercial Standard Reference Solution (1:1).

	Added Bi (III)/Pb (II) [M]	Found Bi (III)			Found Pb (II)		
		ΔA Bi (III) [M]	Recovery %	RSD %	ΔA Pb (II) [M]	Recovery %	RSD %
Standard Reference Solution of bismuth(III)and lead(II) (1:1)	9.57×10^{-7}	9.14×10^{-7}	95.56	6.28	9.49×10^{-7}	99.13	3.77
	4.78×10^{-6}	4.80×10^{-6}	100.45	4.36	4.78×10^{-6}	100.05	2.62
	9.57×10^{-6}	9.59×10^{-6}	100.22	1.73	9.60×10^{-6}	100.27	1.31
Tap water 1	0	< LOD	-	-	< LOD	-	-
	9.57×10^{-7}	9.84×10^{-7}	102.81	6.28	9.70×10^{-7}	101.31	6.53
	4.78×10^{-6}	4.84×10^{-6}	101.17	4.53	4.80×10^{-6}	100.49	2.72
	9.57×10^{-6}	9.63×10^{-6}	100.58	2.26	9.62×10^{-6}	100.48	1.36
Tap water 2	0	< LOD	-	-	< LOD	-	-
	9.57×10^{-7}	9.14×10^{-7}	95.56	8.62	9.28×10^{-7}	96.96	3.77
	4.78×10^{-6}	4.77×10^{-6}	99.72	4.53	4.76×10^{-7}	99.62	2.72
	9.57×10^{-6}	9.56×10^{-6}	99.85	2.26	9.57×10^{-6}	100.05	1.36
Tap water 3	0	< LOD	-	-	< LOD	-	-
	9.57×10^{-7}	9.49×10^{-7}	99.19	5.44	9.38×10^{-7}	98.04	3.27
	4.78×10^{-6}	4.77×10^{-6}	99.72	3.52	4.76×10^{-6}	99.62	2.51
	9.57×10^{-6}	9.59×10^{-6}	100.22	2.88	9.60×10^{-6}	100.27	2.13

described in literature macrocyclic azo derivatives selectively binding bismuth(III). Satisfactory linear relationship between the value of the generated optical signal and the concentration of bismuth(III) and lead (II) optodes at pH 6 was obtained (the range depends on the chromoionophore used). It was also found that it is possible to detect and determine bismuth(III) and lead(II) ions using color measurement applications for mobile devices. Spectrophotometric measurements characterize with lower values of the limit of detection compared to colorimetric measurements based on the measurement of the color change of photos. Membranes with compound **1** generate a greater change in absorbance, and thus also a greater change in color in the presence of bismuth(III) than in the case of compound **2**, which translates into greater sensitivity in the detection and determination of this analyte. The opposite situation takes place in the presence of lead(II), because in this case the optode with compound **2** generates a greater change in absorbance and in color change.

Although the scope of the work in this manuscript does not include studies of the potential use of the described macrocycles in nuclear medicine, we believe they are worthy of such consideration (once the toxicity of the ligands has been determined) by teams specializing in such issues.

CRediT authorship contribution statement

Błażej Galiński: Conceptualization, Data curation, Formal analysis, Investigation, Methodology, Validation, Visualization, Writing – original draft, Writing – review & editing; **Ewa Wagner-Wysiecka**: Conceptualization, Supervision, Visualization, Writing – original draft, Writing – review & editing. **Both authors** discussed the results and commented on the manuscript.

Declaration of Competing Interest

The authors declare that they have no known competing financial interests or personal relationships that could have appeared to influence the work reported in this paper.

Data availability

Data will be made available on request.

Acknowledgments

This work was supported by the Faculty of Chemistry, Gdańsk University of Technology, No. 036277 - an internal grant from statutory funds. The financial support to maintenance of research facilities used in these studies from Gdańsk University of Technology by the DEC-2/2021/IDUB/V.6/Si grant under the SILICIUM SUPPORTING CORE R&D FACILITIES – "Excellence Initiative - Research University" program is gratefully acknowledged. Dr. Katarzyna Szwarc-Karabyka (Gdańsk University of Technology, Faculty of Chemistry, Nuclear Magnetic Resonance Laboratory) is kindly acknowledged for spectra registration. The authors are very grateful to the anonymous Reviewers for their time and comments, which allowed significant improvements to the manuscript.

Appendix A. Supporting information

Supplementary data associated with this article can be found in the online version at doi:10.1016/j.snb.2023.134798.

References

[1] X. Liu, M. Xiao, L. Xu, Y. Miao, R. Ouyang, Characteristics, applications and determination of bismuth, J. Nanosci. Nanotechnol. 16 (2016) 6679–6689, https://doi.org/10.1166/jnn.2016.11371.
[2] R. Wang, H. Li, H. Sun, Bismuth: environmental pollution and health effects, in: J. O. Nriagu (Ed.), Encyclopedia of Environmental Health, second ed., Elsevier, 2019, pp. 415–423, https://doi.org/10.1016/B978-0-444-52272-6.00374-3.
[3] R. Ge, H. Sun, Bioinorganic chemistry of bismuth and antimony: target sites of metallodrugs, Acc. Chem. Res. 40 (2007) 267–274, https://doi.org/10.1021/ar600001b.
[4] H. Li, H. Sun, Recent advances in bioinorganic chemistry of bismuth, Curr. Opin. Chem. Biol. 16 (2012) 74–83, https://doi.org/10.1016/j.cbpa.2012.01.006.
[5] H. Li, R. Wang, H. Sun, Systems approaches for unveiling the mechanism of action of bismuth drugs: new medicinal applications beyond Helicobacter Pylori Infection, Acc. Chem. Res. 52 (2019) 216–227, https://doi.org/10.1021/acs.accounts.8b00439.
[6] C. Wu, Q. Zhang, G. Liu, Z. Zhang, D. Wang, B. Qu, Z. Chen, L. Xiao, From Pb to Bi: a promising family of Pb-free optoelectronic materials and devices, Adv. Energy Mater. 10 (2019), 1902496, https://doi.org/10.1002/aenm.201902496.
[7] A.T. Odularu, Bismuth as smart material and its application in the ninth principle of sustainable chemistry, J. Chem. (2020), 9802934, https://doi.org/10.1155/2020/9802934.
[8] D.M. Griffith, H. Li, M.V. Werrett, P.C. Andrews, H. Sun, Medicinal chemistry and biomedical applications of bismuth-based compounds and nanoparticles, Chem. Soc. Rev. 50 (2021) 12037–12069, https://doi.org/10.1039/D0CS00031K.
[9] Y. Xin, Z. Wang, C. Yao, H. Shen, Y. Miao, Bismuth, a previously less-studied element, is bursting into new hotspots, ChemistrySelect 7 (2022), e202201220, https://doi.org/10.1002/slct.202201220.
[10] S.S. Won, H. Kim, J. Lee, Ch.K. Jeong, S.H. Kim, A.I. Kingon, Lead-free bismuth pyrochlore-based dielectric films for ultrahigh energy storage capacitors, Mater. Today Phys. 33 (2023), 101054, https://doi.org/10.1016/j.mtphys.2023.101054.
[11] Q. Wang, J. Du, R. Ouyang, B. Liu, Y. Miao, Y. Li, Recent advances in functional bismuth chalcogenide nanomaterials: cancer theranostics, antibacterial and biosensing, Coord. Chem. Rev. 492 (2023), 215281, https://doi.org/10.1016/j.ccr.2023.215281.
[12] X. Yang, J. Kuziola, V.A. Beland, J. Busch, M. Leutzsch, J. Bures, J. Cornella, Bismuth-catalyzed amide reduction, Angew. Chem. Int. Ed. (2023), e202306447, https://doi.org/10.1002/anie.202306447.
[13] M. Mato, D. Spinnato, M. Leutzsch, H.W. Moon, E.J. Reijerse, J. Cornella, Bismuth radical catalysis in the activation and coupling of redox-active electrophiles, Nat. Chem. (2023), https://doi.org/10.1038/s41557-023-01229-7.
[14] J. Heine, B. Peerless, S. Dehnen, C. Lichtenberg, Charge makes a difference: molecular ionic bismuth compounds, Angew. Chem. Int. Ed. 62 (2023), 202218771, https://doi.org/10.1002/anie.202218771.
[15] K. Tanimura, M. Gon, K. Tanaka, Effects of hypervalent bismuth on electronic properties of the azobenzene tridentate ligand and roles of lewis acidity in controlling optical properties, Inorg. Chem. 62 (2023) 4590–4597.
[16] J. Yang, Z. Huang, J. Li, Y. Yao, Y. Meng, B. Xie, Z. Ni, S. Xia, Photocatalytic reduction of nitrogen to ammonia by bismuth oxyhalides containing oxygen vacancies, Colloids Surf. A Physicochem. Eng. Asp. 662 (2023), 130995, https://doi.org/10.1016/j.colsurfa.2023.130995.
[17] K.G. Brubakk, E.L.F. Gjengedal, O. Enger, K. Sripada, Ammunition waste pollution and preliminary assessment of risks to child health from toxic metals at the Greek refugee camp Mavrovouni, Int. J. Environ. Res. Public Health 19 (2022) 10086, https://doi.org/10.3390/ijerph191610086.
[18] J. Messerschmidt, A. Von Bohlen, F. Alt, R. Klockenkämper, Determination of arsenic and bismuth in biological materials by total reflection X-ray fluorescence after separation and collection of their hydrides, J. Anal. . Spectrom. 12 (1997) 1251–1254, https://doi.org/10.1039/A705093C.
[19] F. Shemirani, M. Baghdadi, M. Ramezani, M. Reza Jamali, Determination of ultra trace amounts of bismuth in biological and water samples by electrothermal atomic absorption spectrometry (ET-AAS) after cloud point extraction, Anal. Chim. Acta 534 (2005) 163–169, https://doi.org/10.1016/j.aca.2004.06.036.
[20] A.K. Das, R. Chakraborty, M.L. Cervera, M. de la Guardia, Analytical techniques for the determination of bismuth in solid environmental sample, Trends Anal. Chem. 25 (2006) 599–608, https://doi.org/10.1016/j.trac.2006.01.006.
[21] R. Dobrowolski, J. Dobrzyńska, B. Gawrońska, Determination of bismuth in environmental samples by slurry sampling graphite furnace atomic absorption spectrometry using combined chemical modifiers, Environ. Monit. Assess. 187 (2015) 4125, https://doi.org/10.1007/s10661-014-4125-7.
[22] D.J. Arnot, T.N. Lambert, Bismuth detection in alkaline electrolyte via anodic stripping voltammetry for battery separator evaluation, Electroanalysis 33 (2021) 797–803, https://doi.org/10.1002/elan.202060412.
[23] M. Gorska, K. Greda, P. Pohl, Determination of bismuth by optical emission spectrometry with liquid anode/cathode atmospheric pressure glow discharge, J. Anal. . Spectrom. 36 (2021) 165–177, https://doi.org/10.1039/D0JA00401D.
[24] C. McDonagh, C.S. Burke, B.D. MacCraith, Optical Chemical Sensors, Chem. Rev. 108 (2008) 400–422, https://doi.org/10.1021/cr068102g.
[25] A. Lobnik, M. Turel, S.K. Urek, Optical chemical sensors: design and applications, in: W. Wang (Ed.), Advances in Chemical Sensors, InTech, 2012, pp. 3–28, https://doi.org/10.5772/31534.
[26] H.H. Qazi, A. Bakar bin Mohammad, M. Akram, Recent progress in optical chemical sensors, Sensors 12 (2012) 16522–16556.
[27] G. Mistlberger, G.A. Crespo, E. Bakker, Ionophore-based optical sensors, Annu. Rev. Anal. Chem. 7 (2014) 483–512, https://doi.org/10.1146/annurev-anchem-071213-020307.
[28] K.N. Mikhelson, M.A. Peshkova, Advances and trends in ionophore-based chemical sensors, Russ. Chem. Rev. 84 (2015) 555–578, https://doi.org/10.1070/RCR4506.

[29] L. You, D. Zha, E.V. Anslyn, Recent advances in supramolecular analytical chemistry using optical sensing, Chem. Rev. 115 (2015) 7840–7892, https://doi.org/10.1021/cr5005524.
[30] H. Sharma, N. Kaur, A. Singh, A. Kuwar, N. Singh, Optical chemosensors for water sample analysis, J. Mater. Chem. C 4 (2016) 5154–5194, https://doi.org/10.1039/C6TC00605A.
[31] A.V.S. Piriya, P. Joseph, K.S.C.G. Daniel, S. Lakshmanan, T. Kinoshita, S. Muthusamy, Colorimetric sensors for rapid detection of various analytes, Mater. Sci. Eng. C 78 (2017) 1231–1245, https://doi.org/10.1016/j.msec.2017.05.018.
[32] X.-D. Wang, O.S. Wolfbeis, Fiber-optic chemical sensors and biosensors (2015–2019, Anal. Chem. 92 (2020) 397–430, https://doi.org/10.1021/acs.analchem.9b04708.
[33] X. Du, X. Xie, Ion-selective optodes: alternative approaches for simplified fabrication and signaling, Sens. Actuators B Chem. 335 (2021), 129368, https://doi.org/10.1016/j.snb.2020.129368.
[34] P.R. Dongare, A.H. Gore, Recent advances in colorimetric and fluorescent chemosensors for ionic species: design, principle and optical signalling mechanism, ChemistrySelect 6 (2021) 5657–5669, https://doi.org/10.1002/slct.202101090.
[35] J. Kramer, R. Kang, L.M. Grimm, L.D. Cola, P. Picchetti, F. Biedermann, Molecular probes, chemosensors, and nanosensors for optical detection of biorelevant molecules and ions in aqueous media and biofluids, Chem. Rev. 122 (2022) 3459–3636, https://doi.org/10.1021/acs.chemrev.1c00746.
[36] Z. Chen, Z. Zhang, J. Qi, J. You, J. Ma, L. Chen, Colorimetric detection of heavy metal ions with various chromogenic materials: strategies and applications, J. Hazard. Mater. 441 (2023), 129889, https://doi.org/10.1016/j.jhazmat.2022.129889.
[37] K. Yong, M.W. Brechbiel, Towards translation of 212Pb as a clinical therapeutic; getting the lead in, Dalton Trans. 40 (2011) 6068–6076, https://doi.org/10.1039/C0DT01387K.
[38] G. Montavon, A. Le Du, J. Champion, T. Rabungb, A. Morgenstern, DTPA complexation of bismuth in human blood serum, Dalton Trans. 41 (2012) 8615–8623, https://doi.org/10.1039/C2DT30230F.
[39] R. Luckay, I. Cukrowski, J. Mashishi, J.H. Reibenspies, A.H. Bond, R.D. Rogers, R. D. Hancock, Synthesis, stability and structure of the complex of bismuth(III) with the nitrogen-donor macrocycle 1,4,7,10-tetraazacyclododecane. The role of the lone pair on bismuth(III) and lead(II) in determining co-ordination geometry, J. Chem. Soc. Dalton Trans. (1997) 901–908, https://doi.org/10.1039/A605068I.
[40] L.M.P. Lima, M. Beyler, R. Delgado, C. Platas-Iglesias, R. Tripier, Investigating the complexation of the Pb^{2+}/Bi^{3+} pair with dipicolinate cyclen ligands, Inorg. Chem. 54 (2015) 7045–7057, https://doi.org/10.1021/acs.inorgchem.5b01079.
[41] J.L. Lange, P.R.W.J. Davey, M.T. Ma, J.M. White, A. Morgenstern, F. Bruchertseifer, P.J. Blower, B.M. Paterson, An octadentate bis(semicarbazone) macrocycle: a potential chelator for lead and bismuth radiopharmaceuticals, Dalton Trans. 49 (2020) 14962–14974, https://doi.org/10.1039/d0dt02673e.
[42] A. Ullah, F. Shah, I. Khan, M. Anwar, K. Shah, M.T. Muhammad, F. Ahmad, Unprecedented chemosensing behavior of novel tetra-substituted benzimidazole zinc(II) phthalocynine for selective detection of Bi^{3+} ion: synthesis, characterization and ROS generation, Spectrochim. Acta A Mol. Biomol. Spectrosc. 192 (2018) 188–193, https://doi.org/10.1016/j.saa.2017.11.002.
[43] M. Arvand, M. Eskandarnejad, Development of a highly sensitive and selective bismuth optical sensor based on (2*E*,4*E*)-5-(2,4-Dinitrophenyl Amino)penta-2,4-dienal, Anal. Lett. 41 (2008) 2877–2892, https://doi.org/10.1080/00032710802424164.
[44] S. Rastegarzadeh, M. Fatahinia, Design of an optical sensor for determination of bismuth, J. Chin. Chem. Soc. 58 (2011) 136–141, https://doi.org/10.1002/jccs.201190069.
[45] A. Niazi, S.K. Afshar, Design novel optical sensor for determination of bismuth based on immobilization of 4-(4-nitrophenyl)-1-naphthol on a triacetylcellulose membrane, J. Iran. Chem. Res. 4 (2011) 105–111.
[46] H. Khajehsharifi, M.M. Bordbar, P. Esfandiary, Design and evaluation of a novel bismuth optical sensor using PC-ANN application, Anal. Bioanal. Chem. Res. 5 (2018) 159–169, https://doi.org/10.22036/abcr.2018.96082.1163.
[47] P.A. Bizirtsakis, M. Tarara, A. Tsiasioti, P.D. Tzanavaras, G.Z. Tsogas, Development of a paper-based analytical method for the selective colorimetric determination of bismuth in water samples, Chemosensors 10 (2022) 265, https://doi.org/10.3390/chemosensors10070265.
[48] M. Lerchi, E. Bakker, B. Rusterholz, W. Simon, Lead-selective bulk optode based on neutral ionophores with subnanomolar detection limits, Anal. Chem. 64 (1992) 1534–1540, https://doi.org/10.1021/ac00038a007.
[49] E. Anticó, M. Lerchi, B. Rusterholz, N. Achermann, M. Badertscher, M. Valiente, E. Pretsch, Monitoring Pb^{2+} with optical sensing films, Anal. Chim. Acta 388 (1999) 327–338, https://doi.org/10.1016/S0003-2670(99)00085-9.
[50] N. Alizadeh, A. Moemeni, M. Shamsipur, Poly(vinyl chloride)-membrane ion-selective bulk optode based on 1,10-dibenzyl-1,10-diaza-18-crown-6 and 1-(2-pyridylazo)-2-naphthol for Cu^{2+} and Pb^{2+} ions, Anal. Chim. Acta 464 (2002) 187–196, https://doi.org/10.1016/S0003-2670(02)00477-4.
[51] Y. Takahashi, T. Hayashita, T.M. Suzuki, Test strips for lead(II) based on a unique color change of PVC-film containing O-donor macrocycles and an anionic dye, Anal. Sci. 23 (2007) 147–150, https://doi.org/10.2116/analsci.23.147.
[52] A.A. Ensafi, Z.N. Isfahani, Determination of lead ions by an optical sensor based on 2-amino-cyclopentene-1-dithiocarboxylic acid, IEEE Sens. J. 7 (2007) 1112–1117, https://doi.org/10.1109/JSEN.2007.897942.
[53] A.A. Ensafi, M. Fouladgar, Development a simple PVC membrane bulk optode for determination of lead ions in water samples, Sens. Lett. 7 (2009) 177–184, https://doi.org/10.1166/sl.2009.1029.
[54] A.A. Esnafi, A. Katiraei Far, S. Meghdadi, Highly selective optical-sensing film for lead(II) determination in water samples, J. Hazard. Mater. 172 (2009) 1069–1075, https://doi.org/10.1016/j.jhazmat.2009.07.112.
[55] C. Bualoma, W. Ngeontaeb, S. Nitiyanontakita, P. Ngamukota, A. Imyima, T. Tuntulania, W. Aeungmaitrepirom, Bulk optode sensors for batch and flow-through determinations of lead ion in water samples, Talanta 82 (2010) 660–667, https://doi.org/10.1016/j.talanta.2010.05.028.
[56] H. Tavallali, L. Dorostghoal, Design and evaluation of a lead (II) optical sensor based on immobilization of dithizone on triacetylcellulose membrane, Int. J. Chemtech Res. 6 (2014) 3179–3186.
[57] K. Zargoosh, F.F. Babadi, Highly selective and sensitive optical sensor for determination of Pb(II) and Hg^{2+} ions based on the covalent immobilization of dithizone on agarose membrane, Spectrochim. Acta A Mol. Biomol. Spectrosc. 137 (2015) 105–110, https://doi.org/10.1016/j.saa.2014.08.043.
[58] Y. Nur, E. Rohaeti, L.K. Darusman, Optical sensor for the determination of Pb(II) based on immobilization of dithizone onto chitosan-silica membrane, Indones. J. Chem. 17 (2017) 7–14, https://doi.org/10.22146/ijc.23560.
[59] B. Galiński, E. Wagner-Wysiecka, Pyrrole bearing diazocrowns: Selective chromoionophores for lead(II) optical sensing, Sens. Actuators B Chem. 361 (2022), 131678, https://doi.org/10.1016/j.snb.2022.131678.
[60] E. Wagner-Wysiecka, P. Szulc, E. Luboch, J. Chojnacki, D. Laskowska, P. Miklaszewska, P. Sowiński, Do phenyl substituents affect the properties of azobenzocrown derivatives, ChemPlusChem 88 (2023), e202300175, https://doi.org/10.1002/cplu.202300175.
[61] E. Wagner-Wysiecka, E. Luboch, M. Kowalczyk, J.F. Biernat, Chromogenic macrocyclic derivatives of azoles-synthesis and properties, Tetrahedron 59 (2003) 4415–4420, https://doi.org/10.1016/S0040-4020(03)00618-5.
[62] E. Wagner-Wysiecka, M. Jamrógiewicz, M.S. Fonari, J.F. Biernat, Azomacrocyclic derivatives of imidazole: synthesis, structure, and metal ion complexation properties, Tetrahedron 63 (2007) 4414–4421, https://doi.org/10.1016/j.tet.2007.03.095.
[63] M. Kyvala, I. Lukes, Program package "OPIUM" (free access) at ⟨http://www.natur.cuni.cz/kyvala/opium.html⟩.
[64] P. Job, Formation and stability of inorganic complexes in solution, Ann. Chim. 9 (1928) 113–203.
[65] B. Galiński, J. Chojnacki, E. Wagner-Wysiecka, Simple colorimetric copper(II) sensor – spectral characterization and possible applications, Spectrochim. Acta A Mol. Biomol. Spectrosc. 293 (2023), 122472, https://doi.org/10.1016/j.saa.2023.122472.
[66] B. Galiński, E. Luboch, J. Chojnacki, E. Wagner-Wysiecka, Novel diazocrowns with pyrrole residue as lead(II) colorimetric probes, Materials 14 (2021) 7239. ⟨https://10.3390/ma14237239⟩.
[67] W.S. Rasband, ImageJ, U.S. National Institutes of Health, Bethesda, Maryland, USA, ⟨https://imagej.nih.gov/ij/⟩, 1997–2018.
[68] M.D. Abramoff, P.J. Magalhaes, S.J. Ram, Image processing with ImageJ, Biophotonics Int. 11 (2004) 36–42.
[69] C.A. Schneider, W.S. Rasband, K.W. Eliceiri, NIH image to imageJ: 25 years of image analysis, Nat. Methods 9 (2012) 671–675, https://doi.org/10.1038/nmeth.2089.
[70] N.A. Gavrilenko, S.V. Muravyov, S.V. Silushkin, A.S. Spiridonovab, Polymethacrylate optodes: a potential for chemical digital color analysis, Measurement 51 (2014) 464–469, https://doi.org/10.1016/j.measurement.2013.11.027.
[71] S.V. Muravyov, A.S. Spiridonova, N.A. Gavrilenko, P.V. Baranov, L. I. Khudonogovo, A digital colorimetric analyzer for chemical measurements on the basis of polymeric optodes, Instrum. Exp. Tech. 59 (2016) 592–600, https://doi.org/10.1134/S0020441216030210.
[72] S.V. Muravyov, N.A. Gavrilenko, N.V. Saranchina, P.V. Baranov, Polymethacrylate sensors for rapid digital colorimetric analysis of toxicants in natural and anthropogenic objects, IEEE Sens. J. 19 (2019) 4765–4772, https://doi.org/10.1109/JSEN.2019.2903314.

Błażej Galiński (1994) is Ph.D. student at Faculty of Chemistry of Gdańsk University of Technology – M.Sc. in 2018. His scientific interest covers supramolecular chemistry, mainly chromoionophores and their applications in optical sensing.

Ewa Wagner-Wysiecka obtained her Ph.D. (2002) and D.Sc. (2013) in Chemistry from Gdańsk University of Technology (Poland), where now is working as associate professor. The main topic of her research is supramolecular chemistry (organic synthesis, spectroscopic methods, colorimetric receptors and sensors).

P5 – SUPPLEMENTARY MATERIALS

Macrocyclic derivatives of imidazole as chromoionophores for bismuth(III)/lead(II) pair

Błażej Galiński[1], Ewa Wagner-Wysiecka[1,2*]

[1] Department of Chemistry and Technology of Functional Materials, Faculty of Chemistry, Gdańsk University of Technology, Narutowicza Street 11/12, 80-233 Gdańsk, Poland

[2] Advanced Materials Center, Faculty of Chemistry, Gdańsk University of Technology, Narutowicza Street 11/12, 80-233 Gdańsk, Poland

* Corresponding author

Tel.: +48 347 23 59

e-mail: ewa.wagner-wysiecka@pg.edu.pl

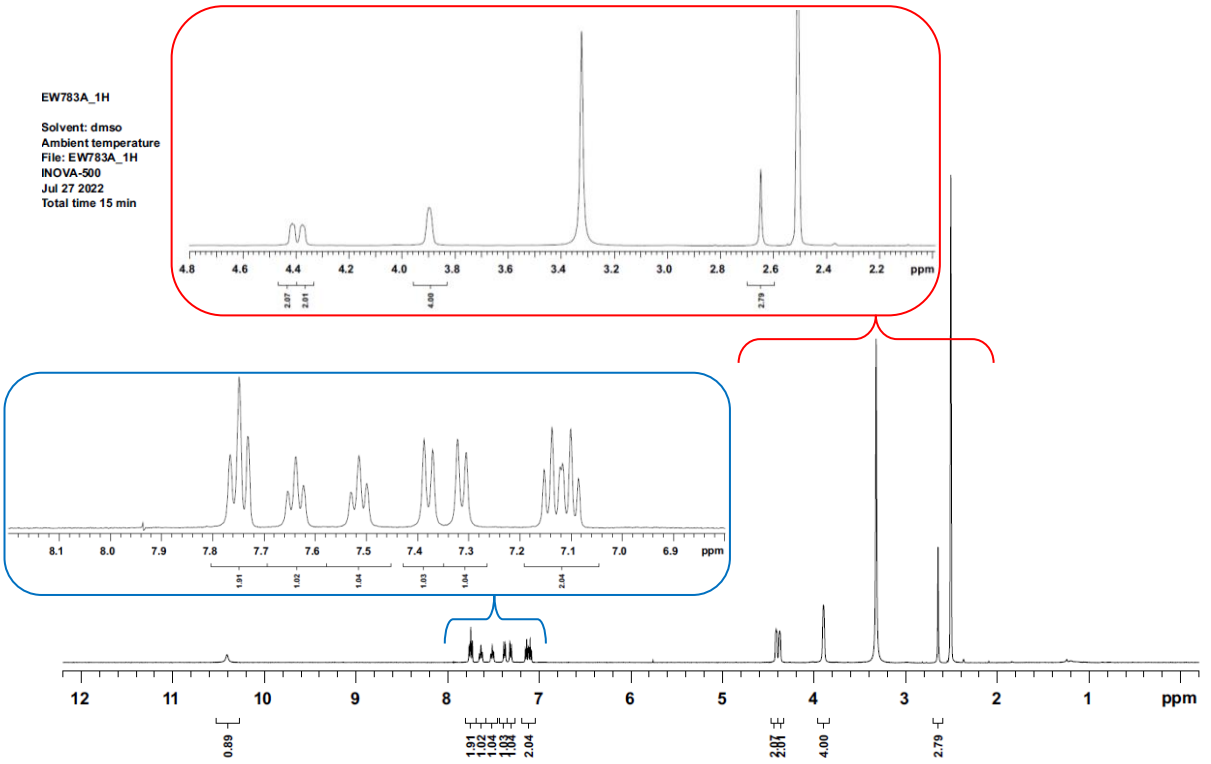

Fig. S1. 1H NMR spectrum of 2 (3.64×10-3 M) in DMSO-d_6.

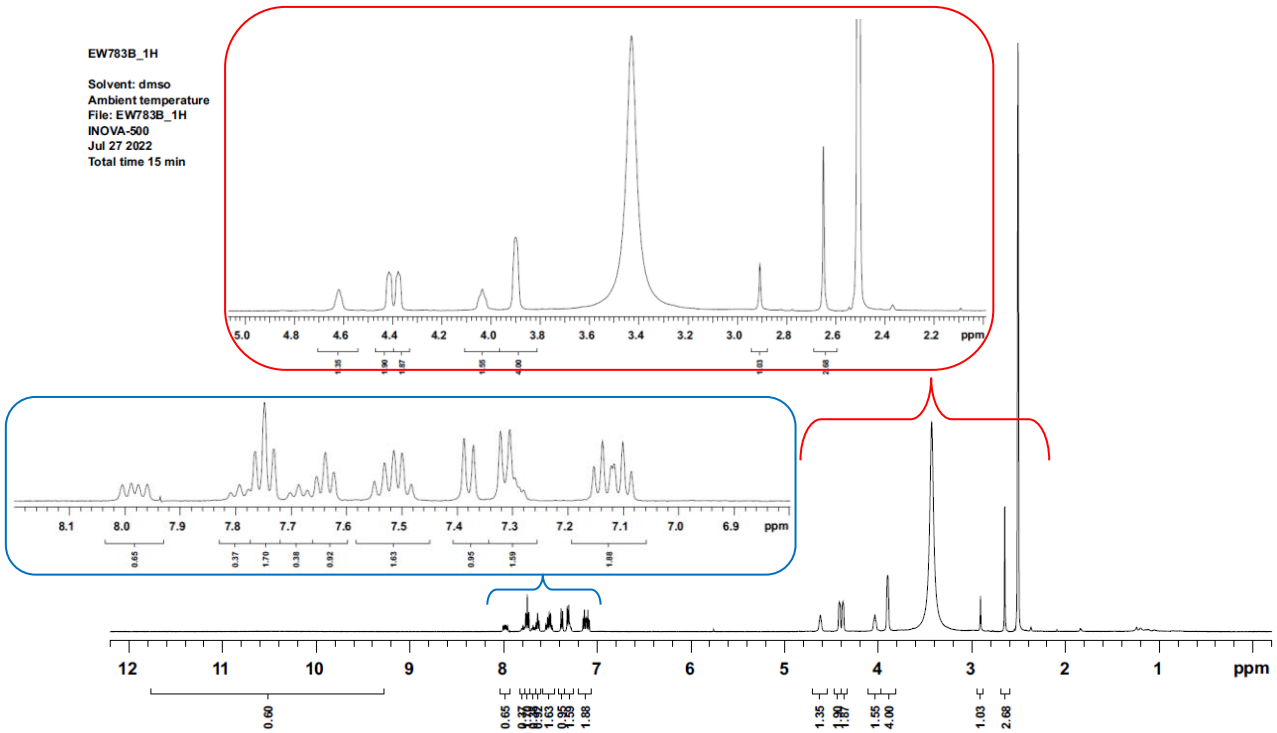

Fig. S2. ^{1}H NMR spectrum of **2** (3.64×10^{-3} M) registered in the presence of equimolar amount of bismuth(III) nitrate in DMSO-d_6.

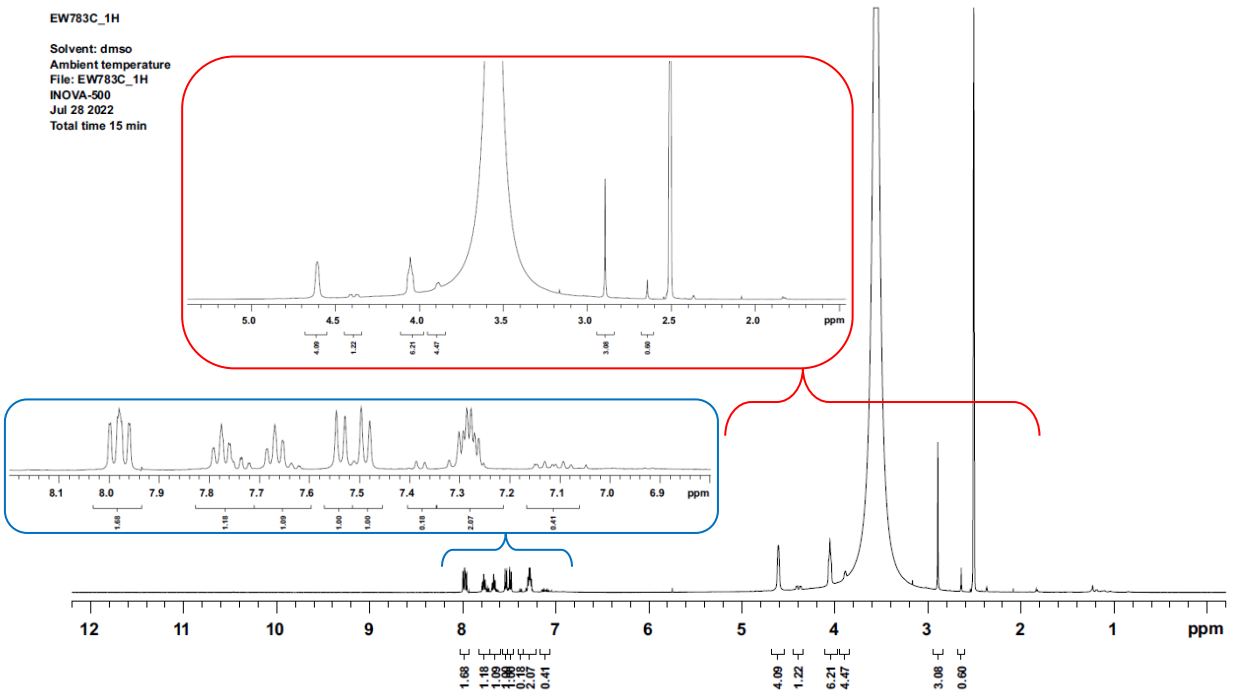

Fig. S3. ^{1}H NMR spectrum of **2** (3.64×10^{-3} M) registered in the presence of 10-fold molar excess of bismuth(III) nitrate in DMSO-d_6.

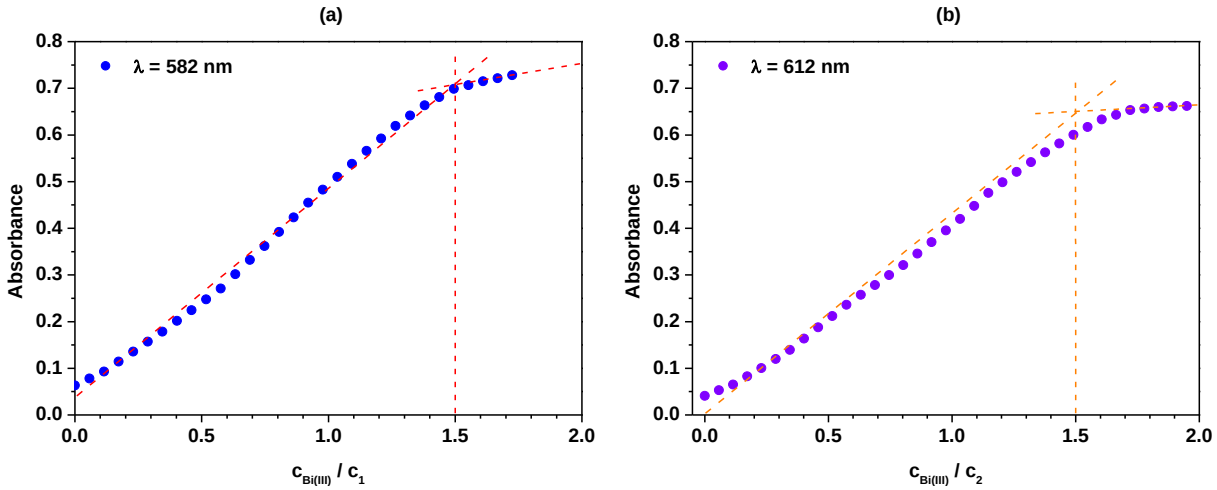

Fig. S4. Molar ratio of compounds with bismuth(III) nitrate in DMSO-water (1:1, v/v) : a) **1** ($c_1 = 4.10\times10^{-5}$ M) ($c_{Bi(III)} = 0 – 6.29\times10^{-5}$ M) and b) **2** ($c_2 = 4.11\times10^{-5}$ M) ($c_{Bi(III)} = 0 – 7.91\times10^{-5}$ M).

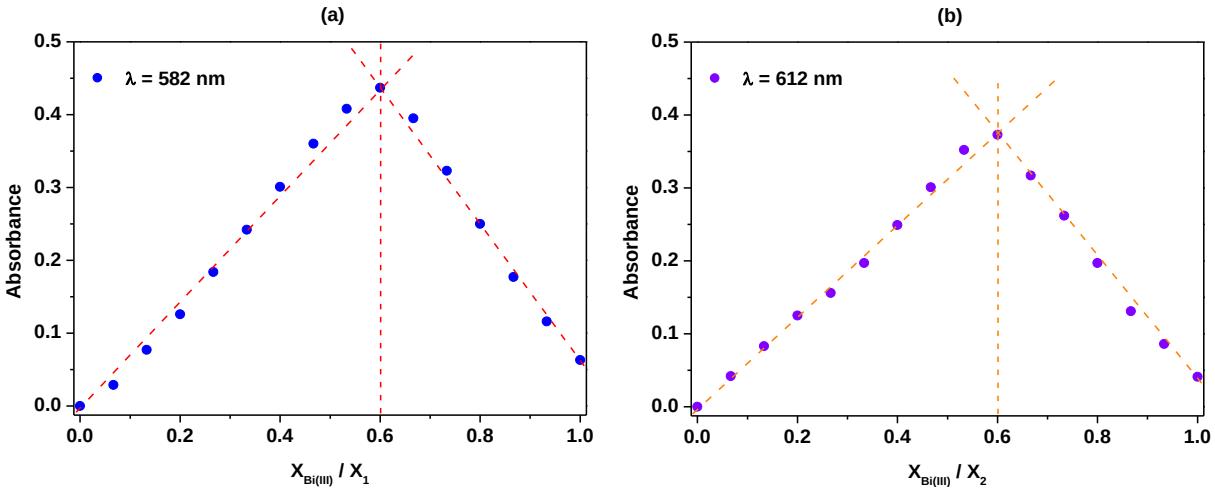

Fig. S5. Job's plots for bismuth(III) nitrate in DMSO-water (1:1, v/v) with compound: a) **1** and b) **2**.

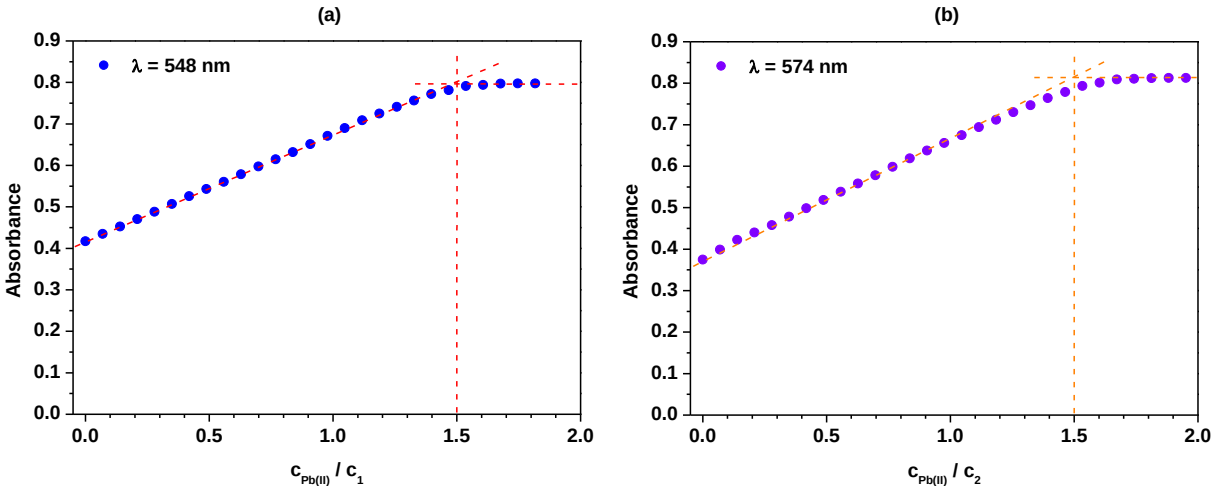

Fig. S6. Molar ratio of compounds with lead(II) nitrate in DMSO-water (1:1,v/v): a) **1** ($c_1 = 4.10\times10^{-5}$ M) ($c_{Pb(II)}$= 0- 7.35×10^{-5} M) and b) **2** ($c_2 = 4.11\times10^{-5}$ M) ($c_{Pb(II)}$= 0 – 7.83×10^{-5} M).

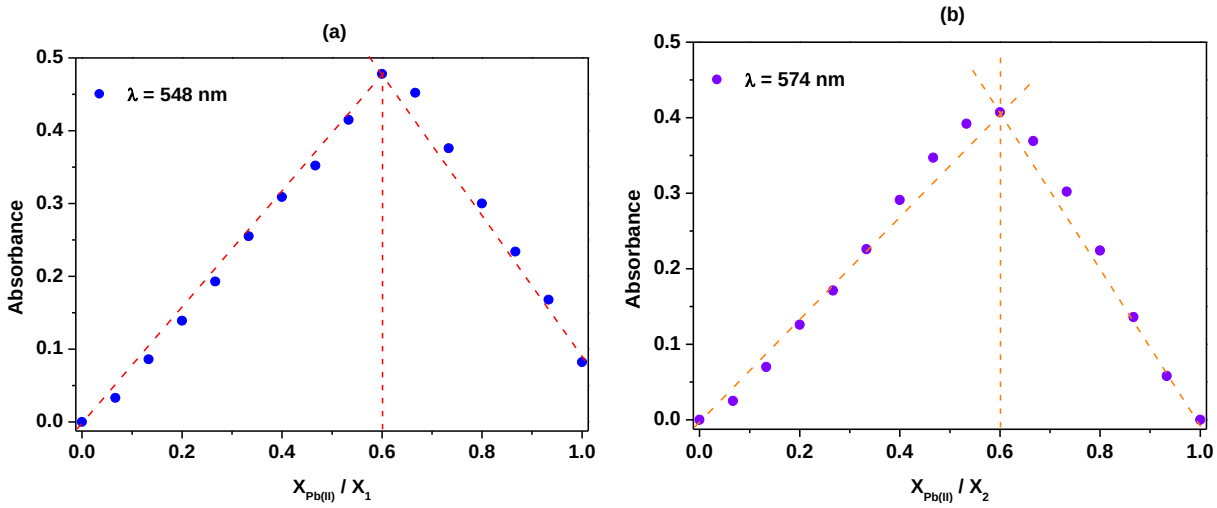

Fig. S7. Job's plots for lead(II) nitrate in DMSO-water (1:1, v/v) with compound: a) **1** and b) **2**.

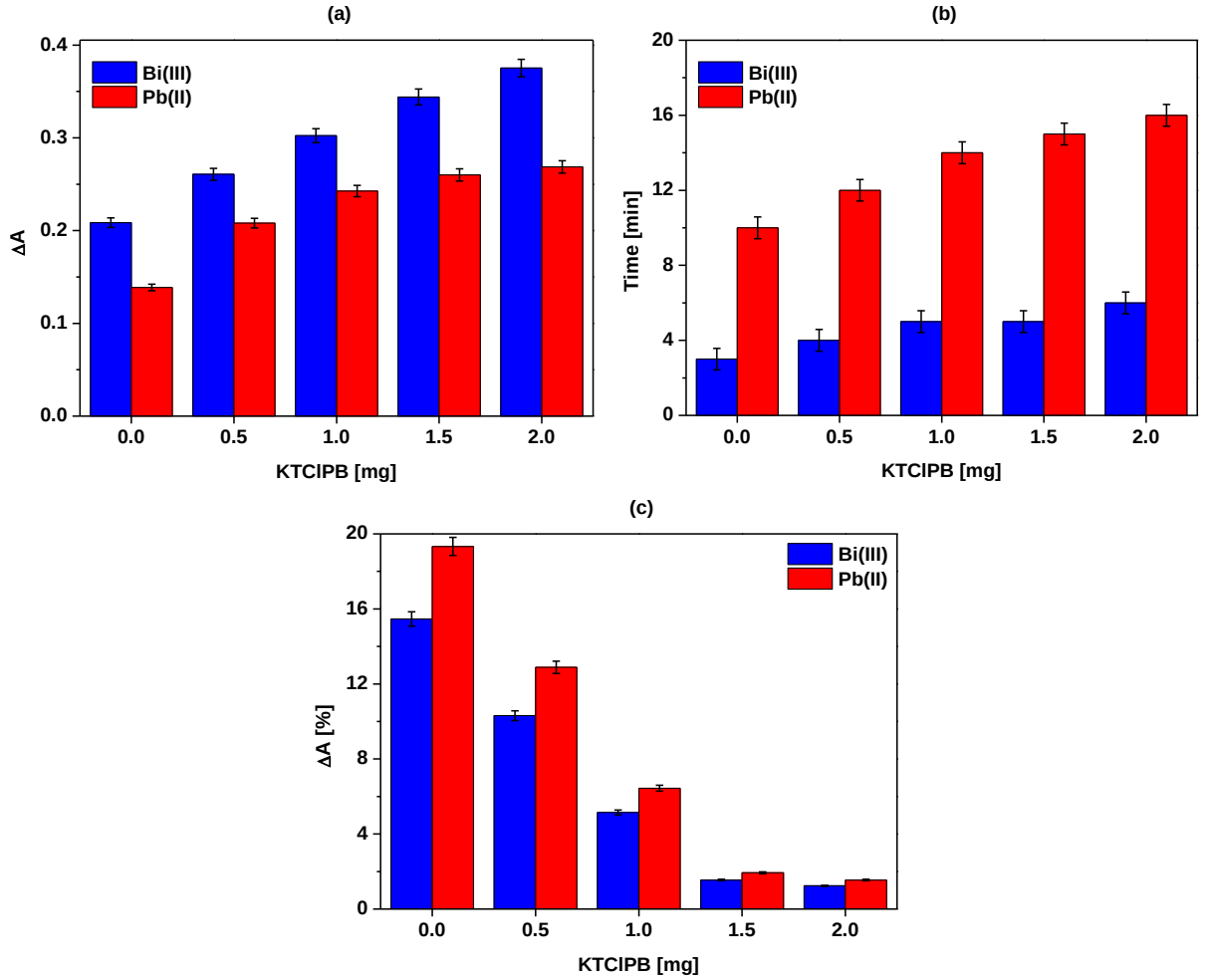

Fig. S8. Effect of the amount of KTClPB on the parameters of optode with compound **1**: a) the value of generated signal (ΔA), b) response time (t_{95}) and c) leaching of chromoinonophores (expressed as a percentage of change in absorbance ΔA%) from membranes after 10 regeneration cycles.

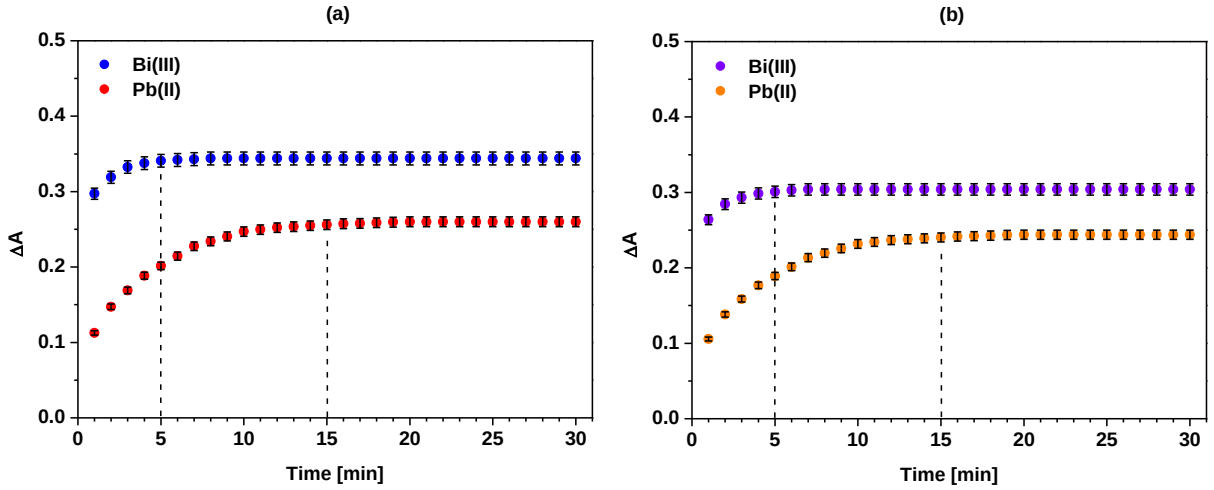

Fig. S9. Response time of the optodes: a) **1** and b) **2**; for the presence of bismuth(III) and lead(II) salts at concentration 1.05×10^{-5} M.

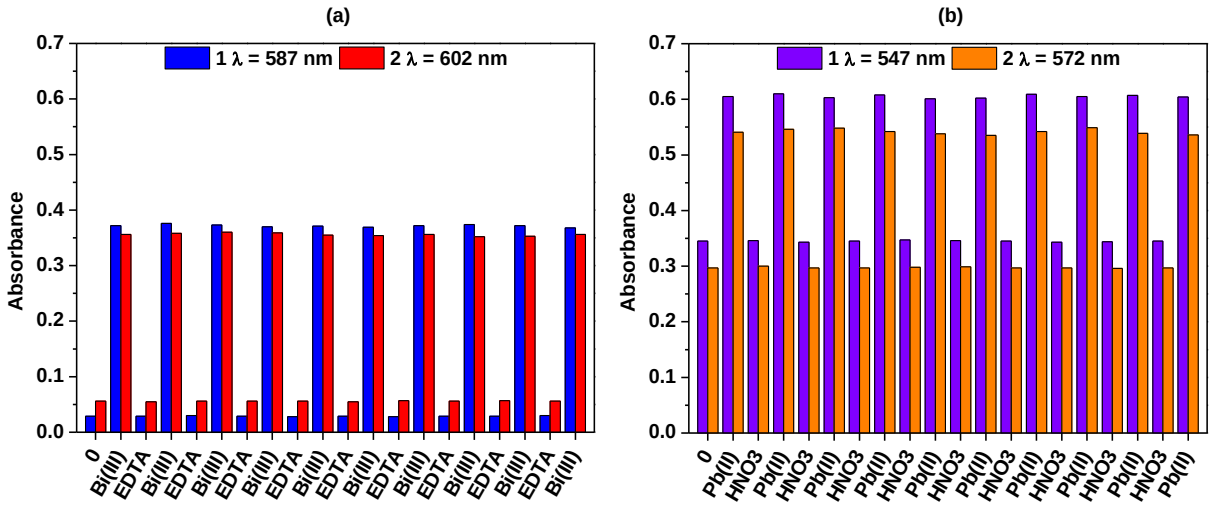

Fig. S10. Regeneration cycles of optodes with compound **1** and **2** after contact with: a) bismuth(III)/EDTA and b) lead(II) nitrates/nitric acid (0 – first time usage).

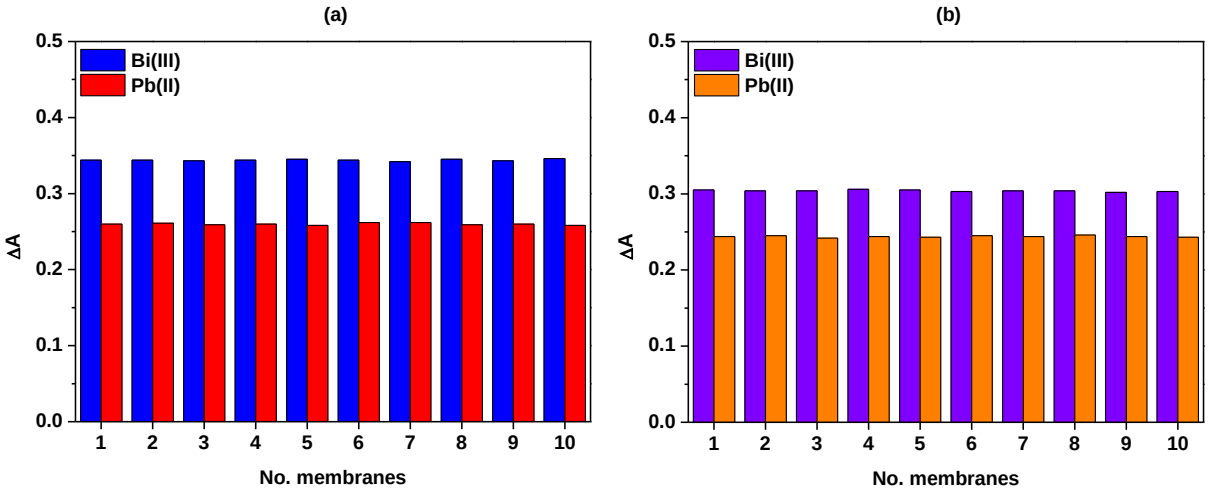

Fig. S11. Reproducibility of optodes with: a) **1** and b) **2**; after contact with bismuth(III) and lead(II) nitrates (1.05×10^{-5} M).

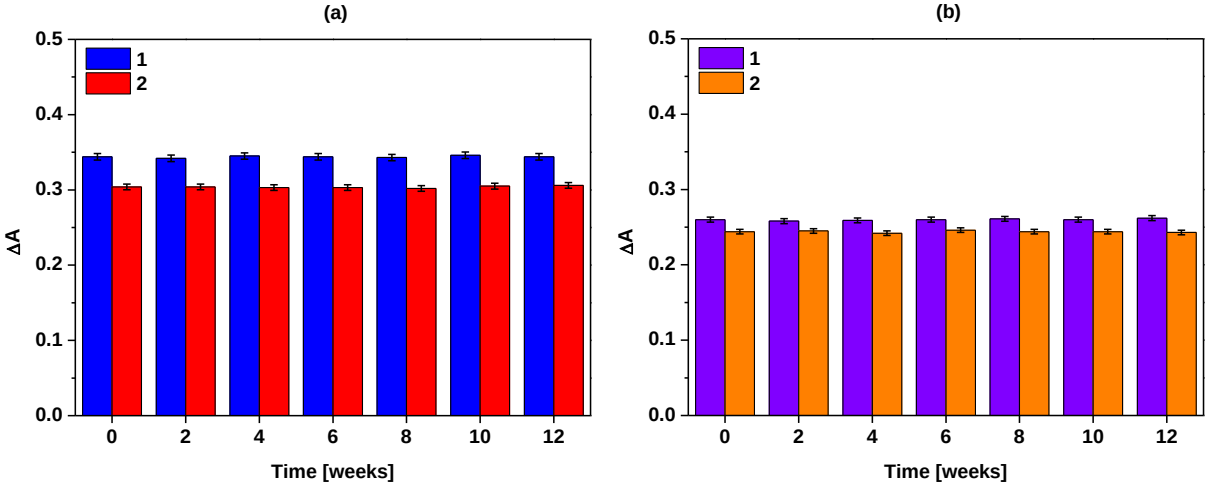

Fig. S12. Response of optodes with compound **1** and **2** after contact with: a) bismuth(III) and b) lead(II) nitrates; storage in a dry and dark place for different time (weeks, 0 – first time usage)

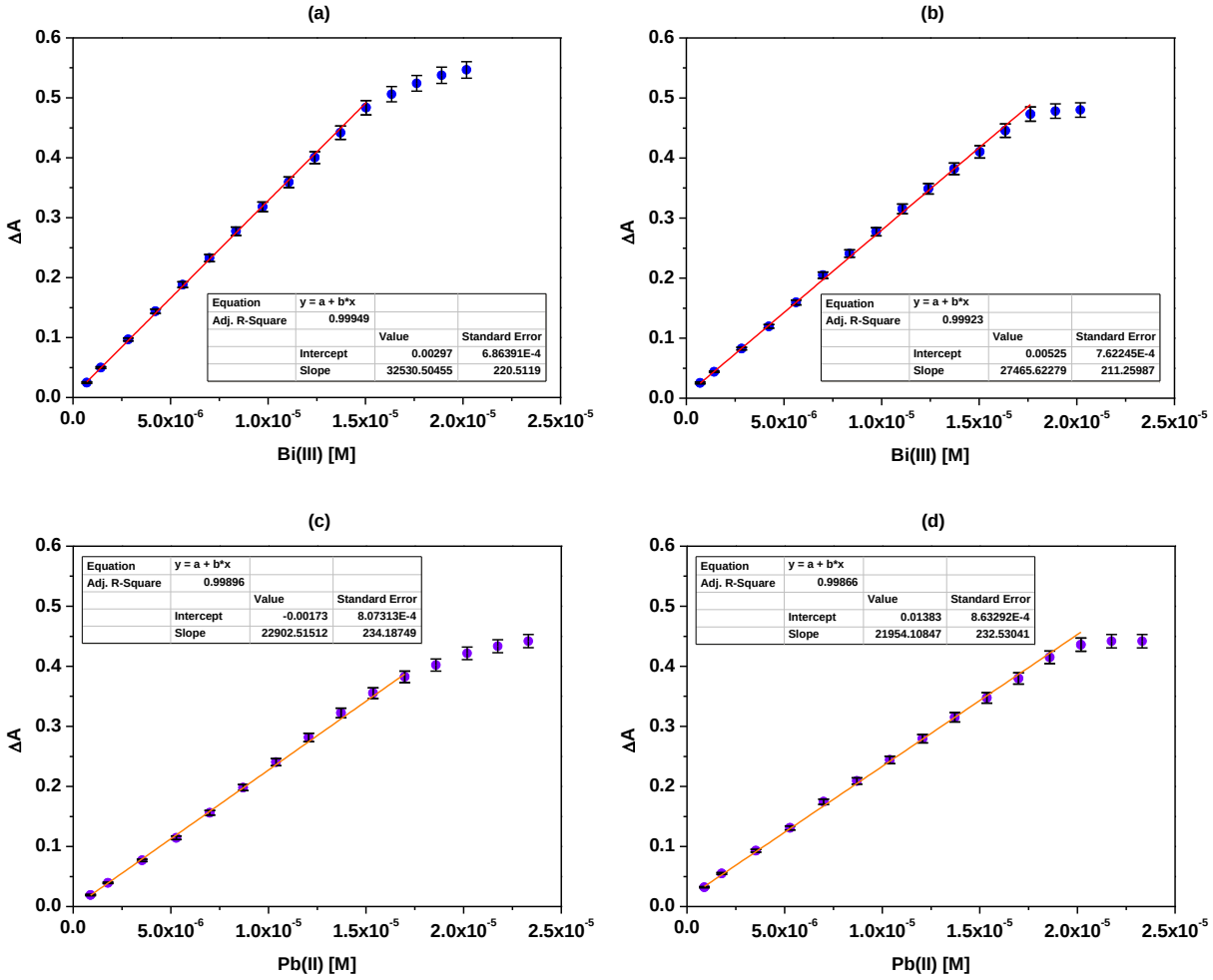

Fig. S13. Dependence of the change in the value of the generated signal (ΔA) of the optodes in the presence of bismuth(III) ($c_{Bi(III)}$ = 0 – 2.02×10^{-5} M): a) **1** and b) **2**; and in the presence of lead(II) ($c_{Pb(II)}$ = 0 – 2.33×10^{-5} M): c) **1** and d) **2**; with marking the range of the linear response.

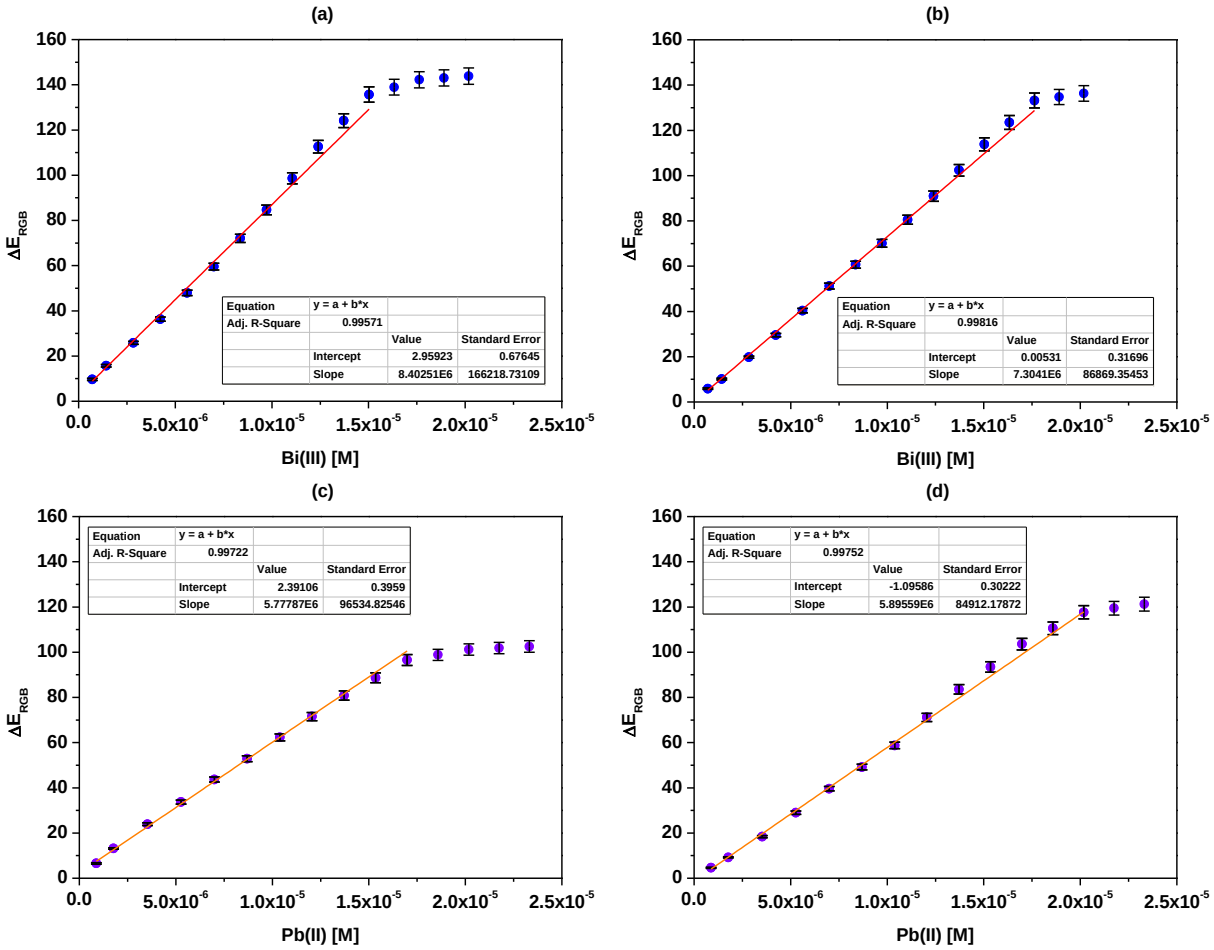

Fig. S14. Dependence of the color change (ΔE_{RGB}) of the optode with bismuth(III) ($c_{Bi(III)}$ = 0 – 2.02×10^{-5} M): a) **1** and b) **2**; and with lead(II) ($c_{Pb(II)}$ = 0 – 2.33×10^{-5} M): c) **1** and d) **2**; with the range of linear response marked.

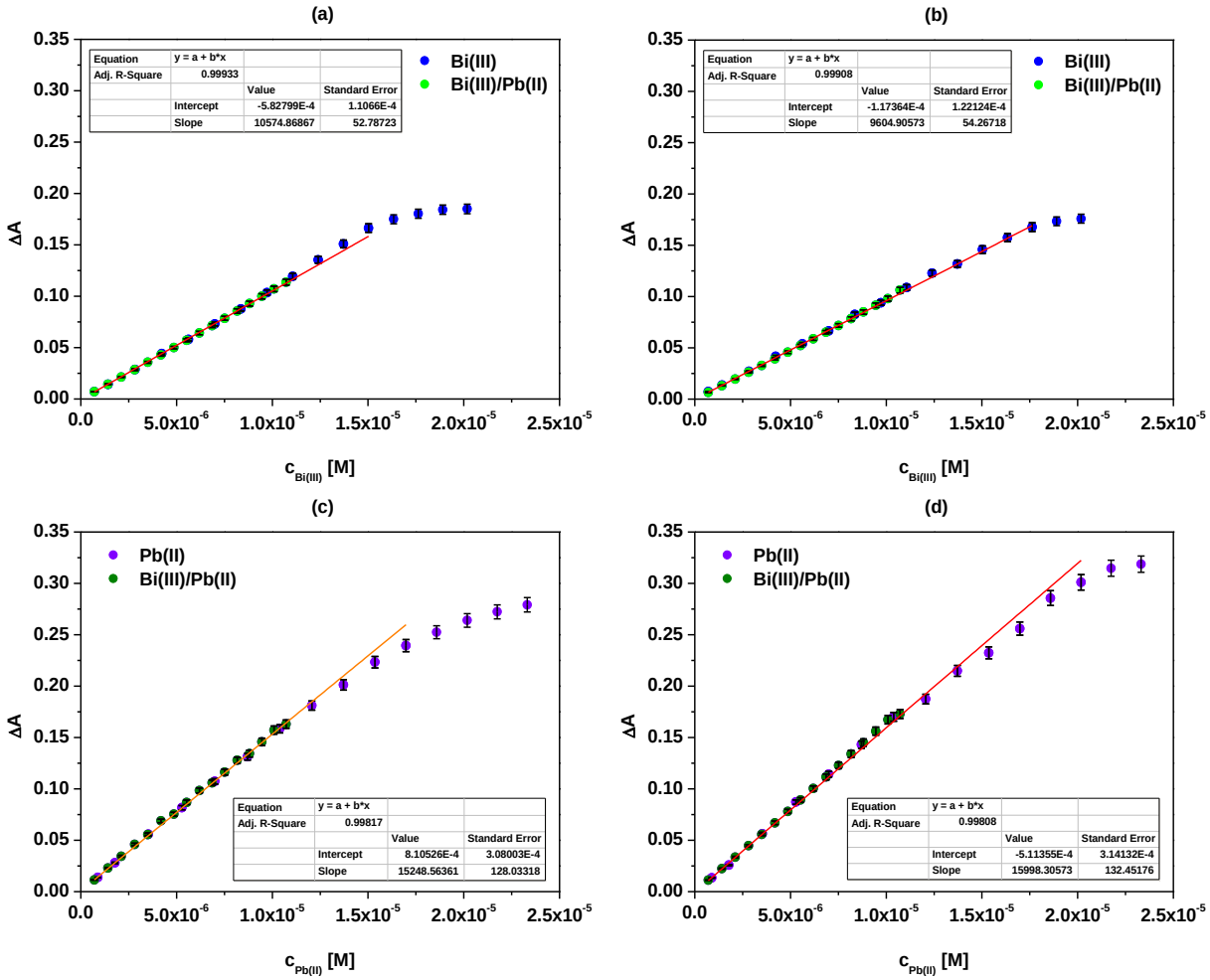

Fig. S15. Dependence of the change in the value of the generated signal (ΔA) of the optodes in the presence of bismuth(III) and lead(II) ($c_{Bi(III)/Pb(II)}$ = 0 – 1.13×10^{-5} M): a) **1** and b) **2** for bismuth(III); c) **1** and d) **2** for lead(II); extended and superimposed on ranges of linear responses for single ions, with the range of the linear response marked.

Table S1. Determination of bismuth(III) by optodes with chromoionophore **1** in real samples and for commercial Standard Reference Solution.

	Added Bi(III) [M]	Found Bi(III)					
		ΔA	Recovery	RSD	ΔE_{RGB}	Recovery	RSD
		Bi(III) [M]	%	%	Bi(III) [M]	%	%
Standard Reference Solution of bismuth(III)	4.78×10^{-7}	4.82×10^{-7}	100.75	3.71	4.85×10^{-7}	101.42	5.18
	9.57×10^{-7}	9.53×10^{-7}	99.58	3.21	9.57×10^{-7}	99.99	3.73
	4.78×10^{-6}	4.80×10^{-6}	100.32	1.29	4.78×10^{-6}	99.94	2.00
	9.57×10^{-6}	9.56×10^{-6}	99.90	0.64	9.57×10^{-6}	99.99	1.44
Tap water 1	0	< LOD	-	-	< LOD	-	-
	4.78×10^{-7}	4.71×10^{-7}	98.61	7.43	4.81×10^{-7}	100.59	7.47
	9.57×10^{-7}	9.63×10^{-7}	100.65	3.41	9.65×10^{-7}	100.81	4.87
	4.78×10^{-6}	4.82×10^{-6}	100.75	1.49	4.79×10^{-6}	100.27	1.51
	9.57×10^{-6}	9.58×10^{-6}	100.11	0.74	9.59×10^{-6}	100.20	1.57
Tap water 2	0	< LOD	-	-	< LOD	-	-
	4.78×10^{-7}	4.71×10^{-7}	98.61	3.91	4.77×10^{-7}	99.76	4.98
	9.57×10^{-7}	9.63×10^{-7}	100.65	1.85	9.57×10^{-7}	99.99	6.49
	4.78×10^{-6}	4.79×10^{-6}	100.11	0.98	4.77×10^{-6}	99.86	1.87
	9.57×10^{-6}	9.55×10^{-6}	99.79	0.49	9.57×10^{-6}	100.03	1.62
Tap water 3	0	< LOD	-	-	< LOD	-	-
	4.78×10^{-7}	4.82×10^{-7}	100.75	6.43	4.81×10^{-7}	100.59	7.80
	9.57×10^{-7}	9.53×10^{-7}	99.58	5.56	9.53×10^{-7}	99.57	3.90
	4.78×10^{-6}	4.80×10^{-6}	100.32	2.23	4.78×10^{-6}	99.94	3.24
	9.57×10^{-6}	9.56×10^{-6}	99.90	1.11	9.57×10^{-6}	100.03	1.50

Table S2. Determination of lead(II) by optodes with chromoionophore **1** in real samples and for commercial Standard Reference Solution.

	Added Pb(II) [M]	Found Pb(II)					
		ΔA	Recovery	RSD	ΔE_{RGB}	Recovery	RSD
		Pb(II) [M]	%	%	Pb(II) [M]	%	%
Standard Reference Solution of lead(II)	4.78×10^{-7}	4.73×10^{-7}	98.96	4.65	4.81×10^{-7}	100.54	5.53
	9.57×10^{-7}	9.75×10^{-7}	101.90	2.63	9.55×10^{-7}	100.85	4.18
	4.78×10^{-6}	4.80×10^{-6}	100.48	1.83	4.78×10^{-6}	99.97	2.45
	9.57×10^{-6}	9.56×10^{-6}	99.92	0.91	9.57×10^{-6}	100.03	1.72
Tap water 1	0	< LOD	-	-	< LOD	-	-
	4.78×10^{-7}	4.80×10^{-7}	100.48	9.13	4.86×10^{-7}	101.74	7.24
	9.57×10^{-7}	9.61×10^{-7}	100.19	4.56	9.54×10^{-7}	99.65	5.43
	4.78×10^{-6}	4.82×10^{-6}	100.79	1.90	4.80×10^{-6}	100.45	2.67
	9.57×10^{-6}	9.59×10^{-6}	100.22	1.05	9.60×10^{-6}	100.27	1.84
Tap water 2	0	< LOD	-	-	< LOD	-	-
	4.78×10^{-7}	4.95×10^{-7}	103.53	5.72	4.86×10^{-7}	101.74	6.27
	9.57×10^{-7}	9.46×10^{-7}	98.85	2.36	9.48×10^{-7}	99.05	2.76
	4.78×10^{-6}	4.77×10^{-6}	99.87	2.11	4.77×10^{-6}	99.85	2.27
	9.57×10^{-6}	9.50×10^{-6}	99.31	1.39	9.51×10^{-6}	99.37	1.64
Tap water 3	0	< LOD	-	-	< LOD	-	-
	4.78×10^{-7}	4.73×10^{-7}	98.44	4.65	4.81×10^{-7}	100.54	5.53
	9.57×10^{-7}	9.61×10^{-7}	100.38	4.56	9.54×10^{-7}	99.65	3.62
	4.78×10^{-6}	4.79×10^{-6}	100.18	1.40	4.78×10^{-6}	99.97	1.81
	9.57×10^{-6}	9.58×10^{-6}	100.07	0.71	9.57×10^{-6}	100.03	1.35

Table S3. Dual determination of bismuth(III) and lead(II) by optodes with chromoionophore **1** in real samples and for commercial Standard Reference Solution (1:1).

	Added Bi(III)/Pb(II) [M]	Found Bi(III)			Found Pb(II)		
		ΔA Bi(III) [M]	Recovery %	RSD %	ΔA Pb(II) [M]	Recovery %	RSD %
Standard Reference Solution of bismuth(III) and lead(II) (1:1)	9.57×10^{-7}	9.38×10^{-7}	97.99	5.70	9.52×10^{-7}	99.52	3.96
	4.78×10^{-6}	4.78×10^{-6}	100.07	3.96	4.80×10^{-6}	100.41	2.74
	9.57×10^{-6}	9.61×10^{-6}	100.38	1.98	9.59×10^{-6}	100.18	1.37
Tap water 1	0	< LOD	-	-	< LOD	-	-
	9.57×10^{-7}	9.69×10^{-7}	101.28	7.50	9.74×10^{-7}	101.81	3.96
	4.78×10^{-6}	4.81×10^{-6}	100.73	4.12	4.82×10^{-6}	100.87	2.86
	9.57×10^{-6}	9.64×10^{-6}	100.71	2.06	9.61×10^{-6}	100.41	1.43
Tap water 2	0	< LOD	-	-	< LOD	-	-
	9.57×10^{-7}	9.06×10^{-7}	94.69	9.88	9.09×10^{-7}	94.95	3.96
	4.78×10^{-6}	4.75×10^{-7}	99.41	4.12	4.78×10^{-7}	99.96	2.86
	9.57×10^{-6}	9.57×10^{-6}	100.05	2.06	9.57×10^{-6}	99.95	1.43
Tap water 3	0	< LOD	-	-	< LOD	-	-
	9.57×10^{-7}	9.53×10^{-7}	99.63	4.94	9.42×10^{-7}	98.38	5.23
	4.78×10^{-6}	4.75×10^{-6}	99.41	3.82	4.78×10^{-6}	99.96	2.58
	9.57×10^{-6}	9.64×10^{-6}	100.71	2.28	9.59×10^{-6}	100.18	2.19